PLANT-WATER RELATIONS FOR SUSTAINABLE AGRICULTURE

EDITED BY: Thorsten M. Knipfer and Italo F. Cuneo

PUBLISHED IN: Frontiers in Plant Science

frontiers Research Topics

frontiers

ISSN 1664-8714
ISBN 978-2-88976-891-2
DOI 10.3389/978-2-88976-891-2

About Frontiers

Frontiers is more than just an open-access publisher of scholarly articles: it is a pioneering approach to the world of academia, radically improving the way scholarly research is managed. The grand vision of Frontiers is a world where all people have an equal opportunity to seek, share and generate knowledge. Frontiers provides immediate and permanent online open access to all its publications, but this alone is not enough to realize our grand goals.

Frontiers Journal Series

The Frontiers Journal Series is a multi-tier and interdisciplinary set of open-access, online journals, promising a paradigm shift from the current review, selection and dissemination processes in academic publishing. All Frontiers journals are driven by researchers for researchers; therefore, they constitute a service to the scholarly community. At the same time, the Frontiers Journal Series operates on a revolutionary invention, the tiered publishing system, initially addressing specific communities of scholars, and gradually climbing up to broader public understanding, thus serving the interests of the lay society, too.

Dedication to Quality

Each Frontiers article is a landmark of the highest quality, thanks to genuinely collaborative interactions between authors and review editors, who include some of the world's best academicians. Research must be certified by peers before entering a stream of knowledge that may eventually reach the public - and shape society; therefore, Frontiers only applies the most rigorous and unbiased reviews.
Frontiers revolutionizes research publishing by freely delivering the most outstanding research, evaluated with no bias from both the academic and social point of view. By applying the most advanced information technologies, Frontiers is catapulting scholarly publishing into a new generation.

What are Frontiers Research Topics?

Frontiers Research Topics are very popular trademarks of the Frontiers Journals Series: they are collections of at least ten articles, all centered on a particular subject. With their unique mix of varied contributions from Original Research to Review Articles, Frontiers Research Topics unify the most influential researchers, the latest key findings and historical advances in a hot research area! Find out more on how to host your own Frontiers Research Topic or contribute to one as an author by contacting the Frontiers Editorial Office: frontiersin.org/about/contact

PLANT-WATER RELATIONS FOR SUSTAINABLE AGRICULTURE

Topic Editors:
Thorsten M. Knipfer, University of British Columbia, Canada
Italo F. Cuneo, Pontificia Universidad Católica de Valparaíso, Chile

Citation: Knipfer, T. M., Cuneo, I. F., eds. (2022). Plant-Water Relations for Sustainable Agriculture. Lausanne: Frontiers Media SA.
doi: 10.3389/978-2-88976-891-2

Table of Contents

frontiers | Frontiers in Plant Science

TYPE Editorial
PUBLISHED 28 July 2022
DOI 10.3389/fpls.2022.979804

OPEN ACCESS

EDITED AND REVIEWED BY
Ingo Dreyer,
University of Talca, Chile

*CORRESPONDENCE
Thorsten Knipfer
thorsten.knipfer@ubc.ca
Italo F. Cuneo
italo.cuneo@pucv.cl

SPECIALTY SECTION
This article was submitted to Plant Biophysics and Modeling, a section of the journal Frontiers in Plant Science

RECEIVED 28 June 2022
ACCEPTED 11 July 2022
PUBLISHED 28 July 2022

CITATION
Knipfer T and Cuneo IF (2022) Editorial: Plant-water relations for sustainable agriculture. *Front. Plant Sci.* 13:979804. doi: 10.3389/fpls.2022.979804

Editorial: Plant-water relations for sustainable agriculture

Thorsten Knipfer[1]* and Italo F. Cuneo[2]*

[1]Faculty of Land and Food Systems, The University of British Columbia, Vancouver, BC, Canada, [2]Facuty of Agriculture and Food Science, Pontificia Universidad Católica de Valparaíso, Valparaíso, Chile

KEYWORDS

plant hydraulics, water relations, irrigation, water use efficiency, drought

Editorial on the Research Topic
Plant-water relations for sustainable agriculture

Ongoing climate change causes unprecedented challenges for agriculture. The modern farmer requires advanced knowledge about plant stress physiology to avoid losses in crop production and quality. This Research Topic on "Plant water relations for Sustainable Agriculture" provides advanced understanding of the mechanisms and responses of crops to water stress by drought and waterlogging.

Crop performance depends on a successful coordination of physiological, anatomical, molecular and morphological processes at root, stem, and leaf level. In this issue, Gervais et al. conducted a large screening study of potato drought stress performance. Authors found differences in tuber yield between drought tolerant and susceptible genotypes and an increase in water use efficiency (WUE) by 2–3-fold in more drought tolerant genotypes. Similarly, Martínez et al. identified differences in physiological performance and productivity in response to soil water availability (i.e., full irrigation and rainfed conditions) among several potato varieties. They found that water stress negatively affects tuber size distribution, reducing overall production by 50–60%. In an effort to improve the selection of drought tolerant rice genotypes, Mahreen et al. combined morpho-physiological and biochemical approaches with infrared thermal imaging technology. Using reliable, fast, and non-destructive technology may accelerate the selection of drought tolerant genotypes in breeding programs. Zheng et al. shows that improving root morphological traits and alleviating root senescence during mid-grain filling are important characteristics that could be used in wheat breeding programs targeting high yield and water use efficiency. For different maize hybrids, Alam et al. reported on the effect of different levels of drought stress on kernel water relations and filling in a tropical environment. On a molecular level, the study of Liang et al. points toward a better understanding of metabolic pathways for improving water management. The authors present a detailed metabolomic depiction of the importance of soil arbuscular mycorrhizal fungi that enhances drought tolerance in trifoliate orange. Similarly, and also in trifoliate orange, Cheng et al. studied the effect of arbuscular mycorrhizal fungi in regulating H+-ATPase activity and gene expression. They showed that inoculated plants exhibit greater photosynthetic rate, stomatal conductance, and

better root characteristics than non-mycorrhizal plants. In contrast, Liu D. et al. reported on problems of water stress by flooding in peanut. The authors used proteomics analysis, and found different metabolic mechanisms that affect the accumulation of toxic substances and enhance anaerobic respiration activity of enzymes. Together, this knowledge facilitates the selection of crop genotypes with improved drought tolerance and the development of sustainable irrigation practices.

Irrigation strategies should be informed by key aspects of plant hydraulics. In this issue, Luo et al. presents a leaf hydraulics model that captures spatiotemporal changes of water potential and flow rates in monocotyledonous and dicotyledonous leaves. The authors point to a substantial contribution of leaf capacitance and resistances that should be acknowledged when interpreting leaf hydraulics in the context of water management on a field scale. For horticultural trees, Sheridan and Nackley used traditional plant hydraulic methods to investigate their desiccation during prolonged cold storage. Their results provide key information to nurseries for improving plant management.

Crop water requirements change daily and annually based on environmental conditions. The pressure chamber provides a tool for measuring plant water status in a cost-effective and robust way. For olive trees, Shackel et al. presents a large data set on stem water potentials and vapor pressure deficit collected over multiple years. The authors established a reference baseline for olives that will allow growers to utilize plant-based irrigation management at olive orchard level. On a related topic, Zhang et al. shows how vapor pressure deficit affects photosynthetic carbon dioxide uptake in a process mediated by foliar abscisic acid content in tomato. This study provides basic information related to the complex water relations at leaf level and how they affect whole plant water relations. Measurements of soil moisture can serve as an indirect indicator of plant water status. Niu et al. used a specific water system to maintain a stable soil moisture level, improving water use efficiency in maize subjected to short-term soil water stress.

For crop production, the meaning of "drought" can be many-fold, but our goal must be to identify ways to maintain production under water-limiting conditions while protecting water as one of our most important natural resources. On this, management becomes crucial, for example, Liu R. et al. presents data that shows that alternate partial root-zone drip nitrogen fertigation improves water use efficiency while reducing the loss of residual nitrate in the soil profile. Also, data presented in this issue shows that specific soil management, such as subsoiling plus organic fertilization, improves water use efficiency by positively impacting soil structure (Yang et al.). The design of orchards with the focus placed in water savings requires key physiological information. Selecting grapevine drought tolerant rootstocks is a complex decision for viticulturists. Villalobos-Soublett et al. present data from naturalized grapevine rootstocks from arid regions of Chile that allows to adapt vineyards to regions with low water availability while maintaining adequate physiological performance for crop production. Stress management at field level requires understanding of key physiological signals of stress such as the balance between reactive oxygen species (ROS) and the antioxidative system (AOS) in plants. Rane et al. provides a thorough review of the role of ROS–AOS relation that ultimately affect photosynthetic efficiency and growth in dryland agricultural crop plants.

Under a fast-changing environment, it is clear that the modern farmer is challenged to make appropriate decisions. This issue highlights that an advanced understanding of crop performance can improve the decision-making process, at least in part. Also, this issue highlights how diverse and multi-layered research in the plant water relations community is to find best solutions to secure crop performance and yield under conditions of water stress. The future will provide extreme challenges for agriculture with water availability as the main driver.

Author contributions

All authors listed have made a substantial, direct, and intellectual contribution to the work and approved it for publication.

Funding

This work was supported by an operating grant from the Natural Sciences and Engineering Research Council of Canada (NSERC, GR019368 awarded to TK).

Conflict of interest

The authors declare that the research was conducted in the absence of any commercial or financial relationships that could be construed as a potential conflict of interest.

Publisher's note

frontiers in Plant Science

ORIGINAL RESEARCH
published: 25 March 2021
doi: 10.3389/fpls.2021.659694

Arbuscular Mycorrhizal Fungi Alleviate Drought Stress in Trifoliate Orange by Regulating H^+-ATPase Activity and Gene Expression

Hui-Qian Cheng[1], Ying-Ning Zou[1], Qiang-Sheng Wu[1,2] and Kamil Kuča[2]**

[1] College of Horticulture and Gardening, Yangtze University, Jingzhou, China, [2] Department of Chemistry, Faculty of Science, University of Hradec Kralove, Hradec Kralove, Czechia

A feature of arbuscular mycorrhiza is enhanced drought tolerance of host plants, although it is unclear whether host H^+-ATPase activity and gene expression are involved in the physiological process. The present study aimed to investigate the effects of an arbuscular mycorrhizal fungus (AMF), *Funneliformis mosseae*, on H^+-ATPase activity, and gene expression of trifoliate orange (*Poncirus trifoliata*) seedlings subjected to well-watered (WW) and drought stress (DS), together with the changes in leaf gas exchange, root morphology, soil pH value, and ammonium content. Soil drought treatment dramatically increased H^+-ATPase activity of leaf and root, and AMF inoculation further strengthened the increased effect. A plasma membrane (PM) H^+-ATPase gene of trifoliate orange, PtAHA2 (MW239123), was cloned. The *PtAHA2* expression was induced by mycorrhization in leaves and roots and also up-regulated by drought treatment in leaves of AMF-inoculated seedlings and in roots of AMF- and non-AMF-inoculated seedlings. And, the induced expression of *PtAHA2* under mycorrhization was more prominent under DS than under WW. Mycorrhizal plants also showed greater photosynthetic rate, stomatal conductance, intercellular CO_2 concentration, and transpiration rate and better root volume and diameter than non-mycorrhizal plants under DS. AMF inoculation significantly increased leaf and root ammonium content, especially under DS, whereas it dramatically reduced soil pH value. In addition, H^+-ATPase activity was significantly positively correlated with ammonium contents in leaves and roots, and root H^+-ATPase activity was significantly negatively correlated with soil pH value. Our results concluded that AMF stimulated H^+-ATPase activity and *PtAHA2* gene expression in response to DS, which resulted in great nutrient (e.g., ammonium) uptake and root growth, as well as low soil pH microenvironment.

Keywords: citrus, H^+-ATPase, mycorrhiza, proton pump, water deficit

OPEN ACCESS

Edited by:
Italo F. Cuneo, Pontificia Universidad Católica de Valparaíso, Chile

Reviewed by:
Yong-ming Huang, Hubei Academy of Agricultural Sciences, China
Xiancan Zhu, Anhui Normal University, China

****Correspondence:***
Qiang-Sheng Wu
wuqiangsh@163.com
Kamil Kuča
kamil.kuca@uhk.cz

Specialty section:
This article was submitted to Plant Abiotic Stress, a section of the journal Frontiers in Plant Science

Received: *28 January 2021*
Accepted: *01 March 2021*
Published: *25 March 2021*

Citation:
Cheng H-Q, Zou Y-N, Wu Q-S and Kuča K (2021) Arbuscular Mycorrhizal Fungi Alleviate Drought Stress in Trifoliate Orange by Regulating H^+-ATPase Activity and Gene Expression. Front. Plant Sci. 12:659694. doi: 10.3389/fpls.2021.659694

INTRODUCTION

Drought is one of the most serious environmental stresses, which severely restrains the growth and productivity of crop by destroying various physiological and biochemical processes such as nutrient absorption, photosynthesis, and cell metabolism (Zhang et al., 2020). As the initial site of damage after stress, changes in cell membrane structure negatively affect transport of various inorganic

ions (Yoshida, 1991). Studies have demonstrated that cells regulated ion balances by changing the transmembrane transport of both ions and small molecules to maintain cell osmotic pressure under drought stress (DS) (Mak et al., 2014). Therefore, it is of profound significance to evaluate the transmembrane transport of key ions for revealing the mechanism of plants in response to DS.

Plasma membrane (PM) H^+-ATPase is a kind of main membrane proteins widely existing in plant organelles (Małgorzata et al., 2018). Based on an electrical gradient inside and outside, H^+ enters and exits the cell PM providing a driving force for the transport of small molecules, which is associated with mineral nutrient (NH_4^+) absorption, metabolite discharge, cytoplasmic pH regulation, cell growth, and stomata opening (Gaxiola et al., 2007). According to the "acid" growth theory, plant growth requires acidification of the cell wall space, and such acidification is derived by H^+ effluxes of PM H^+-ATPase, indicating that the H^+ efflux is regulated by the proton pump, and thus, the acidification of the cell wall is important for root elongation (Staal et al., 2011). Similarly, optimal primary root growth and root hair development also require PM H^+-ATPase to finely regulate H^+ secretion of root tips (Haruta and Sussman, 2012). In *Arabidopsis*, a total of 11 PM H^+-ATPase genes are identified and defined as AHA1–AHA11 (*Arabidopsis* PM H^+-ATPase isoforms) (Palmgren, 2001). Among these isoforms, AHA2 is a housekeeping gene expressed at high levels and is the predominant proton pump in plant roots, contributing to the pH homeostasis and root growth and development (Młodzińska et al., 2014).

Arbuscular mycorrhizal fungi (AMF) form symbiotic association with roots of most terrestrial plants. Host plants transfer carbohydrates to AMF for mycelial growth and spore development; on the other hand, mycorrhizal hyphae enable to absorb nutrients from the soil to the host, thus promoting plant growth and nutrient acquisition (Aggarwal et al., 2011). It has been reported that AMF increased water absorption, nutrient absorption, photosynthesis, root structure, antioxidant defense systems, polyamine and fatty acid homeostasis, osmotic adjustment, aquaporin expression, soil structure, and hormone balance to resist soil water deficit (Wu et al., 2013, 2019; Fernández-Lizarazo and Moreno-Fonseca, 2016; He et al., 2020; Zou et al., 2020). These reactions are the result of a combination of nutritional, physical, and cellular effects. In addition, studies have shown that hyphal H^+ effluxes and spores growth rate were stimulated during the presymbiotic development of *Gigaspora margarita*, which is related to phosphorus and sucrose deficiency (Ramos et al., 2008b). And, in the symbiosis of maize and mycorrhizal fungi, the H^+ pump activity of the host plant was differently regulated by AMF (Ramos et al., 2009). Liu et al. (2020) reported that the tomato AM-specific H^+-ATPase, *SIHA8*, was evolutionarily conserved in maintaining arbuscule development. In tobacco, Gianinazzi-Pearson et al. (2000) reported the expression of *H^+-ATPase* located in cortical parenchyma of AMF-colonized cells only. In addition, two P-type HA genes *GmHA5* and *GmPMA1* were encoded in *Glomus mosseae* (Ferrol et al., 2000; Requena et al., 2003). However, the relationship between AMF and *PM H^+-ATPase* gene (especially *AHA2*) expressions of host plants under water deficit is not yet known.

Here, we hypothesized that AMF potentially regulated PM H^+-ATPase activity and *AHA2* gene expression under DS, thus promoting root growth and nutrient (NH_4^+) acquisition to tolerate soil drought. To confirm the above hypothesis, trifoliate orange (*Poncirus trifoliata* L. Raf., a drought-sensitive citrus rootstock) was selected and inoculated with an AMF *Funneliformis mosseae*. Leaf gas exchange, root morphology, H^+-ATPase activity and *AHA2* gene expression in leaf and root, soil pH value, and ammonium content of trifoliate orange were determined under well-watered (WW) and DS.

MATERIALS AND METHODS

Experimental Design

The experiment was a completely random design with two soil water regimes (WW and DS) and two AMF inoculations (+AMF and -AMF). Each treatment had eight replicates, in a total of 32 pots (three seedlings per pot).

Mycorrhizal Fungal Inoculants

Funneliformis mosseae (Nicol. and Gerd.) C. Walker & A. Schüβler [BGC XJ02] was selected. The arbuscular mycorrhizal fungal strain was provided by the Bank of Glomales in China (BGC) and propagated with white clover as its host for 3 months under greenhouse and potted conditions. At harvest time, the shoot of the white clover was removed, and roots and growth substrates were collected as the mycorrhizal inoculants, which contained the fungal spores (22 spores/g), sporocarps, mycorrhizal hyphae, and colonized roots.

Plant Culture

The four-leaf-old trifoliate orange seedling that was grown in autoclaved sand in an incubator at 26°C was transferred into a 1.4-L plastic pot containing 1.2 kg of autoclaved soil and sand (5:3, vol/vol). The soil properties had been described in detail in Cheng et al. (2021). At the time of transplanting the seedlings, 100 g of mycorrhizal inoculums was applied into trifoliate orange seedlings as the AMF treatment. The non-AMF treatment received 100 g autoclaved (0.11 MPa, 121°C, 1.5 h) mycorrhizal inoculums plus 2-mL filtrates (25-μm filters) of inoculums.

Before soil drought began, potted soil water maintained 75% maximum field water-holding capacity (corresponding to WW) by weighing the pots every day. After 11 weeks, half of the mycorrhizal and non-mycorrhizal plants were exposed to the 55% maximum field water-holding capacity (corresponding to DS) for 8 weeks, and the other half was continued to grow in soil with WW status for 8 weeks. Thereafter, these treated seedlings were harvested. During the experiment, positions of the pots were swapped weekly to reduce the environmental impact. The plants were grown in a greenhouse from March 24 to August 5, 2019, where the day/night temperature was 28°C/21°C, relative humidity 68%, and photon flux density 880 $\mu mol/m^2$ per second.

Determination of Leaf Gas Exchange

On a sunny morning from 9:00 to 11:00 am before the plants were harvested, leaf gas exchange was determined using a Li-6400 Portable Photosynthesis System (Li-Cor Inc., Lincoln, NE, United States) in the fully extended leaf. Photosynthetic rate (Pn), stomatal conductance (g_s), intercellular CO_2 concentration (Ci), transpiration rate (Tr), and leaf temperature were recorded after steady state of gas exchange.

Determination of Root Mycorrhizal Colonization and Root Morphology

Root mycorrhizas were stained by 0.05% trypan blue as described by Phillips and Hayman (1970). Root mycorrhizal colonization degree was assessed as the percentage of root lengths colonized by mycorrhizal fungi against total observed root lengths. The intact roots were carefully scanned by the Epson Perfection V700 Photo Dual Lens System (J221A, Seiko Epson Corporation, Jakarta, Indonesia), and then the obtained root figures were analyzed with a WinRHIZO professional software (Regent Instruments Inc., Quebec, Canada) for root area, volume, and average diameter.

Determination of H+-ATPase Activity in Leaf and Root

The activity of H+-ATPase in leaf and root was determined by the enzyme-linked immunosorbent assay (ELISA). A 0.3-g fresh plant sample was ground under liquid nitrogen, incubated with phosphate buffer (pH 7.4), and centrifuged at 8,000*g* for 30 min. The supernatant was collected, and the H+-ATPase activity was assayed by the H+-ATPase ELISA kits (ml73629, Shanghai Enzyme-linked Biotechnology Co., Ltd., Shanghai, China) according to the user's guide.

Polymerase Chain Reaction Amplification and Sequence Analysis of PtAHA2 (a PM H+-ATPase Gene)

Based on the known *AHA2* (*Arabidopsis* PM H+-ATPase isoform 2) gene sequence (AT4G30190) in *Arabidopsis thaliana* and the BLAST result of sweet orange genome[1], a pair of primers (F: 5′-CCCAACAAGCTAGAA GAGAAAAAG-3′; R: 5′-CGCGAGTAATGTTTTTTCCTTCTG-3′) were designed with the most homologous gene sequence (Cs4g03700.1) for open reading frame amplification.

Total RNA was extracted and purified from leaves and roots of trifoliate orange seedlings with the EASY spin Plus plant RNA kit (RN 38, Aidlab Biotecnolohies Co., Ltd., Beijing, China). After determining the concentration and purity of the isolated RNA by spectrophotometers at 260 and 280 nm, the RNA was reverse-transcribed into cDNA using the kit PrimeScript™ RT reagent kit with a gDNA eraser (PK02006, TaKaRa Bio. Inc., Tokyo, Japan). The polymerase chain reaction (PCR) amplification was initiated using the Planta max super-fidelity DNA polymerase kit (Vazyme Biotech Co., Ltd., Nanjing, China) and recovered the destination fragment by the universal DNA purification kit (TianGen Biotech Beijing Co., Ltd., Beijing, China). The pEASY®-Blunt Zero Cloning Kit (Beijing TransGene Biotech Co., Ltd., Beijing, China) was used for the ligation and transformation of the target fragment. Afterward, it was

[1]http://citrus.hzau.edu.cn/orange/index.php

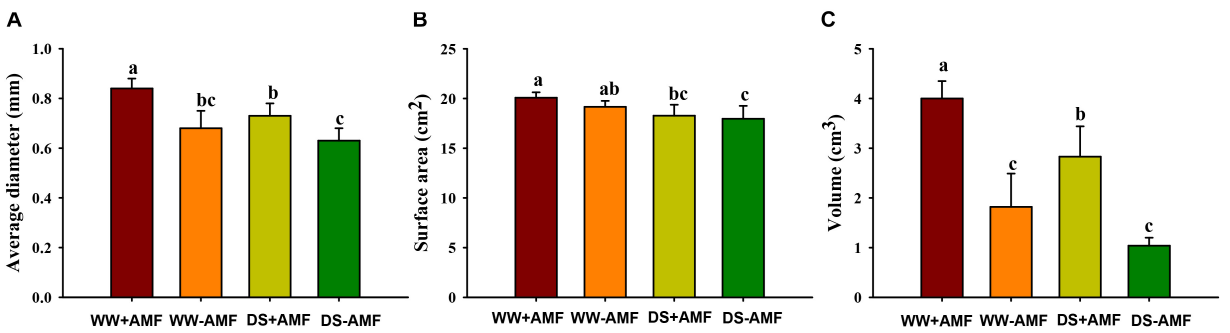

FIGURE 1 | Effects of *Funneliformis mosseae* on root average diameter **(A)**, root surface area **(B)**, and root volume **(C)** of trifoliate orange (*Poncirus trifoliata*) seedlings subjected to well-watered (WW) and drought stress (DS). Data (means ± SD, $n = 4$) followed by different letters above the bars indicate significant differences ($P < 0.05$) between treatments.

TABLE 1 | Effects of *Funneliformis mosseae* on leaf gas exchange of trifoliate orange (*Poncirus trifoliata*) seedlings subjected to well-watered (WW) and drought stress (DS).

Treatments	Pn (μmol/m² per second)	g_s (μmol/m² per second)	Ci (μmol/mol)	Tr (mmol/m² per second)	Leaf temperature (°C)
WW + AMF	5.47 ± 0.90a	96.14 ± 5.80a	339.58 ± 18.28a	2.06 ± 0.47a	34.01 ± 0.62b
WW-AMF	2.50 ± 0.39c	28.45 ± 4.60c	233.22 ± 18.03c	0.61 ± 0.26c	34.69 ± 0.89a
DS + AMF	4.63 ± 1.05b	47.76 ± 6.84b	301.96 ± 10.30b	1.10 ± 0.42b	34.57 ± 0.62a
DS-AMF	1.92 ± 0.68d	23.47 ± 4.41d	187.90 ± 16.53d	0.47 ± 0.10c	34.64 ± 0.82a

Data (means ± SD, n = 4) followed by different letters in the column indicate significant differences (P < 0.05) between treatments.

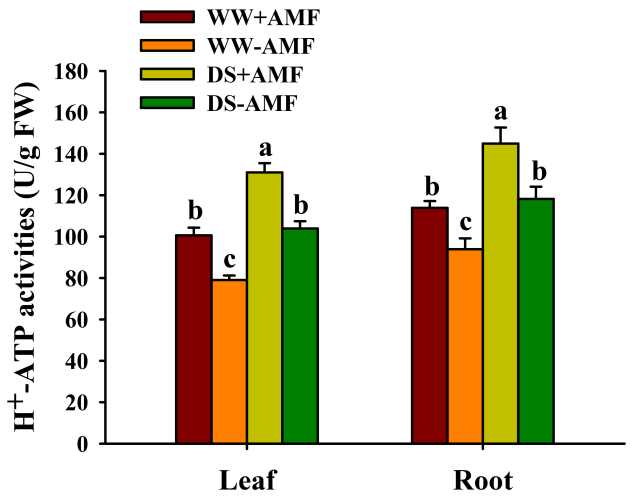

FIGURE 2 | Effects of *Funneliformis mosseae* on leaf and root H^+-ATP activities of trifoliate orange (*Poncirus trifoliata*) seedlings subjected to well-watered (WW) and drought stress (DS). Data (means ± SD, $n = 4$) followed by different letters above the bars indicate significant differences ($P < 0.05$) between treatments.

screened on LB plates coated with kanamycin, and positive clones were isolated by PCR for sequencing. DNAMAN5.2.2 (Lynnon Biosoft, Quebec, Canada) and MEGA 7[2] were used to analyze the sequence alignment and the phylogenetic tree analysis, respectively.

Relative Expressions of *PtAHA2*

The primer was designed based on the predicted PM PtAHA gene sequence. Accumulation of transcript was measured by quantitative real-time PCR (Light Cycler480 System, Roche Diagnostics, Switzerland) using the TB Green premix Ex^{TM} TaqII for fluorescence quantitative analysis. Gene-specific primer sequences of *PtAHA2* gene were as follows: F: 5′-GATGGTAAATGGAGTGAGGAAGAAG-3′; R: 5′-GGATTTTTGGTGACAGGAAGAGAT T-3′. The β-actin gene (Cs1g05000; forward: 5′-CCGACCGTATGAGCAAGGAAA-3′; reverse: 5′-TTCCTGTGGACAATGGATGGA-3′) was used as the housekeeping gene. The expression level of *PtAHA2* was normalized to the expression level of non-AMF plants exposed to WW. The $2^{-\Delta\Delta CT}$ method was used to calculate the relative quantification (Livak and Schmittgen, 2001).

Determination of Soil pH Value

A 10-g air-dried soil sample through 2-mm sieves was mixed with 25 mL distilled water without CO_2 (soil:water = 1:2.5) and shaken well with a magnetic stirrer. After 30 min, the pH value of the supernatant was determined using a pH meter (pH828+, Smart Sensor, Dongguan, China) after precalibration.

[2]www.megasoftware.net

Determination of Ammonium Content in Leaf and Root

Ammonium content in leaf and root was determined by the ninhydrin method described by Tang (1999). A 0.5-g fresh sample was ground with 5 mL of 10% acetic acid and filtered. Afterward, 2-mL filtrate was mixed with 3 mL of the ninhydrin reagent ($C_9H_4O_3 \cdot H_2O$)and 0.1 mL of 1% ascorbic acid solution at 100°C for 15 min. After cooling, the absorbance of the solution was determined at 580 nm.

Statistical Analysis

All the data were analyzed with the analysis of variation according to SAS software (SAS Institute, Inc., Cary, NC, United States), and significant differences between treatments were compared by the Duncan multiple-range tests at $p = 0.05$ level. The Pearson correlation coefficient between two specified variables was analyzed with SAS software.

RESULTS

Changes in Root Mycorrhizal Colonization and Root Morphology

Mycorrhizal fungal colonization was not found in the roots of uninoculated plants, whereas the root mycorrhizal colonization rate of the inoculated plants was 46.91% ± 1.86% under WW and 34.11% ± 7.10% under DS, respectively. The DS treatment significantly reduced root mycorrhizal colonization, compared with the WW treatment. Drought treatment also inhibited root morphology to a certain extent, and *F. mosseae* inoculation partly mitigated the inhibitive effect (**Figures 1A–C**). Compared with non-AMF treatment, AMF inoculation increased root average diameter and volume, respectively, by 23.53 and 119.78% under WW and by 15.87 and 172.11% under DS, respectively (**Figures 1A,C**). Mycorrhizal fungal treatment did not significantly affect root surface area, regardless of soil water regimes (**Figure 1B**).

Changes in Leaf Gas Exchange

Drought treatment significantly decreased leaf Pn, g_s, Ci, and Tr, compared with WW treatment (**Table 1**). Compared with non-mycorrhizal fungal plants, *F. mosseae*–inoculated plants recorded significantly higher leaf Pn, g_s, Ci, and Tr by 118.80, 237.93, 45.61, and 237.70% under WW and by 141.15, 103.49, 60.70, and 134.04% under DS, respectively. In addition, leaf temperature was markedly reduced by *F. mosseae* inoculation by 1.67% under WW only.

Changes in Leaf and Root H^+-ATPase Activity

Soil drought treatment significantly increased H^+-ATPase activity in leaf and root, irrespective of AMF inoculation or not (**Figure 2**). On the other hand, AMF colonization distinctly enhanced H^+-ATPase activity in leaf by 27.37 and 26.06% and in root by 22.14 and 22.61% under WW and DS conditions, respectively, compared with non-AMF colonization.

Sequence Analyses of PtAHA2

A total of 2,965 bp in PM H$^+$-ATPase gene (*PtAHA2*) encoding 885 amino acids were cloned from trifoliate orange, based on sweet orange database and homologous cloning. A GenBank accession number of *PtAHA2* was MW239123. The sequencing of the *PtAHA2* showed that the protein sequence homology between trifoliate orange and sweet orange was 99.66% by DNAMAN (**Supplementary Material 1**), suggesting that trifoliate orange has a high homology with sweet orange. In addition, multiple sequence alignment indicated that the sequence homology of *PtAHA2* proteins with other *AHA2* families was 83.72% (**Figure 3**), indicating that HA2-type proteins have high sequence conservation. Based on the phylogenetic tree analysis of *PtAHA2*, five H$^+$-ATPase genes in *Arabidopsis* (*AtAHA2*, *AtAHA6*, *AtAHA7*, *AtAHA4*, and *AtAHA10*) and five H$^+$-ATPase genes in *Oryza sativa* (*OsAHA7*, *OsAHA6*, *OsAHA8*, *OsAHA1*, and *OsAHA9*) from families I to V by MEGA 7, *PtAHA2* belonged to subfamily I, which was clustered with *OsAHA7* and *AtAHA2* (**Supplementary Material 2**).

Changes in *PtAHA2* Gene Expression

Compared with WW treatment, DS treatment did not affect the *PtAHA2* expression in leaves of non-mycorrhizal plants, while it induced the expression of *PtAHA2* in leaves of mycorrhizal seedlings and in roots of mycorrhizal and non-mycorrhizal seedlings (**Figure 4**). Moreover, the expression of *PtAHA2* in roots was relatively higher than in leaves. In addition, leaf and root *PtAHA2* gene expression was increased under mycorrhization by 1.62- and 9.50-fold under WW and by 5.62- and 20.92-fold under DS, respectively.

Changes in Soil pH Value

Soil pH value was affected by mycorrhization, but not soil drought treatment (**Figure 5**). Compared with non-AMF

FIGURE 3 | Sequence alignments of *PtAHA2* with *HA2* proteins from other plants. *AHA2*: *Arabidopsis thaliana*; *CsHA2*: *Cucumis sativus*; *LHA2*: *Lycopersicon esculentum*; *MxHA2*: *Malus xiaojinensis*; *OSA2*: *Oryza sativa*; *PPA2*: *Prunus persica*; *VHA2*: *Vicia faba*; *PtAHA2*: *Poncirus trifoliata*.

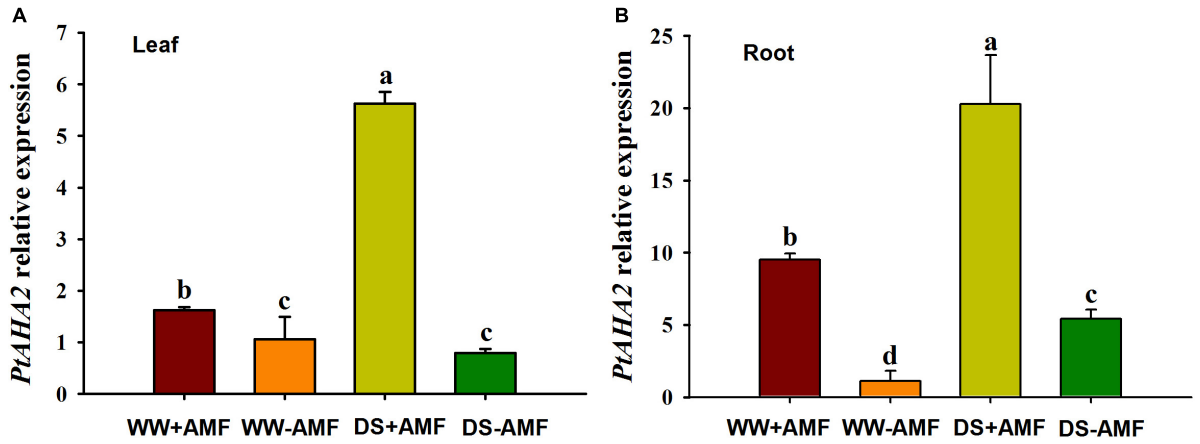

FIGURE 4 | Effects of *Funneliformis mosseae* on relative expression of leaf **(A)** and root **(B)** plasma membrane H^+-ATPase gene *PtAHA2* in trifoliate orange (*Poncirus trifoliata*) seedlings subjected to well-watered (WW) and drought stress (DS). Data (means ± SD, $n = 3$) followed by different letters above the bars indicate significant differences ($P < 0.05$) between treatments.

inoculation, AMF inoculation significantly reduced soil pH value by 12.04 and 14.67% under WW and DS, respectively.

Changes in Leaf and Root Ammonium Content

Leaf and root ammonium contents were not significantly affected by soil DS treatment, irrespective of mycorrhizal and non-mycorrhizal plants (**Figure 6**). AMF colonization significantly enhanced the absorption of ammonium in leaf and root by 26.79 and 43.33% under DS, respectively, compared with non-AMF colonization. Under WW, AMF-inoculated plants recorded 17.65% significantly higher leaf ammonium content than non-AMF-inoculated plants, although no significant difference in root ammonium content was found between AMF- and non-AMF-inoculated plants.

Correlation Studies

Based on the correlation analysis between H^+-ATPase and selective variables, we found that leaf H^+-ATPase activity was significantly ($P < 0.01$) positively correlated with leaf ammonium content (**Figure 7A**). Root H^+-ATPase activity was significantly ($P < 0.05$) positively correlated with root ammonium content (**Figure 7B**) and negatively ($P < 0.01$) correlated with soil pH value (**Figure 7C**).

DISCUSSION

Earlier studies showed that mycorrhizal plants had greater leaf gas exchange capacity than non-mycorrhizal plants subjected to abiotic stress (e.g., DS and salt stress) (Porcel and Ruiz-Lozano,

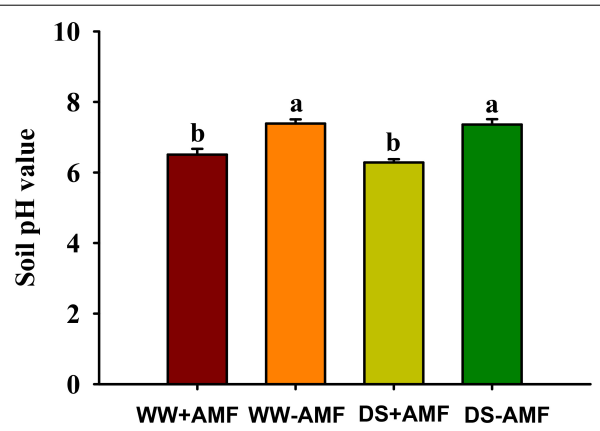

FIGURE 5 | Effects of *Funneliformis mosseae* on soil pH value in trifoliate orange (*Poncirus trifoliata*) seedlings subjected to well-watered (WW) and drought stress (DS). Data (means ± SD, $n = 4$) followed by different letters above the bars indicate significant differences ($P < 0.05$) between treatment.

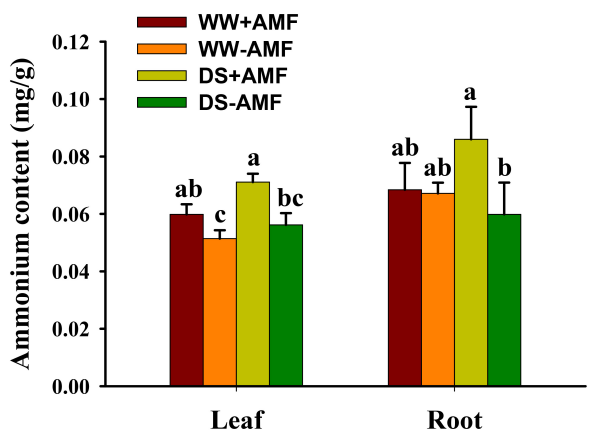

FIGURE 6 | Effects of *Funneliformis mosseae* on leaf and root ammonium contents in trifoliate orange (*Poncirus trifoliata*) seedlings subjected to well-watered (WW) and drought stress (DS). Data (means ± SD, $n = 4$) followed by different letters above the bars indicate significant differences ($P < 0.05$) between treatment.

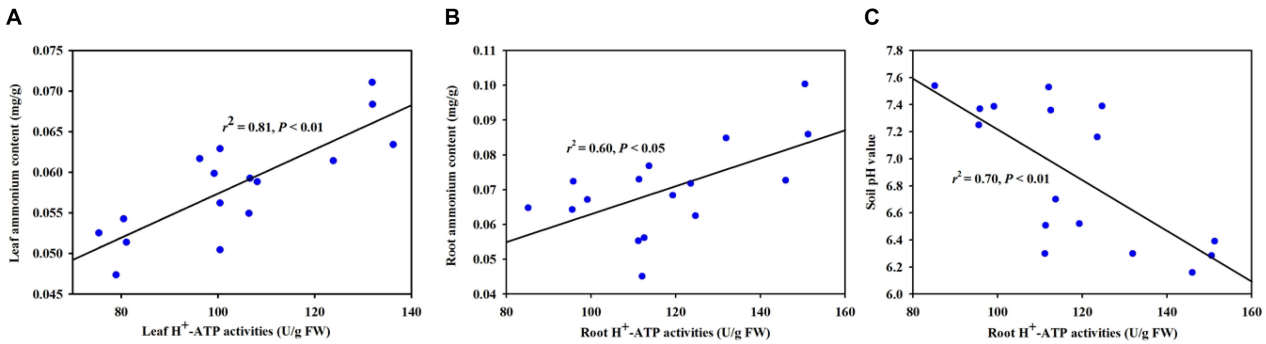

FIGURE 7 | Linear regression between H^+-ATPase activity and ammonium content in leaf **(A)** and root **(B)** and between root H^+-ATPase activity and soil pH value **(C)** (n = 16).

2004; Xiong et al., 2007; Augé et al., 2015). Our study also confirmed that Pn, g_s, Ci, and Tr of mycorrhizal trifoliate orange seedlings were significantly higher than that of non-mycorrhizal seedlings under both WW and DS, implying that mycorrhizal symbiosis has the ability to improve leaf gas exchange of the host under DS. As a result, mycorrhizal plants might produce more carbohydrates for the growth of both the host and the mycorrhizal fungus and also stimulate the transport of water exposed to DS (Hadian-Deljou et al., 2020). In addition, *H^+-ATPase* genes such as *AHA2* were highly expressed in guard cells of *Arabidopsis* for stomatal opening (Ueno et al., 2005). Overexpression of *AHA2* in guard cells of *Arabidopsis* could manipulate stomatal opening, thereby improving plant growth (Wang et al., 2014). In the present study, we concluded that the up-regulated expression of *PtAHA2* in leaf by mycorrhization may be associated with better leaf gas exchange of mycorrhizal plants, especially stomatal opening under DS.

Plant roots contact the soil directly to respond to environmental stress (Ingrain and Malamy, 2010; Franco et al., 2011). The present results showed that the inoculation of *F. mosseae* substantially improved root average diameter and volume under both WW and DS, compared with the non-AMF inoculation. Analogous results have been reported by Zou et al. (2017) in trifoliate orange. It is documented that PM AHA2 is very important for root growth and development, as shown by shorter and lower primary and lateral root length in *aha2* mutant lines of *A. thaliana* versus wild-type plants (Młodzińska et al., 2014). Hence, under WW and DS, *F. mosseae* inoculation induced the activity and gene expression of *PtAHA2* in roots, which potentially stimulates the growth of primary and lateral root, resulting in greater root volume in mycorrhizal plants. As shown in this study, the rhizosphere of mycorrhizal trifoliate orange plants had a low pH environment (**Figure 7**), and indoleacetic acid can be protonized to expand the membrane for transport into the cells, thereby accelerating root growth (Petrasek and Friml, 2009). Therefore, mycorrhizal plants have strong adaptability by optimizing the root morphology to potentially mitigate drought damage (Chu et al., 2014).

In this study, we observed that soil drought treatment dramatically increased leaf and root H^+-ATPase activity in AM and non-AM plants, indicating that trifoliate orange seedlings could rapidly adapt to soil drought environment by enhancing the activity of H^+-ATPase in leaf and root. Furthermore, mycorrhizal trifoliate orange seedlings recorded significantly higher H^+-ATPase activity in leaf and root under both WW and DS conditions, suggesting that H^+-ATPase activity of trifoliate orange could be induced by AMF.

The PM H^+-ATPase is a large gene family that exhibits expression overlap and functional redundancy, but *AHA1* and *AHA2* are highly expressed in almost all tissues and organs (Haruta et al., 2010). Studies by Haruta et al. (2010) showed that single knockout of *AHA1* or *AHA2* did not represent an obvious phenotype, but double knockout is lethal. In our study, *PtAHA2* expression was higher in roots than in leaves, possibly because AHA2 had a strong signal in epidermal and cortex cells of roots, as well as in phloem, xylem, and root hairs (Gianinazzi-Pearson et al., 2000; Fuglsang et al., 2007). The *PtAHA2* expression was induced by soil drought, especially in roots. The AMF-inoculated seedlings recorded dramatically higher expression of *PtAHA2* gene in leaf and root than the non-AMF-inoculated seedlings. And the induced expression of *PtAHA2* under mycorrhization was more prominent under DS than under WW. Thus, *PtAHA2* showed an AMF-specific expression profile. Liu et al. (2016) also analyzed the relative transcript of levels of four tomato *H^+-ATPase* (HA) genes (*SlHA1*, *SlHA2*, *SlHA4*, and *SlHA8*) and found that *SlHA1* and *SlHA4* in leaf and root were not affected by mycorrhization, *SlHA2* was up-regulated by mycorrhization only in root, and *SlHA8* was expressed in root and activated by mycorrhization. This implied that plant *HA* expression could be regulated by mycorrhization, dependent on host plants and HA homologous genes. Further work should analyze the expression of *HA* genes in both host plants and mycorrhizal fungi (e.g., *GmHA5* and *GmPMA1*) in response to DS, which is cooperative or competitive.

In our study, we found lower soil pH value in rhizosphere of mycorrhizal plants versus non-mycorrhizal plant, regardless of soil water regimes. Additionally, soil pH value was significantly negatively correlated with root H^+-ATPase activity, because H^+-ATPase releases protons into rhizosphere, resulting in a low pH environment (Chen et al., 2017). Acidic rhizosphere

under environmental stress conditions is important to the nutrient availability in soil (Ramos et al., 2008a). The H^+ electrochemical gradient generated by H^+-ATPase provides driving forces for nutrients and solutes on the symbiotic membranes and participates in nutrient transfer (Garry et al., 2007). Liu et al. (2020) further analyzed the *SlHA8* expression in tomato and found that the *SlHA8* expression was essential for arbuscule development and symbiotic N uptake. In tobacco, *H^+-ATPase* gene was expressed in AMF-colonized cortical cells only (Gianinazzi-Pearson et al., 2000). In *Medicago truncatula*, a *ha1-2* mutant was isolated and impaired in arbuscule development, but not in root colonization of *Rhizophagus irregularis* (Krajinski et al., 2014). The AMF-induced HA gene was mainly localized in arbuscule-containing cells, where it is the nutrient unloading interface between AMF and hosts. When H^+ ions are released into rhizosphere, plants also absorb ammonium ions into the root to maintain the charge balance (Motte and Beeckman, 2020). Our study also showed that the inoculation with *F. mosseae* dramatically improved ammonium content in leaf under WW and DS and in root under DS, as compared with non-AMF inoculation. Moreover, H^+-ATPase activity was significantly positively correlated with ammonium content. Sun et al. (1999) observed that the activation of the proton pump in mycorrhizal hyphae under drought conditions regulated the rhizospheric microenvironment, resulting in inorganic ions accumulation in the soil. Therefore, the increase of ammonium ions in mycorrhizal plants is related to the induced expression of host *H^+-ATP* gene by mycorrhizal fungi, in addition to mycorrhizal hyphal absorption (Johansen et al., 2010).

CONCLUSION

In short, we cloned a H^+-ATPase gene of trifoliate orange, *PtAHA2*, which is evolutionarily conserved. The *PtAHA2* expression distinctly increased under mycorrhization and soil DS, along with higher H^+-ATPase activity in AM plants versus non-AM plants. The increase in *PtAHA2* gene expression and H^+-ATPase activity under mycorrhization was closely associated with root growth (e.g., root volume and average diameter), nutrient acquisition (ammonium), and leaf gas exchange (e.g., stomatal conductance), which are critical for enhanced drought tolerance of plants. Further analysis of mycorrhiza-specific *PtAHA2* on mycorrhizal plants by molecular techniques such as gene knockout and screening for upstream transcription factors can help us understand the function of *PtAHA2* in response to mycorrhization and DS.

DATA AVAILABILITY STATEMENT

The original contributions presented in the study are included in the article/**Supplementary Material**, further inquiries can be directed to the corresponding authors.

AUTHOR CONTRIBUTIONS

H-QC and Q-SW conceived and designed the experiments. H-QC performed the experiments. H-QC, Y-NZ, Q-SW, and KK analyzed the data. H-QC and Y-NZ prepared the figures. H-QC wrote the manuscript. Q-SW and KK revised the manuscript. All authors contributed to the article and approved the submitted version.

FUNDING

This study was supported by the National Key Research and Development Program of China (2018YFD1000303) and the Plan in Scientific and Technological Innovation Team of Outstanding Young Scientists, Hubei Provincial Department of Education, China (T201604). This work was also supported by the UHK project VT2019-2021.

SUPPLEMENTARY MATERIAL

The Supplementary Material for this article can be found online at: https://www.frontiersin.org/articles/10.3389/fpls.2021.659694/full#supplementary-material

REFERENCES

Aggarwal, A., Kadian, N., Tanwar, A., Yadav, A., and Gupta, K. (2011). Role of arbuscular mycorrhizal fungi (AMF) in global sustainable development. *J. Appl. Nat. Sci.* 3, 340–351. doi: 10.31018/jans.v3i2.211

Augé, R. M., Toler, H. D., and Saxton, A. M. (2015). Arbuscular mycorrhizal symbiosis alters stomatal conductance of host plants more under drought than under amply watered conditions: a meta-analysis. *Mycorrhiza* 25, 13–24. doi: 10.1007/s00572-014-0585-4

Chen, H., Zhang, Q., Cai, H., and Xu, F. (2017). Ethylene mediates alkaline-induced rice growth inhibition by negatively regulating plasma membrane H^+-ATPase activity in roots. *Front. Plant Sci.* 8:1839. doi: 10.3389/fpls.2017.01839

Cheng, H. Q., Giri, B., Wu, Q. S., Zou, Y. N., and Kuča, K. (2021). Arbuscular mycorrhizal fungi mitigate drought stress in citrus by modulating root microenvironment. *Arch. Agron. Soil Sci.* doi: 10.1080/03650340.2021.1878497. [Epub ahead of print].

Chu, G., Chen, T. T., Wang, Z. Q., Yang, J. C., and Zhang, J. H. (2014). Morphological and physiological traits of roots and their relationships with water productivity in water-saving and drought-resistant rice. *Field Crop Res.* 162, 108–119. doi: 10.1016/j.fcr.2013.11.006

Fernández-Lizarazo, J. C., and Moreno-Fonseca, L. P. (2016). Mechanisms for tolerance to water-deficit stress in plants inoculated with arbuscular mycorrhizal fungi. A review. *Agron. Colomb.* 34, 179–189. doi: 10.15446/agron.colomb.v34n2.55569

Ferrol, N., Barea, J. M., and Azcón-Aguilar, C. (2000). The plasma membrane H+-ATPase gene family in the arbuscular mycorrhizal fungus *Glomus mosseae*. *Curr. Genet.* 37, 112–118. doi: 10.1007/s002940050017

Franco, J. A., Bañón, S., Vicente, M. M. J., Miralles, J., and Martínez-Sánchez, J. J. (2011). Review article:root development in horticultural plants grown under abiotic stress conditions-a review. *J. Hort. Sci. Biotechnol.* 86, 543–556. doi: 10.1080/14620316.2011.11512802

Fuglsang, A. T., Guo, Y., Cuin, T. A., Qiu, Q., Song, C., Kristiansen, K. A., et al. (2007). *Arabidopsis* protein kinase PKS5 inhibits the plasma membrane H^+-ATPase by preventing interaction with 14-3-3 protein. *Plant Cell* 19, 1617–1634. doi: 10.1105/tpc.105.035626

Garry, M., Rosewarne, F., Andrew Smith, D. P., and Schachtman, S. E. (2007). Localization of proton-atpase genes expressed in arbuscular mycorrhizal tomato plants. *Mycorrhiza* 17, 249–258. doi: 10.1007/s00572-006-0101-6

Gaxiola, R. A., Palmgren, M. G., and Schumacher, K. (2007). Plant proton pumps. *FEBS Lett.* 581, 2204–2214. doi: 10.1016/j.febslet.2007.03.050

Gianinazzi-Pearson, V., Arnould, C., Oufattole, M., Arango, M., and Gianinazzi, S. (2000). Differential activation of H^+-ATPase genes by an arbuscular mycorrhizal fungus in root cells of transgenic tobacco. *Planta* 211, 609–613. doi: 10.1007/s004250000323

Hadian-Deljou, M., Esna-Ashari, M., and Mirzaie-asl, A. (2020). Alleviation of salt stress and expression of stress-responsive gene through the symbiosis of arbuscular mycorrhizal fungi with sour orange seedlings. *Sci. Hortic.* 268:109373. doi: 10.1016/j.scienta.2020.109373

Haruta, M., Burch, H. L., Nelson, R. B., Barrett-Wilt, G., Kline, K. G., Mohsin, S. B., et al. (2010). Molecular characterization of mutant *Arabidopsis* plants with reduced plasma membrane proton pump activity. *J. Biol. Chem.* 285, 17918–17929. doi: 10.1074/jbc.m110.101733

Haruta, M., and Sussman, M. R. (2012). The effect of a genetically reduced plasma membrane protonmotive force on vegetative growth of *Arabidopsis*. *Plant Physiol.* 158, 1158–1171. doi: 10.1104/pp.111.189167

He, J. D., Zou, Y. N., Wu, Q. S., and Kuča, K. (2020). Mycorrhizas enhance drought tolerance of trifoliate orange by enhancing activities and gene expression of antioxidant enzymes. *Sci. Hortic.* 262:108745. doi: 10.1016/j.scienta.2019.108745

Ingrain, E. A., and Malamy, J. E. (2010). Root system architecture in avoiding chilling-induced water stress. *Adv. Bot. Res.* 55, 76–106.

Johansen, A., Finlay, R. D., and Olsson, P. A. (2010). Nitrogen metabolism of external hyphae of the arbuscular mycorrhizal fungus *Glomus intraradices*. *New Phytol.* 133, 705–712. doi: 10.1111/j.1469-8137.1996.tb01939.x

Krajinski, F., Courty, P. E., Sieh, D., Franken, P., Zhang, H. Q., Bucher, M., et al. (2014). The H^+-ATPase HA1 of *Medicago truncatula* is essential for phosphate transport and plant growth during arbuscular mycorrhizal symbiosis. *Plant Cell* 26, 1808–1817. doi: 10.1105/tpc.113.120436

Liu, J. L., Chen, J. D., Xie, K., Tian, Y., Yan, A. N., Liu, J. J., et al. (2020). A mycorrhiza-specific H^+-ATPase is essential for arbuscule development and symbiotic phosphate and nitrogen uptake. *Plant Cell Environ.* 43, 1069–1083. doi: 10.1111/pce.13714

Liu, J. L., Liu, J. J., Chen, A. Q., Ji, M. J., Chen, J. D., Yang, X. F., et al. (2016). Analysis of tomato plasma membrane H^+-ATPase gene family suggests a mycorrhizal-mediated regulatory mechanism conserved in diverse plant species. *Mycorrhiza* 26, 645–656. doi: 10.1007/s00572-016-0700-9

Livak, K. J., and Schmittgen, T. D. (2001). Analysis of relative gene expression data using real-time quantitative PCR and the $2^{-\Delta\Delta CT}$ method. *Methods* 25, 402–408. doi: 10.1006/meth.2001.1262

Mak, M., Babla, M., Xu, S. C., O'Carrigan, A., Liu, X. H., Gong, Y. M., et al. (2014). Leaf mesophyll K^+, H^+ and Ca^{2+} fluxes are involved in drought-induced decrease in photosynthesis and stomatal closure in soybean. *Environ. Exp. Bot.* 98, 1–12. doi: 10.1016/j.envexpbot.2013.10.003

Małgorzata, J., Wdowikowska, A., and Grażyna, K. (2018). Assay of plasma membrane H^+-ATPase in plant tissues under abiotic stresses. *Meth. Mol. Biol.* 1696, 205–215. doi: 10.1007/978-1-4939-7411-5_14

Młodzińska, E., Kłobus, G., Christensen, M. D., and Fuglsang, A. T. (2014). The plasma membrane H^+-ATPase AHA2 contributes to the root architecture in response to different nitrogen supply. *Physiol. Plant* 154, 270–282. doi: 10.1111/ppl.12305

Motte, H., and Beeckman, T. (2020). A pH antastic ammonium response. *Nature Plants* 6, 1080–1081.

Palmgren, M. G. (2001). Plant plasma membrane H^+-ATPases: powerhouses for nutrient uptake. *Annu. Rev. Plant Physiol. Plant Mol. Biol.* 52, 817–845. doi: 10.1146/annurev.arplant.52.1.817

Petrasek, J., and Friml, J. (2009). Auxin transport routes in plant development. *Development* 136, 2675–2688. doi: 10.1242/dev.030353

Phillips, J. M., and Hayman, D. S. (1970). Improved procedures for clearing roots and staining parasitic and vesicular-arbuscular mycorrhizal fungi for rapid assessment of infection. *Trans. Br. Mycol. Soc.* 55, 158–161. doi: 10.1016/s0007-1536(70)80110-3

Porcel, R., and Ruiz-Lozano, J. M. (2004). Arbuscular mycorrhizal influence on leaf water potential, solute accumulation, and oxidative stress in soybean plants subjected to drought stress. *J. Exp. Bot.* 55, 1743–1750. doi: 10.1093/jxb/erh188

Ramos, A. C., Façanha, A. R., and José, F. (2008a). "Ion dynamics during the polarized growth ofarbuscular mycorrhizal fungi: from presymbiosis to symbiosis," in *Mycorrhiza: State of the Art, Genetics and Molecular Biology, Eco-function, Biotechnology, Eco-physiology, Structure and Systematics*, ed. A. Varma (Berlin: Springer), 241–260. doi: 10.1007/978-3-540-78826-3_12

Ramos, A. C., Façanha, A. R., and José, F. (2008b). Proton (H^+) flux signature for the presymbiotic development of the arbuscular mycorrhizal fungi. *New Phytol.* 178, 177–188. doi: 10.1111/j.1469-8137.2007.02344.x

Ramos, A. C., Martins, M. A., Okorokova-Façanha, A. L., Fábio, L. O., Okorokov, L. A., and Nuno, S. (2009). Arbuscular mycorrhizal fungi induce differential activation of the plasma membrane and vacuolar H^+ pumps in maize roots. *Mycorrhiza* 19, 69–80. doi: 10.1007/s00572-008-0204-3

Requena, N., Breuninger, M., Franken, P., and Ocón, A. (2003). Symbiotic status, phosphate, and sucrose regulate the expression of two plasma membrane H^+-ATPase genes from the mycorrhizal fungus *Glomus mosseae*. *Plant Physiol.* 132, 1540–1549. doi: 10.1104/pp.102.019042

Staal, M., De-Cnodder, T., Simon, D., Vandenbussche, F., Vander Straeten, D., Verbelen, J., et al. (2011). Apoplastic alkalinization is instrumental for the inhibition of cell elongation in the *Arabidopsis* root by the ethylene precursor 1-aminocyclopropane-1-carboxylic acid. *Plant Physiol.* 155, 2049–2055. doi: 10.1104/pp.110.168476

Sun, Y. P., Unestam, T., Lucas, S. D., Johanson, K. J., Kenne, L., and Finlay, R. (1999). Exudation-reabsorption in a mycorrhizal fungus, the dynamic interface for interaction with soil and soil microorganisms. *Mycorrhiza* 9, 137–144. doi: 10.1007/s005720050298

Tang, Z. C. (1999). *A Guide to Modern Plant Physiology Experiments*. Shanghai: Science Press, 138–139.

Ueno, K., Kinoshita, T., Inoue, S., Emi, T., and Shimazaki, K. (2005). Biochemical characterization of plasma membrane H^+-ATPase activation in guard cell protoplasts of *Arabidopsis thaliana* in response to blue light. *Plant Cell Physiol.* 46, 955–963. doi: 10.1093/pcp/pci104

Wang, Y., Noguchi, K., Ono, N., Inoue, S., Terashima, I., and Kinoshita, T. (2014). Overexpression of plasma membrane H^+-ATPase in guard cells promotes light-induced stomatal opening and enhances plant growth. *Proc. Natl. Acad. Sci. U.S.A.* 111, 533–538. doi: 10.1073/pnas.1305438111

Wu, Q. S., He, J. D., Srivastava, A. K., Zou, Y. N., and Kuča, K. (2019). Mycorrhizas enhance drought tolerance of citrus by altering root fatty acid compositions and their saturation levels. *Tree Physiol.* 39, 1149–1158. doi: 10.1093/treephys/tpz039

Wu, Q. S., Srivastava, A. K., and Zou, Y. N. (2013). AMF-induced tolerance to drought stress in citrus: a review. *Sci. Hortic.* 164, 77–87. doi: 10.1016/j.scienta.2013.09.010

Xiong, Y. C., Li, F. M., Zhang, T., and Xia, C. (2007). Evolution mechanism of non-hydraulic root-to-shoot signal during the anti-drought genetic breeding of spring wheat. *Environ. Exp. Bot.* 59, 193–205. doi: 10.1016/j.envexpbot.2005.12.003

Yoshida, S. (1991). Chilling-induced inactivation and its recovery of tonoplast H^+-ATPase in mung bean cell suspension cultures. *Plant Physiol.* 95, 456–460. doi: 10.1104/pp.95.2.456

Zhang, F., Zou, Y. N., Wu, Q. S., and Kuča, K. (2020). Arbuscular mycorrhizas modulate root polyamine metabolism to enhance drought tolerance of trifoliate orange. *Environ. Exp. Bot.* 171:103962.

Zou, Y. N., Wang, P., Li, C. Y., Ni, Q. D., Zhang, D. J., and Wu, Q. S. (2017). Mycorrhizal trifoliate orange has greater root adaptation of morphology and phytohormones in response to drought stress. *Sci. Rep.* 7:41134.

Zou, Y. N., Wu, Q. S., and Kuča, K. (2020). Unravelling the role of arbuscular mycorrhizal fungi in mitigating the oxidative burst of plants under drought stress. *Plant Biol.* doi: 10.1111/plb.13161. [Epub ahead of print].

Conflict of Interest: The authors declare that the research was conducted in the absence of any commercial or financial relationships that could be construed as a potential conflict of interest.

frontiers in Plant Science

ORIGINAL RESEARCH
published: 25 June 2021
doi: 10.3389/fpls.2021.693060

Evaluating the Drought Tolerance of Seven Potato Varieties on Volcanic Ash Soils in a Medium-Term Trial

Ingrid Martínez, Manuel Muñoz, Ivette Acuña and Marco Uribe*

Instituto de Investigaciones Agropecuarias, INIA Remehue, Osorno, Chile

One of the main factors limiting the productivity of potatoes (*Solanum tuberosum* L.) is water stress. Two irrigation systems: full irrigation (I) and rainfed conditions (R), were compared over the growing seasons from 2012–13 to 2019–20. The evaluated varieties were Desiree, Karú-INIA, Patagonia-INIA, Puyehue-INIA, Yagana-INIA, Yaike, and Porvenir. This study determined (i) the yield and tuber size distribution, (ii) their relationship between productivity and environmental conditions, and (iii) the most drought-tolerant varieties based on drought tolerance indices. Nine indices including yield index (YI), tolerance index (TOL), mean productivity (MP), geometric mean productivity (GMP), harmonic mean (Harm), stress tolerance index (STI), harmonic mean productivity (HMP), yield reduction (Yr), and stress susceptible index (SSI) were calculated by using tuber yield under I and R conditions. Tuber yield under R conditions decreased by 27 and 34%. However, the highest yield under R conditions occurred in years with more precipitation between 60 and 120 days after planting (DAP; ±60 mm). Under R conditions, the varieties Porvenir, Patagonia-INIA, Yaike, and Puyehue-INIA showed more tolerance to water stress. Water stress negatively affected tuber size distribution, reducing the production of tubers with size >65 mm by 50–60%. The best indices to study drought tolerance were TOL, MP, GMP, Harm, STI, and HMP. This study suggests that in southern Chile, an area with big yield potential, typically cultivated as rainfed, with cool temperate climate conditions and favorable soil properties for potatoes, as Andisols, available rainfall is still a constraint for yield. Therefore, using more water stress-tolerant varieties and providing supplementary irrigation between 60 and 120 DAP are critical to optimize yield and avoid the failure of the crop in years with remarkably low precipitations, which will be more pronounced in the future according to weather trends. These results exemplify how much we can lose in productivity in rainfed conditions even in one of the most favorable areas for growing potatoes in the world and how risky this situation can be for the performance of the potato farms in the future.

Keywords: drought index, irrigation, tuber size distribution, marketable tuber yield, Andisols, water stress

OPEN ACCESS

Edited by:
Italo F. Cuneo, Pontificia Universidad Católica de Valparaíso, Chile

Reviewed by:
Rahmatollah Karimizadeh, Agricultural Research, Education and Extension Organization (AREEO), Iran
Manuel Gastelo, International Potato Center, Peru

****Correspondence:***
Ingrid Martínez
ingrid.martinez@inia.cl

Specialty section:
This article was submitted to Plant Abiotic Stress, a section of the journal Frontiers in Plant Science

Received: *09 April 2021*
Accepted: *31 May 2021*
Published: *25 June 2021*

Citation:
Martínez I, Muñoz M, Acuña I and Uribe M (2021) Evaluating the Drought Tolerance of Seven Potato Varieties on Volcanic Ash Soils in a Medium-Term Trial. Front. Plant Sci. 12:693060. doi: 10.3389/fpls.2021.693060

INTRODUCTION

The potato (*Solanum tuberosum* L.) is the fourth most important cultivar worldwide, with a global annual yield of 370 Mt, with 17.3 million ha under cultivation (FAOSTAT, 2020). One of the main factors limiting the productivity of potato production is the need for more effective water management (Fleisher et al., 2015). Plants differ in their capacity to use water efficiently. The mechanisms responsible for regulating plant water use remain only partially understood.

Mbava et al. (2020) identified three important factors that account for differences in water use efficiency (WUE): (i) carbon-fixing or C4 plants make more efficient use of water than do C3 plants, (ii) plants in warm, humid climates make more efficient use of water than plants in cold climates, and (iii) soil texture has a significant effect on water retention, clay soils facilitating better WUE than silty soils. Like C3 plants, potatoes make less efficient water use, because of which their productivity varies significantly owing to differences in climate, irrigation, and soil management, with better yields when the availability of water and light are not limiting factors (Zhao et al., 2012; Mi et al., 2015; Mbava et al., 2020). Several authors have shown that water stress affects physiological mechanisms, which can be genotype-dependent. The most severe effects of water stress on potatoes are differences in stolon, tuber formation, yield, and tuber size distribution (Monneveux et al., 2013; Yuan et al., 2013; Aliche et al., 2019, 2020; Gouveia et al., 2019).

Stress factors like drought and excess UV radiation that negatively affect plant yield will be more common in the coming decades due to climate change (Wang and Frei, 2011; Gregory and Marshall, 2012). Environmental stress because of decreased precipitation and changes in temperature affect potato yields, especially in dry regions (Aliche et al., 2019). Although the productivity of irrigated agricultural systems in semiarid areas has increased, water scarcity and the cost of irrigation limit the expansion of these systems (Mbava et al., 2020). Fang and Xiong (2015) argued that plants can be divided into four categories in terms of drought resistance: drought avoidance, drought tolerance, drought escape, and drought recovery. Of these, drought avoidance and drought tolerance are the main survival mechanisms. Zhang et al. (2018) described drought avoidance as the capacity to increase the root/shoot ratio to improve water absorption and close the stomata to reduce transpiration, while the mechanism of drought tolerance is related to the physiological parameters of osmotic adjustment.

To assess genotype responses to water stress, we used indices based on plant resistance or susceptibility. Based on mathematic relationships, selection parameters were used to identify genotypes with high yield potentials under favorable or stressful conditions (Mardeh et al., 2006), as well as genotypes tolerant to high altitudes (Noerwijati and Budiono, 2015), saline soils (Krishnamurthy et al., 2016; Jamshidi and Javanmard, 2018), and contrasting water availability conditions (El-Hendawy et al., 2017; Choudhary et al., 2018). According to Fernandez (1993), genotypes can be divided into four categories based on their associated yields: (1) genotypes with high yields under conditions with or without stress, (2) genotypes with high yields under conditions without stress, (3) genotypes with high yields under stressful conditions, and (4) genotypes with low yields under either condition.

Around 16% of agricultural production in Chile corresponds to potato production (41.268 ha), of which 70% is concentrated in the center-south of this surface area (2018–19, INE). Moreover, a high percentage of this area is dominated by soils derived from volcanic materials, accounting for 50–60%, which is important for agriculture (Valle et al., 2018). Owing to their andic properties, these soils are different from other soils because of their high soil organic carbon and nutrients content, low bulk density, and capacity to store water (Valle et al., 2018; Clunes et al., 2021). Studying the connections between yields, soil and climate shed light on drought resistance mechanisms. The objectives of this study were to assess seven potato varieties (*S. tuberosum* L.) under conditions of irrigation and rainfed in a medium-term trial to determine: (i) the yield and tuber size distribution, (ii) their relationship between productivity and environmental conditions during their development, and (iii) the most water stress-tolerant varieties using drought-tolerant indices in volcanic ash soils.

MATERIALS AND METHODS

Site Description and Field Experiment

Seven potato varieties (*S. tuberosum* L.) were selected to study their water stress tolerance during the 2012–13 to 2019–20 seasons (except for the 2013–14 season) at the Instituto de Investigaciones Agropecuarias (INIA Remehue) in Osorno, Chile (40°35'S, 73°12'W, 72 m.a.s.l.). The selected varieties, except for Desiree (1962, the Netherlands), had been released by INIA: Yagana-INIA (1983), Karú-INIA (2002), Patagonia-INIA (2009), Puyehue-INIA (2011), Yaike (2019), and Porvenir (2019). Due to an institutional decision, the varieties released from 2019 do not have the suffix of INIA, as the case of Yaike and Porvenir. Desiree and Karú-INIA were originally included but were stopped after five seasons (2017–18) to include new genotypes. Porvenir was included in season 2014–15, completing six seasons.

The soil was volcanic in origin, an Andisol of the Osorno series, classified as a Typic Hapludand [Centro de Información de Recursos Naturales (CIREN), 2003], textural class: silty loam, characterized by a high level of phosphorous retention and low bulk density (Valle et al., 2015). To determine soil physical properties, undisturbed soil cores (diameter 5 cm, height 5 cm) were collected in 10 cm increments to 100 cm depth, with three replicates. At the Bromatology Laboratory of INIA Remehue, the cylinders were weighed and dried in an oven at 105°C for 24 h to determine the water content of the soil, based on which the bulk density and porosity were calculated. Colors in the soil profile were identified with the Munsell Soil Color System (Munsell, 2009).

The experiment was carried out with a split-plot randomized design with three replicates; the irrigated (I) condition and rainfed (R) condition were assigned to the main plot and the varieties to the subplots. The size of each subplot was 4.5 m in length by 3 m in width (13.5 m^2 in total area), and the planting pattern was 0.75 m between rows × 0.33 between plants. In the I condition, drip irrigation was homogenously applied after emergence during the crop cycle. The total quantity of water received by the crop cycle over the seven seasons varied between 450 and 600 mm based on climatic conditions. After 1 week from emergence, all plots in the I condition were irrigated weekly with 37.5–50 mm of water. This amount is considered to be enough to satisfy the crop evapotranspiration

estimated during the crop cycle. The R condition (no irrigation applied) was included to represent water-limited conditions for the crop, which considered the rainfall during the growing season. The plots were fertilized with 120 kg of N ha^{-1}, 350 kg of P_2O_5 ha^{-1}, and 160 kg of K_2O ha^{-1}. The duration of the phenological development was between 130 and 150 days. This coincides with the usual crop management in the area, conditioned by the climate requiring potatoes to be harvested before the end of March.

Climatic, Crop Evaluations, and Drought Tolerance Indices

Climatic measurements were taken every day at the experimental station during the period from seeding to harvest. To adjust the determined crop coefficients for a potato to site-specific climatic conditions, a heating unit-based Growing Degree Days (GDD) (McMaster and Wilhelm, 1997), which was calculated with the equation below:

$$\sum = \left\{ \frac{Tmax + Tmin}{2} \right\} - Tbase$$

where Σ is the number of days from emergence to harvest; *Tmax* is the highest temperature; and *Tmin* is the lowest temperature. The monthly accumulated data for the GDD were considered at a *Tbase* of 4°C as the minimum temperature for potato growth (Ahmadvand et al., 2009). Accumulated precipitation, average temperature, and solar radiation at 60 and between 60 and 90, and 90 and 120 days after planting (DAP) were also considered. Weather data (daily maximum and minimum air temperature, precipitation, and solar radiation) were obtained from an automatic weather station at the experimental station at INIA Remehue.

The following yield traits were systematically collected at the harvest date in two internal rows in each subplot, each 4.5 m in length (6.75 m^2 in total area): yield of marketable tubers (>65 mm size), the yield of seed tubers (25–65 mm size) and non-marketable tubers (<25 mm size). In Chile, the seed tuber size to be marketed is regulated by the SAG (The Agricultural and Livestock Service) certification standard. The assessments were conducted in each experimental unit when 70% of the plant leaves were yellowish in color.

Various drought tolerance indices were calculated to estimate the stability in yield under I and R conditions: yield index (YI), tolerance index (TOL), mean productivity (MP), geometric mean productivity (GMP), harmonic mean (HARM), stress tolerance index (STI), harmonic mean productivity (HMP), yield reduction (Yr), and the stress susceptibility index (SSI). The formulas for these indices are presented in **Table 1**.

TABLE 1 | Description of the drought tolerance indices based on tuber yield.

Drought tolerance indices		Formula	References
YI	Yield index	Y_s/X_s	Lin et al., 1986
TOL	Tolerance index	$Y_p - Y_s$	El-Hendawy et al., 2017
MP	Mean productivity	$(Y_s + Y_p)/2$	El-Hendawy et al., 2017
GMP	Geometric mean productivity	$(Y_p \times Y_s)$ $(2 \times Y_s \times Y_p)/$	Krishnamurthy et al., 2016
HARM	Harmonic mean	$(Y_p + Y_s)$	Nikneshan et al., 2019
STI	Stress tolerance index	$(Yp \times Ys)/X_p^2$	Fernandez, 1993
HMP	Harmonic mean productivity	$(2 \times Y_p \times Y_s)/$ $(Yp + Ys)$	Fernandez, 1993
Yr	Yield reduction	$1 - (Y_s/Y_p)$	Golestani and Assad, 1998
SSI	Stress susceptibility index	$[1 - (Y_s/Y_p)]/$ $[1 - (X_p/X_s)]$	Nikneshan et al., 2019

Statistical Analysis

An ANOVA with a split-plot randomized into a three-block design was used to assess the effects of treatments on crop productivity. Means were tested using the Tukey method at a significance level of $p < 0.05$. Regression analyses were performed to assess the associations between variables. Relationships between analyzed variables were established through principal components analysis (PCA) and correlation coefficients ($p > 0.05$) using the Infostat statistical analysis software (Di Rienzo et al., 2009).

RESULTS

Environmental Conditions and Tuber Yield

The physical properties of volcanic soils in the study area showed low bulk density (0.75 ± 0.04 Mg ha^{-1}) and high porosity (67% ± 1.5) in the soil profile (**Table 2**). The study found decreasing trend of accumulated rainfall during the potato growing season across the last 42 years (**Figure 1**). The less frequency of accumulated rainfall higher than 400 mm during the growing season is associated with accumulated rainfall lower than 300 mm. Moreover, the average rainfall in the last 4 decades has decreased around 25% in the last 10 years. **Figure 2** showed that this decreasing rainfall was more intense during the flowering stage. During the experiment (2012–13 to 2019–20), the accumulated rainfall during the growing season was 242.4 mm (**Figure 3**). The ambient temperature was 20.5°C, and the mean daily solar radiation was 19.8 Mj m^{-2}. Around 42% of rainfall took place in the first 2 months after the planting date. Around 24% (58 mm) occurred between January and February, the tuber-filling and maturation period (flowering to ripening stage) when the average temperature was 23.1°C. Radiation was 22.1 Mj m^{-2} (**Figure 3**).

The average yield of the seven varieties during this period under I conditions was 84 Mg ha^{-1}, while the average yield under R conditions was 58 Mg ha^{-1} (**Figure 4**). The varieties with higher productive potential under I conditions were Porvenir, Patagonia-INIA, Yaike, and Puyehue-INIA, with average yields of 100, 97, 89, and 84 Mg ha^{-1}, respectively; in contrast, the varieties Karú-INIA, Yagana-INIA, and Desiree had less productive potential with average yields of 71, 73, and 69 Mg ha^{-1}, respectively. Under R conditions, the varieties with more productive potential were Porvenir, Patagonia-INIA, Puyehue-INIA, and Yaike, with average yields of 69, 65, 60, and 59 Mg ha^{-1}, respectively. In contrast, the varieties with less productive potential were Karú-INIA, Yagana-INIA, and Desiree, with average yields of 52, 52, and 47 Mg ha^{-1}, respectively.

TABLE 2 | Physical properties of soil profile of the field experiment.

Depth	Bulk density	Porosity	Volumetric SWC	Soil color	Color
cm	Mg m^{-3}	%	%	ID	
0–10	0.78 ± 0.01	68 ± 0.34	8.9 ± 1.37	7.5YR 4/4	Brown
10–20	0.78 ± 0.01	68 ± 0.28	14.0 ± 0.71	7.5YR 3/4	Dark yellowish brown
20–30	0.81 ± 0.00	64 ± 0.19	13.6 ± 0.02	7.5YR 4/4	Dark yellowish brown
30–40	0.79 ± 0.00	65 ± 0.14	12.8 ± 1.33	7.5YR 4/4	Dark yellowish brown
40–50	0.76 ± 0.01	66 ± 0.62	15.5 ± 0.65	7.5YR 3/4	Dark yellowish brown
50–60	0.74 ± 0.00	66 ± 0.15	14.7 ± 0.88	7.5YR 3/4	Dark yellowish brown
60–70	0.71 ± 0.01	68 ± 0.26	15.8 ± 0.85	7.5YR 4/4	Dark yellowish brown
70–80	0.71 ± 0.00	68 ± 0.21	16.5 ± 1.52	7.5YR 4/4	Dark brown
80–90	0.69 ± 0.00	69 ± 0.10	19.7 ± 1.36	7.5YR 3/3	Dark brown
90–100	0.72 ± 0.01	67 ± 0.30	24.2 ± 0.47	7.5YR 3/4	Dark brown

SWC, soil water content.

Figure 5 shows the temporal relationship between tuber yield under R conditions and rainfall at 0–60, 60–90, and 90–120 DAP. As can be seen, tuber yield increased in years with higher rainfall in the period 90–120 DAP (±60 mm), as occurred in years 2016 (season 2016–17) and 2019 (season 2019–20). GDD4 was similar from one season to another (**Figure 6**), except the 2014–15 season, which registered the lowest values during the period 90–120 DAP (935) and was also the year with the low tuber yield and precipitation during the same period (**Figure 5**). **Figure 7** shows that when the accumulated rainfall during the crop development exceeded 350 mm, the reduction of tuber yield under rainfed conditions is by 10%. However, when the accumulated rainfall was less than 200 mm, tuber yield decreased by more than 35%.

Stress Indices and Their Correlations With Tuber Yield

A PCA was applied to obtain a visual representation of the correlation between the yields of the varieties and the stress tolerance indices. The biplot analysis shown in **Figure 8** indicates that PC1 and PC2 explain 88.3% of the total variation and that most of this percentage is accounted for by PC1 (65.6%). There was a strong positive correlation between TOL, MP, GMP, Harm, STI, and HMPF (r = >0.92), indicating that these indices are very similar for drought selection. Besides, a weak correlation between YI, Yr, and SSI and the stress indices mentioned before (**Table 3**). The biplot indicates the association between the stress tolerance indices and varieties in productivity and drought tolerance. The varieties Porvenir, Patagonia-INIA, Yaike, and Puyehue-INIA, indicate a close positive relationship between TOL, MP, GMP, HARM, STI, and HMP as most productive and tolerant to drought conditions. In contrast, Desiree, Yagana-INIA, and Karú-INIA are on the opposite end of the PCA, which indicates that these varieties have negative effects on the dependence of the selection indices, which indicates low productivity and more sensitivity to drought conditions. No associations were found between the indices Yr, SSI, and YI and any of the varieties used in this study, which suggests that these indices are not useful for selecting genotypes or varieties studied under contrasting environmental conditions.

In **Figure 9**, the graphs of the average yields of the different varieties in the function of the environmental index (the average yield of all varieties in each environment, considering as an environment the combination of the year and the irrigation or rainfed condition, **Table 4**) show that the varieties Porvenir and Patagonia-INIA have the highest adjusted regression curves, which indicates that these varieties are more tolerant to water deficits and had higher yields over the years of the study and the distinct climatic conditions. This, in turn, indicates that these varieties have higher stress tolerance indices and a good response to improved conditions with irrigation. Coincidentally, the yield regression curve in the context of the environmental indices of varieties Desiree and Karú-INIA, which were less correlated with the drought tolerance index and showed had the lowest curves (**Figure 9**).

The regression between the environmental index and the number of tubers did not result in a significant relationship, indicating that this yield component was not affected by the effects of the irrigated and rainfed conditions in this agroclimatic context (**Table 5**). In contrast, there was a significant relationship between the average weight of the tubers of all the varieties and the environmental index ($p < 0.0001$), with determination coefficients similar to those between the environmental index and yield, indicating that the tuber weight component was affected by differences in water availability.

Drought Effects on the Tuber Size Distribution

The previous results showed that yield was reduced under water limiting conditions depending on the drought severity. However, tuber size was the most affected under water limiting conditions in the different varieties. **Figure 10** shows the average yield for the tuber size distribution of seed (25–65 mm) and marketable tubers (>65 mm) over the years of the study under both conditions (irrigation and rainfed). Drought stress significantly reduced the marketable tubers (>65 mm) by 50–60%. However, under irrigation, not all the varieties were marketable, like Yagana-INIA and Yaike, which are more productive for tuber seed production. The results also indicated that with irrigation, the productivity of Patagonia-INIA and Porvenir differs depending on the tuber size distribution. At the same time, Patagonia-INIA has a higher marketable production by 73%, for Porvenir was by 59%.

DISCUSSION

Tuber Yield Productivity Under Irrigation vs. Rainfed Conditions

The results of the medium-term trial showed the responses of the seven high-yield varieties to water deficit (**Figure 4**),

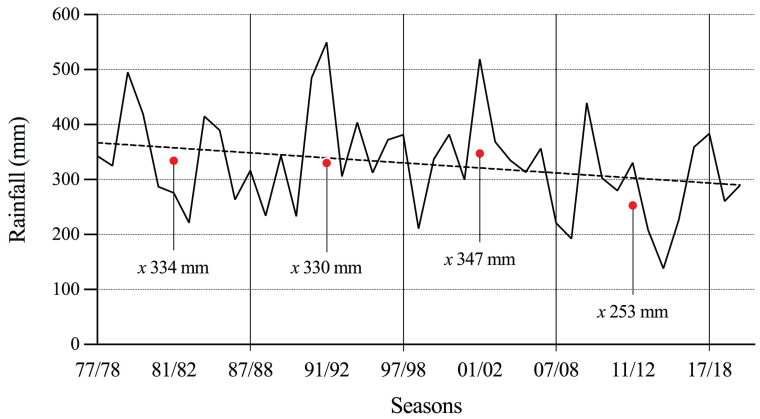

FIGURE 1 | Long-term accumulated rainfall amount during the potato growing season from 1977/78 to 2019/20 in the study area. Each red point represents de average rainfall amount during the last 10 years.

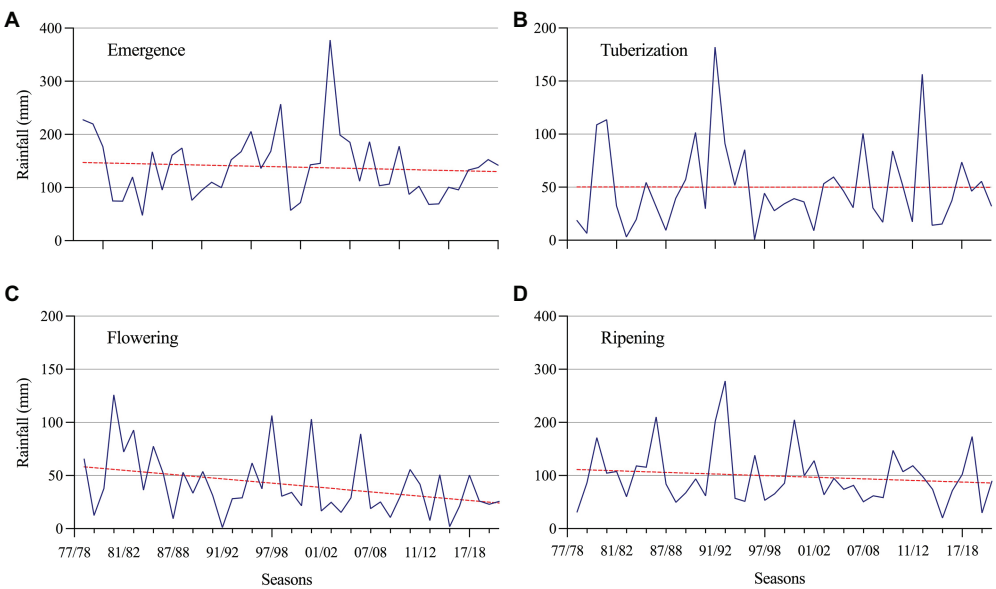

FIGURE 2 | Long-term accumulated rainfall amount in different growth stages of potato: **(A)** Emergence, **(B)** Tuberization, **(C)** Flowering, and **(D)** Ripening from seasons 1977/78 to 2019/20. Each data represent the accumulated rainfall amount during the phenologic stage.

indicating that some varieties are more tolerant to water stress than others. Therefore, variability for drought tolerance is affected differently between cultivars (Aliche et al., 2019). However, it was observed that irrigation can increase yield in these soils by 30% (**Figure 4**). Although Andisols are characterized by the capacity to store and transport water, air, and nutrients, which maximizes plant yield (Valle et al., 2018), the physical properties of the soil capacity (air and water) are sensitive to management practices (Ordoñez et al., 2018), which the limits of storage and transport of water will depend on the pore system (Clunes et al., 2021). Water availability is limiting in the potato growing season in this region, despite the ability of soils to store moisture. Therefore, rainfall during the growing season is pivotal for yield, even in these cool temperate areas with favorable soils for potatoes (Liang et al., 2020). In addition, extremely high soil temperatures and low water content disfavor tuber formation (Liang et al., 2020). Even short periods of water stress can significantly reduce tuber yield, as was observed in our study (Zhang et al., 2018). Comparing yields under irrigation vs. rainfed conditions over seven seasons, the varieties Patagonia-INIA, Puyehue-INIA, Yagana-INIA, and Yaike registered differences in yields of 220, 168, 149, and 210 Mg ha^{-1}, respectively. Over five and six seasons, the varieties Desiree and Karú-INIA registered differences in yields of 110 and 118 Mg ha^{-1}, respectively, while the last variety to be released to the market, Porvenir, registered a difference of 186 Mg ha^{-1} over six seasons. This not only

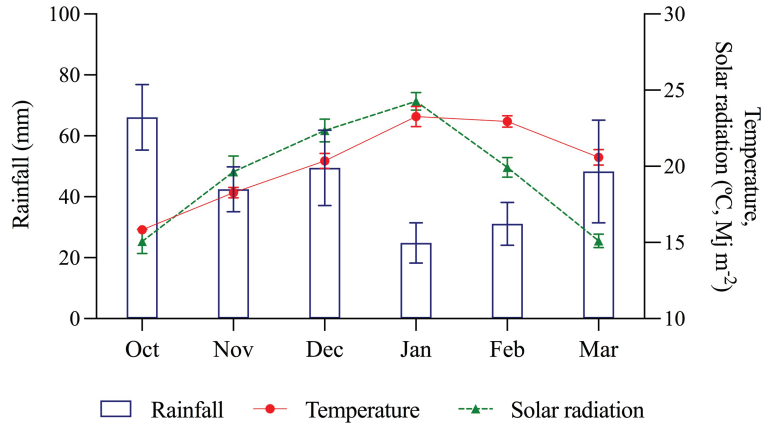

FIGURE 3 | Mean monthly rainfall, temperature, and solar radiation distribution during development stage in potato (2012–13 to 2019–20). Data were provided by the Agrometeorology Network at INIA Remehue. Error bars indicate SE.

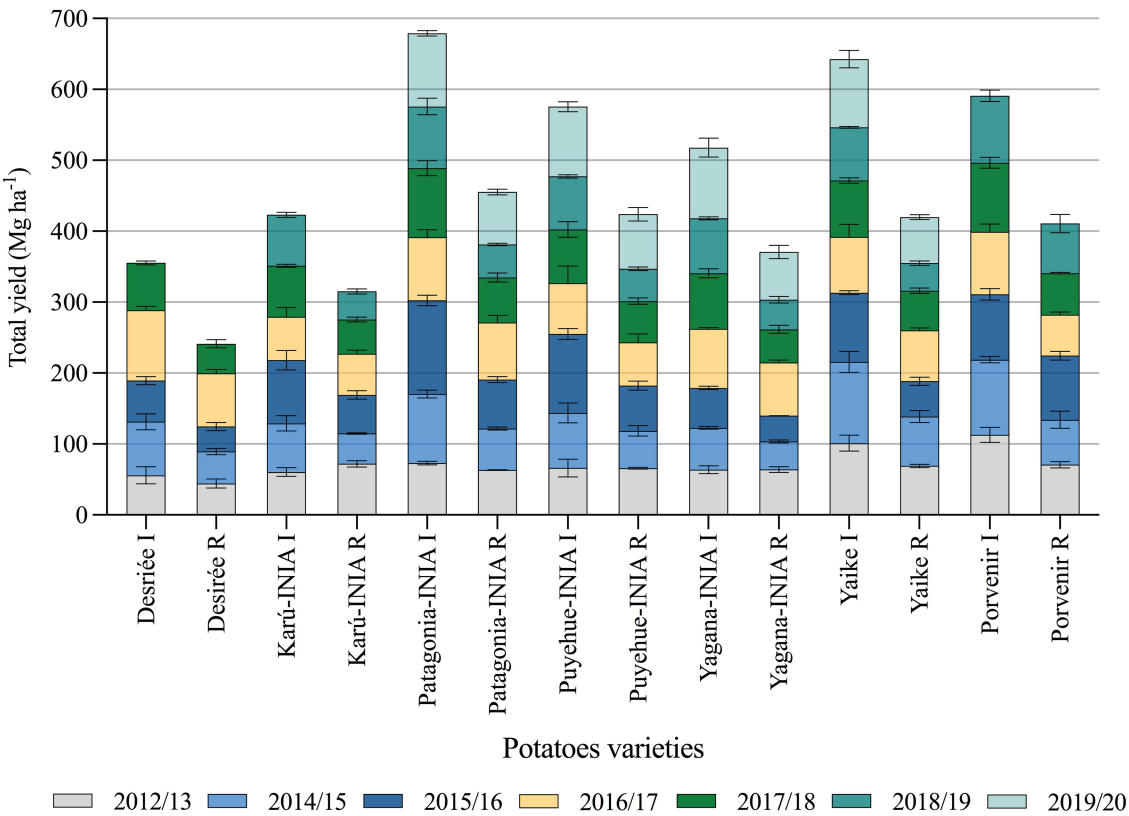

FIGURE 4 | Temporal tuber yield of seven potato varieties under irrigation and rainfed conditions from 2012–13 to 2018–19 season. Desiree and Porvenir with five and six seasons, respectively. Error bars indicate SE. I, irrigation condition; R, rainfed condition.

demonstrates that water deficits significantly affect tuber growth and development (Karam et al., 2014; Ambrosone et al., 2016) but can also cause the loss of yields for one or two seasons over the medium-term. This was observed with the yields of Patagonia-INIA, Yaike, and Puyehue-INIA, which registered accumulated yields of 677, 624, and 591 Mg ha^{-1}, respectively under irrigation. In comparison, Patagonia-INIA reached 601 Mg ha^{-1} over six seasons (**Figure 4**). **Figure 3** shows that the lowest precipitation levels occurred in January and February, which typically

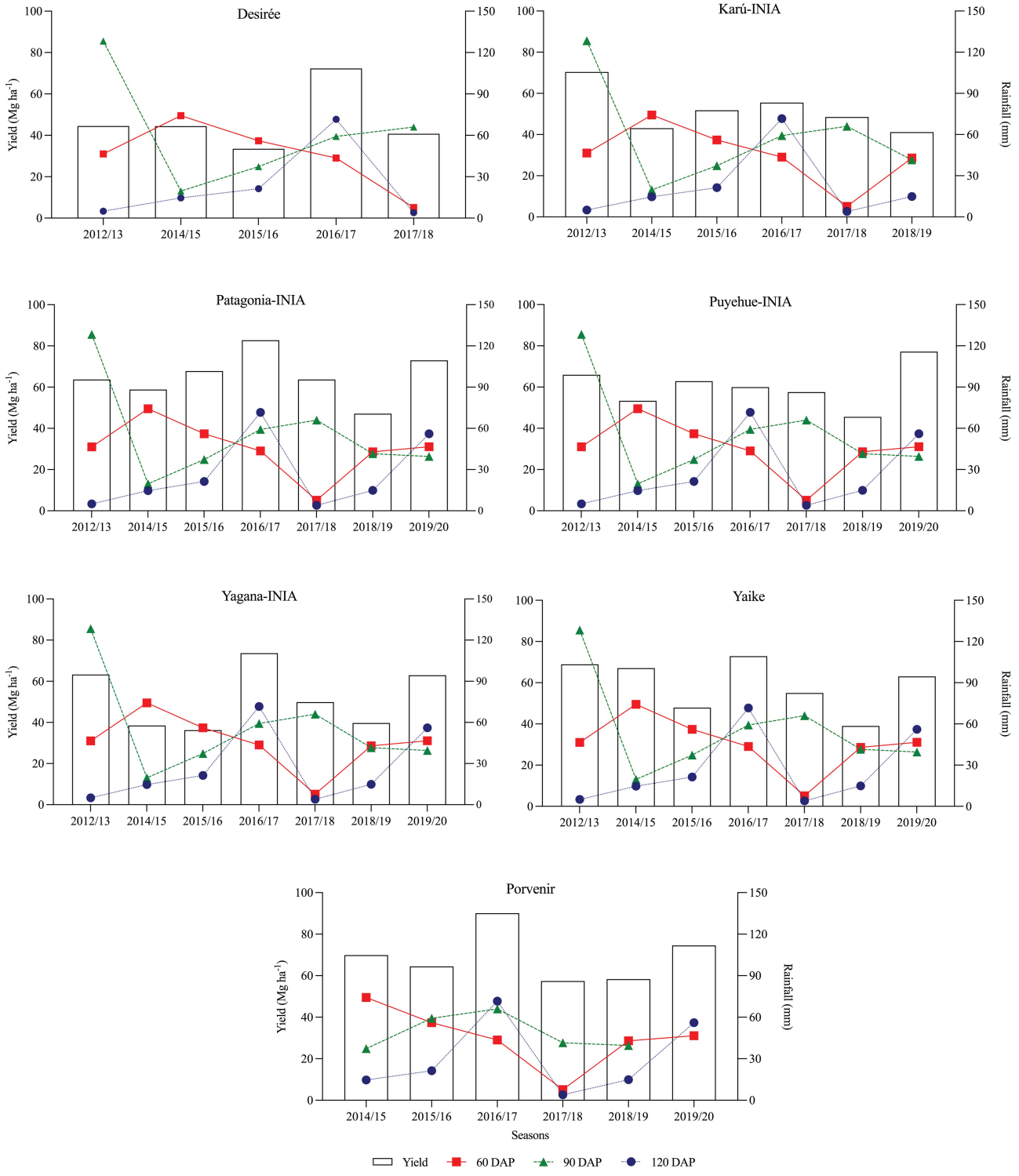

FIGURE 5 | Temporal relationship between potato tuber yield under rainfed conditions and rainfall at 60, 90, and 120 days after planting (DAP), from the 2012–13 to 2019–20 season. 60 DAP: 0–60 days, 90 DAP:60–90 days, and 120 DAP: 90–120 days.

follow flowering in this region. By this time, the number of tubers has already been fixed. Still, during this period, tubers acquire their final weight, which concurs with the environmental index and explains the differences in yields under irrigation and rainfed conditions. The results in a yield of high productive varieties by 7 years indicate an

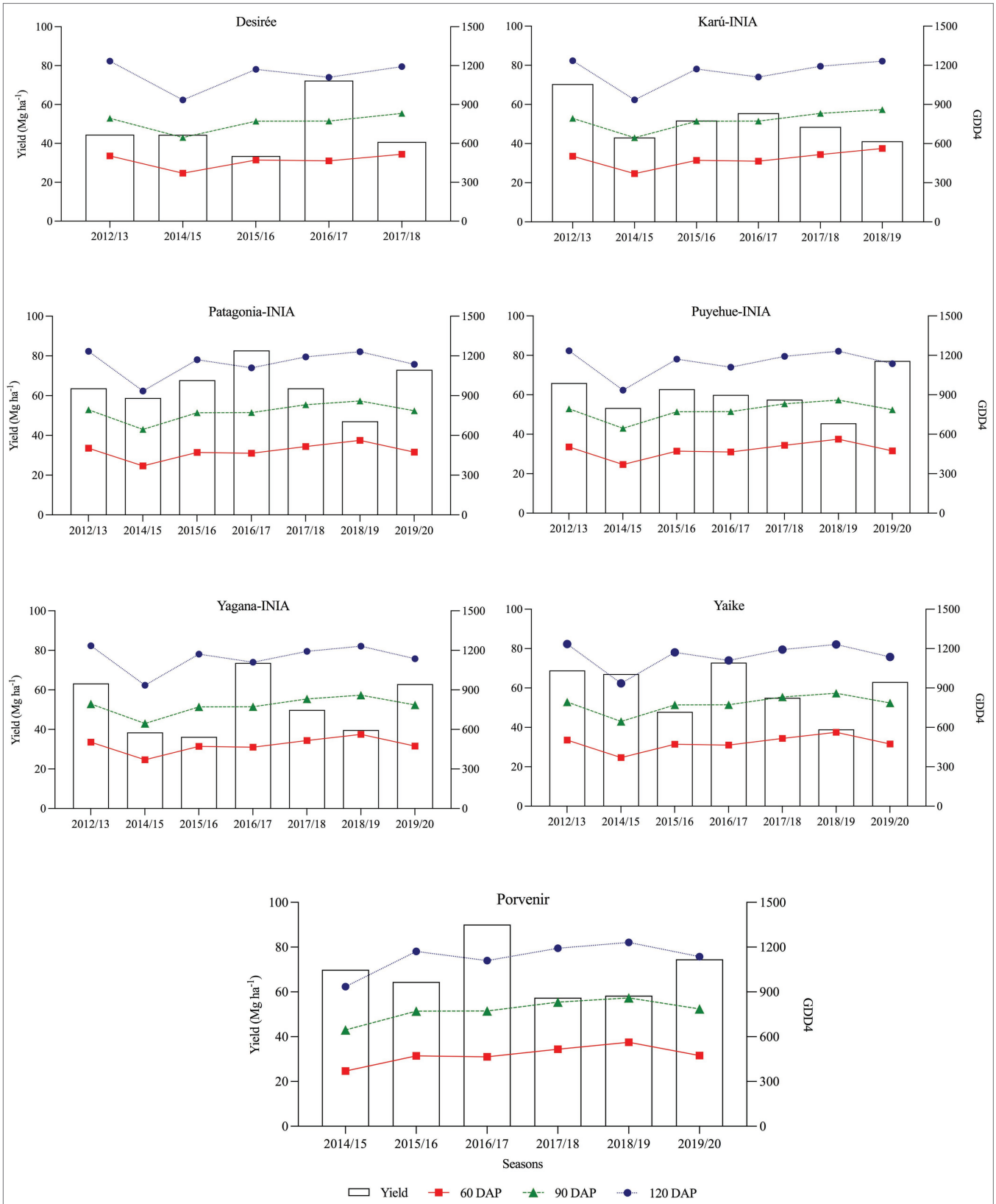

FIGURE 6 | Temporal relationship between potato tuber yield and GDD4 at 60, 90, and 120 DAP, from the 2012–13 to 2019–20 season under rainfed conditions. 60 DAP: 0–60 days, 90 DAP:60–90 days, and 120 DAP: 90–120 days.

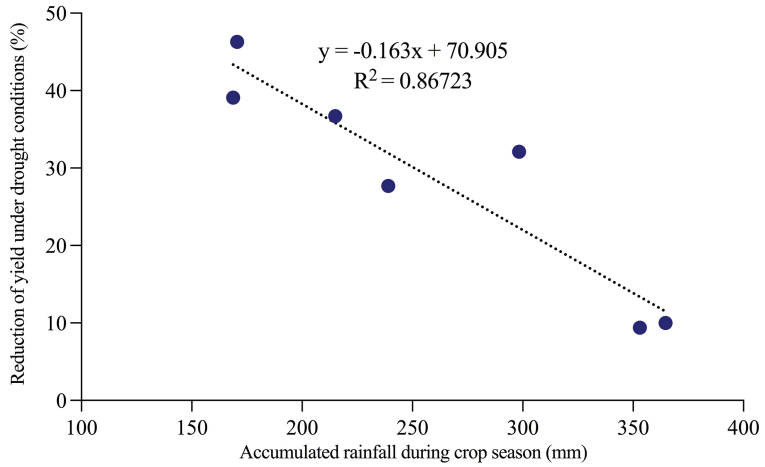

FIGURE 7 | Percentage of reduction of the yield under rainfed conditions compared to irrigated plots concerning the accumulated precipitation during the growing season between 2012–12 and 2019–20 seasons.

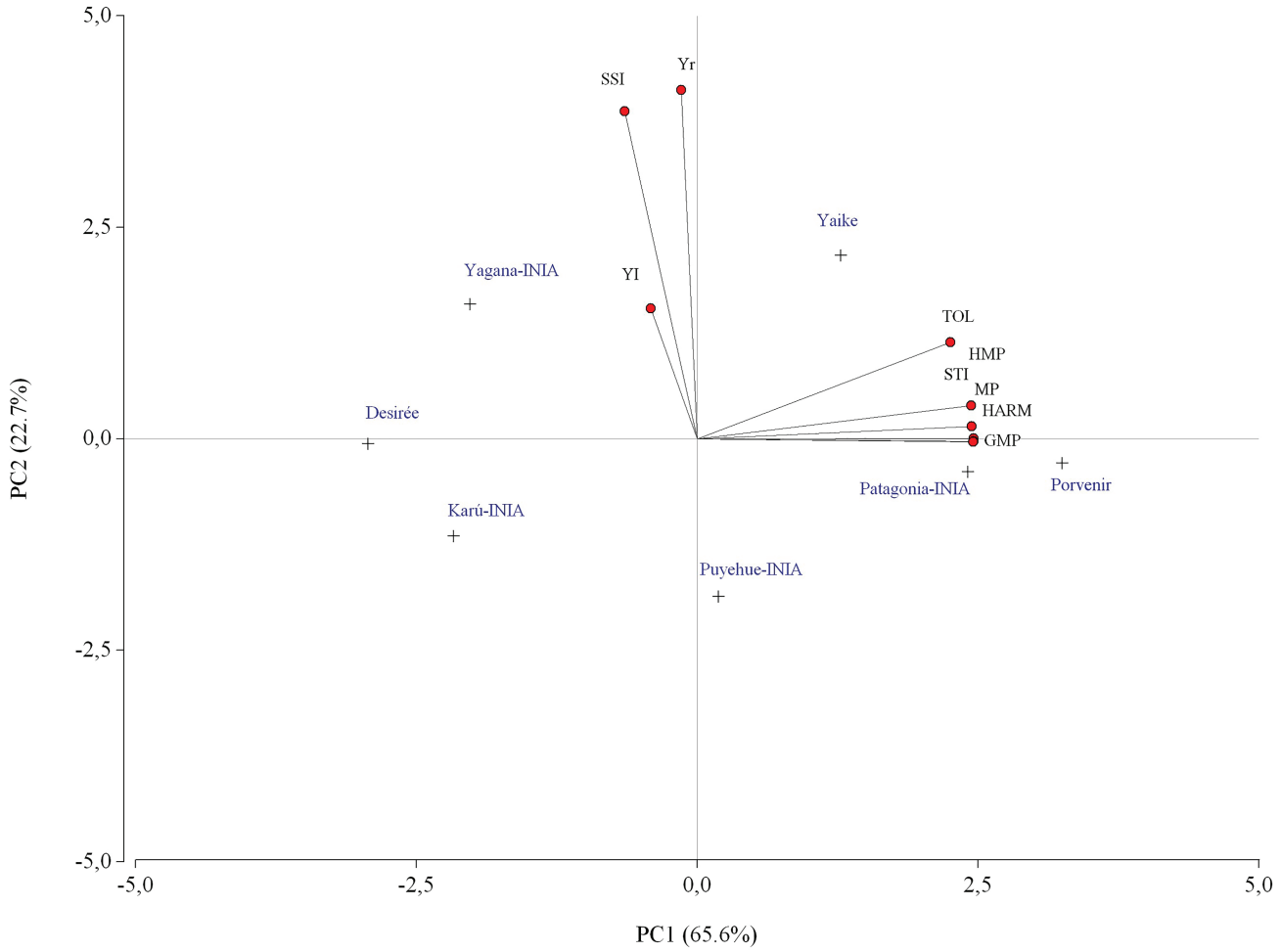

FIGURE 8 | Biplot of the potato varieties under study over different stress tolerance indices under irrigation and rainfed conditions between the 2012–2013 and 2019–2020 seasons.

TABLE 3 | The correlation coefficient between drought stress conditions and drought tolerance indices between 2012–13 and 2019–20.

	YI	TOL	MP	GMP	HARM	STI	HMP	Yr	SSI
YI	1.00								
TOL	0.04	1.00							
MP	−0.17	0.91	1.00						
GMP	−0.18	0.90	1.00	1.00					
HARM	−0.19	0.90	1.00	1.00	1.00				
STI	−0.09	0.92	0.99	0.99	0.99	1.00			
HMP	−0.17	0.88	0.99	1.00	1.00	0.99	1.00		
Yr	0.24	0.21	−0.06	−0.06	−0.06	0.03	−0.02	1.00	
SSI	0.16	−0.04	−0.26	−0.26	−0.26	−0.18	−0.21	0.95	1.00

YI, yield index; TOL, tolerance index; MP, mean productivity; GMP, geometric mean productivity; HARM, harmonic mean; STI, stress tolerance index; HMP, harmonic mean productivity; Yr, yield reduction; and SSI, stress susceptibility index.

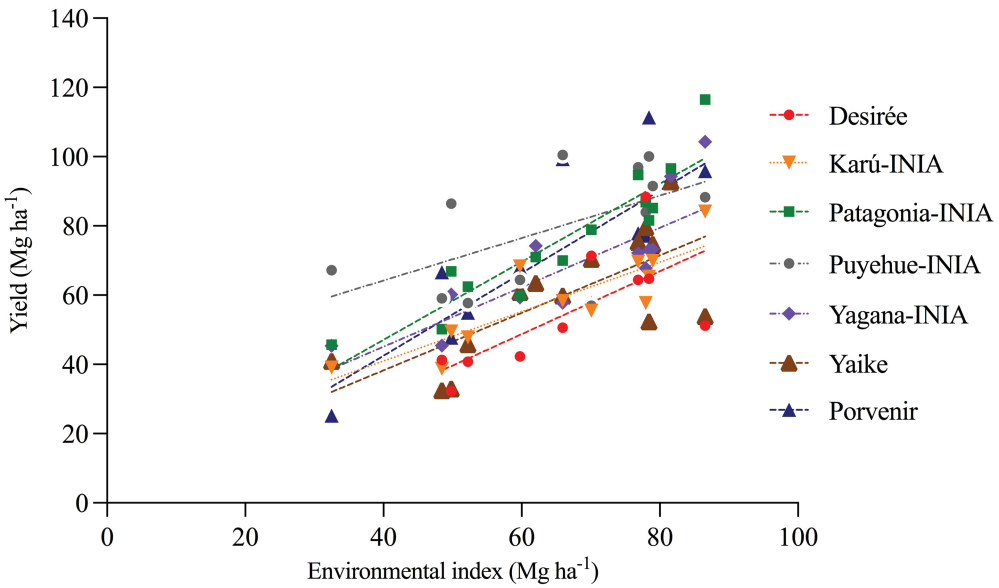

FIGURE 9 | Relationship between yield and environmental index for seven potato varieties.

TABLE 4 | Environmental index (average yield of seven varieties) per year for irrigated and rainfed conditions.

Year	Season pp	E. Index (Mg ha^{-1})	
		Rainfed	Irrigated
2012	353	59.7	65.9
2014	215	49.6	78.4
2015	169	52.7	86.5
2016	365	70.1	77.9
2017	298	52.2	76.9
2018	171	42.3	78.9
2019	239	67.9	93.9
Average	258.6	56.4	79.8

important limiting for yield in no irrigated crops, even considering that south of Chile is an area with big yield potential for potatoes where this species is typically grown in drylands. Data of accumulated rainfall during the potato growing season during the last 40 years (**Figures 1, 2**) show a tendency to lower amounts from past to present. Therefore, potato improvement for drought tolerance and implementation of irrigation systems in this crop is essential to obtain marketable yields and avoid the risk of failure of the crop in years with low precipitation. The situation will probably be more pronounced in the future, given the trends in the last decades (Raymundo et al., 2014; Aliche et al., 2019; Hill et al., 2021). These results exemplify how much we can lose in productivity in dryland conditions even in one of the most favorable areas for growing potatoes globally and how risky this situation can be for the performance of the potato farms in the future.

Effects of Drought Conditions on Tuber Yield

Drought conditions lead to a reduction in total tuber yield and marketable yield (**Figure 10**). The yields of the potato

TABLE 5 | Coefficients of the regression between yield and environmental index for seven potato varieties.

Cultivar	Average yield*	Regression parameters in function of the environmental index (E. index)								
		yield vs. E. index			number of tubers vs. E. index			weight of individual tuber vs. E. index		
		R^2	*b* (slope)	*p*	R^2	*b* (slope)	*p*	R^2	*b* (slope)	*p*
Desiree	54.7 ± 17.5	0.46	0.91	<0.0001	0.28	NC	0.0026	0.5	0.73	<0.0001
Karú-INIA	58.7 ± 14.4	0.58	0.69	<0.0001	0.16	NC	>0.05	0.49	0.58	<0.0001
Patagonia-INIA	76.2 ± 19.9	0.75	1.13	<0.0001	0.05	NC	>0.05	0.86	0.76	<0.0001
Puyehue-INIA	67.25 ± 18.5	0.51	0.86	<0.0001	0.05	NC	>0.05	0.61	0.54	<0.0001
Yagana-INIA	59.69 ± 18.1	0.49	0.83	<0.0001	0.09	NC	>0.05	0.59	0.51	<0.0001
Yaike	73.28 ± 23.4	0.61	1.19	<0.0001	0.05	NC	>0.05	0.81	0.59	<0.0001
Porvenir	79.42 ± 17.9	0.74	0.94	<0.0001	0.06	NC	>0.05	0.67	0.72	<0.0001

**Average yield for all years and treatments.*

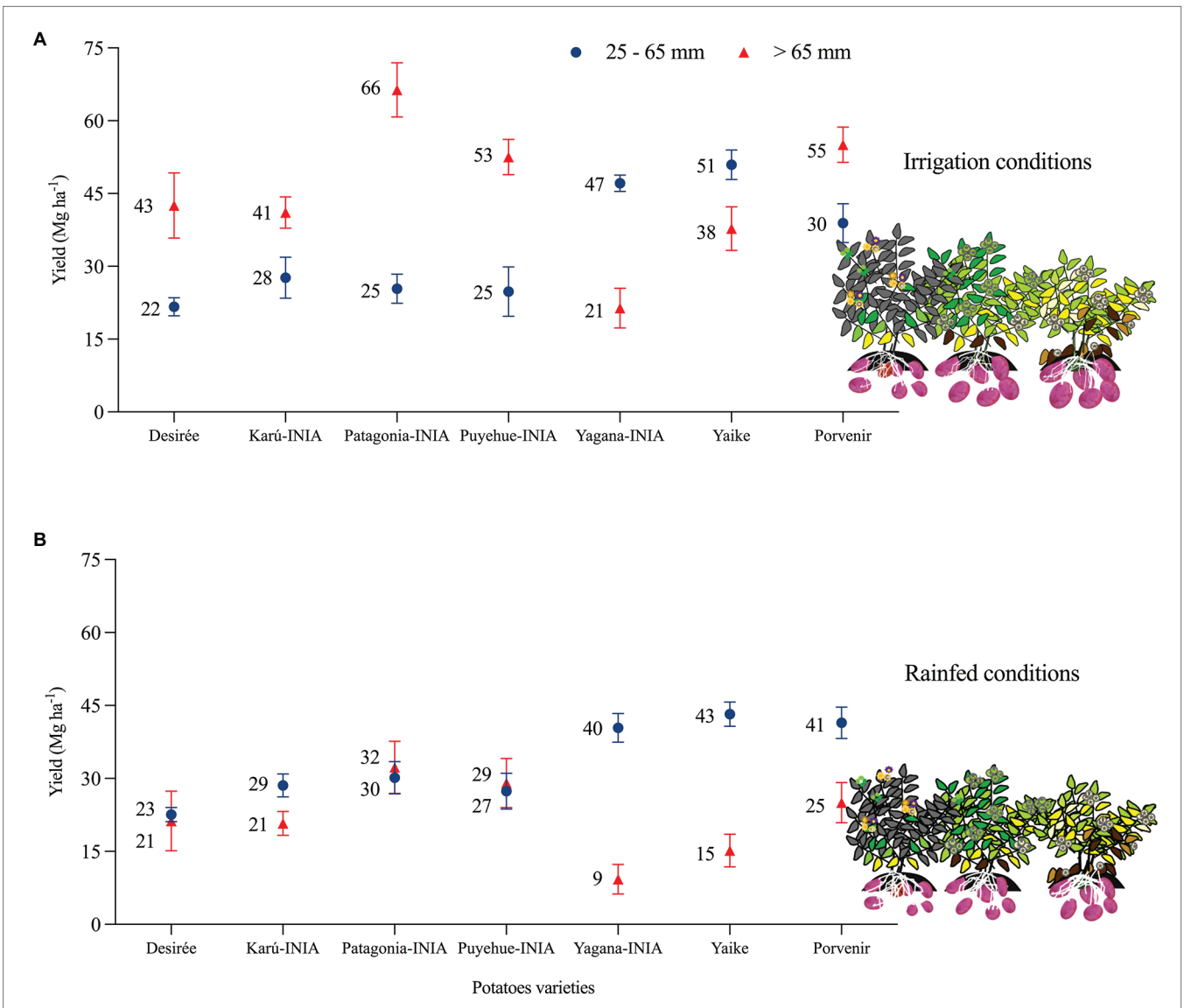

FIGURE 10 | Average tuber size distribution of seven potato varieties under irrigation and rainfed conditions from 2012–14 to 2019–20. **(A)** Yield of marketable tubers: > 65 mm. **(B)** Yield of seed tubers (25–65 mm). Error bars indicate SE ($p < 0.05$).

varieties increased under conditions of water stress when there was precipitation exceeded 60 mm in the first 90–120 DAP (**Figure 5**), which indicates that the important phenological stages and types of varieties should be considered before applying deficit irrigation to maximize productivity (Martínez-Romero et al., 2019). Karam et al. (2014) observed that water deficits during tuber development in semiarid climates can reduce yields by 12%, while water deficits during tuber filling decreased yields by 42%. As observed in **Figure 10**, the effect of drought during the tuber-filling period reduces tuber size distribution and tuber yield (Aliche et al., 2018). Yagana-INIA and Yaike were more productive for tuber seed production across the years of study. Aliche et al. (2019) indicate that cultivars that make more tubers than they can bulk during the growing season would distribute smaller sizes, especially under rainfed conditions.

The highest yields under the I conditions compared to the R conditions occurred in the 2014–15 season (**Figure 4**) and coincided with the lowest rainfall and GDD4 at 90 DAP, and 120 DAP (**Figures 5, 6**) occurred during the tuber-filling period. This could also be associated with the warmest temperature (23°C) and highest levels of solar radiation, 24.3 (Mj m^{-2}), in January (**Figure 3**). Van Harsselaar et al. (2021) mentioned that tuber growth is inhibited under combined drought and heat stress, with elevated temperatures of 30°C during the day. Timlin et al. (2006) indicated that the supply of photosynthates to tuber decreases with higher temperatures since the optimum temperature for biomass accumulation in potato is 20°C (Monneveux et al., 2013; Liang et al., 2020). Moreover, drought on tuberization reduces tuber formation and has a strong effect on tuber yield (Aliche et al., 2018). However, although the climatic conditions, especially precipitation, varied during the phenological period of the crop and during the years of the study, the accumulations of GDD4 were similar in the study area (**Figure 6**). Similar values were observed with the variety Desiree in a Mediterranean climate, indicating a weak correlation between yield and exposure of the plant to GDD (Danieli et al., 2018). Finally, the stress tolerance indices confirmed which varieties are best and least adapted to water deficit. The variables which contributed more positively to PC1 were GMP, HARM, MP, HMP, and TOL, which indicated an association between these indices and the general adaptability of the varieties to stressful environments. The varieties Porvenir, Patagonia-INIA, and Yaike, were the most adaptable (**Figure 8**; **Table 3**) and had the best drought tolerance indices. This confirms that these indices identify genotypes with high yield potential and tolerance to water stress. The GMP was the best-adapted index to assess relative yield (Mohammed and Kadhem, 2017). SSI, Yr, and YI are probably only useful to identify genotypes that behave well under stressful conditions but are not appropriate to identify genotypes that respond to improvements in environmental conditions. Krishnamurthy et al. (2016) indicated that SSI often fails to identify genotypes with high yields and stress tolerance potentials. Thus, Nikneshan et al. (2019) have also indicated that SSI, Yr, and YI work best when the changes in the yield of the genotype are lower and more stable over time.

CONCLUSION

The results in terms of yield-high varieties by 7 years indicate an important limiting in non-irrigated tuber yield, which decreased by 27 and 34% under rainfed conditions. However, tuber size distribution was the most affected under water limiting conditions, significantly reducing the marketable tubers (>65 mm) by 50–60%. The varieties Porvenir, Patagonia-INIA, and Yaike, had higher yields under conditions of irrigation and rainfed. However, it was observed that the varieties had high yields under water stress conditions when precipitation of more than 60 mm occurred between 60 and 120 DAP. The best indices to study drought tolerance were TOL, MP, GMP, Harm, STI, and HMP. Our study suggests that even in cool temperate areas with favorable soil properties for potatoes, as Andisols, low rainfall can produce a serious constraint for productivity. Therefore, combining varieties with more water stress tolerance and providing supplementary irrigation during the dry period can optimize the yield under rainfed conditions.

DATA AVAILABILITY STATEMENT

The original contributions presented in the study are included in the article/supplementary material, further inquiries can be directed to the corresponding author.

AUTHOR CONTRIBUTIONS

IM, MM, and MU contributed to conception and design of the study and organized the database. IM, MM, and IA performed the statistical analysis and wrote sections of the manuscript. IM wrote the first draft of the manuscript. All authors contributed to the article and approved the submitted version.

FUNDING

This research was financed by the Chilean Ministry of Agriculture through the Potato Breeding Program Project N°500057-70 (Fitomejoramiento de papa) and Project N°502783-70 (Evaluación y selección de genotipos de cultivos potencialmente adaptados al estrés hídrico y nutricional para un clima cambiante del sur de Chile).

ACKNOWLEDGMENTS

The authors thank Francisco Salazar for providing access to the INIA Remehue Bromatology Laboratory to take physical soil measurements.

REFERENCES

Ahmadvand, G., Mondani, F., and Golzardi, F. (2009). Effect of crop plant density on critical period of weed competition in potato. *Sci. Hortic.* 121, 249–254. doi: 10.1016/j.scienta.2009.02.008

Aliche, E. B., Oortwihn, M., Theeuwen, T. P. J. M., Bachem, C. W. B., van Eck, H. J., Visser, R. G. F., et al. (2019). Genetic mapping of tuber size distribution and marketable tuber yield under drought stress in potatoes. *Euphytica* 215:186. doi: 10.1007/s10681-019-2508-00123456789

Aliche, E. B., Oortwijn, M., Theeuwen, T. P. J. M., Bachem, C. W. B., Visser, R. G. F., and van der Linden, C. G. (2018). Drought response in field grown potatoes and the interactions between canopy growth and yield. *Agric. Water Manag.* 206, 20–30. doi: 10.1016/j.agwat.2018.04.013

Aliche, E. B., Theeuwen, T. P. J. M., Oortwijn, M., Visser, R. G. F., and van der Linden, C. G. (2020). Carbon partitioning mechanisms in potato under drought stress. *Plant Physiol. Biochem.* 145, 211–219. doi: 10.1016/j.plaphy.2019.11.019

Ambrosone, A., Batelli, G., Bostan, H., D'Agostino, N., Chiusano, M. L., Perotta, G., et al. (2016). Distinct gene networks drive differential response to abrupt or gradual water deficit in potato. *Gene* 597, 30–39. doi: 10.1016/j.gene.2016.10.024

Centro de Información de Recursos Naturales (CIREN) (2003). Estudio agrológico X Reg. Tomo 2, CIREN, Santiago.

Choudhary, A., Sultana, R., Vales, M. I., Saxena, K. B., Kumar, R. R., and Ratnakumar, P. (2018). Integrated physiological and molecular approaches to improvement of abiotic stress tolerance in two pulse crops of the semiarid tropics. *Crop J.* 6, 99–114. doi: 10.1016/j.cj.2017.11.002

Clunes, J., Dörner, J., and Pinochet, D. (2021). How does the functionality of the pore system affects inorganic nitrogen storage in volcanic ash soils? *Soil Tillage Res.* 205:104802. doi: 10.1016/j.still.2020.104802

Danieli, R., Blank, L., Salam, B. B., Malka, S. K., Teper-Bamnolker, P., Daus, A., et al. (2018). Postharvest temperature has a greater impact on apical dominance of potato seed-tuber than field growing-degree days exposure. *Field Crop Res.* 223, 105–112. doi: 10.1016/j.fcr.2018.03.020

Di Rienzo, J. A., Casanoves, F., Balzarini, M. G., Gonzales, L., Tablada, M., and Robledo, C. W. (2009). InfoStat Version. Grupo InfoStat, FCA, Universidad Nacional de Córdoba, Argentina.

El-Hendawy, S. E., Hassan, W. M., Al-Suhaibani, N. A., and Schmidhalter, U. (2017). Spectral assessment of drought tolerance indices and grain yield in advanced spring wheat lines grown under full and limited water irrigation. *Agric. Water Manag.* 182, 1–12. doi: 10.1016/j.agwat.2016.12.003

Fang, Y., and Xiong, L. (2015). General mechanisms of drought response and their application in drought resistance improvement in plants. *Cell. Mol. Life Sci.* 72, 673–689. doi: 10.1007/s00018-014-1767-0

FAOSTAT (2020). FAOSTAT crop data. Food and Agriculture Organization of the United Nations. Available at: http://www.fao.org/faostat/en/#data/QC/visualize (Accessed March 27, 2021).

Fernandez, G. C. J. (1993). "Effective selection criteria for assessing plant stress tolerance," in *Proceedings of the International Symposium on Adaptation of Vegetables and Other Food Crops to Temperature Water Stress*. ed. C. G. Kuo, August 13–18; Taiwan, pp. 257–270.

Fleisher, D. H., Dathe, A., Timlin, D. J., and Reddy, V. R. (2015). Improving potato drought simulations: assessing water stress factors using a coupled model. *Agric. For. Meteorol.* 200, 144–155. doi: 10.1016/j.agrformet.2014.09.018

Golestani, S. A., and Assad, M. T. (1998). Evaluation of four screening techniques for drought resistance and their relationship to yield reduction ratio in wheat. *Euphytica* 103, 293–299. doi: 10.1023/A:1018307111569

Gouveia, C. S. S., Gananca, J. F. T., Slaski, J., Lebot, V., and de Carvalho, M. A. A. P. (2019). Variation of carbon and isotope natural abundances ($\delta^{15}N$ and $\delta^{13}C$) of whole-plant sweet potato (*Ipomoea batatas* L.) subjected to prolonged water stress. *J. Plant Physiol.* 243:153052. doi: 10.1016/j.jplph.2019.153052

Gregory, P. T., and Marshall, B. (2012). Attribution of climate change: a methodology to estimate the potential contribution to increases in potato yield in Scotland since 1960. *Glob. Chang. Biol.* 18, 1372–1388. doi: 10.1111/j.1365-2486.2011.02601.x

Hill, D., Nelson, D., Hammond, J., and Bell, L. (2021). Morphophysiology of potato (*Solanum tuberosum*) in response to drought stress: paving the way forward. *Front. Plant Sci.* 11:597554. doi: 10.3389/fpls.2020.597554

Jamshidi, A., and Javanmard, H. R. (2018). Evaluation of barley (*Hordeum vulgare* L.) genotypes for salinity tolerance under field conditions using the stress indices. *Ain Shams Eng. J.* 9, 2093–2099. doi: 10.1016/j.asej.2017.02.006

Karam, F., Amacha, N., El Asmar, T., and Domínguez, A. (2014). Response of potato to full and deficit irrigation under semiarid climate: agronomic and economic implications. *Agric. Water Manag.* 142, 144–151. doi: 10.1016/j.agwat.2014.05.007

Krishnamurthy, S. L., Gautam, R. K., Sharma, P. C., and Sharma, D. K. (2016). Effect of different salt stresses on agro-morphological traits and utilization of salt stress indices for reproductive stage salt tolerance in rice. *Field Crop Res.* 190, 26–33. doi: 10.1016/j.fcr.2016.02.018

Liang, S.-M., Li, Y.-S., Rehman, M. A., He, S.-D., Wang, P.-J., Yin, Z.-Y., et al. (2020). Effects of planting patterns on rainwater use efficiency and potato tuber yield in seasonally arid areas of southwestern China. *Soil Tillage Res.* 197:104502. doi: 10.1016/j.still.2019.104502

Lin, C. S., Binns, M. R., and Lefkovitch, L. P. (1986). Stability analysis: where do we stand? *Crop Sci.* 26, 894–900. doi: 10.2135/cropsci1986.0011183X002600050012x

Mardeh, A. S., Ahmadi, A., Poustini, K., and Mohammadi, V. (2006). Evaluation of drought resistance indices under various environmental conditions. *Field Crop Res.* 98l, 222–229. doi: 10.1016/j.fcr.2006.02.001

Martínez-Romero, A., Domínguez, A., and Landeras, G. (2019). Regulated deficit irrigation strategies for different potato cultivars under continental mediterranean-Atlantic conditions. *Agric. Water Manag.* 216, 164–176. doi: 10.1016/j.agwat.2019.01.030

Mbava, M., Mutema, M., Zengeni, R., Shimelis, H., and Chaplot, V. (2020). Factors affecting crop water use efficiency: a worldwide meta-analysis. *Agric. Water Manag.* 228:105878. doi: 10.1016/j.agwat.2019.105878

McMaster, G. S., and Wilhelm, W. W. (1997). Growing degree-days: one equation, two interpretations. *Agric. For. Meteorol.* 87, 291–300. doi: 10.1016/S0168-1923(97)00027-0

Mi, X., Ji, Z., Yang, J., Liang, L., Si, H., Wu, J., et al. (2015). Transgenic potato plants expressing cry3A gene confer resistance to Colorado potato beetle. *C. R. Biol.* 338, 443–450. doi: 10.1016/j.crvi.2015.04.005

Mohammed, A. K., and Kadhem, F. A. (2017). Screening drought tolerance in bread wheat genotypes (*Triticum aestivum* L.) using drought indices and multivariate analysis. *Iraqi J. Agric. Sci.* 48:41.51. doi: 10.36103/ijas.v48iSpecial.244

Monneveux, P., Ramírez, D. A., and Pino, M.-T. (2013). Drought tolerance in potato (*S. tuberosum* L.) can we learn from drought tolerance research in cereals? *Plant Sci.* 205-206, 76–86. doi: 10.1016/j.plantsci.2013.01.011

Munsell (2009). *Munsell Soil-Color Charts*. Michigan, USA: Munsell Color, Grand Rapids.

Nikneshan, P., Tadayyon, A., and Javanmard, M. (2019). Evaluating drought tolerance of castor ecotypes in the center of Iran. *Heliyon* 5:e01403. doi: 10.1016/j.heliyon.2019.e01403

Noerwijati, K., and Budiono, R. (2015). Yield and yield components evaluation of cassava (*Manihot esculenta* Crantz) clones in different altitudes. *Energy Procedia* 65, 155–161. doi: 10.1016/j.egypro.2015.01.050

Ordoñez, I., López, I. F., Kemp, P. D., Descalzi, C. A., Horn, R., Zúñiga, F., et al. (2018). Effect of pasture improvement managements on physical properties and water content dynamics of a volcanic ash soil in southern Chile. *Soil Tillage Res.* 178, 55–64. doi: 10.1016/j.still.2017.11.013

Raymundo, R., Asseng, S., Cammarano, D., and Quiroz, R. (2014). Potato, sweet potato, and yam models for climate change: a review. *Field Crop Res.* 166, 173–185. doi: 10.1016/j.fcr.2014.06.017

Timlin, D., Lutfor, S. M., Baker, J., Reddy, V. R., Fleisher, D., and Quebedeaux, B. (2006). Whole plant photosynthesis, development, and carbon partitioning in potato as a function of temperature. *Agron. J.* 98, 1195–1203. doi: 10.2134/agronj2005.0260

Valle, S. R., Carrasco, J., Pinochet, D., Soto, P., and Donald, R. M. (2015). Spatial distribution assessment of extractable Al, (NaF) pH and phosphate retention as tests to differentiate among volcanic soils. *Catena* 127, 17–25. doi: 10.1016/j.catena.2014.12.011

Valle, S. R., Dörner, J., Zúñiga, F., and Dec, D. (2018). Seasonal dynamics of the physical quality of volcanic ash soils under different land uses in southern Chile. *Soil Tillage Res.* 182, 25–34. doi: 10.1016/j.still.2018.04.018

Van Harsselaar, J. K., Claußen, J., Lübeck, J., Wörlein, N., Uhlmann, N., Sonnewald, U., et al. (2021). X-ray CT phenotyping reveals bi-phasic growth phases of potato tubers exposed to combined abiotic stress. *Front. Plant Sci.* 12:613108. doi: 10.3389/fpls.2021.6113108

Wang, Y., and Frei, M. (2011). Stressed food - the impact of abiotic environmental stresses on crop quality. *Agr. Ecosyst. Environ.* 141, 271–286. doi: 10.1016/j.agee.2011.03.017

Yuan, M., Zhang, L., Gou, F., Su, Z., Spiertz, J. H. J., and van der Werf, W. (2013). Assessment of crop growth and water productivity for five C3 species in semiarid Inner Mongolia. *Agric. Water Manag.* 122, 28–38. doi: 10.1016/j.agwat.2013.02.006

Zhang, S., Xu, X., Sun, Y., Zhang, J., and Li, C. (2018). Influence of drought hardening on the resistance physiology of potato seedlings under drought stress. *J. Integr. Agric.* 17, 336–347. doi: 10.1016/S2095-3119(17)61758-1

Zhao, H., Xiong, Y., Li, F., Wang, R., Qiang, S., Yao, T., et al. (2012). Plastic film much for half growing-season maximized WUE and yield of potato via moisture-temperature improvement in a semiarid agroecosystem. *Agric. Water Manag.* 104, 68–78. doi: 10.1016/j.agwat.2011.11.016

Conflict of Interest: The authors declare that the research was conducted in the absence of any commercial or financial relationships that could be construed as a potential conflict of interest.

frontiers in Plant Science

ORIGINAL RESEARCH
published: 12 August 2021
doi: 10.3389/fpls.2021.698060

Potato Response to Drought Stress: Physiological and Growth Basis

*Taylor Gervais, Alexa Creelman, Xiu-Qing Li, Benoit Bizimungu, David De Koeyer and Keshav Dahal**

Fredericton Research and Development Centre, Agriculture and Agri-Food Canada, Fredericton, NB, Canada

Drought poses a major challenge to the production of potatoes worldwide. Climate change is predicted to further aggravate this challenge by intensifying potato crop exposure to increased drought severity and frequency. There is an ongoing effort to adapt our production systems of potatoes through the development of drought-tolerant cultivars that are appropriately engineered for the changing environment. The breeding of drought-tolerant cultivars can be approached through the identification of drought-related physiological and biochemical traits and their deployment in new potato cultivars. Thus, the main objective of this study was to develop a method to identify and characterize the drought-tolerant potato genotypes and the related key traits. To achieve this objective, first we studied 56 potato genotypes including 54 cultivars and 2 advanced breeding lines to assess drought tolerance in terms of tuber yield in the greenhouse experiment. Drought differentially reduced tuber yield in all genotypes. Based on their capacity to maintain percent tuber yield under drought relative to their well-watered controls, potato genotypes differed in their ability to tolerate drought. We then selected six genotypes, Bannock Russet, Nipigon, Onaway, Denali, Fundy, and Russet Norkotah, with distinct yield responses to drought to further examine the physiological and biochemical traits governing drought tolerance. The drought-induced reduction in tuber yield was only 15–20% for Bannock Russet and Nipigon, 44–47% for Onaway and Denali, and 83–91% for Fundy and Russet Norkotah. The tolerant genotypes, Bannock Russet and Nipigon, exhibited about a 2–3-fold increase in instantaneous water-use efficiency (WUE) under drought as compared with their well-watered controls. This stimulation was about 1.8–2-fold for moderately tolerant genotypes, Onaway and Denali, and only 1.5-fold for sensitive genotypes, Fundy, and Russet Norkotah. The differential stimulation of instantaneous WUE of tolerant and moderately tolerant genotypes vs. sensitive genotypes was accounted for by the differential suppression of the rates of photosynthesis, stomatal conductance, and transpiration rates across genotypes. Potato genotypes varied in their response to leaf protein content under drought. We suggest that the rates of photosynthesis, instantaneous WUE, and leaf protein content can be used as the selection criteria for the drought-tolerant potato genotypes.

Keywords: drought tolerance, potato cultivars, growth, yield, tuber number, photosynthesis

OPEN ACCESS

Edited by:
Thorsten M. Knipfer, University of British Columbia, Canada

Reviewed by:
Manuela Zude-Sasse, Leibniz Institute for Agricultural Engineering and Bioeconomy (ATB), Germany
Pradeep Kumar, Central Arid Zone Research Institute (ICAR), India

****Correspondence:***
Keshav Dahal
keshav.dahal@agr.gc.ca

Specialty section:
This article was submitted to Crop and Product Physiology, a section of the journal Frontiers in Plant Science

Received: *10 May 2021*
Accepted: *13 July 2021*
Published: *12 August 2021*

Citation:
Gervais T, Creelman A, Li X-Q, Bizimungu B, De Koeyer D and Dahal K (2021) Potato Response to Drought Stress: Physiological and Growth Basis. Front. Plant Sci. 12:698060. doi: 10.3389/fpls.2021.698060

INTRODUCTION

Potato ranks the first highest produced non-cereal food crops and the fourth highest produced crop after wheat, corn, and rice worldwide (FAOSTAT, 2019). It is cultivated in over 100 countries, and the global production of potatoes was estimated to be 370 million tons in 2019, feeding over a billion people worldwide. Potato is considered to be a healthy source of carbohydrates, dietary fiber, protein, vitamins, antioxidants, and minerals (Beals, 2019). Hence, enhancing the productivity of potato crops can contribute to fulfilling the nutritional requirements of the rising population (Birch et al., 2012). Potato is mainly cultivated for its tuber, which is mainly composed of carbohydrates generated through photosynthesis in the source leaves. The photosynthetic end product, i.e., sucrose, is transported from source leaves to the stolon where it is converted to starch, leading to tuber initiation and growth (Aliche et al., 2020). The effective coordination among these processes is crucial for tuber growth and productivity. The shallow root system of potatoes makes this crop one of the most drought-sensitive species (Zarzynska et al., 2017). Drought strongly inhibits key physiological and biochemical processes, leading to poor plant performance and tuber yield loss. The magnitude of this loss, however, mostly depends on the duration and severity of drought episodes as well as plant growth stage and cultivar (Evers et al., 2010; Stark et al., 2013; Aliche et al., 2018; Plich et al., 2020; Hill et al., 2021). Drought during the early growth stage is considered to be the most harmful as it substantially reduces total leaf area, reduces photosynthetic rates, and assimilates partitioning to tubers leading to poor tuber initiation, bulking, and tuber yield (Evers et al., 2010; Obidiegwu et al., 2015). Drought during tuberization leads to fewer stolon per stem, reflected by lower tuber number and yield (Eiasu et al., 2007). If potato plants experience drought during the tuber bulking stage, they will produce fewer and smaller-sized tubers. Nevertheless, it has been suggested that the initiation of stolon and the formation of tuber are the most critical stages of drought stress (Aliche et al., 2020). The reduction in tuber yield under drought is suggested to be mainly associated with the inhibition of photosynthesis (Plich et al., 2020). The drought-induced stomatal closure, which is aimed at reducing the transpiration water loss and conserving plant water status, also restricts CO_2 diffusion in the leaf making the Calvin cycle CO_2 substrate-limited (Pinheiro and Chaves, 2011; Dahal et al., 2014, Aliche et al., 2020). This may result in the accumulation of ATP and NADPH since their rates of generation by the photosynthetic electron transport chain exceeds their utilization by the Calvin cycle. Consequently, there is an energy imbalance in the chloroplast level that favors the generation of reactive oxygen species leading to oxidative stress and damage of cell components. Thus, plants experience both stomatal and biochemical limitations of photosynthesis in response to drought stress (Lawlor and Tezara, 2009; Pinheiro and Chaves, 2011; Dahal et al., 2015; Dahal and Vanlerberghe, 2017).

Potato plants employ various strategies at the molecular, biochemical, physiological, and whole plant levels to cope with drought stress (Boguszewska-Mańkowska et al., 2018, Dahal et al., 2019). At molecular and genomic levels, drought tolerance has been conferred by the expression of various stress-related genes that encode proteins including transcription factors and enzymes involved in drought stress tolerance (Shinozaki and Yamaguchi-Shinozaki, 2007). The products of drought-related genes play a key role in stimulating initial stress response and in inducing stress tolerance at the cellular level. Drought stress initiates the synthesis and deprotonation of abscisic acid (ABA), a well-known phytohormone (Yao et al., 2018). ABA serves as signaling molecules that induce the expression of several stress-related genes including those involved in closing stomata (Cutler et al., 2010). Drought-related genes are believed to be governed through both ABA-dependent and ABA-independent mechanisms (Takahashi et al., 2018). Although the application of exogenous ABA has confirmed the ABA-induced expression of stress-related genes, several drought-induced genes are insensitive to exogenous ABA application. The ability of the cultivars to tolerate drought stress is considered to be governed by upregulation of the expression of chloroplast-localized antioxidants and molecular chaperones (Vasquez-Robinet et al., 2008). It has been reported that the drought-tolerant capacity of potato cultivars is conferred with the induction of the expression of the dehydration-responsive element-binding protein (DREB1A) regulons (Kasuga et al., 1999; Kudo et al., 2017). For instance, the transgenic potato genotypes overexpressing *AtDREB1a* exhibited an improved drought tolerance in comparison with wild type (Watanabe et al., 2011; Movahedi et al., 2012). Pino et al. (2013) compared *ScCBFI* transgenic potato with non-transgenic lines. Their study suggested an improved drought tolerance in *ScCBFI* transgenic lines as indicated by improved overall plant performance and extensive root development following drought stress (Pino et al., 2013).

At the biochemical level, potato plants display an increased accumulation of compatible solutes in response to drought stress (Chen and Murata, 2008; Evers et al., 2010; Sprenger et al., 2016). These solutes have been believed to decrease the leaf water potential without affecting turgor pressure. As a result, leaf cells are capable of taking up more water from the soil to maintain leaf water status and survive drought. For instance, the elevated accumulation of sugar alcohol (Vasquez-Robinet et al., 2008) and proline levels (Sprenger et al., 2016) has been observed in potato leaves following drought stress. In another study, the increased accumulation of glycine betaine has been reported in higher plants in response to drought, salinity, and low-temperature stress (Rontein et al., 2002). Using transgenic potato genotypes overexpressing betaine aldehyde dehydrogenase—an enzyme required in the biosynthesis of glycine betaine—Zhang et al. (2011) reported improved drought stress tolerance in potatoes.

At the whole plant and physiological levels, potato plants improve instantaneous WUE by minimizing transpiration water loss and concomitantly conserving leaf water status through the decrease in stomatal conductance, leaf number, and leaf area (Liu et al., 2005; Coleman, 2008; Albiski et al., 2012; Ierna and Mauromicale, 2020; Kassaye et al., 2020). However, the associated cost of improved WUE is a reduction in photosynthetic leaf surface area, resulting in a negative impact on carbohydrate synthesis. The leaf develops hair and turns to a narrower size to

lessen the light absorbance and prevent photooxidative damage. A few studies have revealed that potato cultivars exhibit an increase in root/shoot ratio due to the extensive and large root architecture in response to drought stress (Zarzynska et al., 2017; Boguszewska-Mańkowska et al., 2020). The drought tolerance has also been conferred to enhanced water and nutrient uptake efficiency as a result of higher root/plant biomass ratio following drought stress (Wishart et al., 2013; Villordon et al., 2014; Zarzynska et al., 2017; Boguszewska-Mańkowska et al., 2020). Studying five potato cultivars subjected to drought stress, Zarzynska et al. (2017) revealed a correlation between tuber yield to root length and area. Their study suggested that potato cultivars tend to improve drought tolerance with deeper root length and larger root systems. In another study, Banik et al. (2016) reported that severe drought treatment following the drought acclimation cycles reduced leaf wilting, induced thicker cuticular layers, and increased open stomata compared with plants without acclimation treatment. Consequently, potato plants acclimated to mild drought stress exhibited reduced yield losses as compared with non-acclimated controls (Banik et al., 2016).

Research on intensive potato breeding is primarily centered on selecting the drought-resistant cultivars by considering indicators at the whole plant and leaf levels such as yield, plant phenotype, leaf morphology, and leaf water content, with less effort at the physiological and biochemical levels. Although the regulation of the physiological and biochemical traits is critical for drought survival, only a few studies have attempted to integrate changes observed at the leaf and whole plant levels with those at the physiological and biochemical levels during drought. Thus, the main objectives of this study were to develop a method to (1) identify and characterize the drought-tolerant potato genotypes and (2) identify the physiological and biochemical traits governing drought tolerance in potatoes.

MATERIALS AND METHODS

Growth Conditions and Tuber Yield

This study used 56 potato genotypes, including 54 commercial cultivars and 2 advanced breeding lines. Experiments were carried out in the greenhouse at the Fredericton Research and Development Centre, Fredericton, Canada, during 2018 and 2021. Plants were grown in 6-inch clay pots containing a general-purpose growing medium with 4 parts soil (Promix BX; Premier Horticulture) and 1 part vermiculite. The plants were grown at a photosynthetic photon flux density (PPFD) of 300 ± 60 μmol photons/m^2/s, 50 ± 5% relative humidity, at a 16-h photoperiod, and at day/night temperature regimes of 22/16°C. The temperature, relative humidity, irradiance level, and photoperiod in each chamber were computer-controlled, monitored, and recorded continuously. The plants were watered to field capacity every day including nutrient supplementation every second day. The nutrients were provided by using 20-20-20 nitrogen–phosphorus–potassium (NPK) fertilizer, and Fe, Mn, Zn, Cu, B, Mo, EDTA supplements (Plant Products Co., Ltd., Brampton, Ontario, Canada). After 5 weeks, a drought treatment was applied to some plants by withholding water for up to 13 days and rewatered for recovery and tuber yield. Tubers were harvested from both well-watered and drought-stressed plants of 56 genotypes at their maturity, and tuber weight and number were recorded.

Physiological and Biochemical Measurements/Analyses

Out of the 56 potato genotypes, 6 cultivars (i.e., Russet Burbank, Nipigon, Onaway, Denali, Fundy, and Russet Norkotah) with distinct responses to drought stress with respect to tuber yield were further studied for the physiological and biochemical characteristics as described in the following sections. All physiological and biochemical measurements and analyses were subsequently performed on a single fully expanded terminal leaflet (at the third position from the top) of control 5-week-old well-watered plants or drought-stressed plants (analyzed after 6–13 days of withholding watering).

Photosynthesis and Chlorophyll *a* (Chl *a*) Fluorescence Measurements

The rates of photosynthesis were measured on the fully expanded terminal leaflets (at the third position from the top) of each genotype under both well-watered and drought conditions by using the LI-COR 6400 portable IR CO_2 gas analyzer (LI-6400 XRT Portable Photosynthesis System; LI-COR Biosciences, Lincoln, NE, USA) at saturating light (1,600 PPFD). In addition, stomatal conductance and leaf transpiration rates were measured simultaneously with the measurements of CO_2 gas exchange. Leaf instantaneous water-use efficiency (WUE) was calculated as the rate of CO_2 assimilation divided by the rates of transpiration (A/T). The chlorophyll *a* (Chl *a*) fluorescence was measured simultaneously with CO_2 gas exchange on the fully expanded terminal leaflets using an LI-COR 6400. All the measurements of Chl *a* fluorescence were carried out by using the standard fluorescence leaf chamber (2 cm^2). Prior to the fluorescence measurements, the leaflets were dark-adapted for 20 min. The minimum fluorescence (F_o) and maximal fluorescence (F_m) in the dark-adapted leaf and the minimum fluorescence (F'_o), maximal fluorescence (F'_m), and steady-state fluorescence (F_s) in the light-adapted leaf were determined as previously described (Maxwell and Johnson, 2000). The parameters of Chl *a* fluorescence were calculated using the following equations:

i) Maximal quantum yield of photosystem II (PSII) = F_v/F_m (Maxwell and Johnson, 2000).
ii) Linear electron transport rates (ETRs) through PSII = (Φ_{PSII}) (PPFD) (0.84) (0.5), where Φ_{PSII} represents the operating efficiency of PSII (Baker et al., 2007).
iii) Non-photochemical quenching (NPQ), a measure of heat dissipation of excess light energy = $(F_m - F'_m)/F'_m$ (Maxwell and Johnson, 2000).

Determination of Total Leaf Protein

We estimated the total leaf protein to assess the effects of drought stress on leaf protein content. After each measurement of CO_2 gas exchange, the fully expanded terminal leaflets from well-watered and drought-stressed plants were harvested, immediately frozen

in liquid N_2, and stored at −80°C. The frozen leaf samples were ground into a fine powder using liquid N_2 in a mortar and pestle. About 30–35 mg of ground leaf samples were added to 800 µl of cold (4°C) extraction buffer containing 1 M Tris–HCl (pH 6.8), 10% (w/v) SDS, 15% (w/v) sucrose, and 0.5 M DTT. The samples were vortexed briefly, solubilized at 70°C for 10 min, and centrifuged to remove debris. Total leaf protein concentrations of the supernatant were quantified using a modified Lowry method (Larson et al., 1986). While quantifying the total leaf protein content, the addition of 1 µg of bovine serum albumin (Invitrogen, Carlsbad, CA, USA) in the extraction buffer was used as an internal standard.

Other Analyses

Leaf water status was determined by measuring the relative water content (RWC) of terminal leaflets. Five disks were taken from each terminal leaflet, and fresh weight (FW) was taken immediately. The leaf disks were then immersed in water overnight, and turgid weight (TW) was measured. Finally, leaf dry weight (DW) was determined following oven-drying of the leaf disks for 72 h at 70°C. RWC was calculated as RWC = (FW – DW)/(TW – DW). Total chlorophyll, Chl *a*, and chlorophyll *b* (Chl *b*) were determined according to the study of Arnon (1949) using leaf samples that had been snap-frozen in liquid N_2.

Statistical Analysis

The experiments were replicated three times. Thus, the data for all measurements and biochemical analyses were the averages of three replicates. The statistical analyses were performed using ANOVA in Prism 7.0 (GraphPad Software). Significant differences of the means between well-watered and drought-stressed plants within each cultivar were compared at the 5% significance level ($P \leq 0.05$).

RESULTS

Effects of Drought Stress on Tuber Yield and Number

The 56 potato genotypes, including 54 commercial cultivars grown under well-watered conditions for 5 weeks were subjected to water stress for 6 days followed by re-watering until the harvesting of the tubers. Under well-watered conditions, potato genotypes exhibited differences in tuber yield (data not shown). Drought stress significantly inhibited tuber yield in all genotypes; however, the reduction in tuber yield varied across the genotypes. **Table 1** shows the percentage of tuber yield and number for drought-stressed potato genotypes relative to their well-watered counterparts. Drought stress had minimal effects on tuber yield for Bannock Russet (85% of well-watered controls) and had a maximum for Dundord and F11007 (4% of well-watered controls) (**Table 1**). The drought-induced reduction in tuber yield was associated with decreases in total tuber number for the majority of the potato genotypes under drought (**Table 1**). However, the ability of the potato genotypes to maintain higher tuber yield under drought was not associated with its capacity to maintain more tubers (**Table 1**). To further examine the

TABLE 1 | Relative tuber yield and number for drought-stressed plants relative to their well-watered controls (%).

Potato lines	Relative yield (%)	Relative tuber number (%)	Potato lines	Relative yield (%)	Relative tuber number (%)	Potato lines	Relative yield (%)	Relative tuber number (%)
Bannock Russet	85 ± 6	53 ± 17	Kennebec	54 ± 13	39 ± 11	Snowden	36 ± 10	56 ± 8
Grand Falls	83 ± 11	75 ± 12	Denali	53 ± 17	90 ± 14	Bintje	34 ± 7	124 ± 13
Nipigon	79 ± 9	82 ± 23	Brigus	52 ± 8	86 ± 9	Prospect	31 ± 12	50 ± 9
Ivory Crisp	77 ± 11	91 ± 11	Defender	51 ± 6	79 ± 5	Banana	31 ± 16	27 ± 4
Atlantic	73 ± 14	121 ± 24	Norland	49 ± 11	82 ± 12	Eva	31 ± 5	67 ± 10
Jemseg	72 ± 9	60 ± 7	AC Red Island	48 ± 10	33 ± 8	Butte	29 ± 8	28 ± 5
Main Chip	72 ± 4	122 ± 13	Cupids	48 ± 14	104 ± 19	Norchip	29 ± 4	100 ± 7
Congo	71 ± 10	70 ± 14	Ranger Russet	46 ± 9	72 ± 6	Green Mountain	28 ± 7	57 ± 9
Blazer Russet	69 ± 15	44 ± 6	Genstar Russet	44 ± 6	127 ± 22	Shepody	27 ± 5	250 ± 38
F87084	68 ± 3	200 ± 21	Niska	43 ± 8	89 ± 14	Krantz	23 ± 9	67 ± 9
AAC Valley Crisp	68 ± 11	200 ± 33	Red Pontiac	43 ± 11	55 ± 13	Eramosa	22 ± 8	133 ± 14
Blue Mac	66 ± 5	67 ± 11	Belleisle	41 ± 4	73 ± 16	Russet Burbank	18 ± 5	18 ± 4
Glacier Fryer	64 ± 9	35 ± 4	Nooksack	41 ± 15	60 ± 4	Fundy	17 ± 4	61 ± 7
Desiree	63 ± 12	95 ± 6	AC Brador	40 ± 12	33 ± 6	AAC Canada Gold-Dorée	10 ± 9	39 ± 5
Exploits	62 ± 8	82 ± 13	Irish Cobbler	40 ± 9	86 ± 9	Russet Norkotah	9 ± 2	52 ± 8
Goldrush	62 ± 4	96 ± 12	Frontier Russet	39 ± 7	89 ± 3	Yukon Gold	9 ± 4	100 ± 13
AAC Confederation	60 ± 7	59 ± 8	CalWhite	38 ± 10	41 ± 7	Dundord	4 ± 1	44 ± 11
AC Novachip	59 ± 10	85 ± 4	Sangre	37 ± 13	43 ± 4	F11007	4 ± 2	31 ± 6
Onaway	56 ± 8	83 ± 9	Cascade	37 ± 11	100 ± 14			

Drought treatment was applied to some of the 5-week-old well-watered plants by withholding water for 6 days and rewatered for recovery thereafter. Tubers were harvested from both well-watered and drought-stressed plants of 56 genotypes at their maturity. The data represent the mean from three experiments ± SE.

physiological and biochemical regulations of potato drought tolerance, we chose six cultivars, namely, Bannock Russet, Nipigon, Onaway, Denali, Fundy, and Russet Norkotah, with distinct response to drought stress in terms of tuber yield (**Table 1**). Henceforth, we will only present the results observed for these six potato genotypes. The drought-induced reduction in tuber yield was only 15–20% for Bannock Russet and Nipigon, 44–47% for Onaway and Denali, and 83–91% for Fundy and Russet Norkotah (**Figure 1A**). Based on the differential capacity of these genotypes to maintain tuber yield under drought, we will hereafter use the terms "drought-tolerant genotypes" for Bannock Russet and Nipigon, "moderately tolerant genotypes" for Onaway and Denali, and "susceptible genotypes" for Fundy and Russet Norkotah. Drought significantly reduced the total tuber number in all genotypes irrespective of their capacity to maintain the differential tuber yield under drought (**Figure 1B**). To determine whether the differences in tuber yield across potato genotypes under drought stress were due to the differences in plant water content, we measured leaf RWC. Under well-watered conditions, we observed a comparable RWC of 80–87% in all genotypes (**Figure 2**). Drought decreased the RWC by about 25–35% in all potato genotypes, while the RWC under drought was similar in all genotypes. This suggested that the differences in tuber yield across potato genotypes under drought stress were not associated with the differences in RWC but rather associated with the differences in the physiological and biochemical phenomena.

Effects of Drought Stress on Rates of Photosynthesis and Fluorescence Parameters

Gas exchange rates and Chl *a* fluorescence were measured simultaneously to characterize the photosynthesis of the potato genotypes. Under well-watered conditions, the rates of photosynthesis (*A*) varied across the genotypes ranging from ∼12 to 20 μmol/m^2/s (**Table 2**). Drought stress substantially reduced *A* in all genotypes, such that *A* was ∼2.4–5.6 μmol/m^2/s among the genotypes under drought (**Table 2**). This precludes

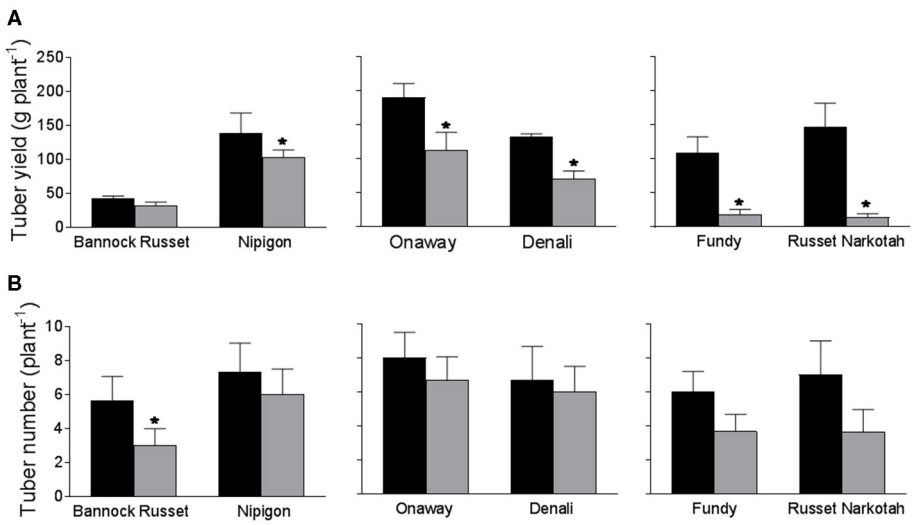

FIGURE 1 | Tuber yield **(A)** and tuber number **(B)** (per plant) of six potato genotypes grown under well-watered and drought conditions. Tubers were harvested from both well-watered and drought-stressed plants at their maturity. The data represent the averages of three experiments ± SE. Significant differences of the means between well-watered and drought-stressed plants within each cultivar are indicated by the symbol * ($P \leq 0.05$).

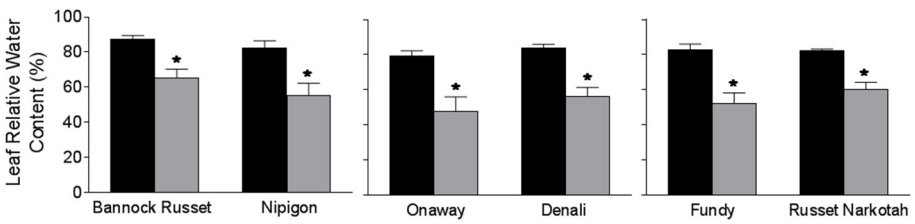

FIGURE 2 | Leaf relative water content (RWC) of six potato genotypes grown under well-watered and drought conditions. RWC was estimated on the fully expanded terminal leaflets of 5-week-old well-watered plants or drought-stressed plants (analyzed after 6 days of withholding watering). The data represent the averages of three experiments ± SE. Significant differences of the means between well-watered and drought-stressed plants within each cultivar are indicated by the symbol * ($P \leq 0.05$).

the previous notion that the ability of potato plants to tolerate drought and thus maintain tuber yield is associated with their capacity to maintain higher *A* under drought (Plich et al., 2020). *In vivo* Chl *a* fluorescence was monitored in combination with the CO_2 gas exchange to estimate (1) the maximum photochemical efficiency of PSII in the dark-adapted state (F_v/F_m), a measure of plant stress condition, (2) the photosynthetic ETRs through PSII, and (3) NPQ, the capacity to dissipate energy as heat. We observed minimal differences across genotypes in the maximum photochemical efficiency of PSII in the dark-adapted state (F_v/F_m) in well-watered plants (**Table 2**). Drought stress decreased F_v/F_m in all genotypes, but there were minimal differences across genotypes subject to drought (**Table 2**). The reduced F_v/F_m suggests that all plants were experiencing stress under drought. Minimal differences were noted across genotypes for ETR in either well-watered or drought-stressed plants, although the ETR was considerably lower by 45–65% in drought-stressed plants as compared with

TABLE 2 | Effects of drought stress on photosynthetic and fluorescence characteristics of six potato genotypes grown under well-watered and drought conditions.

Photosynthetic parameters	Water conditions	Bannock Russet	Nipigon	Onaway	Denali	Fundy	Russet Norkotah
A (μmol CO_2 m^{-2} s^{-1})	WW	20.08 ± 3.24	11.72 ± 2.09	17.83 ± 2.82	17.05 ± 3.14	15.32 ± 3.4	11.94 ± 0.54
	D	5.58* ± 1.10	5.39* ± 2.34	2.44* ± 0.20	4.74* ± 0.78	2.64* ± 0.35	3.92* ± 0.52
ETR (μmol e^- m^{-2} s^{-1})	WW	90 ± 12	67 ± 8	96 ± 6	96 ± 14	95 ± 8	81 ± 16
	D	43* ± 9	38* ± 4	37* ± 8	33* ± 7	50* ± 7	36* ± 2
NPQ	WW	0.39 ± 0.08	0.66 ± 0.14	0.30 ± 0.05	0.57 ± 0.02	0.39 ± 0.05	0.50 ± 0.07
	D	0.74* ± 0.12	0.81 ± 0.06	1.40* ± 0.09	0.89* ± 0.05	1.53* ± 0.11	1.15* ± 0.17
F_v/F_m	WW	0.74 ± 0.03	0.73 ± 0.06	0.76 ± 0.08	0.74 ± 0.02	0.76 ± 0.01	0.73 ± 0.06
	D	0.63* ± 0.02	0.68 ± 0.03	0.72 ± 0.01	0.62* ± 0.05	0.75 ± 0.08	0.63 ± 0.04
Total Chl (mg m^{-2})	WW	362 ± 33	497 ± 61	699 ± 68	510 ± 59	480 ± 30	232 ± 19
	D	296 ± 37	232* ± 12	194* ± 25	232* ± 16	287* ± 45	219 ± 27

*The measurements were performed on the fully expanded terminal leaflets of 5-week-old well-watered plants or drought-stressed plants (analyzed after 6 days of withholding watering). The data represent the mean from three experiments ± SE. Significant differences of the means between well-watered (WW) and drought-stressed (D) plants within each cultivar are indicated by the symbol * ($P \leq 0.05$). ETR, electron transport rate; NPQ, non-photochemical quenching.*

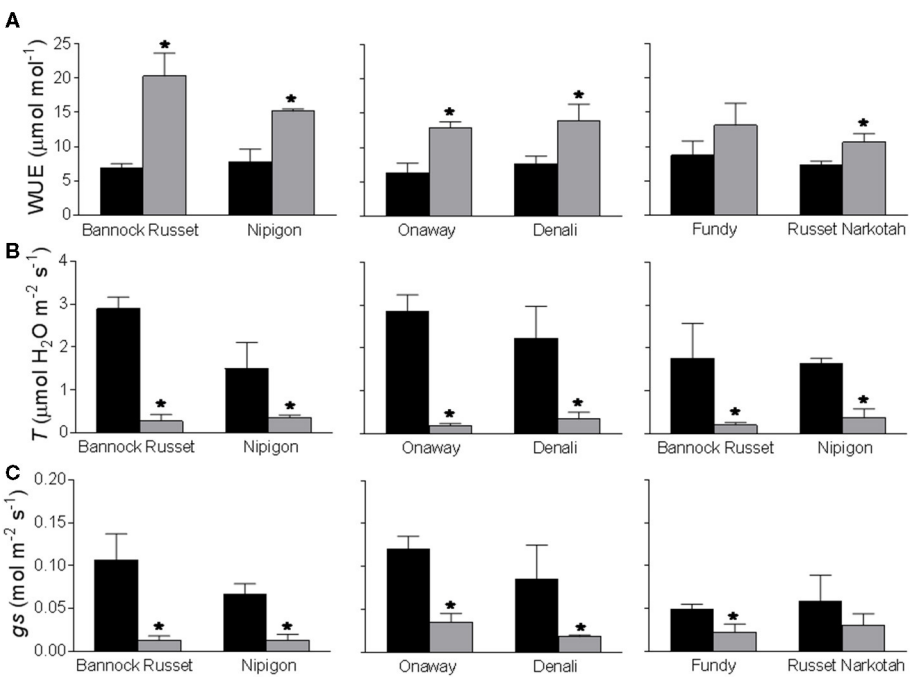

FIGURE 3 | Effects of drought stress on instantaneous water use efficiency **(A)**, transpiration rates **(B)**, and stomatal conductance **(C)** of six potato genotypes. The measurements were performed on the fully expanded terminal leaflets of 5-week-old well-watered plants or drought-stressed plants (analyzed after 6 days of withholding watering). The data represent the averages of three experiments ± SE. Significant differences of the means between well-watered and drought-stressed plants within each cultivar are indicated by the symbol * ($P \leq 0.05$).

their well-watered controls (**Table 2**). The NPQ varied across genotypes under well-watered conditions (**Table 2**). Drought stress substantially increased NPQ by 1.2–5-fold in all genotypes. The differences in NPQ across genotypes observed under well-watered conditions were further magnified under drought (**Table 2**).

Effects of Drought Stress on Instantaneous Water-Use Efficiency, Transpiration, and Stomatal Conductance (g_s)

All six genotypes exhibited comparable instantaneous WUE of 6.2–8.7 μmol/mol under well-watered conditions (**Figure 3A**). Drought stress differentially stimulated WUE in all genotypes. The tolerant genotypes, Bannock Russet and Nipigon, exhibited about a 2–3-fold increase in WUE under drought conditions as compared with well-watered controls (**Figure 3A**). This stimulation was about 1.8–2-fold for moderately tolerant genotypes, Onaway and Denali, and only 1.5-fold for sensitive genotypes, Fundy and Russet Norkotah, when compared with their well-watered controls (**Figure 3A**). The differential stimulation of instantaneous WUE of tolerant and moderately tolerant genotypes vs. sensitive genotypes was associated with the differential suppression of the rates of transpiration (**Figure 3B**) and photosynthesis (**Table 2**) across these genotypes. The rates of transpiration are determined by stomatal aperture size, stomatal density, and opening and closing of stomatal pores, known as stomatal conductance (g_s). In this study, we measured only the stomatal conductance. Drought stress significantly suppressed stomatal conductance in all genotypes (**Figure 3C**). However, this reduction varied across genotypes such that drought-induced reduction in g_s was about 80–90% for tolerant genotypes, Bannock Russet and Nipigon, 70–80% for moderately tolerant genotypes, Onaway and Denali, and 50% for sensitive genotypes, Fundy and Russet Norkotah, when compared with their well-watered controls (**Figure 3C**).

Effects of Drought Stress on Leaf Protein and Chlorophyll Content

When measured on a leaf area basis, we observed a comparable leaf protein content of 12–18 g/m^2 leaf area in all six genotypes tested when grown under well-watered conditions (**Figure 4**). Drought-stressed Bannock Russet and Nipigon exhibited about a 25% increase in total leaf protein content whereas Onaway and Denali exhibited about a 15% increase in the total leaf protein content when compared with their well-watered controls (**Figure 4**). In contrast, drought-stressed Fundy and Russet Norkotah exhibited about a 25% reduction in total leaf protein content relative to their well-watered controls (**Figure 4**). The different stimulation of leaf protein content under drought stress would further magnify when corrected on a chlorophyll basis in tolerant and moderately tolerant genotypes (data not shown). For instance, the protein/chlorophyll ratio (protein/Chl) increased by 2–4-fold for tolerant and moderately tolerant genotypes under drought conditions as compared with their well-watered controls (**Table 2**). However, there was a minimal change in the protein/Chl ratio for sensitive genotypes under drought vs. well-watered conditions (**Table 2**).

DISCUSSION

Plants experience drought stress when they receive insufficient water than their actual demand. The effects of drought stress may range from disruption in the molecular and biochemical functions at the cellular level to the physiological and morphological functions at the leaf and whole plant levels (Shinozaki and Yamaguchi-Shinozaki, 2007). Potato plants use several strategies at the physiological, biochemical, and molecular levels to combat drought stress (Boguszewska-Mańkowska et al., 2018; Dahal et al., 2019). These strategies enable plants either to maintain water potential by escaping the drought or to develop the adaptation mechanisms to tolerate lower water potential.

In this study, we used 56 potato genotypes including commercial cultivars to assess their tolerance to drought stress. Based on their capacity to maintain tuber yield under drought, potato genotypes differed in their ability to tolerate drought stress (**Table 1**). To further examine the drought tolerance mechanisms, we selected six genotypes, namely, Bannock Russet, Nipigon, Onaway, Denali, Fundy, and Russet Norkotah, with diverse response to drought tolerance based on tuber yield (**Table 1**, **Figure 1A**). We measured leaf RWC to determine whether the ability of plants to maintain tuber yield under drought is governed either by drought avoidance or by adaptation mechanism

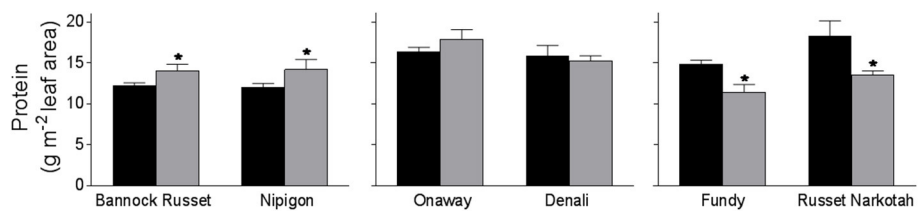

FIGURE 4 | Leaf protein content of six potato genotypes grown under well-watered and drought conditions. Leaf protein content was estimated on the fully expanded terminal leaflets of 5-week-old well-watered plants or drought-stressed plants (analyzed after 6 days of withholding watering). The data represent the averages of three experiments ± SE. Significant differences of the means between well-watered and drought-stressed plants within each cultivar are indicated by the symbol * ($P \leq 0.05$).

to tolerate lower water potential. The comparable leaf RWC across genotypes under drought stress (**Figure 2**) suggests that the ability of the potato genotypes Bannock Russet and Nipigon to tolerate drought was not associated with drought avoidance but rather associated with the physiological and biochemical tolerance mechanisms to lower water potential.

One of the important physiological strategies used by plants to survive drought stress is the improvement in WUE (Liu et al., 2005; Coleman, 2008; Albiski et al., 2012; Ierna and Mauromicale, 2020; Kassaye et al., 2020). The tolerant genotypes, Bannock Russet and Nipigon, exhibited a substantial increase in instantaneous WUE than did moderately tolerant genotypes, Onaway and Denali, and the sensitive genotypes, Fundy and Russet Norkotah, under drought (**Figure 3A**). Consistent with previous findings, our study revealed that the capacity of potato genotypes to enhance WUE under drought stress is reflected in their ability to tolerate drought stress. The differential stimulation of instantaneous WUE of tolerant and moderately tolerant genotypes vs. sensitive genotypes was accounted for by the differential suppression of stomatal conductance and concomitantly transpiration rates across genotypes (**Figures 3B,C**). Another strategy that plants employ following drought stress is a considerable increase in the drought-related proteins (Shinozaki and Yamaguchi-Shinozaki, 2007). Drought induces the expression of numerous stress-related genes that encode proteins including transcription factors and enzymes involved in drought stress tolerance (Shinozaki and Yamaguchi-Shinozaki, 2007). For instance, the ability of potato plants to tolerate drought stress is believed to be governed by upregulation of DREB1A regulons (Movahedi et al., 2012, Pino et al., 2013). In this study, the tolerant genotypes, Bannock Russet and Nipigon, exhibited a considerable increase in leaf proteins relative to moderately tolerant and susceptible genotypes following drought stress (**Figure 4**). The differential stimulation of leaf protein content under drought stress will further magnify when corrected on a chlorophyll basis in tolerant and moderately tolerant genotypes. Future study needs to be focused on the identification of proteins that are upregulated following drought treatment to advance our understanding of molecular mechanisms governing drought tolerance.

Photosynthesis converts CO_2 to carbohydrates in the presence of light energy and with the help of photosynthetic pigments, mainly chlorophylls. The carbohydrate is then translocated to the stolons for tuber initiation and growth. Hence, an enhancement in tuber yield can be expected through the stimulation of photosynthetic carbon fixation and their translocation to stolon. In this study, the drought-induced reduction in tuber yield was mainly related to the strong perturbation of photosynthesis (**Table 2**). However, the reduction in the rates of photosynthesis was similar in all genotypes, regardless of their differential tolerance ability to drought. Therefore, unlike previous findings (Plich et al., 2020), our current study suggests that the ability of the potato genotypes, Bannock Russet and Nipigon, to tolerate drought stress is not associated with the maintenance of photosynthesis under drought as compared with sensitive genotypes. Future research needs to confirm whether the differential ability of potato genotypes to maintain tuber yield under drought is due to the differences in the carbohydrate translocation to the stolon. The reduced F_v/F_m following drought stress indicates that all plants were experiencing stress under drought, which was also mirrored by decreased photosynthesis (**Table 2**). Consequently, all potato genotypes dissipated energy, excess of that used by photosynthesis, through enhanced NPQ under drought (**Table 2**). The precise mechanism that activates NPQ under drought is the area of further research.

The production of potatoes is constrained by frequent and severe drought episodes (Obidiegwu et al., 2015). Improving the productivity of potatoes under such suboptimal growth conditions is important to achieve the nutritional demand of an increasing population. Understanding the stress-related physiological, biochemical, and molecular processes is crucial to develop the screening procedures for selecting potato cultivars that can better adapt to drought. The elucidation of such processes may offer new insights into the identification of specific characteristics that may be useful in breeding new cultivars aimed at maintaining or even enhancing potato yield under the changing climate. Our current study has revealed that leaf protein content, instantaneous WUE, stomatal conductance, and transpiration rates can be used as the screening criteria for selecting the drought-tolerant potato genotypes. We suggest that future research needs to be concentrated on the identification and characterization of signaling molecules and target genes governing drought tolerance and tuber yield potential.

DATA AVAILABILITY STATEMENT

The raw data supporting the conclusions of this article will be made available by the authors, without undue reservation.

AUTHOR CONTRIBUTIONS

KD planned the research and wrote the manuscript. KD and TG planned and designed the experiments. TG and AC conducted the experiments and performed measurements and laboratory analyses. KD and TG analyzed the data. TG, X-QL, BB, and DD revised the manuscript. All authors contributed to the article and approved the submitted version.

ACKNOWLEDGMENTS

KD acknowledges the financial support from the Agriculture and Agri-Food Canada, Government of Canada. The authors also acknowledge John Gillan, Scott Anderson, Margaret McLaughlin, and Ryan Forbes for their assistance in growing and watering plants in the greenhouse.

REFERENCES

Albiski, F., Najla, S., Sanoubar, R., Alkabani, N., and Murshed, R. (2012). *In vitro* screening of potato lines for drought tolerance. *Physiol. Mol. Biol. Plants* 18, 315–321. doi: 10.1007/s12298-012-0127-5

Aliche, E. B., Oortwijn, M., Theeuwen,. T. P. J. M., Bachem, C. W. B., Visser, R. G. F., and van der Linden, C. G. (2018). Drought response in field grown potatoes and the interactions between canopy growth and yield. *Agric. Wat. Man.* 206, 20–30. doi: 10.1016/j.agwat.2018.04.013

Aliche, E. B., Theeuwen, T. P. J. M., Oortwijn, M., Visser, R. G. F., and van der Linden, C. G. (2020). Carbon partitioning mechanisms in potato under drought stress. *Plant Physiol. Biochem.* 146, 211–219. doi: 10.1016/j.plaphy.2019.11.019

Arnon, D.I. (1949). Copper enzymes in isolated chloroplasts: polyphenoloxidases in *Beta vulgaris*. *Plant Physiol.* 24, 1–15. doi: 10.1104/pp.24.1.1

Baker, N.R., Harbinson, J., and Kramer, D.M. (2007). Determining the limitations and regulation of photosynthetic energy transduction in leaves. *Plant Cell Environ.* 30, 1107–1125. doi: 10.1111/j.1365–3040.2007.01680.x

Banik, P., Zeng, W., Tai, H., Bizimungu, B., and Tanino, K. (2016). Effects of drought acclimation on drought stress resistance in potato (*Solanum tuberosum* L.) genotypes. *Environ. Exp. Bot.* 126, 76–89. doi: 10.1016/j.envexpbot.2016.01.008

Beals, K. A. (2019). Potatoes, nutrition and health. *Am. J. Potato Res.* 96, 102–110. doi: 10.1007/s12230-018-09705-4

Birch, P. R. J., Bryan, G., Fenton, B., Gilroy, E., Hein, I., Jones, J. T., et al. (2012). Crops that feed the world. potato: are the trends of increased global production sustainable? *Food Sec.* 4, 477–508. doi: 10.1007/s12571-012-0220-1

Boguszewska-Mańkowska, D., Pieczyński, M., Wyrzykowska, A., Kalaji, H. M., Sieczko, L., Szweykowska-Kulińska, Z., et al. (2018). Divergent strategies displayed by potato (*Solanum tuberosum* L.) cultivars to cope with soil drought. *J. Agron. Crop Sci.* 204, 13–30. doi: 10.1111/jac.12245

Boguszewska-Mańkowska, D., Zarzyńska, K., and Nosalewicz, A. (2020). Drought differentially affects root system size and architecture of potato cultivars with differing drought tolerance. *Am. J. Pot. Res.* 97, 54–62. doi: 10.1007/s12230-019-09755-2

Chen, T., and Murata, N. (2008). Glycinebetaine: an effective protectant against abiotic stress in plants. *Trends Plant Sci.* 13, 499–505. doi: 10.1016/j.tplants.2008.06.007

Coleman, W. K. (2008). Evaluation of wild *Solanum* species for drought resistance: 1. *Solanum gandarillasii* Cardenas. *Environ. Exp. Bot.* 62, 221–230. doi: 10.1016/j.envexpbot.2007.08.007

Cutler, S. R., Rodriguez, P. L., Finkelstein, R. R., and Abrams, S. R. (2010). Abscisic acid: emergence of a core signaling network. *Annu. Rev. Plant Biol.* 61, 651–679. doi: 10.1146/annurev-arplant-042809-112122

Dahal, K., Li, X. Q., Tai, H., Creelman, A., and Bizimungu, B. (2019). Improving potato stress tolerance and tuber yield underclimate change scenario – a current overview. *Front. Plant Sci.* 10:563. doi: 10.3389/fpls.2019.00563

Dahal, K., Martyn, G. D., and Vanlerberghe, G. C. (2015). Improved photosynthetic performance during severe drought in *Nicotiana tabacum* overexpressing a non-energy conserving respiratory electron sink. *New Phytol.* 208, 382–395. doi: 10.1111/nph.13479

Dahal, K., and Vanlerberghe, G. C. (2017). Alternative oxidase respiration maintains both mitochondrial and chloroplast function during drought. *New Phytol.* 213, 560–571. doi: 10.1111/nph.14169

Dahal, K., Wang, J., Martyn, G., Rahimy, F., and Vanlerberghe, G. C. (2014). Mitochondrial alternative oxidase maintains respiration and preserves photosynthetic capacity during moderate drought in *Nicotiana tabacum*. *Plant Physiol.* 166, 1560–1574. doi: 10.1104/pp.114.247866

Eiasu, B. K., Soundy, P., and Hammes, P. S. (2007). Response of potato (*Solanum tuberosum*) tuber yield components to gelpolymer soil amendments and irrigation regimes. *N. Z. J. Crop Hort.* 35, 25–31. doi: 10.1080/01140670709510164

Evers, D., Lefèvre, I., Legay, S., Lamoureux, D., Hausman, J. F., Rosales, R. O., et al. (2010). Identification of drought-responsive compounds in potato through a combined transcriptomic and targeted metabolite approach. *J. Exp. Bot.* 61, 2327–2343. doi: 10.1093/jxb/erq060

FAOSTAT (2019). Available online at: http://www.fao.org/faostat/en/#data/QC (accessed July 07, 2021).

Hill, D., Nelson, D., Hammond, J., and Bell, L. (2021). Morphophysiology of potato (*Solanum tuberosum*) in response to drought stress: paving the way forward. *Front. Plant Sci.* 15:675690. doi: 10.3389/fpls.2021.675690

Ierna, A., and Mauromicale, G. (2020). How moderate water stress can affect water use efficiency indices in potato. *Agronomy* 10:1034. doi: 10.3390/agronomy10071034

Kassaye, K. T., Yilma, W. A., Fisha, M. H., and Haile, D. H. (2020). Yield and water use efficiency of potato under alternate furrows and deficit irrigation. *Int. J. Agron.* 2020:8869098. doi: 10.1155/2020/8869098

Kasuga, M., Liu, Q., and Miura, S. (1999). Improving plant drought, salt, and freezing tolerance by gene transfer of a single stress-inducible transcription factor. *Nat. Biotech.* 17, 287–291. doi: 10.1038/7036

Kudo, M., Kidokoro, S., Yoshida, T., Mizoi, J., Todaka, D., Fernie, A. R., et al. (2017). Double overexpression of DREB and PIF transcription factors improves drought stress tolerance and cell elongation in transgenic plants. *Plant Biotech. J.* 15, 458–471. doi: 10.1111/pbi.12644

Larson, E., Howlett, B., and Jagendorf, A. (1986). Artificial reductant enhancement of the Lowry method for protein determination. *Anal. Biochem.* 155, 243–248. doi: 10.1016/0003-2697(86)90432-X

Lawlor, D. W., and Tezara, W. (2009). Causes of decreased photosynthetic rate and metabolic capacity in water-deficient leaf cells: a critical evaluation of mechanisms and integration of processes. *Ann. Bot.* 103, 561–579. doi: 10.1093/aob/mcn244

Liu, F., Jensen, C. R., Shahanzari, A., Andersen, M. N., and Jacobsen, S. E. (2005). ABA regulated stomatal control and photosynthetic water use efficiency of potato (Solanum tuberosum L.) during progressive soil drying. *Plant Sci.* 168, 831–836. doi: 10.1016/j.plantsci.2004.10.016

Maxwell, K., and Johnson, G. N. (2000). Chlorophyll fluorescence: a practical guide. *J. Exp. Bot.* 51, 659–668. doi: 10.1093/jexbot/51.345.659

Movahedi, S., Sayed Tabatabaei, B. E., and Alizade, H. (2012). Constitutive expression of *Arabidopsis DREB1B* in transgenic potato enhances drought and freezing tolerance. *Biol. Plant* 56, 37–42. doi: 10.1007/s10535-012-0013-6

Obidiegwu, J., Bryan, G., Jones, G., and Prashar, A. (2015). Coping with drought: stress and adaptive responses in potato and perspectives for improvement. *Front. Plant Sci.* 6:542. doi: 10.3389/fpls.2015.00542

Pinheiro, C., and Chaves, M. M. (2011). Photosynthesis and drought: can we make metabolic connections from available data? *J. Exp. Bot.* 60, 869–882. doi: 10.1093/jxb/erq340

Pino, M. T., Avila, A., Molina, A., Jeknic, Z., and Chen, T. H. H. (2013). Enhanced *in vitro* drought tolerance of *Solanum tuberosum* and *Solanum commersonii* plants overexpressing the ScCBF1 gene. *Cienc. Investig. Agrar.* 40, 171–184. doi: 10.4067/S0718-16202013000100015

Plich, J., Boguszewska-Mańkowska, D., and Marczewski, W. (2020). Relations between photosynthetic parameters and drought-induced tuber yield decrease in Katahdin-derived potato cultivars. *Pot. Res.* 63, 463–477. doi: 10.1007/s11540-020-09451-3

Rontein, D., Basset, G., and Hanson, A. (2002). Metabolic engineering of osmoprotectant accumulation in plants. *Metab. Eng.* 4, 49–56. doi: 10.1006/mben.2001.0208

Shinozaki, K., and Yamaguchi-Shinozaki, K. (2007). Gene networks involved in drought stress response and tolerance. *J. Exp. Bot.* 58, 221–227. doi: 10.1093/jxb/erl164

Sprenger, H., Kurowsky, C., Horn, R., Erban, A., Seddig, S., Rudack, K., et al. (2016). The drought response of potato reference cultivars with contrasting tolerance. *Plant Cell Environ.* 39, 2370–2389. doi: 10.1111/pce.12780

Stark, J. C., Love, S. L., King, B. A., Marshall, J. M., Bohl, W. H., and Salaiz, T. (2013). Potato cultivar response to seasonal drought patterns. *Am. J. Potato Res.* 90, 207–216. doi: 10.1007/s12230-012-9285-9

Takahashi, F., Kuromori, T., Sato, H., and Shinozaki, K. (2018). Regulatory gene networks in drought stress responses and resistance in plants. *Adv. Exp. Med. Biol.* 1081, 189–214. doi: 10.1007/978-981-13-1244-1_11

Vasquez-Robinet, C., Mane, S. P., Ulanov, A. V., Watkinson, J. I., Stromberg, V. K., De Koeyer, D., et al. (2008). Physiological and molecular adaptations to drought in Andean potato genotypes. *J. Exp. Bot.* 59, 2109–2123. doi: 10.1093/jxb/ern073

Villordon, A. Q., Ginzberg, I., and Firon, N. (2014). Root architecture and root tuber crop productivity. *Trends Plant Sci.* 19, 419–425. doi: 10.1016/j.tplants.2014.02.002

Watanabe, K. N., Kikuchi, A., Shimazaki, T., and Asahina, M. (2011). Salt and drought stress tolerances in transgenic potatoes and wild species. *Potato Res.* 54, 319–324. doi: 10.1007/s11540-011-9198-x

Wishart, J., George, T. S., Brown, L. K., Ramsay, G., Bradshaw, J. E., White, P. J., et al. (2013). Measuring variation in potato roots in both field and glasshouse: the search for useful yield predictors and a simple screen for root traits. *Plant Soil* 368, 231–249. doi: 10.1007/s11104-012-1483-1

Yao, L., Cheng, X., Gu, Z., Huang, W., Li, S., Wang, L., et al. (2018). The AWPM-19 family protein OsPM1 mediates abscisic acid influx and drought response in rice. *The Plant Cell.* 30, 1258–1276. doi: 10.1105/tpc.17.00770

Zarzynska, K., Boguszewska-Mankowska, D., and Nosalewicz, A. (2017). Differences in size and architecture of the potato cultivars root system and their tolerance to drought stress. *Plant Soil Environ.* 63, 159–164. doi: 10.17221/4/2017-PSE

Zhang, N., Si, H., Wen, G., Du, H., Liu, B., and Wang, D. (2011). Enhanced drought and salinity tolerance in transgenic potato plants with a BADH gene from spinach. *Plant Biotechnol. Rep.* 5, 71–77. doi: 10.1007/s11816-010-0160-1

Conflict of Interest: The authors declare that the research was conducted in the absence of any commercial or financial relationships that could be construed as a potential conflict of interest.

Publisher's Note: All claims expressed in this article are solely those of the authors and do not necessarily represent those of their affiliated organizations, or those of the publisher, the editors and the reviewers. Any product that may be evaluated in this article, or claim that may be made by its manufacturer, is not guaranteed or endorsed by the publisher.

frontiers in Plant Science

ORIGINAL RESEARCH
published: 12 August 2021
doi: 10.3389/fpls.2021.716114

Quantitative Proteomics and Relative Enzymatic Activities Reveal Different Mechanisms in Two Peanut Cultivars (*Arachis hypogaea* L.) Under Waterlogging Conditions

Dengwang Liu[1,2,3], Jian Zhan[1], Zinan Luo[1,2,3], Ningbo Zeng[1,2,3], Wei Zhang[4], Hao Zhang[1,2,3]* and Lin Li[1,2,3]**

[1]College of Agriculture, Hunan Agricultural University, Changsha, China, [2]Hunan Peanut Engineering and Technology Research Center, Hunan Agricultural University, Changsha, China, [3]National Peanut Engineering and Technology Research Center, Hunan Agricultural University, Changsha, China, [4]College of Plant Protection, Hunan Agricultural University, Changsha, China

OPEN ACCESS

Edited by:
Thorsten M. Knipfer, University of British Columbia, Canada

Reviewed by:
Guido Domingo, University of Insubria, Italy
Hadi Pirasteh-Anosheh, Agricultural Research Education and Extention Organization, Iran

***Correspondence:**
Wei Zhang
349187910@qq.com
Hao Zhang
Zhangzhanghaodsm@126.com
Lin Li
lilindw@163.com

Specialty section:
This article was submitted to Crop and Product Physiology, a section of the journal Frontiers in Plant Science

Received: *10 June 2021*
Accepted: *13 July 2021*
Published: *12 August 2021*

Citation:
Liu D, Zhan J, Luo Z, Zeng N, Zhang W, Zhang H and Li L (2021) Quantitative Proteomics and Relative Enzymatic Activities Reveal Different Mechanisms in Two Peanut Cultivars (Arachis hypogaea L.) Under Waterlogging Conditions. Front. Plant Sci. 12:716114. doi: 10.3389/fpls.2021.716114

Peanut is an important oil and economic crop in China. The rainy season (April–June) in the downstream Yangtze River in China always leads to waterlogging, which seriously affects plant growth and development. Therefore, understanding the metabolic mechanisms under waterlogging stress is important for future waterlogging tolerance breeding in peanut. In this study, waterlogging treatment was carried out in two different peanut cultivars [Zhonghua 4 (ZH4) and Xianghua08 (XH08)] with different waterlogging tolerance. The data-independent acquisition (DIA) technique was used to quantitatively identify the differentially accumulated proteins (DAPs) between two different cultivars. Meanwhile, the functions of DAPs were predicted, and the interactions between the hub DAPs were analyzed. As a result, a total of 6,441 DAPs were identified in ZH4 and its control, of which 49 and 88 DAPs were upregulated and downregulated under waterlogging stress, respectively, while in XH08, a total of 6,285 DAPs were identified, including 123 upregulated and 114 downregulated proteins, respectively. The hub DAPs unique to the waterlogging-tolerant cultivar XH08 were related to malate metabolism and synthesis, and the utilization of the glyoxylic acid cycle, such as L-lactate dehydrogenase, NAD^+-dependent malic enzyme, aspartate aminotransferase, and glutamate dehydrogenase. In agreement with the DIA results, the alcohol dehydrogenase and malate dehydrogenase activities in XH08 were more active than ZH4 under waterlogging stress, and lactate dehydrogenase activity in XH08 was prolonged, suggesting that XH08 could better tolerate waterlogging stress by using various carbon sources to obtain energy, such as enhancing the activity of anaerobic respiration enzymes, catalyzing malate metabolism and the glyoxylic acid cycle, and thus alleviating the accumulation of toxic substances. This study provides insight into the mechanisms in response to waterlogging stress in peanuts and lays a foundation for future molecular breeding targeting in the improvement of peanut waterlogging tolerance, especially in rainy area, and will enhance the sustainable development in the entire peanut industry.

Keywords: data-independent acquisition, malate metabolism, data-dependent acquisition, differentially accumulated proteins, protein-protein interaction, anaerobic respiration enzymes

INTRODUCTION

Excessive water in the soil will reduce the rate of gas exchange between the soil and the atmosphere, thus affecting plant growth and development (Andrade et al., 2018; Garcia et al., 2020). Under waterlogging conditions, the oxygen level continues to decrease, but CO_2, H_2S, CH_4, and ethylene continue to accumulate (Kögel-Knabner et al., 2010), which seriously breaks the gas balance and causes a hypoxic or even anoxic environment, reducing the soil reduction potential and affecting the conversion of mineral elements (Ghashghaie et al., 2015). For example, an anoxic environment inhibits aerobic nitrification and nitrifying bacterial activity, resulting in the reduction of nitrate to N_2 and nutrient loss (Walker et al., 2018). In addition, sulfate is easily reduced to H_2S under waterlogging condition, reducing the absorption of sulfur by plants and causing toxicity to plants (Pezeshki and DeLaune, 2012). Waterlogging also reduces oxidized compounds, such as Fe^{2+} and Mn^{4+}, raising up the concentration level of Fe and Mn beyond the nutritional requirements in plants (Khabaz-Saberi et al., 2006; Khabaz-Saberi and Rengel, 2010).

The plant morphology will also be adversely affected under waterlogging stress. The anoxic environment usually decreases leaf resistivity, increases cell electrolyte leakage, and destroys the filtering function of cell membrane. In addition, the chlorophyll level and its synthetic rate were reduced, leading to leaf yellowing and wilting, accelerating the leaf shedding rate, promoting leaf senescence, and hindering the formation of new leaves (Zheng et al., 2009). Waterlogging stress also inhibits root growth, reduces root hair, and decays root tips (Xuewen et al., 2014). In order to adapt to this condition, adventitious roots were formed in large quantities and became the main components of the root system under waterlogging stress, thus expanding the absorption area of plants, improving the absorption and transportation of oxygen, and therefore giving the cells a higher mitotic ability and physiological activity (Zou et al., 2010). Another adaptation in plants under waterlogging stress is to facilitate the accumulation of ethylene concentration (Kim et al., 2018; Zhao et al., 2018), which leads to an increase in cellulase activity, thus resulting in the separation and collapse of root tip cortical cells and the formation of aerenchyma (a gas channel composed of specific cells that can transport oxygen to the root system and alleviate the pressure of oxygen deficiency) (Wang et al., 2016). This adaptation strategy helps maintain the normal physiological metabolism of root cells.

Waterlogging also affects metabolic processes, such as photosynthesis in plants. Under waterlogging stress, the photosynthetic rate in waterlogging-tolerant plants did not change too much, while it dropped rapidly in waterlogging-sensitive plants (Zeng et al., 2020). In addition, waterlogging stress leads to oxygen shortage, which will trigger anaerobic respiration to provide cell energy (da Silva and do Amarante, 2020). Anaerobic respiration usually includes two fermentation pathways: lactic acid and ethanol fermentation. Thus, the enzymes involved in these fermentation pathways, such as lactate dehydrogenase (LDH) and alcohol dehydrogenase (ADH), are changed accordingly as indicators. For example, ADH and LDH will be activated to provide plants with ATP to improve the ability of plants to cope with waterlogging stress (Dennis et al., 2000; Xu et al., 2016).

Most previous studies mainly focused on the effects of waterlogging stress on plant morphology, physiology, dry matter accumulation and distribution, crop yield, and quality characteristics. Few studies have been conducted to unveil the molecular mechanisms under waterlogging stress in peanut. We therefore undertook a quantitative proteomics study to provide a comprehensive understanding of peanut roots in response to waterlogging stress. A number of techniques and strategies can be used for quantitative proteomics study, among which isotopic labeling (e.g., iTRAQ, SILAC, or TMT) and label-free methods are the two techniques with highest popularity (Jylhä et al., 2018). The isotopic labeling strategy relies on binding-specific isobaric labels to peptides for relative quantification of proteins, but it limits the number of different experimental groups (usually only 4–8 samples; Ross et al., 2004; Choe et al., 2012). Data-dependent acquisition (DDA) is often used in iTRAQ, which cannot be applied to large-scale trials due to high cost, setup complexity, and incomplete selection of peptides (Jylhä et al., 2018). However, the sequential windowed acquisition of all theoretical fragment ion mass spectra (SWATH) is a data-independent acquisition (DIA) technique that can overcome this difficulty. SWATH is label-free and not limited to the number of experimental groups, allowing for flexible comparisons and potential savings (Gillet et al., 2012). In addition, SWATH obtains ion spectra containing all the fragments from all the precursor ions within the predefined mass-to-charge (m/z) range (Gillet et al., 2012). The independent datasets obtained from DIA can be re-examined if the library used in the downstream analyses is updated (Jylhä et al., 2018).

In the current study, DIA technique is used to quantitatively analyze the differentially accumulated proteins (DAPs) between two peanut cultivars with different waterlogging tolerance: Xianghua08 (XH08, waterlogging-tolerant) and Zhonghua 4 (ZH4, waterlogging-sensitive). In addition, the effects of waterlogging stress on the relative respiratory enzymes and root morphology were observed and compared between two cultivars. This study provided a theoretical basis for future waterlogging tolerance breeding in peanut and will be of great significance for the sustainable development of the peanut industry.

MATERIALS AND METHODS

Plant Materials and Waterlogging Treatment

The tested peanut cultivars, including waterlogging-sensitive cultivar ZH4 and the waterlogging-tolerant cultivar XH08, were bred by the Arid Land Crops Research Institute of Hunan Agricultural University (Changsha, Hunan). Stainless steel brackets filled with clean fine quartz sand were placed in the PVC basins with a diameter of 20 cm and height of 3 cm, and one seed was sown in each basin in 3 cm depth, with each cultivar replicating three times. When the seedlings germinated to the stage of four leaves and one heart, the flooding treatment was carried out to maintain a flooding depth of 1 cm for different duration time (3, 6, 9, 12, and 15 days). The control group was irrigated normally. The light and dark conditions were alternated with 14-h daylight time and 10-h dark conditions. The temperature was set to 25°C (daylight) and 20°C (night), respectively.

Plant Root Microscopy and Determination of Enzymatic Activities

After waterlogging treatment, paraffin sections of main roots of two cultivars and their controls were made, and the microstructure of the root tissue was observed. The taproots of peanut cultivars (ZH4 and XH08) and their controls were collected for the determination of LDH, ADH, and malate dehydrogenase (MDH) activities as follows: 0.1 g taproot samples of waterlogging-treated cultivars and their control samples were weighed after 12 days and 15 days of waterlogging treatment with each group replicating three times. The supernatants were homogenized on an ice bath with 1 ml of 0.1 M PBS buffer, followed by centrifugation under 4°C at 15,000 rpm for 20 min. The wavelength of the ultraviolet spectrophotometer was set to 340 nm (zero adjustment of ultrapure water). The activities of LDH, ADH, and MDH in peanut taproots were determined using the LDH assay kit (A020-1), the ADH assay kit (A083-2-1), and the MDH assay kit (A021-2-1; Nanjing Jiancheng Bioengineering Research Institute) following the manufacturer's instructions. Exploring changes in enzymatic activities aimed to determine the time point at which the root samples would be collected for the following quantitative proteomics analyses. The collected root samples were immediately frozen in −80°C for further use.

Protein Extraction and Digestion

Proteomic sequencing was performed by the Beijing Genome Institute (Shenzhen, China). The collected peanut roots were first ground using 5-mm magnetic beads, and proteins were extracted using lysis buffer 3 (10 mm Tris–HCl, pH 8.0, 100 mm NaCl, 1 mm EDTA, 0.5 mm EGTA, 0.1% sodium deoxycholate, and 0.5% sodium N-lauroyl sarcosine), with PMSF (protease inhibitor), EDTA, and dithiothreitol (DTT) added to a final concentration of 1 mm, 2 mm, and 10 mm, respectively. The mixture was ground using a tissue grinder for 2 min (power = 50 Hz, time = 120 s), followed by centrifugation at 25,000 g under 4°C for 20 min. After the removal of the supernatant, 10 mm DTT was added, and the mixture was heated at 56°C for 1 h. Iodoacetamide (55 mm) was then added to the mixture and incubated in the dark for 45 min. The protein was precipitated with four volumes of cold acetone for 2 h at −20°C. This step was repeated 2–3 times until the supernatant turned to be transparent. After centrifugation at 25,000 g under 4°C for 20 min, the precipitation was redissolved in lysis buffer 3 and ground using tissue grinder for 2 min (power = 50 Hz, time = 120 s), followed by centrifugation at 25,000 g under 4°C for 20 min. The supernatant was retained for protein quantification using the Bradford method (Kruger, 2009), and the extracted proteins were separated using SDS-PAGE. After electrophoresis, the solution was stained in Coomassie Brilliant Blue for 2 h, followed by decolorization using the decolorizing solution (40% ethanol and 10% acetic acid) for 3–5 times.

Each protein sample (~100 μg protein) was digested twice using trypsin at a 1:40 trypsin-to-protein ratio at 37°C for 4 h, followed by another round at 37°C for 8 h. After trypsin digestion, the peptides were desalted using a Strata-X column (Phenomenex, Los Angeles, United States) and vacuum dried.

HPLC Fractionation and LC MS/MS Under Both DDA and DIA Modes

The peptide samples were fractionated using high-pH reversed-phase high-performance liquid chromatography by using the Gemini C18 column (5 μm, 4.6 mm × 250 mm). Briefly, peptides were first separated with a gradient of 5 to 95% acetonitrile (pH 9.8) over 60 min. Next, they were combined into 10 fractions and freeze-dried by vacuum centrifugation. The dried peptide samples were redissolved with mobile phase A (2% ACN, 0.1% FA) and centrifuged at 20,000 g for 10 min, and the supernatant was retained for MS analysis. LC–MS/MS was carried out in the ultimate 3,000 UHPLC (Thermo scientific, United States). The sample was first enriched and desalted using a trap column and then connected to a self-contained C18 column (150 μm inner diameter, 1.8 μm column material particle size, 25 cm column length) in series. Separation was carried out at a flow rate of 500 nl/min through the following concentration gradient: 0–5 min, 5% mobile phase B (98% ACN, 0.1%). Mobile phase B increased linearly from 5 to 35% from 5 to 160 min, increased from 35 to 80% over 160–170 min, and then increased to 80% over 170–175 min, and finally decreased to 5% over 176–180 min. Afterward, the peptides were injected into a nanoESI ion source followed by a tandem mass spectrometer for both DDA and DIA analyses.

Data-Dependent Acquisition Mass Spectrometry

The separated peptides were ionized by the nanoESI source and injected into a Q-Exactive HF tandem mass spectrometer (Thermo Fisher Scientific, San Jose, CA) under DDA mode. Briefly, intact peptides were detected in the Orbitrap at a resolution of 60,000 with a MS range of 350–1,500 m/z for full scan. The 20 most intense precursor ions per survey scan were selected for higher-energy collisional dissociation (HCD) fragmentation, and the

resulting fragments were analyzed with the Orbitrap at a resolution of 15,000 with a fixed mass of 100 m/z. The MS was operated between MS scan and MS/MS scan with the dynamic exclusion time of 30s. The automatic gain control (AGC) was set as 3E6 for level 1 and 1E5 for level 2.

Data-Independent Acquisition Mass Spectrometry

Another batch of separated peptides was injected into the Q-Exactive HF tandem mass spectrometer (Thermo Fisher Scientific, San Jose, CA) under DIA mode. Briefly, intact peptides were detected in the Orbitrap at a resolution of 120,000 with a MS range of 350–1,500 m/z for full scan, followed by the division of 40 windows for fragmentation and signal acquisition. The fragmentation mode was HCD, and ion fragments were detected with Orbitrap. The dynamic exclusion time was set to 30 s. The AGC was set as follows: 3E6 for level 1 and 1E5 for level 2.

Database Search

The Andromeda engine implemented in MaxQuant was used to process DDA data obtained from the machine.[1] Spectronaut was then used to construct a spectrum library and complete the data deconvolution. The mProphet algorithm was used to complete the data analysis and quality control. Based on the UniProt protein databases, GO, COG/KOG and KEGG pathway annotations were conducted. MSstats software was used to preprocess the data and make comparisons among different group sets. The threshold of significance level for DAPs was set at fold change (FC) ≥ 2 and $p < 0.05$. Finally, enrichment analysis and subcellular localization analysis were performed for DAPs, and protein-protein interaction (PPI) analysis was conducted using STRING database for the functional classification of DAPs.

Data Analysis

SPSS software (v19.0, IBM Corp., Armonk, NY) was used to analyze different respiratory enzymatic activities between two cultivars and their controls. Origin 2019 software was used to draw bar charts and dot charts. The volcano diagram of DAPs between two peanut cultivars and their controls ($|\log2FC| \geq 1$ Magi, $p < 0.05$) was depicted using EXCEL, and the KEGG pathway enrichment bubble diagram was generated by R (R Development Core Team, 2010). The key nodes of DAPs with a confidence score over 500 in the PPI interaction network were selected, and the MCC algorithm implemented in the cytoHubba was used to analyze and identify the hub DAPs using the Cytoscape software (Paul Shannon et al., 1971). The top 100 DAPs with highest confidence levels were used to draw the PPI interaction network diagram.

RESULTS

Effects of Waterlogging Stress on the Morphology of Peanut Taproots

Plant roots are responsible for nutrient and water transportation. When external conditions change, plants adapt to the environment by changing root morphological structure. As shown in **Figure 1A**, after 22 days of waterlogging treatment, the roots of two cultivars became dark brown and rotten, and the growth and development of main roots in controls were better than the treated cultivars. The hypocotyl (**Figure 1B**) of ZH4 generated obvious adventitious roots, while the epicotyl (**Figure 1C**) of XH08 generated obvious adventitious roots.

After 3 days of waterlogging treatment, there was no significant difference in the root growth between ZH4 and XH08, and no ventilatory tissue was found. However, after waterlogging for 6 days, most of the cortical parenchyma cells in ZH4 taproots were dissociated to form ventilatory tissue, while the cortical parenchyma cells in XH08 enlarged and deformed without dissociation, and no obvious ventilatory tissues were formed (**Figures 2A,B**). After 9 days of waterlogging, the xylem in both cultivars showed irregular distribution and a large number of parenchyma cells were damaged. However, the amount of XH08 ventilatory tissue increased without the damage of the cell wall (**Figures 2C,D**).

Functional Analysis of DAPs in Different Peanut Cultivars Under Waterlogging Stress

The DAPs Induced by Waterlogging Stress

Quantitative proteomic analysis of two peanut cultivars with different waterlogging tolerance was carried out by the DIA technique. The analysis of significant DAPs between the treatment and control samples is shown in a volcanic map (**Figure 3**). As shown in **Figure 3A**, a total of 6,441 DAPs were identified between the treated ZH4 and its control group, of which 49 DAPs were significantly upregulated and 88 DAPs were significantly downregulated ($|\log2FC| \geq 1$, $p < 0.05$). As shown in **Figure 3B**, a total of 6,285 DAPs were identified between the treated XH08 and its controls, of which 123 and 114 DAPs were significantly upregulated and downregulated, respectively ($|\log2FC| \geq 1$, $p < 0.05$). Among these DAPs, a total of 156 and 56 specifically existed in XH08 and ZH4, respectively (**Figure 4**), and 81 DAPs shared between two cultivars. In brief, the number of significant DAPs in the waterlogging-tolerant cultivar XH08 was higher than the sensitive cultivar ZH4.

KEGG Pathway Enrichment Analysis

The DAPs related to waterlogging in two peanut cultivars were enriched by KEGG pathway enrichment analysis (**Figure 5**). According to the significance of waterlogging-related DAP enrichment in the signaling pathway, the waterlogging-related DAPs in ZH4 were mainly enriched in the following six metabolic pathways (the number of DAPs enriched in each signaling pathway is in parentheses; **Figure 5A**): glycolysis/gluconeogenesis (16), secondary metabolites (37), fructose and mannose metabolism (6), metabolic pathways (52), pentose phosphate pathway (6), and amino acid biosynthesis (13). The waterlogging-related DAPs in XH08 were mainly enriched in the following six metabolic pathways (**Figure 5B**): glycolysis/gluconeogenesis (22), carbon fixation in photosynthetic organisms (11), carbon metabolism (22), secondary metabolites (56), amino

[1]http://www.maxquant.org

FIGURE 1 | Morphological differences between two treated peanut cultivars and their controls. **(A)** The peanut taproots of treated and the control groups after 22 days of waterlogging treatment. Left two samples were treated ones, and the right one was control sample; **(B)** the peanut hypocotyl produced adventitious roots in Zhonghua 4 (ZH4) after 22 days waterlogging treatment; and **(C)** the peanut epicotyl produced adventitious roots in Xianghua08 (XH08) after 22 days of waterlogging treatment.

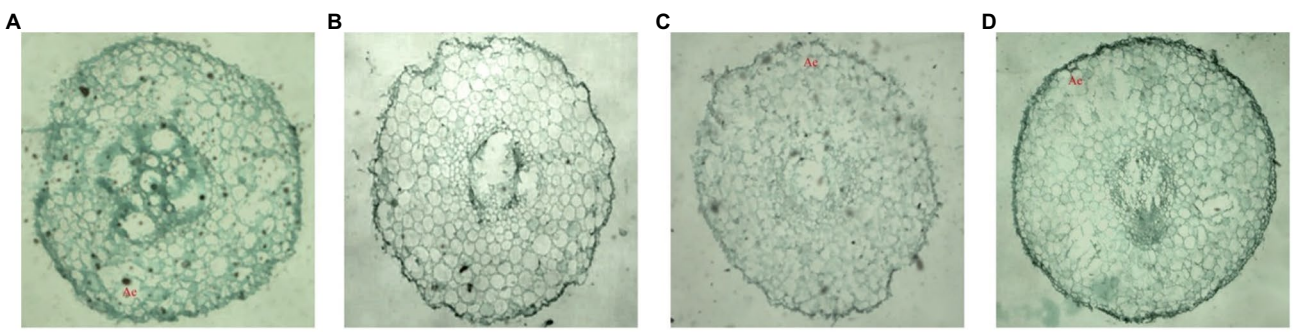

FIGURE 2 | The root tissue micrographs (aerenchyma) of the main roots in two peanut cultivars after waterlogging for 6 days and 9 days. **(A)** Root microscopic map of ZH4 after 6 days of waterlogging treatment; **(B)** root tissue microscopic map of XH08 after 6 days of waterlogging treatment; **(C)** root microscopic map of ZH4 after 9 days of waterlogging treatment; and **(D)** root microscopic map of XH08 after 9 days pf waterlogging treatment.

acid biosynthesis (20), and fatty acid degradation (9). In brief, the main enriched signaling pathways shared between ZH4 and XH08 included metabolic pathways, secondary metabolites, glycolysis/gluconeogenesis, carbon metabolism, amino acid biosynthesis, and phenylpropanoid biosynthesis. The relative up- and downregulated KEGG pathways of the DAPs in both XH08 and ZH4 were indicated in **Figure 6**, indicating that although the trends in upregulated KEGG pathways were similar between two cultivars, more DAPs were downregulated across KEGG pathways in XH08 than ZH4.

Hub DAP PPI Interaction Network Analysis

The key nodes with the confidence score over 500 in the PPI interaction network were selected, and the MCC algorithm

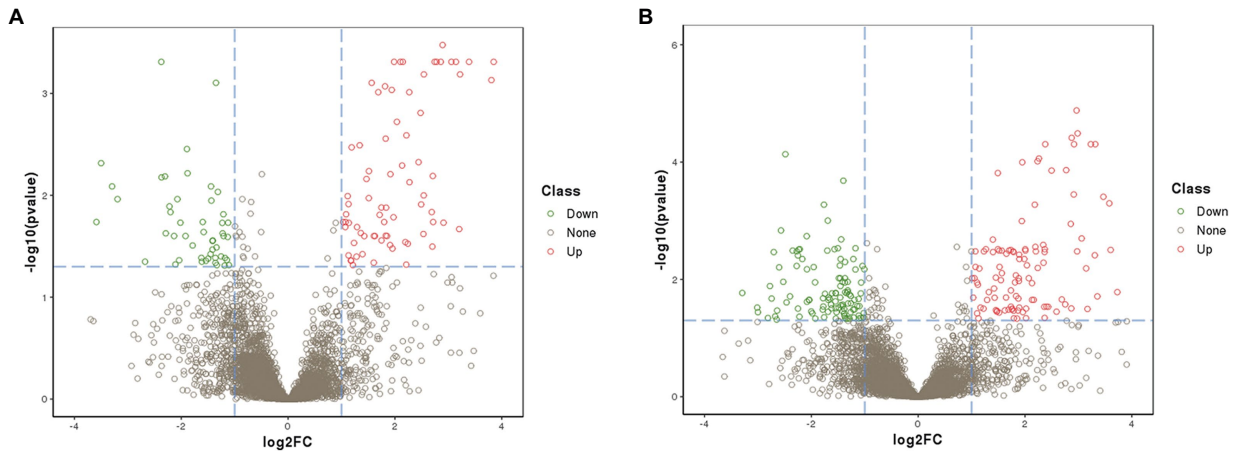

FIGURE 3 | Volcano map of differentially accumulated proteins (DAPs) in two different peanut cultivars after 12 days of waterlogging treatment. **(A)** Volcano map of DAPs between ZH4 and its control group after 12 days of waterlogging treatment. **(B)** Volcano map of DAPs between XH08 and its controls after 12 days of waterlogging treatment.

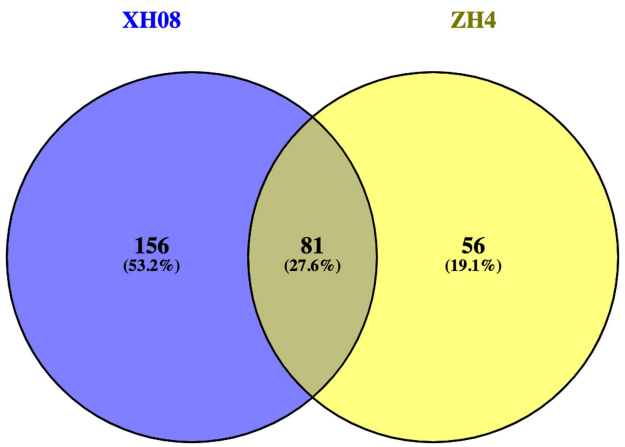

FIGURE 4 | The Venn diagram indicating a comparison of DAPs between XH08 and ZH4.

of the Cytoscape software cytoHubba was used to find the hub DAPs (**Figure 6**). The number of key DAPs (i.e., PPI interaction network key nodes) in XH08 and the number of interactions between key DAPs were higher than ZH4 (**Figure 7**). The hub DAPs related to waterlogging in ZH4 mainly included T2B9M0, A0A444YP93, A0A444YY24, and A0A445B9L1 (**Table 1**; **Figure 7A**). In addition, A0A444YYU4, A0A444XSI4, A0A445BU22, A0A445CFH7, A0A444Y8U1, and A0A445B0R4 also played important roles in response to waterlogging stress, while the only different hub DAP in XH08 from ZH4 was A0A444Y0J8 (**Table 1**; **Figure 7B**). Compared to ZH4, the DAPs, such as A0A444WVT0, A0A445AX60, A0A444ZM03, A0A445B4C1, A0A444X6X2, and A0A445ARZ8, played a key role in the physiological process of XH08 under waterlogging stress (**Table 1**; **Figure 7C**). Under waterlogging stress, the common hub DAPs between XH08 and ZH4 mainly included the enzymes related to glycolysis pathway, such as enolase, fructose-bisphosphate aldolase, glyceraldehyde-3-phosphate dehydrogenase, ATP-dependent 6-phosphofructokinase, and pyruvate kinase, while the unique hub DAPs in XH08 mainly included malate metabolism, such as L-lactate dehydrogenase, NAD^+-dependent malic enzyme, aspartate aminotransferase, and glutamate dehydrogenase as well as the enzymes related to glyoxylic acid cycle. Details of hub DAPs and the corresponding functional predictions between two peanut cultivars are shown in **Table 1**.

Effects of Waterlogging Stress on Enzymatic Activities in Two Peanut Cultivars

The activities of LDH, ADH, and MDH in the main roots of two peanut cultivars were measured after waterlogging treatment for 3, 6, 9, 12, and 15 days, respectively, and the change of enzymatic activities across waterlogging treatment was analyzed (**Tables 2** and **3**; **Figure 8**). The LDH activity of the main roots of ZH4 and XH08 increased slightly slow from 3 to 6 days. However, a sharp increase was observed after treatment for 6 days and reached to a peak on the ninth day in ZH4, while the LDH activity in XH08 continued to increase until reaching a peak on the twelfth day. The LDH activity of in two cultivars showed a downward trend from 12 to 15 days, and a sharper decrease was observed in XH08 than ZH4. However, the ADH activity in both cultivars continuously increased and reached a peak until twelfth day, with the decrease in XH08 being greater than ZH4. Unlike the above two enzymes, the MDH activity in ZH4 and XH08 continuously dropped from 3 to 15 days.

Based on the above results, both ADH and LDH activities reached to a peak at the twelfth day in XH08. At this point of time, the activities of ADH and LDH in both treated cultivars

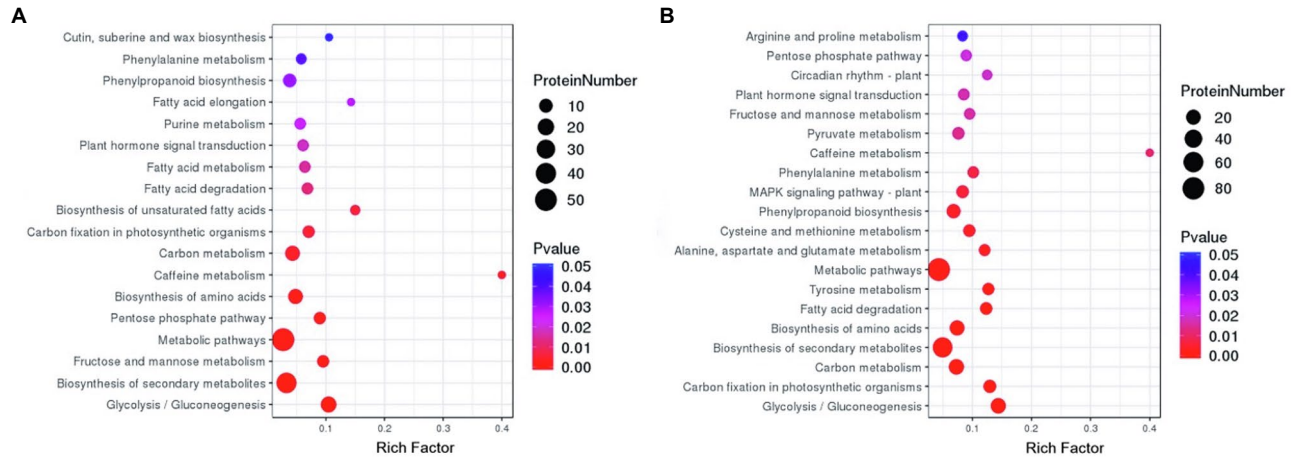

FIGURE 5 | The KEGG signaling pathways of DAPs in two different peanut cultivars were enriched by a bubble map after 12 days of waterlogging treatment. **(A)** Bubble map of the significantly enriched KEGG pathways of DAPs in ZH4 and its controls after 12 days of waterlogging treatment. **(B)** Bubble map of DAPs in KEGG pathways between XH08 and its control samples after 12 days of waterlogging treatment.

were significantly higher than control groups (**Figure 9**), with the *p*-value between treated XH08 and its controls in both ADH and LDH activities smaller than 0.001 and the value of *p* between treated ZH4 and its controls in ADH and LDH smaller than 0.05 and 0.01, respectively.

DISCUSSION

It was found that the production of adventitious roots is an important way for plants to adapt to waterlogging stress. In order to easily obtain oxygen from the environment to maintain normal physiological functions, most of the adventitious roots grow at the base of the stem, on the surface of water or on the surface of soil rich in oxygen after waterlogging stress (Xu et al., 2017). In our study, after 22 days of waterlogging treatment, obvious adventitious roots were grown on both the epicotyl and hypocotyls of main roots in treated peanut cultivars (**Figure 1**). In previous studies, researchers found that under waterlogging stress, plant root parenchyma cells usually died or dissolved to form lytic aerated tissue, which was convenient to transport oxygen from aboveground parts to roots in the soil to maintain the normal physiological functions (Yamauchi et al., 2018; Peng et al., 2020). In agreement with the above findings, our study also found that the dissociation of parenchyma cells from the cortex in ZH4 began to form aerenchyma slightly earlier than XH08 (**Figure 2**), and as the waterlogging treatment time increased, a large number of parenchyma cell walls were damaged, and it was difficult to maintain normal morphology. However, the aerenchyma in XH08, a waterlogging-tolerant cultivar, appeared later, resulting in normal cell wall (**Figure 2**).

The KEGG pathway analysis (**Figure 5**) showed that waterlogging-related DAPs in two peanut cultivars were both significantly enriched in the glycolysis/gluconeogenesis signaling pathway, and the PPI interaction analysis showed that the common function of hub DAPs in two cultivars was also related to the biosynthesis of glycolysis-related enzymes, such as enolase, fructose-bisphosphate aldolase, glyceraldehyde-3-phosphate dehydrogenase, ATP-dependent 6-phosphofructokinase, and pyruvate kinase. Therefore, it is inferred that waterlogging stress induced an anoxic environment and resulted in the anaerobic respiration in peanut root cells to provide energy for life activities through the glycolysis process.

Other than the glycolysis process, the PPI interaction analysis of hub DAPs (**Figure 7**) also showed that waterlogging stress could lead to lactic acid and ethanol fermentation in treated plants. For example, the unique hub DAPs in XH08 were mainly related to lactic acid fermentation, such as L-lactate dehydrogenase, NAD^+-dependent malic enzyme, aspartate aminotransferase, and glutamate dehydrogenase as well as the enzymes related to malic acid metabolism and the glyoxylic acid cycle. In agreement with these, the activities of ADH and LDH in treated cultivars were higher than the control groups (**Figure 8**), suggesting that other than glycolysis process, waterlogging stress induced anaerobic fermentation pathways, including lactic acid and alcohol fermentation (Wu et al., 2020). Lactic acid fermentation produces lactic acid, which would decrease cytosolic pH, thus inhibiting the LDH activity but activating ADH activity, which, as a result, lead to the transition from lactic acid fermentation to alcoholic fermentation (Dennis et al., 2000; An et al., 2016; Famiani et al., 2016; Wu et al., 2020; Pan et al., 2021). However, in waterlogging-tolerant plants, alcohol fermentation is more active than lactic acid fermentation (Dennis et al., 2000; Famiani et al., 2016; Wu et al., 2020; Pan et al., 2021), leading to slow accumulation of lactic acid and slow drop in cytosolic pH, and as a result, prolonged activity of LDH. These can be inferred from **Figures 8A,B, 9**,

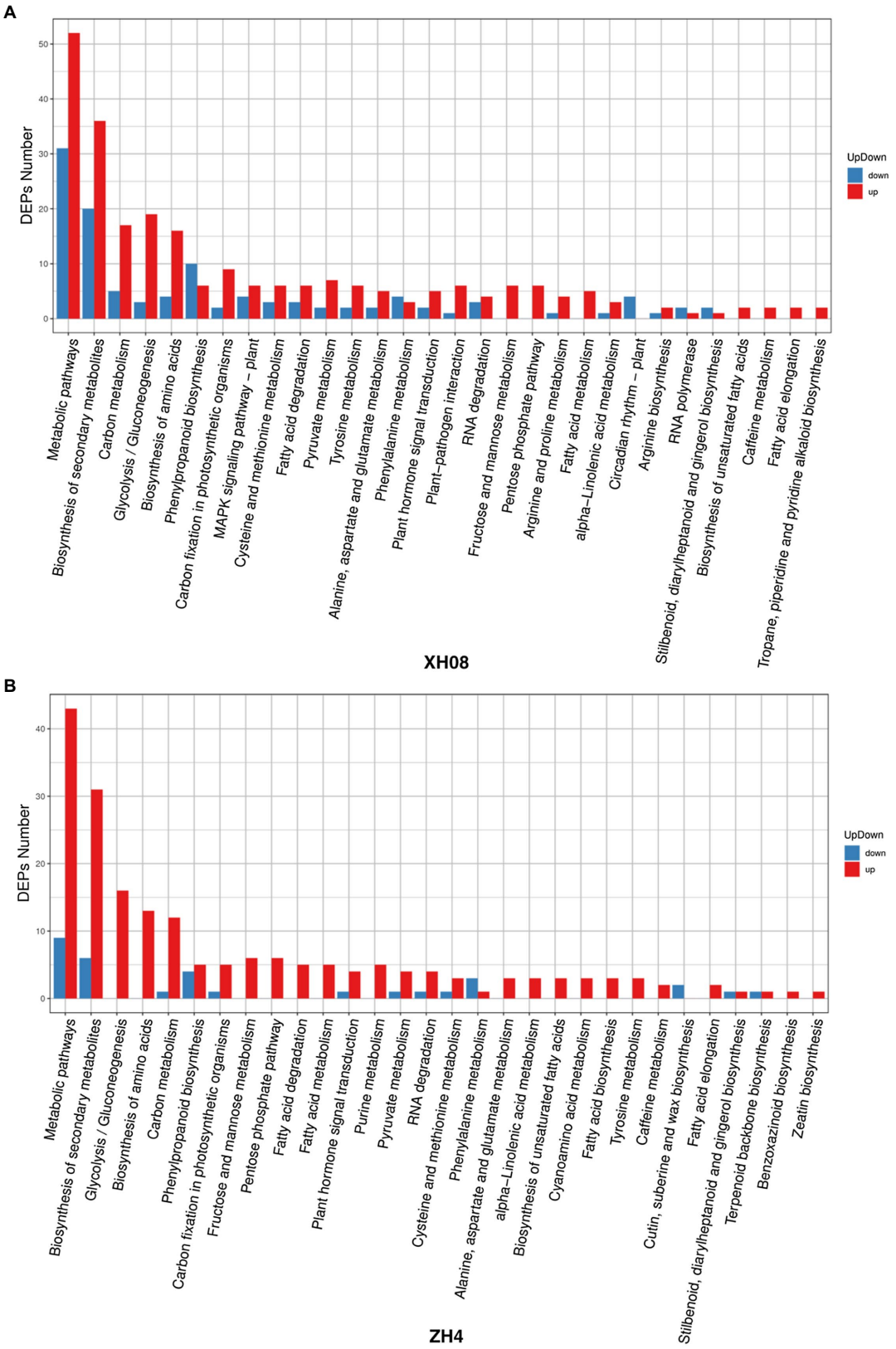

FIGURE 6 | The up- and downregulated DAPs in two peanut cultivars and their controls. **(A)** Up- and downregulated KEGG pathways of DAPs in ZH4 and its controls; **(B)** up- and downregulated KEGG pathways of DAPs in XH08 and its controls.

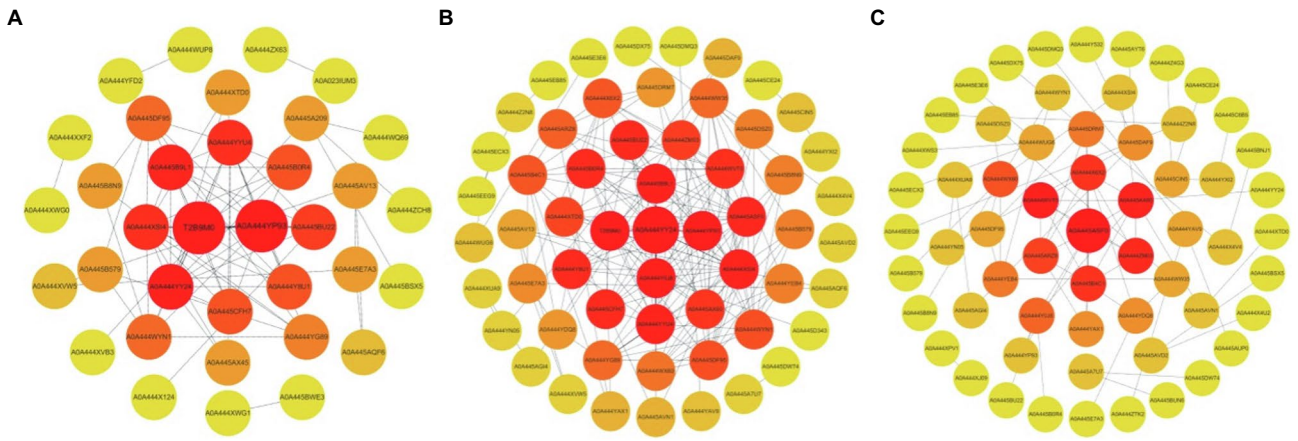

FIGURE 7 | The protein-protein interaction (PPI) network interaction map of the differentially accumulated proteins (DAPs) in two peanut cultivars after 12 days of waterlogging treatment. **(A)** PPI interaction network map of hub DAPs between ZH4 and its control group after 12 days of waterlogging treatment; **(B)** PPI interaction network map of hub DAPs in XH08 and its control group after 12 days of waterlogging treatment; **(C)** PPI interaction network map of hub DAPs between XH08 and ZH4 subjected to waterlogging treatment.

TABLE 1 | The hub DAPs (confidence score ≥ 500) in the interaction network between XH08, ZH4, and their control groups.

Protein ID	SWISS-PROT description (function)	Log2FC(up/down)	Value of *p*
ZH4(sensitive cultivar)hub DAPs			
T2B9M0	Fructose-bisphosphate aldolase, cytoplasmic isozyme	1.1374/Up	0.00024
A0A444YP93	Fructose-bisphosphate aldolase 8, cytosolic	1.1311/Up	0.00012
A0A444YY24	Enolase	2.1478/Up	5.86E-07
A0A445B9L1	Glyceraldehyde-3-phosphate dehydrogenase GAPC2, cytosolic	2.0370/Up	8.28E-06
A0A444YYU4	Pyruvate kinase, cytosolic isozyme	1.4266/Up	0.00042
A0A444XSI4	Pyruvate kinase 1, cytosolic	2.2689/Up	3.93E-06
A0A445BU22	ATP-dependent 6-phosphofructokinase 3	1.8147/Up	2.91E-06
A0A445CFH7	ATP-dependent 6-phosphofructokinase 3	2.7801/Up	9.14E-07
A0A444Y8U1	ATP-dependent 6-phosphofructokinase 3	3.2192/Up	1.52E-06
A0A445B0R4	Pyrophosphate-fructose 6-phosphate 1-phosphotransferase subunit alpha	1.0303/Up	0.00022
XH08(waterlogging-tolerant cultivar) hub DAPs			
A0A444YY24	Enolase	2.3791/Up	7.18E-08
T2B9M0	Fructose-bisphosphate aldolase, cytoplasmic isozyme	1.3983/Up	1.33E-05
A0A444YP93	Fructose-bisphosphate aldolase 8, cytosolic	1.2305/Up	3.62E-05
A0A444Y0J8	Phosphoglycerate kinase 3, cytosolic	1.0122/Up	0.00017
A0A445B9L1	Glyceraldehyde-3-phosphate dehydrogenase GAPC2, cytosolic	2.1833/Up	2.51E-06
A0A444YYU4	Pyruvate kinase, cytosolic isozyme	1.9405/Up	5.32E-06
A0A444XSI4	Pyruvate kinase 1, cytosolic	2.8732/Up	3.68E-08
A0A445ASF0	L-lactate dehydrogenase A	1.1019/Up	0.00022
A0A445CFH7	ATP-dependent 6-phosphofructokinase 3	1.8693/Up	0.00121
A0A444Y8U1	ATP-dependent 6-phosphofructokinase 3	2.1321/Up	0.00061
ZH4 vs. XH08 hub DAPs			
A0A445ASF0	L-lactate dehydrogenase A	1.1019/Up	0.00022
A0A444WVT0	Phosphoenolpyruvate carboxykinase	−1.6541/Down	0.00057
A0A445AX60	Pyruvate, phosphate dikinase, and chloroplastic	3.1700/Up	0.00108
A0A444ZM03	NAD^+-dependent malic enzyme 59 kDa, mitochondrial	1.5232/Up	9.15E-05
A0A445B4C1	Aspartate aminotransferase 1	1.4908/Up	5.38E-07
A0A444X6X2	Aspartate aminotransferase 1	1.7860/Up	3.93E-05
A0A445ARZ8	Glutamate dehydrogenase A	−1.0087/Down	0.000108

in which the ADH activity in XH08 was always higher than ZH4, while the LDH activity of XH08 extended 3 more days than ZH4 until 12 days after waterlogging treatment. It was reasonable to infer that the waterlogging-tolerant cultivar (XH08) had a more active ethanol fermentation activity, which slow down the accumulation of lactate, and

TABLE 2 | Enzymatic activities of LDH, ADH, and MDH in XH08 and ZH4 treated with waterlogging for 3, 6, 9, 12, and 15 days (U mg^{-1} FW).

Enzyme	Cultivar	Waterlogging treatment time (*d*)				
		3d	6d	9d	12d	15d
LDH	XH08	0.037 ± 0.024	0.278 ± 0.037	1.145 ± 0.015	1.406 ± 0.061	0.145 ± 0.018
	ZH4	0.041 ± 0.028	0.287 ± 0.064	1.216 ± 0.053	0.907 ± 0.056	0.283 ± 0.027
ADH	XH08	0.047 ± 0.035	0.514 ± 0.027	0.719 ± 0.023	1.018 ± 0.025	0.330 ± 0.033
	ZH4	0.023 ± 0.035	0.281 ± 0.024	0.484 ± 0.032	0.617 ± 0.042	0.159 ± 0.037
MDH	XH08	0.685 ± 0.021	0.637 ± 0.028	0.606 ± 0.028	0.448 ± 0.041	0.381 ± 0.027
	ZH4	0.631 ± 0.014	0.573 ± 0.026	0.522 ± 0.011	0.392 ± 0.034	0.304 ± 0.022

TABLE 3 | ANOVA analysis of the enzymatic activities (U mg^{-1} FW) of ADH and LDH in XH08 and ZH4 treated with and without waterlogging after 12 days.

Enzyme	Cultivar	Enzyme activity (U mg^{-1} FW)		Significance level
		Treated with waterlogging	Treated without waterlogging (CK)	
LDH	ZH4	0.907 ± 0.056	0.461 ± 0.016	**
	XH08	1.406 ± 0.061	0.791 ± 0.026	***
ADH	ZH4	0.617 ± 0.042	0.024 ± 0.016	*
	XH08	1.018 ± 0.025	0.758 ± 0.024	***

*$p \leq 0.05$; **$p \leq 0.01$; and ***$p \leq 0.001$.

therefore extended the lactic acid fermentation compared to the non-tolerant cultivar (ZH4).

Other than ADH and LDH, the MDH activity in XH08 was also more active than ZH4 throughout the waterlogging treatment process (**Figure 8C**). Coincidently, the expression of NAD^+-dependent malic enzymes in hub DAP in mitochondria unique to XH08 was upregulated in the treated plants (**Table 1**). This coincided with the previous findings that NAD^+-dependent malase could catalyze the decarboxylation of malate to pyruvate in the mitochondria, where the oxidation from malate to CO_2 and NADH appears without going through glycolysis process to generate pyruvate (Famiani et al., 2016; Sun et al., 2019). Driscoll and Finan (1993) also found that NAD^+-dependent malic enzymes produced by *Rhizobium meliloti* were necessary for symbiotic nitrogen fixation (Driscoll and Finan, 1993). Therefore, it is reasonable to infer that the waterlogging-tolerant cultivar might facilitate malic acid metabolism to accumulate pyruvate, producing energy to maintain normal physiological metabolism. It may also facilitate the symbiotic nitrogen fixation in soil microorganisms.

CONCLUSION

Most previous studies mainly focused on the effects of waterlogging stress on plant morphology, physiology, dry matter accumulation and distribution, crop yield, and quality characteristics. Unveiling the molecular mechanisms under waterlogging stress will provide guidance for the future targeted peanut breeding. The current study found that ADH and MDH in XH08 were more active than ZH4, and the activity of LDH was prolonged in XH08 than ZH4, indicating that ethanol fermentation might be the primary anaerobic fermentation pathway in waterlogging-tolerant cultivar. In addition to anaerobic fermentation to provide energy, the waterlogging-tolerant cultivar might also rely on other metabolic pathways, such as malic acid metabolism to generate pyruvate to alleviate the energy shortage under waterlogging stress. This study enriched the current peanut genomics and proteomics resources, which will provide a foundation for future molecular breeding and genetic engineering in breeding for waterlogging-tolerant peanut cultivars.

DATA AVAILABILITY STATEMENT

The datasets "Peanut Root Waterlogging LC-MSMS"presented in this study are deposited to the ProteomeXchange Consortium via the PRIDE (Perez-Riverol et al., 2019) partner repository with the dataset identifier PXD027176.

AUTHOR CONTRIBUTIONS

DL and LL conceived and designed the study. JZ, HZ and NZ prepared samples for quantitative proteomics. WZ and JZ collected, curated the data, and wrote the manuscript. WZ did the data analysis. DL and LL were responsible for funding acquisition. WZ, HZ, ZL, DL, and LL revised the manuscript. All authors read and approved the manuscript.

FUNDING

This work was supported by the National Natural Science Foundation of China (31671634).

ACKNOWLEDGMENTS

We are grateful to the personnel of the College of Plant Protection at Hunan Agricultural University for providing writing guidance. We are also grateful to the editor and the reviewers.

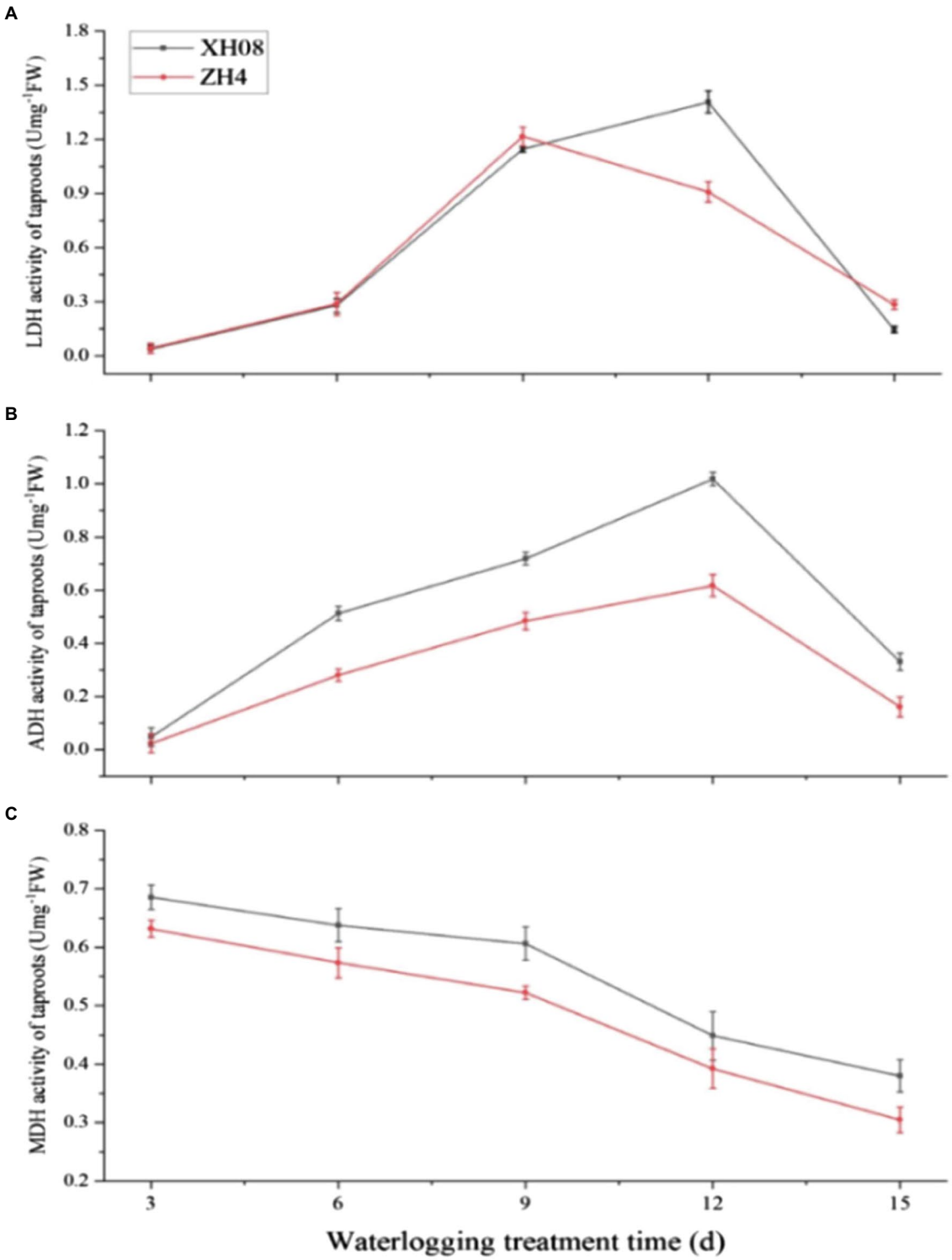

FIGURE 8 | The activities of LDH, alcohol dehydrogenase (ADH), and malate dehydrogenase (MDH) in two peanut cultivars treated with waterlogging for 12 and 15 days. **(A)** The activities of the LDH enzyme in XH08 and ZH4 after waterlogging treatment for 3, 6, 9, 12, and 15 days; **(B)** the activities of the ADH enzyme in XH08 and ZH4 after waterlogging treatment for 3, 6, 9, 12, and 15 days; **(C)** the activities of the MDH enzyme in XH08 and ZH4 after waterlogging treatment for 3, 6, 9, 12, and 15 days.

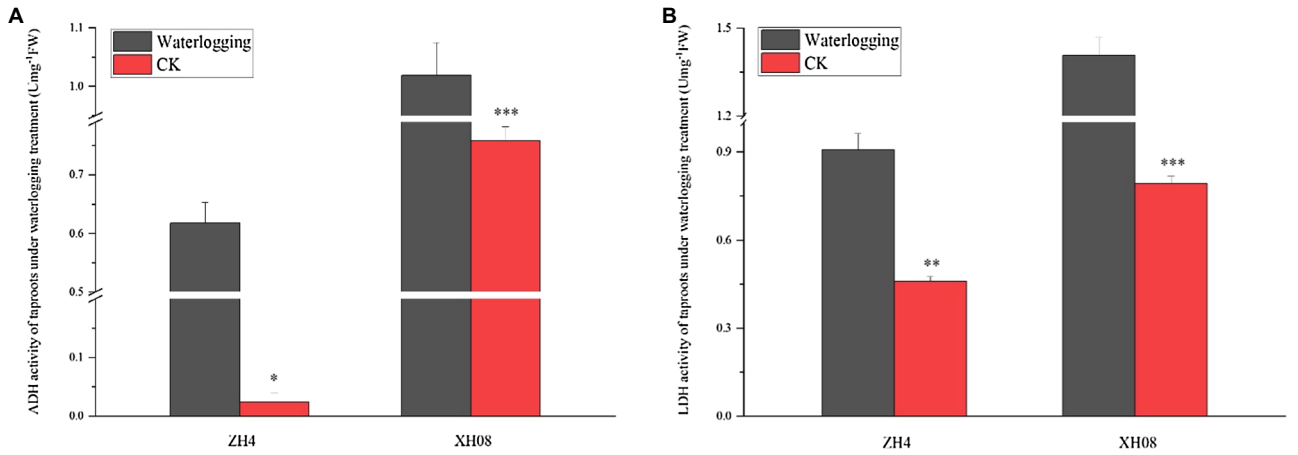

FIGURE 9 | The difference in the activities of ADH and LDH (U mg^{-1} FW) in two different peanut cultivars after 12 days of waterlogging treatment. **(A)** The difference in ADH activity (U mg^{-1} FW) between ZH4 and XH08 after 12 days of waterlogging treatment. **(B)** The difference in LDH activity after 12 days of waterlogging treatment between ZH4 and XH08 ($^{*}p < 0.05$; $^{**}p < 0.01$; $^{***}p < 0.001$).

REFERENCES

An, Y., Qi, L., and Wang, L. (2016). ALA pretreatment improves waterlogging tolerance of fig plants. *PLoS One* 11:e0147202. doi: 10.1371/journal.pone.0147202

Andrade, C. A., de Souza, K. R. D., de Santos, M. O., da Silva, D. M., and Alves, J. D. (2018). Hydrogen peroxide promotes the tolerance of soybeans to waterlogging. *Sci. Hortic.* 232, 40–45. doi: 10.1016/j.scienta.2017.12.048

Choe, L., D'Ascenzo, M., Relkin, N. R., Pappin, D., Ross, P., Williamson, B., et al. (2012). 8-Plex quantitation of changes in cerebrospinal fluid protein expression in subjects undergoing intravenous immunoglobulin treatment for Alzheimer's disease. *Prat. Neurol. FMC* 7, 3651–3660. doi: 10.1002/pmic.200700316

da Silva, C. J., and do Amarante, L. (2020). Short-term nitrate supply decreases fermentation and oxidative stress caused by waterlogging in soybean plants. *Environ. Exp. Bot.* 176:104078. doi: 10.1016/j.envexpbot.2020.104078

Dennis, E. S., Dolferus, R., Ellis, M., Rahman, M., Wu, Y., Hoeren, F. U., et al. (2000). Molecular strategies for improving waterlogging tolerance in plants. *J. Exp. Bot.* 51, 89–97. doi: 10.1093/jexbot/51.342.89

Driscoll, B. T., and Finan, T. M. (1993). NAD^+ −dependent malic enzyme of *Rhizobium meliloti* is required for symbiotic nitrogen fixation. *Mol. Microbiol.* 7, 865–873. doi: 10.1111/j.1365-2958.1993.tb01177.x

Famiani, F., Farinelli, D., Moscatello, S., Battistelli, A., Leegood, R. C., and Walker, R. P. (2016). The contribution of stored malate and citrate to the substrate requirements of metabolism of ripening peach (*Prunus persica* L. Batsch) flesh is negligible. Implications for the occurrence of phosphoenolpyruvate carboxykinase and gluconeogenesis. *Plant Physiol. Biochemist.* 101, 33–42. doi: 10.1016/j.plaphy.2016.01.007

Garcia, N., da Silva, C. J., Cocco, K. L. T., Pomagualli, D., de Oliveira, F. K., da Silva, J. V. L., et al. (2020). Waterlogging tolerance of five soybean genotypes through different physiological and biochemical mechanisms. *Environ. Exp. Bot.* 172:103975. doi: 10.1016/j.envexpbot.2020.103975

Ghashghaie, J., Badeck, F. W., Girardin, C., Sketriené, D., Lamothe-Sibold, M., and Werner, R. A. (2015). Changes in $\delta^{13}C$ of dark respired CO_2 and organic matter of different organs during early ontogeny in peanut plants. *Isot. Environ. Health Stud.* 51, 93–108. doi: 10.1080/10256016.2015.1011635

Gillet, L. C., Navarro, P., Tate, S., Röst, H., Selevsek, N., Reiter, L., et al. (2012). Targeted data extraction of the MS/MS spectra generated by data independent acquisition: a new concept for consistent and accurate proteome analysis. *Image* 11, 1–45. doi: 10.1074/mcp.O111.016717

Jylhä, A., Nättinen, J., Aapola, U., Mikhailova, A., Nykter, M., Zhou, L., et al. (2018). Comparison of itraq and SWATH in a clinical study with multiple time points. *Clin. Proteomics* 15:24. doi: 10.1186/s12014-018-9201-5

Khabaz-Saberi, H., and Rengel, Z. (2010). Aluminum, manganese, and iron tolerance improves performance of wheat genotypes in waterlogged acidic soils. *J. Plant Nutr. Soil Sci.* 173, 461–468. doi: 10.1002/jpln.200900316

Khabaz-Saberi, H., Setter, T. L., and Waters, I. (2006). Waterlogging induces high to toxic concentrations of iron, aluminum, and manganese in wheat varieties on acidic soil. *J. Plant Nutr.* 29, 899–911. doi: 10.1080/01904160600649161

Kim, Y., Seo, C. W., Khan, A. L., Mun, B. G., Shahzad, R., Ko, J. W., et al. (2018). Exo-ethylene application mitigates waterlogging stress in soybean (*Glycine max* L.). *BMC Plant Biol.* 18:254. doi: 10.1186/s12870-018-1457-4

Kögel-Knabner, I., Amelung, W., Cao, Z., Fiedler, S., Frenzel, P., Jahn, R., et al. (2010). Biogeochemistry of paddy soils. *Geoderma* 157, 1–14. doi: 10.1016/j.geoderma.2010.03.009

Kruger, N. J. (2009). The Bradford method for protein quantitation. *Methods Mol. Biol.* 32, 9–15. doi: 10.1385/0-89603-268-X:9

Pan, J., Sharif, R., Xu, X., and Chen, X. (2021). Mechanisms of waterlogging tolerance in plants: research progress and prospects. *Front. Plant Sci.* 11:627331. doi: 10.3389/fpls.2020.627331

Peng, Y. Q., Zhu, J., Li, W. J., Gao, W., Shen, R. Y., and Meng, L. J. (2020). Effects of grafting on root growth, anaerobic respiration enzyme activity and aerenchyma of bitter melon under waterlogging stress. *Sci. Hortic.* 261:108977. doi: 10.1016/j.scienta.2019.108977

Perez-Riverol, Y., Csordas, A., Bai, J., Bernal-Llinares, M., Hewapathirana, S., Kundu, D. J., et al. (2019). The PRIDE database and related tools and resources in 2019: improving support for quantification data. *Nucleic Acids Res.* 47, D442–D450. doi: 10.1093/nar/gky1106

Pezeshki, S. R., and DeLaune, R. D. (2012). Soil oxidation-reduction in wetlands and its impact on plant functioning. *Biology* 1, 196–221. doi: 10.3390/biology1020196

R Development Core Team (2010). R: A language and environment for statistical computing.

Ross, P. L., Huang, Y. N., Marchese, J. N., Williamson, B., Parker, K., Hattan, S., et al. (2004). Multiplexed protein quantitation in *Saccharomyces cerevisiae* using amine-reactive isobaric tagging reagents. *Mol. Cell. Proteomics* 3, 1154–1169. doi: 10.1074/mcp.M400129-MCP200

Shannon, P., Markiel, A., Ozier, O., Baliga, N. S., Wang, J. T., Ramage, D., et al. (1971). Cytoscape: A software environment for integrated models. *Genome Res.* 13:426. doi: 10.1101/gr.1239303.metabolite

Sun, X., Han, G., Meng, Z., Lin, L., and Sui, N. (2019). Roles of malic enzymes in plant development and stress responses. *Plant Signal. Behav.* 14:1644596. doi: 10.1080/15592324.2019.1644596

Walker, R. P., Benincasa, P., Battistelli, A., Moscatello, S., Técsi, L., Leegood, R. C., et al. (2018). Gluconeogenesis and nitrogen metabolism in maize. *Plant Physiol. Biochem.* 130, 324–333. doi: 10.1016/j.plaphy.2018.07.009

Wang, X., Huang, M., Zhou, Q., Cai, J., Dai, T., Cao, W., et al. (2016). Physiological and proteomic mechanisms of waterlogging priming improves tolerance to waterlogging stress in wheat (*Triticum aestivum* L.). *Environ. Exp. Bot.* 132, 175–182. doi: 10.1016/j.envexpbot.2016.09.003

Wu, W. L., Hsiao, Y. Y., Lu, H. C., Liang, C. K., Fu, C. H., Huang, T. H., et al. (2020). Expression regulation of MALATE SYNTHASE involved in glyoxylate cycle during protocorm development in *Phalaenopsis aphrodite* (Orchidaceae). *Sci. Rep.* 10:10123. doi: 10.1038/s41598-020-66932-8

Xu, X., Chen, M., Ji, J., Xu, Q., Qi, X., and Chen, X. (2017). Comparative RNA-seq based transcriptome profiling of waterlogging response in cucumber hypocotyls reveals novel insights into the *de novo* adventitious root primordia initiation. *BMC Plant Biol.* 17:129. doi: 10.1186/s12870-017-1081-8

Xu, B., Cheng, Y., Zou, X., and Zhang, X. (2016). Ethanol content in plants of *Brassica napus* L. correlated with waterlogging tolerance index and regulated by lactate dehydrogenase and citrate synthase. *Acta Physiol. Plant.* 38:81. doi: 10.1007/s11738-016-2098-6

Xuewen, X., Huihui, W., Xiaohua, Q., Qiang, X., and Xuehao, C. (2014). Waterlogging-induced increase in fermentation and related gene expression in the root of cucumber (*Cucumis sativus* L.). *Sci. Hortic.* 179, 388–395. doi: 10.1016/j.scienta.2014.10.001

Yamauchi, T., Colmer, T. D., Pedersen, O., and Nakazono, M. (2018). Regulation of root traits for internal aeration and tolerance to soil waterlogging-flooding stress. *Plant Physiol.* 176, 1118–1130. doi: 10.1104/pp.17.01157

Zeng, R., Chen, L., Wang, X., Cao, J., Li, X., Xu, X., et al. (2020). Effect of waterlogging stress on dry matter accumulation, photosynthesis characteristics, yield, and yield components in three different ecotypes of peanut (*Arachis hypogaea* L.). *Agronomy* 10:1244. doi: 10.3390/agronomy10091244

Zhao, N., Li, C., Yan, Y., Cao, W., Song, A., Wang, H., et al. (2018). Comparative transcriptome analysis of waterlogging-sensitive and waterlogging-tolerant *Chrysanthemum morifolium* cultivars under waterlogging stress and reoxygenation conditions. *Int. J. Mol. Sci.* 19:1455. doi: 10.3390/ijms19051455

Zheng, C., Jiang, D., Liu, F., Dai, T., Jing, Q., and Cao, W. (2009). Effects of salt and waterlogging stresses and their combination on leaf photosynthesis, chloroplast ATP synthesis, and antioxidant capacity in wheat. *Plant Sci.* 176, 575–582. doi: 10.1016/j.plantsci.2009.01.015

Zou, X., Jiang, Y., Liu, L., Zhang, Z., and Zheng, Y. (2010). Identification of transcriptome induced in roots of maize seedlings at the late stage of waterlogging. *BMC Plant Biol.* 10:189. doi: 10.1186/1471-2229-10-189

Conflict of Interest: The authors declare that the research was conducted in the absence of any commercial or financial relationships that could be construed as a potential conflict of interest.

Publisher's Note: All claims expressed in this article are solely those of the authors and do not necessarily represent those of their affiliated organizations, or those of the publisher, the editors and the reviewers. Any product that may be evaluated in this article, or claim that may be made by its manufacturer, is not guaranteed or endorsed by the publisher.

frontiers in Plant Science

ORIGINAL RESEARCH
published: 06 October 2021
doi: 10.3389/fpls.2021.740524

Metabolomics Analysis Reveals Drought Responses of Trifoliate Orange by Arbuscular Mycorrhizal Fungi With a Focus on Terpenoid Profile

Sheng-Min Liang[1†], Fei Zhang[1,2†], Ying-Ning Zou[1], Kamil Kuča[3] and Qiang-Sheng Wu[1,3]*

[1]College of Horticulture and Gardening, Yangtze University, Jingzhou, China, [2]College of Biology and Agricultural Resources, Huanggang Normal University, Huanggang, China, [3]Department of Chemistry, Faculty of Science, University of Hradec Kralove, Hradec Kralove, Czechia

OPEN ACCESS

Edited by:
Italo F. Cuneo,
Pontificia Universidad Católica de Valparaíso, Chile

Reviewed by:
Laura Fernandez Bidondo,
Consejo Nacional de Investigaciones Científicas y Técnicas (CONICET), Argentina
Reza Darvishzadeh,
Urmia University, Iran

***Correspondence:**
Qiang-Sheng Wu
wuqiangsh@163.com

[†]These authors share first authorship

Specialty section:
This article was submitted to Plant Abiotic Stress, a section of journal Frontiers in Plant Science

Received: 13 July 2021
Accepted: 08 September 2021
Published: 06 October 2021

Citation:
Liang S-M, Zhang F, Zou Y-N, Kuča K and Wu Q-S (2021) Metabolomics Analysis Reveals Drought Responses of Trifoliate Orange by Arbuscular Mycorrhizal Fungi With a Focus on Terpenoid Profile. Front. Plant Sci. 12:740524. doi: 10.3389/fpls.2021.740524

Soil water deficit seriously affects crop production, and soil arbuscular mycorrhizal fungi (AMF) enhance drought tolerance in crops by unclear mechanisms. Our study aimed to analyze changes in non-targeted metabolomics in roots of trifoliate orange (*Poncirus trifoliata*) seedlings under well-watered and soil drought after inoculation with *Rhizophagus intraradices*, with a focus on terpenoid profile. Root mycorrhizal fungal colonization varied from 70% under soil drought to 85% under soil well-watered, and shoot and root biomass was increased by AMF inoculation, independent of soil water regimes. A total of 643 secondary metabolites in roots were examined, and 210 and 105 differential metabolites were regulated by mycorrhizal fungi under normal water and drought stress, along with 88 and 17 metabolites being up-and down-regulated under drought conditions, respectively. KEGG annotation analysis of differential metabolites showed 38 and 36 metabolic pathways by mycorrhizal inoculation under normal water and drought stress conditions, respectively. Among them, 33 metabolic pathways for mycorrhization under drought stress included purine metabolism, pyrimidine metabolism, alanine, aspartate and glutamate metabolism, etc. We also identified 10 terpenoid substances, namely albiflorin, artemisinin (–)-camphor, capsanthin, β-caryophyllene, limonin, phytol, roseoside, sweroside, and α-terpineol. AMF colonization triggered the decline of almost all differential terpenoids, except for β-caryophyllene, which was up-regulated by mycorrhizas under drought, suggesting potential increase in volatile organic compounds to initiate plant defense responses. This study provided an overview of AMF-induced metabolites and metabolic pathways in plants under drought, focusing on the terpenoid profile.

Keywords: citrus, metabolite, mycorrhiza, terpenoid, water stress

INTRODUCTION

Crops are often subjected to abiotic stresses in the process of the growth and development, while abiotic stress also activates relevant functional genes and metabolic pathways to mitigate the stress damage of crops (Giordano et al., 2021). Plant stress regulation is a complex network, and it is difficult to fully analyze the responsive mechanisms of plants to stress by studying a single gene or metabolic pathway alone (Li et al., 2017; Yang et al., 2021). Metabolomics is a powerful tool to assess the whole change of organisms at the metabolite level (Alseekh et al., 2018) and also is essential for understanding the chemical signals during plant growth and development (Carrera et al., 2021). In the analysis of metabolomics, metabolites are small molecules that are formed and/or altered during metabolisms, and changes of metabolite profiles can establish a close relationship between genotype and phenotype and also reveal the plant–environment interaction comprehensively and systematically (Bernardo et al., 2019; Carrera et al., 2021).

Arbuscular mycorrhizal fungi (AMF), subphylum Glomeromycotina of the phylum Mucoromycota, are the most widely distributed mycorrhizal fungi in soil, and can colonize the root of host plants to establish arbuscular mycorrhizal symbionts (Kokkoris et al., 2020). Mycorrhizal fungi establish a well-developed network of extraradical mycelium outside the root system, which is directly involved in water and nutrient uptake and therefore responds to various environmental stresses including drought (Meng et al., 2020; Malhi et al., 2021). AMF-induced enhancement of drought tolerance is involved in many metabolic processes, such as proline, indoleacetic acid, polyamines, fatty acids, aquaporins, antioxidant defense system, H^+-ATPase, rhizospheric microenvironment, and so on (Wu et al., 2019; He et al., 2020; Khalil and El-Ansary, 2020; Sheteiwy et al., 2021; Zou et al., 2021; Cheng et al., 2021a,b,c). Metabolomics analysis has been applied to reveal mycorrhiza-associated metabolite changes following AMF inoculation (Rivero et al., 2015). However, very few studies have attempted to use metabolomics tool to analyze metabolite changes caused by AMF inoculation under abiotic stress (e.g., drought and salinity) conditions (Rivero et al., 2018; Bernardo et al., 2019; Yang et al., 2020). For example, Yang et al. (2020) revealed that under saline conditions, inoculation with *Rhizophagus intraradices* induced changes in amino acids, organic acids, flavonoids, sterols, and hormones in *Puccinellia tenuiflora* plants to improve osmoregulation, maintain cell membrane stability, and enhance antioxidant systems. In wheat, *Funneliformis mosseae* mainly triggered sugars, lipids, and oleuropein lactones involved in stress mechanisms under drought stress (Bernardo et al., 2019). These limited studies still revealed that arbuscular mycorrhizal symbionts responded to stress by regulating metabolic plasticity (Rivero et al., 2018).

Terpenoids are the most diverse and widely distributed class of secondary metabolites present in plants. Terpenoids are volatile, serve as mediators of communication between plants and other organisms, and are biologically and ecologically important for the plants' own reproduction and defense (Jiang, 2012). They guarantee the survival of plants in stressed environments by performing several functions, such as protecting plant tissues from pathogens or herbivores and helping reproduction by attracting pollinators or seed dispersers (Quan, 2013). Severe drought dramatically increased total monoterpenes and resin acids in *Pinus sylvestris* and *Picea abies* seedlings (Turtola et al., 2003). In an aromatic plant *Tanacetum vulgare*, root terpenoids were obviously induced by drought, and such increase in root terpenoids would serve as more storage of resources for regrowth (Kleine and Müller, 2014).

Earlier studies have shown that secondary metabolites of many hosts such as terpenoids, flavonoids, and alkaloids were regulated by AMF inoculation under drought conditions (Bernardo et al., 2019). In *P. tenuiflora* seedlings, AMF inoculation under saline conditions significantly altered the relative concentrations of various metabolites, including amino acids, amines, carbohydrates, polyols, phytohormone, steroids, nucleic acids, fatty acids, flavonoids, organic acids, but terpenoids were not reported (Yang et al., 2020). However, in two wheat cultivars, *F. mosseae* caused the change of terpenoids, along with the up-regulation of a limonene-1,2-doil and (20S)-ginsenoside Rh2 and the down-regulation of both 7-deoxyloganate and hemigossypol-6-methyl ether (Bernardo et al., 2019). Kaur and Suseela (2020) reviewed the changes in primary and secondary metabolites of plants induced by mycorrhizal fungi and concluded that host terpene metabolism is specific to the host-associated AMF and terpene species. It was shown that sesquiterpenoid cyclohexenone derivatives could be induced to increase by *Glomus intraradices* (Maier et al., 1997) in the member of Poaceae, but sesquiterpenoid cyclohexenone glycoside was not induced by AMF under biotic and abiotic stresses. Various volatile terpenoids in host plants were also induced by AMF, resulting in an increased emission of these compounds in response to the environment (Rapparini et al., 2007; Fontana et al., 2009). It seems that terpenoids could be regulated by AMF inoculation under stress. Because of the wide variety of terpenoids, metabolomics is the way to clearly outline the response pattern for mycorrhizal inoculation under drought conditions, while how mycorrhizas respond to drought through changes of terpenoid profile is unclear.

The aim of this study was to comprehensively analyze the changes in the metabolome of citrus (a drought-sensitive industrial crop) by AMF inoculation under soil well-watered and soil drought stress through non-targeted metabolomics, with a focus on the response of terpenoids in the differential metabolites to reveal the mechanisms by which mycorrhizas enhance plant drought tolerance.

MATERIALS AND METHODS

Mycorrhizal Inoculum

An arbuscular mycorrhizal fungus, *R. intraradices* (N.C. Schenck & G.S. Smith) C. Walker & A. Schüßler, was used. The mycorrhizal fungal strain (FLR12, Myke®PRO) was provided by the Premier Tech Ltd. (Quebec, Canada), which is a company for the production of commercial mycorrhizal inoculants. The Myke FLR12 strain of *R. intraradices* was

designed for the improved growth of annuals and perennials and also presented positive effects on plant growth performance of trifoliate orange (*Poncirus trifoliata* L. Raf., a citrus rootstock; Cheng et al., 2019). The purchased fungal strain was proliferated by employing white clover as the host plant in pots under the condition of 900 μmol/m^2/s photo density, 28°C/20°C day/night temperatures, and 68% relative air humidity. After 3 months, the white clover plants were harvested, the aboveground parts were removed, and the roots and potting substrates were collected. The roots were cut, mixed well with the growth substrate, dried naturally for 5 days, and collected as mycorrhizal fungal inoculum. Thus, the mycorrhizal inoculum contained AMF-colonized root segments, spores, sporocarps, and mycorrhizal mycelium. Harvested inocula were kept at 4°C for a maximum of 4 months. Prior to the application of AMF inocula, we used sucrose gradient centrifugation (Brundrett et al., 1994) to isolate spores in the inocula and observed 19 spores/g inoculum.

Experimental Design

A 2^2 experimental design was used for this experiment. One factor was AMF inoculations with and without *R. intraradices*; the other factor was soil water regimes, including well-watered (75% of maximum field water holding capacity) and drought stress (55% of maximum field water holding capacity). As a result, there were four treatments in the experiment: the non-inoculated seedlings (non-AMF) under well-watered, the inoculated seedlings (AMF) under well-watered, the non-inoculated seedlings under drought stress, and the inoculated seedlings under drought stress. Each treatment was replicated 8 times, with a total of 32 pots.

Plant Culture

Trifoliate orange seeds were sterilized by 75% alcohol solutions for 5 min, rinsed with distilled water three times, and germinated in sterile sand in an incubator at 28°C/20°C day/night temperature and relative air humidity of 80%. When the seedlings developed four leaves, the seedlings were transplanted into a 2.3-L plastic pot pre-filled with 2.8 kg of autoclaved mixture with soil and sand (1:1, v:v). At transplanting, 100 g of mycorrhizal fungal inoculums was applied into the pot as the AMF treatment, and the non-AMF treatment was correspondingly mixed with an equal amount of autoclaved mycorrhizal inocula. After transplanting, these seedlings were exposed to the condition of 900 μmol/m^2/s photo density, 28°C/20°C day/night temperatures, and 68% relative air humidity and also grew in soil well-watered regime for 11 weeks before soil drought treatment. 3 days prior to soil drought stress, selected pots were stopped from watering and allowed to reach the designed soil moisture content for drought stress. Subsequently, half of the inoculated and non-inoculated plants were subjected to soil drought stress treatment for 9 weeks, and the remaining plants were still grown under soil well-watered regime conditions for 9 weeks. The reduced water of pots was supplemented by weighing daily at 18:00 pm. This study was conducted for 20 weeks.

Determination of Root Mycorrhizal Colonization and Plant Biomass

At harvest plants were divided into shoots and roots, weighted and frozen with liquid nitrogen and immediately stored at−80°C for subsequent analysis.

Five 1-cm-long root segments were cut from each plant, cleared in 10% KOH solution at 95°C for 1.5 h, and stained with 0.05% trypan blue in lactophenol (Phillips and Hayman, 1970). The arbuscular mycorrhizal structure of roots was observed under a light microscope, and the root mycorrhizal colonization rate was estimated according to the following formula:

Extraction of Metabolome Samples

Root tissues were vacuum freeze-dried, and the dried samples were ground into a homogenous powder. Subsequently, 100 mg of the powder was extracted with 70% methanol at 4°C overnight, vortexing and shaking three times during the extracted process. The samples were centrifuged at 10,000 × g/min for 10 min, and the supernatant was filtered through a microporous membrane (0.22 μm), followed by LC–MS/MS analysis.

LC–MS/MS Analysis

Data acquisition systems included Ultra Performance Liquid Chromatography (UPLC; Shim-pack UFLC SHIMADZU CBM20A, Shimadzu Corporation, Kyoto, Japan[1]) and tandem mass spectrometry (Applied Biosystems 6,500 QTRAP, Thermo Fisher Scientific, Waltham, United States).[2] Analytical conditions were as follows: (1) Chromatographic column was Waters ACQUITY UPLC HSS T3 C18 with 1.8 μm and 2.1 mm × 100 mm; (2) mobile phase consisted of ultrapure water (with 0.04% acetic acid added) for the aqueous phase and acetonitrile (with 0.04% acetic acid added) for the organic phase; (3) elution gradient consisted of water and acetonitrile with 95:5 (v/v) at 0–10 min, 5:95 at 11–12 min, 95:5 at 13–15 min; and (4) a flow rate of 0.4 ml/min, a column temperature of 40°C, and an injection volume of 5 μl.

In the LC–MS/MS system, the main parameters of the linear ion trap and triple quadrupole included: the electrospray ionization at 550°C, the mass spectrometry at 5500 V, the curtain gas at 25 psi, the collision-activated dissociation parameters at a high grade. In the triple quadrupole, each ion pair was scanned and detected according to the optimized declustering potential and collision energy. The assay data were analyzed and processed using the Analyst 1.6.3 (AB Sciex, Foster, California, United States) software.

Metabolite Characterization and Quantification

Based on the self-built metware database and the public database of metabolite information, the primary and secondary spectra of mass spectrometry were analyzed qualitatively. The public database of metabolites included the MassBank,[3] the KNAPSAcK,[4]

[1]http://www.shimadzu.com.cn/
[2]https://www.thermofisher.com/us/en/home/brands/applied-biosystems.html
[3]http://www.massbank.jp/
[4]http://kanaya.naist.jp/KNApSAcK/

the HMDB,[5] the MoTo DB,[6] and the METLIN.[7] Metabolite quantification was accomplished using the multiple reaction monitoring mode of triple quadrupole mass spectrometry. After obtaining the metabolite spectra for each sample, the peak areas of the mass spectra of all substances were integrated and corrected for the mass spectra of the same metabolite in different samples. The data were formatted in logarithmic transformation plus centralization using a SIMCA software (V14.1, Sartorius Stedim Data Analytics AB, Umea, Sweden) and then analyzed by automated modeling (Wiklund et al., 2008).

Analysis of Metabolites

Principal component analysis (PCA) was carried out by SIMCA-P software (Umetrics AB, Kinnelon, NJ, United States). The statistical method of orthogonal projections to latent structures-discriminant analysis (OPLS-DA) was utilized to analyze the results of metabolites and to obtain more credible information about the correlation between metabolite group differences and experimental comparison groups. The OPLS-DA modeling analysis was performed on the first principal component. The validity of the model was assessed by the RY (interpretability of the model for categorical variable Y) and Q (predictability of the model) obtained after cross-validation.

Differential Metabolite Screening

By considering the results of both multivariate and univariate statistical analysis methods, we observed the data from different perspectives and draw conclusions, in order to avoid false positive errors or model overfitting caused by using only one type of statistical analysis method. The differential metabolites were defined as per the Student's t-test at $p < 0.05$, along with >1 of the variable importance in the projection of the first principal component of the OPLS-DA model.

KEGG Annotation of Differential Metabolites and Metabolic Pathway Analysis

In this study, all the pathways mapped by the differential metabolites of *Citrus sinensis*, including energy metabolism, substance transport, signaling, and cell cycle regulation, were compiled, in terms of the Kyoto Encyclopedia of Genes and Genomes Pathway database.[8]

Statistical Analysis

Data were analyzed for ANOVA using the SAS software. Bonferroni correction test at 0.05 levels was used to compare the significant differences between treatments.

[5]http://www.hmdb.ca/
[6]https://apbioinf002.wur.nl/
[7]http://metlin.scripps.edu/index.php
[8]http://www.kegg.jp/kegg/pathway.html

RESULTS

Changes in Mycorrhizal Growth

No mycorrhizal colonization was observed in any of the roots of the non-inoculated trifoliate orange plants, and the root colonization of inoculated plants varied from 70 to 85% (**Figure 1A**). The soil drought treatment significantly reduced root AMF colonization by 17.6%, compared to the well-watered treatment.

Changes in Plant Biomass

Drought inhibited root biomass production of inoculated trifoliate orange seedlings, whereas inoculation with AMF significantly promoted shoot and root biomass, independent of soil moisture conditions (**Figures 1B,C**). Compared to non-AMF inoculation, *R. intraradices* inoculation significantly increased shoot and root biomass, as evidenced by a significant increase of 141.27 and 68.52% in shoot and root biomass, respectively, under well-watered conditions and by an increase of 145.89 and 74.11% under drought conditions, respectively.

PCA Analysis of Root Metabolites

A total of 643 secondary metabolites in roots were found in this study. PCA was performed on the quantitative results of metabolites from these samples (including quality control samples; **Figure 2**). A total of 2 principal components were obtained, where the X-axis represented the first principal component, and the Y-axis represented the second principal component. The quality control samples (mix) were clustered together, indicating that the sample mass spectrometry monitoring analysis was stable and the data were reproducible and credible. Samples were clustered across treatments, with the exception of a sample from non-inoculated seedlings under drought stress and a sample from inoculated seedlings under well-watered, which were deviant, probably due to differences in the samples themselves. However, in general, the sample treatments were clearly differentiated, with the first principal component being able to clearly distinguish between AMF inoculation and non-AMF inoculation.

Orthogonal Partial Least Squares-Discriminant Analysis

Orthogonal Partial Least Squares-Discriminant Analysis is a regression method based on characteristic variables. Based on the analysis of OPLS-DA, we obtained reliable information on the degree of correlation between group differences in metabolites and experimental groups, except the orthogonal variables in metabolites not correlated with categorical variables (**Figure 3**). The slope of the OPLS-DA model was positive, and R2Y was close to 1 and Q2 was close to 0 for both the comparison between well-watered and drought stress treatments and between inoculations with AMF and non-AMF, indicating that the model was stable. This indicated that for the results of this metabolomic test, the treatments were grouped very well with significant differences between groups.

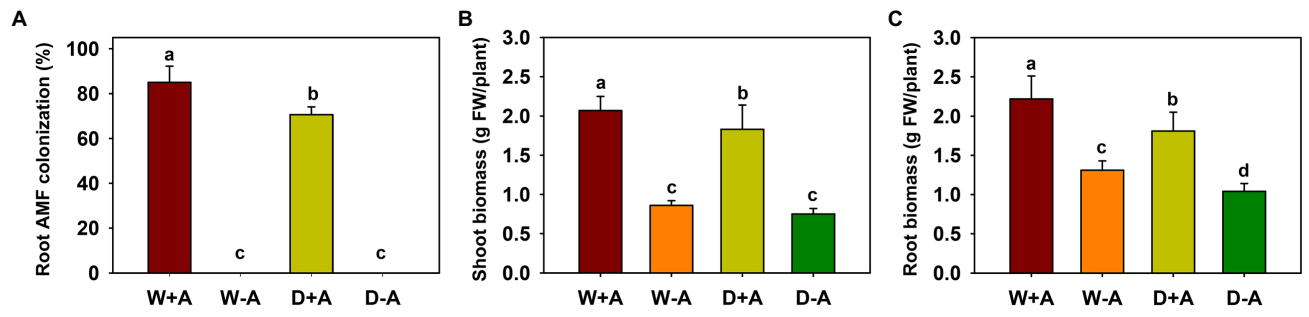

FIGURE 1 | Changes in root mycorrhizal colonization **(A)**, shoot biomass **(B)**, and root biomass **(C)** of trifoliate orange seedlings under well-watered and drought stress conditions after inoculation with *Rhizophagus intraradices*. Different letters above the bar indicate significant differences at $p < 0.05$. Abbreviation: W + A, inoculation with *R. intraradices* under well-watered conditions; W-A, inoculation without *R. intraradices* under well-watered conditions; D + A, inoculation with *R. intraradices* under drought stress conditions; D-A, inoculation without *R. intraradices* under drought stress conditions.

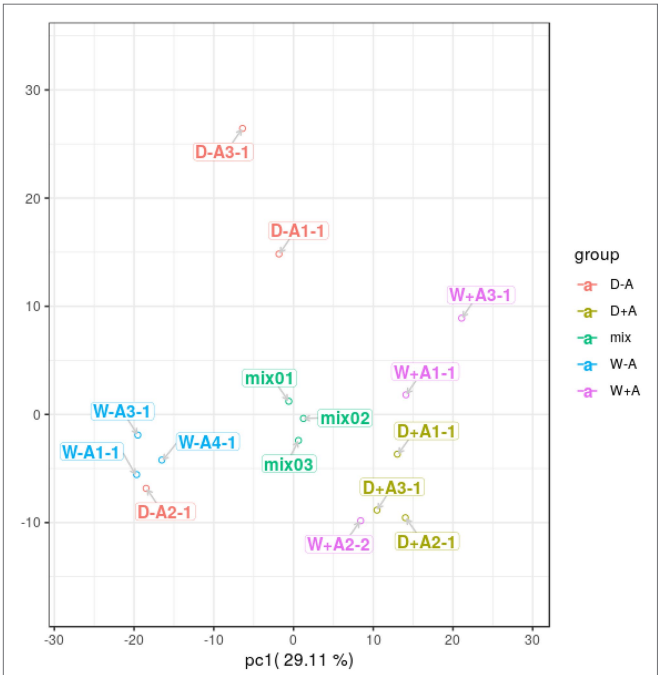

FIGURE 2 | Principal component analysis of metabolites in roots of trifoliate orange seedlings under well-watered and drought stress conditions after inoculation with *Rhizophagus intraradices*. Abbreviation: W + A, inoculation with *R. intraradices* under well-watered conditions; W-A, inoculation without *R. intraradices* under well-watered conditions; D + A, inoculation with *R. intraradices* under drought stress conditions; D-A, inoculation without *R. intraradices* under drought stress conditions; mix, quality control samples.

Screening for Differential Metabolites in Roots

A total of 643 metabolites were compared and screened for differential metabolites between treatments (screening conditions: VIP > 1; $p < 0.05$). The 50 differential metabolites were screened in the non-inoculated seedlings under drought stress versus well-watered, of which 14 differential metabolites were significantly up-regulated and 36 metabolites were significantly down-regulated (**Figure 4A**). Similarly, 76 differential metabolites were screened in the inoculated seedlings under drought stress versus well-watered, of which 39 metabolites were significantly up-regulated and 37 metabolites were down-regulated (**Figure 4B**). We also screened 210 differential metabolites under well-watered conditions after AMF inoculation, of which 86 metabolites were substantially up-regulated and 124 metabolites were down-regulated (**Figure 4C**). Under drought stress conditions, AMF inoculation caused 105 differential metabolites, of which 88 and 17 metabolites were up-regulated and down-regulated, respectively (**Figure 4D**).

KEGG Annotation of Differential Metabolites in Roots

KEGG annotation analysis of differential metabolites showed four, thirty-six, thirty-eight, and thirty-six differential metabolic pathways in the non-inoculated seedlings under drought stress versus well-watered, the inoculated seedlings under drought stress versus well-watered, under well-watered conditions by AMF inoculation versus non-AMF inoculation, and under drought stress conditions by AMF inoculation versus non-AMF inoculation, respectively (**Supplementary Figures 1–4**). Under well-watered conditions, AMF inoculation caused the differential metabolites associated with ABC transporters, biosynthesis of amino acids, nicotinate and nicotinamide metabolism, glycine, serine and threonine metabolism, arginine and proline metabolism, amino sugar and nucleotide sugar metabolism, cysteine and methionine metabolism, histidine metabolism, tryptophan metabolism, beta-alanine metabolism, photosynthesis, arginine biosynthesis, alanine, aspartate and glutamate metabolism, valine, leucine and isoleucine biosynthesis, lysine degradation, tyrosine metabolism, etc (**Supplementary Figure 3**). Under drought stress conditions, AMF triggered differential metabolites involved in biosynthesis of amino acids, arginine biosynthesis, glycine, serine and threonine metabolism, cysteine and methionine metabolism, arginine and proline metabolism, niacin and nicotinamide metabolism, lysine degradation, histidine metabolism, tyrosine metabolism, carbon fixation in photosynthetic organisms, N metabolism, etc (**Supplementary Figure 4**).

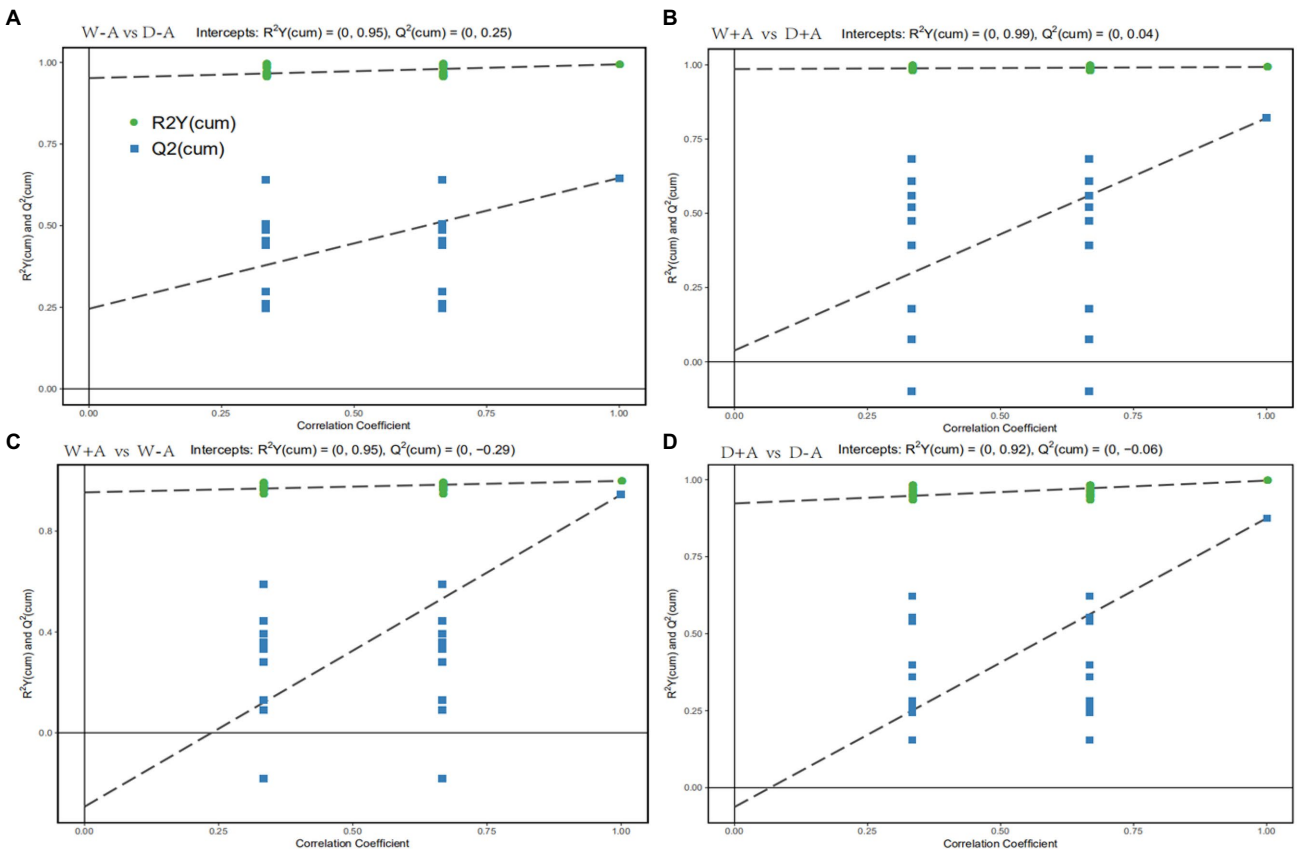

FIGURE 3 | OPLS-DA of metabolites in roots of trifoliate orange seedlings under well-watered and drought stress conditions after inoculation with *Rhizophagus intraradices*. Abbreviation: W + A, inoculation with *R. intraradices* under well-watered conditions; W-A, inoculation without *R. intraradices* under well-watered conditions; D + A, inoculation with *R. intraradices* under drought stress conditions; D-A, inoculation without *R. intraradices* under drought stress conditions; mix, quality control samples.

Analysis of Metabolic Pathways in Differential Metabolites in Roots

In this study, through comprehensive analysis (including enrichment analysis and topological analysis) of the pathways in which the differential metabolites were located, further screening of the pathways could be conducted to find the key pathways with the highest correlation with the difference of metabolites. Based on the comprehensive analysis, differential metabolites of non-inoculated plants under drought stress versus well-watered conditions were mainly annotated to fourteen metabolic pathways, including pyrimidine metabolism, nicotinate and nicotinamide metabolism, glutathione metabolism, arginine and proline metabolism, alanine, aspartate and glutamate metabolism, etc., among them L-glutamic acid was involved in seven metabolic pathways simultaneously (**Figure 5A**). In the inoculated seedlings, compared with well-watered treatment, drought treatment triggered differential metabolites annotated to thirty-one metabolic pathways (e.g., starch and sucrose metabolism and alanine, aspartate and glutamate metabolism), of which L-aspartic acid was involved in ten of these metabolic pathways as a differential metabolite (**Figure 5B**). Under well-watered conditions, mycorrhizal inoculation caused the differential metabolites annotated to thirty-eight metabolic pathways including pyrimidine metabolism, taurine and hypotaurine metabolism, inositol phosphate metabolism, etc (**Figure 5C**). Under drought stress conditions, the differential metabolites were annotated to thirty-three metabolic pathways for mycorrhization compared to non-mycorrhization, including purine metabolism, pyrimidine metabolism, alanine, aspartate and glutamate metabolism, etc (**Figure 5D**).

Changes in Terpenoid Profiles in Roots

Among the differential metabolites, we identified ten terpenoid substances, namely albiflorin, artemisinin (−)-camphor, capsanthin, β-caryophyllene, limonin, phytol, roseoside, sweroside, and α-terpineol, with sweroside belonging to terene and the other nine to terpene (**Table 1**). We also found that in non-inoculated plants, drought triggered a significant accumulation of phytol up to 2.62-fold, but significantly inhibited the relative concentrations of capsanthin, β-caryophyllene, and α-terpineol up to 0.58–0.76-fold; in inoculated plants, soil drought only triggered a significant accumulation of sweroside up to 1.63-fold. In addition, under well-watered conditions, AMF inoculation significantly reduced relative concentrations

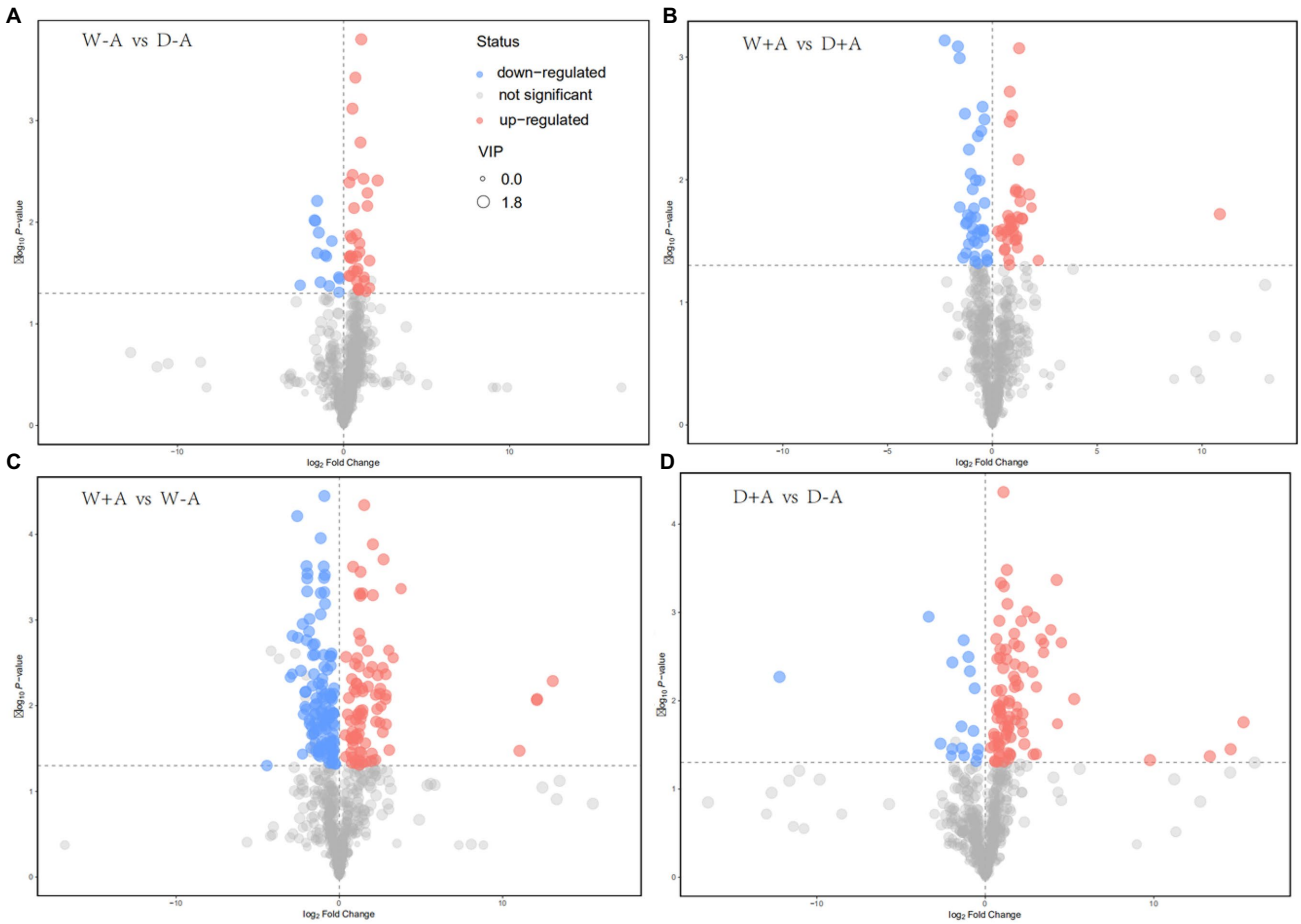

FIGURE 4 | Volcanic map of different metabolites in roots of trifoliate orange seedlings under well-watered and drought stress conditions after inoculation with *Rhizophagus intraradices*. Abbreviation: W + A, inoculation with *R. intraradices* under well-watered conditions; W-A, inoculation without *R. intraradices* under well-watered conditions; D + A, inoculation with *R. intraradices* under drought stress conditions; D-A, inoculation without *R. intraradices* under drought stress conditions; mix, quality control samples.

of capsanthin, α-terpineol, sweroside, limonin, roseoside, albiflorin (−)-camphor, and artemisinin; however, under drought stress conditions, AMF inoculation significantly increased relative concentration of β-caryophyllene, up to 1.78-fold, but significantly reduced relative concentration of phytol, up to 0.38-fold.

DISCUSSION

An important function of arbuscular mycorrhizal symbiosis is to accelerate the growth of the host plant, both under normal and unfavorable environmental conditions (Malhi et al., 2021). Our study also confirmed that *R. intraradices* strongly promoted shoot and root biomass production in trifoliate orange regardless of soil moisture content, and the promoting effect was relatively higher under drought conditions than under well-watered conditions. Zhang et al. (2018) used a device to separate mycorrhizal extraradical hyphae from inoculated trifoliate orange rhizosphere for quantitative estimation of hyphal water absorption rate and found that the hyphal water absorption rate was much higher under soil moisture-limited conditions than under soil moisture-sufficient conditions. This suggests that the improved plant growth of AMF is more important on arid soil than on saturated soil and therefore more attention needs to be paid to mycorrhizas in arid zones (Allen, 2006).

Metabolomic analyses implied changes in root metabolites of trifoliate orange seedlings in response to AMF inoculation. Among them, in non-inoculated plants, 50 differential metabolites were identified and metabolites were predominantly down-regulated. Similarly, in quinoa (without AMF inoculation; *Chenopodium quinoa*), drought stress triggered 60 differential metabolites, 53 of which were down-regulated (Shi et al., 2020); in tall fescue (*Festuca arundinacea*), drought stress caused 282 differential metabolites, 148 of which were down-regulated (Li et al., 2017). However, in the inoculated trifoliate orange plants, 76 differential metabolites were identified, and these metabolites were predominantly up-regulated by drought stress. This result implied an elevated number of differential metabolites and a reversal of the metabolite response pattern from down-regulation (non-inoculated plants) to up-regulation (inoculated plants).

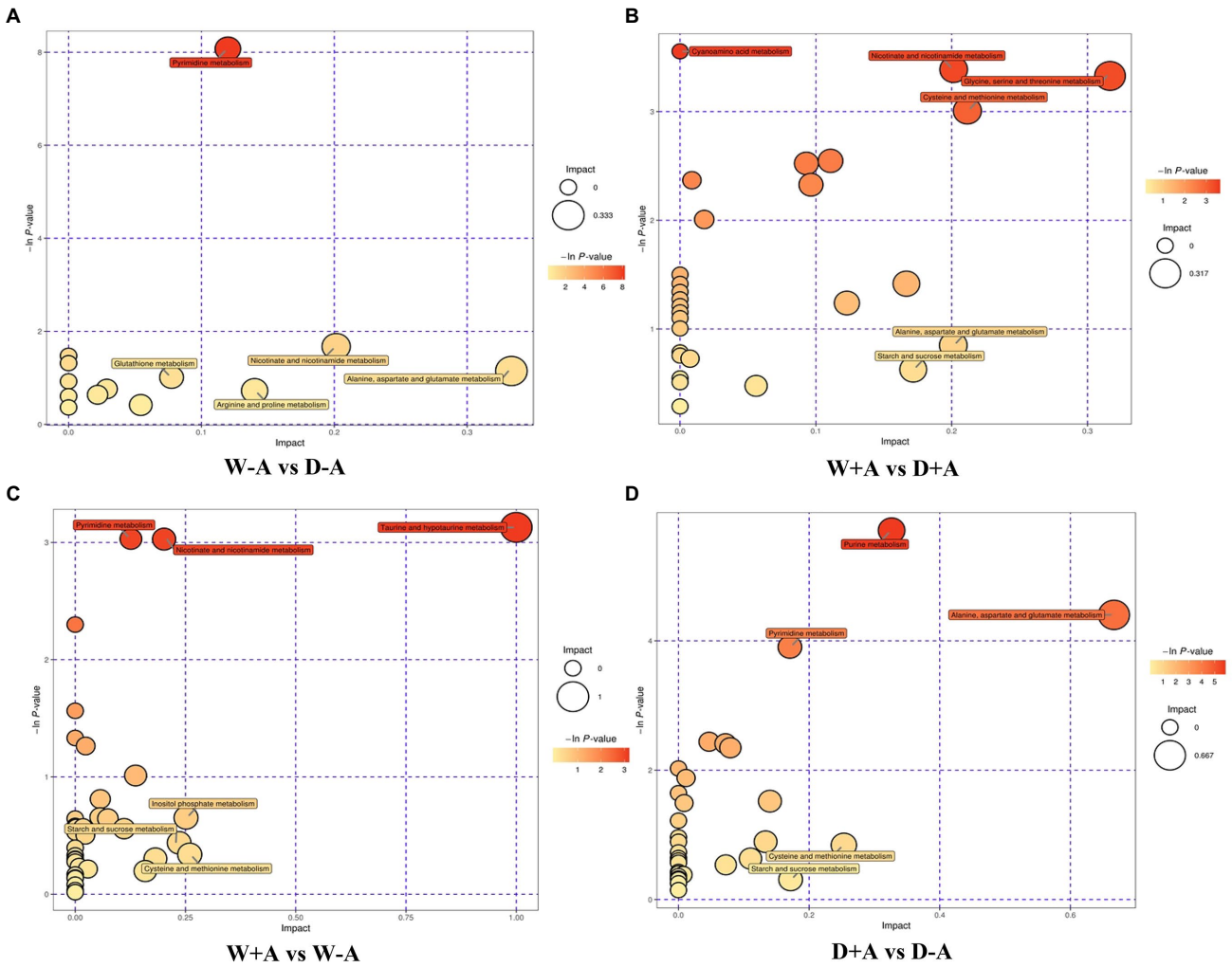

FIGURE 5 | Bubble chart of pathway analysis of different metabolites in different treatment groups of trifoliate orange seedlings under well-watered and drought stress conditions after inoculation with *Rhizophagus intraradices*. Abbreviation: W + A, inoculation with *R. intraradices* under well-watered conditions; W-A, inoculation without *R. intraradices* under well-watered conditions; D + A, inoculation with *R. intraradices* under drought stress conditions; D-A, inoculation without *R. intraradices* under drought stress conditions; mix, quality control samples.

In the analysis of differential metabolite pathway, drought-induced differential metabolites of non-inoculated plants and inoculated plants were annotated to 14 and 31 metabolic pathways, respectively. Among them, non-inoculated plants were dominated by amino acid (e.g., L-glutamic acid) metabolism and inoculated plants were dominated by sugars and amino acids (e.g., L-aspartic acid), showing the different metabolic responses of both. Thus, inoculated plants have stronger metabolic activity in response to drought stress than non-inoculated plants by means of predominant up-regulation, further indicating a higher drought tolerance potential of mycorrhizal plants versus non-mycorrhizal plants.

In addition, the presence of mycorrhizal symbionts strongly stimulated the changes of metabolites in roots of trifoliate orange under well-watered and drought stress, showing, respectively, 210 and 105 differential metabolites, which were predominantly down-regulated under well-watered and up-regulated under soil drought. Yang et al. (2020) also reported more up-regulated differential metabolites of *P. tenuiflora* seedlings under salinity after inoculation with *R. intraradices*. The annotated pathways of these differential metabolites were inconsistent in response to AMF inoculation under well-watered and drought stress, indicating different response mechanisms of mycorrhizal fungi promoting plants under different soil moisture conditions. Among the metabolic pathways, amino acids responded more effectively because they are the basic units of protein synthesis, and changes in them affect protein synthesis and thus interfere with normal physiological metabolism (Yang et al., 2020). AMF induced the increase in 17 amino acids (2-aminoadipic acid (L-homoglutamic acid), N-acetylmethionine, 3-(6-hydroxy-3,4-dioxo-1,5-cyclohexadien-1-yl)-L-alanine, L-glutamic acid, guanidineacetic acid (−)-3-(3,4-dihydroxyphenyl)-2-methylalanine, S-(5′-adenosy)-L-homocysteine, L-pipecolic acid, L-glutamine, L-methionine methyl ester, L-alanine, N-acetyl-L-tyrosine,

TABLE 1 | Changes in relative concentration and fold changes of terpenoids in differential metabolites in roots of trifoliate orange under well-watered (WW) and drought stress (DS) after AMF inoculation.

Comparison of treatments	Terpenoids	Category	KEEG ID	Ionization model	*p*-value	VIP	Fold change
DS vs. WW in non-AMF seedlings	Phytol	Terpene	C01389	[M-H]-	0.039	1.70	2.62↑
	Capsanthin	Terpene	C08584	[M+H]+	0.034	1.55	0.76↓
	β-Caryophyllene	Terpene	C09629	[M+H]+	0.038	1.61	0.58↓
	α-Terpineol	Terpene	C16772	[M+H]+	0.014	1.66	0.71↓
DS vs. WW in AMF seedlings	Sweroside	Terene	C17071	[M+H]+	0.027	1.57	1.63↑
AMF vs. non-AMF under WW	Limonin	Terpene	C03514	[M+H]+	0.003	1.39	0.52↓
	Roseoside	Terpene	–	[M+H]+	0.002	1.32	0.17↓
	Sweroside	Terpene	C17071	[M+H]+	0.008	1.39	0.38↓
	Albiflorin	Terpene	C17457	[M+H]+	0.014	1.30	0.50↓
	(−)-Camphor	Terpene	C00809	[M+H]+	0.025	1.21	0.79↓
	Capsanthin	Terpene	C08584	[M+H]+	0.027	1.22	0.80↓
	Artemisinin	Terpene	C09538	[M+H]+	0.032	1.21	0.61↓
	α-Terpineol	Terpene	C16772	[M+H]+	0.008	1.29	0.70↓
AMF vs. non-AMF under DS	Phytol	Terpene	C01389	[M-H]-	0.034	1.53	0.38↓
	β-Caryophyllene	Terpene	C09629	[M+H]+	0.001	1.60	1.78↑

↑ *and* ↓ *indicate that the variable is increased or decreased.*

N-acetylaspartate, phenylalanine-phenylalanine, S-(5′-adenosyl)-L-methionine, 3-hydroxy-3-methylpentane-1,5-dioic acid, and glutamic acid) and derivatives and the reduction of 3 amino acids and derivatives (3-(2-naphthyl)-D-alanine, aspartic acid-phenylalanine, and L-cysteine) under drought stress conditions. Bernardo et al. (2019) also identified 10 differential amino acids in drought-stressed wheat after AMF inoculation, 7 of which (4-amino-2-methyl-5-phosphomethylpyrimidine, 3-phospho-hydroxypyruvate, imidazole acetol-phosphate, penicillamine, L-methionine/S-ethyl-L-cysteine, O-phospho-L-tyrosine, and 3′-deamino-3′-oxonicotianamine) were up-regulated, and three amino acids (2-amino-3-oxobutanoate, N-acetyl-DL-methionine, and cyclogutamate) were down-regulated. In *P. tenuiflora* seedlings subjected to saline stress, AMF inoculation positively promoted the accumulation of 10 amino acids and amines (Yang et al., 2020). Salvioli et al. (2012) revealed the increase in the amino acid abundance in tomato fruits after inoculation with *G. mosseae.* In white clover, *R. intraradices* accelerated leaf glutamate, aspartate, arginine, and ornithine concentrations, which was associated with changes in N-assimilated enzyme activities (Xie et al., 2021). Mycorrhizal symbiosis accelerated the uptake of various amino acids in *Sorghum bicolor* such as phenylalanine, asparagine, arginine, tryptophan, etc., and the uptake of such neutral or positively charged amino acids was higher than that of negatively charged amino acids (Whiteside et al., 2012). In addition, the increase in amino acids under mycorrhization may originate from the synthesis of mycorrhizal fungi (Govindarajulu et al., 2005). More amino acids were accumulated in mycorrhizal plants after stress, implying more protein synthesis under adversity. This facilitates mycorrhizalized plants to further improve osmoregulation, maintain cytoplasmic membrane permeability and nutrients, and thus enhance the response to stress signals (Teixeira et al., 2020).

Soil drought strongly affected the terpenoid content of plants, usually showing an increasing trend in total terpenes (Turtola et al., 2003; Jiang, 2012). In our study, drought stress induced a significant accumulation of phytol in roots of non-inoculated plants as well as sweroside in inoculated plants, while inhibited the decrease in capsanthin, caryophyllene, and terpineol on non-inoculated plants. Similarly, Podda et al. (2019) also revealed the increase in phytol in *Brassica oleracea* plants in response to drought stress. It seems that phytol, a product of chlorophyll degradation, served as an important indicator of the state of chlorophyll. Other studies in *C. aurantium*, *Eucalyptus camaldulensis*, and *Thymus transcaucasicus* showed diverse changes in metabolites under environmental stresses (drought, salinity, and temperature stresses) conditions, along with the reduction of metabolites more commonly (Eirini et al., 2017; Manukyan, 2019; Amrutha et al., 2021). Thus, these metabolite changes are an adaptive response mechanism in trifoliate orange under drought stress.

The results of the present study showed that AMF inoculation significantly inhibited the relative concentrations of various differential metabolites in almost all cases, except for β-caryophyllene which was increased. Bernardo et al. (2019) also reported the increase of two terpenoids (a limonene-1,2-doil and (20S)-ginsenoside Rh2) and the reduction of another terpenoids (7-deoxyloganate and hemigossypol-6-methyl ether) in wheat plants under drought stress after the colonization by *F. mosseae*. We speculated that mycorrhizal plants possessed more biomass including roots than non-mycorrhizal plants, so there was a dilution effect, which led to the decrease in differential metabolites. Additionally, mycorrhizal fungi may have promoted effects on the amount of volatilization and release of terpenoids under drought conditions. Many terpenes are volatile organic compounds (VOCs), and a small number of studies also displayed that mycorrhizal fungal colonization increased the emission of the green leaf volatile (Z)-3-hexenyl acetate from *Plantago lanceolata* (Fontana et al., 2009) and the emission of limonene and artemisia ketone from *Artemisia annua* (Rapparini et al., 2007). The emission of these terpenoids is almost comparable to the mechanical damage and herbivore damage to plants. These suggest that mycorrhiza-induced reduction of terpenoids may lead to an increased emission of VOCs. VOCs are an indirect way for plants to attract natural enemies to defend against insect herbivores as well as for

VOCs to play a signal to initiate plant defense response (Fontana et al., 2009). More work needs to be carried out around the changes in the emission of VOCs by mycorrhizal versus non-mycorrhizal plants under adversity.

Our results also displayed that AMF inoculation significantly reduced the relative concentration of phytol in roots of trifoliate orange under drought stress, but not under well-watered. In fact, in the process of abiotic stress, a certain amount of chlorophyll is disintegrated, leading to a substantial accumulation of free phytol (Podda et al., 2019). Zhang et al. (2020) also found significantly higher chlorophyll levels in drought-stressed trifoliate orange after inoculation with *F. mosseae*. This implies that mycorrhizal plants have a higher chlorophyll content and therefore reduced phytol levels under drought conditions. It concludes that mycorrhizal plants under drought stress are characterized with a low level of chlorophyll degradation and thus maintain a relatively high accumulation of photosynthates, which is positive for the drought tolerance of plants.

DATA AVAILABILITY STATEMENT

The original contributions presented in the study are included in the article/**Supplementary Material**, further inquires can be directed to the corresponding author.

AUTHOR CONTRIBUTIONS

FZ and Q-SW conceived and designed the experiment. FZ performed the experiments. S-ML, Y-NZ, Q-SW, and KK analyzed the data. S-ML, FZ, and KK prepared the Figures. S-ML wrote the paper. Q-SW and KK revised the paper. All authors contributed to the article and approved the submitted version.

FUNDING

This study was supported by the National Key Research and Development Program of China (2018YFD1000303) and the Plan in Scientific and Technological Innovation Team of Outstanding Young Scientists, Hubei Provincial Department of Education, China (T201604). The authors are also grateful to Excelence project PrF UHK 2011/2021-2022 for the financial support.

SUPPLEMENTARY MATERIAL

The Supplementary Material for this article can be found online at: https://www.frontiersin.org/articles/10.3389/fpls.2021.740524/full#supplementary-material

REFERENCES

Allen, M.F. (2006). "Water dynamics of mycorrhizas in arid soils," in *Fungi in Biogeochemical Cycles*, ed. Gadd, G.M. (Cambridge, UK: Cambridge University Press), 74–97. doi:10.1017/CBO9780511550522.005

Alseekh, S., Bermudez, L., De Haro, L. A., Fernie, A. R., and Carrari, F. (2018). Crop metabolomics: From diagnostics to assisted breeding. *Metabolomics* 14, 1–13. doi: 10.1007/s11306-018-1446-5

Amrutha, S., Parveen, A. B. M., Muthupandi, M., Vishnu, K., Bisht, S. S., Sivakumar, V., et al. (2021). Characterization of *Eucalyptus camaldulensis* clones with contrasting response to short-term water stress response. *Acta Physiol. Plant.* 43, 1–13. doi: 10.1007/s11738-020-03175-0

Bernardo, L., Carletti, P., Badeck, F. W., Rizza, F., Morcia, C., Ghizzoni, R., et al. (2019). Metabolomic responses triggered by arbuscular mycorrhiza enhance tolerance to water stress in wheat cultivars. *Plant Physiol. Bioch.* 137, 203–212. doi: 10.1016/j.plaphy.2019.02.007

Brundrett, M., Melville, L., and Peterson, L. (1994). *Practical Methods in Mycorrhiza Research*. University of Guelph, Guelph, Ontario, Canada: Mycologue Publications.

Carrera, F. P., Noceda, C., Maridueña-Zavala, M. G., and Cevallos-Cevallos, J. M. (2021). Metabolomics, a powerful tool for understanding plant abiotic stress. *Agronomy* 11:824. doi: 10.3390/agronomy11050824

Cheng, H. Q., Fan, Q. F., and Wu, Q. S. (2019). Effects of indigenous and exotic *Rhizoglomus intraradices* strains on trifoliate orange seedlings. *Biotechnology* 18, 42–48. doi: 10.3923/biotech.2019.42.48

Cheng, H. Q., Giri, B., Wu, Q. S., Zou, Y. N., and Kuča, K. (2021a). Arbuscular mycorrhizal fungi mitigate drought stress in citrus by modulating root microenvironment. *Arch. Agron. Soil Sci.*, doi: 10.1080/03650340.2021.1878497

Cheng, H. Q., Zou, Y. N., Wu, Q. S., and Kuča, K. (2021b). Arbuscular mycorrhizal fungi alleviate drought stress in trifoliate orange by regulating H^+-ATPase activity and gene expression. *Front. Plant Sci.* 12:659694. doi: 10.3389/fpls.2021.659694

Cheng, X. F., Wu, H. H., Zou, Y. N., Wu, Q. S., and Kuča, K. (2021c). Mycorrhizal response strategies of trifoliate orange under well-watered, salt stress, and waterlogging stress by regulating leaf aquaporin expression. *Plant Physiol. Biochem.* 162, 27–35. doi: 10.1016/j.plaphy.2021.02.026

Eirini, S., Paschalina, C., Ioannis, T., and Kortessa, D. T. (2017). Effect of drought and salinity on volatile organic compounds and other secondary metabolites of *Citrus aurantium* leaves. *Nat. Prod. Commun.* 12, 193–196.

Fontana, A., Reichelt, M., Hempel, S., Gershenzon, J., and Unsicker, S. B. (2009). The effect of arbuscular mycorrhizal fungi on direct and indirect defense metabolites of *Plantago lanceolata* L. *J. Chem. Ecol.* 35, 833–843. doi: 10.1007/s10886-009-9654-0

Giordano, M., Petropoulos, S. A., and Rouphael, Y. (2021). Response and defence mechanisms of vegetable crops against drought, heat and salinity stress. *Agriculture* 11:463. doi: 10.3390/agriculture11050463

Govindarajulu, M., Pfeffer, P. E., Jin, H., Abubaker, J., Douds, D. D., Allen, J. W., et al. (2005). Nitrogen transfer in the arbuscular mycorrhizal symbiosis. *Nature* 435, 819–823. doi: 10.1038/nature03610

He, J. D., Zou, Y. N., Wu, Q. S., and Kuča, K. (2020). Mycorrhizas enhance drought tolerance of trifoliate orange by enhancing activities and gene expression of antioxidant enzymes. *Sci. Hortic.* 262:108745. doi: 10.1016/j.scienta.2019.108745

Jiang, Y.F. (2012). The regulation and biosynthesis of the terpenoid volatile involved into the floral scent and stress defense in 5 landscape plant species. [doctor's thesis]. [Yangling, Shaanxi, China]: Northwest A & F University.

Kaur, S., and Suseela, V. (2020). Unraveling arbuscular mycorrhiza-induced changes in plant primary and secondary metabolome. *Meta* 10:355. doi: 10.3390/metabo10080335

Khalil, H. A., and El-Ansary, D. O. (2020). Morphological, physiological and anatomical responses of two olive cultivars to deficit irrigation and mycorrhizal inoculation. *Eur. J. Hortic. Sci.* 85, 51–62. doi: 10.17660/eJHS.2020/85.1.6

Kleine, S., and Müller, C. (2014). Drought stress and leaf herbivory affect root terpenoid concentrations and growth of *Tanacetum vulgare*. *J. Chem. Ecol.* 40, 1115–1125. doi: 10.1007/s10886-014-0505-2

Kokkoris, V., Stefani, F., Dalpe, Y., Dettman, J., and Corradi, N. (2020). Nuclear dynamics in the arbuscular mycorrhizal fungi. *Trends Plant Sci.* 25, 765–778. doi: 10.1016/j.tplants.2020.05.002

Li, X. D., Wang, X. L., Wang, Q., Zhang, Y., and Cai, L. (2017). Metabonomics analysis of tall fescue leaves under drought stress. *Chin. J. Grassl.* 9, 122–126. doi: 10.19578/j.cnki.ahfs.2017.02.014

Maier, W., Hammer, K., Dammann, U., Schulz, B., and Strack, D. (1997). Accumulation of sesquiterpenoid cyclohexenone derivatives induced by an

arbuscular mycorrhizal fungus in members of the Poaceae. *Planta* 202, 36–42. doi: 10.1007/s004250050100

Malhi, G. S., Kaur, M., Kaushik, P., Alyemeni, M. N., Alsahli, A. A., and Ahmad, P. (2021). Arbuscular mycorrhiza in combating abiotic stress in vegetables: An eco-friendly approach. *Saudi J. Biol. Sci.* 28, 1465–1476. doi: 10.1016/j.sjbs.2020.12.001

Manukyan, A. (2019). Secondary metabolites and their antioxidant capacity of Caucasian endemic thyme (*Thymus transcaucasicus* Ronn.) as affected by environmental stress. *J. Appl. Res. Med. Aroma. Plants.* 13:100209. doi: 10.1016/j.jarmap.2019.100209

Meng, L. L., He, J. D., Zou, Y. N., Wu, Q. S., and Kuča, K. (2020). Mycorrhiza-released glomalin-related soil protein fractions contribute to soil total nitrogen in trifoliate orange. *Plant Soil Environ.* 66, 183–189. doi: 10.17221/100/2020-PSE

Phillips, J. M., and Hayman, D. S. (1970). Improved procedures for clearing roots and staining parasitic and vesicular-arbuscular mycorrhizal fungi for rapid assessment of infection. *Trans. Br. Mycol. Soc.* 55, 158–161. doi: 10.1016/S0007-1536(70)80110-3

Podda, A., Pollastri, S., Bartolini, P., Pisuttu, C., Pellegrini, E., Nali, C., et al. (2019). Drought stress modulates secondary metabolites in *Brassica oleracea* L. convar. *Acephala* (DC) Alef, var. *sabellica* L. *J. Sci. Food Agric.* 99, 5533–5540. doi: 10.1002/jsfa.9816

Quan, J. X. (2013). The role of terpenoids in plants and its application. *Bot. Res.* 2, 106–108. doi: 10.12677/BR.2013.24018

Rapparini, F., Llusia, J., and Penuelas, J. (2007). Effect of arbuscular mycorrhizal (AM) colonization on terpene emmision and content of *Artemisia annua* L. *Plant Biol.* 10, 108–122. doi: 10.1055/s-2007-964963

Rivero, J., Alvarez, D., Flors, V., Azcon-Aguilar, C., and Pozo, M. J. (2018). Root metabolic plasticity underlies functional diversity in mycorrhiza-enhanced stress tolerance in tomato. *New Phytol.* 220, 1322–1336. doi: 10.1111/nph.15295

Rivero, J., Gamir, J., Aroca, R., Pozo, M. J., and Flors, V. (2015). Metabolic transition in mycorrhizal tomato roots. *Front. Microbiol.* 6:598. doi: 10.3389/fmicb.2015.00598

Salvioli, A., Zouari, I., Chalot, M., and Bonfate, P. (2012). The arbuscular mycorrhizal status has an impact on the transcriptome profile and amino acid composition of tomato fruit. *BMC Plant Biol.* 12:44. doi: 10.1186/1471-2229-12-44

Sheteiwy, M. S., Ali, D. F. I., Xiong, Y. C., Brestic, M., Skalicky, M., Hamoud, Y. A., et al. (2021). Physiological and biochemical responses of soybean plants inoculated with arbuscular mycorrhizal fungi and Bradyrhizobium under drought stress. *BMC Plant Biol.* 21, 1–21. doi: 10.1186/s12870-021-02949-z

Shi, Y. J., Wu, X. Y., Tang, Y., Mi, J. X., and Wan, X. Q. (2020). Metabonomic analysis of *Chenopodium quinoa* under water stress at flowering stage. *J. Henan Agric. Univ.* 54, 921–930.doi: 10.16445/j.cnki.1000-2340.2020.06.003

Teixeira, W. F., Soares, L. H., Fagan, E. B., Mello, S. C., Reichardt, K., and Dourado-Neto, D. (2020). Amino acids as stress reducers in soybean plant growth under different water-deficit conditions. *J. Plant Growth Regul.* 39, 905–919. doi: 10.1007/s00344-019-10032-z

Turtola, S., Manninen, A. M., Rikala, R., and Kainulainen, P. (2003). Drought stress alters the concentration of wood terpenoids in scots pine and Norway spruce seedlings. *J. Chem. Ecol.* 29, 1981–1995. doi: 10.1023/A:1025674116183

Whiteside, M. D., Garcia, M. O., and Treseder, K. K. (2012). Amino acid uptake in arbuscular mycorrhizal plants. *PLoS One* 7:e47643. doi: 10.1371/journal.pone.0047643

Wiklund, S., Johansson, E., Sjoestroem, L., Mellerowicz, E. J., Edlund, U., Shockcor, J. P., et al. (2008). Visualization of GC/TOF-MS-based metabolomics data for identification of biochemically interesting compounds using OPLS class models. *Anal. Chem.* 80, 115–122. doi: 10.1021/ac0713510

Wu, Q. S., He, J. D., Srivastava, A. K., Zou, Y. N., and Kuca, K. (2019). Mycorrhizas enhance drought tolerance of citrus by altering root fatty acid compositions and their saturation levels. *Tree Physiol.* 39, 1149–1158. doi: 10.1093/treephys/tpz039

Xie, M. M., Chen, S. M., Zou, Y. N., Srivastava, A. K., Rahman, M. M., Wu, Q. S., et al. (2021). Effects of *Rhizophagus intraradices* and *rhizobium trifolii* on growth and N assimilation of white clover. *Plant Growth Regul.* 93, 311–318. doi: 10.1007/s10725-020-00689-y

Yang, X., Lu, M., Wang, Y., Wang, Y., Liu, Z., and Chen, S. (2021). Response mechanism of plants to drought stress. *Horticulturae* 7:50. doi: 10.3390/horticulturae7030050

Yang, C. X., Zhao, W. N., Wang, Y. N., Zhang, L., Huang, S. C., and Li, L. X. (2020). Metabolomics analysis reveals the alkali tolerance mechanism in *Puccinellia tenuiflora* plants inoculated with arbuscular mycorrhizal fungi. *Microorganisms* 8:327. doi: 10.3390/microorganisms8030327

Zhang, F., Zou, Y. N., and Wu, Q. S. (2018). Quantitative estimation of water uptake by mycorrhizal extraradical hyphae in citrus under drought stress. *Sci. Hortic.* 229, 132–136. doi: 10.1016/j.scienta.2017.10.038

Zhang, F., Zou, Y. N., Wu, Q. S., and Kuča, K. (2020). Arbuscular mycorrhizas modulate root polyamine metabolism to enhance drought tolerance of trifoliate orange. *Environ. Exp. Bot.* 171:103962. doi: 10.1016/j.envexpbot.2019.103926

Zou, Y. N., Zhang, F., Srivastava, A. K., Wu, Q. S., and Kuča, K. (2021). Arbuscular mycorrhizal fungi regulate polyamine homeostasis in roots of trifoliate orange for improved adaptation to soil moisture deficit stress. *Front. Plant Sci.* 11:600792. doi: 10.3389/fpls.2020.600792

Conflict of interest: The authors declare that the research was conducted in the absence of any commercial or financial relationships that could be construed as a potential conflict of interest.

Publisher's Note: All claims expressed in this article are solely those of the authors and do not necessarily represent those of their affiliated organizations, or those of the publisher, the editors and the reviewers. Any product that may be evaluated in this article, or claim that may be made by its manufacturer, is not guaranteed or endorsed by the publisher.

frontiers in Plant Science

ORIGINAL RESEARCH
published: 12 October 2021
doi: 10.3389/fpls.2021.717178

Kernel Water Relations and Kernel Filling Traits in Maize (*Zea mays* L.) Are Influenced by Water-Deficit Condition in a Tropical Environment

Md. Robiul Alam[1,2], Sutkhet Nakasathien[2], Md. Samim Hossain Molla[3], Md. Ariful Islam[1], Md. Maniruzzaman[1], Md. Akkas Ali[4], Ed Sarobol[2], Vichan Vichukit[2], Mohamed M. Hassan[5]*, Eldessoky S. Dessoky[5], Enas M. Abd El-Ghany[6], Marian Brestic[7,8], Milan Skalicky[8], S. V. Krishna Jagadish[9] and Akbar Hossain[10]**

[1] On-Farm Research Division, Bangladesh Agricultural Research Institute, Pabna, Bangladesh, [2] Department of Agronomy, Faculty of Agriculture, Kasetsart University, Bangkok, Thailand, [3] On-Farm Research Division, Bangladesh Agricultural Research Institute, Rangpur, Bangladesh, [4] On-Farm Research Division, Bangladesh Agricultural Research Institute, Joydebpur, Bangladesh, [5] Department of Biology, College of Science, Taif University, Taif, Saudi Arabia, [6] Department of Genetics, Faculty of Agriculture, Menoufia University, Tanta, Egypt, [7] Department of Plant Physiology, Slovak University of Agriculture, Nitra, Slovakia, [8] Department of Botany and Plant Physiology, Faculty of Agrobiology, Food and Natural Resources, Czech University of Life Sciences Prague, Prague, Czechia, [9] Department of Agronomy, Kansas State University, Manhattan, KS, United States, [10] Bangladesh Wheat and Maize Research Institute, Dinajpur, Bangladesh

OPEN ACCESS

Edited by:
Thorsten M. Knipfer, University of British Columbia, Canada

Reviewed by:
Mozhgan Sepehri, Shiraz University, Iran
Mohsin Tanveer, University of Tasmania, Australia

***Correspondence:**
Md. Robiul Alam
robiula_2013@yahoo.com
Mohamed M. Hassan
m.khyate@tu.edu.sa
Akbar Hossain
akbarhossainwrc@gmail.com

Specialty section:
This article was submitted to Plant Abiotic Stress, a section of the journal Frontiers in Plant Science

Received: *30 May 2021*
Accepted: *25 August 2021*
Published: *12 October 2021*

Citation:
Alam MR, Nakasathien S, Molla MSH, Islam MA, Maniruzzaman M, Ali MA, Sarobol E, Vichukit V, Hassan MM, Dessoky ES, Abd El-Ghany EM, Brestic M, Skalicky M, Jagadish SVK and Hossain A (2021) Kernel Water Relations and Kernel Filling Traits in Maize (Zea mays L.) Are Influenced by Water-Deficit Condition in a Tropical Environment. Front. Plant Sci. 12:717178. doi: 10.3389/fpls.2021.717178

Water deficit is a major limiting condition for adaptation of maize in tropical environments. The aims of the current observations were to evaluate the kernel water relations for determining kernel developmental progress, rate, and duration of kernel filling, stem reserve mobilization in maize. In addition, canopy temperature, cell membrane stability, and anatomical adaptation under prolonged periods of pre- and post-anthesis water deficit in different hybrids was quantified to support observations related to kernel filling dynamics. In this context, two field experiments in two consecutive years were conducted with five levels of water regimes: control (D1), and four water deficit treatments [V10 to V13 (D2); V13 to V17 (D3); V17 to blister stage (D4); blisters to physiological maturity (D5)], on three maize hybrids (Pioneer 30B80, NK 40, and Suwan 4452) in Expt. 1. Expt. 2 had four water regimes: control (D1), three water deficit treatments [V10 to anthesis (D2); anthesis to milk stage (D3); milk to physiological maturity (D4)], and two maize hybrids (NK 40 and Suwan 4452). Water deficit imposed at different stages significantly reduced maximum kernel water content (MKWC), kernel filling duration (KFD), final kernel weight (FKW), and kernel weight ear^{-1} while it increased kernel water loss rate (KWLR), kernel filling rate (KFR), and stem weight depletion (SWD) across maize hybrids in both experiments. The lowest MKWC under water deficit was at D3 in both experiments, indicating that lower KFR results in lowest FKW in maize. Findings indicate that the MKWC (R^2 = 0.85 and 0.41) and KFR (R^2 = 0.62 and 0.37) were positively related to FKW in Expt. 1 and 2, respectively. The KFD was reduced by 5, 7, 7, and 11 days under water deficit at D3, D4 in Expt. 2 and D4, D5 in Expt. 1 as compared to control, respectively. Water deficit at D5 in Expt. 1 and D4 in Expt. 2

increased KWLR, KFR, and SWD. In Expt. 2, lower canopy temperature and electrical conductivity indicated cell membrane stability across water regimes in NK 40. Hybrid NK 40 under water deficit had significantly higher cellular adaptation by increasing the number of xylem vessel while reducing vessel diameter in leaf mid-rib and attached leaf blade. These physiological adjustments improved efficient transport of water from root to the shoot, which in addition to higher kernel water content, MKWC, KFD, KFR, and stem reserve mobilization capacity, rendered NK 40 to be better adapted to water-deficit conditions under tropical environments.

Keywords: water deficit, maize, kernel water relations, kernel filling traits, stem reserve mobilization

INTRODUCTION

Kernel water relations are a good indicator of kernel developmental progress during grain filling in maize (Schnyder and Baum, 1992; Borras and Westgate, 2006). Developing kernels accumulate more water than assimilate reserves early in the development, and both kernel water content (KWC) and kernel dry matter patterns have been shown to be closely related. As such, understanding kernel water relations is a powerful tool for determining and predicting differences in kernel growth and development among hybrids exposed to different environmental conditions (Saini and Westgate, 2000; Borras and Westgate, 2006; Gambin et al., 2007).

Kernel water relations play a key role in controlling kernel growth and development and the duration of grain filling. The maximum water content achieved early in development provides a fairly accurate estimate of potential kernel size and is closely related to the kernel-growth rate (Borras et al., 2003; Borras and Westgate, 2006). Potential kernel weight can be estimated with maximum kernel water content (MKWC), as final kernel weight (FKW) and kernel water relations are strongly associated in maize (Melchiori and Caviglia, 2008). Kernel water accumulation can be used to mark the progress of kernel development during grain filling (Swank et al., 1987; Schnyder and Baum, 1992; Egli and TeKrony, 1997; Borras and Westgate, 2006). Kernel-filling duration is controlled by the relationship between kernel water and biomass accumulation. Several authors have suggested that water loss from kernels during grain filling is merely an exchange between dry matter and water (Millet and Pinthus, 1984; Brooking, 1990; Saini and Westgate, 2000). Grain filling is the final stage of growth in cereals where ovaries that are fertilized at pollination develop into caryopses. Grain filling duration and rate determine the final grain weight, which is a key component that determines overall yield. Water deficit events during the grain filling stage can cause a major reduction in yield by reducing starch accumulation as a result of limited assimilate partitioning to the developing grain (Blum, 1998) or by direct effects on processes of grain growth (Yang et al., 2004). In the early stages of grain fill, endosperm cells determine the maximum amount of starch and protein that can be accumulated in each kernel (Egli, 1998) as influenced by the rate and duration of grain fill. Water stress during grain filling reduces photosynthesis, induces early senescence, and shortens the grain-filling period, which are more highly affected by water stress than grain-filling rate (Brooks et al., 1982; Schnyder and Baum, 1992; Altenbach et al., 2003; Borras et al., 2003). Westgate and Grant (1989) showed that a brief water deficit during linear grain filling had little impact on dry matter accumulation of maize kernels, but did cause a substantial decrease in KWC.

Water deficit stress decreases kernel filling duration (KFD) (Frederick et al., 1991; De Souza et al., 1997), defined as the time from fertilization to physiological maturity (PM), leading to smaller kernels. Prasad et al. (2008) reported that water deficit occurring after flowering has little effect on kernel-filling rate but shortens KFD, leading to smaller kernel size and less yield. Kernel size is largely dependent on photosynthetic reserves that can be mobilized by the plant. Additional reduction in carbohydrates and nitrogen supply, either from a decrease in photosynthetic activity or a reduction in leaf area, would further decrease kernel size and shorten kernel-filling duration, resulting in smaller kernel (Palta et al., 1994). The shortened kernel-filling duration leading to reduced assimilates under water deficit can be compensated through remobilization of stem reserves during grain filling, which is an important supporting process that can largely compensate grain yield decrease (Bdukli et al., 2007). Drought-induced damages on plant cell membranes lead to imbalanced cellular function. The magnitude of plasma membrane damage due to water deficit can be estimated via ionic secretion measurement (Ferrat and Lovatt, 1999; Khan et al., 2007) which can be a good indicator for cell membrane stability. Aslam et al. (2006) reported that relative cell membrane injury (RCI %) could be used as a reliable selection criterion for water deficit tolerance in maize. Balota et al. (2008) concluded that high canopy temperature depression (CTD) tends to have higher grain yield under dry, hot conditions and, therefore, CTD has been used as a selection criterion to improve adaptation to water deficit and heat.

The information on water relations with kernel growth and development and PM under water deficit during different phenological stages is deemed important for better adaptation and phenotyping of maize hybrids in a drought-prone environment. Simultaneously canopy temperature, cell

Abbreviations: BARC, Bangladesh Agricultural Research Council; CTD, canopy temperature depression; EC, electrical conductivity; FC, field capacity; FKW, final kernel weight; KFD, kernel filling duration; KWLR, kernel weight ear^{-1} while increased kernel water loss rate; KDW, kernel dry weight; KFR, kernel filling rate; KGR, kernel growth rate; KU, Kasetsart University; KWC, kernel water content; MKWC, maximum kernel water content; PC, Pak Chong; PM, physiological maturity; SWD, stem weight depletion.

membrane stability, and anatomical adaptation under short and prolonged periods of water deficit might exhibit great significance on the sustainable adaptation of maize in a water deficit environment. In the above context, two independent experiments were conducted to evaluate the kernel water relations for determining kernel developmental progress, rate, and duration of kernel filling, stem reserve mobilization in maize. In addition, canopy temperature, cell membrane stability, and anatomical adaptation under prolonged periods of pre- and post-anthesis water deficit in different hybrids was quantified to support observations related to kernel filling dynamics.

MATERIALS AND METHODS

Experimental Site

Two field experiments were carried out using a randomized complete block design with split-plot arrangement during two growing seasons of 2010–2011 and 2011–12 at the National Corn and Sorghum Research Center (latitude 14.5° N, longitude 101° E, 360 m above sea level) located in Pak Chong, Nakhon Ratchasima, Thailand. Soils at the experimental site belong to the Pak Chong (PC) soil series. Soil details for the experimental site are available in the authors' previous publication (Molla et al., 2019).

Experimental Treatments

In Expt. 1, treatments consisted of five water regimes viz., D1 = Control-soil water status maintained near field capacity (FC), D2 = Water deficit from V10 to V13, D3 = Water deficit from V13 to V17 stage, D4 = Water deficit from V17 to blister stage, and D5 = Water deficit from blister to PM as the main plot factor. Three maize hybrids viz., V1 = Pioneer 30B80, V2 = NK 40, and V3 = Suwan 4452 were selected as subplot factor. Characteristics of all maize hybrids used in the study are given in **Table 1**. Maize growth stage from emergence to maturity are presented in **Figure 1** and growth stage details related to the experimental treatments are presented in **Figure 2**.

In Expt. 2, four water regimes included D1 = Control–soil water status maintained near FC, D2 = Water deficit from V10 to anthesis, D3 = Water deficit from anthesis to milk stage, and D4 = Water deficit from milk to PM stage as the main plot factor and two higher yielding hybrids from Expt. 1 viz., V1 = NK 40 and V2 = Suwan 4452 were assigned as subplot factor.

The water management for the early establishment of crop was through sprinkler irrigation and continued up to 41 days after planting (before the onset of water-deficit treatments). Water deficit under different treatments was imposed on plants at 42 days after planting (V10 stage) by withholding irrigation for a specific duration (mentioned in treatments) followed by re-watering up to PM stage with weekly flood irrigation. To avoid lateral seepage of water around 7.5 m plot to plot distance and a deep trench was dug between main plots to impose different water-deficit treatments. Two tensiometers were installed at 0–30 cm and 0–60 cm depth to monitor daily soil water tension in the experimental plot throughout the crop cycle. Both experiments were carried out during the winter season which was characterized by very low or no rainfall. Therefore, the experiments were not affected by seasonal rainfall.

Field and Crop Management

Soil preparation was performed in accordance with conventional approaches at the Research Station, including disk harrow plow followed by leveler. The plot was finally prepared with ridges and furrows maintaining interrow spacing of 75 cm. Mixed fertilizers (N:P = 16:20) were applied at the rate of 156 kg ha^{-1} during final land preparation and properly incorporated with soil. The kernels of each maize hybrid were sown by a manual operated instrument which maintained two kernels hill^{-1} in 10 rows with each row 7.5 m long, with a spacing of 75 and 25 cm between rows and plant, respectively, on December 1, 2010, and January 14, 2011. The following day after sowing, sprinkler irrigation was applied to the plot to ensure uniform germination, and thereafter irrigation was continued at weekly intervals until maize plants reached the knee-high stage. The plants were thinned at the 4-leaf stage to maintain 1 plant hill^{-1}. The same amount of mixed fertilizers (as basal) was applied as top-dressing with mechanical applicator at 8–10 leaves stage. Sprinkler irrigation was applied immediately after the top dressing of fertilizers.

Physiological Parameters

Canopy Temperature

In both years, the canopy temperature of leaf was monitored at the milk stage of the crops under control and water-deficit treatments between 11:00 and 12:00 a.m by using a hand-held PCS tester (TOA Electronics Ltd., Japan).

Electrical Conductivity of Leaf Tissue

The electrical conductivity (EC) of the leaves was measured at the end of each water-deficit treatment. Twenty leaf disk punches were randomly obtained from young leaves and then put into 20 ml distilled water. Later, these samples were placed in a refrigerator (about 5°C) and after 24 h EC of the leaves was recorded using YOA EC meter (CM 14P, TOA Electronics Ltd., Japan). Eventually, EC of the distilled water (as control) was subtracted from these rates and the EC of leaves under different treatments were obtained.

Leaf Anatomy

Ear leaf of maize was collected from control and water-deficit treatments and immediately preserved in a humified box and then transported to the Central Laboratory, Faculty of Agriculture, Kasetsart University (UK) for studying the leaf anatomy. After preparing the slide of leaf mid-rib and attached leaf blade tissue, anatomical view was taken with a digital camera Moticam 2500 (Bettlachstrasse 2, 2540 Grenchen, Switzerland) connected to a microscope Olympus CX21 (Manufacturer: Quality Report Co., Ltd., Thailand).

Measurement of Kernel-Related Traits

Measurement of kernel number and kernel weight was done after pollination. Four plants per treatment under control and water deficit were sampled on the day of 50% pollination and at 7-day intervals thereafter. The entire ear with surrounding husks were

TABLE 1 | Characteristics of maize hybrids used in Expt. 1 and 2. [Source: National Corn and Sorghum Research Center, Thailand (2010)].

Hybrids	Description	Duration (days)	Grain yield (kg ha^{-1})	Released by
Pioneer 30B80	Single cross hybrid Highly adapted to major maize growing areas	100–150	7083	Pioneer Hi-Bred (Thailand) Co., Ltd.
NK 40	Single cross hybrid Widely adapted	105–115	7209	Syngenta Seeds Ltd.
Suwan 4452	Single cross hybrid Widely adapted	100–120	7747	National Corn and Sorghum Research Center

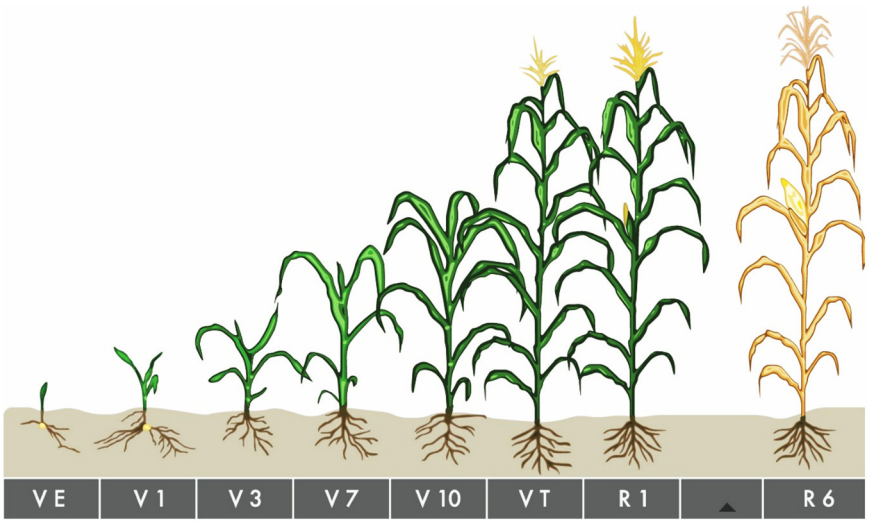

FIGURE 1 | Maize growth stage from emergence to maturity. VE About 4–5 days after planting under ideal conditions, but up to 2 weeks or longer under cool or dry conditions. V1–V5 At V1, round-tipped leaf on first collar appears, nodal roots elongate. By V2, plant is 2–4 inches tall and relies on the energy in the kernel. V3 begins 2–4 weeks after VE and V5, the number of potential number of leaf and ears are determined. V6–V8 Beginning 4–6 weeks after VE. V9–V11 Around 6–8 weeks after VE. V12–Vnth By V12, the plant is about 4 feet tall or more. VT Beginning around 9–10 weeks after emergence. R Corn plants enter reproductive growth after completing tassel emergence, although reproductive stages are determined by kernel development, instead of plant collars. R6 Black Layer Attained about 60 days after silking stage.

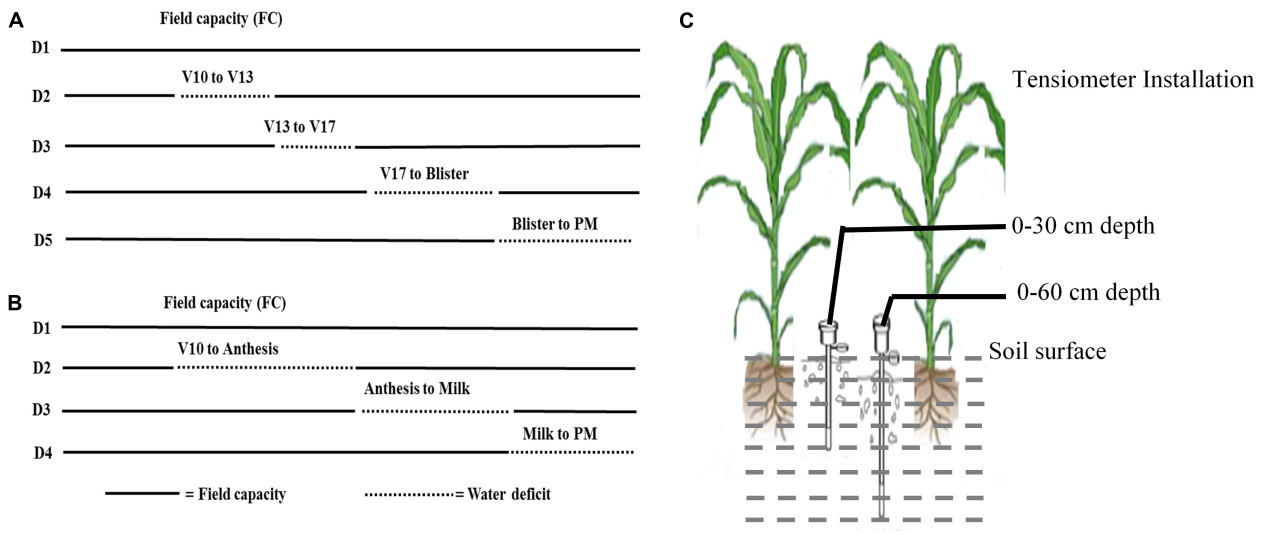

FIGURE 2 | Five water regimes imposed at different growth stages of maize in experiment I **(A)** and four water regimes at different growth stages of maize in experiment II **(B)**. Tensiometers were installed at 0–30 and 0–60 cm depth to monitor soil water potential **(C)**. Sample (-) soil moisture at FC (<–40 KPa) and (—) indicates the period of water deficit.

immediately enclosed in an airtight plastic bag and transported to the lab. Immediately after counting kernel number from the ear of the selected plants, 50 kernels were excised from the ear at floret positions 10–15 from the bottom of the ear within a humidified box. Fresh weight was recorded immediately after sampling, and kernel dry weight (KDW) was determined after drying samples at 70°C for at least 96 h.

Kernel water content was measured throughout kernel development starting from pollination and until kernels reached physiological maturity. Fresh and dry weight was used to calculate KWC (mg kernel^{-1}). Kernel water content was calculated as the difference between kernel fresh weight and dry weight. Maximum KWC and maximum dry weight were taken as the maximum value measured for each hybrid by treatment combination during the grain-filling period. The rate of kernel water loss was estimated as the ratio between difference of maximum water content and water content at PM and the duration. The ratio between dry matter and water content in the kernel was calculated at each sampling date as described by Sala et al. (2007).

The average rate of grain filling was determined as maximum grain weight divided by duration (day), assuming grain weight to be zero at anthesis. The duration of grain filling was estimated as the difference between days to PM and days to anthesis.

Statistical Analysis

The experiment was conducted following a randomized complete block design with a split-plot arrangement and replicated three times. Data were analyzed using MSTATC software (Mstatc, 1990). The significant differences between treatment means were compared with the critical difference at 5% probability level by the Duncan's Multiple Range Test.

RESULTS AND DISCUSSION

Kernel Water Content and Kernel Dry Weight

Kernel water relations are a good indicator of kernel growth and development progress during grain filling

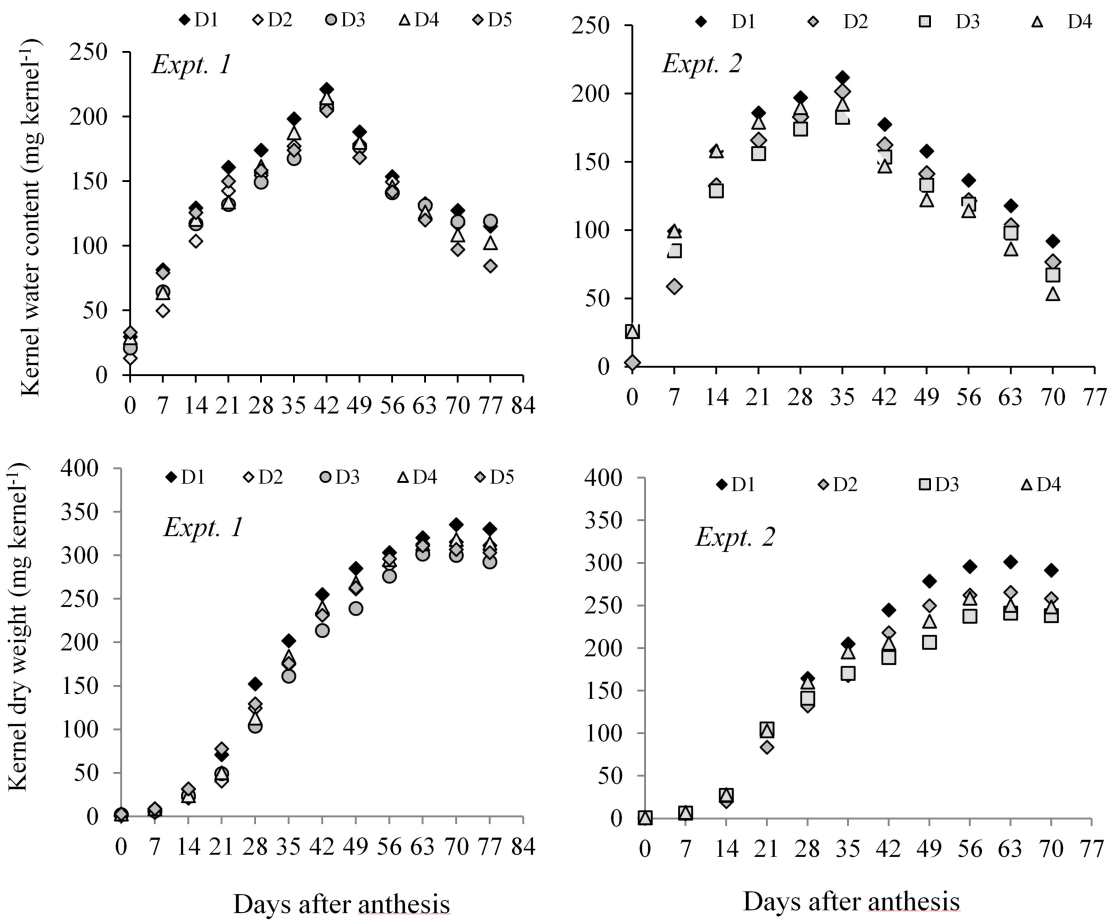

FIGURE 3 | Kernel water content and kernel dry weight of maize hybrids from anthesis to PM at 7 days interval under different water regimes averaged across hybrids in Expt. 1 and Expt. 2. In Expt. 1, D1–Control-soil water status maintained near FC, D2–Water deficit from V10 to V13, D3–Water deficit from V13 to V17 stage, D4–Water deficit from V17 to blister stage, and D5–Water deficit from blister to PM; In Expt. 2, D1–Control–soil water status maintained near FC, D2–Water deficit from V10 to anthesis stage, D3–Water deficit from anthesis to milk stage, and D4–Water deficit from milk to physiological maturity stage.

(Schnyder and Baum, 1992; Borras and Westgate, 2006). Kernel water content and KDW was estimated after anthesis to quantify the progress in kernel development in maize hybrids exposed to water deficit. The developmental dynamics of kernel water and kernel dry mass accumulation under two field experiments (Expt. 1 and Expt. 2) with short and long periods of water deficit at different phenological stages has been highlighted.

Both in Expt. 1 and Expt. 2, higher KWC and KDW was sustained in D1 (control) during the grain-filling period. Water deficit at different periods resulted in relatively lower KWC and dry weight measured after anthesis to PM in all three maize hybrids (**Figure 3**). A general observation was that the KWC under water-deficit condition did not follow a distinct development pattern. However, water deficit at the early vegetative stage gradually sustains a slightly higher water content in the kernel during grain filling as compared to post-anthesis water deficit. Post-anthesis water deficit showed relatively lower kernel water at the later grain-filling stage.

In Expt. 2, water deficit either before anthesis or prolonged water deficit at post-anthesis resulted in lower KDW. This result indicates that water deficit imposed before or after anthesis causes reduced dry mass accumulation in the kernel. All hybrids under different water regimes showed more or less similar response. However, NK 40 contained relatively higher kernel water and KDW under control and water deficit treatments in both experiments as compared to Pioneer 30B80 and Suwan 4452 (**Figure 4**). Among the hybrids, NK 40 showed its superiority over Suwan 4452 and Pioneer 30B80, based on the progressive

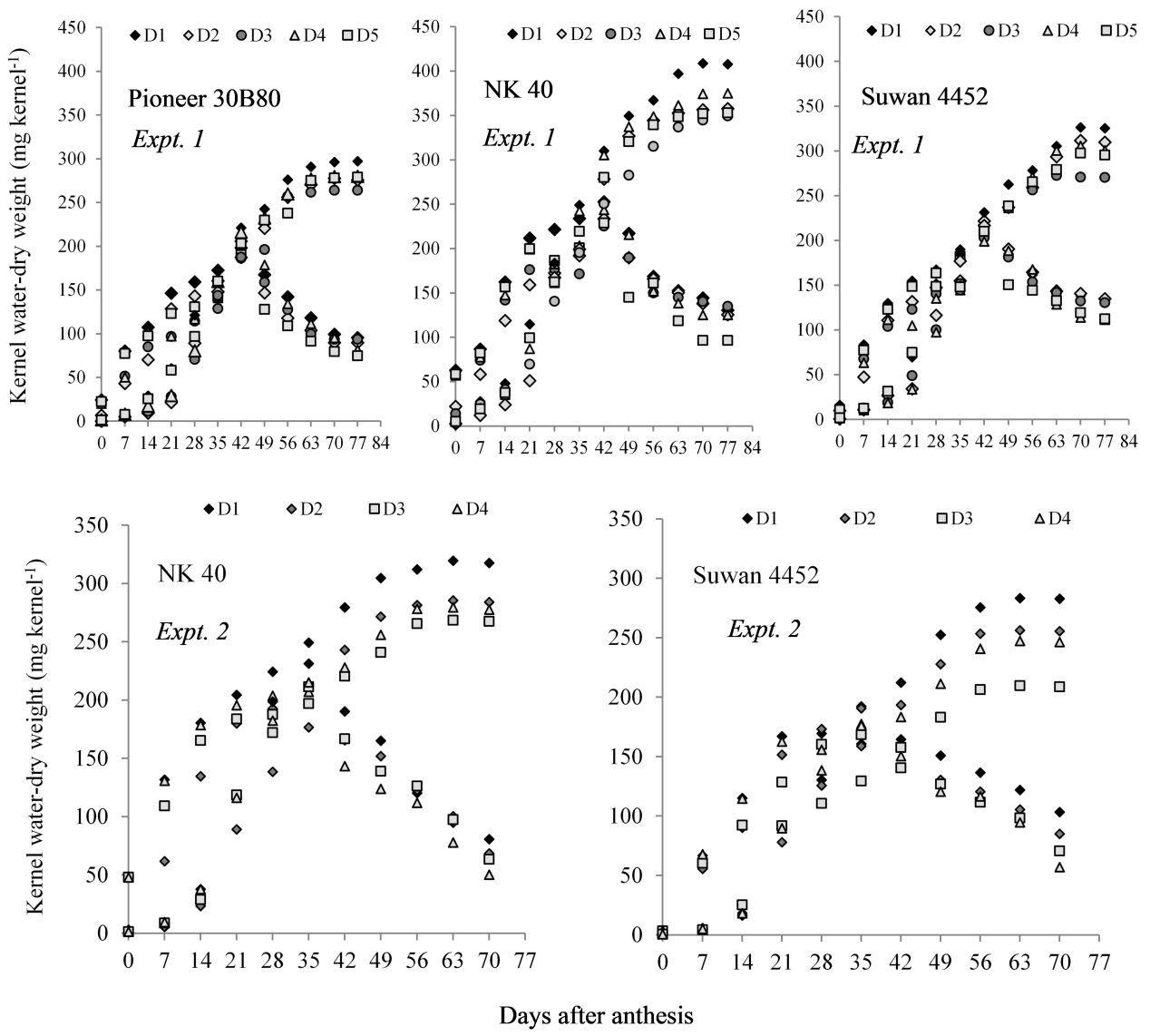

FIGURE 4 | Kernel water content and kernel dry weight of three hybrids (Pioneer 30B80, NK 40, and Suwan 4452) under five water regimes in Expt. 1 and two hybrids (NK 40 and Suwan 4452) under four water regimes in Expt. 2. For treatment details see **Figure 3** legend.

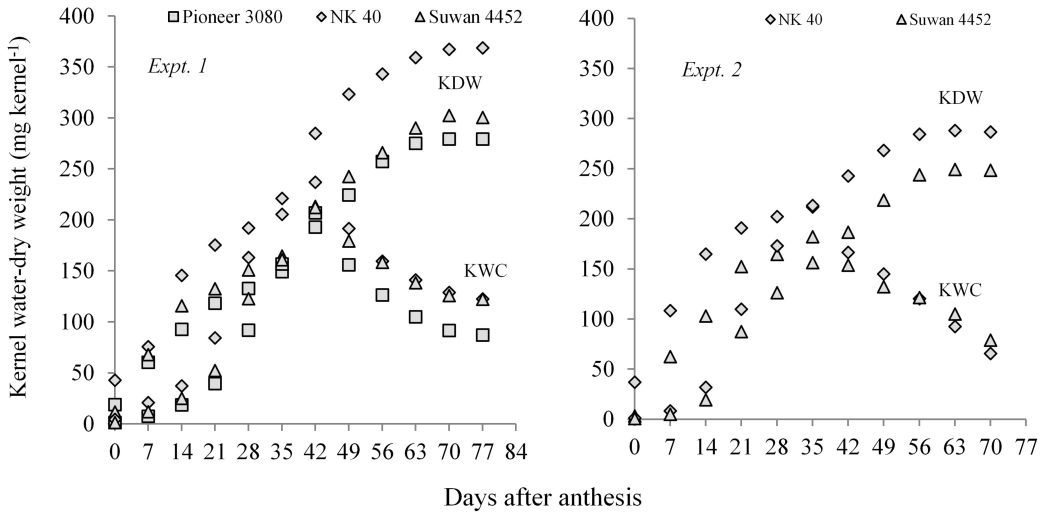

FIGURE 5 | Kernel water content (KWC) and kernel dry weight (KDW) of field maize hybrids after anthesis to physiological maturity at 7 days interval irrespective of water regimes in Expt. 1 and Expt. 2, respectively.

development of kernel water and KDW during kernel filling irrespective of water-deficits treatments (**Figure 5**).

In Expt. 1, water regimes showed significant differences in MKWC. Maximum water content ranged from 225.10 to 206.62 mg kernel^{-1}. Well-watered treatment recorded the highest value of MKWC whereas water deficit induced at D3 and D4 accumulated the lowest MKWC (**Table 2**). Hybrids differed significantly in the maximum water content per kernel achieved during mid grain fill ($P \leq 0.05$, **Table 2**).

NK 40 achieved significantly higher MKWC during the mid grain-filling phase, compared to the average of the other two hybrids. The hybrid Pioneer 30B80 attained the lowest amount of MKWC. It indicates that water shortage before the anthesis stage causes more reduction in water accumulation in Pioneer 30B80 kernels. Interaction of hybrid and water regimes revealed that NK 40 accumulated significantly higher maximum water content in control (D1) compared to water deficit stress treatments, except D5. NK 40 consistently accumulated higher maximum water content as compared to Pioneer 30B80 and Suwan 4452, across all water regimes. Maximum KWC exhibited a significant positive relationship with FKW (**Figure 6A**). Borras et al. (2003) and Gambin et al. (2007) also reported a significant positive relationship between MKWC and FKW.

In Expt. 2, the maximum water content of the kernel also varied significantly due to water regimes. Maximum water content per kernel ranged from 211.81 to 182.80 mg kernel^{-1} (**Table 3**). Control and water deficit imposed at milk to physiological stage had the highest value of maximum water content whereas water deficit from anthesis to milk stage recorded the lowest MKWC (**Table 3**). After anthesis, water deficit up to milk stage limits water uptake by the crops and the subsequent effect would have resulted in lower accumulation of water by the kernel as compared to control or water deficit at other stages. Hybrids showed significant variation in maximum water content (MWC) per kernel ($P \leq 0.05$, **Table 3**). NK 40 exhibited significantly higher MKWC as compared to Suwan 4452. NK 40 accumulated significantly higher MKWC across the water regimes as compared to Suwan 4452 (**Table 3**) suggesting this hybrid has the potential to accumulate higher KWC in control and water-deficit environments. Similar to Expt. 1, MKWC exhibited a positive relationship with FKW (**Figure 6B**).

Loss of Kernel Water

For maize kernel growth, the effective grain-filling period is more important for active dry matter accumulation and actual kernel size determination (Borras et al., 2009). During this phase, KWC reaches its maximum value and then begins to decline closely coordinated with dry matter deposition. A difference in the duration of kernel filling is a consequence of variations in the relationship between kernel water loss and dry matter accumulation after attaining maximum water content. In the present study, the water loss rate from the kernel was determined after attaining maximum water content.

In Expt. 1, water regimes showed significant differences in dynamics of kernel water loss after attaining maximum water content. The maximum rate of water loss per day from the kernel (5.77 mg kernel^{-1} day^{-1}) was observed in D5 treatment. The control showed a significantly lower rate of water loss per day compared to the average of all the water-deficit treatments (**Table 2**). This result indicates that water deficit imposed during grain filling increases the rate of water loss as compared to water deficit at vegetative stage and control. Hybrids also exerted significant variation on kernel water loss per day. Pioneer 30B80 showed the maximum rate of kernel water loss (4.54 mg kernel^{-1} day^{-1}) while Suwan 4452 demonstrated the minimum rate (3.83 mg kernel^{-1} day^{-1}) (**Table 2**).

The rate of kernel water loss varied across water regimes and the maize hybrids. The kernel water loss rate of NK 40 at D5 was significantly higher, and the lowest was recorded with Suwan 4452 at D2 stage followed by Suwan 4452 at

TABLE 2 | Effect of water regimes on kernel filling components of maize hybrids in Expt. 1.

Treatments	Maximum water content (mg kernel^{-1})	Kernel water loss rate (mg kernel^{-1} day^{-1})	Kernel filling duration (days)	Kernel filling rate (mg day^{-1})
Water regimes				
D1	225.10^{a}	3.06^{c}	72^{a}	4.84^{b}
D2	214.80^{b}	3.98^{b}	70^{b}	4.94^{ab}
D3	206.62^{c}	4.11^{b}	68^{c}	4.38^{c}
D4	209.41^{c}	4.16^{b}	65^{d}	4.99^{ab}
D5	215.21^{b}	5.77^{a}	61^{e}	5.36^{a}
LSD ($P \leq 0.05$)	5.040	0.482	1.637	0.418
Hybrids				
Pioneer 30B80	193.00^{c}	4.54^{a}	65^{b}	4.45^{b}
NK 40	236.50^{a}	4.27^{b}	70^{a}	5.52^{a}
Suwan 4452	213.21^{b}	3.83^{c}	66^{b}	4.74^{b}
LSD ($P \leq 0.05$)	6.272	0.251	1.511	0.292
Interaction effect of water regimes and hybrids				
D1				
Pioneer 30B80	202.50^{ghi}	3.52^{de}	70^{cd}	4.15^{hi}
NK 40	250.91^{a}	3.13^{de}	75^{ab}	5.78^{ab}
Suwan 4452	221.90^{cdef}	2.54^{fg}	72^{bc}	4.60^{efghi}
D2				
Pioneer 30B80	198.11^{hij}	4.87^{c}	63^{e}	5.11^{bcdef}
NK 40	233.60^{bc}	4.83^{c}	76^{a}	5.45^{abc}
Suwan 4452	212.70^{efgh}	2.23^{g}	71^{cd}	4.26^{ghi}
D3				
Pioneer 30B80	186.40^{f}	3.56^{de}	62^{ef}	3.89^{i}
NK 40	225.40^{cde}	3.04^{ef}	68^{d}	4.93^{cdefg}
Suwan 4452	208.12^{fgh}	5.72^{b}	73^{abc}	4.31^{ghi}
D4				
Pioneer 30B80	190.50^{ij}	5.33^{bc}	68^{d}	4.40^{fghi}
NK 40	228.82^{cd}	3.74^{d}	70^{cd}	5.43^{abc}
Suwan 4452	208.91^{fgh}	3.40^{de}	57^{g}	5.15^{bcde}
D5				
Pioneer 30B80	187.30^{ij}	5.43^{bc}	63^{e}	4.69^{defgh}
NK 40	243.73^{ab}	6.62^{a}	62^{ef}	6.03^{a}
Suwan 4452	214.62^{defg}	5.27^{bc}	59^{fg}	5.36^{abcd}
LSD ($P \leq 0.05$)	14.02	0.562	3.378	0.901
CV (%)	3.84	7.81	2.95	7.82

FC, field capacity; PM, physiological maturity.
*Treatment abbreviated as in **Figure 3**.*
Means in each column with the same letter are not significantly different from each other at $p \leq 0.05$.

control (**Table 2**). It was observed that the genotypic response across water regimes did not follow a distinct pattern with the rate of water loss from the kernel after attaining maximum water content. Variation of assimilate availability generally regulates the kernel water uptake and expansion in maize hybrids (Borras et al., 2003; Westgate et al., 2004). It has been investigated that source reduction during the effective grain-filling period accelerates the rate of water loss from kernels, accelerates desiccation, and reduces the grain-filling duration without affecting the biomass accumulation rate (Barlow et al., 1980; Brooks et al., 1982; Jones and Simmons, 1983; Egli, 1990; Westgate, 1994).

In Expt. 2, the maximum rate of water loss per day from the kernel (4.07 mg kernel^{-1} day^{-1}) was observed in water deficit at D4 stage. The control recorded significantly lowest rate of water loss per day (2.72 mg kernel^{-1} day^{-1}) (**Table 3**). This result indicates that water deficit imposed after anthesis and successive stages enhance the rate of water loss, reaches peak rate of water loss leading to water shortage after milk stage as compared to water deficit at vegetative stage and control. Hybrids also exerted significant variation on kernel water loss per day. NK 40 showed a significantly higher kernel water loss rate per day compared to Suwan 4452 (**Table 3**).

Kernel water loss rate significantly differed across water regimes and the hybrids. NK 40 demonstrated a significantly higher rate of kernel water loss per day under different periods of water deficit as compared to Suwan 4452 (**Table 3**). Kernel water loss rate exhibited a significant negative relationship with

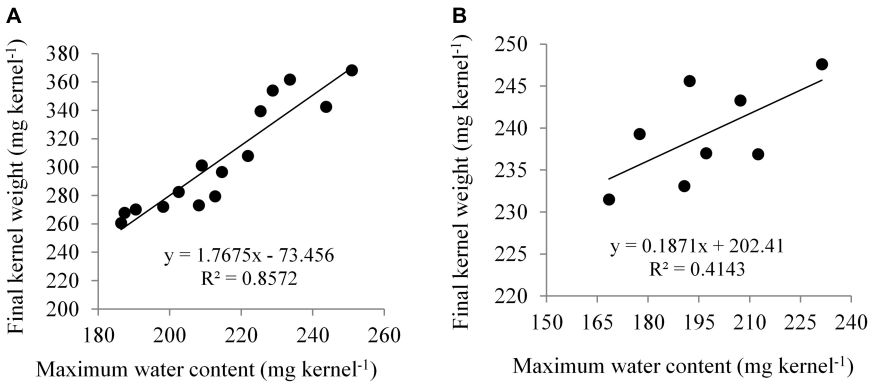

FIGURE 6 | Relationship between maximum kernel water content (MKWC) and final kernel weight (FKW) in Expt. 1 **(A)** and Expt. 2 **(B)**.

TABLE 3 | Effect of water regimes on grain filling components of maize hybrids in Expt. 2.

Treatment	Maximum water content (mg kernel^{-1})	Kernel water loss rate (mg kernel^{-1} day^{-1})	Kernel filling duration (days)	Kernel filling rate (mg day^{-1})
Water regimes				
D1	211.81^{a}	2.72^{d}	69.50^{a}	4.19
D2	192.32^{bc}	3.44^{c}	64.35^{ab}	4.34
D3	182.80^{c}	3.88^{b}	64.00^{b}	3.72
D4	201.60^{ab}	4.07^{a}	62.50^{b}	4.06
LSD ($P \leq 0.05$)	11.34	0.178	5.183	ns
Hybrids				
NK 40	212.03^{a}	4.40^{a}	66	4.44^{a}
Suwan 4452	182.21^{b}	2.65^{b}	65	3.71^{b}
LSD ($P \leq 0.05$)	23.75	0.97	ns	0.492
Interaction effect of water regimes and hybrids				
D1				
NK 40	231.30^{a}	3.54^{bc}	72^{a}	4.27^{ab}
Suwan 4452	192.20^{bc}	1.90^{d}	67^{b}	4.10^{ab}
D2				
NK 40	207.20^{ab}	4.21^{ab}	65^{bc}	4.90^{a}
Suwan 4452	177.50^{bc}	2.67^{cd}	64^{bc}	3.77^{ab}
D3				
NK 40	197.10^{abc}	4.80^{a}	64^{bc}	4.26^{ab}
Suwan 4452	168.40^{c}	2.95^{bcd}	64^{bc}	3.18^{b}
D4				
NK 40	212.40^{ab}	5.05^{a}	62^{c}	4.32^{ab}
Suwan 4452	190.70^{bc}	3.08^{bcd}	63^{bc}	3.86^{ab}
LSD ($P \leq 0.05$)	33.40	1.191	3.706	1.284
CV (%)	9.00	17.94	3.02	16.73

FC, field capacity; PM, physiological maturity.
*Treatment abbreviated as in **Figure 3**.*
Means in each column with the same letter are not significantly different from each other at $P \leq 0.05$.

the days from maximum KWC to PM stage in both experiments (**Figure 7**). Similar findings have also been reported by Westgate (1994) and Pepler et al. (2006).

Rate and Duration of Kernel Filling

In Expt. 1, water deficit imposed at different stages of crop showed significant influence on grain filling duration and the rate of grain filling. Water management at FC (control) demonstrated the maximum duration of grain filling (72 days) whereas the minimum grain filling duration (61 days) was with water-deficit stress imposed at D5 stage (**Table 2**). It was generally observed that water deficit at grain-filling stages had a more negative impact than that of vegetative stages, in terms of grain-filling duration. Grain filling was shortened by 2, 4, 7, and 11 days under water deficit from D2, D3, D4, and D5 stages, respectively, as compared to control. Water deficit at reproductive stages

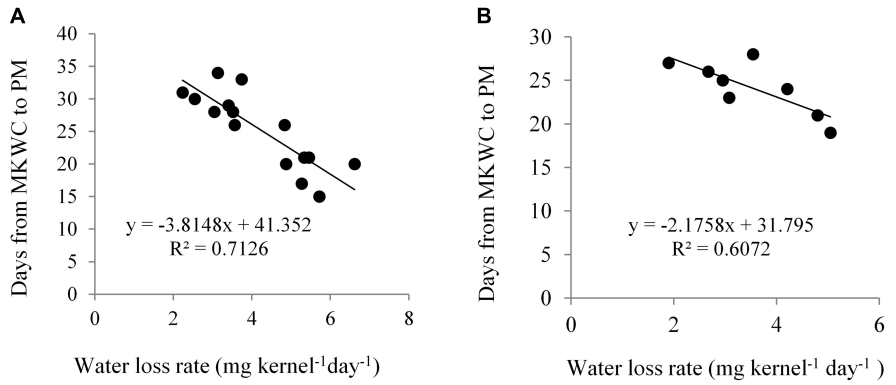

FIGURE 7 | Relationship between kernel water loss rate and days from maximum kernel water content (MKWC) to physiological maturity (PM) in Expt. 1 **(A)** and Expt. 2 **(B)**.

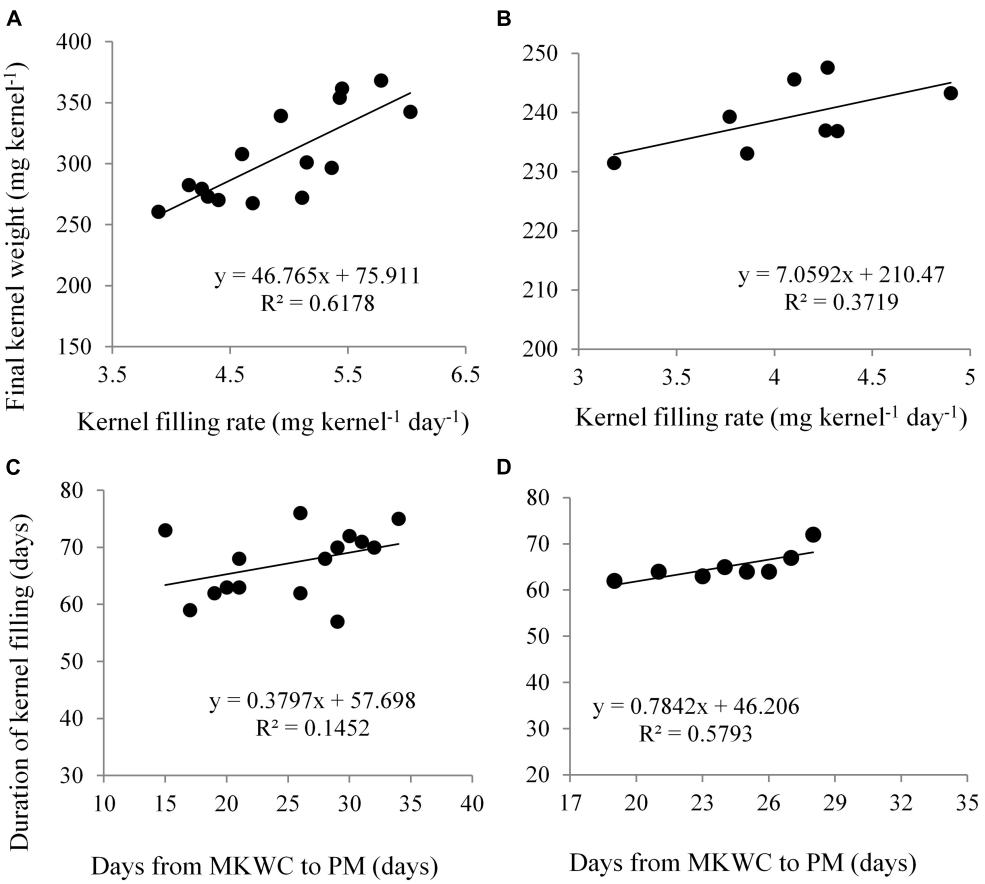

FIGURE 8 | Relationship between kernel filling rate and final kernel weight in Expt. 1 **(A)** and Expt. 2 **(B)**; days from maximum kernel water content (MKWC) to physiological maturity (PM) and duration of kernel filling in Expt. 1 **(C)** and Expt. 2 **(D)**.

shortens the grain-filling duration because of inhibition of current photosynthetic assimilates, i.e., limited source capacity. The rate of grain filling was also significantly affected by water deficit treatments. The highest rate of grain filling was recorded in D5 and D4 stages. Control and D2 stages exhibited the lowest rate of grain filling. Hybrids showed a significant variation in duration and rate of grain filling in maize. NK 40 exhibited a significantly higher duration of grain filling as compared to Pioneer 30B80 and Suwan 4452. A similar result was obtained in the case of rate of grain filling (**Table 2**). The higher grain filling duration accompanied by a higher rate of grain filling made this hybrid attain higher yield potential. Irrespective of water deficit

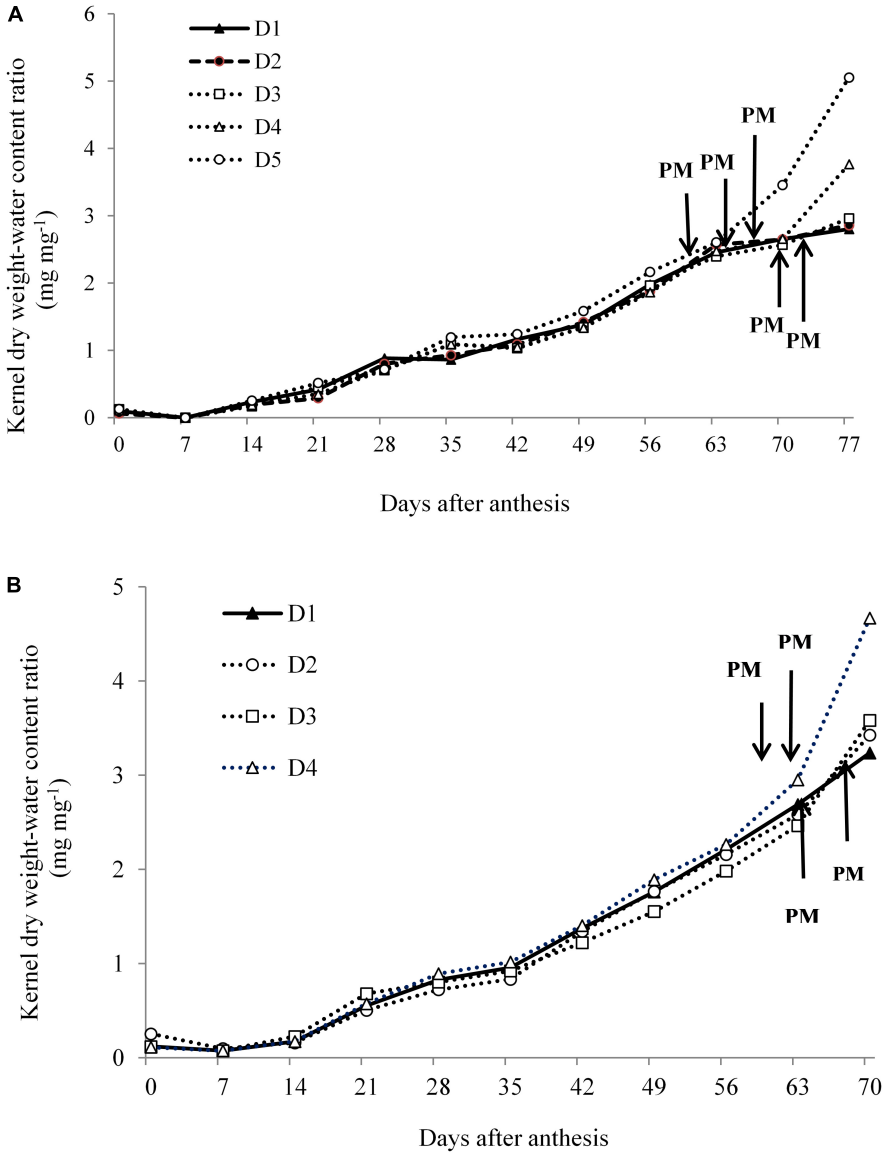

FIGURE 9 | Kernel dry weight-water content ratio under different water regimes at 7 days intervals from days after anthesis to physiological maturity in Expt. 1 **(A)** and Expt. 2 **(B)**.

at different stages of the crop, NK 40 demonstrated superiority over two other maize hybrids. Potential physiological traits such as higher relative water content, chlorophyll content, MKWC, dry matter translocation, and translocation efficiency of NK 40 could have resulted in optimum grain filling and higher grain yield (Molla et al., 2019).

The results indicated that maximum grain-filling duration was attained by NK 40 at D1, D2, and D4 stages. Generally, Pioneer 30B80 recorded relatively lower grain-filling duration under control and stress periods as compared to NK 40 and Suwan 4452, except in D4 and D5 compared to Suwan 4452 (**Table 2**). Under optimum irrigation condition and water deficit at the early grain-filling stage, NK 40 exhibited its potential capacity to fill the kernel for a relatively long period as compared to other hybrids. The rate of grain filling recorded a significant difference due to water deficit and hybrids interaction. The grain filling rate of NK 40 at D5 was significantly higher which was statistical similar to NK 40 at D1, D2, and D4, and the lowest grain filling rate of Pioneer 30B80 was recorded at D3. In general, NK 40 showed higher efficiency of grain filling under optimum water management and water-deficit conditions imposed at different stages.

In Expt. 2, the highest duration of grain filling (69.50 and 64.53 days) was noted in control and water deficit from V10 to anthesis stage, respectively (**Table 3**). Water deficit from D3 and D4 stage recorded the lowest duration of grain filling in maize. This result indicated that water deficit at the vegetative stage has a similar response in grain filling as in control. Control condition

TABLE 4 | The effect of water regimes and hybrids on final kernel weight, kernel weight reduction, kernel weight ear^{-1}, reduction in kernel weight ear^{-1}, and stem weight depletion (% of kernel weight ear^{-1}) in Expt. 1.

Treatment	Final kernel weight (mg kernel^{-1})	Reduction in kernel weight (%)	Kernel weight ear^{-1} (g)	Reduction in kernel weight ear^{-1} (%)	Stem weight depletion (% of kernel weight ear^{-1})
Water regimes					
D1	319.50^{a}	–	180.60^{a}	–	1.730^{e}
D2	304.40^{c}	4.73	158.40^{cd}	6.95	2.343^{d}
D3	291.10^{d}	8.89	152.60^{d}	8.76	5.090^{c}
D4	308.50^{b}	3.44	168.80^{b}	3.69	6.130^{a}
D5	302.30^{c}	5.38	162.60^{bc}	5.63	5.310^{b}
LSD ($P \leq 0.05$)	3.380		6.832		0.203
Hybrids					
Pioneer 30B80	270.70^{c}	–	162.20^{b}	–	3.474^{b}
NK 40	353.20^{a}	–	167.80^{a}	–	5.510^{a}
Suwan 4452	291.70^{b}	–	163.80^{b}	–	3.378^{b}
LSD ($P \leq 0.05$)	5.794		3.685		0.138
Interaction effect of water regimes and hybrids					
D1					
Pioneer 30B80	282.50^{f}	–	176.85b	–	1.36^{i}
NK 40	368.23^{a}	–	177.59b	–	1.86^{h}
Suwan 4452	307.94^{e}	–	187.51a	–	1.97^{h}
D2					
Pioneer 30B80	272.11^{fgh}	3.68	158.63^{ef}	10.30	2.02^{h}
NK 40	361.70^{ab}	1.77	166.06^{cde}	6.49	3.56^{g}
Suwan 4452	279.53^{fg}	9.22	150.65^{fg}	19.66	1.45^{i}
D3					
Pioneer 30B80	260.72^{h}	7.72	149.38^{g}	15.53	4.04^{f}
NK 40	339.41^{d}	7.82	160.20^{de}	9.79	5.28^{d}
Suwan 4452	273.23^{fgh}	11.27	148.07^{g}	21.03	5.95^{c}
D4					
Pioneer 30B80	270.34^{fgh}	4.32	166.78^{cde}	5.69	5.31^{d}
NK 40	354.13^{bc}	3.83	170.68^{bc}	3.89	9.01^{a}
Suwan 4452	301.21^{e}	2.18	168.97^{bcd}	9.89	4.08^{f}
D5					
Pioneer 30B80	267.80^{gh}	5.20	159.34^{e}	9.90	4.64^{e}
NK 40	342.52^{cd}	6.98	164.62^{cde}	7.30	7.85^{b}
Suwan 4452	296.71^{e}	3.64	163.71^{cde}	12.69	3.44^{g}
LSD ($P \leq 0.05$)	12.960		8.239		0.309
CV (%)	2.49		2.94		4.40

FC, field capacity; PM, physiological maturity.
*Treatment abbreviated as in **Figure 3**.*
Means in each column with the same letter are not significantly different from each other at $p \leq 0.05$.

and water deficit during vegetative stages do not restrict source capacity for grain filling compared to during grain filling. Water deficit during grain-filling stages reduces assimilate supply to the growing kernel which results in shortened duration of grain filling. Severe moisture deficit in soil did not have a significant influence on the rate of grain filling (**Table 3**). The duration of grain filling was not influenced by the hybrids. The rate of grain filling was found significantly higher in NK 40 as compared to Suwan 4452 (**Table 3**). Under both water deficit conditions, the higher grain filling rate of NK 40 indicates that it has the potentiality to supply assimilate for meeting the demand of growing kernel. Kernel filling rate (KFR) exhibited a positive relationship with FKW in both experiments (**Figures 8A,B**). Days from MKWC to PM showed a positive relationship with the duration of kernel filling (**Figures 8C,D**).

Kernel Water Content-Dry Weight Ratio

In Expt. 1, dry weight-KWC ratio under water deficit is a coordinated process and is considered important for evaluating the dynamics of dry matter deposition during effective grain filling. **Figure 9A** indicates that KDW-water content ratio among water deficit treatments including control was similar during the kernel filling period until they reached the PM stage. After reaching PM, i.e., D5 and D4 treatments, the dry weight-KWC started to increase rapidly than that of D1. This surprising increase in the dry weight-KWC was associated with a decline

TABLE 5 | The effect of water regimes and hybrids on final kernel weight, kernel weight reduction, kernel weight ear^{-1}, reduction in kernel weight ear^{-1}, and stem weight depletion (% of kernel weight ear^{-1}) in Expt. 2.

Treatment	Final kernel weight (mg kernel^{-1})	Reduction in kernel weight (%)	Kernel weight ear^{-1} (g)	Reduction in kernel weight ear^{-1} (%)	Stem weight depletion (% of kernel weight ear^{-1})
Water regimes					
D1	246.60^{a}	–	162.40^{a}	–	16.80^{c}
D2	241.30^{a}	2.15	136.80^{b}	15.76	7.26^{d}
D3	234.30^{b}	4.99	120.90^{c}	25.55	33.86^{b}
D4	235.00^{b}	4.70	131.10^{b}	19.27	46.74^{a}
LSD ($P \leq 0.05$)	5.903		9.459		1.240
Hybrids					
NK 40	241.27	–	141.91	–	33.80
Suwan 4452	237.42	–	133.68	–	18.54
LSD ($P \leq 0.05$)					
Interaction effect of water regimes and hybrids					
D1					
NK 40	247.60^{a}	–	159.33^{a}	–	26.15^{c}
Suwan 4452	245.70^{ab}	–	165.53^{a}	–	7.45^{e}
D2					
NK 40	243.30^{ab}	1.74	147.36^{b}	7.51	7.91^{e}
Suwan 4452	239.30^{ab}	2.60	126.15^{d}	23.79	6.61^{e}
D3					
NK 40	237.00^{ab}	4.28	124.38^{d}	21.94	49.85^{a}
Suwan 4452	231.50^{b}	5.78	117.45^{d}	29.05	17.88^{d}
D4					
NK 40	236.90^{ab}	4.32	136.53^{c}	14.31	51.27^{a}
Suwan 4452	233.10^{ab}	5.13	125.59^{d}	24.13	42.20^{b}
LSD ($P \leq 0.05$)	13.72		9.461		3.354
CV (%)	3.05		3.65		6.81

FC, field capacity; PM, physiological maturity.
Means in each column with the same letter are not significantly different from each other at $p \leq 0.05$.

in KWC after cessation of kernel growth (**Figure 8A**). Water deficit during reproductive stages (D5, D4, and D3 treatments) limits assimilate supply which eventually shortens grain filling duration by advancing PM, and this result is consistent with rapid increases of dry weight-KWC ratio. Sala et al. (2007) also reported that the dry weight-water content ratio of kernel during grain filling of maize germplasm was affected by the source-sink relationship. In Expt. 2, KDW-water content ratio was quite similar for all treatments, and after attaining PM this ratio sharply increased in case of D4 treatment. This result suggests that limited assimilate supply shortens kernel filling by advancing PM and increasing dry weight-KWC ratio that leads to cessation of kernel growth (**Figure 9B**).

Kernel Weight and Stem Reserve Mobilization

In Expt. 1, the FKW was significantly different under water regimes and hybrids. All hybrids attained higher kernel weight under control condition. Kernel weight under control was significantly higher in NK 40, compared to the average of other two hybrids, indicating higher yield potential with increased kernel weight in NK 40 (**Table 4**). Reduction in FKW was higher in moderate water deficit at D3 stage for all hybrids with a maximum of 11.27% in Suwan 4452 followed by the same hybrid at D2 stage (**Table 4**). Water deficit at D5 stage recorded slightly higher reduction in kernel weight compared to D4 stage in all hybrids. Kernel weight per ear in the control was significantly higher in Suwan 4452 than NK 40 and Pioneer 30B80, indicating a relatively higher potential ear productivity in Suwan 4452. Reduction in kernel weight per ear was higher in all hybrids at the water deficit imposed from D3 with a higher reduction (21.03%) in Suwan 4452 followed by D2 stage in the same hybrid (19.66%).

In general, a decrease in kernel weight per ear under water deficit at different stages was found to be relatively low in NK 40. This could be due to the supplementation of assimilates from the stem reserves when current photosynthesis is limited during water deficit. Moderate water deficit during D3 stage, i.e., before flowering results in a higher reduction in the kernel weight. Reduction in kernel setting might be one of factor that can be attributed to this response. Stem weight depletion (SWD) at D4 and D5 stages in NK 40 was significantly higher as compared to other hybrids. Pioneer 30B80 exhibited a similar pattern of SWD at different stages as in NK 40 but with significantly lower values. Higher depletion of stem weight in Suwan 4452 was noted with water deficit from D3 stage. Stem dry weight depletion as a percentage of grain weight per ear in all hybrids tended to increase under-water deficit imposed at different stages as compared to control (**Table 4**). However, the SWD and the

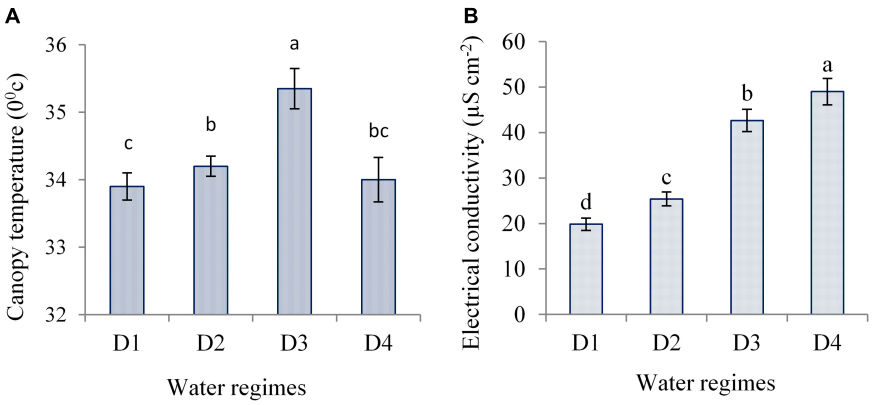

FIGURE 10 | Canopy temperature **(A)** and electrical conductivity **(B)** of ear leaf of maize measured during mid grain filling as affected by water regimes in Expt. 2. Different letters on bars are significantly different from each other at $p \leq 0.05$.

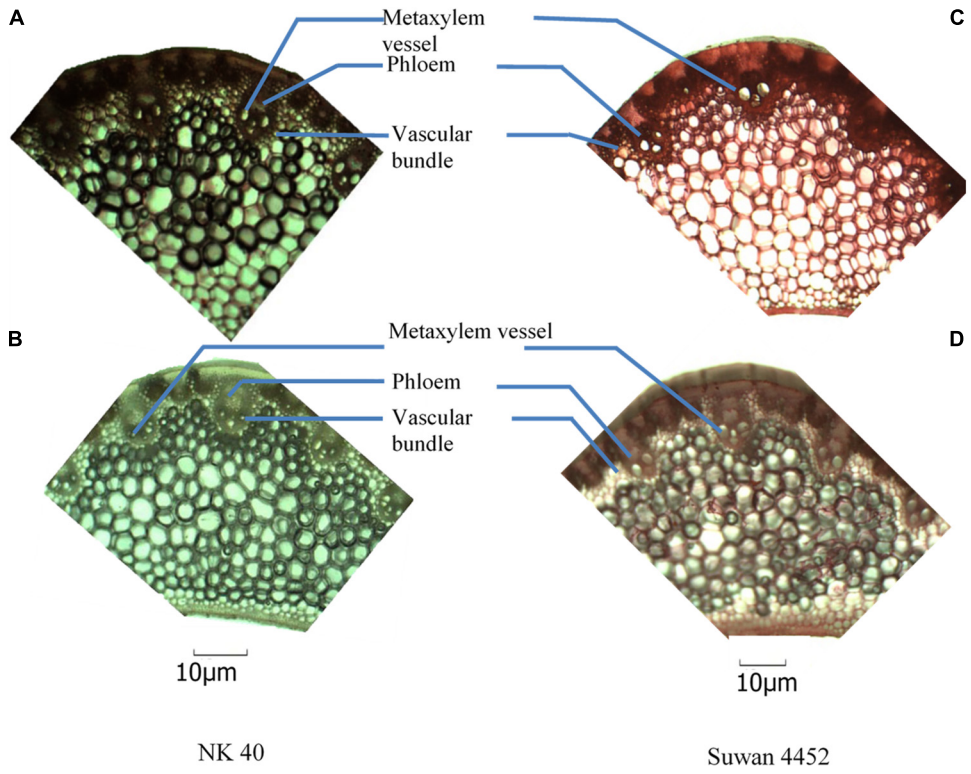

FIGURE 11 | Anatomical view of leaf blade attached to the mid-rib of NK 40 and Suwan 4452 under control **(A,C)** and water deficit **(B,D)** during mid grain-filling stage.

potential increase in assimilate translocation to grains was higher in NK 40 than other two hybrids.

In Expt. 2, FKW and kernel weight per ear in controls (**Table 5**) were lower as compared to Expt. 1. This could be associated to climatic variation (delayed planting of 2nd experiment). The first experiment was planted in the first week of December while the prevailing temperature was quite low, whereas the 2nd experiment was planted in mid-January with comparatively higher temperature. So the growth and development of the crop in the 2nd experiment was relatively faster than in Expt. 1. However, NK 40 still maintained its superiority over Suwan 4452 in potential kernel weight whereas Suwan 4452 demonstrated higher productivity in kernel weight per ear over NK 40 only in the control condition. Water deficit at the grain-filling stage exhibited higher reduction in kernel weight in both hybrids (**Table 5**). Under severe water deficit the reduction in kernel weight was comparatively higher in Suwan 4452 than in NK 40 (**Table 5**).

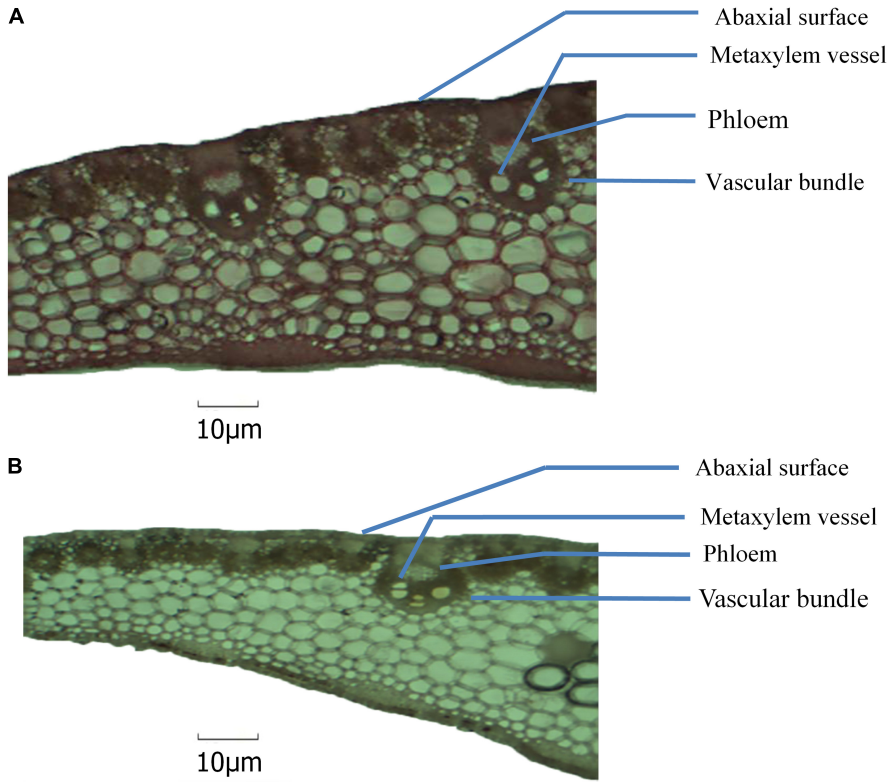

FIGURE 12 | Anatomical view of leaf blade attached with mid-rib of NK 40 under control **(A)** and water deficit **(B)** after milking stage.

Imposing water stress at anthesis to milk stage accounted for 29.05 and 21.94% kernel weight reduction per ear in Suwan 4452 and NK 40, respectively. In Expt. 2, severe water deficit at D3 accounts for higher kernel weight reduction probably due to higher kernel abortion. Higher SWD was recorded at D4 stage in both hybrids. Both hybrids showed similar pattern of SWD with a higher overall reduction in NK 40.

Stem weight loss under water deficit at D3 and D4 stages accounted for 49.85 and 51.27% of grain weight per ear in NK 40 followed by 42.20% at D4 in Suwan 4452. This finding indicates that stem dry matter reserves may have accounted for about half of the grain weight per ear in NK 40 under severe water-deficit condition, while it was lower in Suwan 4452 (**Table 5**). Clearly, the contribution of stem reserves to grain mass was consistently higher in NK 40 than in other hybrids under both experiments, indicating an efficient and stable assimilate translocation despite inter annual differences in climatic conditions.

Canopy Temperature and Cell Membrane Stability Under Water Deficit

Canopy temperature varied significantly due to water regimes. Water deficit imposed at anthesis to milk showed significantly higher canopy temperature (CT) as compared to other water-deficit periods and control (**Figure 10A**). However, control under well-watered condition exhibited the lowest CT. This suggests that optimum water management helps regulate water uptake by roots and induce efficient transpiration cooling through the stomatal regulation leading to lower CT. Conversely, during the periods of water deficit, water shortage in the root zone induces stomatal closure and inhibits water loss through transpiration leading to relatively higher CT. Canopy temperature also differed significantly due to the interaction of hybrids and water regimes. NK 40 and Suwan 4452 showed significantly lower CT under control (33.40 and 34.40°C) and higher (34.80 and 35.90°C) in D3 treatment of Expt. 2. NK 40 recorded significantly lower CT under control and all water deficit treatments as compared to Suwan 4452, indicated that NK 40 sustained relatively higher RWC (%) under control and water-deficit conditions and we hypothesize this to be associated with partially opening of stomata resulting in continued transpirational cooling.

Water-deficit stress causes damages to plasma membranes of plant cell and results in leaking of electrolytes from the cell. The magnitude of plasma membrane damage due to water deficit can be estimated via measuring the proportion of ion leakage (Khan et al., 2007). In the present study, the electrolyte leakage in terms of EC was monitored at the late grain-filling stage of maize exposed to severe water deficit. Water deficit at different stages significantly increased EC as compared to control (**Figure 10B**). Hybrids showed a significant variation on EC across water regimes. Both hybrids showed significantly lower EC under control as compared to water deficit treatments. NK 40 exhibited relatively lower EC under severe water deficit, which indicated lower membrane damage as compared to Suwan 4452. It has been

suggested that the critical feature of tolerance to dehydration depends on the ability of the plant to limit membrane damage during dehydration and to regain membrane integrity and membrane-bound activities quickly upon rehydration (Tripathy et al., 2000). This result suggests that NK 40 showed relatively more water-deficit tolerance than Suwan 4452. Blum and Ebercon (1981) also reported that the changes in membrane permeability following exposure to water-deficit stress can be used to estimate water-deficit tolerance in crop plants.

Changes in Leaf Anatomy

In Expt. 2, severe water deficit induced some changes in mid-rib of leaf and attached leaf blade of NK 40 and Suwan 4452. From the anatomic view, it clearly shows that the number of xylem vessel in leaf blade increased under water deficit relative to control treatment in both maize cultivars (**Figures 11**, **12**). The increase in the number of xylem vessels under water deficit is quite consistent in NK 40 compared to Suwan 4452. In contrast, a decrease in the diameter of xylem vessels was observed under water deficit, with higher xylem diameter observed under control. De Souza et al. (2010) also reported a decrease in diameter of metaxylem of maize leaf under water stress condition. The decrease in the diameter of the metaxylem vessel is an adaptation mechanism by the plant under water deficit to avoid cavitation. This change in leaf anatomy is also supported by other studies which have reported that vessels with greater caliber are more prone to cavitation than vessels with smaller caliber (Vasellati et al., 2001). Mostajeran and Rahimi-Eechi (2008) reported that the cavitation process can diminish the plant capacity in transporting water and fixing carbon. A decrease in metaxylem vessel diameter can avoid cavitation and embolism due to the increase in the number of water molecules in contact to xylem cell walls per unit water volume (Hacke and Sperry, 2001). So the increase in the number of metaxylem vessels with narrow diameter could protect the water transportation system, possibly by favoring the water absorption in the root, the flow, and the distribution of water in the leaves.

The relative area of phloem in leaf mid-rib was found to be slightly higher in NK 40 under water deficit compared with control (**Figures 11A,B**). Though the phloem area in Suwan 4452 is not well visualized in anatomic view, under water deficit phloem area is quite evident. Comparing Suwan 4452, NK 40 exhibited relatively higher phloem area under water deficit indicating more mobilization of photosynthates during grain filling, supporting the higher SWD in both experiments (**Tables 4**, **5**). Souza et al. (2010) also revealed an increased phloem thickness in maize leaf under water stress. A relatively higher number of vascular bundle with smaller inter vascular bundle distance in mid-rib of both hybrids was observed under water deficit as compared to control. It was also an evidence of adaptation under water deficit to maintain a continuous stream of water.

In summary, the major physiological differences that rendered NK 40 to be more tolerant during post-anthesis water-deficit stress compared to other tested hybrids could be due to NK 40 having lower canopy temperature and EC indicated cell membrane stability across, higher kernel water, KDW, and stem reserve mobilization capacity as compared to Pioneer 30B80 and Suwan 4452 across water regimes in both experiments. Under water deficit at milk to PM, NK 40 had significantly higher cellular adaptation by increasing the number of xylem vessel while reducing vessel diameter in leaf mid-rib and attached leaf blade. These physiological adjustments improved efficient transport of water from root to the shoot, which in addition to higher kernel water content, MKWC, KFD, KFR, and stem reserve mobilization capacity, rendered NK 40 to be better adapted to water-deficit conditions under tropical environments.

CONCLUSION

Water deficit at different phenological stages exhibited significant variation on kernel water and kernel filling traits of field-grown maize. Water deficit at different periods resulted in relatively lower KWC and KDW measured after anthesis to PM, irrespective of hybrids. Water deficit advanced PM by reducing KFD by 5, 7, 7, and 11 days when maize plants were subjected to water deficit at D3 and D4 in Expt. 2, D4 and D5 in Expt.1, respectively, as compared to control. NK 40 had higher kernel water, KDW, and stem reserve mobilization capacity as compared to Pioneer 30B80 and Suwan 4452 across water regimes in both experiments. In addition, water deficit at milk to PM increased the number of xylem vessel in leaf mid-rib attached leaf blade of NK 40 relative to control which favored better adaptation under water-deficit environment. In addition, imporved vascular physiology, higher kernel water content, MKWC, KFD, KFR, and stem reserve mobilization capacity, helped NK 40 to be better adapted to water-deficit conditions under tropical environments.

DATA AVAILABILITY STATEMENT

The original contributions presented in the study are included in the article/supplementary material, further inquiries can be directed to the corresponding author/s.

AUTHOR CONTRIBUTIONS

MRA, SN, MSM, ES, and VV: conceptualization, methodology, and investigation. MRA, SN, MAI, MM, and AH: software. MRA and SN: validation. MRA, SN, MSM, and AH: formal analysis. SN: resources and supervision. MRA, SN, MSM, ES, VV, and AH: data curation. MRA, SN, MSM, MAI, ES, VV, and MM: writing–original draft preparation. MRA, MH, ED, MA, MB, MS, SJ, MAI, and AH: writing–review and editing. SN, ES, and MH: project administration. SN, MH, ED, MA, and AH: funding acquisition. All authors have read and agreed to publish the current version of the manuscript.

FUNDING

This current work was funded by NATP Phase 1, Bangladesh Agricultural Research Council (BARC), Dhaka, Bangladesh and

the Taif University Researches Supporting Project number (TURSP-2020/85), Taif University, Taif, Saudi Arabia.

ACKNOWLEDGMENTS

The authors wish to acknowledge the NATP Phase 1, Bangladesh Agricultural Research Council for the Fellowship and also Department of Agronomy, Kasetsart University (KU), Thailand for providing the research facility. The authors also thank Pasajee Kongsil, Department of Agronomy, KU for her help in the process of statistical analysis. The authors also extend their appreciation to Taif University for funding current work by Taif University Researches Supporting Project number (TURSP-2020/85), Taif University, Taif, Saudi Arabia. Contribution number 21-282-J from Kansas Agricultural Experiment Station.

REFERENCES

Altenbach, S. B., DuPont, F. M., Kothari, K. M., Chan, R., Johnson, E. L., and Lieu, D. (2003). Temperature, water and fertilizer influence the timing of key events during grain development in a US spring wheat. *J. Cereal Sci.* 37, 9–20. doi: 10.1006/jcrs.2002.0483

Aslam, M., Khan, I. A., Saleem, M., and Ali, Z. (2006). Assessment of water tolerance in different maize accessions at germination and early growth stage. *Pak. J. Bot.* 38, 1571–1579.

Balota, M., Payne, W. A., Evett, S. R., and Peters, T. R. (2008). Morphological and physiological traits associated with canopy temperature depression in three closely related wheat lines. *Crop Sci.* 48, 1897–1910. doi: 10.2135/cropsci2007.06.0317

Barlow, E. W. R., Lee, J. W., Munns, R., and Smart, M. G. (1980). Water relations of the developing wheat grain. *Aust. J. Plant Physiol.* 7, 519–525. doi: 10.1071/pp9800519

Bdukli, E. N., Celik, M., Turk, G., and Bayram, B. T. (2007). Effects of post anthesis drought stress on the stem–reserve mobilization supporting grain filling of two rowed barley cultivars at different levels of nitrogen. *J. Biol. Sci.* 7, 949–953. doi: 10.3923/jbs.2007.949.953

Blum, A. (1998). Improving wheat grain filling under stress by stem reserve mobilisation. *Euphytica* 100, 77–83.

Blum, A., and Ebercon, A. (1981). Cell membrane stability as a measure of drought and heat tolerance in wheat. *Crop Sci.* 21, 43–47. doi: 10.2135/cropsci1981.0011183x002100010013x

Borras, L., and Westgate, M. E. (2006). Predicting maize kernel sink capacity early in development. *Field Crops Res.* 95, 223–233. doi: 10.1016/j.fcr.2005.03.001

Borras, L., Westgate, M. E., and Otegui, M. E. (2003). Control of kernel weight and kernel water relations by post-flowering source-sink ratio in maize. *Ann. Bot.* 91, 857–867. doi: 10.1093/aob/mcg090

Borras, L., Zinselmeier, C., Lynn Senior, M., Westgate, M. E., and Muszynski, M. G. (2009). Characterization of grain filling patterns in diverse maize germplasm. *Crop Sci.* 49, 999–1009. doi: 10.2135/cropsci2008.08.0475

Brooking, I. R. (1990). Maize ear moisture during grain-filling, and its relation to physiological maturity and grain drying. *Field Crops Res.* 23, 55–68. doi: 10.1016/0378-4290(90)90097-u

Brooks, A., Jenner, C. F., and Aspinall, D. (1982). Effects of water deficit on endosperm starch granules and on grain physiology of wheat and barley. *Aust. J. Plant Physiol.* 9, 423–436. doi: 10.1071/pp9820423

De Souza, P. I., Egli, D. B., and Bruening, W. P. (1997). Water stress during seed filling and leaf senescence in soybean. *Agron. J.* 89:807. doi: 10.2134/agronj1997.00021962008900050015x

De Souza, T. C., Magalhaes, P. C., Pereira, F. J., de Castro, E. M., da Silva Junior, J. M., and Parentoni, S. N. (2010). Leaf plasticity in successive selection cycles of 'Saracura' maize in response to periodic soil flooding. *Pesq. Agropec. Bras.* 45, 6–24.

Egli, D. B. (1990). Seed water relations and the regulation of the duration of seed growth in soybean. *J. Exp. Bot.* 41, 243–248. doi: 10.1093/jxb/41.2.243

Egli, D. B. (1998). *Seed Biology and the Yield of Grain Crops*. Wallingford: CAB International.

Egli, D. B., and TeKrony, D. M. (1997). Species differences in seed water status during seed maturation and germination. *Seed Sci. Res.* 7, 3–11. doi: 10.1017/s0960258500003305

Ferrat, I. L., and Lovatt, C. J. (1999). Relationship between RWC, nitrogen pools and growth of *Phaseolus vulgaris* L. and P. acutifolius A. Grag during water deficit. *Crop Sci.* 39, 467–475. doi: 10.2135/cropsci1999.0011183x0039000200028x

Frederick, J. R., Woolley, J. T., Hesketh, J. D., and Peters, D. B. (1991). Seed yield and agronomic traits of old and modern soybean cultivars under irrigation and soil water-deficit. *Field Crops Res.* 27, 71–82. doi: 10.1016/0378-4290(91)90023-o

Gambin, B. L., Borras, L., and Otegui, M. E. (2007). Kernel water relations and duration of grain filling in maize temperate hybrids. *Field Crops Res.* 101, 1–9. doi: 10.1016/j.fcr.2006.09.001

Hacke, U. G., and Sperry, J. S. (2001). Functional and ecological xylem anatomy. *Perspect. Plant Ecol. Evol. Syst.* 4, 97–115.

Jones, R. J., and Simmons, S. R. (1983). Effect of altered source–sink ratio on growth of maize kernels. *Crop Sci.* 23, 129–134. doi: 10.2135/cropsci1983.0011183x002300010038x

Khan, H. U., Link, W., Hocking, T., and Stoddard, F. (2007). Evaluation of physiological traits for improving drought tolerance in faba bean (*Vicia faba* L.). *Plant Soil* 292, 205–213. doi: 10.1007/s11104-007-9217-5

Melchiori, R. J. M., and Caviglia, O. P. (2008). Maize kernel growth and kernel water relations as affected by nitrogen supply. *Field Crops Res.* 108, 198–205. doi: 10.1016/j.fcr.2008.05.003

Millet, E., and Pinthus, M. J. (1984). The association between grain volume and grain weight in wheat. *J. Cereal Sci.* 2, 31–35. doi: 10.1016/s0733-5210(84)80005-3

Molla, M. S. H., Nakasathien, S., Ali, M. A., Khan, A. S. M. M. R., Alam, M. R., Hossain, A., et al. (2019). Influence of nitrogen application on dry biomass allocation and translocation in two maize varieties under short pre-anthesis and prolonged bracketing flowering periods of drought. *Archiv. Agron. Soil Sci.* 65, 928–944. doi: 10.1080/03650340.2018.1538557

Mostajeran, A., and Rahimi-Eechi, V. (2008). Drought stress effects on root anatomical characteristics of rice cultivars (*Oryza sativa* L.). *Pak. J. Biol. Sci.* 11, 2173–2183. doi: 10.3923/pjbs.2008.2173.2183

Mstatc (1990). *A Microcomputer Program for the Design, Management, and Analysis of Agronomic Research Experiments*. East Lansing, MI: Michigan State University.

Palta, J. A., Kobata, T., Turner, N. C., and Fillery, I. R. (1994). Remobilization of carbon and nitrogen in wheat as influenced by post-anthesis water deficits. *Crop Sci.* 34, 118–124. doi: 10.2135/cropsci1994.0011183x003400010021x

Pepler, S., Gooding, M. J., and Ellis, R. H. (2006). Modeling simultaneously water content and dry matter dynamics of wheat grains. *Field Crops Res.* 95, 49–63. doi: 10.1016/j.fcr.2005.02.001

Prasad, P. V. V., Pisipati, S. R., Mutava, R. N., and Tuinstra, M. R. (2008). Sensitivity of grain sorghum to high temperature stress during reproductive development. *Crop Sci.* 48, 1911–1917. doi: 10.2135/cropsci2008.01.0036

Saini, H. S., and Westgate, M. E. (2000). Reproductive development in grain crops during drought. *Adv. Agron.* 68, 59–96. doi: 10.1016/s0065-2113(08)60843-3

Sala, R. G., Andrade, F. H., and Westgate, M. E. (2007). Maize kernel moisture at physiological maturity as affected by the source–sink relationship during grain filling. *Crop Sci.* 47, 711–716. doi: 10.2135/cropsci2006.06.0381

Schnyder, H., and Baum, U. (1992). Growth of the grain of wheat (*Triticum aestivum* L.). The relationship between water content and dry matter accumulation. *Eur. J. Agron.* 1, 51–57. doi: 10.1016/s1161-0301(14)80001-4

Souza, T. C., Magalhães, P. C., Pereira, F. J., Castro, E. M., Silva-Junior, J. M., and Parentoni-Neto, S. (2010). Leaf plasticity in successive selection cycles of 'saracura' maize in response to periodic soil flooding. *Pesqui. Agropecu. Bras.* 45, 16–24. doi: 10.1590/s0100-204x2010000100003

Swank, J. C., Egli, D. B., and Pfeiffer, T. W. (1987). Seed growth characteristics of soybean hybrids differing in duration of seed fill. *Crop Sci.* 27, 85–89. doi: 10.2135/cropsci1987.0011183x002700010022x

Tripathy, J. N., Zhang, J., Robin, S., Nguyen, Th.T, and Nguyen, H. T. (2000). QTLs for cell-membrane stability mapped in rice (*Oryza sativa* L.) under drought stress. *Theor. Appl. Genet.* 100, 1197–1202. doi: 10.1007/s001220051424

Vasellati, V., Oesterhelds, M., Medan, D., and Loreti, J. (2001). Effects of flooding and drought on the anatomy of *Paspalum dilatatum*. *Ann. Bot.* 88, 355–360. doi: 10.1006/anbo.2001.1469

Westgate, M. E. (1994). Water status and development of the maize endosperm and embryo during drought. *Crop Sci.* 34:76. doi: 10.2135/cropsci1994.0011183x003400010014x

Westgate, M. E., and Grant, D. L. T. (1989). Water deficits and reproduction in maize. Response of the reproductive tissue to water deficits at anthesis and mid-grain fill. *Plant Physiol.* 91, 862–867. doi: 10.1104/pp.91.3.862

Westgate, M. E., Otegui, M. E., and Andrade, F. H. (2004). "Physiology of the corn plant," in *Corn: Origin, History, Technology, and Production*, eds W. C. Smith, J. Betran, and E. Runge (Hoboken, NJ: Wiley), 235–271.

Yang, J., Zhang, J., Wang, Z., Xu, G., and Zhu, Q. (2004). Activities of key enzymes in sucrose-to-starch conversion in wheat grains subjected to water deficit during grain filling. *Plant Physiol.* 135, 1621–1629. doi: 10.1104/pp.104.041038

Conflict of Interest: The authors declare that the research was conducted in the absence of any commercial or financial relationships that could be construed as a potential conflict of interest.

Publisher's Note: All claims expressed in this article are solely those of the authors and do not necessarily represent those of their affiliated organizations, or those of the publisher, the editors and the reviewers. Any product that may be evaluated in this article, or claim that may be made by its manufacturer, is not guaranteed or endorsed by the publisher.

frontiers in Plant Science

ORIGINAL RESEARCH
published: 13 October 2021
doi: 10.3389/fpls.2021.722459

Alternate Partial Root-Zone Drip Nitrogen Fertigation Reduces Residual Nitrate Loss While Improving the Water Use but Not Nitrogen Use Efficiency

Rui Liu[1,2], *Peng-Fei Zhu*[2], *Yao-Sheng Wang*[3], *Zhen Chen*[1], *Ji-Rong Zhu*[2], *Liang-Zuo Shu*[1,2]* and *Wen-Ju Zhang*[4]*

[1] Zhejiang Provincial Key Laboratory of Plant Evolutionary and Conservation, School of Life Science, Taizhou University, Taizhou, China, [2] Anhui Key Laboratory of Resource and Plant Biology, School of Life Sciences, Huaibei Normal University, Huaibei, China, [3] Laboratory of Dryland Agriculture, Institute of Environment and Sustainable Development in Agriculture, Chinese Academy of Agricultural Sciences, Beijing, China, [4] National Engineering Laboratory for Improving Quality of Arable Land, Institute of Agricultural Resources and Regional Planning, Chinese Academy of Agricultural Sciences, Beijing, China

OPEN ACCESS

Edited by:
Thorsten M. Knipfer, University of British Columbia, Canada

Reviewed by:
Zhen Wang, China Institute of Water Resources and Hydropower Research, China
Harby Mostafa, Benha University, Egypt

***Correspondence:**
Liang-Zuo Shu
shulz69@163.com
Wen-Ju Zhang
zhwenju@163.com

Specialty section:
This article was submitted to Crop and Product Physiology, a section of the journal Frontiers in Plant Science

Received: *08 June 2021*
Accepted: *15 September 2021*
Published: *13 October 2021*

Citation:
Liu R, Zhu P-F, Wang Y-S, Chen Z, Zhu J-R, Shu L-Z and Zhang W-J (2021) Alternate Partial Root-Zone Drip Nitrogen Fertigation Reduces Residual Nitrate Loss While Improving the Water Use but Not Nitrogen Use Efficiency. Front. Plant Sci. 12:722459. doi: 10.3389/fpls.2021.722459

The efficient utilization of irrigation water and nitrogen is of great importance for sustainable agricultural production. Alternate partial root-zone drip irrigation (APRD) is an innovative water-saving drip irrigation technology. However, the coupling effects of water and nitrogen (N) supply under APRD on crop growth, water and N use efficiency, as well as the utilization and fate of residual nitrates accumulated in the soil profile are not clear. A simulated soil column experiment where 30–40 cm soil layer was $^{15}NO_3$-labeled as residual nitrate was conducted to investigate the coupling effects of different water [sufficient irrigation (W_1), two-thirds of the W_1(W_2)] and N [high level (N_1), 50% of N_1 (N_2)] supplies under different irrigation modes [conventional irrigation (C), APRD (A)] on tomato growth, irrigation water (IWUE) and N use efficiencies (NUE), and the fate of residual N. The results showed that, compared with CW_1N_1, AW_1N_1 promoted root growth and nitrogen absorption, and increased tomato yield, while the N absorption and yield did not vary significantly in AW_2N_1. The N absorption in AW_2N_2 decreased by 16.1%, while the tomato yield decreased by only 8.8% compared with CW_1N_1. The highest IWUE appeared in AW_2N_1, whereas the highest NUE was observed in AW_2N_2, with no significant difference in NUE between AW_2N_1 and CW_1N_1 at the same N supply level. The ^{15}N accumulation peak layer was almost the same as the originally labeled layer under APRD, whereas it moved 10–20 cm downwards under CW_1N_1. The amount of ^{15}N accumulated in the 0-40 cm layer increased with the decreasing irrigation water and nitrogen supply, with an increase of 82.9–141.1% in APRD compared with that in CW_1N_1. The utilization of the ^{15}N labeled soil profile by the tomato plants increased by 9–20.5%, whereas the loss rate of ^{15}N from the plant-soil column system decreased by 21.3–50.1% in APRD compared with the CW_1N_1 treatment. Thus, APRD has great potential in saving irrigation water, facilitating water use while reducing the loss of residual nitrate accumulated in the soil profile, but has no significant effect on the NUE absorbed.

Keywords: root growth, fruit yield, irrigation water use efficiency, nitrogen use efficiency, ^{15}N

INTRODUCTION

Water shortage is a great concern that is jeopardizing sustainable development globally, including in China. Water crisis coexists with the low efficiency of irrigation water in agricultural production, which consumes ∼70% of the total freshwater (Mancosu et al., 2015; Kang et al., 2017). Developing water-saving irrigation technologies is an essential and urgent requirement to support the high food demand for the increasing world population. Deficit irrigation and alternate partial root-zone irrigation (APRI) are two water-saving irrigation strategies currently investigated (Kang and Zhang, 2004; Dodd, 2009; Sezen et al., 2019). In deficit irrigation, the amount of water supplied to the whole root zone is less than that of plant evapotranspiration, inducing moderate water stress in the plant which has marginal effects on yield formation (Dodd, 2009). In APRI, irrigation is supplied only to half of the root system, leaving the other half dry till the next irrigation occurs. The repeated alternation of wetting/drying in the two root zones in APRI induces an abscisic acid (ABA)-based root-to-shoot chemical signaling, hydraulic signals, and an increased xylem sap pH to regulate the stomatal opening thereby increasing water use efficiency (WUE) (Kang and Zhang, 2004; Hu et al., 2011; Pérez-Pérez et al., 2018). For many plant species including cotton, corn, tomato, potato, cucumber, grape, and apple, APRI has been demonstrated to be an efficient water-saving irrigation technology that outperforms deficit irrigation by maintaining the yield and improving the WUE substantially (Kang and Zhang, 2004; Shahnazari et al., 2007; Dodd, 2009; Yactayo et al., 2013; Jovanovic and Stikic, 2018; Sarker et al., 2019). The main form in APRI application is the alternate furrow irrigation or alternate watering to different sides of the plants (Yactayo et al., 2013; Zhang et al., 2014; Sarker et al., 2019, 2020; Khalili et al., 2020). However, it is a time-consuming and laborious process to manipulate the furrows or to manually switch the irrigation sides, which limits its use in practice. With the popularization of drip fertilization technology, an emerging new kind of APRI, named alternate partial root-zone drip irrigation (APRD) is formed by combining drip irrigation with APRI (Du et al., 2008a,b; Topak et al., 2016; Sezen et al., 2019). This form of APRI is not only easy to implement but also potentially has the advantages of both APRI and drip irrigation in improving WUE and yield (Topak et al., 2016; Sezen et al., 2019; Liu et al., 2020).

Nitrogen is an important macro-nutrient for crop growth and yield. However, the excessive application of nitrogen (N) fertilizer not only reduces fertilizer use efficiency but also produces many environmental problems, adversely impacting the quality of vegetables and fruit trees (Zhu and Chen, 2002; Gong et al., 2011). In addition, excessive fertilization leads to the accumulation of high amounts of residual nitrate in the soil profile of farmlands, which could leach into the groundwater, causing environmental problems (Zhu and Chen, 2002; Gathumbi et al., 2003). Therefore, increasing the N use efficiency (NUE) and reducing the soil residual nitrate accumulation and its leaching into the groundwater is an important issue to be resolved (Gathumbi et al., 2003).

Alternate partial root-zone irrigation can facilitate the accumulation of nitrate in the topsoil, promote the absorption of N by plants, and reduce the potential risk of nitrate leaching (Tafteh and Sepaskhah, 2012; Wang et al., 2014, 2020; Hou et al., 2017). However, whether the NUE in plants has improved under APRI is unclear. Although APRD is a promising new technology, the coupling effects of different water and N supplies on the movement and utilization of the residual nitrate accumulated in the soil profile under APRD are not known. Furthermore, the residual nitrate accumulated 30–40 cm under APRI also received little attention. Root growth and distribution decreased sharply beneath 20 cm, while it accumulated higher amounts of residual nitrate in the 20–40 cm layer (Zhang et al., 2014; Liu et al., 2020). Therefore, in the present study, a soil column experiment was conducted with the ^{15}N-labeled $K^{15}NO_3$ as the residual nitrate in the 30–40 cm soil layer, to investigate the effects of different water and nitrogen supply on the growth, WUE, NUE, and the fate of residual nitrate accumulated in the soil profile of tomato plants, a common greenhouse vegetable, under APRD. The outcome of this study would be of great significance to guide efficient utilization of water and N resources and reduce environmental risk by sustainable agricultural production.

MATERIALS AND METHODS

Experimental Site

The experimental site is located in a steel-framed vegetable greenhouse in Xuji Village (116°46′E, 33°58′N), Duji District, Huaibei City, Anhui Province, China. It belongs to a typical temperate humid climate, with an average annual relative humidity of 71%, an annual average frost-free period of 202 days, and sunshine hours of 2315.8 h. The experiment was initiated on February 28 and finished on June 25, 2017. The experimental soil was sandy loam (Shu et al., 2020). The pH of the soil was 7.3, with 26.2% (gravimetric) or 0.341 cm^{-3} field water capacity, 1.6 g kg^{-1} total N, 37.4 mg kg^{-1} nitrate N, 0.6 g kg^{-1} total phosphorus (P), and 1.3 g cm^{-3} soil bulk density.

Experimental Treatments

The experiment was performed using soil columns which were made using cylindrical aluminum drums (**Figure 1**) as described in our previous studies (Wang et al., 2019, 2020; Liu et al., 2020). A ditch was dug in the center of the greenhouse and the soil from the layers 0–20, 20–40, 40–60, and 60–100 cm were separated. Eighteen homemade bottomless cylindrical aluminum drums with a height of 105 cm and a diameter of 45 cm were put vertically to a depth of 100 cm along the ditch, 15 cm apart from each other. Then the sieved dry soil (passed through a 2 mm sieve) from the original layers was backfilled to the drums and watered to its 90% field capacity layer by layer. While filling the soil columns, the ditch area outside the drums was also filled. In the 30–40 cm layer of each column, the soil was mixed and labeled with 11.9 g $K^{15}NO_3$ (the abundance of ^{15}N was 20.3%, provided by the Shanghai Research Institute of Chemical Industry). All the P and potassium fertilizers were supplied as basal fertilizers and were mixed with the top 0–20 cm soil layer as KH_2PO_4 and K_2SO_4 at the rate of 200 mg P_2O_5 kg^{-1} and 300 mg K_2O kg^{-1},

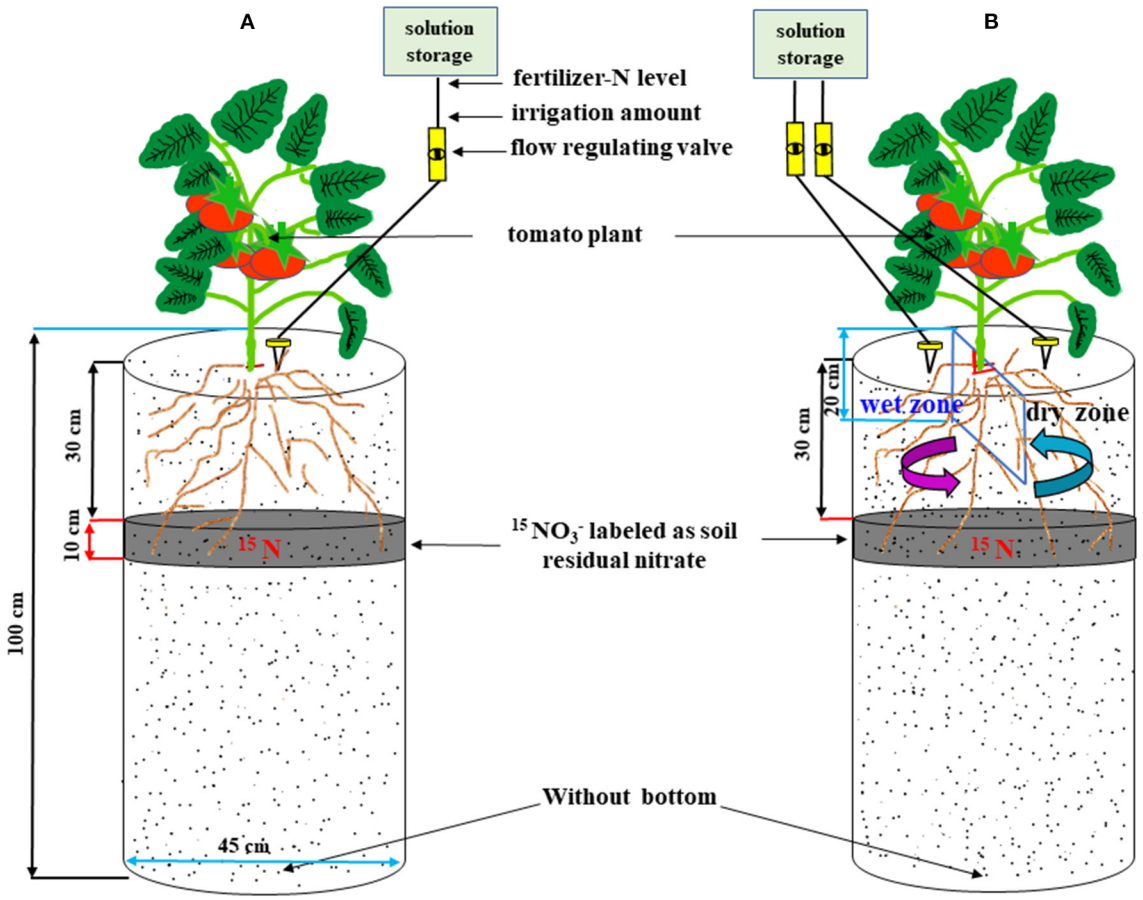

FIGURE 1 | The schematic view of the soil column design for conventional drip irrigation **(A)** and alternate partial root-zone drip irrigation **(B)**.

respectively. Nitrogen fertilizer was supplied by fertigation while planting the tomatoes. To avoid the surface flow of irrigated water between the root compartments as indicated previously in the pot APRI experiments (Li et al., 2010; Wang et al., 2010), the top 0-20 cm soil in the APRD column was separated into two equal compartments by inserting a plastic film vertically in the center (Hou et al., 2017; Liu et al., 2020). A gap of 5 × 5 cm size was cut in the center of the plastic film to allow the transplanting of tomato seedlings.

The method for supplying water and N was the same as in our previous study (Liu et al., 2020). Briefly, a 5 L plastic bucket was suspended at a height of 1.8 m above the soil column (**Figure 1**). The water and N fertilizers were delivered from the bucket to the surface of the soil column through a medical infusion tube with needles (specification 16G, aperture 1.3 mm). On February 28, 2017, 50-day-old tomato (*Lycopersicon esculentum* Mill., cv. Zhongyan No. 958) seedlings of uniform size were transplanted in the center of the columns, with one seedling for each column. The surface layer of the column was covered with a plastic film after transplanting to reduce water evaporation. The plants were watered with conventional drip irrigation during the plant re-establishment stage. The water and N fertilizer treatments were initiated 18 days after transplantation (March 18). The four treatments included CW_1N_1, AW_1N_1, AW_2N_1, and AW_2N_2, where C represented conventional drip irrigation, A represented APRD, W_1 and W_2 represented sufficient and deficient irrigation, and N_1 and N_2 represented high N and low N application rate, respectively. Each treatment was replicated four times.

In the CW_1N_1 treatment, the soil in 0–20 cm (seedling stage) or 0–30 cm (after flowering stage) was irrigated to 90% of the field capacity whenever the soil water content dropped to 65% of the field capacity. The irrigation amount of W_1 (CW_1N_1) was calculated according to the method described by Liu et al. (2020). Irrigation was applied to all treatments when CW_1N_1 was irrigated. For the deficient irrigation treatment, two-thirds of the W_1 (W_2) irrigation amount was applied. For the N application amount, N_1 was calculated as supplying N at 240 mg kg^{-1} to the 0–20 cm soil layer in the column, and N_2 received 50% of the N_1 level. The N fertilizer was supplied as urea at 8.30 g urea per column for the N_1 level during the experiment. In the CW_1N_1 treatment, fertigation was supplied to a location 5-cm away from the plants through needles (**Figure 1A**). In the APRD treatment (AW_1N_1, AW_2N_1, and AW_2N_2), fertigation was supplied alternately to only one compartment in the center

of each irrigation event, letting the other soil compartment dry. At the next irrigation, the fertigation was shifted to the previously dry compartment, letting the previously irrigated compartment dry (**Figure 1B**). The N fertigation interval was at 4–10 days depending on the soil water content in the soil columns. There were a total of fourteen drip fertigation events in the present study, with 0.593 or 0.296 g urea at each fertigation for the N_1 or N_2 treatment, respectively, forming seven alternating wetting–drying fertigation cycles in each root compartment of the AW_1N_1-, AW_2N_1-, and AW_2N_2-treated soil columns.

To monitor the changes in the soil water content and to determine when to start the irrigation, two soil columns without the ^{15}N labeling were set as the reference and were managed as the CW_1N_1 treatment. A time-domain reflection meter (TDR) instrument (TRIME-PICO-IPH-TDR, IMKO, Germany) was buried in the reference column at a depth of 0–100 cm. In addition, a portable TDR soil moisture meter was also used for examining the soil water content in the 0–20 cm soil layer. When the soil moisture content declined to 65% of the field capacity, irrigation was applied to all columns. The amount of water supplied was 8.5 L for each column before different drip fertigation treatments were initiated. After that, 42.7 L or 28.2 L of irrigation water was supplied to the treatments as W_1 and W_2, respectively. Therefore, the W_2 treatment saved 28.3% of irrigation water in the whole plant growth period compared with that of W_1. The plants had five ears of fruit per plant and there were three fruits per ear. The tomato plants were finally harvested on June 25, 2017.

Measurements and Methods

On May 5, after removing the apical buds, the plant height and stem diameter were measured. The plant height was measured with a tape. The diameter of the stem (3 cm above the ground) was measured with a 0.01 mm precision digital vernier caliper (Shanghai Meinaite Industrial Inc., Shanghai, China).

The fallen leaves on the ground were collected during plant growth, and the fruits were harvested successively to maturity. The plants were harvested on June 25, 2017, and were divided into leaves, stems, and fruits. All the fresh samples were weighed and then oven-dried at 105°C for 30 min immediately after sampling and thereafter dried at 70°C to constant mass. The biomass of the leaves included the fallen leaves. The fruit yield was the cumulative value of fruits collected in different batches.

After harvest, the soil outside the soil columns was dug out, then the aluminum drum was exposed and cut longitudinally. About 20 cm per layer of soil was taken out from the drums horizontally. The roots were collected carefully using tweezers and then cleaned with distilled water. After root samples in each layer were collected, the soil was mixed thoroughly in a basin and soil samples were taken. A subsample was used to determine the soil water content immediately. The remaining soil samples were air-dried and then used for determining the total N content and the soil ^{15}N.

The roots were scanned by a root scanner (Epson Perfection V700 Photo, Epson, Japan), and the root length, diameter, and surface area were analyzed with a WinRhizoPro Vision 5.0 (Regent Instruments, Inc., Quebec, Canada). After scanning, the roots in each layer were dried in the oven to constant mass.

Both the plant and soil samples were ground and passed through a 0.25-mm sieve. The concentrations of the total N and ^{15}N were analyzed using mass spectrometry (isoprime100, Elementar Analysensysteme GmbH, Germany) coupled with an elemental analyzer (Vario pyro cube, Analysensysteme GmbH, Germany). The total N absorption was calculated by N concentration and the dry mass of each organ.

Irrigation water use efficiency ($kg \cdot m^{-3}$) = fresh mass of tomato fruit/total irrigation water used. NUE ($g \cdot g^{-1}$) = dry mass of tomato fruit/N accumulated in the plant. ^{15}N absorption (mg) = (atom% ^{15}N excess of total N in plant) × (total N in the plant). The utilization of ^{15}N by the plants (%) = (atom% ^{15}N excess of total N in the plant) × (total N in the plant)/(amount of ^{15}N labeled). Soil ^{15}N accumulation (mg) = (atom% ^{15}N excess of soil total N) × (total N per soil layer).

Statistical Analysis

The experimental data were analyzed using a one-way ANOVA with the SPSS software (IBM, Armonk, NY, USA) and average comparisons were made using Duncan's multiple range test at $P \leq 0.05$. The data were expressed as mean ± standard error.

RESULTS

Effects of Irrigation and Nitrogen Supply on Plant Growth

The irrigation methods and the amount of irrigation water or N supplied did not affect the height of the tomato plants (**Figure 2A**), but significantly affected the stem diameter (**Figure 2B**). Compared with the CW_1N_1 treatment, the stem diameter under the AW_1N_1 treatment increased by 1.6%, whereas it decreased by 3.3 and 5.5% under the AW_2N_1 and AW_2N_2 treatment, respectively. Under APRD, a reduction in one-third of the irrigation water decreased the stem diameter by 4.8% in the AW_2N_1 treatment compared with AW_1N_1.

Compared with CW_1N_1, the leaf and total biomass and fruit mass in the AW_1N_1 treatment increased significantly except for the stem dry mass (**Table 1**). Under APRD, the stem, leaf, and total dry biomass and fruit mass in the AW_2N_1 treatment were significantly lower than those of AW_1N_1. Compared with the CW_1N_1 treatment, the total biomass in the AW_2N_1 treatment decreased by 5.8%, while the fruit mass did not decrease significantly. Under the APRD with W_2 and a reduction in N fertilizer by 50%, there were no significant effects on the fruit yield and leaf biomass but decreased the stem biomass and total biomass by 8.4% on average (AW_2N_2 vs. AW_2N_1). Compared with CW_1N_1, the fruit yield in AW_2N_2 decreased by only 8.8%, even though the irrigation amount and nitrogen application rate were both decreased substantially in the AW_2N_2.

Effects of Irrigation and Nitrogen Supply on Root Growth and Distribution

Compared with CW_1N_1, AW_1N_1 increased the root length and surface area by 6.8 and 8.7%, respectively, while there was no significant difference in the root dry mass (**Table 2**). There was

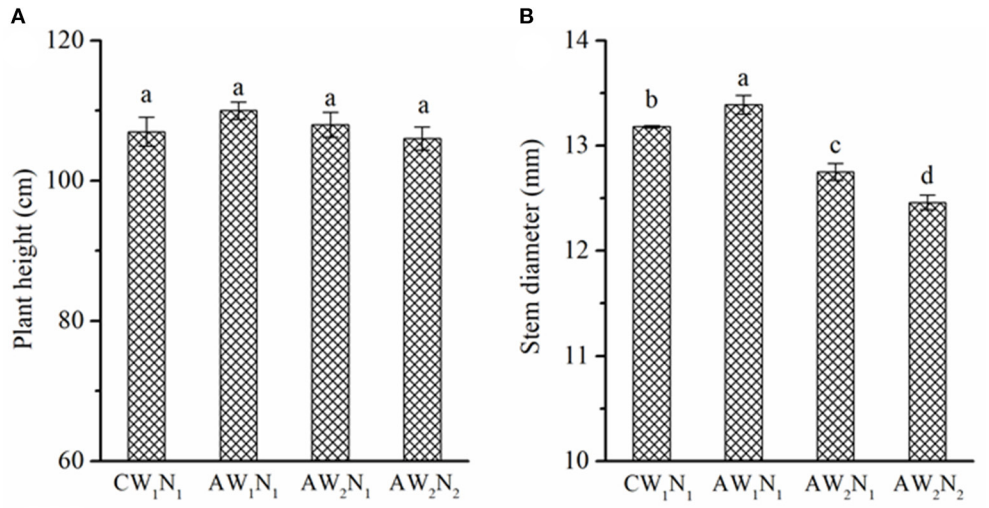

FIGURE 2 | The effects of irrigation and nitrogen (N) supply on the plant height (**A**, cm) and stem diameter (**B**, mm) of tomato plants under alternate partial root-zone drip irrigation. Values are the means ± SE. Different lowercase letters in the columns denote significant differences among the treatments ($P \leq 0.05$).

TABLE 1 | Effects of irrigation and nitrogen (N) supply on tomato biomass (g plant^{-1}) and yield (g plant^{-1}) under alternate partial root-zone drip N fertigation.

Treatments	Stem dry mass	Leaf dry mass	Fruit dry mass	Fruit fresh mass	Total biomass*
CW_1N_1	91.0 ± 2.8ab	80.7 ± 1.0b	220.9 ± 3.9b	4270 ± 29b	403.2 ± 5.4b
AW_1N_1	95.3 ± 0.8a	88.0 ± 0.7a	259.5 ± 2.5a	4573 ± 24a	453.9 ± 3.2a
AW_2N_1	87.6 ± 0.3b	72.7 ± 2.7c	208.9 ± 7.8bc	4117 ± 64b	379.7 ± 7.1c
AW_2N_2	77.8 ± 1.8c	68.0 ± 1.6c	202.6 ± 2.7c	3874 ± 38c	358.0 ± 2.5d

**The total biomass was the sum of the dry mass of root, stem, leaf, and fruit. Values are the means ± SE. The different lowercase letters in the column denote significant differences among the treatments ($P \leq 0.05$).*

TABLE 2 | The effects of irrigation and N supply on the mass, length, and surface area of tomato roots under alternate partial root-zone drip N fertigation.

Treatments	Dry mass (g plant^{-1})	Length (m plant^{-1})	Surface area (cm^2 plant^{-1})
CW_1N_1	10.60 ± 0.12a	226.3 ± 0.6b	9009 ± 153b
AW_1N_1	11.11 ± 0.09a	241.8 ± 4.3a	9792 ± 150a
AW_2N_1	10.58 ± 0.13a	230.6 ± 3.8b	9243 ± 118b
AW_2N_2	9.60 ± 0.39b	221.6 ± 1.2b	7882 ± 160c

The values are the means ± SE. The different lowercase letters in the columns denote significant differences among the treatments ($P \leq 0.05$).

no significant difference in the root dry mass, length, and surface area between the AW_2N_1 and CW_1N_1 treatments. However, the root length and root surface area were lower in AW_2N_1 than those of AW_1N_1. The AW_2N_2 treatment had no significant influence on the root length but decreased the root dry mass by 9.4% and the root surface area by 12.5% compared with the CW_1N_1 treatment.

Compared with the CW_1N_1 treatment, the root mass in the AW_1N_1 treatment increased significantly in the 0–40 cm soil layer, which was similar in the 40–80 cm but decreased in the 80–100 cm soil layer (**Figure 3A**). The AW_2N_1 had a similar root mass in the 0–60 cm soil layer compared with the CW_1N_1 treatment. The root mass under APRD in the 80–100 cm soil layer was reduced by 21.4–45.8% compared with that under the CW_1N_1 treatment.

Compared with the CW_1N_1 treatment, the root length in the AW_1N_1 treatment showed no significant difference in the 0–40 cm soil layer but increased by 8.2% significantly in the 40–100 cm (**Figure 3B**). There was no significant difference in the total root length or root length in different soil layers between AW_2N_1 and AW_2N_2 except in the 60–80 cm soil layer, where the root length increased significantly in AW_2N_1. However, the root length below 40 cm in the soil profile decreased significantly in AW_2N_1 and AW_2N_2 compared with that of AW_1N_1 (**Table 2** and **Figure 3B**).

Compared with CW_1N_1, the root diameter tended to decrease under the APRD treatments (**Figure 3C**), by 6.5% on average in AW_1N_1 in the 20–80 cm layer, and 10 and 14.4% in 0–100 cm in AW_2N_1 and AW_2N_2, respectively.

The variations of the root surface area among the treatments were similar to that of the root length (**Figure 3D**). Compared with CW_1N_1, the root surface area in the soil profile of AW_1N_1

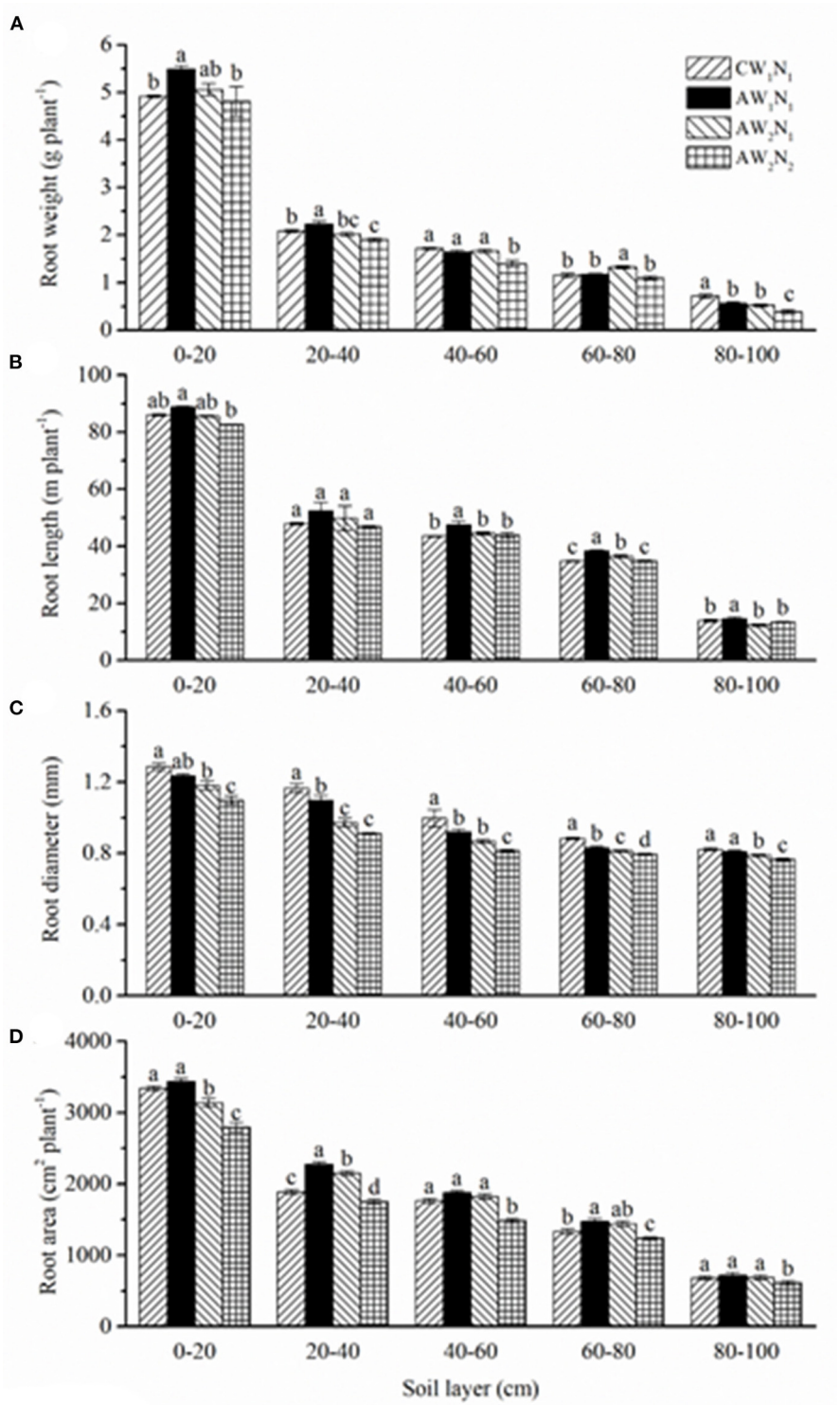

FIGURE 3 | The effects of irrigation and N supply on root growth and distribution in soil layers under alternate partial root-zone drip irrigation. **(A)** Root weight (g plant^{-1}), **(B)** root length (m plant^{-1}), **(C)** toot diameter (mm) and **(D)** root area (cm^2 plant^{-1}). Values are the means ± SE. Different lowercase letters in the columns denote significant differences among the treatments ($P \leq 0.05$).

tended to increase in the 0–80 cm layer and showed a significant difference in 20–80 cm. Reduction of water and/or N fertilizer under APRD decreased the root surface area, but this decrease became less obvious with the increase in soil depth. Compared with CW_1N_1, the root surface area in the AW_2N_2 treatment decreased significantly in different soil layers except in 60–80 cm.

Effects of Irrigation and Nitrogen Supply on Water, Nitrogen, and ^{15}N Use Efficiency

At the same fertigation level, AW_1N_1 increased the N absorption by 13.8%, and irrigation water use efficiency (IWUE) by 7.1% compared with that of CW_1N_1. However, there was no significant difference in the NUE between CW_1N_1 and AW_1N_1 (**Table 3**). Under APRD, the total N absorption by the tomato plants decreased with a reduction in irrigation amount and N level, with the highest N absorption observed in AW_1N_1. The IWUE of plants treated with AW_2N_1 was highest among the treatments. Compared with CW_1N_1, AW_2N_1 increased the IUWE by 35.6%, but no significant difference in NUE was observed. The AW_2N_2 treatment had the highest NUE among all treatments, being 9.4% higher than that of CW_1N_1. Similarly, the IWUE was also higher in AW_2N_2 than those in CW_1N_1 and AW_1N_1 treatments.

There was no significant difference in the total ^{15}N absorption and ^{15}N recovery rate between the treatments CW_1N_1 and AW_1N_1 (**Figure 4**). The ^{15}N absorption and recovery rate in AW_2N_1 was the highest among all the treatments, which increased by 20.5% compared with that of CW_1N_1. The total ^{15}N absorption and recovery rate showed no significant difference among the treatments of AW_2N_2, AW_1N_1, and CW_1N_1.

TABLE 3 | The effects of irrigation and N supply on the total plant N absorption, irrigation water (IWUE), and N (NUE) use efficiency under alternate partial root-zone drip N fertigation.

Treatments	Total N (g plant^{-1})	NUE (g·g^{-1})	IWUE (kg·m^{-3})	IWUE (kg·ha^{-1}·mm^{-1})
CW_1N_1	8.41 ± 0.10b	26.26 ± 0.31bc	83.41 ± 0.56d	834 ± 6d
AW_1N_1	9.57 ± 0.11a	27.12 ± 0.31b	89.34 ± 0.47c	893 ± 5c
AW_2N_1	8.21 ± 0.23b	25.43 ± 0.32c	113.12 ± 1.44a	1131 ± 14a
AW_2N_2	7.06 ± 0.14c	28.74 ± 0.49a	105.53 ± 1.86b	1055 ± 19b

The values are the means ± SE. The different lowercase letters in the columns denote significant differences among the treatments ($P \leq 0.05$).

Effects of Irrigation and Nitrogen Supply on ^{15}N Distribution in Different Soil Layers

The ^{15}N was labeled in the 30–40 cm layer of the soil columns. However, ^{15}N was also found in the 0–20 cm layer after harvest (**Figure 5**), indicating that ^{15}N has moved upward and was taken up by plants. In the 0–20 cm soil layer, the ^{15}N accumulation in the CW_1N_1 treatment was significantly lower than that of the APRD treatment. In the 20–40 cm soil layer, the ^{15}N accumulation of CW_1N_1 accounted for only 19.3% of the total ^{15}N labeled, while AW_1N_1, AW_2N_1, and AW_2N_2 accounted for 36.6, 38.6, and 49.7% of the applied ^{15}N, respectively.

The distance between the soil layer where the ^{15}N accumulation peak appeared after plant harvest and the layer labeled with $K^{15}NO_3$ at the beginning of the experiment was considered the movement distance of the residual nitrogen in a specific layer (Wang et al., 2014; Liu et al., 2020). The ^{15}N accumulation in the CW_1N_1 treatment peaked in the 40–60 cm layer, indicating the downward movement distance of 10–20 cm; while the ^{15}N accumulation in all the APRD treatments in 20–40 cm, indicating a slow movement of ^{15}N in the soil profile or it moved upward only within 10 cm (as we did not take soil samples every 10 cm per layer) as reported previously (Wang et al., 2014, 2019, 2020). In the layers where the ^{15}N accumulation peaked, the ^{15}N accumulation in CW_1N_1 decreased by 2.1, 8, and 17.7%, respectively, compared with those in AW_1N_1, AW_2N_1, and AW_2N_2 treatments. In APRD with the same nitrogen supply level (N_1), the ^{15}N accumulation increased in the 0–20 and 20–40 cm soil layers, while decreased in the layers below 40 cm in the AW_2N_1 treatment as compared with AW_1N_1. Under deficient soil water level, the reduction in 50% of the nitrogen

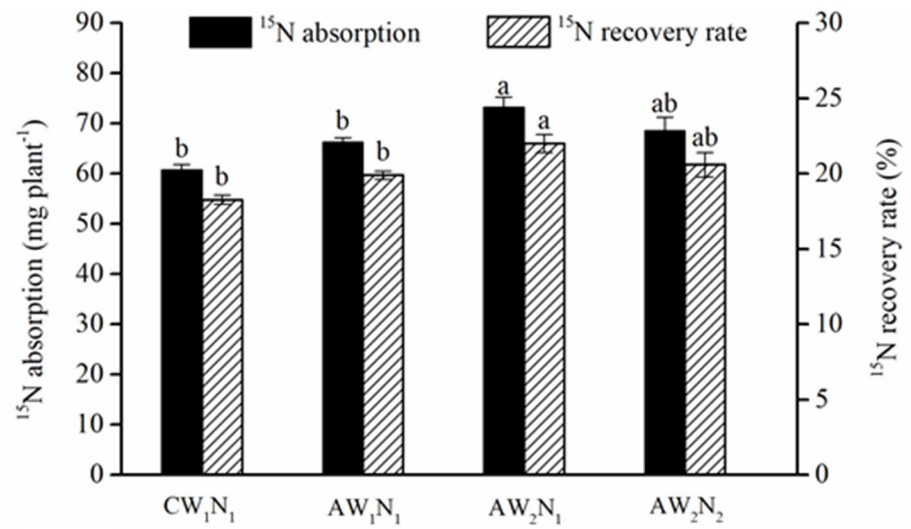

FIGURE 4 | The effects of water and N supply on ^{15}N absorption and recovery rate by tomato plants under alternate partial root-zone drip irrigation. Values are the means ± SE. Different lowercase letters in the columns denote significant differences among the treatments ($P \leq 0.05$).

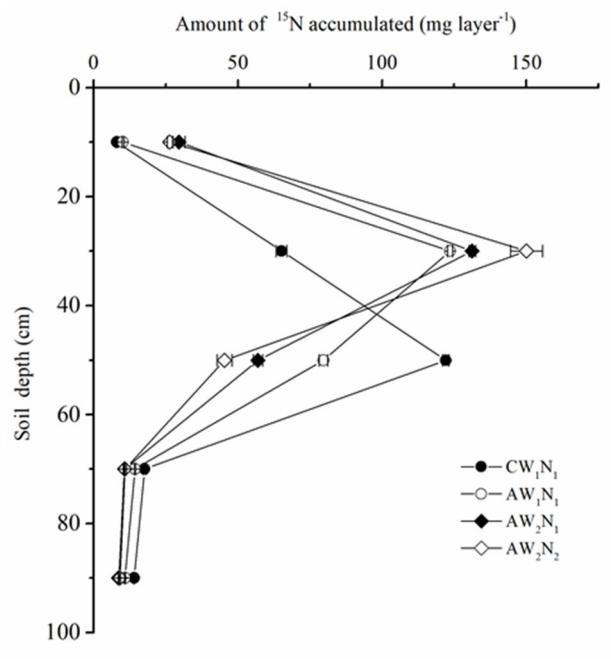

FIGURE 5 | The effects of irrigation and N supply on the distribution of labeled ^{15}N in different soil layers under alternate partial root-zone drip irrigation. Values are the means ± SE.

supply (AW_2N_2) increased the ^{15}N accumulation significantly in the 20-40 cm layer, but decreased in the 40–60 cm, with no significant difference observed in ^{15}N accumulation in the other layers compared with AW_2N_1.

Effects of Irrigation and Nitrogen Supply on the ^{15}N Accumulation and Recovery and Its Loss From the Soil Column

Under the same amount of water and nitrogen supply, the AW_1N_1 treatment increased the total ^{15}N recovery by 3.7%, while the ^{15}N loss rate decreased by 21.3%, and with no significant effects on the ^{15}N accumulation in the 0–100 cm soil profile compared with CW_1N_1 (**Table 4**). Under APRD, the reduction in both the water and N fertilizer significantly increased the ^{15}N recovery and accumulation in the soil profile, while the ^{15}N loss and loss rate decreased by 30%. However, the recovery amount, loss amount, and loss rate were similar between AW_2N_2 and AW_2N_1.

TABLE 4 | The effects of irrigation and N treatments on ^{15}N accumulation and recovery and ^{15}N loss from the top 0–100 cm soil layer under alternate partial root-zone drip N fertigation.

Treatments	Accumulation amount (mg column^{-1})	Recovery amount (mg column^{-1})	Loss amount (mg column^{-1})	Loss rate (%)
CW_1N_1	226.66 ± 1.60b	287.47 ± 2.46c	50.33 ± 2.46a	14.90 ± 0.73a
AW_1N_1	231.85 ± 3.07b	298.21 ± 2.49b	39.59 ± 2.49b	11.72 ± 0.74b
AW_2N_1	239.95 ± 2.15a	310.71 ± 1.54a	25.09 ± 1.64c	7.43 ± 0.56c
AW_2N_2	241.62 ± 2.14a	310.19 ± 0.72a	27.61 ± 0.92c	8.17 ± 0.22c

11.9 gram of ^{15}N-labeled $K^{15}NO_3$ with the ^{15}N abundance of 20.3% provided 337.8 mg ^{15}N to the 30–40 cm soil layer in each column. The total recovery amount of ^{15}N was included in the ^{15}N accumulated in the 0–100 cm soil and absorbed by the plant. The total loss of ^{15}N was calculated from the difference between labeled ^{15}N introduced by $K^{15}NO_3$ and the total recovery amount. The data in the table are the means ± SE. The different lowercase letters in the columns denote significant differences among different treatments ($P \leq 0.05$).

DISCUSSION

Effect of Irrigation and Nitrogen Supply on Plant Growth, WUE, and NUE

In the present study, the crop growth and yield were significantly affected by the water and N application levels and methods. Compared with CW_1N_1, APRD significantly increased the plant biomass and fruit mass under the same level of irrigation and N application (AW_1N_1) (**Table 1**). Reducing the irrigation water by one-third decreased the plant biomass significantly, while the fruit yield was not affected in AW_2N_1 (**Table 1**). Therefore, APRD improved the IWUE by 35.6% without any significant yield reduction (**Tables 1**, **3**). This result is in agreement with the advantages of APRD on saving irrigation water reported in several previous studies (Topak et al., 2016; Sezen et al., 2019; Shu et al., 2020). In addition to the improved IUWE, N absorption was also enhanced under APRD (**Table 3**). Even though the biomass decreased significantly, the total N absorption varied little in AW_2N_1 when compared with that in CW_1N_1 whereas it decreased by only 16% in AW_2N_2, where a 50% reduction in the nitrogen fertilizer occurred (**Tables 1**, **3**).

Several reasons could account for the improved IUWE and N absorption under APRD. Under APRI (including APRD), roots could sense the drying soil, and thus generated root-sourced signals to reduce stomatal opening (Kang and Zhang, 2004; Dodd et al., 2006; Liu et al., 2006). It has been demonstrated that the moderate closure of the stomata significantly inhibited the transpiration rate, but showed little effect on photosynthesis, which can stabilize crop growth and yield and improve WUE under APRI with a substantial reduction in irrigation water (Kang and Zhang, 2004). Moreover, under APRI, the root system in the irrigated side can absorb enough water and nutrients to meet the demands of the plants. The roots under APRD became thinner, which increased the root length and surface area in different layers of the soil profile, especially in the middle and lower layers (**Figure 3**), which is consistent with our previous reports (Chen et al., 2016; Wang et al., 2019; Liu et al., 2020). Several studies reported that APRI could promote the compensatory and balanced growth of roots in different root zones, stimulate the growth and development of root hairs, and induce more root distribution deeper in the soil [refer to review by Kang and Zhang (2004) and Zhang et al. (2014)]. In addition, the repeated drying/wetting cycles improved the soil aeration, which was conducive to

root activity. The increased root growth and root activity could promote the absorption of water and nutrients by plants (Kang and Zhang, 2004; Sarker et al., 2020). Furthermore, APRI could stimulate organic carbon and N mineralization and release more mineral N into the soil solution, which could promote the absorption of N by plants (Sun et al., 2013; Liu et al., 2020). It was reported that APRI (including APRD) could increase the recovery rate of both the fertilizer-N and residual N accumulated in the soil (Wang et al., 2014; Hou et al., 2017; Liu et al., 2020). However, the NUE was not improved in the plants under APRD compared with the conventional irrigation at the same N supply level (AW_1N_1, AW_2N_1 vs. CW_1N_1, **Table 3**), indicating that APRI-plants absorbed excessive N to ensure growth and yield formation. The NUE increased by 9.4% in AW_2N_2 compared with that in CW_1N_1 (**Table 3**). However, it is a general response that the NUE is higher at N_2 than at N_1 (Xu et al., 2012), indicating that the increased NUE in AW_2N_2 is not an APRD-specific response.

In AW_2N_1, the reduced irrigation water decreased the total biomass, but the yield was similar compared with that of the conventional drip irrigation (**Table 1**). This indicated that the carbon allocation and remobilization from vegetative organs to fruits was enhanced under APRD. Abscisic acid was suggested to play a vital role in the regulation of plant senescence and carbon remobilization (Yang et al., 2000). Higher leaf ABA concentrations were observed throughout the growing season under APRI compared with that under other treatments (Kirda et al., 2004). The enhanced remobilization of photosynthates and higher harvest index induced by APRD were also observed in our previous studies (Zhang et al., 2014; Shu et al., 2020).

Effect of Irrigation and Nitrogen Supply on Residual Nitrate Loss and Utilization

It was found that when the ^{15}N was labeled in the 30–40 cm layer, APRD reduced the ^{15}N leaching in the soil column and increased the ^{15}N accumulation in the 0–40 cm soil layer by 82.9–141.1% compared with the conventional drip irrigation (**Figure 5**). Moreover, APRD increased the absorption and utilization of the labeled N significantly under W_2 coupled with N_2 application, and the ^{15}N loss rate was decreased by 21.3–50.1%, which was the lowest under the deficient irrigation treatments (AW_2N_1, AW_2N_2) (**Table 4**). These changes were mainly because under APRI (including in APRD form), the water movement in the soil was different from that of conventional irrigation (Kang and Zhang, 2004; Sarker et al., 2019). The heterogeneous distribution of soil moisture induced by APRI reduced the vertical leakage and promoted the lateral infiltration of soil water. In addition, the irrigation amount has been reduced in most cases under APRI (Kang and Zhang, 2004; Zhang et al., 2014; Wang et al., 2019). All these factors contributed to the reduction in nitrate leaching and N loss under APRI (Wang et al., 2014, 2019). The changes in the ^{15}N accumulation peaked soil layer also indicated that the leaching of soil nitrate was weakened by APRI (**Figure 5**). Root activity and root compensatory growth can be increased by APRI, which can lead to an enhanced nutrient absorption (Chen et al., 2016). In addition to the reduced leaching, APRI or APRD could reduce N loss from the plant-soil system by reducing denitrification and ammonia volatilization (Lei et al., 2009; Han et al., 2014). In the present study, compared with conventional drip irrigation, the total plant biomass, fruit yield, and total N absorption decreased, whereas the absorption and utilization of labeled N increased significantly by decreasing the amount of irrigation water and nitrogen application under APRD (AW_2N_2 treatment) (**Tables 1**, **3** and **Figure 4**).

Wang et al. (2014, 2019) labeled ^{15}N in both the 10–20 and 40–50 cm layers and found that with lowering the ^{15}N labeled layer in the soil profile, the absorption and utilization of ^{15}N by plants also decreased, while the loss rate of ^{15}N from the plant-soil column system increased. The downward leaching distance of ^{15}N was shortened under APRI, and even in the case of labeling the ^{15}N in the 40–50 cm soil layer, the ^{15}N accumulation peaked layer moved upward by 10 cm (Wang et al., 2014; Hou et al., 2017). However, the recovery and loss rate of ^{15}N were different between the results reported by Wang et al. (2014, 2019) and Hou et al. (2017), probably due to the differences in the plant growth seasons, ^{15}N labeling amount used, and plant growth conditions. In the present study, ^{15}N was labeled in the 30–40 cm layer, which was different from the above previous reports, but close to the depth of 40–50 cm as reported by Wang et al. (2014) with a close amount of ^{15}N labeled and the same plant growing season. The results showed that under the AW_2N_1 treatment, the ^{15}N absorption and loss rate from the plant-soil column system was at 22.01 and 7.43% (**Figure 4** and **Table 4**), which was 46.7% higher while 40.8% lower than those of APRI where ^{15}N was labeled in the 40–50 cm layer, and even close to those of APRI where ^{15}N was labeled in the 10–20 cm layer with the same level of water and N supply as reported by Wang et al. (2014). The distribution of the tomato roots was mainly concentrated at the top 0–20 cm layer (**Figure 3**) (Wang et al., 2014, 2019; Liu et al., 2020; Shu et al., 2020), thus, the ^{15}N labeled in the 10–20 cm layer was more conducive to plant absorption and utilization and to reduce its loss from the plant-soil system (Wang et al., 2014). In the present study, although ^{15}N was labeled in the 30-40 cm layer, the ^{15}N absorption, utilization, and loss rate in the CW_1N_1 were close to those of the conventional irrigation with ^{15}N labeled in the 10–20 cm layer as reported by Wang et al. (2014). These results showed that drip irrigation and APRD are more conducive to reducing the leaching and loss of nitrate accumulated in the soil profile, thus promoting plant absorption and its accumulation in soil than the conventional irrigation and APRI (not in the form of APRD here), respectively.

CONCLUSIONS

Compared with CW_1N_1, under the same amount of water and N supply, AW_1N_1 showed a reduced ^{15}N leaching in the soil, promoted root growth, and enhanced the absorption of residual nitrate, thus promoted the tomato growth and yield formation. Compared with CW_1N_1, decreasing the irrigation

water by 34.1% under APRD (AW_2N_1) maintained the total N absorption, tomato yield, and increased the IWUE by 35.6%, the utilization rate of labeled ^{15}N by 20.5%, while the loss rate of ^{15}N from the plant-soil column was decreased by 50.1%. AW_2N_2 increased the absorption of the labeled ^{15}N by 12.8%, IWUE by 26.5%, but reduced the yield by 8.8% compared with those under CW_1N_1. Even though the N absorption was enhanced, the absorbed-NUE had not improved, indicating that a luxurious absorption of N occurred under APRD compared with the CW_1N_1 at the same N supply level. Therefore, it is concluded that APRD can significantly increase IWUE and N absorption, promote its utilization, and thus, reduce the loss of residual N that is accumulated in the soil profile. Thus, APRD is a promising technology for sustainable agriculture production even though the NUE in plants has not been improved.

DATA AVAILABILITY STATEMENT

The raw data supporting the conclusions of this article will be made available by the authors, without undue reservation.

AUTHOR CONTRIBUTIONS

L-ZS and W-JZ conceived and designed the experiments. RL, P-FZ, and J-RZ performed the experiments. RL and ZC analyzed the data and wrote the manuscript. Y-SW designed the experiments and improved the manuscript. All the authors contributed to the article and approved the submitted version.

FUNDING

This study was financially supported by the National Natural Science Foundation of China [Grant No. 31572202], the Agricultural Science and Technology Innovation Program [CAAS-ZDRW202002], and the Basic Public Welfare Projects of Zhejiang Province [2017C32082].

ACKNOWLEDGMENTS

We would like to thank Mr. Ming-Ji Du and Mrs. Shu-Xia Jiang for their assistance in routine management and their other help with the experiment.

REFERENCES

Chen, C., Xu, F., Zhu, J. R., Wang, R. F., Xu, Z. H., Shu, L. Z., et al. (2016). Nitrogen forms affect root growth, photosynthesis, and yield of tomato under alternate partial root-zone irrigation. *J. Plant Nutr. Soil Sci.* 179, 102–110. doi: 10.1002/jpln.201500179

Dodd, I. C. (2009). Rhizosphere manipulations to maximize 'crop per drop' during deficit irrigation. *J. Exp. Bot.* 60, 2454–2459. doi: 10.1093/jxb/erp192

Dodd, I. C., Theobald, J. C., Bacon, M. A., and Davies, W. J. (2006). Alternation of wet and dry sides during partial root zone drying irrigation alters root-to-shoot signaling of abscisic acid. *Funct. Plant Biol.* 33, 1081–1089. doi: 10.1071/FP06203

Du, T. S., Kang, S. Z., Zhang, J. H., and Li, F. S. (2008a). Water use and yield responses of cotton to alternate partial root-zone drip irrigation in the arid area of north-west China. *Irrigation Sci.* 26, 147–159. doi: 10.1007/s00271-007-0081-0

Du, T. S., Kang, S. Z., Zhang, J. H., Li, F. S., and Yan, B. Y. (2008b). Water use efficiency and fruit quality of table grape under alternate partial root-zone drip irrigation. *Agricult. Water Manage.* 95, 659–668. doi: 10.1016/j.agwat.2008.01.017

Gathumbi, S. M., Cadisch, G., Buresh, R. J., and Giller, K. E. (2003). Subsoil nitrogen capture in mixed legume stands as assessed by deep nitrogen-15 placement. *Soil Sci. Soc. Am. J.* 67, 573–582. doi: 10.2136/sssaj2003.5730

Gong, P., Liang, L., and Zhang, Q. (2011). China must reduce fertilizer use too. *Nature* 473, 284–285. doi: 10.1038/473284e

Han, K., Zhou, C., and Wang, L. (2014). Reducing ammonia volatilization from maize fields with separation of nitrogen fertilizer and water in an alternating furrow irrigationsystem. *J. Integr. Agric.* 13, 1099–1112. doi: 10.1016/S2095-3119(13)60493-1

Hou, M. M., Jin, Q., Lu, X. Y., Li, J. Y., Zhong, H. Z., and Gao, Y. (2017). Growth, water use, and nitrate-15N uptake of greenhouse tomato as influenced by different irrigation patterns, 15N labeled depths, and transplant times. *Front. Plant Sci.* 8:666. doi: 10.3389/fpls.2017.00666

Hu, T. T., Kang, S. Z., Li, F. S., and Zhang, J. H. (2011). Effects of partial root-zone irrigation on hydraulic conductivity in the soil-root system of maize plant. *J. Exp. Bot.* 62, 4163–4172. doi: 10.1093/jxb/err110

Jovanovic, Z., and Stikic, R. (2018). Partial root-zone drying technique: from water saving to the improvement of a fruit quality. *Front. Sustain. Food Syst.* 1:3. doi: 10.3389/fsufs.2017.00003

Kang, S. Z., Hao, X. M., Du, T. S., Tong, L., Su, X. L., Lu, H. N., et al. (2017). Improving agricultural water productivity to ensure food security in china under changing environment: from research to practice. *Agricult. Water Manage.* 179, 5–17. doi: 10.1016/j.agwat.2016.05.007

Kang, S. Z., and Zhang, J. H. (2004). Controlled alternate partial root zone irrigation: Its physiological consequences and impact on water use efficiency. *J. Exp. Bot.* 55, 2437–2446. doi: 10.1093/jxb/erh249

Khalili, F., Aghayari, F., and Ardakani, M. R. (2020). Effect of alternate furrow irrigation on maize productivity in interaction with different irrigation regimes and biochar amendment. *Commun. Soil Sci. Plant Anal.* 51, 1532–2416. doi: 10.1080/00103624.2020.1733001

Kirda, C., Cetin, M., Dasgan, Y., Topcu, S., Kaman, H., Ekici, B., et al. (2004). Yield response of greenhouse grown tomato to partial root drying and conventional deficit irrigation. *Agricult. Water Manage.* 69, 191–201. doi: 10.1016/j.agwat.2004.04.008

Lei, Y., Wang, L., Xue, L., Li, Z., and Shang, H. (2009). Effect of alternative irrigation and fertilization on soil ammonia volatilization of summer maize. *Transact. Chin. Soc. Agricult. Eng.* 25, 41–46.

Li, F., Yu, J., Nong, M., Kang, S., and Zhang, J. (2010). Partial root-zone irrigation enhanced soil enzyme activities and water use of maize under different ratios of inorganic to organic nitrogen fertilizers. *Agricult. Water Manage.* 97, 231–239. doi: 10.1016/j.agwat.2009.09.014

Liu, F. L., Shahnazari, A., Andersen, M. N., Jacobsen, S. E., and Jensen, C. R. (2006). Physiological responses of potato (*Solanum tubersum* L.) to partial root-zone drying: ABA signaling, leaf gas exchange, and water use efficiency. *J. Exp. Bot.* 57, 3727–3735. doi: 10.1093/jxb/erl131

Liu, R., Yang, Y., Wang, Y. S., Wang, X. C., Rengel, Z., Zhang, W. J., et al. (2020). Alternate partial root-zone drip irrigation with nitrogen fertigation promoted tomato growth, water and fertilizer -nitrogen use efficiency. *Agricult. Water Manage.* 233:106049. doi: 10.1016/j.agwat.2020.106049

Mancosu, N., Snyder, R., Kyriakakis, G., and Spano, D. (2015). Water scarcity and future challenges for food production. *Water* 7, 975–992. doi: 10.3390/w7030975

Pérez-Pérez, J. G., Navarro, J. M., Robles, J. M., and Dodd, I. C. (2018). Prolonged drying cycles stimulate ABA accumulation in Citrus macrophylla seedlings exposed to partial rootzone drying. *Agricult. Water Manage.* 210, 271–278. doi: 10.1016/j.agwat.2018.08.020

Sarker, K. K., Hossain, A., Timsina, J., Biswas, S. K., Kundu, B. C., Barman, A., et al. (2019). Yield and quality of potato tuber and its water productivity are

influenced by alternate furrow irrigation in a raised bed system. *Agricult. Water Manage*. 224:105750. doi: 10.1016/j.agwat.2019.105750

Sarker, K. K., Hossain, A., Timsina, J., Biswas, S. K., Malone, S. L., Alam, M. K., et al. (2020). Alternate furrow irrigation can maintain grain yield and nutrient content, and increase crop water productivity in dry season maize in sub-tropical climate of South Asia. *Agricult. Water Manage*. 238:106229. doi: 10.1016/j.agwat.2020.106229

Sezen, S. M., Yazar, A., and Tekin, S. (2019). Physiological response of red pepper to different irrigation regimes under drip irrigation in the Mediterranean region of Turkey. *Sci. Hortic*. 245, 280–288. doi: 10.1016/j.scienta.2018.10.037

Shahnazari, A., Liu, F. L., Andersen, M. N., Jacobsen, S. E., and Jensen, C. R. (2007). Effects of partial root-zone drying on yield, tuber size and water use efficiency in potato under field conditions. *Field Crops Res*. 100, 117–124. doi: 10.1016/j.fcr.2006.05.010

Shu, L. Z., Liu, R., Min, W., Wang, Y. S., and Zhu, J. R. (2020). Regulation of soil water threshold on tomato plant growth and fruit quality under alternate partial root-zone drip irrigation. *Agricult. Water Manage*. 238:106200. doi: 10.1016/j.agwat.2020.106200

Sun, Y., Yan, F., and Liu, F. (2013). Drying/rewetting cycles of the soil under alternate partial root-zone drying irrigation reduce carbon and nitrogen retention in the soil-plant systems of potato. *Agricult. Water Manage*. 128, 85–91. doi: 10.1016/j.agwat.2013.06.015

Tafteh, A., and Sepaskhah, A. R. (2012). Yield and nitrogen leaching in maize field under different nitrogen rates and partial root drying irrigation. *Int. J. Plant Prod*. 6, 93–114.

Topak, R., Acar, B., Uyanöz, R., and Ceyhan, E. (2016). Performance of partial root-zone drip irrigation for sugar beet production in a semi-arid area. *Agricult. Water Manage*. 176, 180–190. doi: 10.1016/j.agwat.2016.06.004

Wang, C. H., Shu, L. Z., Yu, H. M., Zhu, P. F., Tang, J. H., and Zhou, Q. W. (2020). Effects of partial root-zone irrigation and nitrogen forms on the movement of nitrate in deep subsoil and its utilization by tomato plants. *Eur. J. Soil Sci*. 71, 448–458. doi: 10.1111/ejss.12850

Wang, C. H., Shu, L. Z., Zhou, S. L., Yu, H. M., and Zhu, P. F. (2019). Effects of alternate partial root-zone irrigation on the utilization and movement of nitrates in soil by tomato plants. *Sci. Hortic*. 243, 41–47. doi: 10.1016/j.scienta.2018.08.006

Wang, C. H., Zhu, P. F., Shu, L. Z., Zhu, J. Z., and Yu, H. M. (2014). Effects of alternate partial root-zone irrigation and nitrogen forms on utilization and movement of nitrate in soil. *Transact. Chin. Soc. Agricult. Eng.* 30, 92–101. doi: 10.3969/j.issn.1002-6819.2014.11.012

Wang, Y., Liu, F., Neergaard, A. D., Jensen, L. S., Luxhi, J., and Jensen, C. R. (2010). Alternate partial root-zone irrigation induced dry/wet cycles of soils stimulate N mineralization and improve n nutrition in tomatoes. *Plant Soil* 337, 167–177. doi: 10.1007/s11104-010-0513-0

Xu, G. H., Fan, X. R., and Miller, A. J. (2012). Plant nitrogen assimilation and use efficiency. *Annu. Rev. Plant Biol.* 63: 153–182. doi: 10.1146/annurev-arplant-042811-105532

Yactayo, W., Ramírez, D. A., Gutiérrez, R., Mares, V., Posadas, A., and Quiroz, R. (2013). Effect of partial root-zone drying irrigation timing on potato tuber yield and water use efficiency. *Agricult. Water Manage*. 123, 65–70. doi: 10.1016/j.agwat.2013.03.009

Yang, J. C., Zhang, J. H., Huang, Z. L., Zhu, Q., and Wang, L. (2000). Remobilization of carbon reserves is improved by controlled soil-drying during grain filling of wheat. *Crop Sci*. 40, 1645–1655. doi: 10.2135/cropsci2000.4061645x

Zhang, Q., Wu, S., Chen, C., Shu, L. Z., Zhou, X. J., and Zhu, S. N. (2014). Regulation of nitrogen forms on growth of eggplant under partial root-zone irrigation. *Agricult. Water Manage*. 142, 56–65. doi: 10.1016/j.agwat.2014.04.015

Zhu, Z. L., and Chen, D. L. (2002). Nitrogen fertilizer use in China contributions to food production, impacts on the environment and best management strategies. *Nutr. Cycling Agroecosyst*. 63, 117–127. doi: 10.1023/A:1021107026067

Conflict of Interest: The authors declare that the research was conducted in the absence of any commercial or financial relationships that could be construed as a potential conflict of interest.

Publisher's Note: All claims expressed in this article are solely those of the authors and do not necessarily represent those of their affiliated organizations, or those of the publisher, the editors and the reviewers. Any product that may be evaluated in this article, or claim that may be made by its manufacturer, is not guaranteed or endorsed by the publisher.

frontiers in Plant Science

ORIGINAL RESEARCH
published: 14 October 2021
doi: 10.3389/fpls.2021.725995

Leaf Water Storage and Robustness to Intermittent Drought: A Spatially Explicit Capacitive Model for Leaf Hydraulics

Yongtian Luo[1]*, *Che-Ling Ho*[2], *Brent R. Helliker*[2] and *Eleni Katifori*[1]*

[1] Department of Physics and Astronomy, University of Pennsylvania, Philadelphia, PA, United States, [2] Department of Biology, University of Pennsylvania, Philadelphia, PA, United States

Leaf hydraulic networks play an important role not only in fluid transport but also in maintaining whole-plant water status through transient environmental changes in soil-based water supply or air humidity. Both water potential and hydraulic resistance vary spatially throughout the leaf transport network, consisting of xylem, stomata and water-storage cells, and portions of the leaf areas far from the leaf base can be disproportionately disadvantaged under water stress. Besides the suppression of transpiration and reduction of water loss caused by stomatal closure, the leaf capacitance of water storage, which can also vary locally, is thought to be crucial for the maintenance of leaf water status. In order to study the fluid dynamics in these networks, we develop a spatially explicit, capacitive model which is able to capture the local spatiotemporal changes of water potential and flow rate in monocotyledonous and dicotyledonous leaves. In electrical-circuit analogs described by Ohm's law, we implement linear capacitors imitating water storage, and we present both analytical calculations of a uniform one-dimensional model and numerical simulation methods for general spatially explicit network models, and their relation to conventional lumped-element models. Calculation and simulation results are shown for the uniform model, which mimics key properties of a monocotyledonous grass leaf. We illustrate water status of a well-watered leaf, and the lowering of water potential and transpiration rate caused by excised water source or reduced air humidity. We show that the time scales of these changes under water stress are hugely affected by leaf capacitance and resistances to capacitors, in addition to stomatal resistance. Through this modeling of a grass leaf, we confirm the presence of uneven water distribution over leaf area, and also discuss the importance of considering the spatial variation of leaf hydraulic traits in plant biology.

Keywords: biophysical modeling, leaf hydraulics, vascular network, water stress, xylem, transpiration, water-storage capacitance, monocot

OPEN ACCESS

Edited by:
Thorsten M. Knipfer, University of British Columbia, Canada

Reviewed by:
Roberto L. Salomon, Polytechnic University of Madrid, Spain
Fulton Rockwell, Harvard University, United States

***Correspondence:**
Yongtian Luo
yongtian@sas.upenn.edu
Eleni Katifori
katifori@sas.upenn.edu

Specialty section:
This article was submitted to Plant Biophysics and Modeling, a section of the journal Frontiers in Plant Science

Received: *16 June 2021*
Accepted: *20 September 2021*
Published: *14 October 2021*

Citation:
Luo Y, Ho C-L, Helliker BR and Katifori E (2021) Leaf Water Storage and Robustness to Intermittent Drought: A Spatially Explicit Capacitive Model for Leaf Hydraulics. Front. Plant Sci. 12:725995. doi: 10.3389/fpls.2021.725995

1. INTRODUCTION

Fluid flows in the plant vascular tissue system, which consists of xylem vessels for water transport and phloem vessels for the transport of photosynthetic products from leaves, are by no means isolated from other plant tissues. This is especially prominent in leaf hydraulic networks, which are typically the terminal portions of water flow through xylem. The xylem vessels making up these

networks not only connect to phloem through leaf tissue, but also deliver water to an extra-xylary network of living cells from which water is evaporated and transpired to the atmosphere through leaf-surface pores (stomata) (Sack and Holbrook, 2006; Stroock et al., 2014). Photosynthetic carbon assimilation requires stomata to remain open for the exchange of carbon dioxide with air, while transpiration simultaneously leads to a large sum of water loss, resulting in water-use efficiency (CO_2 uptake per water molecule loss) as low as 1/500 (Taiz and Zeiger, 2002). Implementation of water stress by a shortage of water source at the leaf base or decreasing atmospheric humidity around the leaf will cause stomata to close, thus suppressing transpirational water loss, but also reducing photosynthesis (Brodribb, 2009; Choat et al., 2018). The maintenance of leaf water status, which changes spatially in the xylem hydraulic vascular network, is therefore critical to keeping stomata open and sustaining photosynthesis.

Water storage functions of certain plant cells help to maintain plant water status, and supports the resilience and survival of a plant experiencing water stress (Tyree and Ewers, 1991; Jones, 2013). Succulent plants are perhaps the most obvious example, where water-storage parenchyma cells play the role of hydraulic capacitors, storing water when water supply is sufficient and providing water to sustain water status under stress (Smith et al., 1987). Most theoretical examinations of capacitance have focused on trees and how the substantial water storage in wood, ray parenchyma and embolized xylem conduits (Hölttä et al., 2009; Meinzer et al., 2009; Pfautsch et al., 2015; Mencuccini et al., 2017) offer a water source for continued transpiration and/or the maintenance of plant-water potential above safety margins during seasonal changes in soil or atmospheric drought (Salomón et al., 2017; Bryant et al., 2021). Less attention has been paid to the capacitance of leaves, and how local capacitance may buffer the transpiration stream through the relatively rapid vagaries of environment to which a leaf is subjected.

In grass leaves, bulliform cells, water-storage parenchyma, and vascular bundle sheaths could all play the role of dynamic local capacitors (Raven et al., 2005). Previous theoretical work on the water-storage capacitance was typically from the perspective of whole leaf or whole plant, such as in a lumped-element model using electrical-circuit analogs, where a whole system-wide capacitor is used as well as other whole-system elements including resistors (Jones, 1978). This whole-system approach extends also to the interpretation of pressure-volume curve measurements where capacitance, determined for both pre- and post-turgor-loss points, is necessarily assigned to the whole leaf and not specific cells (Bartlett et al., 2012). The more cell-specific, leaf-level models of fluid (and vapor) flow in leaves do not explicitly include water-storage capacitance (Buckley, 2015). Water reservoir cells are distributed along water pathways in the network, which means capacitance is spatially dependent and could affect the water status locally. Transpiration also occurs locally through stomata all over the leaf surface, making vessels in the network behave as leaking pipes. The competing effects of transpiration and water storage under stress will thus be more appropriately investigated in terms of spatially explicit network systems. In grass leaves, the unbalanced distribution of water content from leaf base to tip is illustrated by the fact that the area near tip is disproportionately disadvantaged and dries out faster than the area near the base (water source) when subject to water shortage or even a transient change in atmospheric humidity. Even in a static, fully hydrated environment, the uneven spatial water distribution in a grass leaf is measurable by gravimetric methods (see section 2), as illustrated in section 3.

The plant or leaf water status, generally described by water potential ψ which is regarded as the driving force of water flow, has been theoretically studied by two classes of models. In both classes, the water transport through leaf xylem is treated as laminar following the Hagen-Poiseuille law, in which the hydraulic resistance of a xylem vessel is equal to the water potential difference between its two ends divided by the flow rate (van den Honert, 1948; Altus et al., 1985; Tyree and Ewers, 1991). The first type of model considers the small-scale spatial variations of leaf vascular networks, by implementing a network system consisting of only resistors, while ignoring the water-storage capacitance, for both monocot (Wei et al., 1999; Martre et al., 2001) and dicot (Cochard et al., 2004; Katifori, 2018) leaf modeling. In the second modeling type, large-scale tissue or organ-level properties including both resistance and capacitance are considered, while ignoring any spatially explicit architecture within a leaf (Cowan, 1965, 1972; Smith et al., 1987; Steppe et al., 2006). In such a model, the water flow through leaf or plant is commonly driven by a current source representing transpiration, which can be adjusted arbitrarily or according to experimentally measured transpiration rate, without an explicit, direct mechanistic input from water potential deficit (or vapor pressure deficit) between the leaf and air. Here, we bridge these two classes of models by developing a spatially explicit leaf hydraulic network model with local capacitance. While our model is general and can be applied to any type of vascularized leaf, we focus on grass leaf examples as they almost ubiquitously have water storage cells, and the parallel vein structure of grasses leads to water being lost throughout the length of the blade. While this too occurs in dicots over short distances (Zwieniecki et al., 2002), the process occurs along the entirety of a grass leaf. By conducting computation and simulation on a uniform grass leaf model, we study the dependence of transpiration rate on leaf hydraulic traits and water potentials in the environment.

We illustrate and discuss how capacitance increases the robustness of a leaf in a changing environment and maintains leaf water status, so that stomata can remain open to potentially sustain photosynthesis along the entire leaf blade. To examine this, we assume a condition that might appear unorthodox to a plant physiologist, that of static stomatal resistance. While constant stomatal resistance is not typically observed, this is not simply an academic assumption or a model convenience. First, rapid changes in leaf-to-air evaporative gradients, such as those coming from increases in wind speed, can expose the leaf to high transpirational demands before stomata respond by closing. Second, not all stomata respond the right way. A large number of species display a "wrong-way" stomatal response and temporarily increase opening with increasing evaporative demand, a response that can last 10s of minutes and further exacerbate transpirational demand (Buckley et al., 2011). In such scenarios, local capacitance could conceivably

allow for continued transpiration and photosynthesis without dropping leaf-water potentials to damaging levels. Our modeling results, which are based on idealized theoretical assumptions, are not directly comparable with any known experimental measurements of spatial variations of water potential, but can be indirectly validated by our gravimetric measurements of water content distribution in the leaves of grass *Anthaenantia villosa*. See section 4 for discussions on experimental validation and biological applications.

2. METHODS OF THEORETICAL MODELING AND EXPERIMENTAL MEASUREMENT

2.1. The Spatially Explicit Model of Capacitive Leaf Hydraulics

We use a capacitive electrical circuit analog to model the spatial variation of hydraulic traits of a simple plant leaf model (such as a monocot leaf). A one-dimensional network model analogous to an electrical circuit is illustrated in **Figure 1**, consisting of nodes $i = 1, 2, \ldots, N$. In this example only one xylem conduit is shown as the midline. The water potential in the atmosphere ψ_a, which is more negative than the water potentials in the xylem ($\psi_0, \psi_1, \ldots, \psi_N$), is related to relative humidity (RH) in the air through the relationship:

$$\psi_a = \frac{\bar{R}T}{v} \ln\left(\frac{\mathrm{RH}}{100\%}\right) \tag{1}$$

with ideal gas constant $\bar{R}$ =8.3145 J·mol^{-1}·K^{-1}, room temperature T =298.15 K, and liquid water molar volume v ≈18 mL/mol (Buckley and Sack, 2019). The water potential ψ_s underneath capacitors is the baseline osmotic potential of leaf water storage, which is specifically defined as the plant root potential plus the most negative osmotic potential of water-storage cells, when the cell water content is at the minimum for the cells to behave like linear capacitors. With this definition, ψ_s is always more negative than water potential ψ_i in the xylem, and the voltage V_i across each capacitor C_i is considered to be the positive hydrostatic pressure (turgor) (Smith et al., 1987; Jones, 2013), for which the plus and minus signs label the direction of V_i in the diagram. We assume the atmospheric condition outside the leaf and the baseline osmotic potential of reservoir cells inside are both uniform along the leaf blade, and thus have a single wire for ψ_a and ψ_s, respectively in the diagram.

Figure 1 represents a well-watered leaf, where the water source potential ψ_0 at the leaf base keeps charging the water-storage capacitors C_i, and stomata are wide-open so that water is being released into the atmosphere through transpiration. When the direction of current $I_i^{(c)}$ is reversed, the corresponding capacitor is discharged and loses water content, while the polarity of its voltage V_i does not change. The resistors $R_i^{(c)}$ represent the resistance in the water-storage pathways, and resistors $R_i^{(a)}$ are the total resistance from xylem to the atmosphere, including outside-xylem resistance (mainly through mesophyll) for liquid water inside the leaf and stomatal resistance for water vapor. At steady state, the capacitors are not being charged and all $I_i^{(c)} = 0$, when the water status is in equilibrium and turgor and water content are at the maximum. When stomata are closed, $R_i^{(a)} \to \infty$ and all $I_i^{(a)} = 0$. The summation of all $I_i^{(a)}$ gives the total transpiration current $E = \sum_i I_i^{(a)}$.

The fundamental equations of the electrical analog are:

$$I_{i-1,i} = I_{i,i+1} + I_i^{(a)} + I_i^{(c)} \tag{2}$$

$$\psi_{i-1} - \psi_i = R_{i-1,i} I_{i-1,i} \tag{3}$$

$$\psi_i - \psi_a = R_i^{(a)} I_i^{(a)} \tag{4}$$

$$I_i^{(c)} = \frac{\partial}{\partial t}[C_i(\psi_i - \psi_s - R_i^{(c)} I_i^{(c)})]. \tag{5}$$

At the terminal note (end of the xylem), $I_{N-1,N} = I_N^{(a)} + I_N^{(c)}$. With time-independent C_i and $R_i^{(c)}$, the last equation becomes:

$$I_i^{(c)} = C_i \frac{\partial \psi_i}{\partial t} - C_i R_i^{(c)} \frac{\partial I_i^{(c)}}{\partial t}. \tag{6}$$

If we also assume the transpiration resistance $R_i^{(a)}$ is time-independent, we can obtain the following equation by substituting Expressions (4) and (6) into the first derivative of Equation (2) with respect to time ($\partial I_{i-1,i}/\partial t = \partial I_{i,i+1}/\partial t + \partial I_i^{(a)}/\partial t + \partial I_i^{(c)}/\partial t$):

$$\frac{\partial I_{i-1,i}}{\partial t} - \frac{\partial I_{i,i+1}}{\partial t} = \left(\frac{1}{R_i^{(a)}} + \frac{1}{R_i^{(c)}}\right)\frac{\partial \psi_i}{\partial t} - \frac{1}{C_i R_i^{(c)}}\left(I_{i-1,i} - I_{i,i+1} - \frac{\psi_i - \psi_a}{R_i^{(a)}}\right). \tag{7}$$

We will demonstrate how such a spatially uniform, one-dimensional network can be treated as a continuous model when the number of nodes N is large, and can be studied through analytical calculation under certain circumstances. We will also design a numerical method to simulate both the steady state and the time-dependent behavior of a general capacitive network model, which is not necessarily uniform or one-dimensional.

2.2. Analytical Calculation of the One-Dimensional Model

We assume the size of a node l is small compared to the total length of the network L, so that the number of nodes $N = L/l$ is large. At node i we define a normalized location $x = i/N$ ($\Delta x = l/L$ so that $0 \leqslant x \leqslant 1$) which changes continuously, and in the xylem the water potential ψ and current I also change continuously which means $(\psi_{i-1} - \psi_i)/\Delta x \to -\partial\psi/\partial x$ and $(I_{i-1,i} - I_{i,i+1})/\Delta x \to -\partial I/\partial x$. In this normalized continuous model, we assume the resistances and capacitances are uniformly distributed and time-independent throughout the network ($R_{i-1,i} = R^{(o)}$, $R_i^{(a)} = R^{(a)}$, $R_i^{(c)} = R^{(c)}$ and $C_i = C^{(o)}$

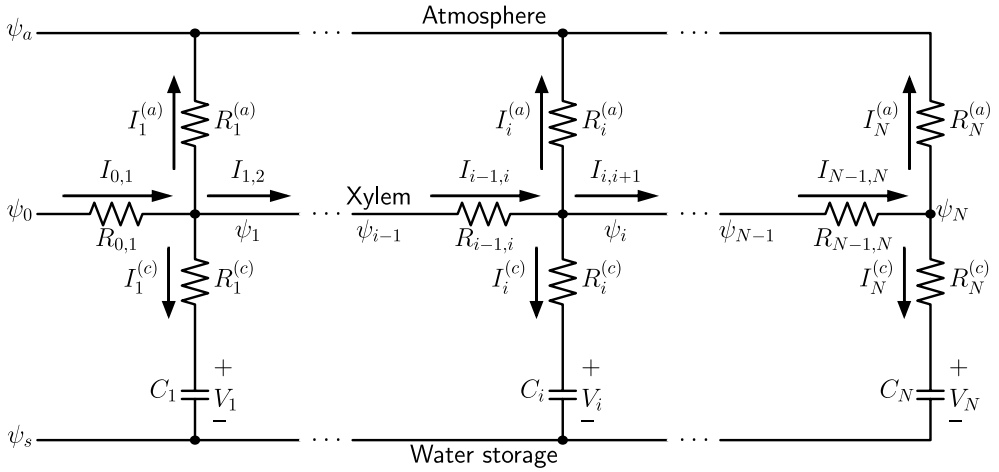

FIGURE 1 | A one-dimensional capacitive network model, where ψ_a is the water potential in the atmosphere, ψ_s is the baseline osmotic potential of water storage, ψ_0 is the water source potential at the leaf base, and ψ_i ($i = 1, 2, \ldots, N$) are water potentials at different nodes of the xylem. Currents $I_i^{(a)}$ are transpiration currents through stomata, and $I_i^{(c)}$ are charging capacitors C_i, which represent leaf water storage function.

are all constants), and we define $R = NR^{(o)}$, $R_a = R^{(a)}/N$, $R_c = R^{(c)}/N$ and $C = NC^{(o)}$ as combined parameters for the whole system. Considering $\partial\psi/\partial x = -RI$, we derive the following basic equation from Equation (7):

$$\frac{\partial^3\psi}{\partial t\partial x^2} = R\Big(\frac{1}{R_a}+\frac{1}{R_c}\Big)\frac{\partial\psi}{\partial t} - \frac{1}{CR_c}\frac{\partial^2\psi}{\partial x^2} + \frac{R}{CR_cR_a}\psi - \frac{R\psi_a}{CR_cR_a}. \quad (8)$$

We outline the general time-dependent solution of this equation in **Supplementary Section 1**. The steady-state average potential in the xylem is:

$$\bar{\psi} = I_0R_a + \psi_a \quad (9)$$

where $I_0 = I(x = 0)$ is the current entering through the base (see Equation S8 in **Supplementary Material** for expression), which is equal to the total transpiration current E at steady state.

For a nontrivial, time-dependent water potential boundary condition (dynamic ψ_0 or ψ_a induced by the change of water supply or air humidity), in **Supplementary Section 2** we illustrate the solution for a dynamic water source $\psi(x = 0, t) = A\cos(\omega_0 t + \varphi)$ that oscillates with time. We also consider an excised leaf xylem which is initially at the fully hydrated steady state and is cut off at the leaf base at $t = 0$, when the base water source is turned off. The calculation is detailed in **Supplementary Section 3**. It turns out that both average xylem potential $\bar{\psi}$ and total transpiration current E are exponential decay functions with time at $t > 0$, where time constant is $\tau = C(R_c + R_a)$:

$$\bar{\psi}(t) = \psi_a + I_0R_a\exp\Big(-\frac{t}{C(R_c+R_a)}\Big) \quad (10)$$

$$E(t) = I_0\exp\Big(-\frac{t}{C(R_c+R_a)}\Big) \quad (11)$$

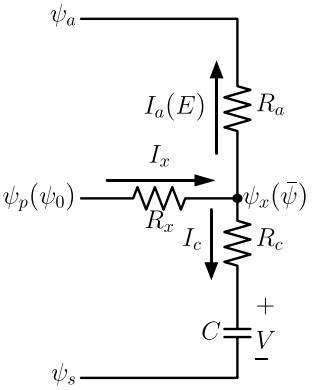

FIGURE 2 | A lumped-element model which is equivalent to the one-dimensional network in **Figure 1**. Here $\psi_p = \psi_0$ is the water source potential at the leaf base, and $\psi_x = \bar{\psi}$ is the average potential in the xylem. Currents $I_a = E$ and I_c are total transpiration current and capacitor charging current, respectively.

which means the existence of capacitance C as well as transpiration resistance R_a (which is static) and water-storage pathway resistance R_c slows down the process of losing water in a drought condition where the leaf loses its water source, illustrating the function of capacitance in a plant's resilience against drought.

A highly lumped-element model can be derived from the one-dimensional network in **Figure 1** and validated by analytical calculations of the continuous model. The diagram of the model, which is similar to lumped models commonly found in literature on whole-plant or whole-leaf modeling, is in **Figure 2**, in which the water source potential ψ_0 at the leaf base is relabeled as ψ_p, ψ_x is the average water potential in the xylem ($\bar{\psi} = \sum_i \psi_i/N$),

and V is the average capacitor voltage ($\bar{V} = \sum_i V_i/N$). The current I_x is the incoming current I_0 through leaf base, while $I_a = \sum_i I_i^{(a)}$ is the total transpiration current E and $I_c = \sum_i I_i^{(c)}$ is the total capacitor charging (or discharging) current. With R_a and R_c defined previously as grouped elements for the whole system, we demonstrate in **Supplementary Section 4** the equivalence of the lumped model in **Figure 2** and the uniform model based on **Figure 1**, for which we need to define the effective xylem hydraulic resistance $R_x = R/3$ where R is the total xylem resistance. We also show that the time constant $\tau = C(R_c + R_a)$ of an excised leaf can be obtained from the lumped model. When studying changing stomata whose conductance depends on leaf water status, we can use this lumped model to investigate the importance of stomatal sensitivity to local water content in transpiration control. See section 4 for relevant discussions.

2.3. Numerical Simulation of General Capacitive Networks

The one-dimensional model in **Figure 1** can be generalized into two- or higher-dimensional networks, which can include branches and loops. If node i is a node in such a network, and its neighboring nodes are labeled by $n(i)$, we use $I_{n(i),i}$ and $R_{n(i),i}$ to label the current from $n(i)$ to i and the resistance between $n(i)$ and i, respectively. Starting from the current relation:

$$\sum_{n(i)} \frac{\partial I_{n(i),i}}{\partial t} = \frac{\partial I_i^{(a)}}{\partial t} + \frac{\partial I_i^{(c)}}{\partial t}, \tag{12}$$

we derive the water potential relation at i:

$$\Big(\sum_{n(i)} \frac{1}{R_{n(i),i}} + \frac{1}{R_i^{(a)}} + \frac{1}{R_i^{(c)}}\Big)\frac{\partial \psi_i}{\partial t} - \sum_{n(i)} \frac{1}{R_{n(i),i}} \frac{\partial \psi_{n(i)}}{\partial t} = \frac{1}{C_i R_i^{(c)}}\Big(\frac{\psi_a - \psi_i}{R_i^{(a)}} + \sum_{n(i)} \frac{\psi_{n(i)} - \psi_i}{R_{n(i),i}}\Big) \tag{13}$$

where $\psi_{n(i)}$ is the water potential at node $n(i)$. The problem of solving the time-dependent behavior of ψ_i is organized into a matrix equation $\boldsymbol{Ax} = \boldsymbol{b}$, where at time t, the vector to be solved is:

$$\boldsymbol{x} = \left(\frac{\partial \psi_1}{\partial t}, \frac{\partial \psi_2}{\partial t}, \ldots, \frac{\partial \psi_i}{\partial t}, \ldots, \frac{\partial \psi_N}{\partial t}\right)^{\mathrm{T}} \tag{14}$$

which contains the time derivatives of water potential at all nodes. The ith element of vector $\boldsymbol{b}$ is:

$$\boldsymbol{b}_i = \frac{1}{C_i R_i^{(c)}}\Big(\frac{\psi_a - \psi_i(t)}{R_i^{(a)}} + \sum_{n(i)} \frac{\psi_{n(i)}(t) - \psi_i(t)}{R_{n(i),i}}\Big) \tag{15}$$

and the elements in the invertible and symmetric matrix $\boldsymbol{A}$ are determined by:

$$\boldsymbol{A}_{i,j} = \begin{cases} \sum_{n(i)} 1/R_{n(i),i} + 1/R_i^{(a)} + 1/R_i^{(c)} & i = j \\ -1/R_{j,i} & j \text{ is neighbor of } i \\ 0 & i \neq j \,\&\, j \text{ is not neighbor of } i \end{cases}. \tag{16}$$

If the node i is connected to one or more water sources, the external water potentials must be included in the evaluation of $\boldsymbol{b}_i$ and $\boldsymbol{A}_{i,j}$. For example, if node i is connected to a base potential ψ_p, we have $\boldsymbol{b}_i = 1/(C_i R_i^{(c)})[(\psi_p - \psi_i)/R_{p,i} + (\psi_a - \psi_i)/R_i^{(a)} + \sum_{n(i)}(\psi_{n(i)} - \psi_i)/R_{n(i),i}]$ and $\boldsymbol{A}_{i,i} = 1/R_{p,i} + \sum_{n(i)} 1/R_{n(i),i} + 1/R_i^{(a)} + 1/R_i^{(c)}$, where $R_{p,i}$ is the resistance between i and base (location of water source).

To simulate the dynamics of the network, we start from an initial water status $\psi_i(t = 0)$, calculate $\boldsymbol{b}$ and then $\boldsymbol{x} = \boldsymbol{A}^{-1}\boldsymbol{b}$ at the current time t, and update the water potentials after a small time step Δt:

$$\psi_i(t + \Delta t) = \psi_i(t) + \frac{\partial \psi_i}{\partial t}\Delta t. \tag{17}$$

To numerically calculate the steady state where all $\partial \psi_i/\partial t = 0$, we organize the equation $(\psi_a - \psi_i)/R_i^{(a)} + \sum_{n(i)}(\psi_{n(i)} - \psi_i)/R_{n(i),i} = 0$ into another matrix equation $\boldsymbol{By} = \boldsymbol{a}$, where $\boldsymbol{y}_i = \psi_i$, $\boldsymbol{a}_i = \psi_a/R_i^{(a)}$ (or $\boldsymbol{a}_i = \psi_p/R_{p,i} + \psi_a/R_i^{(a)}$ if i is connected to a water source ψ_p), and $\boldsymbol{B}_{i,j} = \boldsymbol{A}_{i,j}$ if $i \neq j$ while $\boldsymbol{B}_{i,i} = \sum_{n(i)} 1/R_{n(i),i} + 1/R_i^{(a)}$ (or $\boldsymbol{B}_{i,i} = 1/R_{p,i} + \sum_{n(i)} 1/R_{n(i),i} + 1/R_i^{(a)}$). By solving $\boldsymbol{y} = \boldsymbol{B}^{-1}\boldsymbol{a}$ we can calculate the steady-state water potentials in the network.

2.4. Experimental Measurements of the Spatial Distribution of Water Content Along Grass Leaf Blades

As an indirect validation of our theoretical modeling prediction that water content decreases spatially from leaf base to tip (because of the tapering of water potential), the C4 grass species *Anthaenantia villosa* (*A. villosa*) was used for measuring the local distribution of water amount in its leaves. For light treatment, the species was exposed to light ($\sim$500 μmol·m^{-2}·s^{-1}) for 1 h prior to the measurement. For dark treatment, the species was kept in the lab without a light source. Leaf lengths were measured and divided into five segments of equal length marked with sharpies. Sample leaves were cut sequentially from the tip to the base and placed in bags with moist air (except for the dark + 1 h equilibrium treatment). Leaf fresh mass (FM, g) was measured soon after leaf excision. Segments were dried in a 40 °C oven for $>$ 24 h for leaf dry mass (DM, g) measurement. For the dark + 1 h equilibrium treatment, the whole leaf was cut at the base and placed in double bags with moist air for 1 h in the dark prior to the procedure described above. The purpose of the dark + 1 h equilibrium treatment was to compare with the dark treatment results to rule out any possible statistical difference caused by extra equilibration after excision. (The leaves equilibrated for an extra hour after excision do not show statistically significant difference from dark treatment results in **Supplementary Figure 7**). The measurement result of water amount per unit dry mass (= (FM − DM)/DM, g/g) is calculated for each segment, used to characterize the spatial variations of water content along leaf blades to account for the effects of both leaf area and thickness on water storage.

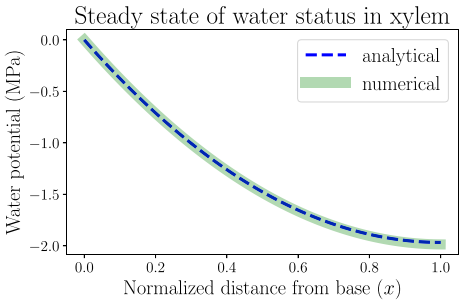

FIGURE 3 | The spatially dependent water potential in a living, uniform model leaf at the steady state. The water potential decreases from 0 ($x = 0$, the leaf base) to about −2MPa ($x = 1$, the leaf tip). The one-dimensional numerical simulation result follows the analytical expression. Parameters used in the modeling are listed in **Table 1**. The steady-state transpiration rate of this model leaf is $E = 1.97\ \text{mmol} \cdot m^{-2} \cdot s^{-1}$.

3. COMPUTATION AND SIMULATION RESULTS OF UNIFORM MODEL LEAF

3.1. The Well-Watered Steady State of a Uniform Leaf

In this section we apply the analytical calculation (for one-dimensional continuous models) and numerical simulation methods (for discretized network models) introduced in section 2 to the study of hydraulic behaviors of a model leaf, by making use of biologically relevant parameters. One of these results is the spatially dependent water potential profile at the steady state of a living uniform leaf shown in **Figure 3**. We assume the plant is well watered and estimate that the water potential at the leaf base $\psi(x = 0)$ is approximately $\psi_0 = 0$ where x is the normalized distance from base ($x = 0$) to tip ($x = 1$). In order to generate a clear spatial pattern of water status with significant spatial variations, we select an atmospheric water potential $\psi_a = -100$ MPa, which represents moderately dry air conditions outside the leaf stomata. Through Equation (1), the relative humidity is estimated to be RH $\approx$ 48%. The RH can be used to calculate the vapor pressure deficit (VPD) between the inner air space of the leaf and the outside atmosphere (across stomata), which is estimated to be VPD $= (1 - \text{RH})P \approx 1.64$ kPa, where $P = 3.17$ kPa is the saturation vapor pressure of water (RH = 100%) at room temperature. The concept of VPD is usually used in plant biology as the driving force of transpiration.

Other modeling parameters used in this section, though not directly found in previous measurements, are selected to mimic the general trends of static or dynamic behaviors of leaf hydraulics. For example, the resulting steady-state water potential profile in **Figure 3** illustrates a monotonically decreasing trend from base to tip, so that the water flow is unidirectional in this uniform model leaf. With the hydraulic resistance parameters we choose, including xylem total resistance $R = 2\ \text{MPa}\cdot\text{m}^2\cdot\text{s}\cdot\text{mmol}^{-1}$ and resistance from xylem to air $R_a = 50\ \text{MPa}\cdot\text{m}^2\cdot\text{s}\cdot\text{mmol}^{-1}$ (so that xylem conductance is 25 times the conductance into air), the leaf water potential is maintained above −2 MPa, below which xylem conduits may embolize and flow may start to cease. The analytical solution in **Figure 3** as obtained from Equation S3 in **Supplementary Material** is a monotonically decreasing function. The numerical simulation of network is conducted by discretizing the leaf into $N = 100$ nodes from base to tip. The parameters for each node are derived from whole system parameters through the relationships introduced in subsection 2.2, e.g., $R^{(o)} = R/N$ and $R^{(a)} = NR_a$. The simulation result reproduces the spatial distribution of water potential described by the analytical solution, also validating the usefulness of the simulation method which can be used for a more general, expanded network model. With these parameters, the average xylem water potential and total transpiration rate are calculated as $\bar{\psi} = -1.31$ MPa and $E = I_0 = 1.97\ \text{mmol}\cdot\text{m}^{-2}\cdot\text{s}^{-1}$ according to Equations S7 and S8 in **Supplementary Material**, which are of the same order of magnitude as typical experimental values (which can be found in textbooks like Jones, 2013). If the distribution of water-storage capacitance is also uniform along the leaf, the local leaf water content will also similarly taper toward the tip, which can be tested by our gravimetric measurements. Parameters used in all the modeling work in this section are summarized in **Table 1**.

3.2. Exactly Solvable Model: Dehydration of an Excised Leaf

We consider the analytically solved situation of excising a living uniform model leaf in steady state from plant (see **Supplementary Section 3**). The results in Equations (10) and (11) show that the time dependence of both average xylem water potential and total transpiration current is characterized by a time constant $\tau = C(R_c + R_a)$ in an exponentially decaying trend in the dehydration process, as long as the stomatal resistance is kept unchanged. **Figure 4** illustrates the time dependence of total transpiration rate E, which continuously decreases from the steady-state value 1.97 mmol m^{-2} s^{-1} instead of going through a drastic change because of the existence of capacitance. In addition to the same parameters ψ_a, R and R_a used in **Figure 3**, we use different sets of capacitance value C and resistance R_c from xylem to capacitor for the whole leaf as labeled in each subplot of **Figure 4**. The discretized numerical results, which are obtained by conducting the simulation in a 100-node network where $C^{(o)} = C/N$ and $R^{(c)} = NR_c$ at each node (relationships from subsection 2.2 where $N = 100$) with time interval $\Delta t = 0.01 min$, match the analytical expressions with time constant τ, revalidating the simulation method. These results are based on the critical assumption that all hydraulic elements are constant including transpiration resistance R_a, which leads to a large drop of average xylem water potential $\bar{\psi}$ to very negative, non-physiological values in a matter of minutes (see **Supplementary Figure 1**). The decrease of transpiration rate, which would become nearly 0 ultimately as $\bar{\psi}$ drops to nearly ψ_a, is entirely induced by the huge decline of $\bar{\psi}$ instead of closing stomata, as the E–$\bar{\psi}$ plot shows in **Supplementary Figure 2**. The calculations shown here are mainly used to explore the function of capacitors in the adjustment of leaf water status, emphasizing their importance for the stabilization and resilience of plant hydraulics, while ignoring other factors such as R_a.

TABLE 1 | Summary of modeling parameters used in this section.

Parameter	Steady state (3.1)	Excised leaf (3.2)	Changing VPD (3.3)
Water source potential ψ_0 (MPa)	0	Removed	0
Atmospheric potential ψ_a (MPa)	−100	−100	−50 or −150
Baseline osmotic potential ψ_s	Not used	Not used	Not used
Xylem hydraulic resistance R (MPa· m^2· s· mmol^{-1})	2	2	2
Xylem-to-air resistance R_a (MPa· m^2· s· mmol^{-1})	50	50	50
Water-storage capacitance C (mmol· m^{-2}· MPa^{-1})	Not used	30 or 120	60 or 120
Xylem-to-capacitor resistance R_c (MPa· m^2·s· mmol^{-1})	Not used	1 or 50	25 or 50

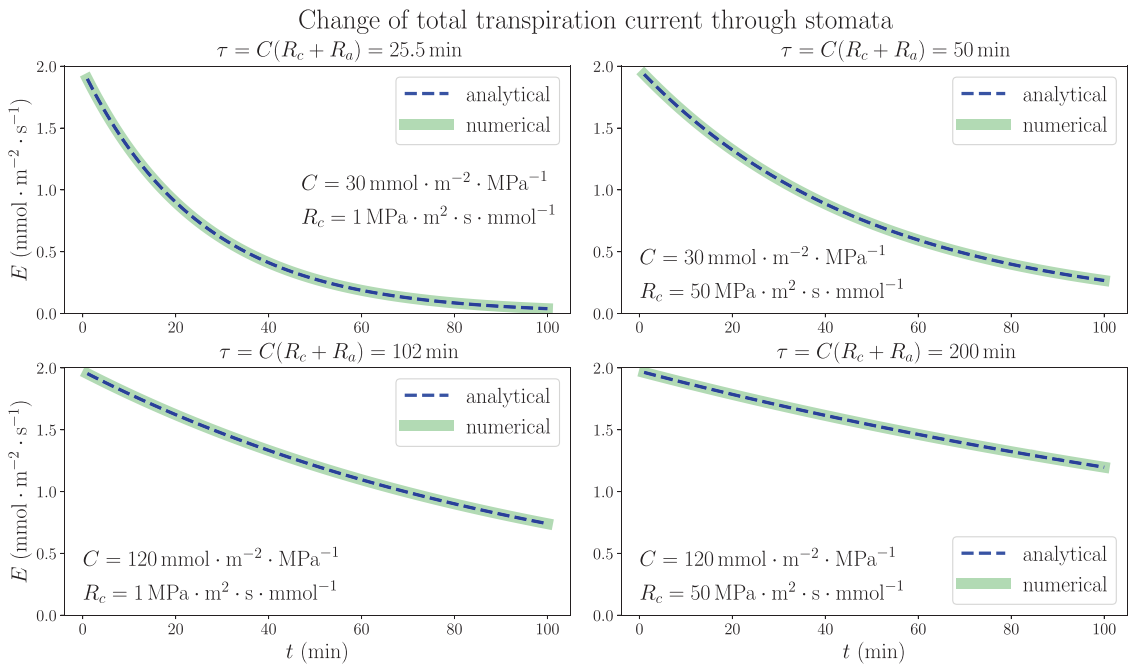

FIGURE 4 | The time dependence of total transpiration rate through stomata when a living, uniform model leaf in steady state is removed from a plant and the water source is closed at the base. The 1D simulation results match the analytical exponential decay expressions, with time constants $\tau = C(R_c + R_a)$. The temporal variations of average water potential in xylem are similar. Various sets of whole-leaf capacitance C and xylem-to-capacitor resistance R_c values are used, while other parameters are the same as those in **Figure 3**. The effect of increasing (or decreasing) the capacitance C on the rate of change is shown to be much larger than that of the increase (or decrease) of R_c.

As predicted by the theoretical calculations and proven by the numerical simulations, both capacitance C and resistance R_c are shown to play an important role in the dehydration dynamics of a model leaf experiencing the removal of water source, which models the behavior of plant water status in a severe drought condition. It turns out that within the ranges of parameters we choose, the variation of C, which is directly proportional to τ, would exert a much larger influence on the time scale and rate of change in the dehydration process than the effect of varying R_c. While R_c increases from 1 MPa·m^2·s·mmol^{-1} (same order of magnitude as R) to 50 MPa·m^2·s·mmol^{-1} (comparable to R_a), which is a fifty times increase, the time constant τ is only increased by less than two times. These observations of a model leaf indicate that an effective strategy for a plant to be more resilient under water stress and to survive a drought would be to enlarge its water-storage capacitance, the ability to contain large amount of water, rather than to increase the resistance of pathways connecting xylem and capacitors. In a real-life plant, whose stomatal resistance is changeable and sensitive to the water status, a drought stressed condition and decreasing water content would trigger the closing of stomata, drastically increasing R_a, which also prolongs the time constant and slows down the decrease of water potential (while ceasing transpiration), providing another effective strategy to overcome water stress.

3.3. Numerical Simulations of Leaf Water Status in Changing Environments

We consider the response of a living, fully hydrated plant leaf to an instant change of atmospheric conditions, such as a

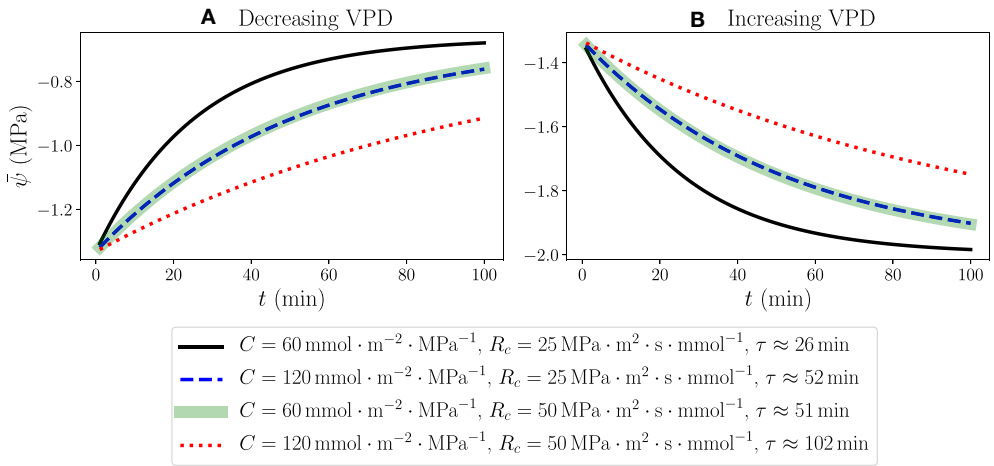

FIGURE 5 | The time dependence of average water potential in xylem, when ψ_a is abruptly increased from −100MPa to −50MPa **(A)** where the air is wetted and VPD is decreased from 1.64 to 0.965kPa, or decreased from −100MPa to −150MPa **(B)** where the air is dried and VPD is increased from 1.64kPa to about 2.1kPa. Various sets of C and R_c values are used, while other parameters are the same as those in **Figure 3**. In both situations, the time constants τ corresponding to the same C and R_c values are identical as labeled in the legend.

sudden increase or decrease of relative humidity (RH) in the air, which is related to a rise or drop of atmospheric water potential through Equation (1). The results are generated by simulating the 100-node discretized network (with simulation time step $\Delta t = 0.01\ min$). We start from modeling a well-watered leaf in the steady state using the parameters for **Figure 3** ($\psi_a = -100$ MPa, RH $\approx$ 48% and VPD $\approx$1.64 kPa), which is the same initial state in **Figure 4**, and at time $t = 0$ instantly change the value of ψ_a, resulting in a continuous change of average water potential in xylem starting from −1.31 MPa as shown in **Figure 5**. As ψ_a is raised to −50 MPa, when the air is more humid (RH $\approx$ 70%) and the vapor pressure deficit across stomata becomes smaller (VPD $\approx$0.965 kPa), $\bar{\psi}$ also increases gradually toward a new steady-state value −0.656 MPa, which is determined by the new ψ_a value through Equations S7 and S8 in **Supplementary Material** with constant resistance values R and R_a. Similarly, as ψ_a is dropped to −150 MPa, when the air is drier (RH $\approx$ 34%) and VPD becomes larger (2.1 kPa), $\bar{\psi}$ will decrease with time to an ultimate steady-state value −1.97 MPa. The analytical expressions for the time dependence of $\bar{\psi}$, as illustrated in **Figures 5A,B** for increasing and decreasing ψ_a, respectively, are not explicitly available, but we can fit the profiles of $\bar{\psi}$ to exponential decay curves with time constant τ shown in the legend. The time constant for a certain set of C and R_c values turns out to be identical in both air wetting and drying situations, proving that the specific dynamics of leaf water status depends only on the internal hydraulic traits rather than external environments. In **Supplementary Figure 3**, the total transpiration rate E obtained in this modeling changes with time in a slightly different way, in which E would abruptly jump from its original steady-state value 1.97 $\mathrm{mmol \cdot m^{-2} \cdot s^{-1}}$ to a new lower (decreasing VPD) or higher value (increasing VPD), and then gradually change with the same exponentially decaying trend and time constant as $\bar{\psi}$, to steady-state values 0.987 $\mathrm{mmol \cdot m^{-2} \cdot s^{-1}}$ and 2.96 $\mathrm{mmol \cdot m^{-2} \cdot s^{-1}}$ for cases in **(A)** and **(B)**, respectively.

The continuous change of average xylem water potential and the avoidance of drastic variation in a short time are another illustration of the functions of leaf water-storage capacitance C, as well as resistance R_c from xylem to capacitors, in stabilizing the plant hydraulics and reducing the variation of water content. The instant changes of ψ_a and VPD are used to model the effects of transient changes of wind condition, which would cause the leaf to lose water and dehydrate under the influence of a drying atmosphere even when the plant is well watered. It turns out that the effects of changing C and changing R_c on the time dependence of $\bar{\psi}$ are similar in this case within the ranges of parameters we choose. While making the capacitance twice as large will exactly increase the time constant to two times, suggesting a direct proportionality between C and τ, we find that doubling R_c will also make τ increase to a little lower than two folds. The weaker effect of R_c is possibly related to the presence of unchanging R_a. This observation once again points to the effective strategy for a plant to overcome hydraulic destabilization and water loss due to negative environmental disturbances, by increasing either C or R_c of the leaf.

The stabilization of $\bar{\psi}$, however, only represents an average effect over the whole leaf from base to tip. The local xylem water potential ψ, which varies spatially in the leaf, would stay close to 0 near the base ($x = 0$) but would still become very negative near the tip ($x = 1$). An example is demonstrated in **Figure 6**, where the dynamics of spatially dependent water potential is simulated and its snapshots are plotted at multiple time points along the simulation. The figure shows the detailed changes of ψ according to the same hydraulic parameters and

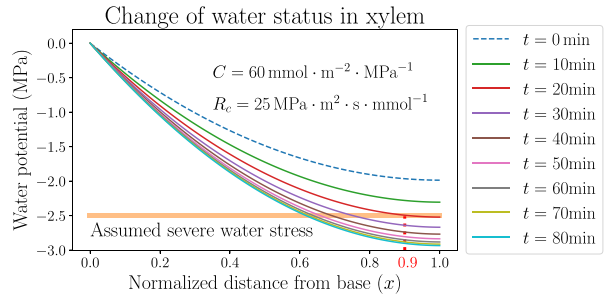

FIGURE 6 | The temporal variation of spatially dependent water potential in xylem, when the atmospheric water potential ψ_a is instantly decreased from −100MPa to −150MPa where the air is dried. Parameters used are identical to those used for the black curves in **Figure 5**. The horizontal line labels the upper limit of presumed water potential under severe stress.

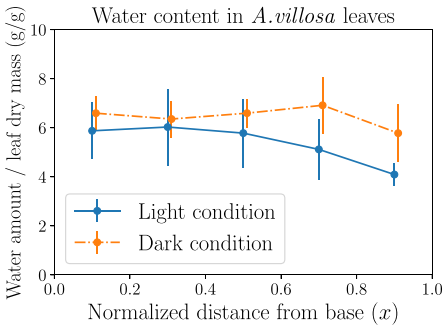

FIGURE 7 | The experimental measurements of the mass of water content averaged over leaf dry mass (both in grams), in each of the five leaf portions of equal length. Six leaves of the grass *Anthaenantia villosa* in light conditions and six leaves of the same species in dark conditions are used in the measurements. Error bars represent standard deviations. A more even distribution in leaves in darkness and a tapering trend from base to tip in leaves exposed to light are observed. The two sets of data are plotted with a horizontal shift of 0.01 to show error bars.

atmospheric condition of the black solid line in **Figure 5B**, where ψ_a decreases from –100 to −150 MPa instantly at $t = 0$ and VPD increases from 1.64 kPa to about 2.1 kPa. Within tens of minutes, the average potential $\bar{\psi}$ is stabilized at around −2 MPa (specifically −1.97 MPa) which is the new steady state at the lower ψ_a, while the profile of ψ maintains a monotonically declining trend but lowers quantitatively with time. The rate of the lowering of ψ is initially faster and slows down later, corresponding to the exponential decay of $\bar{\psi}$. Even though the xylem average water potential is always higher than −2 MPa, the local water potential near the tip would experience severe water stress (which is assumed to be lower than −2.5 MPa here) after a short time. This severely stressed water potential is presumably lower than the value required for the normal functioning of a plant leaf, and would thoroughly dehydrate the leaf portion under this negative potential, making it lose physiological functions. For example, in about 20 min after the instant change of ψ_a and VPD, the leaf portion at $x > 0.9$ (between the vertical dotted line and the tip at $x = 1.0$ in **Figure 6**) would experience the low water potential and severe stress, and would be quickly dehydrated even when the average water status of the whole leaf is still relatively high. As the simulation proceeds with time, the leaf portion near the tip undergoing severe water stress would enlarge and the left boundary of this region (the vertical dotted line) would move to smaller x. This discovery calls for caution when studying the average water status of a leaf, which may be in a safe range for the leaf tissue to stay healthy, while the local water potential (especially at the tip) may be very negative and the leaf can be partly dehydrated, losing part of its functionality. A large capacitance C, and also large resistances R_c and R_a, could help to delay the lowering of water potential by increasing the time scale τ, so that even the tip potential could be held at a high level to avoid dehydration for a relatively long time. A real-life living plant leaf would most likely close stomata and immediately raise R_a, when facing dry wind in the air and going through quickly rising VPD.

3.4. Experimental Measurement Results of Water Content Distribution in *A. villosa* Leaves

The experimental data of the spatial variation of leaf water potential is usually difficult to obtain by using common techniques, while the measurement of local water content distribution is quantifiable by gravimetric methods. **Figure 7** shows the different measurement results of local water amount averaged over leaf dry mass (to account for both leaf area and thickness) in leaves of the grass *A. villosa* when exposed to light or in dark conditions. It is observed that the leaves in darkness (where stomata are presumed to be closed) sustain a more evenly distributed water content, while leaves in light conditions (where stomata are presumed to be open) hold more water near the base but gradually decreasing water amount toward the tip, reflecting the declining trend of water potential. The statistical difference between the dark and light measurement results is most significant in the rightmost leaf segment nearest to the tip. Both observations as well as their difference actually demonstrate the usefulness of our modeling methods. The light treatment result indirectly confirms the finding in **Figure 3**. The dark treatment result, on the other hand, matches the prediction from **Figure 1** that when stomata are closed and transpiration is stopped ($I_i^{(a)} = 0$), in a fully hydrated steady state all currents (water flow) would also stop, leading to xylem water potential $\psi_i = \psi_0$ throughout the xylem vessel and water content uniformly distributed along the leaf. See **Supplementary Material** for additional measurement data.

4. DISCUSSION

One of the central assumptions of our theoretical modeling work on uniform grass leaf model is the constant resistance

R_a from xylem to the atmosphere. This assumption implies that the stomatal resistance to water vapor flow is steady and independent of environmental changes within the modeled time period, a highly hypothetical stomatal behavior which is usually not accurate in a living plant. However, this idealized behavior is most helpful for focusing on the effects of water-storage capacitance and its associated resistance while avoiding the complication of a changeable stomatal resistance. This assumption is not trivial or baseless even from a plant biological point of view when studying short-term behaviors. It is shown that beginning with a well-watered state, both stomatal conductance and transpiration rate are stabilized and would not decrease significantly even when leaf water potential starts to drop, as long as the potential is higher than a threshold that causes stomata to react, increasing their resistance and ultimately closing (Brodribb, 2009; Choat et al., 2018). In fact, the dynamic processes modeled in this work all start from a well-watered steady state, and the results are meaningful for the study of initial changes and reactions of a leaf blade in response to instant or short-time variations of water conditions, which are exactly what is considered in the hypothesized dynamic scenarios.

In order to model the long-term dehydration dynamics, we would need to incorporate the dependence of stomatal resistance (and thus R_a), on the leaf water status. The large R_a used in our modeling (compared with xylem hydraulic resistance) in the pathway from xylem to the atmosphere is mainly comprised of two parts, namely the stomatal resistance R_s and the outside-xylem resistance R_{ox} which is mostly through mesophyll and is also referred to as mesophyll resistance (Xiao and Zhu, 2017; Xiong et al., 2017). If we consider R_a as a variable dependent on water content W, we can assume $R_a(W) = R_s(W) + R_{ox}$ in which R_s is a function of W and R_{ox} is a constant. We assume that the water content of the leaf when well-watered is W_0, so that $R_s(W_0) = 0$ and $R_a(W_0) = R_{ox}$ when the leaf is fully hydrated ($W = W_0$) and stomata are open, and thus R_{ox} between xylem and stomata provides the minimum resistance in the transpiration pathway. The lumped model in **Figure 2** is helpful for estimating the importance of the stomatal sensitivity to leaf water content (contained by capacitors) in controlling the transpiration rate. We suppose that when the leaf is slightly dehydrated from W_0 to a water content $W < W_0$, both whole-leaf lumped capacitor and stomatal resistance depend linearly on W (effectively expanded to the first order). For the linear capacitor, we have its voltage $V(W) = W/C$ as a function of W, where C is the regular capacitance. For the linear stomatal resistance, we have $R_a(W) = R_{ox} + s(W_0 - W)$ in which $R_s(W) = s(W_0 - W)$ where s is a positive linear measure of the sensitivity of R_a (and R_s) to W, so that R_a and R_s increase with decreasing W according to the expected behavior of real-life stomata. From Equations S22–S25 in **Supplementary Material**, we calculate the expressions of ψ_x, I_x, I_a and I_c (all found in **Figure 2**) in terms of given terminal water potentials (ψ_p and ψ_a) and electrical traits including $V(W)$ and $R_a(W)$. From the dependence of I_c on W and the relation $I_c = \mathrm{d}W/\mathrm{d}t$, we calculate a steady-state expression for W which represents the static water status of a living leaf. Furthermore, by substituting this steady-state W into the expression of I_a, we obtain the following estimate of the relationship between terminal potentials and I_a (showing the highest-order term):

$$\psi_p - \psi_a \approx CR_x s \cdot I_a^2 + \cdots \tag{18}$$

which emphasizes the essential functions of leaf capacitance C, xylem hydraulic resistance R_x and the stomatal sensitivity to water content in limiting the increase of transpiration current I_a with an increasing water potential deficit $\psi_p - \psi_a$ between inside and outside of the leaf. In this way both capacitance and stomatal control are shown to be helpful for keeping water content and reducing water loss in transpiration.

If the dehydration lasts longer and the leaf approaches severe stress (such as water potential below the limit of severe water tress in **Figure 6**), the xylem hydraulic conductance would also start to decrease due to the formation of embolism or cavitation, air bubbles blocking water flow in xylem vessels (Tyree and Ewers, 1991; Sack and Holbrook, 2006; Choat et al., 2012, 2018; Jones, 2013; Stroock et al., 2014). The dependence of xylem conductance on water potential is conventionally approximated as a logistic function with the shape of a sigmoid curve, in which the loss of conductance is negligible at relatively high potential and grows more rapidly with further lowering potential. Indeed, the incorporation of xylem and stomatal conductances dependent on water potential is applied in several theoretical models, in which the stomatal dependence is also treated as sigmoidal or approximately piecewise linear functions (Mencuccini et al., 2019). Alternatively, a more direct stomatal dependence on VPD can also be established and implemented (Grossiord et al., 2020). Most recently, the sigmoidal behaviors of both xylem and stomatal conductances are applied in a spatially explicit study (Jain et al., 2021). The specific biophysical and biochemical mechanisms that control stomatal opening through water status, including the turgor pressure of guard cells and epidermal cells around stomata and the use of plant hormone abscisic acid, are broadly explored by existing literature (Buckley, 2005). If the spatial variation of stomatal conductance (or resistance) along leaf surface is also included, the model would need to take into account anatomical data over leaf blade, including sizes and spatial distributions of stomata and xylem vessels (Ocheltree et al., 2012; Rockwell and Holbrook, 2017). It would be necessary to incorporate not only the overall dependences of whole-system hydraulic traits on average water status in the large scale (such as sigmoid), but also small-scale quantitative relationships between stomatal and xylem resistances at fine spatial resolution and their local water potential or content, to make full use of our spatially explicit capacitive model. We expect to experimentally measure these fine-resolution quantities and implement the experimental inputs in future modeling. For the completeness of the current work, we have uploaded the source code of grass leaf simulations for interested readers to try simulating leaves with extra spatial variations or stomatal features. (See the data availability statement.)

Under the assumption of constant stomatal opening, our computation and simulation results indicate that both capacitance C and the resistance R_c from xylem to capacitors play significant roles in defining the time constant τ, which determines the rate of change in a dehydration (or hydration) dynamics. Both C and R_c are positively related to τ, and thus a plant with large C or R_c can effectively slow down dehydration under short-term water stresses and maintain leaf-water potential higher than the threshold which causes stomata to close and so that photosynthesis and other physiological functioning can proceed. Similar time constants (as product of whole-system hydraulic resistance and capacitance) were described in previous literature (Chuang et al., 2006; Meinzer et al., 2009). This maintenance of water status can be observed in experimental studies of grass leaves. Specifically, in a leaf that dehydrates slowly (possibly due to larger capacitance), stomatal conductance would change less with atmospheric humidity and VPD by a smaller magnitude of slope compared to a leaf showing faster dehydration dynamics. The two types of water-storage cells in grass leaves, bulliform and bundle sheath, are different in their specific capacitance values C, which are related to cell wall rigidity or elasticity, and also in R_c values. Bundle sheaths are much closer to xylem conduits which are contained in vascular bundles, while bulliform cells are mostly distributed in the epidermis on the upper side of a leaf. The longer water pathways from xylem to bulliform may lead to larger R_c and greater contribution to the delay of water loss. In our simulation, using two sets of capacitors and resistors could be feasible when dealing with the cell types. In certain plants, a variable capacitance depending on water status was observed (Salomón et al., 2017) and could be additionally applied. The baseline osmotic potential ψ_s of water storage, which is determined by the most negative osmotic potential due to the presence of aqueous solutes in leaf cells and does not play an explicit part in this study, can be obtained by measuring C and water content $W = C(\psi_x - \psi_s)$ where ψ_x is the steady-state mean potential in xylem. These measurements can be achieved through pressure-volume (PV) curves, which measure the interdependence between leaf potential and water content (Abrams, 1988; Jones, 2013). Another factor worth considering when studying water flows outside of xylem, both to stomata for transpiration or to leaf cells for storage, is the actual form of water transport. Recent modeling efforts have specifically investigated the relative importance of symplastic (through cell cytoplasm), apoplastic (inside cell wall but outside cell membrane), and gaseous pathways (especially in transpiration), as well as the exact site of exiting water evaporation (either near vascular bundle or near stomata and epidermis) which may complicate the hydraulic condition inside a leaf (Rockwell et al., 2014; Buckley, 2015; Buckley et al., 2017).

Our spatially explicit modeling methods provide a new theoretical approach to the study of fluid dynamics of general flow networks with fluid-storage function. Such networks are not necessarily hydraulic vascular networks found in plant leaves, but could also be found in other water transport systems such as river networks. The applicability of the modeling methods to plant biology has been illustrated in the computation and simulation results of grass leaf hydraulics. The use of grass leaves as a model benefits from not only simpler stomata and venation arrangements than dicots, but also the clear presence of water-storage cells (capacitors). The spatially dependent xylem water potential profile, which decreases from base to tip in well-watered steady state (**Figure 3**) when capacitors are static, compares qualitatively well with earlier calculation results of wheat leaves by Altus et al. (1985) and most recent experimental measurements (using a novel method) and theoretical predictions of maize leaves by Jain et al. (2021), as well as water potential gradients along sugarcane stems (Meinzer et al., 1992). By tuning the biologically relevant parameters we choose, we can reproduce quantitatively matching results, though these previous studies considered local resistances without explicit water storage. The measurement results of the spatial distribution of water content in *A. villosa* leaves in **Figure 7**, which are statistically different toward leaf tip between light and dark conditions, also support key predictions and the effectiveness of the model.

To further improve the ability of our model to accurately predict leaf hydraulic behaviors, we can implement the grass leaf vascular architecture with hierarchy, where major lateral veins and minor intermediate veins are parallel and connected by transverse veins, as shown by Altus et al. In fact, hierarchical structures exist among all plant leaf networks, especially dicotyledonous leaves whose veins are not parallel but instead form branches and loops. It has been experimentally found in dicot leaves that major veins (with high conductivity) are useful for distributing water throughout the leaf blade evenly in a fast manner, and minor veins (with high resistivity) are used to deliver water to leaf cells (Zwieniecki et al., 2002). This observation has also been simulated by a resistor-only model to verify the functions of multiple levels of veins with different resistances in a mesh network (Cochard et al., 2004). Our modeling could help to reveal the function of capacitance in water flow dynamics and balancing of water distribution in similar networked systems. At each level of the hierarchy, the continuous anatomical narrowing of xylem conduits from leaf base to tip can also affect the water potential pattern (Lechthaler et al., 2020) and can be implemented in our model with a large number of nodes. Along with hierarchical considerations, and guided by empirical sub-leaf scale data, we plan to apply more biologically realistic anatomical and physiological inputs in future simulation studies based on our current model. We can then gain a better understanding of the importance of capacitance in time-dependent leaf hydraulic behavior in both natural and agricultural settings to help explain evolutionary adaptations of plants to manage water, and, eventually inspire more efficient agricultural practices.

DATA AVAILABILITY STATEMENT

The original contributions presented in the study are publicly available. The code used

for the numerical simulations can be found at https://github.com/yongtianluo/Leaf-capacitive-hydraulics.

AUTHOR CONTRIBUTIONS

YL developed the theoretical methods, analyzed the results, and wrote the manuscript. C-LH performed the experiments. BRH designed the research and revised the manuscript. EK conceived and designed the research and revised the manuscript. All authors contributed to the article and approved the submitted version.

FUNDING

The authors acknowledge support from NSF-IOS, Award 1856587.

SUPPLEMENTARY MATERIAL

The Supplementary Material for this article can be found online at: https://www.frontiersin.org/articles/10.3389/fpls.2021.725995/full#supplementary-material

REFERENCES

Abrams, M. D. (1988). Sources of variation in osmotic potentials with special reference to North American tree species. *Forest Sci.* 34, 1030–1046.

Altus, D. P., Canny, M. J., and Blackman, D. R. (1985). Water pathways in wheat leaves. II: Water-conducting capacities and vessel diameters of different vein types, and the behaviour of the integrated vein network. *Aust. J. Plant Physiol.* 12, 183–199. doi: 10.1071/PP9850183

Bartlett, M. K., Scoffoni, C., and Sack, L. (2012). The determinants of leaf turgor loss point and prediction of drought tolerance of species and biomes: a global meta-analysis. *Ecol. Lett.* 15, 393–405. doi: 10.1111/j.1461-0248.2012.01751.x

Brodribb, T. J. (2009). Xylem hydraulic physiology: the functional backbone of terrestrial plant productivity. *Plant Sci.* 177, 245–251. doi: 10.1016/j.plantsci.2009.06.001

Bryant, C., Fuenzalida, T. I., Brothers, N., Mencuccini, M., Sack, L., Binks, O., et al. (2021). Shifting access to pools of shoot water sustains gas exchange and increases stem hydraulic safety during seasonal atmospheric drought. *Plant Cell Environ.* 44, 2898–2911. doi: 10.1111/pce.14080

Buckley, T. N. (2005). The control of stomata by water balance. *New Phytol.* 168, 275–292. doi: 10.1111/j.1469-8137.2005.01543.x

Buckley, T. N. (2015). The contributions of apoplastic, symplastic and gas phase pathways for water transport outside the bundle sheath in leaves. *Plant Cell Environ.* 38, 7–22. doi: 10.1111/pce.12372

Buckley, T. N., John, G. P., Scoffoni, C., and Sack, L. (2017). The sites of evaporation within leaves. *Plant Physiol.* 173, 1763–1782. doi: 10.1104/pp.16.01605

Buckley, T. N., and Sack, L. (2019). The humidity inside leaves and why you should care: implications of unsaturation of leaf intercellular airspaces. *Am. J. Bot.* 106, 618–621. doi: 10.1002/ajb2.1282

Buckley, T. N., Sack, L., and Gilbert, M. E. (2011). The role of bundle sheath extensions and life form in stomatal responses to leaf water status. *Plant Physiol.* 156, 962–973. doi: 10.1104/pp.111.175638

Choat, B., Brodribb, T. J., Brodersen, C. R., Duursma, R. A., López, R., and Medlyn, B. E. (2018). Triggers of tree mortality under drought. *Nature.* 558, 531–539. doi: 10.1038/s41586-018-0240-x

Choat, B., Jansen, S., Brodribb, T. J., Cochard, H., Delzon, S., Bhaskar, R., et al. (2012). Global convergence in the vulnerability of forests to drought. *Nature* 491, 752–755. doi: 10.1038/nature11688

Chuang, Y.-L., Oren, R., Bertozzi, A. L., Phillips, N., and Katul, G. G. (2006). The porous media model for the hydraulic system of a conifer tree: linking sap flux data to transpiration rate. *Ecol. Modell.* 191, 447–468. doi: 10.1016/j.ecolmodel.2005.03.027

Cochard, H., Nardini, A., and Coll, L. (2004). Hydraulic architecture of leaf blades: where is the main resistance? *Plant Cell Environ.* 27, 1257–1267. doi: 10.1111/j.1365-3040.2004.01233.x

Cowan, I. R. (1965). Transport of water in the soil-plant-atmosphere system. *J. Appl. Ecol.* 2, 221–239. doi: 10.2307/2401706

Cowan, I. R. (1972). Oscillations in stomatal conductance and plant functioning associated with stomatal conductance: observations and a model. *Planta* 106, 185–219. doi: 10.1007/BF00388098

Grossiord, C., Buckley, T. N., Cernusak, L. A., Novick, K. A., Poulter, B., Siegwolf, R. T., et al. (2020). Plant responses to rising vapor pressure deficit. *New Phytol.* 226, 1550–1566. doi: 10.1111/nph.16485

Hölttä, T., Cochard, H., Nikinmaa, E., and Mencuccini, M. (2009). Capacitive effect of cavitation in xylem conduits: results from a dynamic model. *Plant Cell Environ.* 32, 10–21. doi: 10.1111/j.1365-3040.2008.01894.x

Jain, P., Liu, W., Zhu, S., Chang, C. Y.-Y., Melkonian, J., Rockwell, F. E., et al. (2021). A minimally disruptive method for measuring water potential in planta using hydrogel nanoreporters. *Proc. Natl. Acad. Sci. U.S.A.* 118, e2008276118. doi: 10.1073/pnas.2008276118

Jones, H. G. (1978). Modelling diurnal trends of leaf water potential in transpiring wheat. *J. Appl. Ecol.* 15, 613–626. doi: 10.2307/2402615

Jones, H. G. (2013). *Plants and Microclimate: A Quantitative Approach to Environmental Plant Physiology, 3rd Edn.* Cambridge, UK: Cambridge University Press.

Katifori, E. (2018). The transport network of a leaf. *Comptes Rendus Physique* 19, 244–252. doi: 10.1016/j.crhy.2018.10.007

Lechthaler, S., Kiorapostolou, N., Pitacco, A., Anfodillo, T., and Petit, G. (2020). The total path length hydraulic resistance according to known anatomical patterns: what is the shape of the root-to-leaf tension gradient along the plant longitudinal axis? *J. Theor. Biol.* 502:110369. doi: 10.1016/j.jtbi.2020.110369

Martre, P., Cochard, H., and Durand, J.-L. (2001). Hydraulic architecture and water flow in growing grass tillers (Festuca arundinacea Schreb.). *Plant Cell Environ.* 24, 65–76. doi: 10.1046/j.1365-3040.2001.00657.x

Meinzer, F. C., Goldstein, G., Neufeld, H. S., Grantz, D. A., and Crisosto, G. M. (1992). Hydraulic architecture of sugarcane in relation to patterns of water use during plant development. *Plant Cell Environ.* 15, 471–477. doi: 10.1111/j.1365-3040.1992.tb00998.x

Meinzer, F. C., Johnson, D. M., Lachenbruch, B., McCulloh, K. A., and Woodruff, D. R. (2009). Xylem hydraulic safety margins in woody plants: coordination of stomatal control of xylem tension with hydraulic capacitance. *Funct. Ecol.* 23, 922–930. doi: 10.1111/j.1365-2435.2009.01577.x

Mencuccini, M., Manzoni, S., and Christoffersen, B. (2019). Modelling water fluxes in plants: from tissues to biosphere. *New Phytol.* 222, 1207–1222. doi: 10.1111/nph.15681

Mencuccini, M., Salmon, Y., Mitchell, P., Hölttä, T., Choat, B., Meir, P., et al. (2017). An empirical method that separates irreversible stem radial growth from bark water content changes in trees: theory and case studies. *Plant Cell Environ.* 40, 290–303. doi: 10.1111/pce.12863

Ocheltree, T. W., Nippert, J. B., and Prasad, P. V. V. (2012). Changes in stomatal conductance along grass blades reflect changes in leaf structure. *Plant Cell Environ.* 35, 1040–1049. doi: 10.1111/j.1365-3040.2011.02470.x

Pfautsch, S., Hölttä, T., and Mencuccini, M. (2015). Hydraulic functioning of tree stems-fusing ray anatomy, radial transfer and capacitance. *Tree Physiol.* 35, 706–722. doi: 10.1093/treephys/tpv058

Raven, P. H., Evert, R. F., and Eichhorn, S. E. (2005). *Biology of Plants, 7th Edn.* New York, NY: W. H. Freeman.

Rockwell, F. E., and Holbrook, N. M. (2017). Leaf hydraulic architecture and stomatal conductance: a functional perspective. *Plant Physiol.* 174, 1996–2007. doi: 10.1104/pp.17.00303

Rockwell, F. E., Holbrook, N. M., and Stroock, A. D. (2014). The competition between liquid and vapor transport in transpiring leaves. *Plant Physiol*. 164, 1741–1758. doi: 10.1104/pp.114.236323

Sack, L., and Holbrook, N. M. (2006). Leaf hydraulics. *Annu. Rev. Plant Biol*. 57, 361–381. doi: 10.1146/annurev.arplant.56.032604.144141

Salomón, R. L., Limousin, J.-M., Ourcival, J.-M., Rodríguez-Calcerrada, J., and Steppe, K. (2017). Stem hydraulic capacitance decreases with drought stress: implications for modelling tree hydraulics in the Mediterranean oak Quercus ilex. *Plant Cell Environ*. 40, 1379–1391. doi: 10.1111/pce.12928

Smith, J. A. C., Schulte, P. J., and Nobel, P. S. (1987). Water flow and water storage in Agave deserti: osmotic implications of crassulacean acid metabolism. *Plant Cell Environ*. 10, 639–648. doi: 10.1111/j.1365-3040.1987.tb01846.x

Steppe, K., De Pauw, D. J. W., Lemeur, R., and Vanrolleghem, P. A. (2006). A mathematical model linking tree sap flow dynamics to daily stem diameter fluctuations and radial stem growth. *Tree Physiol*. 26, 257–273. doi: 10.1093/treephys/26.3.257

Stroock, A. D., Pagay, V. V., Zwieniecki, M. A., and Holbrook, N. M. (2014). The physicochemical hydrodynamics of vascular plants. *Annu. Rev. Fluid Mech*. 46, 615–642. doi: 10.1146/annurev-fluid-010313-141411

Taiz, L., and Zeiger, E. (2002). *Plant Physiology, 3rd Edn*. Sunderland, MA: Sinauer Associates.

Tyree, M. T., and Ewers, F. W. (1991). The hydraulic architecture of trees and other woody plants. *New Phytol*. 119, 345–360. doi: 10.1111/j.1469-8137.1991.tb00035.x

van den Honert, T. H. (1948). Water transport in plants as a catenary process. *Discuss Faraday Soc*. 3, 146–153. doi: 10.1039/df9480300146

Wei, C., Tyree, M. T., and Steudle, E. (1999). Direct measurement of xylem pressure in leaves of intact maize plants. A test of the cohesion-tension theory taking hydraulic architecture into consideration. *Plant Physiol*. 121, 1191–1205. doi: 10.1104/pp.121.4.1191

Xiao, Y., and Zhu, X.-G. (2017). Components of mesophyll resistance and their environmental responses: a theoretical modelling analysis. *Plant Cell Environ*. 40, 2729–2742. doi: 10.1111/pce.13040

Xiong, D., Flexas, J., Yu, T., Peng, S., and Huang, J. (2017). Leaf anatomy mediates coordination of leaf hydraulic conductance and mesophyll conductance to CO_2 in Oryza. *New Phytol*. 213, 572–583. doi: 10.1111/nph.14186

Zwieniecki, M. A., Melcher, P. J., Boyce, C. K., Sack, L., and Holbrook, N. M. (2002). Hydraulic architecture of leaf venation in *Laurus nobilis* L. *Plant Cell Environ*. 25, 1445–1450. doi: 10.1046/j.1365-3040.2002.00922.x

Conflict of Interest: The authors declare that the research was conducted in the absence of any commercial or financial relationships that could be construed as a potential conflict of interest.

Publisher's Note: All claims expressed in this article are solely those of the authors and do not necessarily represent those of their affiliated organizations, or those of the publisher, the editors and the reviewers. Any product that may be evaluated in this article, or claim that may be made by its manufacturer, is not guaranteed or endorsed by the publisher.

frontiers in Plant Science

ORIGINAL RESEARCH
published: 10 November 2021
doi: 10.3389/fpls.2021.745110

Physiological and Transcriptomic Analyses Revealed the Implications of Abscisic Acid in Mediating the Rate-Limiting Step for Photosynthetic Carbon Dioxide Utilisation in Response to Vapour Pressure Deficit in *Solanum Lycopersicum* (Tomato)

Dalong Zhang[1,2,3], *Qingjie Du*[4], *Po Sun*[1], *Jie Lou*[1], *Xiaotian Li*[1], *Qingming Li*[1,2,3] *and Min Wei*[1,2,3]*

[1] College of Horticultural Science and Engineering, Shandong Agricultural University, Tai'an, China, [2] State Key Laboratory of Crop Biology, Tai'an, China, [3] Scientific Observing and Experimental Station of Environment Controlled Agricultural Engineering in Huang-Huai-Hai Region, Ministry of Agriculture, Beijing, China, [4] College of Horticulture, Henan Agricultural University, Zhengzhou, China

OPEN ACCESS

Edited by:
Thorsten M. Knipfer,
University of British Columbia, Canada

Reviewed by:
Wencheng Wang,
Huazhong Agricultural University, China
Dimitrios Fanourakis,
Technological Educational Institute of Crete, Greece

***Correspondence:**
Min Wei
minwei@sdau.edu.cn

Specialty section:
This article was submitted to Crop and Product Physiology, a section of the journal Frontiers in Plant Science

Received: 21 July 2021
Accepted: 24 September 2021
Published: 10 November 2021

Citation:
Zhang D, Du Q, Sun P, Lou J, Li X, Li Q and Wei M (2021) Physiological and Transcriptomic Analyses Revealed the Implications of Abscisic Acid in Mediating the Rate-Limiting Step for Photosynthetic Carbon Dioxide Utilisation in Response to Vapour Pressure Deficit in Solanum Lycopersicum (Tomato). Front. Plant Sci. 12:745110. doi: 10.3389/fpls.2021.745110

The atmospheric vapour pressure deficit (VPD) has been demonstrated to be a significant environmental factor inducing plant water stress and affecting plant photosynthetic productivity. Despite this, the rate-limiting step for photosynthesis under varying VPD is still unclear. In the present study, tomato plants were cultivated under two contrasting VPD levels: high VPD (3–5 kPa) and low VPD (0.5–1.5 kPa). The effect of long-term acclimation on the short-term rapid VPD response was examined across VPD ranging from 0.5 to 4.5 kPa. Quantitative photosynthetic limitation analysis across the VPD range was performed by combining gas exchange and chlorophyll fluorescence. The potential role of abscisic acid (ABA) in mediating photosynthetic carbon dioxide (CO_2) uptake across a series of VPD was evaluated by physiological and transcriptomic analyses. The rate-limiting step for photosynthetic CO_2 utilisation varied with VPD elevation in tomato plants. Under low VPD conditions, stomatal and mesophyll conductance was sufficiently high for CO_2 transport. With VPD elevation, plant water stress was gradually pronounced and triggered rapid ABA biosynthesis. The contribution of stomatal and mesophyll limitation to photosynthesis gradually increased with an increase in the VPD. Consequently, the low CO_2 availability inside chloroplasts substantially constrained photosynthesis under high VPD conditions. The foliar ABA content was negatively correlated with stomatal and mesophyll conductance for CO_2 diffusion. Transcriptomic and physiological analyses revealed that ABA was potentially involved in mediating water

transport and photosynthetic CO_2 uptake in response to VPD variation. The present study provided new insights into the underlying mechanism of photosynthetic depression under high VPD stress.

Keywords: abscisic acid, evaporative demand, mesophyll conductance, plant water status, stomatal conductance

INTRODUCTION

Carbon dioxide (CO_2) is significant for plant photosynthesis, growth, and yield production. Although CO_2 fertilisation and globally elevated trends are expected to improve crop photosynthesis and yield, large evidence has shown that the magnitude of such enhancement is constrained by other climate change-derived phenomena, such as more extreme and frequent environmental stress (Norby, 2002). The bottlenecks constraining the CO_2 utilisation efficiency are limited CO_2 acquisition and assimilation. It has been recognised that CO_2 movement and carbon fixation are regulated by environmental factors. There is increasing evidence from physiology and crop production that high vapour pressure deficit (VPD) induces plant water stress and inhibits photosynthetic productivity (Lu et al., 2015; Zhang et al., 2015). Few previous studies have quantitatively addressed the components of photosynthetic limitation across a series of VPD. The rate-limiting step for photosynthetic CO_2 transport and utilisation under different VPD conditions was highly uncertain. A quantitative limitation analysis consisting of stomatal, mesophyll, and biochemical limitations is essential to reveal the underlying mechanism by which the VPD affects the photosynthetic process.

Photosynthetic CO_2 uptake and transport are constrained by a series of resistances, which have been simplified into stomatal and mesophyll resistance (Tholen and Zhu, 2011). Guard cells of stomata are the first barrier for gas exchange and modulate photosynthetic CO_2 uptake and transpiration (Lawson and Blatt, 2014). Large evidence has shown that CO_2 movement from the substomatal cavity to the carbon fixation site is constrained by great mesophyll resistance (Niinemets et al., 2009; von Caemmerer and Evans, 2010; Flexas et al., 2012; Kaldenhoff, 2012; Sharkey, 2012; Li et al., 2019b). In addition to stomatal resistance, mesophyll resistance also substantially constrains the photosynthetic rate, especially for C_3 plants. Environmental fluctuations are thought to profoundly affect CO_2 uptake and transport. Leaf anatomical properties determine the maximum potential conductance for gas or liquid phase diffusion. Some studies attributed photosynthetic limitations to anatomical adaptations under high VPD stress, such as reduced stomatal size, stomatal density, vein density, and mesophyll surface area (Fanourakis et al., 2016, 2020; Du et al., 2019). CO_2 uptake and water loss share some common pathways, such as stomatal and intercellular spaces. Anatomical adaptations prevent excessive water loss, which simultaneously increases diffusion resistance for CO_2 uptake. In addition to the anatomical determination over long-term adaptations, much evidence has shown that stomatal and mesophyll conductance respond rapidly and sensitively to external environmental variation (Xiong et al., 2015; Li et al., 2019a,b). The field and greenhouse VPD fluctuate dramatically over the diurnal course, which significantly affects the photosynthetic process. However, less attention has been given to reveal the mechanism of the rapid response of CO_2 diffusion conductance across a series of VPD.

It has been widely reported that the plant hormone abscisic acid (ABA) is involved in various abiotic stresses and acts as a signalling molecule in response to drought, salinization, heat, and so on (Fang et al., 2019). Cellular ABA accumulation is an important dehydration-sensing and water balance-maintaining mechanism, which has special implications in stomatal closure and the decline of hydraulic conductance (Sack et al., 2018). ABA prevents excessive water loss and enhances crop drought tolerance by signalling pathways. As a C_3 plant species, the photosynthetic and yield potential of tomato plants is greatly limited by the low CO_2 availability inside chloroplasts. The excessive evaporative demand under high VPD exceeds root water uptake capacity and triggers plant water deficit in tomato plants, which contributes to photosynthetic depression and yield loss (Zhang et al., 2017, 2018; Li et al., 2019b). We hypothesised that ABA plays a significant role in preventing transpiration under high VPD-induced plant water deficit, which simultaneously constrains photosynthetic CO_2 uptake and acquisition. Identifying the rate-limiting step for photosynthetic CO_2 acquisition under contrasting VPD and revealing the mechanism has significant implications for both basic plant sciences and crop production.

To investigate the effect of long-term acclimation on the short-term rapid VPD response, the implications of leaf anatomical properties and ABA in modulating CO_2 transport across a series of VPD ranges were addressed by physiological and transcriptomic analyses. Three questions were addressed in the present study: (1) How did stomatal and mesophyll conductance tune with the VPD? (2) How did the contribution of stomatal and mesophyll limitation to photosynthesis vary with the VPD? (3) How did ABA tune with the VPD and correlate with stomatal and mesophyll conductance?

Abbreviations: VPD, vapour pressure deficit; Ψ_{leaf}, leaf water potential; Ψ_{soil}, soil water potential; Ψ_{air}, air-water potential; $\Delta\Psi_{leaf-air}$, the drawdown of water potential between leaf and air; $\Delta\Psi_{soil-leaf}$, the drawdown of water potential between soil and leaf; V_{cmax}, Maximum carboxylation rate; J_{max}, maximum electron transport rate; CE, carboxylation efficiency; g_s, stomatal conductance; g_m, mesophyll conductance; g_{tot}, total conductance; C_a, ambient CO_2 concentration; C_i, intracellular CO_2 concentration; C_C, CO_2 concentration of carboxylation sites inside chloroplast; L_s, stomatal limitations imposed on the photosynthetic rate; L_m, mesophyll limitations imposed on the photosynthetic rate; L_b, biochemical limitations imposed on the photosynthetic rate; LMA, leaf mass area; P_n, net photosynthetic rate; R_d, the rate of mitochondrial respiration in the light; Γ, chloroplastic CO_2 compensation point.

MATERIALS AND METHODS

Plant Materials and Growth Conditions

The experiment was conducted in two environmentally controlled greenhouses with the same characteristics (15 m in length, 10 m in width, and 3.5 m in height, north-south oriented) under spring-summer climatic conditions from May to August 2018. Two widely grown tomato cultivars (JinPeng NO.1, CV1, JinPeng & Co., Ltd., China; FenGuan, CV2, ZhongYa & Co., Ltd., China) with relatively distinct VPD responses were examined (Du et al., 2020). Seeds were sown in plugs for germination and transplanted at the four-leaf stage to 4.5 L plastic pots containing the same amount of organic substrate and perlite mixture in a 3:1 proportion (v/v). Soil moisture was maintained at ∼90% container capacity according to a previous method (Zhang et al., 2017). Plants were periodically trimmed to maintain rapid vegetative growth throughout experiments. Plants were grown in two environmentally controlled greenhouses and maintained under the same growth conditions but contrasting VPD. A high VPD was achieved in a natural greenhouse environment, with a VPD of ∼3–5 kPa around midday, while low VPD was maintained in the range of.5–1.5 kPa by humidification. A high-pressure micro-fog system was activated when the VPD exceeded the target values, and the characteristics of the system were described in detail in a previous study by Zhang et al. (2018). The average daily meteorological data inside the greenhouse during the growth period were ∼maintained at a temperature of 20–32°C, relative humidity of 50–75%, and photosynthetically active radiation of 45–65 Wm^{-2}.

The effects of VPD perturbations on leaf photosynthetic performance and plant water status were investigated ∼50 days after treatments. Afterward, 15 uniform plants from each treatment were selected as samples and transferred to growth cabinets in the evening prior to photosynthetic measurements. The light and temperature of the growth cabinets were controlled steadily at normal levels throughout the experiment.

Leaf Gas Exchange and Chlorophyll Fluorescence

Leaf gas exchange and chlorophyll fluorescence were measured simultaneously on healthy and expanded leaflets at the same nodes by portable gas exchange systems equipped with a leaf chamber fluorometer (LI-6400, Li-Cor, Inc., Lincoln, NE, USA). All portable gas exchange systems were enclosed in growth cabinets. The VPD inside cabinets and the leaf chamber was simultaneously controlled across a series gradient of 0.5, 1.5, 2.5, 3.5, and 4.5 kPa. The temperature, light, and CO_2 concentrations were controlled at the following constant and steady conditions throughout the experiment: temperature of 28 ± 1°C; saturating photosynthetic photon flux density (PPFD) of 1,100 μmol m^{-2} s^{-1}; CO_2 concentration of 400 μmol mol^{-1}. The VPD was increased stepwise across the gradients for at least 60 min until photosynthesis and the plant water status achieved a new steady state.

The curve of the photosynthetic rate (P_n) vs. intercellular CO_2 concentration (C_i) was determined using a previous procedure (Li et al., 2019b), across the VPD range of 0.5–4.5 kPa. Briefly, a P_n-C_i curve was generated by controlling the ambient CO_2 concentration (C_a) from 400 to 300, 200, 150, 100, and 50 μmol mol^{-1} and then increased to 400 μmol mol^{-1}. After re-achieving a steady-state at 400 μmol mol^{-1}, C_a was increased gradually from 400 μmol mol^{-1} to 1,200 μmol mol^{-1}. The carboxylation efficiency (CE) was estimated according to linear regression of the P_n-C_i curve in the range of $C_a \leq 200$ μmol mol^{-1} (Sun et al., 2016). The maximum rate of Rubisco carboxylation capacity (V_{cmax}) and maximal rate of electron transport (J_{max}) were determined according to the FvCB model (Farquhar et al., 1980).

Estimation of Photosynthetic CO_2 Diffusion Conductance

Carbon dioxide diffuses *via* stomatal and mesophyll barriers in a series circuit, which was driven by the CO_2 partial pressure gradient (Li et al., 2019b). Stomatal conductance for CO_2 diffusion (g_{sc}) was determined according to the water diffusion conductance (g_{sw}) and the ratio between molecular diffusivities of water and CO_2 in gas (Giuliani et al., 2013). The mesophyll conductance (g_m) was estimated by the variable J method (Harley et al., 1992):

$$g_m = \frac{P_n}{C_i - \frac{\Gamma^*(J+8(P_n+R_d))}{J-4(P_n+R_d)}} \quad (1)$$

where P_n is the net photosynthetic rate and C_i is the intercellular CO_2 concentration. P_n and C_i were measured by steady-state gas exchange. R_d is the mitochondrial respiration rate in the light, and Γ* is the CO_2 compensation point inside the chloroplast. R_d and Γ* were calculated according to a previous study by Laisk and Oja (1998). Briefly, P_n-C_i curves were measured at two light intensities (75 and 500 μmol m^{-2} s^{-1}) at CO_2 concentrations of 30–120 μmol mol^{-1}. Γ* (x-axis) and R_d (y-axis) were derived according to the intersection point of the P_n-C_i curves. J is the electron transport rate, which was calculated as described by a previous study (Tomas et al., 2013).

According to the series circuit, the total CO_2 diffusion resistance ($1/g_{tot}$) can be determined as $1/g_{tot} = 1/g_s + 1/g_m$ (Niinemets et al., 2009). Therefore, g_{tot} can be determined as:

$$g_{tot} = \frac{1}{1/g_s + 1/g_m} \quad (2)$$

Partitioning of the Photosynthetic Limitation

The photosynthetic limitation was divided into the components of stomatal limitation (L_s), mesophyll limitation (L_m), and biochemical limitation (L_m). The proportions of individual components imposed on photosynthesis were determined as follows (Muir et al., 2014; Li et al., 2019b):

$$L_s = \frac{g_{tot}/g_s \times \partial A/\partial C_c}{g_{tot} + \partial A/\partial C_c}$$
$$L_m = \frac{g_{tot}/g_m \times \partial A/\partial C_c}{g_{tot} + \partial A/\partial C_c}$$
$$L_b = \frac{g_{tot}}{g_{tot} + \partial A/\partial C_c} \quad (3)$$

By definition, $L_s + L_m + L_b = 1$; $\partial A/\partial C_c$ was determined as the slope of the P_n-C_c curves at CO_2 concentrations of 40–110 μmol mol^{-1}.

Determination of the Plant Water Status

Once photosynthetic measurements were completed, the adjacent leaflets were harvested for the determination of the water status of the plant. The leaf water potential (Ψ_{leaf}) was measured by a pressure chamber (PMS-1000, PMS Instruments Inc., Corvallis, OR, USA). An extra test was performed where Ψ_{leaf} of adjacent leaflets was compared, and no differences in Ψ_{leaf} were detected between two adjacent leaflets. Some plants were kept in dark conditions for ∼8–10 h for the determination of the soil water potential (Ψ_{soil}) (Tsuda and Tyree, 2000). Since water movement was ∼zero under dark conditions, Ψ_{soil} remained relatively constant and can be assumed to equal the xylem pressure potential of leaves under dark conditions.

Leaf Morphology

After determination of the plant water status, the leaflet area was measured by a leaf area metre. The leaflet samples were dried at 80°C in an oven to a constant dry mass and weighed. The leaf mass area (LMA) was determined as the ratio of leaf dry mass to leaf area.

Leaf ABA Concentration

After reaching the steady-state of photosynthesis, leaflets were harvested for ABA detection and transcriptome sequencing. Phytohormone contents were determined by a liquid chromatography electrospray ionisation tandem mass spectrometry (LC-ESI-MS/MS) system (HPLC, Shim-pack UFLC SHIMADZU CBM30A system, www.shimadzu.com.cn/; MS, Applied Biosystems 6500 Triple Quadrupole, www.appliedbiosystems.com.cn/). Briefly, the leaflets for photosynthetic measurements were harvested and frozen in liquid nitrogen. The samples were extracted with methanol/water/formic acid and filtered before LC-MS/MS analysis. The detailed protocol was described on MetWare (http://www.metware.cn/) based on the AB Sciex QTRAP 6500 LC-MS/MS platform. Samples were detected with three biological replicates.

RNA Extraction and Transcriptome Sequencing

Total RNA was extracted from leaflet samples for transcriptome sequencing, according to a previous study (Zhang et al., 2019b). Sequencing libraries were constructed using the Ultra^{TM} RNA Library Prep Kit for Illumina (NEB, USA) according to the instructions of the manufacturer. The detailed protocol was described in a previous study, which was briefly described in a simplified diagram.

Sequencing Data Analysis

The clean data were obtained by processing the raw data through in-house Perl scripts. The low-quality data and sequencing adapters were trimmed. The fragments per kilobase of transcript per million fragments mapped (FPKM) was calculated based on gene length and read counts. Differentially expressed genes (DEGs) were assigned according to the adjusted P <0.05. Gene ontology (GO) enrichment was determined by submitting DEGs to the GO database to classify the genes. Kyoto Encyclopaedia of Genes and Genomes (KEGG; https://www.genome.jp/kegg) was used to perform pathway enrichment analysis. Terms with corrected $P < 0.05$ were identified as significantly enriched by DEGs. To confirm the reliability of transcriptome sequencing, 10 candidates expressed genes in RNA-seq were simultaneously evaluated by qRT–PC analysis. The qRT–PCR values were linearly correlated with the RNA-seq FPKM values ($P < 0.001$).

Statistical Analyses

All statistical analyses were performed using SPSS 19. One-way ANOVA was used to determine the significant difference of average values according to Tukey's test ($P < 0.05$). Regression analysis was performed by Microsoft Excel.

RESULTS

Effect of VPD on Water Transport Forces Along the Soil-Plant-Atmospheric Continuum

Vapour pressure deficit significantly affected the distribution of water potential along the soil-plant-atmospheric pathway (**Figure 1**). Atmospheric evaporative demand increased with VPD elevation, which triggered plant water stress and a linear decline in the leaf water potential (**Figure 1A**). With VPD elevation, the drawdown of Ψ_{leaf} in high-VPD-grown plants was less than that in low-VPD-treated plants according to the slope of linear regression (**Figure 1A**). The driving force for passive water flow between the soil and leaf ($\Delta\Psi_{soil-leaf}$) increased with the VPD, and the magnitude of the increase was greater in low-VPD-grown plants than high-VPD-grown plants (**Figure 1B**). Since Ψ_{leaf} was negligible compared with the large negative air potential, the water driving force at the leaf-air boundary ($\Delta\Psi_{leaf-air}$) increased dramatically with an increase in the VPD (**Figure 1C**). The magnitude of the increase in $\Delta\Psi_{leaf-air}$ was considerably greater than that of $\Delta\Psi_{soil-leaf}$, and the difference between $\Delta\Psi_{leaf-air}$ and $\Delta\Psi_{soil-leaf}$ was enlarged with the VPD: the ratio of $\Delta\Psi_{leaf-air}$ to $\Delta\Psi_{soil-leaf}$ increased logarithmically from ∼50 at 0.5 kPa to 150 at 1.5 kPa and then maintained at a steady level (**Figure 1D**). The statistical analyses of the plant water status are shown in **Supplementary Table 1**.

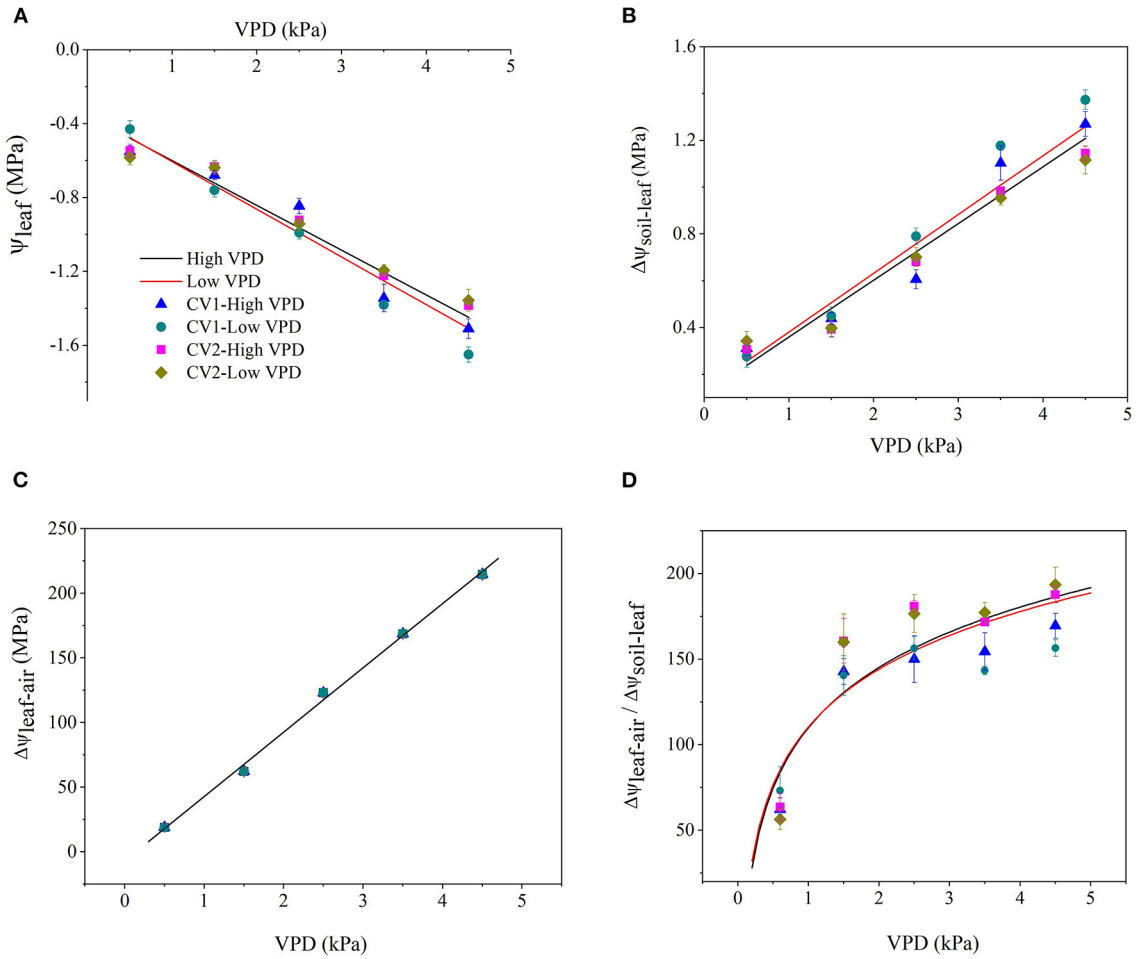

FIGURE 1 | Effect of the vapour pressure deficit (VPD) on the spatial distribution of the water potential and driving force ($\Delta\Psi$) between two spatial positions. Values are the mean ± SE (n = 4~6 replicates). The regression lines shown are: **(A)** HVPD, $\Psi_{leaf} = -0.242$ VPD -0.358, $R^2 = 0.92$; LVPD, $\Psi_{leaf} = -0.258$ VPD -0.347, $R^2 = 0.93$. **(B)** HVPD, $\Delta\Psi_{soil-leaf} = 0.242$ VPD + 0.118, $R^2 = 0.94$; LVPD, $\Delta\Psi_{soil-leaf} = 0.251$ VPD + 0.13, $R^2 = 0.93$. **(C)** HVPD, $\Delta\Psi_{leaf-air} = 49.8$ VPD -6.86, $R^2 = 0.98$; LVPD, $\Delta\Psi_{leaf-air} = 49.8$ VPD-6.86, $R^2 = 0.98$. **(D)** HVPD, $\Delta\Psi_{leaf-air}/\Delta\Psi_{soil-leaf} = 50.82$ ln (VPD) + 109.95, $R^2 = 0.85$; LVPD, $\Delta\Psi_{leaf-air}/\Delta\Psi_{soil-leaf} = 48.63$ ln (VPD) + 110.41, $R^2 = 0.8$.

Effect of VPD on the Photosynthetic Parameters of Tomato Plants

The photosynthetic rate responded to CO_2 elevation in similar patterns regardless of cultivar and VPD growth conditions: the photosynthetic rate rose rapidly across low CO_2 concentrations and then reached a steady state (**Supplementary Figure 1**). The maximum steady-state photosynthetic rate declined as the VPD increased from 0.5 to 4.5 kPa (**Supplementary Figure 1**). The maximum carboxylation rate (V_{cmax}), maximum electron transport rate (J_{max}), and CE declined linearly with VPD elevation (**Supplementary Figure 2**). The drawdown of V_{cmax}, J_{max}, and CE with VPD elevation was moderated in high-VDP-grown plants compared with low-VPD-grown plants according to the slope of linear regression (**Supplementary Figure 2**). The statistical analyses of photosynthetic parameters across VPD ranges are shown in **Supplementary Table 2.**

Effect of VPD on the Photosynthetic CO_2 Uptake and Transport

The stomatal, mesophyll, and total conductance for CO_2 diffusion decreased linearly with VPD elevation, regardless of the cultivar and VPD growth conditions (**Figure 2**). The magnitudes of drawdown in the stomatal, mesophyll, and total conductance were lower in high-VPD-grown plants than in low-VPD-grown plants for two cultivars (**Figure 2**).

The CO_2 concentration along the "source-path-sink" was reduced to different extents with VPD elevation (**Figures 3A,B**). The drawdowns of C_i and C_c caused by VPD elevation were relatively lower in high-VPD-grown plants than in low-VPD-grown plants (**Figures 3A,B**). Consequently, the CO_2 transport efficiency of C_i/C_a, C_c/C_a and C_c/C_i decreased linearly with VPD elevation. The declining slopes of C_i/C_a, C_c/C_a, and C_c/C_i vs. VPD were lower in

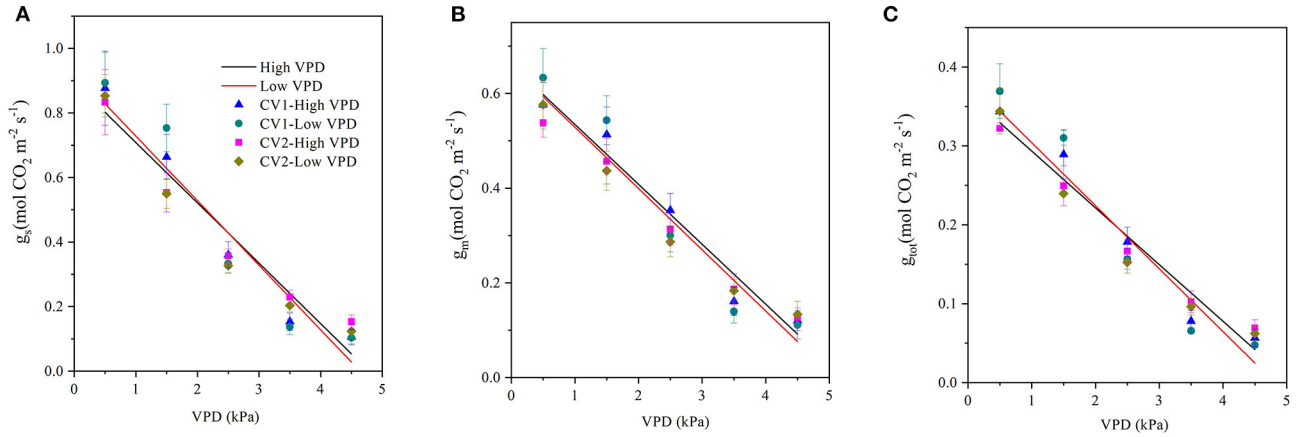

FIGURE 2 | Effect of the VPD on the stomatal conductance (g_s), mesophyll conductance (g_m), and total conductance (g_{tot}) for photosynthetic carbon dioxide (CO_2) diffusion. Values are the mean ± SE ($n = 4$ replicates). The regression lines shown are: **(A)** HVPD, $g_s = -0.187$ VPD + 0.895, $R^2 = 0.94$; LVPD, $g_s = -0.200$ VPD + 0.928, $R^2 = 0.92$. **(B)** HVPD, $g_m = -0.126$ VPD + 0.661, $R^2 = 0.95$; LVPD, $g_m = -0.129$ VPD + v0.658, $R^2 = 0.94$. **(C)** HVPD, $g_{tot} = -0.0719$ VPD +0.365, $R^2 = 0.95$; LVPD, $g_{tot} = -0.0798$ VPD + 0.384, $R^2 = 0.94$.

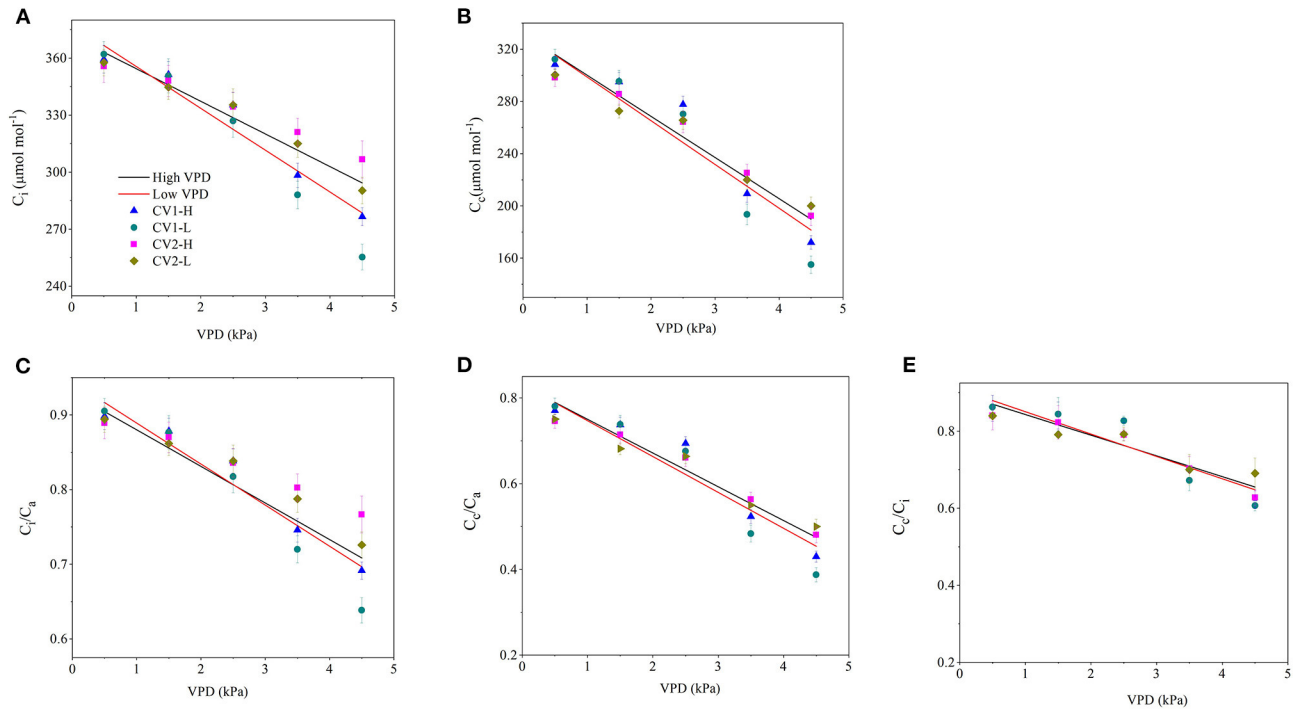

FIGURE 3 | Effect of the VPD on the intracellular CO_2 concentration [**(A)**; C_i], carboxylation sites inside chloroplasts CO_2 concentration [**(B)**; C_C], the ratio of the intercellular to ambient CO_2 concentration [**(C)**; C_i/C_a], the ratio of the chloroplast to ambient CO_2 concentration [**(D)**; C_c/C_a] and the ratio of the chloroplast to intercellular CO_2 concentration [**(E)**; C_c/C_i]. The regression lines shown are: **(A)** HVPD, $C_i = -17.2$ VPD + 371.6, $R^2 = 0.86$; LVPD, $C_i = -22$ VPD + 377.6, $R^2 = 0.87$. (B) HVPD, $C_C = -31.5$ VPD + 331.6, $R^2 = 0.91$; LVPD, $C_C = -33.5$ VPD + 332.2, $R^2 = 0.88$. **(C)** HVPD, $C_i/C_a = -0.0429$ VPD + 0.93, R^2 =0.86; LVPD, $C_i/C_a = -0.055$ VPD + 0.94, $R^2 = 0.87$. **(D)** HVPD, $C_c/C_a = -0.0788$VPD + 0.83, $R^2 = 0.92$; LVPD, $C_c/C_a = -0.0837$VPD + 0.83, $R^2 = 0.87$. **(E)** HVPD, $C_c/C_i = -0.0537$ VPD + 0.89, $R^2 = 0.82$; LVPD, $C_c/C_i = -0.058$VPD + 0.91, $R^2 = 0.89$.

high-VPD-grown plants than in low-VPD-grown plants (**Figures 3C–E**). The statistical analyses of CO_2 concentrations along the "source-path-sink" across VPD ranges are shown in **Supplementary Table 3**.

Partial Photosynthetic Limitation

The fractions of stomatal, mesophyll, and biochemical limitations imposed on photosynthesis varied with VPD elevation (**Figure 4**). Under low VPD conditions, the stomatal and

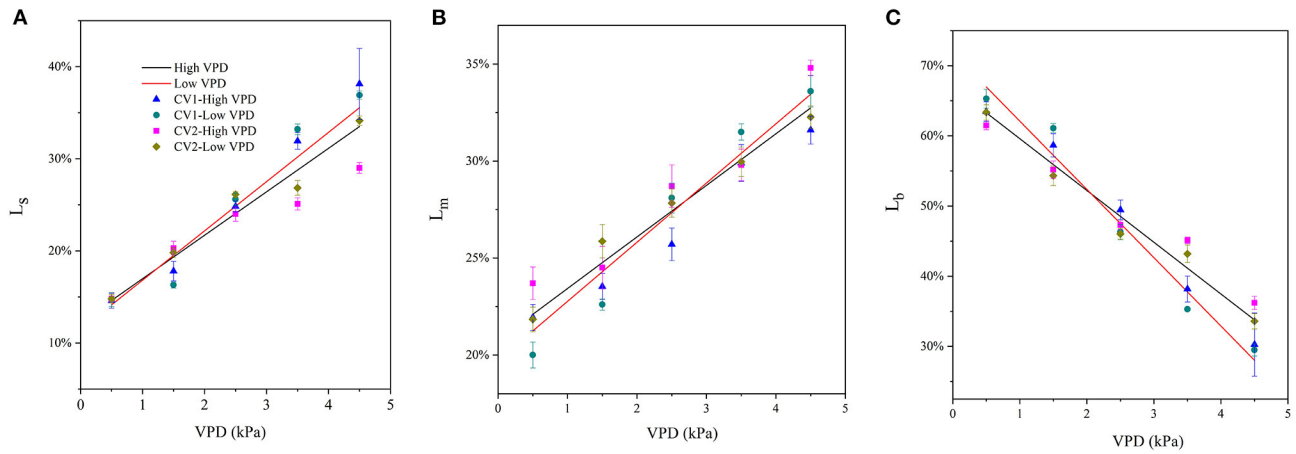

FIGURE 4 | Quantitative limitation analysis comparing stomatal [**(A)**; L_s], mesophyll [**(B)**; L_m], and biochemical [**(C)**; L_b] limitations imposed on the photosynthetic rate under varying VPD. The regression lines shown are: **(A)** HVPD, Ls = 0.0472 VPD + 0.122, R^2 = 0.86; LVPD, Ls = 0.0535 VPD + 0.115, R^2 = 0.89. **(B)** HVPD, L_m = 0.0266 VPD + 0.208, R^2 = 0.88; LVPD, L_m = 0.0305 VPD + 0.197, R^2 = 0.91.

mesophyll conductance for CO_2 diffusion were high and imposed relatively minor limitations on photosynthesis. The stomatal and mesophyll conductance accounted for a low proportion of photosynthetic limitation, while biochemical carboxylation for carbon fixation was the most significant limitation for photosynthetic processes under low VPD conditions (**Figure 4**). The fraction of stomatal limitation increased linearly with the VPD, from ∼15% at 0.5 kPa to 35% at 4.5 kPa (**Figure 4A**). A similar pattern was observed in the mesophyll limitation: the fraction of mesophyll limitation also increased linearly with VPD elevation, from ∼23% at 0.5 kPa to 33% at 4.5 kPa (**Figure 4B**). The increments in the fractions of stomatal and mesophyll limitations tended to be less marked in high-VPD-grown plants. In contrast, the fraction of total limitations attributed to the biochemical limitation of carbon fixation gradually decreased linearly with VPD elevation, from ∼65% at.5 kPa to 35% at 4.5 kPa (**Figure 4C**). The statistical analyses of stomatal, mesophyll, and biochemical limitation fractions across VPD ranges are shown in **Supplementary Table 4**.

Biochemical limitation accounted for the greatest limitation on photosynthesis under low VPD conditions, regardless of the cultivar and growth conditions (**Figure 5**). The limitations that stomatal and mesophyll conductance imposed on photosynthesis gradually increased and predominated under high VPD stress (**Figure 5**). Diffusion limitations, i.e., the sum of the stomatal and mesophyll resistance, were the rate-limiting step for the photosynthetic process under high VPD conditions, which imposed the greatest limitation on photosynthesis in tomato plants (**Figure 5**).

Correlations Among g_m, g_s, Leaf Water Status, and LMA

The mesophyll conductance was significantly and positively correlated with the stomatal conductance (**Supplementary Figure 3A**). Meanwhile, the stomatal and mesophyll conductance for CO_2 diffusion were closely linked to the leaf water status, wherein significant and positive correlations were found in the leaf water potential vs. the stomatal and mesophyll conductance (**Supplementary Figures 3B,C**). Acclimation to VPD modified leaf structural traits, wherein LMA tended to be slightly greater in high-VPD-grown plants than in low-VPD-grown plants (**Supplementary Figure 4A**). A significant and negative correlation between g_m and LMA was observed (**Supplementary Figure 4B**).

Leaf ABA Concentration and Correlation With CO_2 Diffusion Conductance

With VPD elevation, the foliar ABA content increased exponentially (**Figure 6A**). The leaf ABA content was linearly and negatively correlated with the CO_2 diffusion conductance of g_s and g_m (**Figure 6B**). The slope of linear regression in g_s was more negative than that in g_m, indicating that g_s was more sensitive to ABA in response to VPD stress (**Figure 6B**).

Transcriptomic Analysis of Plant Response Across Series of VPD Ranges

Kyoto Encyclopaedia of Genes and Genomes analysis showed that physiological processes of "metabolic pathway" and "plant hormone signal transduction" were involved in the response to VPD and were potentially associated with ABA biosynthesis and signal transduction (**Figure 7**). "Metabolic pathway" was the dominant pathway in response to VPD elevation. "Plant hormone signal transduction" also exhibited a significant pathway in response to VPD stress in the range from 1.5 to 3.5 kPa (**Figure 7**).

The enriched genes in the comparison between different VPD treatments were annotated in three main GO categories: biological process, cellular component, and molecular function.

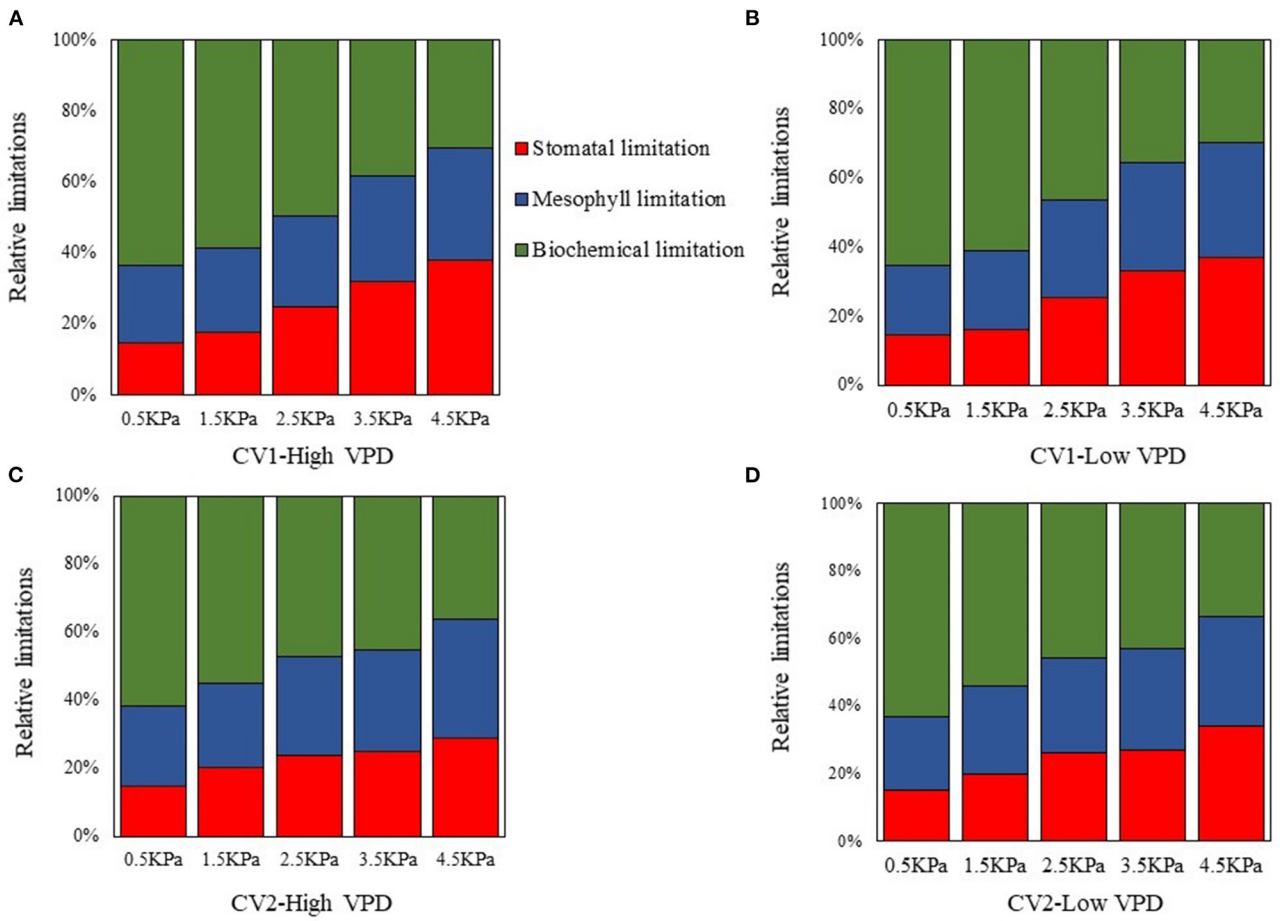

FIGURE 5 | The dynamic changes in the relative proportions of individual components of photosynthetic limitations across VPD ranges: **(A)** CV1 grown under high VPD condition; **(B)** CV1 grown under low VPD condition; **(C)** CV2 grown under high VPD condition; and **(D)** CV2 grown under low VPD condition.

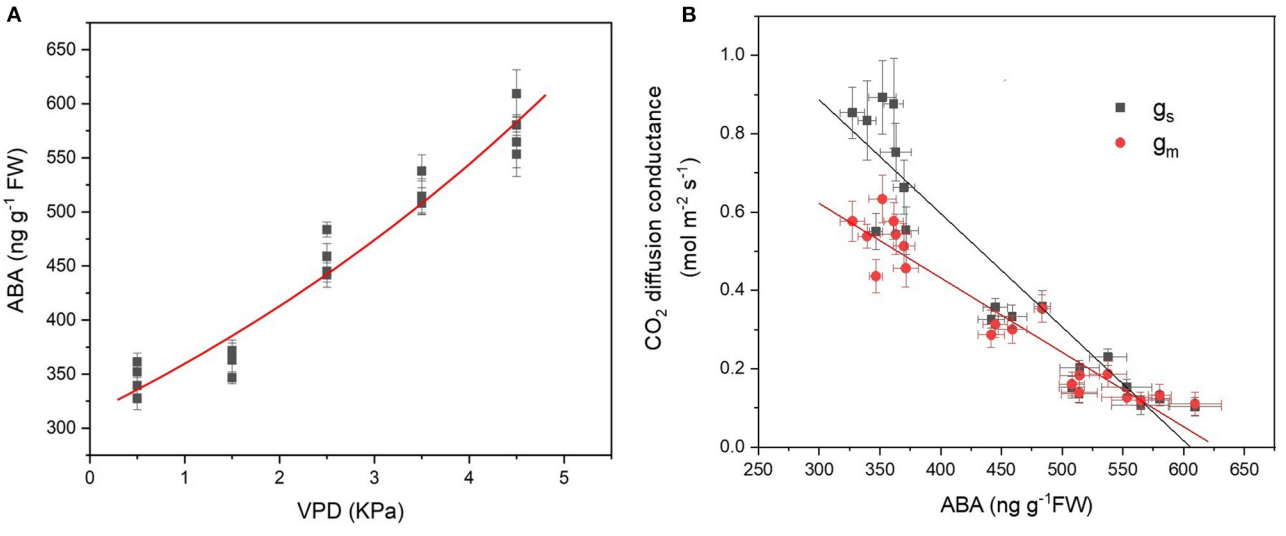

FIGURE 6 | Leaf ABA content in response to the VPD **(A)** and its correlation with the CO_2 diffusion conductance of g_s and g_m **(B)**. The regression lines shown are ABA = $301.3e^{0.15VPD}$, $R^2 = 0.96$, $P < 0.01$; $g_s = -0.0029$ ABA + 1.76, $R^2 = 0.85$, $P < 0.01$; $g_m = -0.0019$ ABA + 1.19, $R^2 = 0.88$, $P < 0.01$.

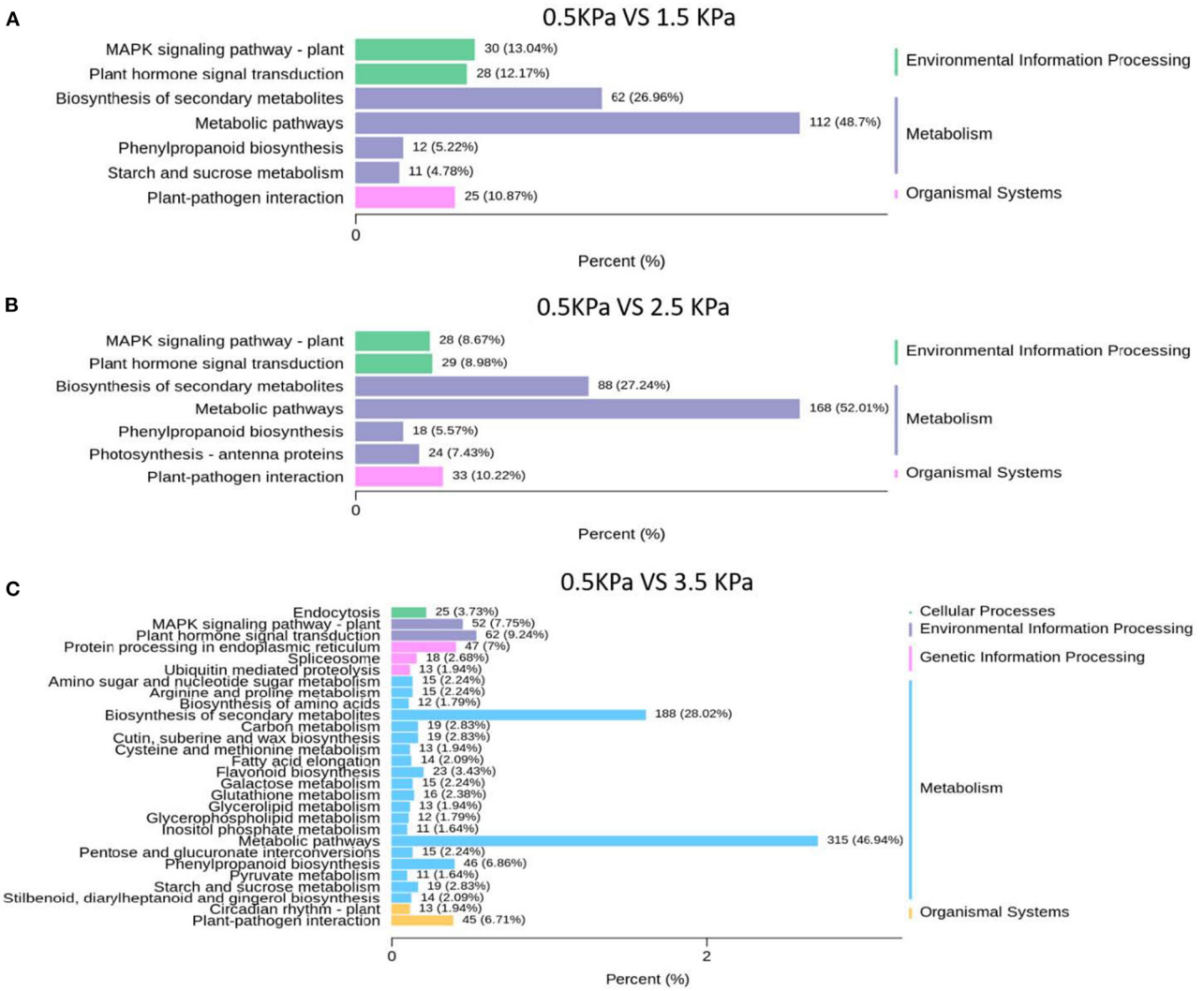

FIGURE 7 | KEGG classification analysis of differentially expressed genes under different VPD conditions: **(A)** 0.5 kPa versus 1.5 kPa; **(B)** 0.5 kPa versus 2.5 kPa; and **(C)** 0.5 kPa versus 3.5 kPa.

A great difference in the top 50 GO enrichment terms was observed between different VPD conditions (**Figure 8**). In the comparison of 0 with 1.5 kPa and 0.5 kPa with 3.5 kPa, the "ABA-activated signalling pathway" was significantly enriched and was involved in the VPD response (**Figures 9A,C**). In the comparison of 0.5 kPa with. 2.5 kPa, ABA was potentially involved according to the enriched terms of "cellular hormone metabolic process," "hormone biosynthetic process," and "hormone metabolic process". Gene expression with rising VPD can be classified into 10 patterns according to K-means analysis (**Figure 9**). Gene expression patterns were mostly classified into the pattern of "Subclass 6" with 768 genes, wherein gene expression remained relatively stable under mild VPD stress and increased dramatically under high VPD water stress (**Figure 9**). The genes associated with ABA biosynthesis and signal transduction followed different patterns.

DISCUSSION

The present study assessed the rate-limiting step for tomato plant photosynthesis across a series of VPD ranges and evaluated ABA-mediated regulatory mechanisms according to physiological and transcriptomic analyses. The key rate-limiting step for photosynthetic performance varied with the VPD: under low VPD conditions, stomatal, and mesophyll conductance was high for efficient CO_2 transport, which facilitated sufficiently high CO_2 availability inside chloroplasts for carbon fixation (**Figures 2**, **3**). With VPD elevation, the stomatal and mesophyll conductance for CO_2 transport declined gradually. Consequently, photosynthesis was substantially constrained by the low chloroplast CO_2 concentration under high VPD conditions (**Figure 3**). Therefore, the CO_2 diffusion limitation in a series of stomatal and mesophyll resistances was

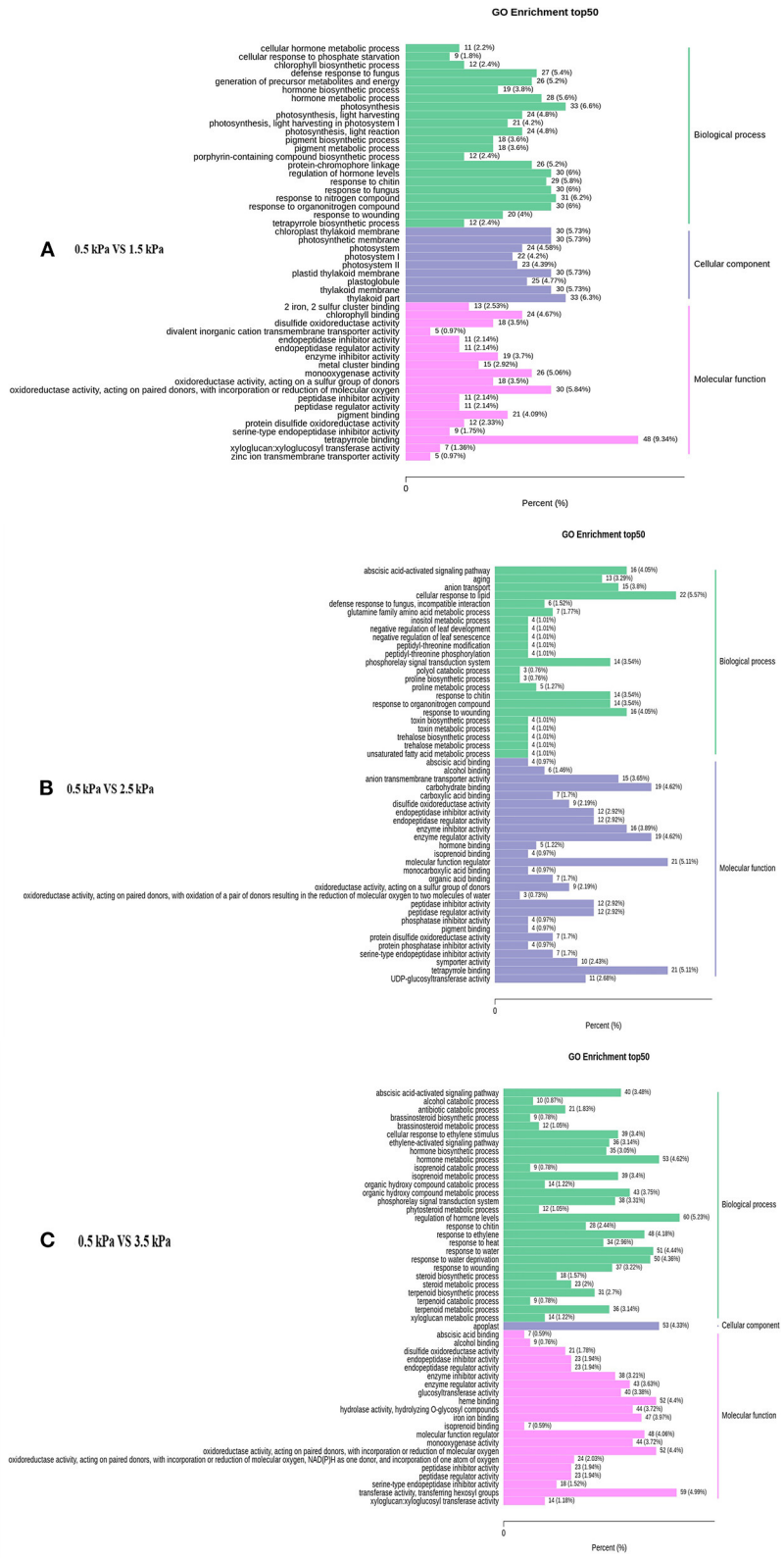

FIGURE 8 | Top 50 enriched GO terms of the differentially expressed genes under different VPD conditions: **(A)** 0.5 kPa versus 1.5 kPa; **(B)** 0.5 kPa versus 2.5 kPa; and **(C)** 0.5 kPa versus 3.5 kPa.

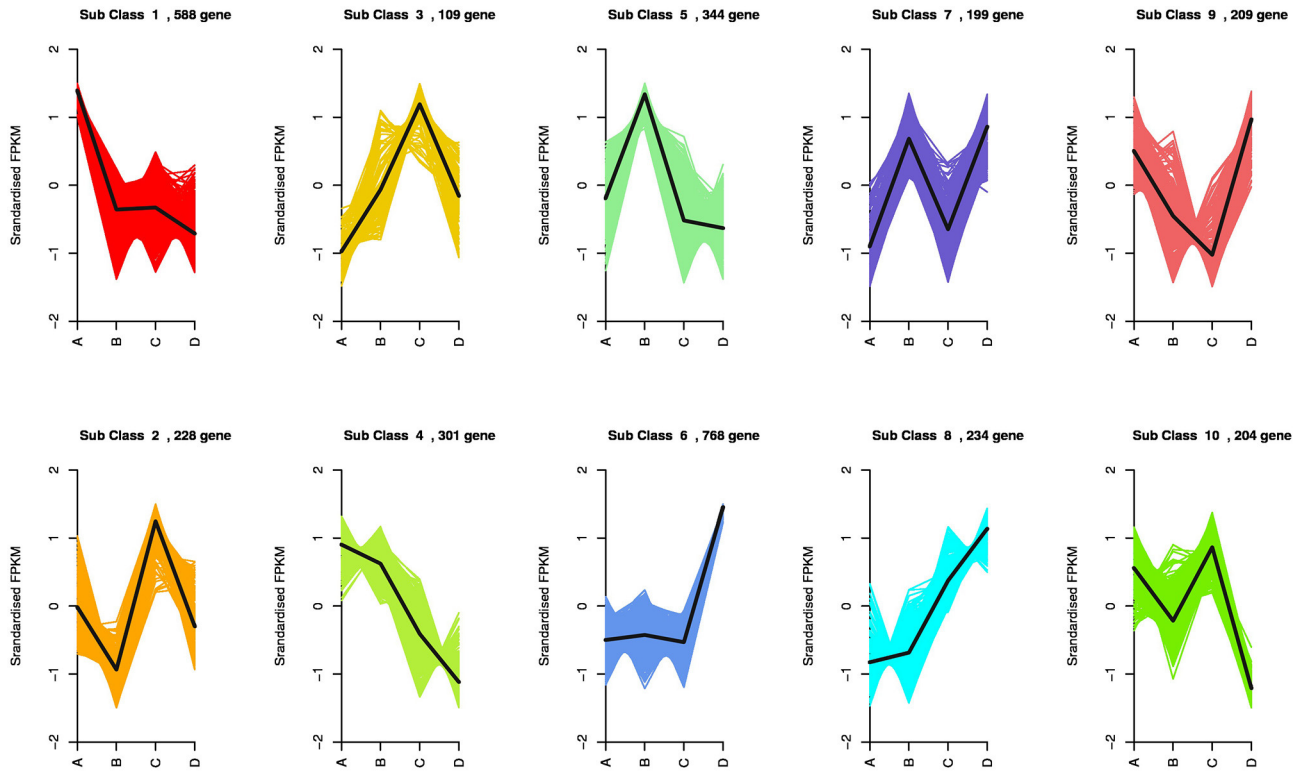

FIGURE 9 | Expression model of DEGs across a series of VPD ranges. A, B, C, and D in the X-axis in the figures represent 0.5, 1.5, 2.5, and 3.5 kPa, respectively.

the key rate-limiting step for photosynthesis under high VPD conditions (**Figure 4**). In addition to anatomical determination, ABA accumulation and signal transduction were involved in maintaining the water balance in response to VPD. ABA accumulation was negatively correlated with CO_2 diffusion conductance (**Figure 6**). Three steps were involved in the potential mechanism accounting for the increased limitation of stomatal and mesophyll conductance imposed on tomato plant photosynthesis with VPD elevation (**Supplementary Figure 5**): (I) VPD elevation caused plant water stress by disrupting the mass balance between the soil water supply and atmospheric evaporative demand; (II) plants maintained the water balance by regulating ABA accumulation and signal transduction in response to high VPD stress; (III) ABA in combination with leaf anatomical adaptation modulated CO_2 uptake and transport.

VPD Elevation Triggers Plant Water Stress by Disrupting the Mass Balance Between Soil Water Supply and Atmospheric Evaporative Demand

Passive water movement was driven by the gradient of free energy along the soil-plant-atmospheric continuum, which could be quantified as the gradient in water potential in the liquid phase. Water movement at the leaf-air boundary in the gas phase was driven by the difference in the VPD. Based on physical principles, excessive air desiccation triggered a high VPD and great negative air-water potential. $\Delta\psi_{leaf-air}$ was substantially > $\Delta\psi_{soil-leaf}$, which drove transpiration. The substantial difference between $\Delta\psi_{leaf-air}$ and $\Delta\psi_{soil-leaf}$ was logarithmically enlarged with an increase in the VPD (**Figure 1**). Quantitatively, the atmospheric driving force at the leaf-air boundary could be >100-fold larger than the soil-leaf component under high VPD conditions (**Figure 1**). The great asymmetry between the atmospheric evaporative demand and soil water supply triggered disruption in the water balance despite plants being well irrigated. Root water uptake and supply were inadequate to keep pace with the great atmospheric driving force under high VPD conditions, which consequently triggered leaf dehydration and decline in water potential. Therefore, the VPD is a crucial external stimulus moving water through a soil-plant-environment continuum. VPD fluctuates dramatically over the diurnal course in crop production, especially for greenhouse cultivation. Soil moisture is relatively stable over the short term compared with the VPD (Caldeira et al., 2014). Plant-water relations are regulated to a greater extent by the VPD and to a lesser extent by soil moisture. Similar to soil drought, VPD-induced plant water stress is also an important factor triggering photosynthetic depression.

Plants Maintain the Water Balance by Regulating ABA Accumulation and Signal Transduction in Response to High VPD Stress

The stoma is the "gatekeeper" for the exchange of water vapour and CO_2. Guard cells surrounding the stomatal pore

respond to perturbations of the soil-plant-atmospheric hydraulic continuum, which is putatively transduced into stomatal movements by feedback and feedforward mechanisms (Buckley, 2005, 2017, 2019). Stomatal control of transpired water loss is critical for sustaining physiological processes, such as leaf water status and photosynthetic CO_2 uptake. It has been recognised that plants respond to drought by closing guard cells to prevent the development of water dehydration in plant tissues (Novick et al., 2016). In the present study, the atmospheric driving force was an order of magnitude greater than the water supply, which led to a great dissymmetry between the water supply and evaporative demand. The dissymmetry between the water supply and evaporative demand triggered declines in the leaf water potential and stomatal closure. However, the mechanism of VPD-triggered stomatal closure is still uncertain and is a "black box" (Buckley, 2016). Some hypotheses hold that stomatal closure in angiosperms under high VPD conditions is an active process that is regulated by hormonal and hydraulic signals (Merilo et al., 2018; Pantin and Blatt, 2018). The plant stress hormone ABA is continuously produced and delivered with a transpiration stream to guard cells (Qiu et al., 2017; Merilo et al., 2018). In the present study, leaf ABA rapidly accumulated with the rise in the VPD. Transcriptome analysis suggested that ABA biosynthesis and signal transduction were potentially involved in the response to the VPD. Based on the theory of ion channel-mediated guard cell signal transduction (Julian et al., 2001), hypothetical mechanisms of the ABA-mediated stomatal closure response to high VPD-induced water stress are proposed in **Supplementary Figure 6**. Ions and water flowed into guard cells under low VPD conditions and sustained turgor for stomatal openness. Under high VPD-induced water stress, ABA rapidly accumulated and promoted stomatal closure by altering ion channel activities.

Although stomatal closure prevented excess water loss to maintain physiological processes by passive or active mechanisms, closed "gatekeepers" simultaneously increased stomatal resistance for photosynthetic CO_2 uptake from air to intercellular. The intercellular CO_2 concentration was gradually reduced with VPD elevation (**Figure 3**). Consequently, the stomatal limitation imposed on photosynthesis gradually became pronounced with VPD elevation (**Figure 4**). The declines in the leaf water potential and stomatal conductance with VPD elevation were less marked in high-VPD-grown plants in the present research. The distinct response to the VPD is potentially modulated by physiological acclimation to growth conditions (Fanourakis et al., 2019). In contrary to the previous study, no significant differences were observed in the photosynthetic parameters across VPD ranges between the two examined cultivars. The distinct responses of two cultivars between the previous and present study were potentially caused by the examined VPD conditions. The dynamic VPD response of the present and previous studies were performed under cabinets and greenhouse conditions, respectively.

Anatomical Properties and ABA Modulate Mesophyll Conductance Under Contrasting VPD Conditions

In addition to the first barrier of stomata, CO_2 movement from intercellular to carboxylation sites is constrained by mesophyll resistance. The present study demonstrated that mesophyll resistance was a significant component of diffusion resistance from air to Rubisco in tomato plants. A strong positive correlation between the mesophyll and stomatal conductance was observed among treatments (**Figure 6**). Similar to the stomatal conductance, the mesophyll conductance of tomato plants was also linearly reduced with VPD elevation (**Figure 2**). Under low VPD conditions, stomatal conductance coupled with mesophyll conductance was high for efficient CO_2 transport to carboxylation sites within chloroplasts. High diffusion conductance facilitated high chloroplast CO_2 concentrations for carbon fixation (**Figure 3**). With VPD elevation, the CO_2 concentration inside chloroplasts was substantially reduced under high VPD conditions. The limitation of mesophyll conductance imposed on photosynthesis gradually dominated with VPD elevation (**Figure 5**). Leaf anatomical traits from the substomatal cavity to the carbon fixation site determine the maximum potential of mesophyll conductance (Muir et al., 2014; Xiong et al., 2017; Earles et al., 2018; Han et al., 2018; Carriqui et al., 2019). The LMA is a composite of underlying traits such as the lamina thickness, mesophyll thickness, cell wall thickness, cell shape, and bulk leaf density, which anatomically regulate the mesophyll conductance (Muir et al., 2014). The LMA determines the upper limit on mesophyll conductance. Meanwhile, the LMA is closely linked to abiotic stress tolerance (Xiong and Flexas, 2018; Xiong et al., 2018). Generally, a higher LMA is a good indicator of greater stress tolerance. In the present study, the LMA of high-VPD-grown plants was lower but higher than that of low-VPD-grown plants (**Supplementary Figure 4**). Long-term acclimation to a high VPD facilitates enhanced drought tolerance to prevent dehydration by regulating the leaf thickness, cuticular permeability, stomatal morphology, and other anatomical features (Fanourakis et al., 2016, 2020). Long-term exposure to a VPD also affects stomatal sensitivity and morphological features such as the stomatal size, density, index, and spacing, which consequently modulate transpired water loss (Fanourakis et al., 2016, 2020). As mentioned above, root water uptake and supply are inadequate to keep pacing with the great atmospheric driving force under high VPD conditions. A higher LMA indicated dense structural traits, which buffered cellular transpired water loss and prevented leaf tissue dehydration under high VPD conditions. However, CO_2 and water transport share pathways through the mesophyll cell walls and perhaps plasma membranes within leaves (Barbour, 2017; Groszmann et al., 2017; Zhao et al., 2017; Drake et al., 2019). Although dense structural traits improved drought tolerance, the resistance of CO_2 diffusion was simultaneously increased. The LMA was negatively correlated with mesophyll conductance in the present study, which is consistent with previous studies (Hassiotou et al., 2009).

In addition to anatomical determinations, biochemical regulations such as ABA, carbonic anhydrase, and aquaporin facilitate rapid mesophyll conductance responses to short-term changing environmental factors (Momayyezi et al., 2020). The mesophyll conductance is negatively correlated with the leaf ABA content in tomato plants, which is in accordance with a previous study (Sorrentino et al., 2016; Qiu et al., 2017). The foliar ABA content rapidly increased upon long-term and short-term exposure to a high VPD, which is in accordance with a previous study (McAdam and Brodribb, 2016). However, the ABA-mediated regulatory mechanism has rarely been reported. CO_2 entering from intercellular to carboxylation sites inside chloroplasts must pass through plasma membranes. The resistance of transport across the membrane accounts for a great proportion of the mesophyll resistance. It is now well established that aquaporins function as water pores for water transport across membranes and play significant roles in maintaining water homeostasis in response to drought and salinity (Qian et al., 2015; Zhang et al., 2019a). There is increasing evidence that some specific aquaporins (which localise to the plasma membrane and chloroplast inner envelope membrane) are permeable to CO_2 and contribute to the mesophyll conductance (Uehlein et al., 2012; Groszmann et al., 2017; Zhao et al., 2017). Similar to guard cells, some *PIPs* pores mediate CO_2 uptake and water transport across the plasma membrane (Zhang et al., 2021). Therefore, the specific *PIPs* potentially reconciled the trade-off between carbon gain and water loss in response to VPD-induced water stress. *PIPs* were sensitive to drought signals and responded rapidly to enclose gating and inhibit activity.

Gating is a general mechanism of membrane-mediated channels for controlling the permeability of water and CO_2. Although the inhibition of *PIPs* channels prevents water loss under high VPD stress, CO_2 uptake across the membrane is also restricted by the gating enclosure. ABA has been reported as a signal-inducing variation in the aquaporin content and activity (Fang et al., 2019). Therefore, VPD potentially modulated *PIPs* gating for CO_2 and water permeability *via* ABA signalling, which contributed to mesophyll conductance and the photosynthetic rate.

CONCLUSIONS

The present study revealed the rate-limiting step for photosynthetic CO_2 utilisation under contrasting VPD conditions and proposed ABA-mediated regulatory mechanisms according to transcriptomic and physiological evidence. The photosynthetic performance of tomato plants was gradually constrained with VPD elevation. The key rate-limiting steps for photosynthetic performance varied with the rise in the VPD. With VPD elevation, plant water stress was gradually pronounced and triggered linear declines in the stomatal and mesophyll conductance. The contributions of stomatal and mesophyll limitations to photosynthesis increased gradually with VPD elevation. Consequently, the low CO_2 availability inside chloroplasts substantially constrained photosynthesis under high VPD conditions. Leaf ABA accumulated rapidly with pronounced water stress under a high VPD and negatively correlated with the stomatal and mesophyll conductance for CO_2 diffusion. Transcriptomic combined with physiological analyses revealed that ABA biosynthesis and signal transduction were potentially involved in mediating CO_2 transport in response to the VPD.

DATA AVAILABILITY STATEMENT

The original contributions presented in the study are publicly available. This data can be found here: National Center for Biotechnology Information (NCBI) BioProject database under accession number PRJNA762604.

AUTHOR CONTRIBUTIONS

DZ, QL, and MW conceived and designed the experiments. PS, JL, and XL conducted the experiments. QD analysed the data and wrote the draft. All the authors reviewed and approved the manuscript.

FUNDING

This project was supported by the National Natural Science Foundation of China (32102466), the Natural Science Foundation of Shandong Province (ZR2019BC035), and the Major Scientific Innovation Project of Shandong Province (2019JZZY010715).

SUPPLEMENTARY MATERIAL

The Supplementary Material for this article can be found online at: https://www.frontiersin.org/articles/10.3389/fpls.2021.745110/full#supplementary-material

REFERENCES

Barbour, M. M. (2017). Understanding regulation of leaf internal carbon and water transport using online stable isotope techniques. *New phytol.* 213, 83–88. doi: 10.1111/nph.14171

Buckley, T. N. (2005). The control of stomata by water balance. *New phytol.* 168, 275–292. doi: 10.1111/j.1469-8137.2005.01543.x

Buckley, T. N. (2016). Stomatal responses to humidity: has the 'black box' finally been opened? *Plant Cell Environ.* 39, 482–484. doi: 10.1111/pce.12651

Buckley, T. N. (2017). Modeling stomatal conductance. *Plant physiol.* 174, 572–582. doi: 10.1104/pp.16.01772

Buckley, T. N. (2019). How do stomata respond to water status? *New phytol.* 224, 21–36 doi: 10.1111/nph.15899

Caldeira, C. F., Bosio, M., Parent, B., Jeanguenin, L., Chaumont, F., and Tardieu, F. (2014). A hydraulic model is compatible with rapid changes in leaf elongation under fluctuating evaporative demand and soil water status. *Plant Physiol.* 164, 1718–1730. doi: 10.1104/pp.113.228379

Carriqui, M., Roig-Oliver, M., Brodribb, T. J., Coopman, R., Gill, W., Mark, K., et al. (2019). Anatomical constraints to nonstomatal diffusion

conductance and photosynthesis in lycophytes and bryophytes. *New phytol*. 222, 1256–1270 doi: 10.1111/nph.15675

Drake, P. L., Boer, H. J. D., Schymanski, S. J., and Veneklaas, E. J. (2019). Two sides to every leaf: water and CO_2 transport in hypostomatous and amphistomatous leaves. *New Phytolol*. 222, 1179–1187. doi: 10.1111/nph.15652

Du, Q., Song, X., Bai, P., Jiao, X., Ding, J., Zhang, J., et al. (2020). Effect of different vapor pressure deficits on gas exchange parameters and growth of tomatoes and comprehensive evaluation. *Acta Agriculturae Boreli-occidentalis Sinica*. 29, 66–74.

Du, Q., Liu, T., Jiao, X., Song, X., Zhang, J., and Li, J. (2019). Leaf anatomical adaptations have central roles in photosynthetic acclimation to humidity. *J. Exp. Bot*. 70, 4949–4962. doi: 10.1093/jxb/erz238

Earles, J. M., Theroux-Rancourt, G., Roddy, A. B., Gilbert, M. E., McElrone, A. J., and Brodersen, C. R. (2018). Beyond porosity: 3D leaf intercellular airspace traits that impact mesophyll conductance. *Plant Physiol.* 178, 148–162. doi: 10.1104/pp.18.00550

Fang, L., Abdelhakim, L. O. A., Hegelund, J. N., Li, S., Liu, J., Peng, X., et al. (2019). ABA-mediated regulation of leaf and root hydraulic conductance in tomato grown at elevated CO_2 is associated with altered gene expression of aquaporins. *Hortic. Res.* 6,1–10. doi: 10.1038/s41438-019-0187-6

Fanourakis, D., Aliniaeifard, S., Sellin, A., Giday, H., Korner, O., Rezaei Nejad, A., et al. (2020). Stomatal behavior following mid- or long-term exposure to high relative air humidity: A review. *Plant Physiol. Biochem.* 153, 92–105.doi: 10.1016/j.plaphy.2020.05.024

Fanourakis, D., Bouranis, D., Giday, H., Carvalho, D. R., Rezaei Nejad, A., and Ottosen, C. O. (2016). Improving stomatal functioning at elevated growth air humidity: A review. *J. Plant Physiol.* 207, 51–60. doi: 10.1016/j.jplph.2016.10.003

Fanourakis, D., Giday, H., Hyldgaard, B., Bouranis, D., Körner, O., and Ottosen, C. O. (2019). Low air humidity during cultivation promotes stomatal closure ability in rose. *Eur. J. Hortic. Sci*. 84, 245–252. doi: 10.17660/eJHS.2019/84.4.7

Farquhar, G. D., von Caemmerer, S., and Berry, J. A. (1980). A biochemical model of photosynthetic CO_2 assimilation in leaves of C_3 species. *Planta*. 149, 78–90. https://doi.org/10.1007/BF00386231.

Flexas, J., Barbour, M. M., Brendel, O., Cabrera, H. M., Carriqui, M., Diaz-Espejo, A., et al. (2012). Mesophyll diffusion conductance to CO_2: an unappreciated central player in photosynthesis. *Plant Sci.* 193–194, 70–84. doi: 10.1016/j.plantsci.2012.05.009

Giuliani, R., Koteyeva, N., Voznesenskaya, E., Evans, M. A., Cousins, A. B., and Edwards, G. E. (2013). Coordination of leaf photosynthesis, transpiration, and structural traits in rice and wild relatives (Genus *Oryza*). *Plant Physiol*. 162, 1632–1651. doi: 10.1104/pp.113.217497

Groszmann, M., Osborn, H. L., and Evans, J. R. (2017). Carbon dioxide and water transport through plant aquaporins. *Plant Cell Environ.* 40, 938–961. doi: 10.1111/pce.12844

Han, J., Lei, Z., Flexas, J., Zhang, Y., Carriqui, M., Zhang, W., et al. (2018). Mesophyll conductance in cotton bracts: anatomically-determined internal CO_2 diffusion constraints on photosynthesis. *J. Exp. Bot.* 69, 5433–5443. doi: 10.1093/jxb/ery296

Harley, P. C., Loreto, F., Di Marco, G., and Sharkey, T. D. (1992). Theoretical considerations when estimating the mesophyll conductance to CO_2 flux by analysis of the response of photosynthesis to CO_2. *Plant Physiol.* 98, 1429–1436. doi: 10.1104/pp.98.4.1429

Hassiotou, F., Ludwig, M., Renton, M., Veneklaas, E. J., and Evans, J. R. (2009). Influence of leaf dry mass per area, CO_2, and irradiance on mesophyll conductance in sclerophylls. *J. Exp. Bot*. 60, 2303–2314. doi: 10.1093/jxb/erp021

Julian, I., Schroeder, Gethyn, J., Allen, Veronique, H.ugouvieux, June, M., Kwak, a., and Waner, D. (2001). Guard cell signal transduction. *Annu. Rev. Plant Physiol. Plant Mol.Biol.* 52, 627–658. doi: 10.1146/annurev.arplant.52.1.627

Kaldenhoff, R. (2012). Mechanisms underlying CO_2 diffusion in leaves. *Curr Opin Plant Biol.*15, 276–281. doi: 10.1016/j.pbi.2012.01.011

Laisk, A., and Oja, V. (1998). *Dynamics of leaf photosynthesis*. Australia: CSIRO Publishing.

Lawson, T., and Blatt, M. R. (2014). Stomatal size, speed, and responsiveness impact on photosynthesis and water use efficiency. *Plant Physiol.* 164, 1556–1570. doi: 10.1104/pp.114.237107

Li, Q., Liu, Y., Tian, S., Liang, Z., Li, S., Li, Y., et al. (2019a). Effect of supplemental lighting on water transport, photosynthetic carbon gain and water use efficiency in greenhouse tomato. *Sci. Hortic*. 256, 108630. doi: 10.1016/j.scienta.2019.108630

Li, Q., Wei, M., Li, Y., Feng, G., Wang, Y., Li, S., et al. (2019b). Effects of soil moisture on water transport, photosynthetic carbon gain and water use efficiency in tomato are influenced by evaporative demand. *Agric. Water Manage.* 226, 105818. doi: 10.1016/j.agwat.2019.105818

Lu, N., Nukaya, T., Kamimura, T., Zhang, D., Kurimoto, I., Takagaki, M., et al. (2015). Control of vapor pressure deficit (VPD) in greenhouse enhanced tomato growth and productivity during the winter season. *Sci. Hortic.* 197, 17–23. doi: 10.1016/j.scienta.2015.11.001

McAdam, S. A., and Brodribb, T. J. (2016). Linking turgor with ABA biosynthesis: implications for stomatal responses to vapor pressure deficit across land plants. *Plant Physiol.* 171, 2008–2016.doi: 10.1104/pp.16.00380

Merilo, E., Yarmolinsky, D., Jalakas, P., Parik, H., Tulva, I., Rasulov, B., et al. (2018). Stomatal VPD response: there is more to the story than ABA. *Plant Physiol.* 176, 851–864. doi: 10.1104/pp.17.00912

Momayyezi, M., McKown, A. D., Bell, S. C. S., and Guy, R. D. (2020). Emerging roles for carbonic anhydrase in mesophyll conductance and photosynthesis. *Plant J.* 101, 831–844. doi: 10.1111/tpj.14638

Muir, C. D., Hangarter, R. P., Moyle, L. C., and Davis, P. A. (2014). Morphological and anatomical determinants of mesophyll conductance in wild relatives of tomato (*Solanum* sect. Lycopersicon, sect. Lycopersicoides; Solanaceae). *Plant Cell Environ*. 37, 1415–1426. doi: 10.1111/pce.12245

Niinemets, U., Diaz-Espejo, A., Flexas, J., Galmes, J., and Warren, C. R. (2009). Role of mesophyll diffusion conductance in constraining potential photosynthetic productivity in the field. *J. Exp. Bot.* 60, 2249–2270. doi: 10.1093/jxb/erp036

Norby, R. J. (2002). Plant water relations at elevated CO_2-implications for water-limited environments. *Plant Cell Environ*.25, 319–331. doi: 10.1046/j.1365-3040.2002.00796.x

Novick, K. A., Miniat, C. F., and Vose, J. M. (2016). Drought limitations to leaf-level gas exchange: results from a model linking stomatal optimization and cohesion-tension theory. *Plant Cell Environ.* 39, 583–596. doi: 10.1111/pce.12657

Pantin, F., and Blatt, M. R. (2018). Stomatal response to humidity: blurring the boundary between active and passive movement. *Plant Physiol.* 176, 485–488, doi: 10.1104/pp.17.01699

Qian, Z. J., Song, J. J., Chaumont, F., and Ye, Q. (2015). Differential responses of plasma membrane aquaporins in mediating water transport of cucumber seedlings under osmotic and salt stresses. *Plant Cell Environ*. 38, 461–473, doi: 10.1111/pce.12319

Qiu, C., Ethier, G., Pepin, S., Dube, P., Desjardins, Y., and Gosselin, A. (2017). Persistent negative temperature response of mesophyll conductance in red raspberry (*Rubus idaeus* L.) leaves under both high and low vapour pressure deficits: a role for abscisic acid? *Plant Cell Environ.* 40, 1940–1959, doi: 10.1111/pce.12997

Sack, L., John, G. P., and Buckley, T. N. (2018). ABA accumulation in dehydrating leaves is associated with decline in cell volume, not turgor pressure. *Plant Physiol* 176, 489–495. doi: 10.1104/pp.17.01097

Sharkey, T. D. (2012). Mesophyll conductance: constraint on carbon acquisition by C_3 plants. *Plant Cell Environ.*35, 1881–1883. doi: 10.1111/pce.12012

Sorrentino, G., Haworth, M., Wahbi, S., Mahmood, T., Zuomin, S., and Centritto, M. (2016). Abscisic acid induces rapid reductions in mesophyll conductance to carbon dioxide. *PloS ONE.* 11, e0148554. doi: 10.1371/journal.pone.0148554

Sun, J., Ye, M., Peng, S., and Li, Y. (2016). Nitrogen can improve the rapid response of photosynthesis to changing irradiance in rice (*Oryza sativa* L.) plants. *Sci Rep.* 6, 31305. doi: 10.1038/srep31305

Tholen, D., and Zhu, X. G. (2011). The mechanistic basis of internal conductance: a theoretical analysis of mesophyll cell photosynthesis and CO_2 diffusion. *Plant Physiol.*156, 90–105. doi: 10.1104/pp.111.172346

Tomas, M., Flexas, J., Copolovici, L., Galmes, J., Hallik, L., Medrano, H., et al. (2013). Importance of leaf anatomy in determining mesophyll diffusion conductance to CO_2 across species: quantitative limitations and scaling up by models. *J. Exp. Bot*. 64, 2269–2281. doi: 10.1093/jxb/ert086 (2013)

Tsuda, M., and Tyree, M. T. (2000). Hydraulic conductance measured by the high pressure flow meter in crop plants. *J. Exp. Bot.* 51, 823–828. doi: 10.1093/jexbot/51.345.823

Uehlein, N., Sperling, H., Heckwolf, M., and Kaldenhoff, R. (2012). The Arabidopsis aquaporin *PIP1;2* rules cellular CO_2 uptake. *Plant Cell Environ*. 35, 1077–1083. doi: 10.1111/j.1365-3040.2011.02473.x

von Caemmerer, S., and Evans, J. R. (2010). Enhancing C_3 photosynthesis. *Plant Physiol*.154, 589–592. doi: 10.1104/pp.110.160952

Xiong, D., Douthe, C., and Flexas, J. (2018). Differential coordination of stomatal conductance, mesophyll conductance, and leaf hydraulic conductance in response to changing light across species. *Plant Cell Environ*. 41, 436–450. doi: 10.1111/pce.13111

Xiong, D., and Flexas, J. (2018). Leaf economics spectrum in rice: leaf anatomical, biochemical, and physiological trait trade-offs. *J. Exp. Bot*. 69, 5599–5609. doi: 10.1093/jxb/ery322

Xiong, D., Flexas, J., Yu, T., Peng, S., and Huang, J. (2017). Leaf anatomy mediates coordination of leaf hydraulic conductance and mesophyll conductance to CO_2 in *Oryza*. *New Phytol*. 213, 572–583. doi: 10.1111/nph.14186

Xiong, D., Liu, X., Liu, L., Douthe, C., Li, Y., et al. (2015). Rapid responses of mesophyll conductance to changes of CO_2 concentration, temperature and irradiance are affected by N supplements in rice. *Plant Cell Environ*. 38, 2541–2550. doi: 10.1111/pce.12558

Zhang, D., Du, Q., Zhang, Z., Jiao, X., Song, X., and Li, J. (2017). Vapour pressure deficit control in relation to water transport and water productivity in greenhouse tomato production during summer. *Sci. Rep*. 7, 43461. doi: 10.1038/srep43461

Zhang, D., Jiao, X., Du, Q., Song, X., and Li, J. (2018). Reducing the excessive evaporative demand improved photosynthesis capacity at low costs of irrigation via regulating water driving force and moderating plant water stress of two tomato cultivars. *Agric. Water Manag*. 199, 22–33. doi: 10.1016/j.agwat.2017.11.014

Zhang, D., Li, Y., and Li, Y. (2021). The potential implications of a plasma membrane aquaporin in improving CO2 transport capacity, photosynthetic potential and water use efficiency under contrasting CO_2 source in *Solanum lycopersicum* (tomato). *Sci. Hortic*. 283: 110122. doi: 10.1016/j.scienta.2021.110122

Zhang, D., Zhang, Z., Li, J., Chang, Y., Du, Q., and Pan, T. (2015). Regulation of vapor pressure deficit by greenhouse micro-fog systems improved growth and productivity of tomato via enhancing photosynthesis during summer season. *PLoS ONE*. 10, e0133919. doi: 10.1371/journal.pone.0133919

Zhang, S., Feng, M., Chen, W., Zhou, X., Lu, J., Wang, Y., et al. (2019a). In rose, transcription factor PTM balances growth and drought survival via *PIP2;1* aquaporin. *Nat Plants*. 5, 290–299. doi: 10.1038/s41477-019-0376-1

Zhang, Z., Cao, B., Li, N., Chen, Z., and Xu, K. (2019b). Comparative transcriptome analysis of the regulation of ABA signaling genes in different rootstock grafted tomato seedlings under drought stress. *Environ Exp Bot*. 166, 103814. doi: 10.1016/j.envexpbot.2019.103814

Zhao, M., Tan, H. T., Scharwies, J., Levin, K., Evans, J. R., and Tyerman, S. D. (2017). Association between water and carbon dioxide transport in leaf plasma membranes: assessing the role of aquaporins. *Plant Cell Environ*. 40, 789–801, doi: 10.1111/pce.12830

Conflict of Interest: The authors declare that the research was conducted in the absence of any commercial or financial relationships that could be construed as a potential conflict of interest.

Publisher's Note: All claims expressed in this article are solely those of the authors and do not necessarily represent those of their affiliated organizations, or those of the publisher, the editors and the reviewers. Any product that may be evaluated in this article, or claim that may be made by its manufacturer, is not guaranteed or endorsed by the publisher.

frontiers in Plant Science

ORIGINAL RESEARCH
published: 26 November 2021
doi: 10.3389/fpls.2021.791711

Establishing a Reference Baseline for Midday Stem Water Potential in Olive and Its Use for Plant-Based Irrigation Management

Ken Shackel[1], Alfonso Moriana[2,3], Giulia Marino[1], Mireia Corell[2,3], David Pérez-López[4], Maria Jose Martin-Palomo[2,3], Tiziano Caruso[5], Francesco Paolo Marra[5], Luis Martín Agüero Alcaras[6], Luke Milliron[7], Richard Rosecrance[8], Allan Fulton[9] and Peter Searles[10]*

[1] Department of Plant Sciences, University of California, Davis, Davis, CA, United States, [2] Departamento de Agronomía, ETSIA, Universidad de Sevilla, Seville, Spain, [3] Unidad Asociada al CSIC de Uso Sostenible del Suelo y el Agua en la Agricultura (Universidad de Sevilla-IRNAS), Seville, Spain, [4] Departamento de Producción Agraria, CEIGRAM, Universidad Politécnica de Madrid, Madrid, Spain, [5] Department of Agricultural, Food and Forest Sciences (SAAF), University of Palermo, Palermo, Italy, [6] Agencia de Extensión Rural Aimogasta, Instituto Nacional de Tecnología Agropecuaria, Aimogasta, Argentina, [7] University of California Cooperative Extension, Oroville, CA, United States, [8] College of Agriculture, California State University, Chico, Chico, CA, United States, [9] University of California Cooperative Extension, Red Bluff, CA, United States, [10] Centro Regional de Investigaciones Científicas y Transferencia Tecnológica de La Rioja (CRILAR-Provincia de La Rioja-UNLaR-SEGEMAR-UNCa-CONICET), Anillaco, Argentina

OPEN ACCESS

Edited by:
Thorsten M. Knipfer, University of British Columbia, Canada

Reviewed by:
Maria Isabel Hernández Pérez, EAFIT University, Colombia
Eduardo Rafael Trentacoste, Instituto Nacional de Tecnología Agropecuaria, Argentina

***Correspondence:**
Ken Shackel
kashackel@ucdavis.edu

Specialty section:
This article was submitted to Plant Biophysics and Modeling, a section of the journal Frontiers in Plant Science

Received: *08 October 2021*
Accepted: *01 November 2021*
Published: *26 November 2021*

Citation:
Shackel K, Moriana A, Marino G, Corell M, Pérez-López D, Martin-Palomo MJ, Caruso T, Marra FP, Agüero Alcaras LM, Milliron L, Rosecrance R, Fulton A and Searles P (2021) Establishing a Reference Baseline for Midday Stem Water Potential in Olive and Its Use for Plant-Based Irrigation Management. Front. Plant Sci. 12:791711. doi: 10.3389/fpls.2021.791711

Midday stem water potential (SWP) is rapidly becoming adopted as a standard tool for plant-based irrigation management in many woody perennial crops. A reference or "baseline" SWP has been used in some crops (almond, prune, grape, and walnut) to account for the climatic influence of air vapor pressure deficit (VPD) on SWP under non-limiting soil moisture conditions. The baseline can be determined empirically for field trees maintained under such non-limiting conditions, but such conditions are difficult to achieve for an entire season. We present the results of an alternative survey-based approach, using a large set of SWP and VPD data collected over multiple years, from irrigation experiments in olive orchards located in multiple countries [Spain, United States (California), Italy, and Argentina]. The relation of SWP to midday VPD across the entire data set was consistent with an upper limit SWP which declined with VPD, with the upper limit being similar to that found in *Prunus*. A best fit linear regression estimate for this upper limit (baseline) was found by selecting the maximum R^2 and minimum probability for various upper fractions of the SWP/VPD relation. In addition to being surprisingly similar to the *Prunus* baseline, the olive baseline was also similar (within 0.1 MPa) to a recently published mechanistic olive soil-plant-atmosphere-continuum (SPAC) model for "super high density" orchard systems. Despite similarities in the baseline, the overall physiological range of SWP exhibited by olive extends to about −8 MPa, compared to about −4 MPa for economically producing almond. This may indicate that, despite species differences in physiological responses to low water

availability (drought), there may be convergent adaptations/acclimations across species to high levels of water availability. Similar to its use in other crops, the olive baseline will enable more accurate and reproducible plant-based irrigation management for both full and deficit irrigation practices, and we present tentative SWP guidelines for this purpose.

Keywords: deficit irrigation, *Olea europaea*, stem water potential, vapor pressure deficit, baseline

INTRODUCTION

Crop productivity is closely linked to crop water use (e.g., Howell, 1990) and improving the efficiency of water use in agriculture has been an ongoing focus of research worldwide (e.g., Velasco-Muñoz et al., 2018). For some woody perennial crops, reducing or eliminating irrigation during specific periods of development (e.g., Chalmers et al., 1981) has been shown to produce economically beneficial effects, such as an improved fruit drying ratio in prunes (Lampinen et al., 1995), decreased fruit drop in peach (Li et al., 1989), and increased control of hull rot disease in almonds (Teviotdale et al., 2001). Hence, these crops may be good candidates for deficit water management strategies to increase overall water use efficiency. In woody perennial crops, however, the effect of any given deficit irrigation regime can depend strongly on soil conditions (e.g., Lampinen et al., 1995). Hence, the plant-based approach of midday stem water potential (SWP; Shackel, 2011) has become a widely accepted tool for deficit irrigation management.

Olive (*Olea europaea* L.) is considered to be a drought resistant species (Connor, 2005) and also exhibits a wide range of SWP under cultivated conditions. However, olive also exhibits differential sensitivity of yield to SWP at different periods of crop development. Olive trees are an evergreen species most often grown in Mediterranean climate regions with shoot growth and bloom occurring during spring in mature orchards. Fruit set occurs as evaporative demand increases, with fruit growth and oil accumulation occurring under fairly high evaporative demand conditions in the summer and fall, and with harvest varying from the end of summer to early winter. In addition to occurring under different environmental conditions, all of these processes exhibit different levels of sensitivity to low SWP. Shoot growth and flowering are very sensitive to water limited conditions, and while these processes normally occur at a time in the season when soil water is not limiting, supplemental irrigation may be needed under drought conditions or in locations with delayed growth cycles (Moriana et al., 2003; Pérez-López et al., 2007). SWP of around −2 MPa reduced fruit size due to reduced endocarp growth (Gómez del Campo, 2013; Gómez del Campo et al., 2014) with more severe SWP deficits (−4 MPa at predawn) affecting bud development and reducing next season bloom (Gucci et al., 2019). Once endocarp growth finishes, the number of fruits is relatively constant and pit hardening occurs (Rapoport et al., 2013). After this phase, the sensitivity of yield to water stress is reduced (Goldhamer, 1999; Moriana et al., 2003; Fernández et al., 2013; Girón et al., 2015; Ahumada-Orellana et al., 2017; Corell et al., 2020). Even under very severe water stress conditions (SWP below −5 MPa) yield may only be slightly reduced, particularly if there is an adequate recovery in SWP before harvest (Moriana et al., 2003; Fernández et al., 2013; Ahumada-Orellana et al., 2017). Oil accumulation prior to harvest is usually coincident with autumn rains under Mediterranean climate conditions, but several authors have suggested that moderate water stress does not substantially reduce oil accumulation (Moriana et al., 2003; Lavee et al., 2007; Ben-Gal et al., 2021) and improves oil extractability. Reduction in oil accumulation is likely to occur only with SWP values consistently below −2 MPa (Hueso et al., 2019). Postharvest irrigation is not commonly studied, but Agüero-Alcaras et al. (2021) reported no significant differences in next season yield over a wide range of postharvest water stress conditions.

The above values provide some guidance for an allowable lower range of SWP, but from a practical as well as scientific standpoint it is important to understand this physiological range in the context of both upper and lower limits. McCutchan and Shackel (1992) were the first to propose SWP as a reliable physiological indicator of water stress, in part because a stable relation over much of the growing season was found between SWP and vapor pressure deficit (VPD) under non-limiting soil moisture conditions. This relation enabled a reliable prediction of SWP for a "fully irrigated state or condition" (i.e., from an irrigation perspective). In essentially all previous and many current irrigation studies, the highest irrigation level is simply assumed to be non-water-limiting. However, localized water application systems (e.g., micro-irrigation) create zones of wet and dry soil, and, particularly for woody perennials, there are typically roots present in both zones throughout the season. If roots in dry soil influence overall plant water relations, then irrigation at 100% of crop evapotranspiration (ET_c) in the wetted soil zones may not establish a physiologically non-soil-water-limited condition for the plant. To the authors knowledge, other than the McCutchan and Shackel (1992) study in *Prunus*, there has only been one study in olive (Morales-Sillero et al., 2013) in which the entire soil volume was maintained at a high moisture content over the growing season. Morales-Sillero et al. (2013) measured leaf rather than SWP in olive trees, but also did not report any relation of water potential to VPD. A number of studies in olive have found a linear relation of SWP to VPD (Morales-Sillero et al., 2013; Corell et al., 2016, 2020; Martin-Palomo et al., 2020), indicating that a relationship exists, but may be influenced by a number of factors, potentially including unintended effects of dry soil areas.

Based on the principle that the majority of water movement in soils and plants is driven primarily by differences in water potential (e.g., Kramer and Boyer, 1995), it is expected that SWP will depend on a large number of independent physical and biological factors such as soil, root, and stem hydraulic properties as well as plant transpiration as determined by stomatal and

atmospheric conditions. Hence, it is not clear that an upper limit to SWP should exist, that it should be largely independent of soil and tree conditions, and that it should have a reproducible relation simply to VPD. However, the experimentally determined upper limit reported by McCutchan and Shackel (1992) produced a robust estimate for an upper limit of SWP that was supported by further studies in both prune (Shackel, 2011) and almond (Shackel et al., 2010) orchards. The objective of the current study in olive was to determine if a large survey of SWP and VPD values from olive orchards in multiple countries might produce an upper limit reference SWP baseline.

MATERIALS AND METHODS

Survey Sites and Measurements

Much of the data used for this survey study was obtained from previous publications, and **Table 1** summarizes the locations and additional characteristics of each of the survey sites. All orchards were managed commercially and drip irrigated. The multi-year and multi-location studies provided a large data set with variable ranges in VPD and SWP. References are listed in **Table 1** where further information on particular sites may be obtained. Five different table (Manzanillo, Noceralla de Belice, and Olivo di Mandanici) and oil (Arbequina and Cornicabra) cultivars were used in these experiments in Argentina, Italy, Spain, and United States (California). Most data were from Arbequina and Manzanillo cvs but in different locations and management systems. Orchard age ranged from 2 to more than 10 years-old, but most orchards would be considered mature based on yield. Only the youngest in Coria del Rio (Spain) and Sciacca (Italy) were orchards with less yield than mature conditions and could be considered young. Tree density varied from high density (HD; around 300–350 trees per ha) to super high density (SHD), hedgerow orchards (>1000 trees per ha).

Stem water potential was typically measured over multiple years as part of irrigation experiments. SWP was determined on individual trees as described previously (Fulton et al., 2001). Briefly, a shaded leaf or short stem located near the main trunk within the tree canopy was covered with a reflective plastic bag for longer than 10 min (typically 1–2 h) to allow equilibration with the water potential of the stem at the point of attachment. A Scholander-type pressure chamber was then used to measure SWP. Olive trees are a Mediterranean species, typically growing under hot and dry summer and relatively warm winter conditions. However, even in these regions, climatic conditions can be very different. For instance, the experiments in Ciudad Real (central Spain, Pérez-López et al., 2007) are in a production zone with a shorter and cooler summer than that in Dos Hermanas (south Spain, Corell et al., 2020). In all experiments, hourly climatic data were measured with automated stations either at the experimental plots, or in nearby locations with the same environment as the experimental plots. Hourly, mid-afternoon climatic measurements were used to calculate hourly air VPD (Tetens, 1930) that coincided with the period of SWP measurement.

Data Assumptions and Analysis

Based on the hypothesis that there may be a practical upper limit to SWP at a given level of VPD for trees under non-soil-water-limited conditions (i.e., the "baseline" relation of Shackel, 2011), a total of 837 (SWP, VPD) values over all sites, years, and experimental treatments, were divided into groups based on 0.5 kPa classes of VPD. Assuming that each class would contain SWP values that were at or near the upper limit (i.e., if rain or irrigation had resulted in non-soil-water-limited conditions for that site and date) as well as SWP values below this limit, a range of uppermost (least negative) fractions (0.02–0.16) of SWP and the corresponding VPD values were averaged, and the average points used in a regression analysis of SWP on VPD. Since there was only one average (SWP, VPD) point per VPD class, each fraction contained the same number of (SWP, VPD) points, so the uppermost fraction which exhibited the highest regression R^2 and lowest probability was used as the best fit estimate of the non-water-limited ("baseline") relation of SWP to VPD. All statistical analyses were conducted in SAS 9.4 (SAS institute, Cary, NC, United States).

Comparison to Data From the Literature

First, the baseline estimate for olive was compared to that found in prune and almond (Shackel, 2011). Second, a set of SWP and VPD values obtained from a multi-compartment hydraulic model for olive under simulated non-soil-water-limiting conditions for two contrasting planting densities (García-Tejera et al., 2021) was kindly provided by the authors. The relation of SWP to VPD for this set of data was determined and compared to the baseline estimate for olive. Lastly, previously published data of leaf conductance (Gs) to SWP in almond (Spinelli et al., 2016) was also compared to data in olive as reported by Marino et al. (2018) and Ahumada-Orellana et al. (2019). The raw data for each was kindly provided by the authors and fitted using a smoothed spline function (Proc Transreg, SAS 9.4) in order to avoid any *a priori* assumptions regarding the functional form of the (Gs, SWP) relation.

RESULTS

Relation of Stem Water Potential to Vapor Pressure Deficit

Olive SWP values from the entire data set varied over a wide range (−0.5 to about −6 MPa), but the highest (least negative) values exhibited a pattern of decline with increasing VPD that was similar to the previously reported *Prunus* baseline (McCutchan and Shackel, 1992; **Figure 1**). Overall, SWP values in Spain tended to be closest to the *Prunus* baseline, but some SWP values from other countries were also close to this baseline. The maximum midday air VPD in this data set was about 6.5 kPa, which allowed for a total of 13 groups of 0.5 kPa classes in VPD, having a mode of 2.5 kPa (inset, **Figure 1**). Because there were relatively few SWP values in each VPD group below 1.5 and above 3.5 kPa (inset, **Figure 1**), in order to obtain a comparable upper fraction sample from every group, only data from the

TABLE 1 | Description of the sites used in the survey.

Country	Site	References	GPS	Year	CV	AGE	Soil	Density	Use
Argentina	Aimogasta (La Rioja)	Correa-Tedesco et al., 2010	28°33′S, 66°49′W	2005–2007	Manzanillo	6	Loamy sand	8 × 4	Table
Argentina	Aimogasta (La Rioja)	Agüero-Alcaras et al., 2021	28°35′S, 66°42′W	2009–2010	Manzanillo	10	Loamy sand	8 × 4	Table
Argentina	Chilecito (La Rioja)	Unpublished	29°09′S, 67°26′W	2017–2018	Arbequina	4	Gravelly sand	4 × 1.5	Oil
Spain	Ciudad Real	Unpublished	39°N, 5°6′W	2012–2015	Cornicabra	14	Shallow clay loam	7 × 4.76	Oil
Spain	Coria del Rio (Seville)	Martin-Palomo et al., 2020	37°N, 6°3′W	2014–2016	Manzanillo	43	Sandy loam	7 × 5	Table
Spain	Dos Hermanas (Seville)	Corell et al., 2020	37°25′N,5°95′W	2015–2017	Manzanillo	30	Sandy loam	7 × 4	Table
Spain	Carmona (Seville)	Unpublished	37.5°N, 5.7°W	2017–2019	Arbequina	11	Sandy loam	4 × 1.5	Oil
Spain	Coria del Rio (Seville)	Unpublished	37°N, 6°3′W	2015	Manzanillo	2	Sandy loam	4 × 1.5	Table
Italy	Marsala	Marra et al., 2016	37°46′28″N, 12°30′19″E	2008–2009	Arbequina	4	Sandy clay loam	1.5 × 3.5	Oil
Italy	Sciacca	Marino et al., 2016, 2021	37°32′N, 13°02′E	2014–2015	Nocellara del Belice and Olivo di Mandanici	3–4	Sandy clay loam	5 × 3, 5 × 2, 7 × 7	Oil, table
United States (CA)	Genoa	Unpublished	39°54′16.04″N, 122°17′14.20″W	2011	Manzanillo	>10	Loam, gravelly loam	7.7 × 3.6	Table
United States (CA)	Haro	Unpublished	39°49′N, 122°23′W	2011	Manzanillo	>10	Gravelly loam, sandy loam	9.0 × 5.8	Table
United States (CA)	Nielsen	Unpublished	39°44′59.36″N, 122°8′51.97″W	2009, 2011	Manzanillo	6, 8	Sandy loam	3.6 × 5.5	Table

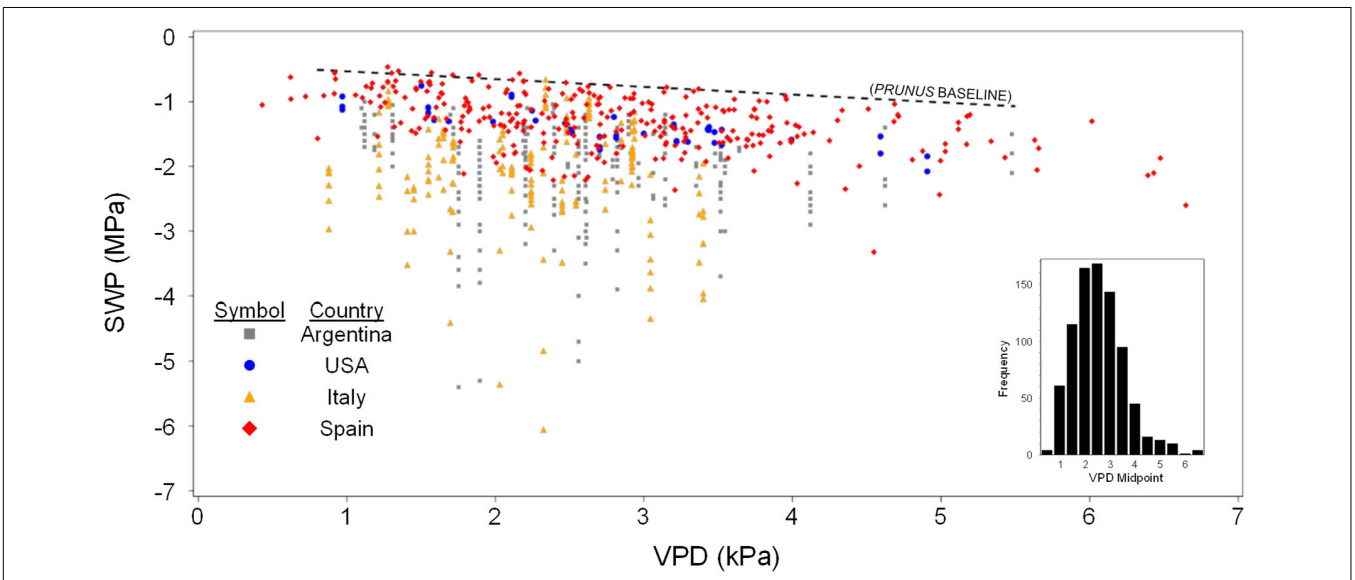

FIGURE 1 | All survey data of SWP to midday VPD from four countries. Each point is an individual measurement, with vertical lines of points indicating SWP values that were collected at the same site and time. Also shown for reference is the baseline relation found for *Prunus* (dashed line). Equation for the *Prunus* baseline is SWP (MPa) = –0.12 × VPD – 0.41. Inset shows the number of SWP measurements associated with each 0.5 kPa class of VPD.

five central VPD groups (1.5–3.5 kPa) were further analyzed. A regression analysis of average SWP on average VPD for the upper 0.02–0.16 fractions (2–16%) of SWP values exhibited a relatively linear decrease in SWP with increasing VPD regardless of the fraction selected (**Figure 2**). As expected, selecting greater fractions of the upper SWP values in each VPD group resulted in a progressive decrease in the regression intercept, but no clear trend was apparent in the regression slope (**Figure 2**). For all fractions from 0.02 to 0.16, the regression R^2 was maximum and the *P*-value minimum for fractions of 0.07 and 0.08, with a

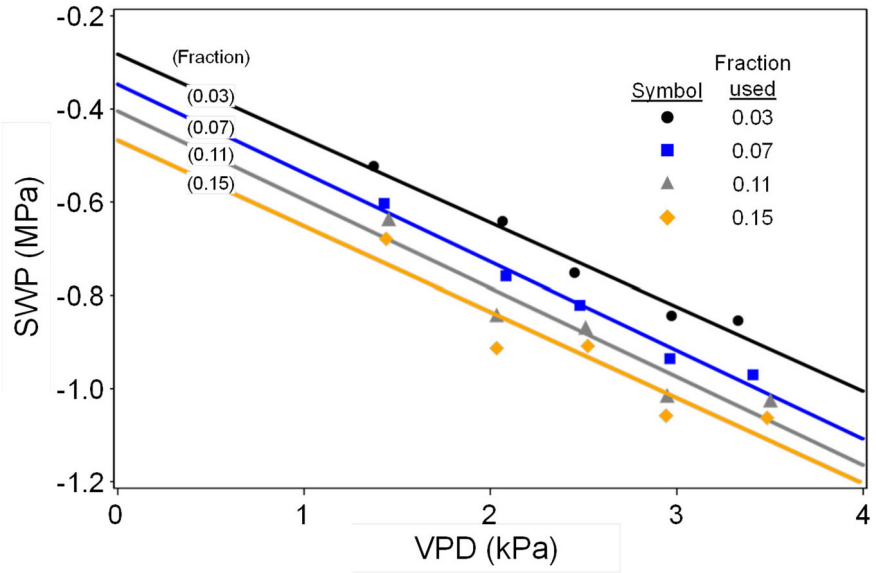

FIGURE 2 | Relation of average SWP to average VPD for representative upper fractions of SWP values from 0.5 kPa classes of VPD. Also shown are the regression lines for each fraction. Only SWP data from the central 5 VPD classes (1.5–3.5 kPa midpoints) were used. Slopes were –0.17, –0.18, –0.19, and –0.18, and intercepts were –0.29, –0.34, –0.40, and –0.46, respectively for fractions of 0.03, 0.07, 0.11, and 0.15.

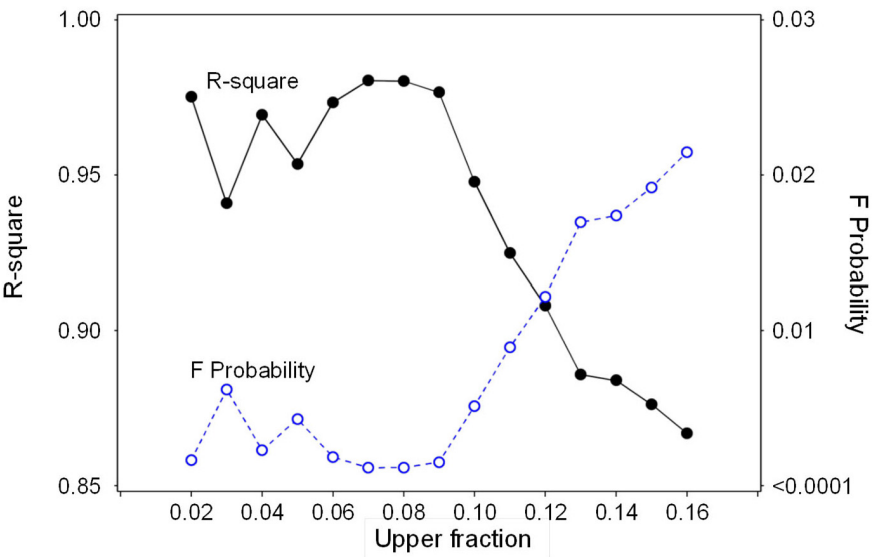

FIGURE 3 | Regression statistics (R-square and F Probability) for the relation between average SWP and average VPD (as in **Figure 2**) for a range of upper fractions of SWP values.

clear decline in R^2 and increase in P-value as fractions increased above about 0.09 (**Figure 3**). It should be noted that these R^2 and P-values are only used for purposes of comparison, and even though the total number of observations increased with higher fractions, since the regression analysis was performed on the mean (SWP, VPD) values, the number of points (5) for each regression was constant (as shown in **Figure 2**). Since a decrease in the regression intercept was expected as the fraction of upper SWP values increased, the relation corresponding to an upper fraction of 0.07 was considered the most appropriate estimate for a linear upper limit of olive SWP to air VPD. The slope and intercept for this relation (−0.18 and −0.34, **Figure 2**), were similar to those reported for *Prunus* (−0.12 and −0.41, respectively, **Figure 1**).

Comparison to Model Data

The soil-plant-atmosphere-continuum (SPAC) model of García-Tejera et al. (2021), which was not based on an explicit link

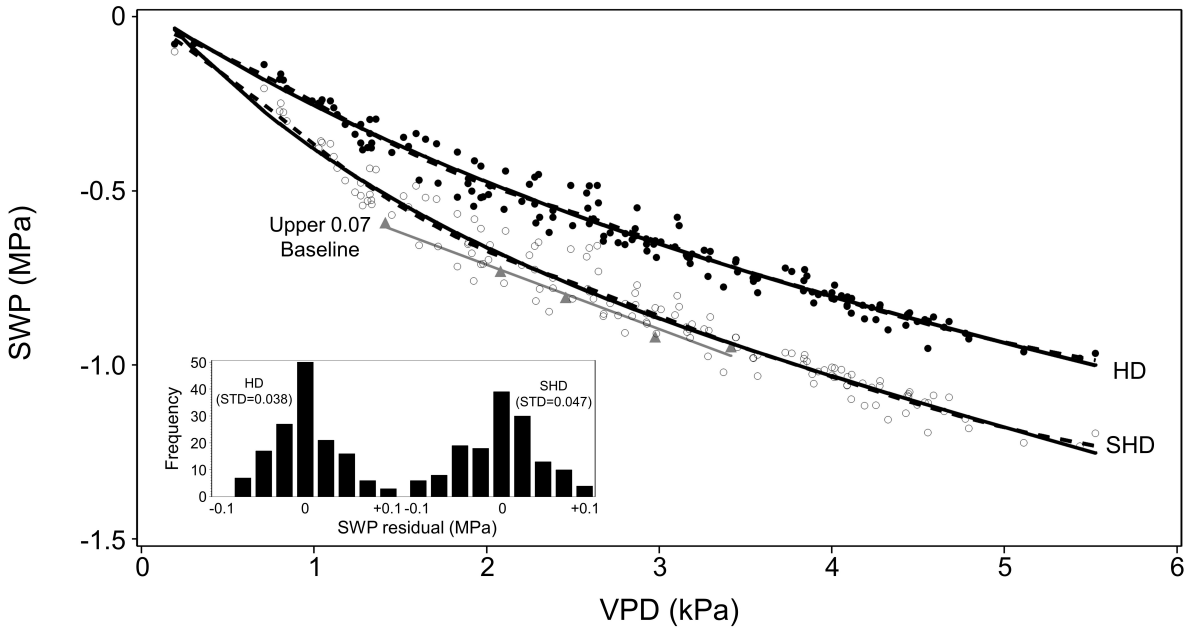

FIGURE 4 | Relation of SWP to midday VPD modeled by García-Tejera et al. (2021) for high density (HD, filled circle) and super-high density (SHD, empty circle) orchard conditions, as well as the same relation for the upper 0.07 fraction of SWP (filled triangles) found in the current study. The dashed lines for HD and SHD models are 50% smoothed spline functions (Proc Transreg SAS 9.4) and the solid lines are a combined linear and exponential function (see **Table 2** for parameters) fit to the data. A linear fit (also shown in **Figure 2**) for the upper 0.07 fraction is shown for reference. Inset shows the distribution and standard deviation (STD) of the residuals from the HD and SHD points to the combined linear/exponential fit. Both distributions were normal.

between SWP and VPD, exhibited a clear negative overall relation between SWP and VPD under non-soil-water-limiting conditions, with a similar shape for both HD and SHD orchard conditions (**Figure 4**). The relation of SWP to VPD was well fit by a smoothed spline function, which involves no *a priori* assumption about the shape of the relation but cannot be easily parameterized, and equally well fit by an exponential decay to a linear dependence of SWP on VPD for both HD and SHD (**Figure 4**). The residuals to the exponential + linear fit for HD and SHD exhibited a relatively low variation (0.038–0.047 MPa) and a normal distribution (Shapiro–Wilk $P = 0.37$ and 0.74), respectively, and the slope (change in SWP per 1 kPa change in VPD) of the linear component for SHD (−0.13, m in **Table 2**) was in the same range as that for the strictly linear olive (−0.18, **Figure 2**) and *Prunus* (−0.12, **Figure 1**) baselines. One conceptual advantage of the García-Tejera et al. (2021) model over a strictly linear model is that it allows SWP values to approach 0 as VPD's approach 0, which would be expected for non-soil-water-limited conditions. The relation of SWP to various temperatures and relative humidities for the exponential + linear fit of the García-Tejera et al. (2021) SHD model is presented in **Table 3**.

The data used for the olive survey included a wide range of planting densities (**Table 1**), but the linear estimate for the baseline was much closer to the SHD than to the HD model (**Figure 4**). All individual survey values that contributed to the upper 0.07 fraction for the linear estimate were categorized based on orchard density, and the least squares mean SWP (i.e., SHD model adjusted mean) for each density was compared (**Figure 5**). There were no statistically significant differences in the adjusted SWP means from different densities (ANCOVA not

TABLE 2 | Parameters and fit statistics for combined linear + exponential fit shown in **Figure 4**.

Density	Equation parameters				Fit statistics		
	A	B	C	m	TSS	Model SS	Fit
HD	0.556	2.47	0.0266	−0.096	6.81	6.59	0.97
SHD	0.613	1.37	0.0685	−0.13	9.57	9.25	0.97

$SWP = m*VPD + C - A*(1 - e^{(-\frac{VPD}{B})})$.

TABLE 3 | Baseline SWP (MPa) for various combinations of air temperature and relative humidity, based on the equation and parameters for SHD density shown in **Table 2**.

Air temperature (°C)	Air relative humidity (%)					
	10	20	30	40	50	60
5	−0.30	−0.27	−0.23	−0.19	−0.16	−0.11
10	−0.41	−0.37	−0.33	−0.28	−0.23	−0.18
15	−0.54	−0.50	−0.44	−0.39	−0.33	−0.26
20	−0.69	−0.63	−0.57	−0.51	−0.44	−0.36
25	−0.84	−0.78	−0.71	−0.64	−0.56	−0.47
30	−1.00	−0.93	−0.86	−0.78	−0.69	−0.59
35	−1.19	−1.11	−1.02	−0.93	−0.83	−0.72
40	−1.40	−1.30	−1.20	−1.10	−0.98	−0.86

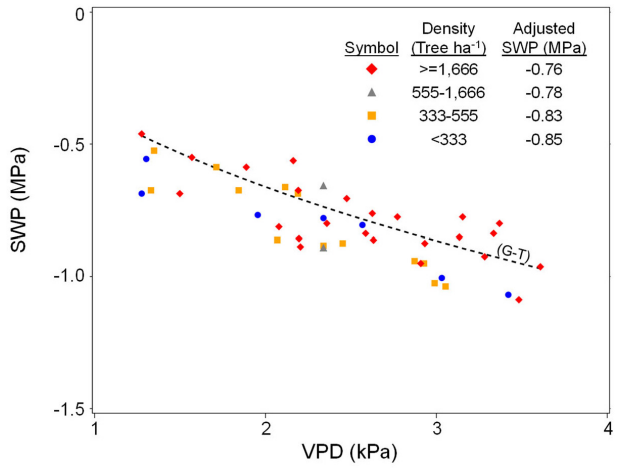

FIGURE 5 | Relation of SWP to VPD for all individual points of the upper 0.07 fraction, classified into groups representing different orchard tree densities, and the adjusted SWP means corresponding to each group. Also shown for reference is the linear/exponential fit for the García-Tejera et al. (2021, GT) SHD model (also shown in **Figure 4**).

shown) but the trend was for an increase in SWP at higher densities (**Figure 5**), rather than the decrease predicted by the García-Tejera et al. (2021) model (**Figure 4**).

Within the context of the overall range in SWP exhibited by olive under field conditions, the difference between the empirical linear fit and the SHD model fit can be considered relatively minor (**Figure 6**), with both being surprisingly close to the *Prunus* linear relation (**Figure 1**). Based on data from the literature, a similar overall relation of Gs to SWP in almond and olive was also found for the upper range of SWP, with close to a linear increase in Gs from about −1.1 to −0.5 MPa in almond and a similar linear increase in Gs from about −1.6 to −0.9 MPa in olive (**Figure 7**). However, a clear difference between the species was apparent in the lower range of SWP, with almond exhibiting a Gs close to 0 by about −3 MPa, whereas olive maintaining a measurable Gs to about −7 MPa (**Figure 7**).

DISCUSSION

As originally proposed (McCutchan and Shackel, 1992), the baseline SWP was intended to serve as a plant-based reference SWP value indicating non-soil-water-limited ("wet soil") conditions, rather than a plant-based reference value indicating non-physiologically limiting ("non-stressed") conditions. For instance, a plant under wet soil (baseline) conditions may exhibit the same SWP at high VPD as does a plant under dry soil conditions exhibits at low VPD. In this case, the baseline predicts that irrigation should cause an increase in SWP for the plant at low VPD, but not for the plant at high VPD. However, it does not predict that the increase in SWP at low VPD will have a meaningful impact on plant physiological activity. Thus, as a reference value for irrigation management under field conditions, observed SWP values at or close to the baseline SWP would indicate that soil water was not limiting and hence that no irrigation was needed. Presumably, irrigation under these circumstances may also have an undesirable negative effect on root health. It is also important to consider baseline SWP in order to avoid problems associated with the use of a simple threshold SWP to trigger irrigation, as considered by García-Tejera et al. (2021). Under field conditions, short term (day-to-day) as well as medium term (weather system) patterns in VPD will result in a range of SWP for any given level of soil moisture. Hence, if a desired or "target" SWP has been established for a particular crop and time of year (e.g., prunes: Lampinen et al., 2001; almond: Stewart et al., 2011), then this target must be considered as having a normal range of variation associated with weather (VPD) conditions. Considering the trend of both SWP and baseline SWP over time is required in order to avoid over-reacting to unusually high or low VPD conditions, especially as the target SWP is approached. Observed SWP typically exhibits changes in parallel with baseline SWP over time even at different irrigation levels (e.g., Figure 5 in Shackel, 2011). Hence, the difference between observed SWP and baseline SWP can be used as a more stable plant-based indicator of any trend in the effects of soil water availability. For instance, it may be possible to combine this trend with a forecasted VPD in order to forecast when SWP will reach a given threshold.

Independently of its use as a baseline index of soil water limitations, SWP itself should be a measure of physiological water limitations, although this assumption has not been without controversy (e.g., Sinclair and Ludlow, 1985). SWP should be mechanistically dependent on multiple physical and biological factors (e.g., water transport properties of the soil and plant, as well as stomatal and atmospheric influences on transpiration), and hence it is somewhat surprising that a similar and relatively straightforward dependence of SWP on VPD should be found for both olive (evergreen) and *Prunus* (deciduous). This, as well as the fact that the baseline relation appears to apply across multiple soil types, planting densities, and environmental conditions, may indicate a convergence of plant adaptations/acclimations related to balancing plant water demand to soil water supply, at least for high levels of soil water availability. In both olive and *Prunus*, the range of baseline SWP is relatively small (to −1.2 and −1.0 MPa at a VPD of 5 kPa, respectively, **Figures 1**, **4**) compared to the range of observed SWP. SWP has been reported to range to about −3 MPa in commercial prune (Shackel, 2011) and almond (Shackel et al., 2010) orchards, and to about −4.5 MPa in almond drought studies (Shackel, 2011). SWP of olives in this and other studies show a somewhat wider range (to about −7 MPa; Marino et al., 2018), and for all of these crops the observed range of SWP should be considered as representative of the crops physiological range. In a number of deciduous crops, reductions in SWP over their physiological range have been closely associated with reductions in various measures of physiological activity such as vegetative (cherry) and reproductive (pear and apple) growth (e.g., Shackel et al., 1997; Naor, 2006) and stomatal conductance and/or photosynthesis (e.g., Spinelli et al., 2016). In fact, most of the above studies have found a nearly linear relation between long term average SWP and long-term average or integrative measures of physiological

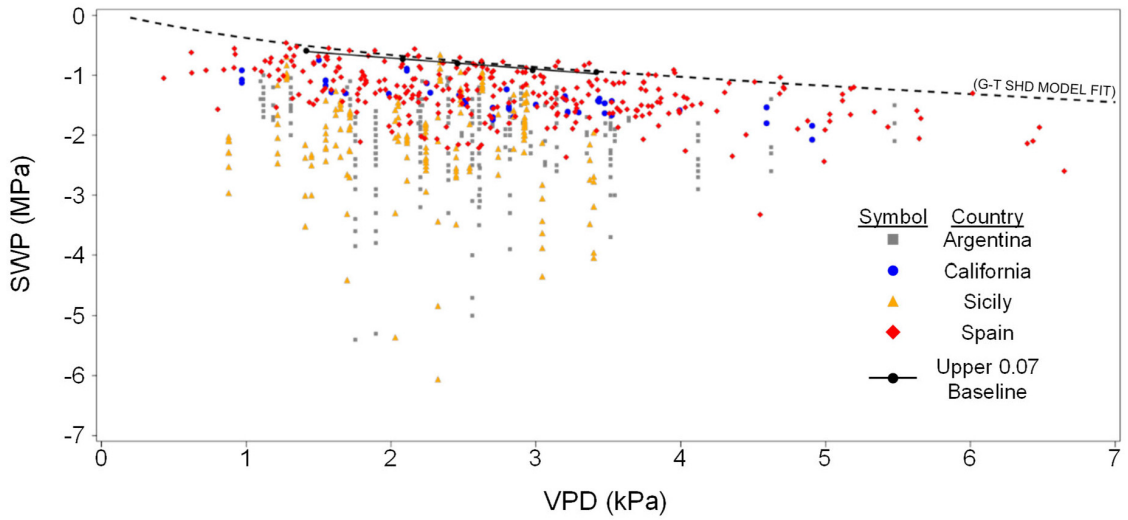

FIGURE 6 | Pooled relation of SWP to midday VPD for all countries, as in **Figure 2**, showing the combined linear/exponential relation for the SHD data of García-Tejera et al. (2021, dashed line), as well as the points and linear fit for the upper 0.07 fraction found in the current study. Equation for linear fit is SWP = –0.18 × VPD – 0.34.

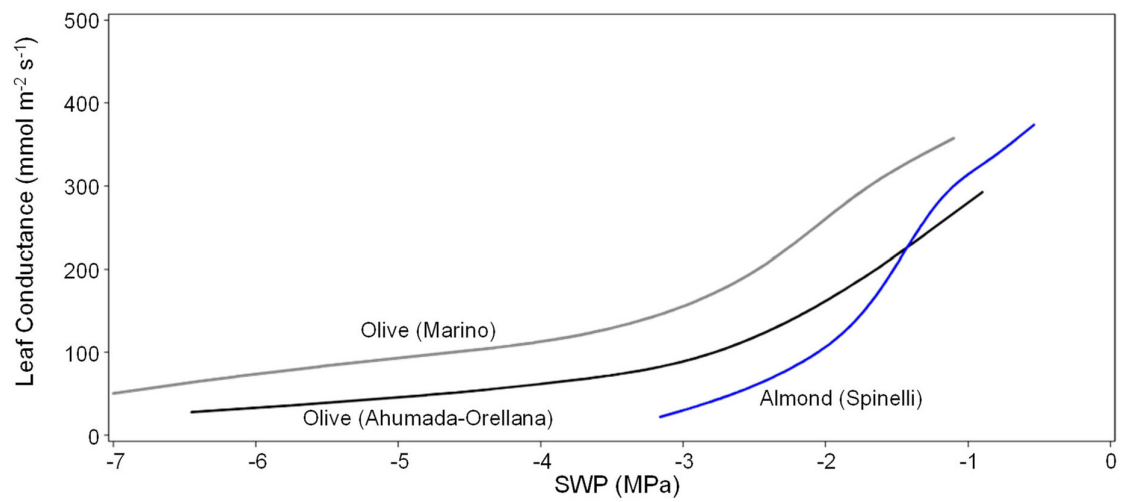

FIGURE 7 | Relation of leaf conductance to SWP for almond reported by Spinelli et al. (2016), for olive reported by Marino et al. (2018), and for olive reported by Ahumada-Orellana et al. (2019). Each line is a 60% smoothed spline function fit to the raw data (Proc Transreg SAS 9.4).

activity such as final tree or fruit size after multiple or single seasons, respectively. Measures of more dynamic (short-term) physiological properties such as Gs have shown a substantial amount of variability in the level of Gs at any particular SWP, with the relation of Gs to SWP in olive described as exponential (Marino et al., 2018) or segmented linear (Ahumada-Orellana et al., 2019). Using an empirical (smoothed spline) approach, we found that a positive linear trend of Gs with SWP occurred at high SWP in both olive and almond (**Figure 7**). Since this trend occurred within the baseline range, it may indicate that plant water availability can be physiologically limiting, even if soil water availability is not, but further research will be needed to determine whether these limitations are of any practical importance (i.e., limit plant growth or productivity) for irrigation management. For instance, reductions in Gs due to mild water stress may not affect photosynthesis, but could reduce vegetative growth (Bradford and Hsiao, 1982), potentially resulting in an increase in carbohydrate availability for reproductive processes.

In woody perennials, crop yield and quality are the result of growth, developmental, and biochemical processes that occur over relatively long time frames (seasonal or multi-seasonal). Hence, appropriate target or threshold SWP levels for irrigation management in these crops will depend on which processes contribute to yield and quality at which times, as well as the sensitivity of each process to deficit levels of SWP. **Table 4** summarizes the range of SWP for regulated deficit irrigation

TABLE 4 | Guidelines for the use of SWP for deficit irrigation management in olive trees.

Phenological stage	Response	SWP range	References
PHASE I			
Vegetative growth	Maximum growth	At or near baseline, (> about −1 MPa)	Pérez-López et al., 2007; Pierantozzi et al., 2020; Hueso et al., 2021
	Significant growth reduction	−1.0 to −1.2 MPa	Moriana et al., 2012; Gómez del Campo, 2013
	Strong growth reduction	−2 Mpa	Moriana et al., 2012; Gómez del Campo, 2013
Flower/inflorescence development	Maximum inflorescence development and flowering	At or near baseline, (> about −1 MPa)	Rapoport et al., 2012; Hueso et al., 2021
	Significant reduction in flowers and inflorescences	−2 MPa	Beyá-Marshall et al., 2018
Fruit set/endocarp growth	Maximum fruit set	At or near baseline, (> about −1 MPa)	Rapoport et al., 2012
	Little or no effect on endocarp growth	−2 MPa	Gómez del Campo, 2013; Gómez del Campo et al., 2014
	Reduction in endocarp growth and fruit size at harvest	−3 MPa	Gómez del Campo, 2013; Gómez del Campo et al., 2014
	Reduction in endocarp growth and fruit size at harvest; possible effect on the flower induction of next season	Lower than −3 MPa; −4 MPa (predawn stem water potential values)	Gucci et al., 2019
PHASE II			
Endocarp schlerification (pit hardening)	No significant yield reduction with rehydration next phase. Negligible fruit drop.	−2 to −3 MPa	Moriana et al., 2003, 2012; Fernández et al., 2013; Girón et al., 2015; Ahumada-Orellana et al., 2017
	Significant yield reduction. Fruit drop.	−3 to −4 MPa	Moriana et al., 2003; Gómez del Campo, 2013; Ahumada-Orellana et al., 2017; Corell et al., 2020
	Fruit shrinkage. Permanent injury to table olives.	Below −4 MPa	
PHASE III			
Fruit growth due to cell expansion (table and oil olives)	No significant yield reduction. No significantly lower fruit size.	At or near baseline, (> about −1.5 MPa)	Girón et al., 2015; Corell et al., 2020; Martin-Palomo et al., 2020
Oil quantity and quality (oil olives)	No significant effect on oil accumulation	> −2 MPa	Moriana et al., 2003; Hueso et al., 2019
	Increase in phenolic compounds	Linear increase from −2 to −3 MPa	Sánchez-Rodríguez et al., 2019
	Increase in oil extractability	−3 MPa	Fernández et al., 2011; García et al., 2013
	Decrease phenolic compounds	Below −3 MPa	Sánchez-Rodríguez et al., 2019

Phenological phases are based on Goldhamer (1999) and Fernández et al. (2013).

in olive and the observed crop response during different phenological stages. These threshold values may serve as an approximate guide, but it is recognized that the duration of a given water stress is also likely to be important (Girón et al., 2015; Corell et al., 2020).

Although differences may occur by region, the irrigation season is commonly divided into three phases in mature orchards. Phase I is the most water-sensitive part of the season because shoot growth and flower development occur. For both processes, irrigation scheduling should be performed such that SWP is near the baseline. Even under such conditions, vegetative growth may not be optimal due to the high water stress sensitivity of growth to reductions in SWP (Pérez-López et al., 2007). In young orchards, crown development is very important for reaching maximum yields per hectare, but in mature orchards with super high densities, moderate water stress (−1 to −1.2 MPa SWP; Moriana et al., 2012; Gómez del Campo, 2013) could reduce pruning costs and increase yields by reducing shading (Trentacoste et al., 2019). Maintaining SWP near the baseline would be the best strategy during these phenological stages because fruit and oil yield is strongly affected by early water stress (Rapoport et al., 2012). However, some evidence suggests that only SWP below −2 MPa in the spring will decrease flower number and its quality (Beyá-Marshall et al., 2018). Allowing trees to reach this level of stress before irrigation could provide significant water savings and allow for a greater number of management options at the farm scale under drought conditions.

Endocarp sclerification occurs during Phase II (Goldhamer, 1999; Rapoport et al., 2012). In this period, low SWP values can be tolerated (−2 to −3 MPa) with minor reductions in yield (Goldhamer, 1999). This too could be important when managing drought impacts at a farm scale.

During the last phase, fruit growth occurs principally due to cell expansion and oil accumulation. In this period, different irrigation strategies for table and oil cultivars are necessary, especially if harvesting is done for green table olives. Fruit size

is one of the main quality features of table olives and optimum water status is desirable if previous deficit irrigation has been applied (Girón et al., 2015; Corell et al., 2020). SWP might not be the best indicator for detecting a final effect on fruit size during recovery from water stress because no differences in SWP were related to slight differences in fruit size (Girón et al., 2015; Corell et al., 2020). However, if no previous deficit irrigation has been applied, a moderate water stress could be applied with no fruit size reduction (Martin-Palomo et al., 2020). Oil accumulation is more tolerant than fruit growth to water deficit (Gómez del Campo et al., 2014). Furthermore, optimum water status could increase fruit moisture and decrease oil extractability under commercial conditions (Fernández et al., 2011, 2013; García et al., 2013). Evidence suggests that oil accumulation is not affected until SWP is less than −2 MPa (Hueso et al., 2019). The influence of water deficits on oil quality and sensory characteristics is not completely clear yet, but the best quality oil would be well below the SWP baseline (Grattan et al., 2006; Sánchez-Rodríguez et al., 2019). For example, water deficit often increases total phenols, which is an important component of oil quality.

CONCLUSION

Across multiple sites and years, an upper limit of olive midday SWP, presumably corresponding to non-limiting soil moisture (i.e., baseline) conditions in the field, was found to have a negative linear relation with midday air VPD for VPD's above about 1.5 kPa. This relation was very close (within 0.1 MPa) to that of a recently published olive hydraulic model for non-limiting soil moisture and VPD's above about 2 kPa. This relation was also remarkably similar across the entire range of VPD's (0 to 6 kPa) to the SWP baseline in *Prunus*. This similarity between *Prunus* and olive, despite many fundamental physiological differences (e.g., *Prunus* being deciduous and olive being evergreen), may indicate a convergence in woody perennial plant adaptations/acclimations that impact the balance between plant water demand on one hand and soil water supply on the other, at least under high levels of soil water availability. The proposed baseline should serve as a reference for olive SWP under non-limiting soil moisture conditions, and it may be important for irrigation management to maintain trees near this reference during stress sensitive periods (e.g., spring). Tentative SWP guidelines for irrigation management during potentially less stress sensitive periods are also presented.

DATA AVAILABILITY STATEMENT

The raw data supporting the conclusions of this article will be made available by the authors, without undue reservation.

AUTHOR CONTRIBUTIONS

KS, AM, GM, MC, and PS substantially contributed to the conception and design of the study. KS wrote the manuscript with assistance from AM, GM, and PS. KS analyzed the full data set from the four countries. DP-L, MM-P, TC, FPM, LMA, LM, RR, and AF were all involved in field measurements, data processing, and supervision of these tasks in the different countries. All authors contributed to the article and approved the submitted version.

FUNDING

In addition to the authors institutions, this research was supported by the Olive Oil Commission of California and the California Olive Committee.

ACKNOWLEDGMENTS

We would like to thank Omar García Tejera for sharing his model output of SWP and VPD. Samuel Ortega-Farías kindly provided leaf conductance data for olive.

REFERENCES

Agüero-Alcaras, L. M., Rousseaux, M. C., and Searles, P. S. (2021). Yield and water productivity responses of olive trees (cv Manzanilla) to postharvest deficit irrigation in a non-Mediterranean climate. *Agric. Water Manag.* 245:106562. doi: 10.1016/j.agwat.2020.106562

Ahumada-Orellana, L. E., Ortega-Farias, S., Searles, P. S., and Retamales, J. B. (2017). Yield and water productivity responses to irrigation cut-off strategies after fruit set using stem water potential thresholds in a super-high density olive orchard. *Front. Plant Sci.* 8:1280. doi: 10.3389/fpls.2017.01280

Ahumada-Orellana, L., Ortega-Farías, S., Poblete-Echeverría, C., and Searles, P. S. (2019). Estimation of stomatal conductance and stem water potential threshold values for water stress in olive trees (cv. Arbequina). *Irrig. Sci.* 37, 461–467. doi: 10.1007/s00271-019-00623-9

Ben-Gal, A., Ron, Y., Yermiyahu, U., Zipori, I., Naoum, S., and Dag, A. (2021). Evaluation of regulated deficit irrigation strategies for oil olives: a case study for two modern Israeli cultivars. *Agric. Water Manag.* 245:106577. doi: 10.1016/j.agwat.2020.106577

Beyá-Marshall, V., Herrera, J., Fichet, T., Trestaconte, E. R., and Kremer, C. (2018). The effct of water status on productive and flowering variables in young "Arbequina" olive trees under limited irrigation water availability in a semiarid region of Chile. *Hortic. Environ. Biotechnol.* 59, 815–826.

Bradford, K. J., and Hsiao, T. C. (1982). "Physiological responses to moderate water Stress," in *Encyclopedia of Plant Physiology, Physiological Plant Ecology B. Water Relations and Photosynthetic Productivity*, eds O. L. Lange, P. S. Nobel, C. B. Osmond, and H. Ziegler (Berlin: Springer Verlag).

Chalmers, D. J., Mitchell, P. D., and van Heek, L. (1981). Control of peach tree growth and productivity by regulated water supply, tree density, and summer pruning. *J. Am. Soc. Hortic. Sci.* 106, 307–312.

Connor, D. J. (2005). Adaptation of olive (*Olea europaea* L.) to water-limited environments. *Aust. J. Agric. Res.* 56, 1181–1189.

Corell, M., Martín-Palomo, M. J., Girón, I., Andreu, L., Galindo, A., Centeno, A., et al. (2020). Stem water potential-based regulated deficit irrigation scheduling for olive table trees. *Agric. Water Manag.* 242:106418. doi: 10.1016/j.agwat.2020.106418

Corell, M., Pérez-López, D., Martín-Palomo, M. J., Centeno, A., Girón, I., Galindo, A., et al. (2016). Comparison of the water potential baseline in different locations: usefulness for irrigation scheduling of olive orchards. *Agric. Water Manag.* 177, 308–316.

Correa-Tedesco, G., Rousseaux, M. C., and Searles, P. S. (2010). Plant growth and yield responses in olive (*Olea europaea*) to different irrigation levels in an arid region of Argentina. *Agric. Water Manag.* 97, 1829–1837. doi: 10.1016/j.agwat.2010.06.020

Fernández, J. E., Perez-Martin, A., Torres-Ruiz, J. M., Cuevas, M. V., Rodriguez-Dominguez, C. M., Elsayed-Farag, S., et al. (2013). A regulated deficit irrigation strategy for hedgerow olive orchards with high plant density. *Plant Soil* 372, 279–295. doi: 10.1002/jsfa.7828

Fernández, J. E., Torres-Ruiz, J. M., Diaz-Espejo, A., Montero, A., Alvarez, R., Jimenez, M. D., et al. (2011). Use of máximum trunk diameter measurements to detect wáter stress in mature "Arbequina" olive trees under deficit irrigation. *Agric. Water Manag.* 98, 1813–1821. doi: 10.1016/j.agwat.2011.06.011

Fulton, A., Buchner, R., Olson, B., Schwankl, L., Gilles, C., Bertagna, N., et al. (2001). Rapid equilibration of leaf and stem water potential under field conditions in almonds, walnuts, and prunes. *HortTechnology* 11, 609–615. doi: 10.21273/horttech.11.4.609

García, J. M., Cuevas, M. V., and Fernandez, J. E. (2013). Production and oil quality in "Arbequina" olive (*Olea europaea*, L) trees under two deficit irrigation strategies. *Irrig. Sci.* 31, 359–370. doi: 10.1007/s00271-011-0315-z

García-Tejera, O., Lopez-Bernal, A., Orgaz, F., Testi, L., and Villalobos, F. J. (2021). The pitfalls of water potential for irrigation scheduling. *Agric. Water Manag.* 243:106522. doi: 10.1093/jxb/erh213

Girón, I. F., Corell, M., Martín-Palomo, M. J., Galindo, A., Torrecillas, A., Moreno, F., et al. (2015). Feasibility of trunk diameter fluctuations in the scheduling of regulated deficit irrigation for table olive trees without reference trees. *Agric. Water Manag.* 161, 114–126. doi: 10.1016/j.agwat.2015.07.014

Goldhamer, D. A. (1999). Regulated deficit irrigation for California canning olives. *Acta Hortic.* 474, 369–372. doi: 10.17660/actahortic.1999.474.76

Gómez del Campo, M. (2013). Summer deficit-irrigation strategies in a hedgerow olive orchard cv "Arbequina": effect on fruit characteristics and yield. *Irrig. Sci.* 31, 259–269. doi: 10.1007/s00271-011-0299-8

Gómez del Campo, M., Perez-Exposito, M. A., Hammami, S. B. M., Centeno, A., and Rapoporrt, H. F. (2014). Effect of varied summer déficit irrigation on components of olive fruit growth and development. *Agric. Water Manag.* 137, 84–91. doi: 10.1016/j.agwat.2014.02.009

Grattan, S. R., Berenguer, M. J., Connell, J. H., Polito, V. S., and Vossen, P. M. (2006). Olive oil production as influenced by different quantities of applied water. *Agric. Water Manag.* 85, 133–140. doi: 10.1016/j.agwat.2006.04.001

Gucci, R., Caruso, G., Gennani, C., Esposto, S., Urbani, S., and Servili, M. (2019). Fruit growth, yield and oil quality changes induced by deficit irrigation at different stages of olive fruit development. *Agric. Water Manag.* 212, 88–98.

Howell, T. A. (1990). "Relationships between crop production and transpiration, evaporation, and irrigation," in *Irrigation of Agricultural Crops*, Chap. 14, eds E. B. Stewart and D. Nielsen (Madison, WI: American Society of Agronomy, Crop Science Society of America, and Soil Science Society of America), 391–434. doi: 10.1016/j.scitotenv.2018.11.176

Hueso, A., Camacho, G., and Gomez-del-Campo, M. (2021). Spring deficit irrigation promotes significant reduction on vegetative growth, flowering, fruit growth and production in hedgerow olive orchards (cv Arbequina). *Agric. Water Manag.* 248:106695. doi: 10.1016/j.agwat.2020.106695

Hueso, A., Trentacoste, E. R., Junquera, P., Gomez-Miguel, V., and Gomez del Campo, M. (2019). Differences in stem wáter potential during oil synthesis determine fruit characteristics and production but not vegetative growth or return bloom in an olive hedgerow orchard (cv Arbequina). *Agric. Water Manag.* 223:105589. doi: 10.1016/j.agwat.2019.04.006

Kramer, P. J., and Boyer, J. S. (1995). *Water Relations of Plants and Soils*. Cambridge, MA: Academic Press Inc.

Lampinen, B. D., Shackel, K. A., Southwick, S. M., and Olson, W. H. (2001). Deficit irrigation strategies using midday stem water potential in prune. *Irrig. Sci.* 20, 47–54. doi: 10.1007/s002710000028

Lampinen, B. D., Shackel, K. A., Southwick, S. M., Olson, B., Yeager, J. T., and Goldhamer, D. (1995). Sensitivity of yield and fruit quality of French prune to water deprivation at different fruit growth stages. *J. Am. Soc. Hortic. Sci.* 120, 139–147. doi: 10.21273/jashs.120.2.139

Lavee, S., Hanoch, E., Wodner, M., and Abramowitch, H. (2007). The effect of predetermined deficit irrigation on the performance of cv Muhasan olives (*Olea europaea* L) in the eastern coastal plain of Israel. *Sci. Hortic.* 112, 156–163.

Li, S. H., Huguet, J. C., Schoch, P. G., and Orlando, P. (1989). Response of peach tree growth and cropping to soil water deficit at various phenological stages of fruit development. *J. Hortic. Sci.* 61, 531–552.

Marino, G., Caruso, T., Ferguson, L., and Paolo Marra, F. (2018). Gas exchanges and stemwater potential define stress thresholds for efficient irrigation management in olive (*Olea europea* L.). *Water* 10:342. doi: 10.3390/w10030342

Marino, G., Pernice, F., Marra, F. P., and Caruso, T. (2016). Validation of an online system for the continuous monitoring of tree water status for sustainable irrigation managements in olive (*Olea europaea* L.). *Agric. Water Manag.* 177, 298–307.

Marino, G., Scalisi, A., Guzmán-Delgado, P., Caruso, T., Marra, F. P., and Lo Bianco, R. (2021). Detecting mild water stress in olive with multiple plant-based continuous sensors. *Plants* 10:131. doi: 10.3390/plants10010131

Marra, F. P., Marino, G., Marchese, A., and Caruso, T. (2016). Effects of different irrigation regimes on a super-high density olive grove cv. 'Arbequina': vegetative growth, productivity and polyphenol content of the oil. *Irrig. Sci.* 34, 313–325.

Martin-Palomo, M. J., Corell, M., Girón, I., Andreu, L., Galindo, A., Centeno, A., et al. (2020). Absence of yield reduction after controlled water stress during preharvest period in table olive trees. *Agronomy* 10:258.

McCutchan, H., and Shackel, K. A. (1992). Stem-water potential as a sensitive indicator of water stress in prune trees (*Prunus domestica* L. cv. French). *J. Am. Soc. Hortic. Sci.* 117, 607–611. doi: 10.21273/jashs.117.4.607

Morales-Sillero, A., García, J. M., Torres-Ruiz, J. M., Montero, A., Sánchez-Ortiz, A., and Fernández, J. E. (2013). Is the productive performance of olive trees under localized irrigation affected by leaving some roots in drying soil? *Agric. Water Manag.* 123, 79–92.

Moriana, A., Orgaz, F., Fereres, E., and Pastor, M. (2003). Yield responses of a mature olive orchard to water deficits. *J. Am. Soc. Hortic. Sci.* 128, 425–431. doi: 10.21273/jashs.128.3.0425

Moriana, A., Pérez-López, D., Prieto, M. H., Ramírez-Santa-Pau, M., and Pérez-Rodriguez, J. M. (2012). Midday stem water potential as a useful tool for estimating irrigation requirements in olive trees. *Agric. Water Manag.* 112, 43–54. doi: 10.1016/j.agwat.2012.06.003

Naor, A. (2006). Irrigation scheduling and evaluation of tree water status in deciduous orchards. *Hortic. Rev.* 32, 111–165. doi: 10.1002/9780470767986.ch3

Rapoport, H. F., Pérez-López, D., Hammami, S. B. M., Aguera, J., and Moriana, A. (2013). Fruit pit hardening: physical measurements during olive growth. *Ann. Appl. Biol.* 163, 200–208. doi: 10.1111/aab.12046

Pérez-López, D., Ribas, F., Moriana, A., Olmedilla, N., and De Juan, A. (2007). The effect of irrigation schedules on the water relations and growth of a young olive (*Olea europaea* L.) orchard. *Agric. Water Manag.* 89, 297–304. doi: 10.1016/j.agwat.2007.01.015

Pierantozzi, P., Torres, M., Tivani, M., Contreras, C., Gentili, L., Parera, C., et al. (2020). Spring deficit irrigation in olive (cv. Genovesa) growing under arid continental climate: effects on vegetative growth and productive parameters. *Agric. Water Manag.* 238:106212. doi: 10.1016/j.agwat.2020.106212

Rapoport, H. F., Hammami, S. B. M., Martins, P., Perez-Priego, O., and Orgaz, F. (2012). Influence of water deficits at different times during olive tree inflorescence and flower development. *Environ. Exp. Bot.* 77, 227–233. doi: 10.1016/j.envexpbot.2011.11.021

Sánchez-Rodríguez, L., Kranjac, M., Marijanovic, Z., Jerkovic, I., Corell, M., Moriana, A., et al. (2019). Quality attributes and fatty acid, volatile and sensory profiles of "Arbequina" hydroSOStainable olive oil. *Molecules* 24:2148. doi: 10.3390/molecules24112148

Shackel, K. A. (2011). A plant-based approach to deficit irrigation in trees and vines. *Hortic. Sci.* 46, 173–177. doi: 10.21273/hortsci.46.2.173

Shackel, K. A., Ahmadi, H., Biasi, W., Buchner, R., Goldhamer, D., Gurusinghe, S., et al. (1997). Plant water status as an index of irrigation need in deciduous fruit trees. *HortTechnology* 7, 23–29. doi: 10.21273/horttech.7.1.23

Shackel, K. A., Buchner, R., Connell, J., Edstron, J., Fulton, A., Holtz, B., et al. (2010). "Midday stem water potential as a basis for irrigation scheduling," in *Proceedings of the 5th National Decennial Irrigation Conference, 5-8 December 2010, Phoenix Convention Center*, (Phoenix, ARI). doi: 10.1093/treephys/28.8.1255

Sinclair, T. R., and Ludlow, M. M. (1985). Who taught plants thermodynamics? The unfulfilled potential of plant water potential. *Aust. J. Plant Physiol.* 12, 213–217.

Spinelli, G. M., Snyder, R. L., Sanden, B. L., and Shackel, K. A. (2016). Water stress causes stomatal closure but does not reduce canopy evapotranspiration in almond. *Agric. Water Manag.* 168, 11–22.

Stewart, W. L., Fulton, A. E., Krueger, W. H., Lampinen, B. D., and Shackel, K. A. (2011). Regulated deficit irrigation reduces water use of almonds without affecting yield. *Calif. Agric.* 65, 90–99. doi: 10.1016/j.scitotenv.2021.146148

Tetens, V. O. (1930). Uber einige meteorolgische. *Begriffe Z. Geophys.* 6, 297–309.

Teviotdale, B. L., Goldhamer, D. A., and Viveros, M. (2001). Effects of deficit irrigation on hull rot disease of almond trees caused by *Monilinia fructicola* and *Rhizopus stolonifer*. *Plant Dis.* 85, 399–403. doi: 10.1094/PDIS.2001.85.4.399

Trentacoste, E. R., Calderón, F. J., Contreras-Zanessi, O., Galarza, W., Banco, A. P., and Puertas, C. M. (2019). Effect of regulated deficit irrigation during the vegetative growth period on shoot elongation and oil yield components in olive hedgerows (cv. Arbosana) pruned annually on alternate sides in San Juan, Argentina. *Irrig. Sci.* 37, 533–546. doi: 10.1007/s00271-019-00632-8

Velasco-Muñoz, J. F., Aznar-Sánchez, J. A., Belmonte-Ureña, L. J., and Román-Sánchez, I. M. (2018). Sustainable water use in agriculture: a review of worldwide research. *Sustainability* 10:1084. doi: 10.3390/su10041084

Conflict of Interest: The authors declare that the research was conducted in the absence of any commercial or financial relationships that could be construed as a potential conflict of interest.

Publisher's Note: All claims expressed in this article are solely those of the authors and do not necessarily represent those of their affiliated organizations, or those of the publisher, the editors and the reviewers. Any product that may be evaluated in this article, or claim that may be made by its manufacturer, is not guaranteed or endorsed by the publisher.

frontiers in Plant Science

REVIEW
published: 10 January 2022
doi: 10.3389/fpls.2021.778270

Effective Use of Water in Crop Plants in Dryland Agriculture: Implications of Reactive Oxygen Species and Antioxidative System

Jagadish Rane[1], Ajay Kumar Singh[1], Manish Tiwari[2], P. V. Vara Prasad[2] and S. V. Krishna Jagadish[2]*

[1] ICAR-National Institute of Abiotic Stress Management, Baramati, India, [2] Department of Agronomy, Kansas State University, Manhattan, KS, United States

OPEN ACCESS

Edited by:
Italo F. Cuneo, Pontificia Universidad Católica de Valparaíso, Chile

Reviewed by:
Manzer H. Siddiqui, King Saud University, Saudi Arabia
Paulo Eduardo Ribeiro Marchiori, Universidade Federal de Lavras, Brazil

***Correspondence:**
Jagadish Rane
jagrane@hotmail.com;
jagadish.rane@icar.gov.in

Specialty section:
This article was submitted to Crop and Product Physiology, a section of the journal Frontiers in Plant Science

Received: *16 September 2021*
Accepted: *02 December 2021*
Published: *10 January 2022*

Citation:
Rane J, Singh AK, Tiwari M, Prasad PVV and Jagadish SVK (2022) Effective Use of Water in Crop Plants in Dryland Agriculture: Implications of Reactive Oxygen Species and Antioxidative System. Front. Plant Sci. 12:778270. doi: 10.3389/fpls.2021.778270

Under dryland conditions, annual and perennial food crops are exposed to dry spells, severely affecting crop productivity by limiting available soil moisture at critical and sensitive growth stages. Climate variability continues to be the primary cause of uncertainty, often making timing rather than quantity of precipitation the foremost concern. Therefore, mitigation and management of stress experienced by plants due to limited soil moisture are crucial for sustaining crop productivity under current and future harsher environments. Hence, the information generated so far through multiple investigations on mechanisms inducing drought tolerance in plants needs to be translated into tools and techniques for stress management. Scope to accomplish this exists in the inherent capacity of plants to manage stress at the cellular level through various mechanisms. One of the most extensively studied but not conclusive physiological phenomena is the balance between reactive oxygen species (ROS) production and scavenging them through an antioxidative system (AOS), which determines a wide range of damage to the cell, organ, and the plant. In this context, this review aims to examine the possible roles of the ROS-AOS balance in enhancing the effective use of water (EUW) by crops under water-limited dryland conditions. We refer to EUW as biomass produced by plants with available water under soil moisture stress rather than per unit of water (WUE). We hypothesize that EUW can be enhanced by an appropriate balance between water-saving and growth promotion at the whole-plant level during stress and post-stress recovery periods. The ROS-AOS interactions play a crucial role in water-saving mechanisms and biomass accumulation, resulting from growth processes that include cell division, cell expansion, photosynthesis, and translocation of assimilates. Hence, appropriate strategies for manipulating these processes through genetic improvement and/or application of exogenous compounds can provide practical solutions for improving EUW through the optimized ROS-AOS balance under water-limited dryland conditions. This review deals

with the role of ROS-AOS in two major EUW determining processes, namely water use and plant growth. It describes implications of the ROS level or content, ROS-producing, and ROS-scavenging enzymes based on plant water status, which ultimately affects photosynthetic efficiency and growth of plants.

Keywords: water productivity, antioxidant system, reactive oxygen species, crop plants, drought tolerance

INTRODUCTION

Drought is a challenging natural phenomenon frequently occurring in arid, semiarid, and sub-humid dryland environments. However, agricultural drought is typically defined in terms of soil moisture deficit relative to the needs of crops at particular growth and developmental stages. Drought stress for plants results from insufficient amount of water available for the maintenance of normal physiological processes, such as photosynthesis, respiration, and cell, tissue, organ, and plant homeostasis (Lawas et al., 2019a,b). By adversely affecting vital physiological processes, drought leads to a substantial reduction in the productivity of crops. With the predicted increase in precipitation variability across the globe, the intensity and duration of extreme drought stress are likely to increase, adding more pressure on agri-food systems to meet the increasing demand by a growing population. In countries like India and sub-Saharan Africa, major proportion of the crop production area is drought prone, and drought stress can lead to significant productivity losses in annual and perennial crops (Hyland and Russ, 2019; Choudhury et al., 2021). Nearly 68% of total arable land in India is prone to drought stress due to erratic and irregular rainfall (Das et al., 2020). Similarly, in Africa, about 70% of arable land includes 66% of the cereal-producing area, and 80% of livestock holdings, which are under dryland conditions and prone to drought stress (Morris et al., 2015; Halilou et al., 2020). Not only in underdeveloped or developing countries but also substantial arable areas in developed countries, including the United States (Stewart et al., 2006), Australia (Howden et al., 2014), and Mediterranean regions (Ryan et al., 2006) are prone to drought stress. Recently, a modeling study by Williams et al. (2020) has shown that the period from 2000 to 2018 was the driest phase since the late 1500s, and, consequently, many regions in the United States may be on the verge of entering a mega drought period. Severe drought has already been experienced in western parts of the United States in the last few years. Model projections show robust drying and increases in extreme drought in many regions around the world by the end of the 21st century, including regions in America, Europe, Asia, and Australia (Cook et al., 2020). Hence, sustaining the productivity of crops under drought stress is crucial for income-generating and sustaining livelihoods of farmers across developing and developed countries. Increasing demand for food, with limited resources and predicted adverse effects of climate change, has emphasized the need for sustaining productivity under dryland agriculture. Hence, scientific interventions are necessary to develop and produce genetically improved drought-tolerant crop varieties (Pareek et al., 2020). To achieve targeted levels of drought tolerance, it is necessary to revisit and decipher the mechanisms associated with survival, tolerance, and recovery of drought-affected plants at molecular, cellular, and at the whole plant levels.

To survive under water-limited conditions, crop plants have evolved three different mechanisms, namely escape, avoidance, and tolerance (Kaya and Zeki, 2017; Blumenthal et al., 2020). One of the immediate responses of crops to drought is the partial closure of stomata, which can reduce water loss through transpiration and limit the entry of CO_2 (Ranjbar et al., 2021). Apart from morphological changes in response to drought, several intrinsic molecular mechanisms are activated upon stress signaling and perception. One of the well-established stress responses includes the generation of reactive oxygen species (ROS), such as hydrogen peroxides (H_2O_2), superoxide (O_2^-), hydroxyl radical (OH^-), and singlet oxygen ($^1O_2$) (Srivastava and Suprassana, 2015). ROS production is directly related to stress in plants and leads to membrane damage and subsequent stress signaling (Mishra et al., 2017, 2018). ROS production takes place in the reaction centers of photosystem I (PSI) and PSII in chloroplast thylakoids (Foyer, 2018; Mishra et al., 2021a). ROS species formation is a result of the direct transfer of the excitation energy from chlorophyll to produce singlet oxygen, or by oxygen reduction in the Mehler reaction (Foyer, 2018). In addition to the chloroplast, ROS are generated in mitochondria (Moller et al., 2007), peroxisomes (del Río and López-Huertas, 2016), and even in intercellular space of the cells, the apoplast (Moschou et al., 2008; Miller et al., 2009). Antioxidant system (AOS) is the "first line of defense" against ROS generated by environmental stimuli (Srivastava and Suprassana, 2015). The ROS species are interchangeably produced by redox reactions involving several enzymes. The univalent reduction of O_2^- in the presence of enzyme superoxide dismutase (SOD) produces H_2O_2, and a molecule of oxygen or H_2O_2 in the presence of Fe^{2+} gives rise to hydroxyl radical (Fukai and Ushio-Fukai, 2011). H_2O_2 inactivates most of the enzymes by oxidizing their thiol groups, and, because of its long-life span compared to other ROS (half-life of milliseconds to seconds) (Marinho et al., 2014) and high permeability across membranes, H_2O_2 is considered as a secondary messenger at low concentrations; however, at high concentrations, it causes programmed cell death (Quan et al., 2008; Zheng et al., 2020). H_2O_2 metabolism and signaling cascades play important roles during plant growth and development, such as xylem differentiation, development of root hair, reinforcement of a plant cell wall by structural cross-linking, and loosening, leading to stomatal control (Saxena et al., 2016). Similar to H_2O_2, OH^- free radical can interact with all biological macromolecules and play a signaling role during plant development. The oxidative

power of OH^- is utilized during vegetative growth, reproduction, and adaptation to stress by stomatal closure (Richards et al., 2015). Due to the lack of an enzymatic mechanism, it is hard to eliminate this highly reactive radical, and its enhanced accumulation leads to cell death (Das and Roychoudhury, 2014). The enzymes, namely catalase (CAT), and different types of peroxidases can scavenge H_2O_2 from the cell (Mishra et al., 2021a). Similar to the enzymatic antioxidant defense system, the plant also possesses non-enzymatic antioxidants like carotenoids, flavonoids, and ascorbate, which are synthesized in response to excess light stress and complement the antioxidant enzymes in mitigating ROS (Hatier and Gould, 2008; Agati et al., 2009, 2011). Compounds such as phenylpropanoids have tremendous potential to reduce ROS concentration and are synthesized in response to different abiotic stresses, including drought (Agati and Tattini, 2010; Pollastri and Tattini, 2011; Ding et al., 2021).

It is evident from previous reviews that a lot of knowledge has been generated on ROS-AOS in the context of different stresses, including drought (Henmi et al., 2007; Claeys and Inze, 2013; Song et al., 2014; You and Chan, 2015; Ullah et al., 2017; Devireddy et al., 2020; Hasanuzzaman et al., 2020). In addition, various cellular processes that lead to the generation of ROS and scavenging or detoxification of these deleterious hyper reactive molecules and their relevance to perception of drought stress in crops have been reviewed (Noctor et al., 2014; Verma et al., 2019).

This review complements previous reports and covers the ROS-AOS system in facilitating effective water use (EUW). Furthermore, it provides an optimistic insight into scientific investigations, particularly on critical cellular mechanisms, which can be translated into tools or products for alleviating oxidative stress. We refer to EUW as biomass produced by plants with available water under soil moisture stress rather than per unit of water (WUE). Blum (2009) introduced that EUW implies maximum utilization of soil moisture through transpiration by minimizing direct water loss by soil evaporation or other non-stomatal mechanisms. Thus, EUW-associated traits promise to allow judicious use of the available soil moisture by plant and retaining moisture during critical and sensitive crop growth and development stages. While mining for drought tolerance traits in crops is in progress, considering EUW to complement WUE has been recommended for increased genetic gains and enhanced crop productivity under drought stress (Blum, 2009). Emphasis on EUW is based on the argument that many traits that contribute to WUE come at the cost of plants performance under favorable conditions. It is well-known that stomatal mechanisms that determine water use are influenced by ROS (Noctor et al., 2014). On the other hand, cell division and cell expansion, in addition to photosynthesis, the primary processes of biomass accumulation, are also affected. In this context, we discuss the role of ROS-AOS in two major EUW-determining processes, namely stomatal regulation of water use and plant growth. This review aims to analyze information and knowledge related to ROS-AOS in plants for facilitating EUW, particularly for drought stress management in crops.

INFLUENCE OF REACTIVE OXYGEN SPECIES-ANTIOXIDATIVE SYSTEM ON PLANT PROCESSES

Plant Water Relations

Water stress severely impacts routine plant functionality and triggers molecular, biochemical, morphological, and physiological mechanisms to compensate for water limitation (Mitchell et al., 2013; Lee et al., 2016). Water limitation causes a surge in the production of ROS species such as H_2O_2, and superoxide anion radicals (O_2^-) resulting in lipid peroxidation, reduced photosynthetic capacity (Deeba et al., 2012), enhanced programmed cell death (Gill and Tuteja, 2010), and retarded growth (Wallace et al., 2016). The ROS-scavenging antioxidant enzymes, such as SOD, POD, CAT, glutathione reductase (GR), and ascorbate peroxidase (APX), can be triggered to neutralize excessive ROS accumulation. Alterations in these enzyme activities are the primary pathway in plants for inducing drought stress tolerance (Gill and Tuteja, 2010; Nikoleta-Kleio et al., 2020). ROS-AOS can act through root as well as shoot components, associated with water uptake and transpiration (Zhang et al., 2019). Besides, root and shoot, one of the well-characterized physiological responses under drought stress is ABA-induced leaf stomatal closure (Cruz de Carvalho, 2008). An insight into the diurnal and seasonal implication of such action by ROS-AOS can help us tailor management options to optimize water use by plants. Hence, this section discusses the role of ROS-AOS in processes regulating water relations.

It is well established that water relations at the shoot level are primarily determined by stomatal mechanisms that regulate transpiration. ROS can influence guard cell functions in leaves' in plants, including *Arabidopsis*, bean (*Phaseolus* sp.), and pea (*Pisum* sp.) (Song et al., 2014). Most of the ROS-related actions appear to be associated with abscisic acid (ABA). The phytohormone ABA is synthesized in shoots, roots, particularly in seeds, and leaves (veins, and guard cells) (Boursiac et al., 2013), and plays a critical role in stomatal regulation in response to abiotic stresses. ABA actions involve methyl jasmonate (MeJA), which evokes ROS and NO (nitrous oxide) production in guard cells as shown in *A. thaliana* (Islam et al., 2009; Nazareno and Hernandez, 2017). Zhu et al. (2014) found that disruption of partially redundant Nicotinamide Adenine Dinucleotide Phosphate-reduced form (NADPH) oxidase catalytic subunit genes expressed in guard cells stops Methyl Jasmonate (MeJA)-induced stomatal closure and ROS production. This indicated that the two NADPH oxidases are chief ROS sources in guard cell MeJA signaling. However, it does not cause MeJA-induced cytosolic alkalization in *Arabidopsis* guard cells, suggesting the possible role of MeJA-induced ROS and NO in stomatal closure and drought tolerance (Ye et al., 2013; Nazareno and Hernandez, 2017). Another NADPH oxidase-interacting gene, *OPEN STOMATA 1* (*OST1*), acts upstream of ROS signaling to mediate ABA-induced stomatal closure (Acharya et al., 2013; Ali et al., 2019). The *OST1* regulates ROS generation through direct interaction and phosphorylation of the NADPH oxidase

subunit of RBOHF (respiratory burst oxidase homologs) in *Arabidopsis* (Sirichandra et al., 2009; Han et al., 2019). MeJA also elicits NO production in the guard cells for induction of stomatal closure through the release of Ca^{2+} (Han et al., 2019). Besides NADPH oxidases, other ROS-producing enzymes (cell wall bound-peroxidase and copper amine oxidase) have been shown to regulate stomatal movement (Khokon et al., 2011). Several genes have been characterized, which reveal the role of ROS species in stomatal closure under stress conditions. The RING finger ubiquitin E3 ligase, OsHTAS, can promote H_2O_2-induced stomatal closure, leading to ABA-dependent drought, heat, and salt tolerance (Liu et al., 2016). *Arabidopsis* CYCLIN H;1 (CYCH;1) positively regulates blue light-induced stomatal opening by controlling ROS homeostasis (Zhou et al., 2014). Another critical interaction involved in stomatal closure during drought stress includes biological gas transmitter H_2S (hydrogen sulfide), which promotes *de novo* ABA synthesis and activation of AOS to provide drought stress tolerance in *Arabidopsis* and rice (Jin et al., 2013; Zhou et al., 2020).

Water uptake and transport are the crucial processes determining the use of water by plants. Osmotic and hydrostatic forces are the major determinants of water uptake through the root. Osmotic force results from accumulation of solutes, and, furthermore, addition of root pressure and hydrostatic force produced mainly by transpiration stream drives movement of water (Kim et al., 2018). Adverse effect of ROS on functions of roots, the major component of plant water uptake structure, can negatively influence the water relations in plants (An et al., 2018). Under different abiotic stress conditions, root tissue produces ROS, and, among them, the role of H_2O_2 in root water uptake has been extensively investigated (Boursiac et al., 2008). It is shown that exogenous application of H_2O_2 inhibited cell and root hydraulic conductivity by closing aquaporin pores (Ye and Steudle, 2006) or accumulation of plasma membrane intrinsic proteins (PIPs) in internal structures called vesicles and vacuoles (Boursiac et al., 2008). Lack of function of genes associated with oxidative burst in the root can lead to accumulation of ROS in root vascular system and the xylem vessel of *Arabidopsis* subjected to salinity that creates osmotic stress similar to the one caused by soil moisture stress (Jiang et al., 2012). Production of ROS in maize (*Zea mays*) and *Arabidopsis* roots is associated with wall loosening and growth *via* cell elongation (Mangano et al., 2017). RAC/ROP-regulated production of NADPH-dependent H_2O_2 has been implicated in the secondary cell wall differentiation (Oh et al., 2018). Drought stress tolerance can be achieved by expressing genes involved in enhanced root growth and minimizing ROS levels. In this context, a multiple stress-responsive *WRKY* gene, *GmWRKY27*, interacts with *GmMYB174* to suppress *GmNAC29* expression, resulting in reduced ROS levels. The transgenic hairy roots of soybean (*Glycine max*) overexpressing *GmWRKY27* displayed better root growth and enhanced tolerance to drought and salt stress than control plants (Wang et al., 2015). ROS can act as signals to regulate root hydraulic conductivity under stress conditions and increase or decrease root hydraulic conductivity, depending on the cellular concentration of ROS (Kaneko et al., 2015). This hypothesis is supported by the observations that applying exogenous antioxidants can modify ROS levels and the response of ABA on root hydraulic conductivity (Xu et al., 2015). Additionally, ROS-triggered intracellular trafficking of aquaporin negatively impacts water transport (Boursiac et al., 2008; Quiroga et al., 2018). The effect is caused by direct ROS-mediated closure or by more indirect signaling pathways, and the latter possibly involves salicylic acid (Ye and Steudle, 2006; Boursiac et al., 2008; Quiroga et al., 2018). Apart from ROS-mediated regulation of aquaporins, water transport can also be influenced by the activity of ROS in other pathways involving genes implicated in the regulation of root growth and development under drought stress (Janiak et al., 2015; Dalal et al., 2018). Furthermore, exogenous application of putrescine (Put) exhibited reduced water loss by transpiration and increased drought tolerance. The effect can be attributed to antioxidant or ROS scavenging action in roots and activation of stress-related genes (Alcazar et al., 2010; Mahdavian et al., 2021). Putrescine is also known to alleviate the inhibitory action of aluminum-induced ROS and provide tolerance against excess aluminum and heat stress (Fini et al., 2012; Yu et al., 2019; Kolupaev et al., 2021). Proper functioning of stomata requires coordination between ABA, ROS, and Ca^{2+}-based signaling systems. Alteration in this may disturb the gaseous balance and plant water status, which ultimately affects the photosynthetic efficiency and growth of plants (Srivastava and Suprassana, 2015).

In summary, the ROS-AOS system under water-limited conditions functionally regulates the growth and development of plant organs, including roots and shoots. The stomatal closure in leaves is a crucial process that provides drought tolerance to plants. ROS-mediated actions involving a key player, ABA in its nexus, govern stomatal movements during stress. Not only ABA but another phytohormone MeJA is recruited by ABA to induce ROS machinery and NO production in guard cells, resulting in stomatal closure during drought conditions. NADPH oxidases work under the ABA-MeJA nexus and upstream of ROS system to critically elevate ROS levels under drought. In addition to the effect on aboveground parts, i.e., leaves, ROS-AOS system defines root water uptake and transport functionality under water stress. Interestingly, a large knowledge gap exists in determining the role of ABA-MeJA-NADPH-oxidase circuitry in root tissue to regulate ROS levels. Future studies targeting this regulatory network in root tissue may lead to better water uptake and transport under water-limited conditions. Such regulations, if fine-tuned to extend the availability of water, can extend the life of crop plants till the subsequent spell of water supply either through natural precipitation or life-saving irrigation and, hence, can substantially improve EUW, particularly in the events of mid-season drought

Plant Growth

When subjected to soil moisture stress, generally, plants cease their growth, and much of the plant processes and assimilates are diverted for survival or for ensuring a successful reproductive cycle (Mi et al., 2018; Chadha et al., 2019). This strategy allows plants to save water by reducing the size of leaves associated with transpiration or curtailing the duration of growth to escape

severe stress (Mi et al., 2018). Annual crops are featured by distinct growth phases for vegetative and reproductive stages, often separated by the time of flowering, which is highly critical to adapting to the prevailing environment (Craufurd and Wheeler, 2009). On the other hand, perennials, including forage grasses and fruit crops, have different growing habits where both vegetative and reproductive parts grow simultaneously (Skinner and Moore, 2007). Hence, the time of occurrence of soil moisture stress determines the differences in responses and impacts on biomass production and productivity among these crops (Lelievre et al., 2011). Plant growth, reflected by an increase in biomass, results from a set of primary processes, which include cell division and expansion, assimilate accumulation through photosynthesis, and transport of these assimilates to growing parts (Gonzalez et al., 2013). Any factor influencing these processes favorably or adversely can impact growth and overall productivity. Furthermore, there is ample information about the protective role of different antioxidants in plant growth and development (Henmi et al., 2007).

Reactive oxygen species interacts with key-signaling components like calcium (Ca^{2+}), kinases (CDPKs and MAPKs), cyclic nucleotides, G-proteins, several transcription factors (TFs), and other regulators (Devireddy et al., 2021). The intricate interaction between ROS and these signaling cues orchestrate a cardinal response involving an appropriate molecular, metabolic, and physiological acclimation responses, allowing the plant to survive under adverse environmental conditions (Zhu et al., 2016; Waszczak et al., 2018; Kollist et al., 2019; Zandalinas et al., 2020). The cell division and expansion are critical events of the plant growth process that are often affected by environmental stresses and are under the control of ROS, phytohormones, transcription factors, kinases, and small RNAs (Huang et al., 2019; Mishra et al., 2021b; Tiwari et al., 2021a,b,c). The role of ROS in cell proliferation is also evident from reports that reveal manganese superoxide dismutase (MnSOD) regulating a redox cycle within the cell cycle (Sarsour et al., 2014). Zhang et al. (2013) observed that *OsAPX2*-overexpressing plants were more tolerant to drought stress than wild-type plants at the booting stage, as revealed by a significant increase in spikelet fertility under abiotic stresses. ABA-independent pathways that regulate growth and development of rice (*Oryza sativa*) at both seedling and panicle emergence involve STRESS-RESPONSIVE NAC1 (SNAC1)-regulated downstream *PP2C* genes such as *OsPP18*, which confers drought and oxidative stress tolerance by regulating ROS homeostasis (You et al., 2014). Mitogen-activated protein kinase (MAPK) cascades mediate cell differentiation and development, hormonal activity, and abiotic stress responses (Komis et al., 2018). MAPK kinases have been characterized to impart stress resistance and ROS equilibrium in cotton (*Gossypium* sp.) (Lu et al., 2014) and pepper (*Capsicum* sp.) (Jeong et al., 2020). Overexpression of *GhMKK1* leads to significant accumulation of antioxidant enzymes and enhanced ROS scavenging activities, thereby improving tolerance of tobacco (*Nicotiana* sp.) plants to salt and drought stresses (Lu et al., 2014). During drought, the expression levels of MAPKs, *MdMAPK16-2*, *MdMAPK17*, and *MdMAPK20-1* were elevated compared to those in apple (*Malus domestica*) seedlings under control conditions (Huang et al., 2020). Huang et al. (2020) reported that arbuscular mycorrhizal fungi (AMF) could utilize the MAPKs signaling pathway to enhance drought tolerance by using MAPK signaling as an intermediate pathway for interactions between AMF and their host apple plant. Besides, the extensive role of MAPKs, other kinases such as histidine kinases, CDPKs, leucine-rich repeat-receptor-like kinases, and serine-threonine protein kinases are also at the center of stress tolerance (Mishra et al., 2021a; Tiwari et al., 2021a,b). Early leaf development is regulated by genes-encoding *OsSIK2*, a protein kinase located in rice leaf and sheath plasma membrane. The *OsSIK2* was suggested as a candidate gene for manipulation to facilitate crop improvement. It is hypothesized to integrate stress signals, predictably through ROS, into a developmental program for improved adaptation under stress conditions (Chen et al., 2013). Overexpression of calcium-dependent protein kinase gene, *OsCPK4*, results in increased tolerance to salt and drought stresses in rice plants. This was possibly due to the higher expression of several genes that regulate protection against oxidative stress and lipid metabolism, and thus determining cell membrane stability under stress conditions (Campo et al., 2014). The zinc finger super family transcription factors regulate multiple aspects of plant development and abiotic stress tolerance (Liu et al., 2021). Zinc Finger 2 (SlZF2) is rapidly induced by drought in cultivated tomatoes (*Solanum lycopersicum*), and its ectopic expression provides tolerance against salinity stress (Hichri et al., 2014). The chrysanthemum (*Chrysanthemum grandiflorum*) Zinc Finger Protein 1 (*CgZFP1*) shows enhanced expression under drought and salinity, and its heterologous expression in *Arabidopsis* revealed increased tolerance to both stresses.

The plant response to limited water availability varies with developmental growth stages of plants, which influence the final yield. There is ample evidence to support that ROS-AOS system influences on the cell division and expansion. Furthermore, many of the genes associated with growth and development of plants are linked to ROS-AOS. Some of the key genes include kinases such as MAPKs and those involved in Ca^{2+} signaling. Association of genes with ROS-AOS-mediated control of cell division and expansion could be genetically engineered appropriately to express or silence genes in response to sufficient or deficit soil moisture. Genetically engineered plants employ mechanisms in a way that cell division and expansion are continued or ceased based on water availability to ensure survival and productivity of plants. To counter mid-season dry spells, it would be appropriate to choose plants that have AOS-ROS system and associated traits tuned for survival till the next spell of water supply. Alternatively, exogenous application of ROS-scavenging biostimulants can be recommended as an effective management practice. A combination of the optimized AOS-ROS mechanism and external application of effective biostimulants have the potential to facilitate EUW by plants.

Assimilate Synthesis

Cellular events associated with cell division and expansion are followed by the accumulation of assimilates during the growth

process. Alteration in the photosynthetic process can affect plant growth (Weraduwage et al., 2016). Chloroplast is one of the major sites of ROS production, with photosynthesis affected directly due to the ROS-induced impact on photosynthetic apparatus and indirectly due to altered stomatal mechanisms. The ROS can cause protein breakdown, chlorophyll degradation, and lipid peroxidation in leaves, resulting in a loss of photosynthetic electron transport chain, membrane integrity, and cell death (Slooten et al., 1995; Ekmekci and Terzioglu, 2005). Higher levels of ROS are generated in plants when drought is accompanied with high solar irradiation and temperatures (Munne-Bosch et al., 2001; Jubany-Mari et al., 2010). Damage to cell membranes and reduction in CO_2 intake due to closure of stomata restrict the capacity of plants to use photosynthetically active radiation (PAR) under soil moisture stress (Bota et al., 2004; Flexas et al., 2004; Chaves et al., 2009). This can be prevented by reducing the ROS generation and enhancing the detoxification of ROS (Das and Roychoudhury, 2014). The *OsCPK4* protects cellular membranes from stress-induced oxidative damage and thereby positively regulates salt and drought stress responses in rice (Campo et al., 2014). Previously, attempts have been made to improve the tolerance of plants under various abiotic stresses through protecting photosynthetic machinery by manipulating antioxidant enzymes, including the overexpression of SOD, GR, and dehydroascorbate reductase (DHAR) through genetic engineering (Logan et al., 2006). The strengthening of chloroplast antioxidant defenses could be the key protective mechanism for plant cells toward enhancing abiotic stress tolerance (Mishra et al., 2021b).

Drought-induced loss of chlorophyll accompanied by an elevated ratio of the violaxanthin pigment in chlorophyll effectively helps in mitigating oxidative load in the chloroplast by reduction of light-absorption centers (Brunetti et al., 2018). Carotenoids, particularly xanthophyll pigments, are substantially affected by drought stress, which play an effective role as singlet oxygen scavengers (Krieger-Liszkay, 2005). The ROS-detoxifying antioxidant enzymes and ascorbic acid are upregulated to protect membrane lipids from oxidation (Munne-Bosch et al., 2001; Du et al., 2010). Protection of photosynthetic system against excess H_2O_2 produced by photorespiration during drought was observed in tobacco due to overexpression of gene-coding ascorbate peroxidase (Yan et al., 2003). Mitochondrial Alternative Oxidase (AOX) has been hypothesized to aid photosynthetic metabolism by acting as an additional electron sink for the photogenerated reductant or by dampening ROS generation. This was essential for maintaining photosynthesis under mild drought in *Nicotiana tabacum* (Dahal et al., 2014).

Other metabolites, such as galactinol and raffinose, can function as osmoprotectants in plant cells. Transgenic *Arabidopsis* plants overexpressing galactinol synthases (*GolS1* and *GolS2*) exhibited increased accumulation of these oligosaccharides and increased tolerance to oxidative damage induced upon exposure to chilling and osmotic stress (Nishizawa et al., 2008). Biosynthesis of compatible solute glycinebetaine enhances the tolerance of plants to soil moisture stress (Chen and Murata, 2008). Glycinebetaine synthesis activates ROS-scavenging antioxidant enzymes and thus alleviates oxidative stress. Intriguingly, the elevated levels of glycinebetaine seem to be more effective in the chloroplasts compared to cytosol, indicating its competency to protect the photosynthetic machinery (Chen and Murata, 2008). Trehalose, a non-reducing disaccharide, accumulates to higher levels in some desiccation-tolerant plants like *Myrothamnus flabellifolius* and functions as an osmolyte and stabilizes proteins and membranes (Iordachescu and Imai, 2008).

Chloroplast acts as a site of photosynthesis as well as ROS production. Stress-mediated ROS generation impacts the membrane and also activates signaling related to stomatal closure. Therefore, the site of synthesis and accumulation of photosynthates are consistently associated with ROS-AOS system, which is evident from the literature cited in this section. Drought stress effect on chlorophyll is largely mitigated by accessory pigments, such as carotenoids and violaxanthin. They primarily scavenge ROS molecules to provide membrane stability and protection to maintain pigment system. The challenge is to design strategies at the molecular level to fine-tune best combinations of players for the light-trapping system to cease/decelerate their function when stomata tend to close for saving water. Although such a system might exist in nature, phenotyping methods to identify such genotypes may play a crucial role in improving the photosynthesis per unit available water, ultimately contributing to EUW.

Assimilate Transport

Phloem transport plays an important role in maintaining homeostasis between plant growth and abiotic stress responses by providing an uninterrupted pathway of carbon distribution and signaling to all organs (Dinant and Lemoine, 2010; Ainsworth and Bush, 2011). Hydrostatic pressure gradient between the source and sink organs created during this process drives the mass flow of phloem sap. The phloem transport is maintained by a positive pressure energized and regulated by a dynamic loading between bundle sheath cells at source locations and the sieve element companion cell complex (Orians et al., 2015). The electrical signals involving Ca^{2+}, Cl^{-}, and K^{+} fluxes are transmitted rapidly along the length of the sieve element cell as well as laterally from parenchyma cells to sieve an element *via* companion cells through plasmodesmata (Borges, 2008) in response to stress and ultimately impact mobilization of carbohydrates.

Remobilization of pre-stored carbohydrates from wheat (*Triticum aestivum*) stems to grain results in a significant contribution to yield during terminal drought conditions (Bazargani et al., 2011). Studies conducted to underpin the molecular nexus responsible for stem reserve utilization during drought conditions in two contrasting wheat landraces (N49 and N14) revealed differential expressions of proteins with the highest levels in efficient landrace N49 at 20 days after anthesis. This is in conjunction with active remobilization of dry matter, indicating a probable involvement of these differential proteins in effective stem reserve remobilization in N49 (Bazargani et al., 2011). Furthermore, some proteins associated with this process were

related to oxidative stress defense, suggesting ROS-AOS playing a role in remobilization of stem reserves (Bazargani et al., 2011).

Despite abundant stored reserves in stems, plants may fail to produce grains if environmental stresses affect reproductive organs. The maize transcriptome analysis involving well-watered and drought-treated fertilized ovary and basal leaf meristem tissue displayed a significantly decreased abundance of transcripts involved in the cell cycle and cell division only in the drought-stressed ovary (Kakumanu et al., 2012). Many of the genes were related to sucrose and starch metabolism changes in the ovary, consistent with a decrease in sucrose transporter function and starch levels. Possible mechanisms for adaptive responses included repression of a phospholipase C-mediated signaling pathway, activation of programmed cell death-mediated senescence, and arrest of the cell cycle in the stressed ovary a day after pollination (Kakumanu et al., 2012; Zhang et al., 2017). Furthermore, an elevated invertase level was observed in the stressed leaf meristem, resulting in maintenance of hexose levels at an "unstressed" level in that tissue, accompanied with lower ABA levels, providing drought resistance (Kakumanu et al., 2012). A possible role of ROS-AOS in this process cannot be ruled out as ROS are associated with programmed cell death. Other evidence that hints at the association of ROS-AOS emerges from studies on *AtSUC9*, a gene associated with sucrose transport in the cell. This gene gets induced by low sucrose levels and then mediates the balance of sucrose distribution and promotes ABA accumulation to enhance resistance to abiotic stresses in *Arabidopsis* (Jia et al., 2015). Similarly, the role of carbohydrate metabolism, carbohydrate profile, and sugar cleavage and transport determined pollen sterility in grain sorghum (*Sorghum bicolor*) exposed to heat stress (Jain et al., 2007). Increased membrane damage and enhanced ROS in pollen grains under heat stress result in loss of pollen viability in sorghum (Djanaguiraman et al., 2014). Increased ROS and decreased antioxidant enzymes in pollen and pistils were observed under heat stress in sorghum (Djanaguiraman et al., 2018a) and pearl millet (*Pennisetum glaucum*) (Djanaguiraman et al., 2018b). Impact of heat stress becomes more pronounced in the absence of sufficient soil moisture.

Assimilate transport through phloem directly determines the quantity and quality of yield. Drought stress affects cell division and cell cycle-related genes in addition to starch and sucrose metabolism. Sugar metabolism is required for cell growth, expansion, and division. Thus, ROS-AOS system plays a dual control on plant growth by regulating the cell cycle as well as sugar metabolism. Since there is a possible involvement of ROS-AOS both in assimilate transport from stems to reproductive parts and also in reproductive physiology, it can be hypothesized that these critical aspects of grain developmental process offer new dimension to develop strategies to manage ROS-AOS through genetic improvement or through exogenous application of promising formulations that can quench ROS. The dual regulation of starch metabolism and the cell cycle are very important in pollen or ovary development as these processes depend extensively on cell division as well as cell expansion. Higher EUW can be expected in genotypes identified based on their potential to manage ROS-AOS for facilitating better protection of pollen and ovary, in addition to supporting stem reserve mobilization during reduced soil moisture.

Leaf Senescence

Photosynthesis can also be affected by leaf senescence induced by ROS, depending on the age of the leaf (Rosenwasser et al., 2013). Under limited or excess irradiation, coordinated biochemical, molecular, and physiological processes are required for photosynthetic apparatus acclimation and simultaneous achievement of optimal and effective photosynthetic functioning (Kreslavski et al., 2018). Due to these processes, leaves usually display a high ability to adjust to alteration of microclimate conditions. Leaf senescence is a genetically programmed process that leads to a decline in various cellular processes, including photosynthesis, and involves the remobilization of macromolecules, such as proteins and lipids (Tamary et al., 2019). It is mainly governed by the developmental age and is reprogrammed by environmental stresses, such as drought, salinity, heat, and other stresses. An overview of chloroplast protein degradation during leaf senescence and the roles of ROS has been reviewed earlier (Khanna-Chopra, 2012). Membrane proteins can be crucial as they are involved in leaf senescence through ROS (Jespersen et al., 2015). Genetic modification of genes such as *OsTZF1* could delay leaf senescence as this gene regulates genes associated with the ROS-AOS balance (Maruyama et al., 2013). Stress-induced leaf senescence under heat stress is associated with increased membrane damage, increased ROS, and reduced activity of antioxidant enzymes in soybean (Djanaguiraman and Prasad, 2010; Djanaguiraman et al., 2011) and sorghum (Djanaguiraman et al., 2014). While leaf senescence is an ultimate solution for reducing water loss through transpiration, other mechanisms keep the leaves functional under soil moisture stress. It is speculated that vacuolar phenylpropanoids may act as a secondary antioxidant system, which acts upon the depletion of primary antioxidant defenses to keep whole-cell H_2O_2 within sub-lethal concentration (Fini et al., 2012). The photoprotection mechanism against ROS was more conspicuous in younger than in mature leaves of common figs (*Ficus carica*) in response to a combination of high irradiation ($\sim$1,300 $\mu molm^{-2}$ s^{-1}) and increased temperature ($\sim$35°C) at midday. Photo protective strategies in young leaves enabled them to minimize oxidative damage due to a competent antioxidative system relative to mature leaves (Mlinaric et al., 2016).

As leaves are the sites for photosynthesis as well as ROS production, maintaining a homeostasis during stress determines the survival of plants. There is sufficient evidence to support involvement of ROS in leaf senescence through programmed cell death and cell membrane damage, and hence altering physiological processes and functions in plants. The inherent strategy of plants to survive under drought involves reduction in transpiration through reduced leaf size or load on plants. When inevitable, systematic elimination of older leaves rather than young leaves can substantially contribute to reduction in consumption of water by plants, particularly during terminal drought. Therefore, genetic manipulation of genes for optimized

ROS-AOS functionality and photosynthesis under water-limited conditions is much needed. The strategy should also involve simultaneous facilitation of stem reserve mobilization for grain development in crop plants.

CONCEPTUAL FRAMEWORK OF REACTIVE OXYGEN SPECIES-ANTIOXIDATIVE SYSTEM FOR EFFECTIVE USE OF WATER

We conceptualized that the strategy for enhancing EUW by the plant should prioritize water use-driven biomass production over biomass-driven water use under depleting or restricted soil moisture stress environments. As shown in **Figure 1**, the key components of this strategy should include a fine control over plant structure (shoots and roots), processes such as photosynthesis, cell expansion/proliferation, functions associated with water use, and biomass production. It is well-known that plants avoid water stress by extracting water through need-based extension and architecture of roots, often supported by tissue osmotic adjustment at root and shoot levels (Siddiqui et al., 2021; Strock et al., 2021). On the other hand, plants can save water by stomatal closure, reduced leaf expansion, leaf curling, and leaf rolling (Wang et al., 2020). Therefore, the EUW needs processes and structures that facilitate efficient usage of water that can contribute to survival during stress when soil moisture is deficit and maximum use for biomass production when sufficient water is available (Kosova et al., 2019). The conceptual framework encompasses major water use and growth processes, which is influenced by processes detailed in previous sections. The genes and endogenous substances addressed in this review are not exhaustive; instead, an attempt to reveal integrated ROS-AOS regulation governing adaptive mechanisms in plants exposed to drought has been presented. It needs to be critically examined if ROS-AOS facilitates selective switches for these processes and functions, depending on the type and growing habits of crop plants and the nature of drought stress. We discuss here the possible options for promoting water use-driven biomass production that underpins EUW of crop plants and hence improve productivity under drought stress conditions, such as early drought, mid-season or recurrent, and terminal drought.

Mid-season drought occurs when the depleting soil moisture is not replenished by natural precipitation and in the absence of irrigation. Since planting is carried out by the farmers only when there is optimum moisture in the soil, crop performance depends on the early establishment by utilizing available moisture (Fahad et al., 2017). Plants that develop their canopy rapidly have the advantage of enhancing the effective use of water by reducing moisture loss due to evaporation (Fahad et al., 2017; Sofi et al., 2019). Hence, ROS-mediated switches promoting biomass production processes and their distribution should be critical at the beginning of the soil moisture depletion curve (Laxa et al., 2019). The shoot growth has to be prioritized over roots for ensuring rapid ground cover at this phase to effectively utilize moisture at the top soil, followed by root proliferation to extract soil moisture from deeper layers of the soil profile. This preparedness for risk should be modulated by switches that impart endurance against limited soil moisture until the next opportunity emerges to replenish soil moisture. Under these conditions, cell division could continue, cell expansion could cease, but leaves continue to be functionally active. Plant growth can continue with partial closure of stomata, which facilitates carbon assimilation with minimum water loss (Zhang et al., 2018). This can happen if ROS-AOS switches are regulated to favor processes leading to increased growth under low vapor pressure deficit (VPD) periods within the diurnal cycle. This would induce a favorable response, as inactivation of chloroplast enzymes is known to occur under excess excitation energy, particularly during midday under tropical conditions (Foyer, 2018). Conditions during midday can lead to concomitant exposure to water stress, high sunlight irradiance, and high temperature, which significantly reduce the activity of enzymes aimed at detoxifying H_2O_2 (Sharma and Dubey, 2005; Guidi et al., 2008; Liu et al., 2011; Foyer, 2018; Aliyeva et al., 2020). Hence, an increase in violaxanthin pigments such as zeaxanthin from predawn to midday may avoid ROS generation by enhancing the capacity of thermal dissipation of excess radiant energy in the chloroplast (Kono and Terashima, 2014) and preserve thylakoid membranes from oxidation (Niinemets et al., 2003; Havaux et al., 2007). This may partially counter the depression of antioxidant enzymes activity.

Plants' performance under intermittent drought is determined by water saving for survival and quick recovery after the cessation of drought stress. Roots can absorb water with less restriction early in the day, but the water demand would be greater than the supply during the latter part of the day (Neumann, 2008; Teran et al., 2019). With time, soil moisture is further depleted, and moisture stress tends to occur earlier and with higher intensity, affecting growth until replenishment of soil moisture. Thus, conservation of soil water by reduced transpiration would delay the onset of severe plant water-deficit stress and cessation of growth both diurnally and over a longer time period (Kulkarni et al., 2017). The concept of limited transpiration is based on plants modulation of water use through hydraulic conductivity during the early stages of crop development so that more water is available during the latter phase of the plant growth and development, which are more sensitive to stress conditions (Gholipoor et al., 2010, 2012). It has also been established that the effect of stomatal closure is less on carbon dioxide diffusion into the leaf than on water diffusion out of the leaf (Kono and Terashima, 2014; Qi et al., 2018). In this context, ROS switches need to be explored for promoting inherent or bio-regulator-induced water saving capacity at a critical stress period and efficient water uptake and utilization during favorable conditions. This is crucial for most dryland plants wherein the timing of water stress majorly determines the plant performance compared to the quantity of available water.

Terminal drought at the final stages of annual crops needs strategies that favor functional stay green with delayed senescence (Jagadish et al., 2015). Furthermore, under terminal drought, ROS-AOS is involved in the developmental shift from vegetative

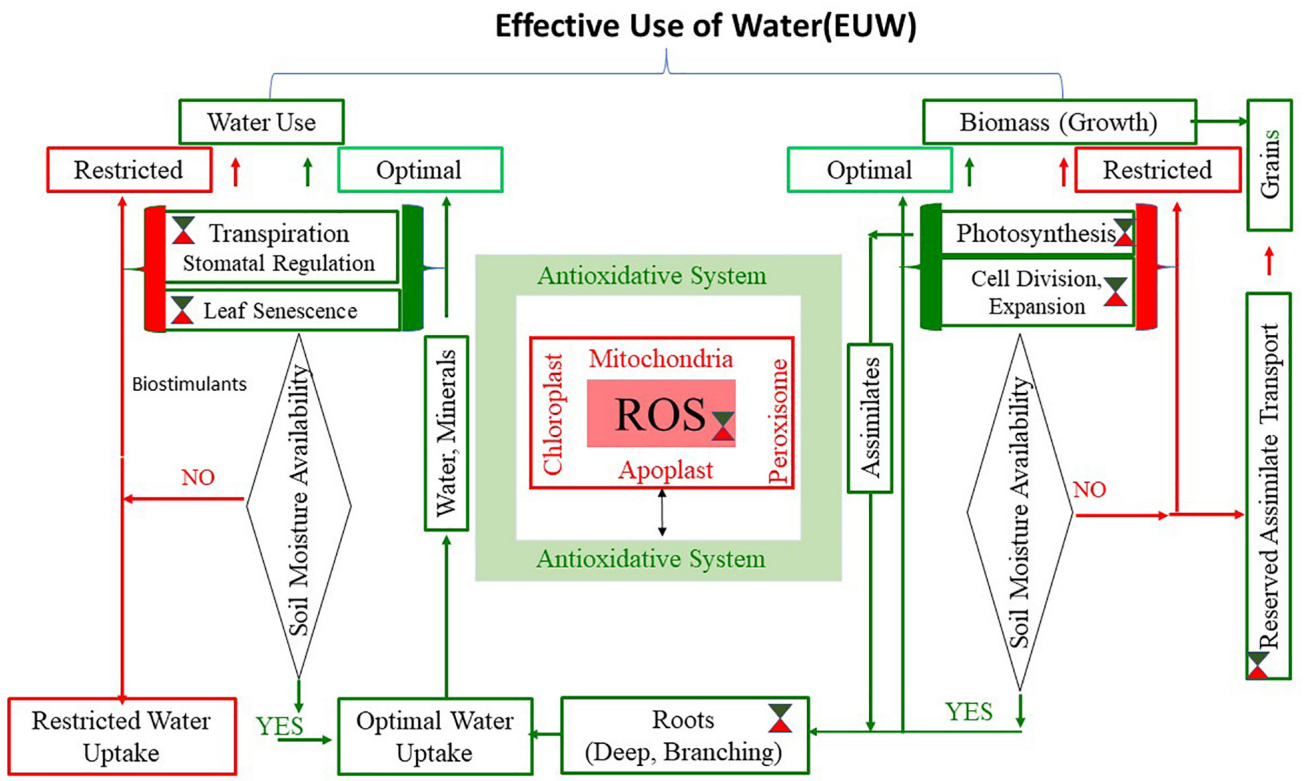

FIGURE 1 | Water use by plants and biomass production are the two major components of Effective Use of Water (EUW). The figure is based on the fact that enhanced EUW is possible if water use by plants drives biomass production rather than biomass produced at a given time drives water use. The implications of reactive oxygen species and anti-oxidative system (ROS-AOS) that operates at mitochondria, chloroplast, peroxisome, and apoplast (shown at the center of the figure) are evident from scientific leads. The green/red symbol (indicates opportunities to use ROS-AOS as feasible switches to put on or off the processes and functions required to achieve high EUW during optimal (green lines) and restricted (red lines) phases of soil moisture regime during the drought cycle. As shown in the **Table 1**, association of ROS-AOS is evident in the stomatal mechanism, water uptake and transport, and leaf senescence, which contribute to water use regulation while photosynthesis, cell division, and expansion assimilate transport, which are all linked with biomass production. Alternatively, exogenous bioactive compounds may be evaluated to get desired effect on each of the components to achieve maximum EUW based on the soil moisture regime, plant growth stage, and nature of drought.

to the reproductive, particularly flowering and grain-filling stages (Jagadish et al., 2015). It is interesting to know that the control over genes (*SOC1* and *FUL*) associated with a shift from the vegetative to reproductive stage in *Arabidopsis* can significantly prolong the lifecycle of the plants, and, often, ROS-AOS is associated with these genes (Melzer et al., 2008; Lens and Melzer, 2012). Another gene, *Ghd7*, has been regarded as a critical regulator of heading date and yield potential in rice. This gene regulates yield traits through modulating panicle branching independent of the heading date. Drought is one among several factors that strongly repress the expression of *Ghd7* that maximizes the reproductive success of the rice plant (Weng et al., 2014). Furthermore, ROS-AOS switches need to be optimized to prevent damages to reproductive organs like pollens and ovules that may occur due to soil moisture stress (Kakumanu et al., 2012). In addition, plants could benefit from the action of ROS-AOS by promoting stem reserves for grain development and delayed senescence of roots for extracting soil moisture from deeper profiles of soil (Jagadish et al., 2015). This is crucial to maintain the normal physiological function of plants to support reproductive growth that can result in higher EUW. Possibilities of achieving this emerge from the fact that ROS-AOS are involved in the accumulation of compounds like oligosaccharides during the stress, which can be diverted for grain growth when photosynthesis ceases due to desiccation in plants (Cui et al., 2020; Ma et al., 2021). Annual crops are likely to benefit from opportunities with favorable periods in a diurnal cycle or intermittent precipitation during their short-life cycle. The physiological and molecular basis of ROS-AOS can help facilitate genetic improvement targeting traits for improved water relations in plants. Furthermore, the enhanced balance of ROS-AOS during critical growth stages can help tolerate drought episodes with minimal impact on biomass or economic yield (Aslam et al., 2015; Fang et al., 2015; Fang and Xiong, 2015; Salehi-Lisar and Bakhshayeshan-Agdam, 2016). The ROS-AOS facilitated acceleration or deceleration of processes associated with water uptake, and tissue water maintenance are crucial for optimum crop productivity under limited water conditions.

The proposed conceptual framework for translating ROS-AOS information for improvement in EUW is based on genetic

TABLE 1 | Some of the ROS-AOS genes associated with processes governing water use and biomass production.

S. No	Gene/ TFs	Mode of action	Plant/ Transformation receptor	References
(A) Genes associated with water use and ROS-AOS: Stomatal closure				
1.	Ca^{2+} ATPase gene (*OsACA6*)	Changes in several physiological indices	Tobacco	Huda et al. (2013)
2.	*OsCPK4* (Calcium dependent protein kinase)	ABA-induced antioxidant defense	Rice	Campo et al. (2014)
3.	*ZmCPK11* (Calcium dependent protein kinase)	Abscisic acid (ABA)-mediated stomatal movement	Maize	Ding et al. (2013)
4.	ZFP36 (abscisic acid (ABA)- and hydrogen peroxide (H_2O_2)-responsive C_2H_2-type ZFP gene)	ABA-induced upregulation of the expression and the activities antioxidant system Regulated by protein kinases (MAPKs) in ABA signaling (ABA-induced antioxidant defense)	Rice	Zhang et al. (2014)
5.	*OsTZF1* (CCCH-type zinc finger gene family)	Induced by abscisic acid, methyl jasmonate, salicylic acid and H_2O_2; Delays leaf senescence	Rice	Jan et al. (2013)
6.	Guard Cell Hydrogen Peroxide-Resistant 1 (GHR1)	ABA and hydrogen peroxide regulated stomatal movement under drought stress	*Arabidopsis* Soybean	Hua et al. (2012) and Tripathi et al. (2016)
7.	Cyclin H-I (CYCH-I)	Positively regulate stomatal opening by controlling ROS homeostasis	*Arabidopsis*	Zhou et al. (2014)
8.	Ring finger ubiquitin E3 ligase (*OsHTAS*)	Stomatal closure and ABA induced drought tolerance	Rice	Liu et al. (2016)
9.	Heme oxygenase (HY1)	ABA hypo/hyper sensitive regulation of stomatal closure	*Arabidopsis*	Xie et al. (2015)
(B) Genes associated with water use and ROS-AOS: Root architecture				
1.	NAC ANAC054/CUC1 (Downregulation)	Shoot apical meristem formation and auxin-mediated lateral root formation	*Arabidopsis*	Balazadeh et al. (2012)
2.	MADS AGL6/RSB1 (Downregulation)	Involved in axillary bud formation; control of flowering time and lateral organ development	*Arabidopsis*	Balazadeh et al. (2012)
3.	MYB MYB2	Inhibits cytokine-mediated branching	*Arabidopsis*	Balazadeh et al. (2012)
4.	Ca^{2+} ATPase gene (*OsACA6*)	Changes in several physiological indices	Tobacco	Huda et al. (2013)
5.	NAC2	Increase in root length	*Arabidopsis*	Gunapati et al. (2016)
(C) Genes associated with water use and ROS-AOS: Leaf senescence				
1.	MYB44	Regulates ethylene signaling	*Arabidopsis*	Balazadeh et al. (2012)
2.	NAC ANAC092/ORE1	Regulator of leaf senescence	*Arabidopsis*	Balazadeh et al. (2012)
3.	*GhTZF1* (cotton CCCH-type tandem zinc finger gene)	Delays leaf senescence by inhibiting reactive oxygen species accumulation	*Arabidopsis*	Zhou et al. (2014)
4.	MYB37/RAX1 (Downregulation)	Regulates axillary meristem formation	*Arabidopsis*	Balazadeh et al. (2012)
5.	*OsTZF1* (CCCH-type zinc finger gene family)	Induced by abscisic acid, methyl jasmonate, salicylic acid and H_2O_2; Delays leaf senescence	Rice	Jan et al. (2013)
6.	SNAC3 (ONAC003, LOC_Os01g09550)	Reduces levels of H_2O_2, malondialdehyde (MDA), and relative electrolyte leakage	Rice	Fang et al. (2015)
7.	Ca^{2+} ATPase gene (*OsACA6*)	Changes in several physiological indices	Tobacco	Huda et al. (2013)
(D) Genes associated with growth and ROS-AOS: Photosynthesis				
1.	NAC ANAC054/CUC1 (Downregulation)	Shoot apical meristem formation and auxin-mediated lateral root formation	*Arabidopsis*	Balazadeh et al. (2012)
2.	MYB37/RAX1 (Downregulation)	Regulates axillary meristem formation	*Arabidopsis*	Balazadeh et al. (2012)

(Continued)

TABLE 1 | (Continued)

S. No	Gene/ TFs	Mode of action	Plant/ Transformation receptor	References
3.	MYB44	Regulates ethylene signaling	*Arabidopsis*	Balazadeh et al. (2012)
4.	NAC ANAC092/ORE1	Regulator of leaf senescence	*Arabidopsis*	Balazadeh et al. (2012)
5.	*GhTZF1* (cotton CCCH-type tandem zinc finger gene)	Delays leaf senescence by inhibiting reactive oxygen species accumulation	*Arabidopsis*	Zhou et al. (2014)
6.	HB (HB2/HAT4)	Involved in cell expansion and cell proliferation	*Arabidopsis*	Balazadeh et al. (2012)
7.	(NAC) ANAC068	Mediates cytokine signaling during cell division	*Arabidopsis*	Balazadeh et al. (2012)
8.	(*PsAOX1* gene) Alternate oxidase gene	Regulated ROS by affecting alternate oxidase pathways	Pea	Dinakar et al. (2016)
9.	Ca^{2+} ATPase gene (*OsACA6*)	Changes in several physiological indices	Tobacco	Huda et al. (2013)
10.	*OsCPK4* (Calcium dependent protein kinase)	ABA-induced antioxidant defense	Rice	Campo et al. (2014)
11.	SNAC3 (ONAC003, LOC_Os01g09550)	Reduces levels of H_2O_2, malondialdehyde (MDA), and relative electrolyte leakage	Rice	Fang et al. (2015)
(E) Genes associated with growth and ROS-AOS: Cell division and expansion				
1.	Ca^{2+}ATPase gene *(OsACA6*)	Changes in several physiological indices	Tobacco	Huda et al. (2013)
2.	MYB MYB37/RAX1 (Downregulation)	Regulates axillary meristem formation	*Arabidopsis*	Keller et al. (2006)
3.	NAC ANAC054/CUC1 (Downregulation)	Shoot apical meristem formation and auxin-mediated lateral root formation	*Arabidopsis*	Balazadeh et al. (2012)
4.	HB (HB2/HAT4)	Involved in cell expansion and cell proliferation	*Arabidopsis*	Balazadeh et al. (2012)
5.	(NAC) ANAC068	Mediates cytokinin signaling during cell division	*Arabidopsis*	Balazadeh et al. (2012)
6.	KUODA1 (KUA1)	Leaf development, decreases peroxidase activity	*Arabidopsis*	Lu et al. (2014)
7.	SNAC3 (ONAC003, LOC_Os01g09550)	Reduces levels of H_2O_2, malondialdehyde (MDA), and relative electrolyte leakage	Rice	Fang et al. (2015)
8.	*OsCPK4* (Calcium dependent protein kinase)	ABA-induced antioxidant defense	Rice	Campo et al. (2014)
(F) Genes associated with growth and ROS-AOS: Shift from vegetative to reproductive phase				
1.	MADS AGL6/RSB1 (Downregulation)	Involved in axillary bud formation; control of flowering lateral organ development	*Arabidopsis*	Balazadeh et al. (2012)
2.	MYB21	Petal and stamen development	*Arabidopsis*	Balazadeh et al. (2012)
3.	SEP2/AGL4 (Downregulation)	Flower and ovule development	*Arabidopsis*	Balazadeh et al. (2012)
4.	SEP1/AGL2 (Downregulation)	Flower and ovule development	*Arabidopsis*	Balazadeh et al. (2012)
5.	AP2/EREBP (RAV2/TEM2)	Repressor of flowering	*Arabidopsis*	Balazadeh et al. (2012)
6.	(NAC) ANAC089	Negative regulator of floral initiation	*Arabidopsis*	Balazadeh et al. (2012)
7.	AP2/EREBP (SNZ)	Represses flowering	*Arabidopsis*	Balazadeh et al. (2012)
8.	ABI3/VP1 AP2/B3-like	Seed development	*Arabidopsis*	Balazadeh et al. (2012)
9.	MADS SEP2/AGL4 (Downregulation)	Flower and ovule development	*Arabidopsis*	Balazadeh et al. (2012)

(Continued)

TABLE 1 | (Continued)

S. No	Gene/ TFs	Mode of action	Plant/ Transformation receptor	References
10.	MADS SEP1/AGL2 (Downregulation)	Involved in flower and ovule development	*Arabidopsis*	Balazadeh et al. (2012)
11.	WRKY51	Repression of jasmonate-mediated signaling	*Arabidopsis*	Balazadeh et al. (2012)
12.	WRKY25	Involved in response to various abiotic stresses	*Arabidopsis*	Balazadeh et al. (2012)
13.	SgNCED1	ABA-induced antioxidant defense (Drought and salt stress)	*Arabidopsis*	Zhang et al. (2009)
14.	*TaOPR1* (12-oxo-phytodienoic acid reductases)	ABA-induced antioxidant defense	*Arabidopsis*	Dong et al. (2013)
15.	Anther gene (Ghd7)	Regulates heading and yield potential	Rice	Weng et al. (2014)

improvement and traits identification that can alleviate stress. In addition to scientific leads that have emerged from physiological an molecular biology investigation on the role of ROS-AOS (**Table 1**) and access to evidence-based genetic variability is crucial for genetic improvement of tolerance of crop plants to abiotic stresses. Genetic variability in ROS production has been reported in grass species (Jespersen et al., 2015) and doubled haploid maize (Darko et al., 2009). Furthermore, genes identified through single-nucleotide polymorphism (SNP) and methylated quantitative trait locus (MQTL) approaches for genetic improvement of abiotic stress tolerance in wheat include those associated with scavenging of ROS and abscisic-acid-induced stomatal closure (Acuna-Galindo et al., 2015). Identified MQTL and candidate genes should be targeted for future studies and genetic improvement of abiotic stress tolerance. Recently, it has been observed that genes inhibiting anthocyanin synthesis at short high light exposure lose their action after prolonged exposure of plants to high light intensity, suggesting that these mechanisms might be facilitating acclimation to oxidative stress (Viola et al., 2016). Levels of antioxidants can be enhanced by silencing genes such as *OsSRFP*, which codes for stress-related RING Finger Protein 1 in rice (Fang et al., 2015; Fang and Xiong, 2015), and this can contribute to drought stress tolerance. Elevated antioxidant capacity may contribute to the paraquat tolerance of the paraquat-selected DH2 lines, and *in vitro* microspore selection represents a potential way to improve oxidative stress tolerance in maize (Darko et al., 2009).

Among the endogenous substances that can alleviate oxidative stress, polyamines such as putrescine reduce ROS activity in roots of red kidney bean (*Phaseolus vulgaris*) and alleviate Al-induced inhibition of root elongation. This was mediated by inhibition of NADPH oxidase activity (Wang et al., 2013), suggesting that deeper understanding of ROS-AOS switches can help in identifying useful bioregulators to achieve desired results in promoting EUW. Anthocyanins protect plant tissues against excess light and ROS by absorbing light and thus reducing the amount of energy that reaches the photosynthetic apparatus. Therefore, bio-regulators that promote anthocyanin production or protection can possess the potential to alleviate the soil moisture stress that accompanies exposure to high light (Hughes et al., 2013). Anthocyanins may also act as antioxidant compounds in plants since they are ROS scavengers (Nakabayashi et al., 2014).

Possibilities of employing ROS-AOS insights for management of drought are evident from a series of recent studies conducted with biostimulants in crops, including tomato (Casadesús et al., 2019; Antonucci et al., 2021, Francesca et al., 2021), capsicum (Agliassa et al., 2021), soybean (do Rosário Rosa et al., 2021), and lettuce (Zhou et al., 2022). Exogenous application of 16 tannin-based biostimulants having antioxidant properties improved root system architecture of tomato under salt stress (Campobenedetto et al., 2021). Additionally, *Late embryogenesis abundant protein (LEA) family proteins* were found to be upregulated, which are associated with water-limited stress tolerance. Thus, osmotic stress in crop plants can be managed, and this could be extended to managing drought stress. A commercial glycine-betaine-based biostimulant improved EUW in tomato under water stress condition. Moreover, elicitation of stress priming through induction of H_2O_2-mediated antioxidant mechanisms was suggested as one of the primary reasons behind the beneficial effect (Antonucci et al., 2021). Antioxidant properties of biostimulants are attributed to improvement in crop productivity under water stress (Malik et al., 2021). Studies reveal the potential of timely application of biostimulants (depending on the growth stage) either through foliar approaches or fertigation to improve drought tolerance. These recommendations can immensely help in improving effective use of water, as biostimulants can improve tolerance to water-deficit conditions and also facilitate recovery from drought stress.

WAY FORWARD

This review is central to contemporary demand for scientific interventions that can improve productivity of dryland crops, particularly when various environmental constraints challenge food security of millions of people. Dryland agriculture

will play an increasingly important role in meeting food security challenges (Ng et al., 2012; Temam et al., 2019), mainly because of two reasons: First, only about 7% of the agricultural land across the world is equipped with irrigation (FAO et al., 2019), and the substantial remaining proportion of the area depends on rains and provides an opportunity to use technological advances to enhance productivity and support the most vulnerable populations; second, the world's supply of freshwater for irrigation is insufficient to meet the targeted food production with current technology. Therefore, any technological interventions that can enhance the productivity of crops under limited water stress conditions will be critical to drylands that routinely encounter varying levels of drought stress (Rao and Gopinath, 2016; Rane and Minhas, 2017; Zuniga et al., 2021). Variability rather than the amount of total rainfall determines crop growth, development, and yield under dryland conditions. Therefore, we need location-specific drought-adaptive mechanisms or traits to develop crop varieties with improved resilience. In this context, adaptive mechanisms based on ROS-AOS are perceived to play important roles due to their involvement in almost all growth, development, and yield-determining processes throughout the crop growth cycle. Genotypes are known to differ in their response to drought stress, including the production of ROS and AOS mechanisms. Targeted traditional and molecular breeding programs using both conventional and novel genomic tools are essential to enhance drought-tolerant genotypes and hybrids in major food crops and address food and nutritional security around the world.

Knowing the ubiquitous and complex nature of ROS-AOS in plants (Noctor et al., 2014), it is important to advance scientific investigations in optimizing ROS-AOS under severe drought stress conditions to facilitate EUW in both annuals and perennial crops under dryland and rainfed environments. The majority of damage and losses in dryland are due to time and duration of occurrence rather than net soil moisture throughout the crop season. Therefore, fine-tuning of ROS-AOS mechanisms either genetically or through exogenous application of bio-regulators can help in optimizing the use of water for biomass production, crucial for maintaining productivity of crops. Such suggestions derive support from the evidence that the antioxidant machinery of plants can be more effective under mild than severe stress conditions (Guidi et al., 2011). A lot of promise emerges from the fact that several master regulators controlling the balance between growth and survival have been identified. Possibilities of association of ROS and antioxidant systems through these regulators have been predicted but are yet to be experimentally elucidated. If proven, this can open up new opportunities to promote plant growth and development without compromising on protective tolerance mechanisms (Claeys and Inze, 2013). Hence, it is necessary to explore the possibilities of exogenous bioregulators to ensure need-based neutralization of apoplastic-ROS that accumulate outside the cell membrane during drought. The need may be to reduce transpiration loss of water for survival of perennial fruits crops during prolonged drought or to keep the leaves of annuals photosynthetically and physiologically functional under mild stress. This will help promote rapid recovery after the stress is released or to provide sufficient time for assimilate transport to developing grains as stem reserve mobilization is crucial for grain growth (Bazargani et al., 2011; Jagadish et al., 2015). The role of optimized ROS-AOS in processes associated with the transport of assimilates in plants needs to be further investigated. Drought has been reported to either enhance or depress the activity of antioxidant enzymes, depending on species, genotypes, and stress severity (Ren et al., 2007; Liu et al., 2011; Oladosu et al., 2019). The issue of osmotic stress-induced changes in antioxidant enzymes activity and low molecular weight antioxidants, such as ascorbic acid, needs to be elucidated.

Novel findings from the leaf level under controlled environment have to be validated at the whole plant level in crops under field conditions as expression of transcripts depends on growth conditions as illustrated in case of inhibition of cell death-inducing genes such as LESION SIMULATING DISEASE 1 (LSD1) null mutant (lsd1), which are shown to improve tolerance to combined drought and high-light stress in *Arabidopsis* (Wituszynska et al., 2013). Furthermore, it is necessary to elucidate the role of such genes with those associated with apoptosis or phenoptosis, where the programmed death of cells, organs or organisms occurs (Skulachev and Skulachev, 2018). Furthermore, the control over genes such as *SOC1* and *FUL* associated with a shift from vegetative to the reproductive stage that prolongs the lifecycle of the plants through ROS-AOS needs attention. It is hypothesized that regulation of such genes may help accelerate or delay the leaf senescence based on the time of occurrence of the drought stress in the life cycle of plants. Despite the lack of significant links at the cellular level for the execution of several functions for appropriately manipulating the ROS-AOS, there are ample indications of its involvement in water use and growth (**Table 1**). This new knowledge and understanding provide the platform for an optimistic approach for effective scientific intervention for managing crops under dryland conditions through genetic improvement of crop adaptation through bioactive compounds, or a combination of both, for mitigating water-stress-induced loss in crop productivity.

AUTHOR CONTRIBUTIONS

JR, AS, SJ, and PP: conceptualization, review of literature, and preparation of manuscript. MT: review of literature. All authors contributed to the article and approved the submitted version.

FUNDING

JR and AS acknowledge the support extended by the ICAR-NICRA (Project No. OXX01737) and ICAR-NIASM. The authors also acknowledge the support provided by the DBT-BBSRC project, Contribution No. 22-085-J from the Kansas Agricultural Experiment Station.

REFERENCES

Acharya, B. R., Jeon, B. B., Zhang, W., and Assmann, S. M. (2013). Open stomata 1 (OST1) is limiting in abscisic acid responses of Arabidopsis guard cells. *New Phytol.* 200, 1049–1063. doi: 10.1111/nph.12469

Acuna-Galindo, M. A., Mason, R. E., Subramanian, N. K., and Hays, D. B. (2015). Meta-analysis of wheat QTL regions associated with adaptation to drought and heat stress. *Crop Sci.* 55, 477–492. doi: 10.2135/cropsci2013.11.0793

Agati, G., and Tattini, M. (2010). Multiple functional roles of flavonoids in photoprotection. *New Phytol.* 186, 786–793. doi: 10.1111/j.1469-8137.2010.03269.x

Agati, G., Biricolti, S., Guidi, L., Ferrini, F., Fini, A., and Tattini, M. (2011). The biosynthesis of flavonoids is enhanced similarly by UV radiation and root zone salinity in L. vulgare leaves. *Plant Physiol.* 168, 204–212. doi: 10.1016/j.jplph.2010.07.016

Agati, G., Stefano, G., Biricolti, S., and Tattini, M. (2009). Mesophyll distribution of 'antioxidant' flavonoids glycosides in *Ligustrum vulgare* leaves under contrasting sunlight irradiance. *Ann. Bot.* 104, 853–861. doi: 10.1093/aob/mcp177

Agliassa, C., Mannino, G., Molino, D., Cavalletto, S., Contartese, V., Bertea, C. M., et al. (2021). A new protein hydrolysate-based biostimulant applied by fertigation promotes relief from drought stress in *Capsicum annuum* L. *Plant Physiol. Biochem.* 166, 1076–1086. doi: 10.1016/j.plaphy.2021.07.015

Ainsworth, E. A., and Bush, D. R. (2011). Carbohydrate export from the leaf: a highly regulated process and target to enhance photosynthesis and productivity. *Plant Physiol.* 155, 64–69. doi: 10.1104/pp.110.167684

Alcazar, R., Planas, J., Saxena, T., Zarza, X., Bortolotti, C., Cuevas, J., et al. (2010). Putrescine accumulation confers drought tolerance in transgenic Arabidopsis plants over-expressing the homologous Arginine decarboxylase 2 gene. *Plant Physiol. Biochem.* 48, 547–552. doi: 10.1016/j.plaphy.2010.02.002

Ali, A., Kim, J. K., Jan, M., Haris, H. A., Khan, I. U., Shen, M., et al. (2019). Rheostatic control of ABA signaling through HOS15-Mediated OST1 degradation. *Mol. Plant.* 12, 1447–1462. doi: 10.1016/j.molp.2019.08.005

Aliyeva, D. R., Aydinli, L. M., Zulfugarov, I. S., and Huseynova, I. M. (2020). Diurnal changes of the ascorbate-glutathione cycle components in wheat genotypes exposed to drought. *Funct. Plant Biol.* 47, 998–1006. doi: 10.1071/FP19375

An, J., Cheng, C., Hu, Z., Chen, H., Cai, W., and Yu, B. (2018). The Panax ginseng PgTIP1 gene confers enhanced salt and drought tolerance to transgenic soybean plants by maintaining homeostasis of water, salt ions and ROS. *Environ. Exp. Bot.* 155, 45–55.

Antonucci, G., Croci, M., Miras-Moreno, B., Fracasso, A., and Amaducci, S. (2021). Integration of gas exchange with metabolomics: high-throughput phenotyping methods for screening biostimulant-elicited beneficial responses to short-term water deficit. *Front. Plant Sci.* 12:678925. doi: 10.3389/fpls.2021.678925

Aslam, M., Maqbool, M. A., and Cengiz, R. (2015). *Drought Stress in Maize (Zea mays L.): Effects, Resistance Mechanism, Global Achievements and Biological Strategies for Improvement*, 74. doi: 10.1007/978-3-319-25442-5

Balazadeh, S., Jaspert, N., Arif, M., Mueller-Roeber, B., and Maurino, V. G. (2012). Expression of ROS-responsive genes and transcription factors after metabolic formation of H2O2 in chloroplasts. *Front. Plant Sci.* 3:234. doi: 10.3389/fpls.2012.00234

Bazargani, M. M., Sarhadi, E., Bushehri, A. A. S., Matros, A., and Mock, H. P. (2011). A proteomics view on the role of drought-induced senescence and oxidative stress defense in enhanced stem reserves remobilization in wheat. *J. Proteomics* 74, 1959–1973. doi: 10.1016/j.jprot.2011.05.015

Blum, A. (2009). Effective use of water (EUW) and not water-use efficiency (WUE) is the target of crop yield improvement under drought stress. *Field Crops Res.* 112, 119–123.

Blumenthal, D. M., Mueller, K. E., Kray, J. A., Ocheltree, T. W., Augustine, D. J., and Wilcox, K. R. (2020). Traits link drought resistance with herbivore defence and plant economics in semi-arid grasslands: the central roles of phenology and leaf dry matter content. *J. Ecol.* 108, 2336–2351. doi: 10.1111/1365-2745.13454

Borges, R. M. (2008). Plasticity comparisons between plants and animals: concepts and mechanisms. *Plant Signal. Behav.* 36, 367–375. doi: 10.4161/psb.3.6.5823

Bota, J., Medrano, H., and Flexas, J. (2004). Is photosynthesis limited by decreased rubisco activity ad RuBP content under progressive water stress? *New Phytol.* 162, 671–681. doi: 10.1111/j.1469-8137.2004.01056.x

Boursiac, Y., Boudet, J., Postaire, O., Luu, D. T., Tournaire-Roux, C., and Maurel, C. (2008). Stimulus-induced down regulation of root water transport involves reactive oxygen species-activated cell signaling and plasma membrane intrinsic protein internalization. *Plant Physiol.* 56, 207–218. doi: 10.1111/j.1365-313X.2008.03594.x

Boursiac, Y., Leran, S., Corratge-Faillie, C., Gojon, A., Krouk, G., and Lacombe, B. (2013). ABA transport and transporters. *Trends Plant Sci.* 18, 325–333. doi: 10.1016/j.tplants.2013.01.007

Brunetti, C., Loreto, F., Ferrini, F., Guidi, L., Remorini, D., et al. (2018). Metabolic plasticity in the hygrophyte *Moringa oleifera* exposedto water stress. *Tree Physiol.* 38, 1640–1654. doi: 10.1093/treephys/tpy089

Campo, S., Baldrich, P., Messeguer, J., Lalanne, E., Coca, M., and San Segundo, B. (2014). Overexpression of a calcium-dependent protein kinase confers salt and drought tolerance in rice by preventing membrane lipid peroxidation. *Plant Physiol.* 165, 688–704. doi: 10.1104/pp.113.230268

Campobenedetto, C., Mannino, G., Beekwilder, J., Contartes, V., Karlova, R., Bertea, C. M., et al. (2021). The application of a biostimulant based on tannins affects root architecture and improves tolerance to salinity in tomato plants. *Sci. Rep.* 11:354. doi: 10.1038/s41598-020-79770-5

Casadesús, A., Polo, J., and Munné-Bosch, S. (2019). Hormonal effects of an enzymatically hydrolyzed animal protein-based biostimulant (pepton) in water-stressed tomato plants. *Front. Plant Sci.* 10:953. doi: 10.3389/fpls.2019.00758

Chadha, A., Florentine, S. K., Chauhan, B. S., Long, B., and Jayasundera, M. (2019). Influence of soil moisture regimes on growth, photosynthetic capacity, leaf biochemistry and reproductive capabilities of the invasive agronomic weed; Lactucaserriola. *PLoS One* 14:e0218191. doi: 10.1371/journal.pone.0218191

Chaves, M. M., Flexas, J., and Pinheiro, C. (2009). Photosynthesis under drought and salt stress: regulation mechanisms from whole plant to cell. *Ann. Bot.* 103, 551–560. doi: 10.1093/aob/mcn125

Chen, L.-J., Wuriyanghan, H., Zhang, Y. Q., Duan, K. X., Chen, H. W., Li, Q. T., et al. (2013). An S-domain receptor-like kinase, OsSIK2, confers abiotic stress tolerance and delays dark-induced leaf senescence in rice. *Plant Physiol.* 163, 1752–1765. doi: 10.1104/pp.113.224881

Chen, T. H., and Murata, N. (2008). Glycinebetaine: an effective protectant against abiotic stress in plants. *Trends Plant Sci.* 13, 499–505. doi: 10.1016/j.tplants.2008.06.007

Choudhury, A., Dutta, D., Bera, D., and Kundu, A. (2021). Regional variation of drought parameters and long-term trends over India using standardized precipitation evapotranspiration index. *J. Environ. Manag.* 296:113056. doi: 10.1016/j.jenvman.2021.113056

Claeys, H., and Inze, D. (2013). The agony of choice: how plants balance growth and survival under water-limiting conditions. *Plant Physiol.* 162, 1768–1779. doi: 10.1104/pp.113.220921

Cook, B. I., Mankin, J. S., Marvel, K., Williams, A. P., Smerdon, J. E., and Anchukaitis, K. J. (2020). Twenty-first century drought projections in the CMIP6 forcing scenarios. *Earths Future* 8:e2019EF00161.

Craufurd, P. Q., and Wheeler, T. R. (2009). Climate change and the flowering time of annual crops. *J. Exp. Bot.* 60, 2529–2539. doi: 10.1093/jxb/erp196

Cruz, and de Carvalho, M. H. (2008). Drought stress and reactive oxygen species: production, scavenging and signalling. *Plant Signal. Behav.* 3, 156–165. doi: 10.4161/psb.3.3.5536

Cui, J., Sun, T., Chen, L., and Zhang, W. (2020). Engineering salt tolerance of photosynthetic cyanobacteria for seawater utilization. *Biotechnol. Adv.* 43:107578. doi: 10.1016/j.biotechadv.2020.107578

Dahal, K., Wang, J., Martyn, G. D., Rahimy, F., and Vanlerberghe, G. C. (2014). Mitochondrial alternative oxidase maintains respiration and preserves photosynthetic capacity during moderate drought in *Nicotiana tabacum*. *Plant Physiol.* 166, 1560–1574. doi: 10.1104/pp.114.247866

Dalal, M., Sahu, S., Tiwari, S., Rao, A. R., and Gaikwad, K. (2018). Transcriptome analysis reveals interplay between hormones, ROS metabolism and cell wall biosynthesis for drought-induced root growth in wheat. *Plant Physiol. Biochem.* 130, 482–492. doi: 10.1016/j.plaphy.2018.07.035

Darko, E., Ambrus, H., Fodor, J., Kiraly, Z., and Barnabas, B. (2009). Enhanced tolerance to oxidative stress with elevated antioxidant capacity in doubled haploid maize derived from microspores exposed to paraquat. *Crop Sci.* 49, 628–639.

Das, J., Jha, S., and Goyal, M. K. (2020). Non-stationery and copula-based approach to assess the drought characteristics encompassing climate indices over the Himalayan states in India. *J. Hydrol.* 580:124356. doi: 10.1016/j.jhydrol.2019.124356

Das, K., and Roychoudhury, A. (2014). Reactive oxygen species (ROS) and response of antioxidants as ROS-scavengers during environmental stress in plants. *Front. Environ. Sci.* 2:53.

Deeba, F., Pandey, A. K., Ranjan, S., Mishra, A., Singh, R., Sharma, Y. K., et al. (2012). Physiological and proteomic responses of cotton (*Gossypium herbaceum* L.) to drought stress. *Plant Physiol. Biochem.* 53, 6–18. doi: 10.1016/j.plaphy.2012.01.002

del Río, L. A., and López-Huertas, E. (2016). ROS generation in peroxisomes and its role in cell signaling. *Plant Cell Physiol.* 57, 1364–1376. doi: 10.1093/pcp/pcw076

Devireddy, A. R., Arbogast, J., and Mittler, R. (2020). Coordinated and rapid whole-plant systemic stomatal responses. *New Phytol.* 225, 21–25. doi: 10.1111/nph.16143

Devireddy, A. R., Zandalinas, S. I., Fichman, Y., and Mittler, R. (2021). Integration of reactive oxygen species and hormone signaling during abiotic stress. *Plant J.* 105, 459–476. doi: 10.1111/tpj.15010

Dinakar, C., Vishwakarma, A., Raghavendra, A. S., and Padmasree, K. (2016). Alternative oxidase pathway optimizes photosynthesis during osmotic and temperature stress by regulating cellular ROS, malate valve and antioxidative systems. *Front. Plant Sci.* 7:68. doi: 10.3389/fpls.2016.00068

Dinant, S., and Lemoine, R. (2010). The phloem pathway: new issues and old debates. *C. R. Biol.* 333, 307–319. doi: 10.1016/j.crvi.2010.01.006

Ding, X., Zhu, X., Zheng, W., Li, F., Xiao, S., and Duan, X. (2021). BTH treatment delays the senescence of postharvest Pitaya fruit in relation to enhancing antioxidant system and phenylpropanoid Pathway. *Foods* 10:846. doi: 10.3390/foods10040846

Ding, Y., Cao, J., Ni, L., Zhu, Y., Zhang, A., Tan, M., et al. (2013). ZmCPK11 is involved in abscisic acid-induced antioxidant defence and functions upstream of ZmMPK5 in abscisic acid signaling in maize. *J. Exp. Bot.* 64, 871–884. doi: 10.1093/jxb/ers366

Djanaguiraman, M., and Prasad, P. V. V. (2010). Ethylene production under high temperature stress causes premature leaf senescence. *Func. Plant Biol.* 37, 1071–1084.

Djanaguiraman, M., Perumal, R., Ciampitti, I. A., Gupta, S. K., and Prasad, P. V. V. (2018a). Quantifying pearl millet response to high temperature stress: thresholds, sensitive stages, genetic variability and relative sensitivity of pollen and pistil. *Plant Cell Environ.* 41, 993–117. doi: 10.1111/pce.12931

Djanaguiraman, M., Perumal, R., Jagadish, S. K., Ciampitti, I. A., and Prasad, P. V. V. (2018b). Sensitivity of sorghum pollen and pistil to high-temperature stress. *Plant Cell Environ.* 41, 1065–1082. doi: 10.1111/pce.13089

Djanaguiraman, M., Prasad, P. V. V., and Al-Khatib, K. (2011). Ethylene perception inhibitor 1-MCP decreases oxidative damage of leaves through enhanced oxidant defense mechanisms in soybean plants grown under high temperature stress. *Environ. Exp. Bot.* 71, 215–223. doi: 10.1016/j.envexpbot.2010.12.006

Djanaguiraman, M., Prasad, P. V. V., Murugan, M., Perumal, R., and Reddy, U. K. (2014). Physiological differences among sorghum (*Sorghum bicolor* L. Moench) genotypes under high temperature stress. *Environ. Exp. Bot.* 100, 43–54. doi: 10.1016/j.envexpbot.2013.11.013

do Rosário Rosa, V., Farias dos Santos, A. L., Alves da Silva, A., Sab, M. P. V., Germino, G. H., and Cardoso, F. B. (2021). Increased soybean tolerance to water deficiency through biostimulant based on fulvic acids and *Ascophyllum nodosum* (L.) seaweed extract. *Plant Physiol. Biochem.* 158, 228–243. doi: 10.1016/j.plaphy.2020.11.008

Dong, W., Wang, M., Xu, F., Quan, T., Peng, K., Xiao, L., et al. (2013). Wheat oxophytodienoate reductase geneTaOPR1 confers salinity tolerance via enhancement of abscisic acid signalling and reactive oxygen species scavenging. *Plant Physiol.* 161, 1217–1228. doi: 10.1104/pp.112.211854

Du, H., Wang, N., Cui, F., Li, X., Xiao, J., and Xiong, L. (2010). Characterization of the carotene hydroxylase gene DSM2 conferring drought and oxidative stress resistance by increasing the xanthophylls and abscisic acid synthesis in rice. *Plant Physiol.* 154, 1304–1318. doi: 10.1104/pp.110.163741

Ekmekci, Y., and Terzioglu, S. (2005). Effects of oxidative stress induced by paraquat on wild and cultivated wheat. *Pestic. Biochem. Physiol.* 83, 69–81. doi: 10.1016/j.pestbp.2005.03.012

Fahad, S., Bajwa, A. A., Nazir, U., Anjum, S. A., Farooq, A., Zophaib, A., et al. (2017). Crop production under drought and heat stress: plant responses and management options. *Front. Plant Sci.* 8:1147. doi: 10.3389/fpls.2017.01147

Fang, Y., and Xiong, L. (2015). General mechanisms of drought response and their application in drought resistance improvement in plants. *Cell Mol. Life Sci.* 72, 673–689. doi: 10.1007/s00018-014-1767-0

Fang, Y., Liao, K., Du, H., Xu, Y., Song, H., Li, X., et al. (2015). A stress- responsive NAC transcription factor SNAC3 confers heat and drought tolerance through modulation of reactive oxygen species in rice. *J. Exp. Bot.* 66, 6803–6817. doi: 10.1093/jxb/erv386

FAO, IFAD, UNICEF, WFP, and WHO (2019). *The State of Food Security and Nutrition in the World 2019. Safeguarding Against Economic Slowdowns and Downturns*. Rome: FAO.

Fini, A., Guidi, L., Ferrini, F., Brunetti, C., Ferdinando, M. D., Biricolti, S., et al. (2012). Drought stress has contrasting effects on antioxidant enzymes activity and phenylpropanoid biosynthesis in *Fraxinus ornus* leaves: an excess light stress affair? *Plant Physiol.* 169, 929–939. doi: 10.1016/j.jplph.2012.02.014

Flexas, J., Bota, J., Loreto, F., Cornic, G., and Sharkey, T. D. (2004). Diffusive and metabolic limitations to photosynthesis under drought and salinity in C3 plants. *Plant Biol.* 6, 269–279. doi: 10.1055/s-2004-820867

Foyer, C. H. (2018). Reactive oxygen species, oxidative signaling and the regulation of photosynthesis. *Environ. Exp. Bot.* 154, 134–142. doi: 10.1016/j.envexpbot.2018.05.003

Francesca, S., Cirillo, V., Raimondi, G., Maggio, A., Barone, A., and Rigano, M. M. (2021). A novel protein hydrolysate-based biostimulant improves tomato performances under drought stress. *Plants* 10:783. doi: 10.3390/plants10040783

Fukai, T., and Ushio-Fukai, M. (2011). Superoxide dismutases: role in redox signaling, vascular function, and diseases. *Antioxid. Redox Signal.* 15, 1583–1606. doi: 10.1089/ars.2011.3999

Gholipoor, M., Prasad, P. V. V., Mutava, R. N., and Sinclair, T. R. (2010). Genotypic variability of transpiration response to vapor pressure deficit among sorghum genotypes. *Field Crop Res.* 119, 85–90.

Gholipoor, M., Sinclair, T. R., and Prasad, P. V. V. (2012). Genotypic variation within sorghum for transpiration response to drying soils. *Plant Soil* 357, 35–40. doi: 10.1007/s11104-012-1140-8

Gill, S. S., and Tuteja, N. (2010). Reactive oxygen species and antioxidant machinery in abiotic stress tolerance in crop plants. *Plant Physiol. Biochem.* 48, 909–930. doi: 10.1016/j.plaphy.2010.08.016

Gonzalez, A., Castro, J., Vera, J., and Moenne, A. (2013). Seaweed oligosaccharides stimulate plant growth by enhancing carbon and nitrogen assimilation, basal metabolism, and cell division. *J. Plant Growth Regul.* 32, 443–448. doi: 10.1007/s00344-012-9309-1

Guidi, L., Degl'IE, Remorini, D., Massai, R., and Tattini, M. (2008). Interaction of water stress and solar irradiance on the physiology and biochemistry of *Ligustrum vulgare*. *Tree Physiol.* 28, 873–883. doi: 10.1093/treephys/28.6.873

Guidi, L., Degl'Innocenti, E., Carmassi, G., Massa, D., and Pardossi, A. (2011). Effects of boron on leaf chlorophyll fluorescence of greenhouse tomato grown with saline water. *Environ. Exp. Bot.* 73, 57–63. doi: 10.1016/j.envexpbot.2010.09.017

Gunapati, S., Naresh, R., Ranjan, S., Nigam, D., Hans, A., Verma, P. C., et al. (2016). Expression of GhNAC2 from G. herbaceum, imparts root growth and imparts tolerance to drought in transgenic cotton and Arabidopsis. *Sci. Rep.* 6:24978.

Halilou, O., Assefa, Y., Falalou, H., Abdou, H., Achirou, B. F., Karami, S. M. A., et al. (2020). Agronomic performance of pearl millet genotypes under variable phosphorus, water, and environmental regimes. *Agrosys. Geosci. Environ.* 3:e20131.

Han, J.-P., Koster, P., Drerup, M. M., Scholz, M., Li, S., Edel, K. H., et al. (2019). Fine-tuning of RBOHF activity is achieved by differential phosphorylation and Ca2+ binding. *New Phytol.* 221, 1935–1949. doi: 10.1111/nph.15543

Hasanuzzaman, M., Bhuyan, M. H. M. B., Zulfiqar, F., Raza, A., Mohsin, S. M., Mahmud, J. A., et al. (2020). Reactive oxygen species and antioxidant defense in plants under abiotic stress: revisiting the crucial role of a universal defense regulator. *Antioxidants* 9:681. doi: 10.3390/antiox9080681

Hatier, J. H. B., and Gould, K. S. (2008). Foliar anthocyanins as modulators of stress signals. *Theor. Biol.* 253, 625–627. doi: 10.1016/j.jtbi.2008.04.018

Havaux, M., Dall', O. L., and Bassi, R. (2007). Zeaxanthin has enhanced antioxidant capacity with respect to all other xanthophylls in Arabidopsis leaves and

functions independent of binding to PSII antennae. *Plant Physiol.* 145, 1506–1520. doi: 10.1104/pp.107.108480

Henmi, K., Yanagida, M., and Ogawa, K. (2007). Role of reactive oxygen species and glutathione in plant development. *Plant. Dev. Biol.* 1, 185–210.

Hichri, I., Muhovski, Y., Žižková, E., Dobrev, P. I., Franco-Zorrilla, J. M., Solano, R., et al. (2014). The Solanum lycopersicum Zinc finger2 cysteine-2/histidine-2 repressor-like transcription factor regulates development and tolerance to salinity in tomato and Arabidopsis. *Plant Physiol.* 164, 1967–1990. doi: 10.1104/pp.113.225920

Howden, M., Schroeter, S., Crimp, S., and Hanigan, I. (2014). The changing roles of science in managing Australian droughts: an agricultural perspective. *Weather Clim. Extrem.* 3, 80–89. doi: 10.1016/j.wace.2014.04.006

Hua, D., Wang, C., He, J., Liao, H., Duan, Y., Zhu, Z., et al. (2012). A plasma membrane receptor kinase, GHR1, mediates abscisic acid- and hydrogen peroxide regulated stomatal movement in Arabidopsis. *Plant Cell* 24, 2546–2561. doi: 10.1105/tpc.112.100107

Huang, D., Ma, M. N., Wang, Q., Zhang, M. X., Jing, G. Q., Li, C., et al. (2020). Arbuscular mycorrhizal fungi enhanced drought resistance in apple by regulating genes in the MAPK pathway. *Plant Physiol. Biochem.* 149, 245–255. doi: 10.1016/j.plaphy.2020.02.020

Huang, H., Ullah, F., Zhou, D.-X., Yi, M., and Zhao, Y. (2019). Mechanisms of ROS regulation of plant development and stress responses. *Front. Plant Sci.* 10:800. doi: 10.3389/fpls.2019.00800

Huda, K. M., Banu, M. S., Garg, B., Tula, S., Tuteja, R., and Tuteja, N. (2013). OsACA6, a P-type IIB Ca2+ ATPase promotes salinity and drought stress tolerance in tobacco by ROS scavenging and enhancing the expression of stress-responsive genes. *Plant J.* 76, 997–1015. doi: 10.1111/tpj.12352

Hughes, N. M., Carpenter, K. L., and Cannon, J. G. (2013). Estimating contribution of anthocyanin pigments to osmotic adjustment during winter leaf reddening. *J. Plant Physiol.* 170, 230–233. doi: 10.1016/j.jplph.2012.09.006

Hyland, M., and Russ, J. (2019). Water as destiny – the long-term impacts of drought in sub-Saharan Africa. *World Dev.* 115, 30–45. doi: 10.1016/j.worlddev.2018.11.002

Iordachescu, M., and Imai, R. (2008). Trehalose biosynthesis in response to abiotic stresses. *J. Integr. Biol.* 50, 1223–1229. doi: 10.1111/j.1744-7909.2008.00736.x

Islam, M. M., Tani, C., Watanabe-Sugimoto, M., Uraji, M., Jahan, M. S., Masuda, C., et al. (2009). Myrosinases, TGG1 and TGG2, redundantly function in ABA and MeJA signaling in Arabidopsis guard cells. *Plant Cell Physiol.* 50, 1171–1175. doi: 10.1093/pcp/pcp066

Jagadish, S. V. K., Kishor, P. B. K., Bahuguna, R. N., von Wiren, N., and Sreenivasulu, N. (2015). Alive or going to die during terminal senescence - an enigma surrounding yield stability. *Front. Plant Sci.* 6:1070. doi: 10.3389/fpls.2015.01070

Jain, M., Prasad, P. V. V., Boote, K. J., Allen, L. H. Jr., and Chourey, P. S. (2007). Effect of season-long high temperature growth conditions on sugar-to-starch metabolism in developing microspores of grain sorghum (*Sorghum bicolor* L. Moench). *Planta* 227, 67–79. doi: 10.1007/s00425-007-0595-y

Jan, A., Maruyama, K., Todaka, D., Kidokoro, S., Abo, M., Yoshimura, E., et al. (2013). OsTZF1, a CCCH-Tandem zinc finger protein, confers delayed senescence and stress tolerance in rice by regulating stress-related genes. *Plant Physiol.* 161, 1202–1216.

Janiak, A., Kwaśniewski, M., and Szarejko, I. (2015). Gene expression regulation in roots under drought. *J. Exp Bot.* 67, 1003–1014. doi: 10.1093/jxb/erv512

Jeong, S., Lim, C. W., and Lee, S. C. (2020). The pepper MAP Kinase CaAIMK1 positively regulates ABA and drought stress responses. *Front. Plant Sci.* 11:720. doi: 10.3389/fpls.2020.00720

Jespersen, D., Xu, C., and Huang, B. (2015). Membrane proteins associated with heat-induced leaf senescence in a cool-season grass species. *Crop Sci.* 55, 10–11.

Jia, W., Lijun, Z., Di, W., Shan, L., Xue, G., Zhenhai, C., et al. (2015). Sucrose transporter AtSUC9 mediated by a low sucrose level is involved in Arabidopsis abiotic stress resistance by regulating sucrose distribution and ABA accumulation. *Plant Cell Physiol.* 56, 1574–1587. doi: 10.1093/pcp/pcv082

Jiang, C., Belfield, E. J., Mithani, A., Visscher, A., Ragoussis, J., Mott, R., et al. (2012). ROS-mediated vascular homeostatic control of root-to-shoot soil Na delivery in Arabidopsis. *EMBO J.* 31, 4359–4370. doi: 10.1038/emboj.2012.273

Jin, Z., Xue, S., Luo, Y., Tian, B., Fang, H., Li, H., et al. (2013). Hydrogen sulfide interacting with abscisic acid in stomatal regulation responses to drought stress in Arabidopsis. *Plant Physiol. Biochem.* 62, 41–46. doi: 10.1016/j.plaphy.2012.10.017

Jubany-Mari, T., Prielsen, E., Munne-Bosch, S., and Alegre, L. (2010). The timing of methyl jasmonate, hydrogen peroxide and ascorbate accumulation during water deficit and subsequent recovery in the Mediterranean shrub *Cistus albidus* L. *Environ. Exp. Bot.* 69, 47–55. doi: 10.1016/j.envexpbot.2010.02.003

Kakumanu, A., Ambavaram, M. M. R., Klumas, C., Krishnan, A., Batlang, U., Myers, E., et al. (2012). Effects of drought on gene expression in maize reproductive and leaf meristem tissue revealed by RNA-Seq. *Plant Physiol.* 160, 846–867. doi: 10.1104/pp.112.200444

Kaneko, T., Horie, T., Nakahara, Y., Tsuji, N., Shibasaka, M., and Katsuhara, M. (2015). Dynamic regulation of the root hydraulic conductivity of barley plants in response to salinity/osmotic stress. *Plant Cell Physiol.* 56, 875–882. doi: 10.1093/pcp/pcv013

Kaya, K., and Zeki, Y. (2017). Gene regulation network behind drought escape, avoidance and tolerance strategies in black poplar (*Populus nigra* L.). *Plant Physiol. Biochem.* 115, 183–199. doi: 10.1016/j.plaphy.2017.03.020

Keller, T., Abbott, J., Moritz, T., and Doerner, P. (2006). *Arabidopsis* REGULATOR OF AXILLARY MERISTEMS1controls a leaf axil stem cell niche and modulates vegetative development. *Plant Cell* 18, 598–611. doi: 10.1105/tpc.105.038588

Khanna-Chopra, R. (2012). Leaf senescence and abiotic stresses share reactive oxygen species-mediated chloroplast degradation. *Protoplasma* 249, 469–481. doi: 10.1007/s00709-011-0308-z

Khokon, A. R., Okuma, E., Hossain, M. A., Munemasa, S., Uraji, M., Nakamura, Y., et al. (2011). Involvement of extracellular oxidative burst in salicylic acid-induced stomatal closure in Arabidopsis. *Plant Cell Environ.* 34, 434–443. doi: 10.1111/j.1365-3040.2010.02253.x

Kim, Y. X., Ranathunge, K. R., Lee, S., Lee, Y., Lee, D., and Sung, J. (2018). Composite transport model and water and solute transport across plant roots: an update. *Front. Plant Sci.* 9:193. doi: 10.3389/fpls.2018.00193

Kollist, H., Zandalinas, S. I., Sengupta, S., Nuhkat, M., Kangasjärvi, J., and Mittler, R. (2019). Rapid responses to abiotic stress: priming the landscape for the signal transduction network. *Trends Plant Sci.* 24, 25–37. doi: 10.1016/j.tplants.2018.10.003

Kolupaev, Y. E., Kokorev, A. I., Shkliarevskyi, M. A., Lugovaya, A. A., Karpets, V., Ivanchenko, E., et al. (2021). Role of NO synthesis modification in the protective effect of putrescine in wheat seedlings subjected to heat stress. *Appl. Biochem. Microbiol.* 57, 384–391.

Komis, G., Samajová, O., Ovecka, M., and Samaj, J. (2018). Cell and developmental biology of plant mitogen-activated protein kinases. *Annu. Rev. Plant Biol.* 69, 237–265. doi: 10.1146/annurev-arplant-042817-040314

Kono, M., and Terashima, I. (2014). Long-term and short-term responses of the photosynthetic electron transport to fluctuating light. *J. Photochem. Photobiol. B Biol.* 137, 89–99. doi: 10.1016/j.jphotobiol.2014.02.016

Kosova, K., Vítámvás, P., Klíma, M., and Prášil, I. T. (2019). Breeding drought-resistant crops: G×E interactions, proteomics and pQTLS. *J. Exp. Bot.* 70, 2605–2608. doi: 10.1093/jxb/erz116

Kreslavski, V. D., Los, D. A., Schmitt, F.-J., Zharmukhamedov, S. K., Kuznetsov, V. V., and Allakhverdiev, S. I. (2018). The impact of the phytochromes on photosynthetic processes. *Biochim. Biophys. Acta Bioenergy* 1859, 400–408. doi: 10.1016/j.bbabio.2018.03.003

Krieger-Liszkay, A. (2005). Singlet oxygen production in photosynthesis. *J. Exp. Bot.* 56, 337–346.

Kulkarni, M., Soolanayakanahally, R., Ogawa, S., Uga, Y., Selvaraj, M. G., and Kagale, S. (2017). Drought response in wheat: key genes and regulatory mechanisms controlling root system architecture and transpiration efficiency. *Front. Chem.* 5:106. doi: 10.3389/fchem.2017.00106

Lawas, L. M. F., Erban, A., Kopka, J., Jagadish, S. V. K., Zuther, E., and Hincha, D. K. (2019a). Metabolic responses of rice source and sink organs during recovery from combined drought and heat stress in the field. *Gigascience* 8:giz102. doi: 10.1093/gigascience/giz102

Lawas, L. M. F., Li, X., Erban, A., Kopka, J., Jagadish, S. V. K., Zuther, E., et al. (2019b). Metabolic responses of rice cultivars with different tolerance to combined drought and heat stress under field conditions. *Gigascience* 8:giz050. doi: 10.1093/gigascience/giz050

Laxa, M., Liebthal, M., Telman, W., Chibani, K., and Dietz, K. J. (2019). The role of the plant antioxidant system in drought tolerance. *Antioxidants* 8:94. doi: 10.3390/antiox8040094

Lee, D. K., Jung, H., Jang, G., Jeong, J. S., Kim, Y. S., Ha, S. H., et al. (2016). Overexpression of the OsERF71 transcription factor alters rice root structure and drought resistance. *Plant Physiol.* 172, 575–588. doi: 10.1104/pp.16.00379

Lelievre, F., Seddaiu, G., Ledda, L., Porqueddu, C., and Volaire, F. (2011). Water use efficiency and drought survival in Mediterranean perennial forage grasses. *Field Crops Res.* 121, 333–342. doi: 10.1016/j.fcr.2010.12.023

Lens, F., and Melzer, S. (2012). Stem anatomy supports *Arabidopsis thaliana* as a model for insular woodiness. *New Phytol.* 193, 12–17. doi: 10.1111/j.1469-8137.2011.03888.x

Liu, C., Liu, Y., Guo, K., Fan, D., Li, G., Zheng, Y., et al. (2011). Effect of drought on pigments, osmotic adjustment and antioxidant enzymes in six woody plant species in karst habitats of southwestern China. *Environ. Exp. Bot.* 71, 174–183.

Liu, H., Yang, Y., and Zhang, L. (2021). Zinc finger-homeodomain transcriptional factors (ZF-HDs) in wheat (*Triticum aestivum* L.): identification, evolution, expression analysis and response to abiotic stresses. *Plants* 10:593. doi: 10.3390/plants10030593

Liu, J., Zhang, C., Wei, C., Liu, X., Wang, M., Yu, F., et al. (2016). The ring finger ubiquitin E3 ligase oshtas enhances heat tolerance by promoting H2O2-induced stomatal closure in rice. *Plant Physiol.* 170, 429–443. doi: 10.1104/pp.15.00879

Logan, B. A., Kornyeyev, D., Hardison, J., and Holaday, A. S. (2006). The role of antioxidant enzymes in photoprotection. *Photosynthesis Res.* 88, 119–132.

Lu, D., Wang, T., Persson, S., Mueller-Roeber, B., and Schippers, J. H. M. (2014). Transcriptional control of ROS homeostasis by KUODA1 regulates cell expansion during leaf development. *Nat. Commun.* 5:3767. doi: 10.1038/ncomms4767

Ma, S., Lv, J., Li, X., Ji, T., Zhang, Z., and Gao, L. (2021). Galactinol synthase gene 4 (CsGolS4) increases cold and drought tolerance in *Cucumis sativus* L. by inducing RFO accumulation and ROS scavenging. *Environ. Exp. Bot.* 185:104406. doi: 10.1016/j.envexpbot.2021.104406

Mahdavian, M., Sarikhani, H., Hadadinejad, M., and Dehestani, A. (2021). Exogenous application of putrescine positively enhances the drought stress response in two citrus rootstocks by increasing expression of stress-related genes. *J. Soil Sci. Plant Nutr.* 20, 244–252.

Malik, A., Mor, V. S., Tokas, J., Punia, H., Malik, S., Malik, K., et al. (2021). Biostimulant-treated seedlings under sustainable agriculture: a global perspective facing climate change. *Agronomy* 2021:14. doi: 10.3390/agronomy11010014

Mangano, S., Paola, S., Juarez, D., Cho, H. S., Marzol, E., Hwang, Y., et al. (2017). Molecular link between auxin and ROS-mediated polar growth. *Proc. Natl. Acad. Sci.* 114, 5289–5294. doi: 10.1073/pnas.1701536114

Marinho, H. S., Real, C., Cyrne, L., Soares, H., and Antunes, F. (2014). Hydrogen peroxide sensing, signaling and regulation of transcription factors. *Redox Biol.* 2, 535–562. doi: 10.1016/j.redox.2014.02.006

Maruyama, J. A., Todaka, K., Kidokoro, D., Abo, S., Yoshimura, M., Shinozaki, E., et al. (2013). OsTZF1, a CCCH-tandem zinc finger protein, confers delayed senescence and stress tolerance in rice by regulating stress-related genes. *Plant Physiol.* 161, 1202–1216. doi: 10.1104/pp.112.205385

Melzer, S., Lens, F., Gennen, J., Vanneste, S., Rohde, A., and Beeckman, T. (2008). Flowering-time genes modulate meristem determinacy and growth form in *Arabidopsis thaliana*. *Nat. Genet.* 40, 1489–1492. doi: 10.1038/ng.253

Mi, N., Cai, F., Zhang, Y., Ji, R., Zhang, S., and Wang, Y. (2018). Differential responses of maize yield to drought at vegetative and reproductive stages. *Plant Soil Environ.* 64, 260–267. doi: 10.1007/s10142-021-00773-0

Miller, G., Suzuki, N., Ciftci-Yilmaz, S., and Mittler, R. (2009). Reactive oxygen species homeostasis and signaling during drought and salinity stresses. *Plant Cell Environ.* 33, 453–467. doi: 10.1111/j.1365-3040.2009.02041.x

Mishra, D., Shekhar, S., Agrawal, L., Chakraborty, S., and Chakraborty, N. (2017). Cultivar-specific high temperature stress responses in bread wheat (*Triticum aestivum* L.) associated with physicochemical traits and defense pathways. *Food Chem.* 221, 1077–1087. doi: 10.1016/j.foodchem.2016.11.053

Mishra, D., Shekhar, S., Chakraborty, S., and Chakraborty, N. (2021a). Wheat 2-Cys peroxiredoxin plays a dual role in chlorophyll biosynthesis and adaptation to high temperature. *Plant J.* 105, 1374–1389. doi: 10.1111/tpj.15119

Mishra, D., Suri, G. S., Kaur, G., and Tiwari, M. (2021b). Comprehensive analysis of structural, functional, and evolutionary dynamics of Leucine Rich Repeats-RLKs in Thinopyrumelongatum. *Intl. J. Biol. Macromol.* 183, 513–527. doi: 10.1016/j.ijbiomac.2021.04.137

Mishra, D., Shekhar, S., Singh, D., Chakraborty, S., and Chakraborty, N. (2018). "Heat shock proteins and abiotic stress tolerance in plants," in *Regulation of Heat Shock Protein Responses. Heat Shock Proteins*, Vol 13, eds A. Asea and P. Kaur (Cham: Springer).

Mitchell, P. J., O'Grady, A. P., Tissue, D. T., White, D. A., Ottenschlaeger, M. L., and Pinkard, E. A. (2013). Drought response strategies define the relative contributions of hydraulic dysfunction and carbohydrate depletion during tree mortality. *New Phytol.* 197, 862–872. doi: 10.1111/nph.12064

Mlinaric, S., Antunović, D. J., Štolfa, I., Cesar, V., and Lepeduš, H. (2016). High irradiation and increased temperature induce different strategies for competent photosynthesis in young and mature fig leaves. *S. Afr. Bot.* 103, 25–31.

Moller, I. M., Jensen, P. E., and Hanson, A. (2007). Oxidative modifications to cellular components in plants. *Annu. Rev. Plant Biol.* 58, 459–481. doi: 10.1146/annurev.arplant.58.032806.103946

Morris, M., Raffaello, C., Zhe, G., and Jawoo, K. (2015). "The central role of drylands in Africa's development challenge," in *Confronting Drought in Africa's Drylands: Opportunities for Enhancing Resilience*, eds R. Cervigni and M. Morris (Washington, DC: International Bank for Reconstruction and Development).

Moschou, P. N., Paschalidis, K. A., Delis, I. D., Andripoulou, A. H., Lagiotis, G. D., Yakomakis, D. L., et al. (2008). Spermidine exodus and oxidation in the apoplast induced by abiotic stress is responsible for H2O2 signatures that direct tolerance response in tobacco. *Plant Cell* 20, 1708–1724. doi: 10.1105/tpc.108.059733

Munne-Bosch, S., Jubany-Mari, T., and Alegre, L. (2001). Drought-induced senescence is characterized by a loss of antioxidant defences in chloroplasts. *Plant Cell Environ.* 24, 1319–1327.

Nakabayashi, R., Yonekura-Sakakibara, K., UranoK, Suzuki, M., Yamada, Y., Nishizawa, T., et al. (2014). Enhancement of oxidative and drought tolerance in Arabidopsis by overaccumulation of antioxidant flavonoids. *Plant J.* 77, 367–379. doi: 10.1111/tpj.12388

Nazareno, A. L., and Hernandez, B. S. (2017). A mathematical model of the interaction of abscisic acid, ethylene and methyl jasmonate on stomatal closure in plants. *PLoS One* 12:e0171065. doi: 10.1371/journal.pone.0171065

Neumann, P. M. (2008). Coping mechanisms for crop plants in drought-prone environments. *Ann. Bot.* 101, 901–907. doi: 10.1093/aob/mcn018

Ng, J. P., Hollister, E. B., Gonzalez-Chavez, M. C. A., Hons, F. M., Zuverer, D. A., Aitkenhead-Peterson, J. A., et al. (2012). Impacts of cropping systems and long-term tillage on soil microbial population levels and community composition in dryland agricultural setting. *Intl. Scholarly Res. Network* 2012, 1–11.

Niinemets, U., Kollist, H., Garcia-Plazaola, J. I., Hernandez, A., and Becerril, J. M. (2003). Do the capacity and kinetics for modification of xanthophyll cycle pool size depend on growth irradiance in temperate trees? *Plant Cell Environ.* 26, 1787–1801.

Nikoleta-Kleio, D., Theodoros, D., and Roussos, P. A. (2020). Antioxidant defense system in young olive plants against drought stress and mitigation of adverse effects through external application of alleviating products. *Sci. Hortic.* 259:108812.

Nishizawa, A., Yabuta, Y., and Shigeoka, S. (2008). Galactinol and raffinose constitute a novel function to protect plants from oxidative damage. *Plant Physiol.* 147, 251–1263. doi: 10.1104/pp.108.122465

Noctor, G., Mhamdi, A., and Foyer, C. H. (2014). The roles of reactive oxygen metabolism in drought: not so cut and dried. *Plant Physiol.* 164, 1636–1648. doi: 10.1104/pp.113.233478

Oh, E., Seo, P. J., and Kim, J. (2018). Signaling peptides and receptors coordinating plant root development. *Trend. Plant Sci.* 23, 337–351. doi: 10.1016/j.tplants.2017.12.007

Oladosu, Y., Rafii, M. Y., Samuel, C., Fatai, A., Magaji, U., Kareem, I., et al. (2019). Drought resistance in rice from conventional to molecular breeding: a review. *Int. J. Mol. Sci.* 20:3519. doi: 10.3390/ijms20143519

Orians, C. M., Babst, B., and Zanne, A. E. (2015). "Vascular constraints and long distance transport in dicots," in *Physiological Ecology, Vascular Transport in Plants*, eds N. M. Holbrook and M. A. Zwieniecki (Cambridge, MA: Academic Press).

Pareek, A., Dhankher, O. P., and Foyer, C. H. (2020). Mitigating the impact of climate change on plant productivity and ecosystem sustainability. *J. Exp. Bot.* 71, 451–456. doi: 10.1093/jxb/erz518

Pollastri, S., and Tattini, M. (2011). Flavonols: old compounds for old roles. *Ann. Bot.* 108, 1225–1233. doi: 10.1093/aob/mcr234

Qi, J., Song, C. P., Wang, B., Zhou, J., Kangasjärvi, J., Zhu, J. K., et al. (2018). Reactive oxygen species signaling and stomatal movement in plant responses to drought stress and pathogen attack. *J. Integr. Plant Biol.* 60, 805–826. doi: 10.1111/jipb.12654

Quan, L. J., Zhang, B., Shi, W. W., and Li, H. Y. (2008). Hydrogen peroxide in plants: a versatile molecule of the reactive oxygen species network. *J. Integr. Plant Biol.* 50, 2–18. doi: 10.1111/j.1744-7909.2007.00599.x

Quiroga, G., Erice, G., Aroca, R., Zamarreño, A. M., García-Mina, J. M., and Ruiz-Lozano, J. M. (2018). Arbuscular mycorrhizal symbiosis and salicylic acid regulate aquaporins and root hydraulic properties in maize plants subjected to drought. *Agric. Water Manag.* 202, 271–284. doi: 10.1016/j.agwat.2017.12.012

Rane, J., and Minhas, P. S. (2017). "Agriculture drought management options: scope and opportunities," in *Abiotic Stress Management for Resilient Agriculture*, eds P. Minhas, J. Rane, and R. Pasala (Singapore: Springer).

Ranjbar, A., Imani, A., Piri, S., and Abdossi, V. (2021). Drought effects on photosynthetic parameters, gas exchanges and water use efficiency in almond cultivars on different rootstocks. *Plant Physiol. Rep.* 26, 95–108. doi: 10.1007/s40502-021-00568-2

Rao, C. S., and Gopinath, K. A. (2016). Resilient rainfed technologies for drought mitigation and sustainable food security. *Mausam* 67, 169–182.

Ren, J., Dai, W., Xuan, Z., Yao, Y., Korpelainen, H., and Li, C. (2007). The effect of drought and enhanced UV-B radiation on the growth and physiological traits of two contrasting poplar species. *Forest Ecol. Manag.* 239, 112–119.

Richards, S. L., Wilkins, K. A., Swarbreck, S. M., Anderson, A. A., Habib, N., and Smith, A. G. (2015). The hydroxyl radical in plants: from seed to seed. *J. Exp. Bot.* 66, 37–46. doi: 10.1093/jxb/eru398

Rosenwasser, S., Fluhr, R., Joshi, J. R., Leviatan, N., Sela, N., Hetzroni, A., et al. (2013). ROSMETER: a bioinformatic tool for the identification of transcriptomic imprints related to reactive oxygen species type and origin provides new insights into stress responses. *Plant Physiol.* 163, 1071–1083. doi: 10.1104/pp.113.218206

Ryan, J., Eddy, de, P., Humberto, G., and Rachid, M. (2006). Drylands of the Mediterranean zone: biophysical resources and cropping systems. *Agron. Monograph.* 23, 577–624. doi: 10.2134/agronmonogr23.2ed.c15

Salehi-Lisar, S. Y., and Bakhshayeshan-Agdam, H. (2016). "Drought stress in plants: causes, consequences, and tolerance," in *Drought Stress Tolerance in Plants*, Vol 1, eds M. Hossain, S. Wani, S. Bhattacharjee, D. Burritt, and L. S. Tran (Cham: Springer).

Sarsour, E. H., Amanda, L. K., Prabhat, C., and Goswami, L. (2014). Role of ROS in cell proliferation is also evident from report that manganese superoxide dismutase regulates a redox cycle within the cell cycle. *Antioxidants RedoxSignalling* 20, 1618–1627.

Saxena, I., Srikanth, S., and Chen, Z. (2016). Cross talk between H2O2 and interacting signal molecules under plant stress response. *Front. Plant Sci.* 7:570. doi: 10.3389/fpls.2016.00570

Sharma, P., and Dubey, R. S. (2005). Modulation of nitrate reductase activity in rice seedlings under aluminium toxicity and water stress: role of osmolytes as enzyme protectants. *Plant Physiol.* 16, 854–864. doi: 10.1016/j.jplph.2004.09.011

Siddiqui, M. N., Léon, J., Naz, A. A., and Ballvora, A. (2021). Genetics and genomics of root system variation in adaptation to drought stress in cereal crops. *J. Exp. Bot.* 72, 1007–1019. doi: 10.1093/jxb/eraa487

Sirichandra, C., Gu, D., Hu, H. C., Davanture, M., Lee, S., Djaoui, M., et al. (2009). Phosphorylation of the Arabidopsis AtrbohF NADPH oxidase by OST1 protein kinase. *FEBS Lett.* 583, 2982–2986. doi: 10.1016/j.febslet.2009.08.033

Skinner, R. H., and Moore, K. J. (2007). "Growth and development of forage plants," in *Forages, the Science of Grassland Agric*, eds R. F. Barnes, C. J. Nelson, and K. J. Moore (Hoboken, NJ: Wiley).

Skulachev, M. V., and Skulachev, V. P. (2018). "Phenoptosis: programmed death of an organism," in *Apoptosis and Beyond: The Many Ways Cells Die*, ed. J. A. Radosevich (Hoboken, NJ: John Wiley & Sons).

Slooten, L., Capiau, K., van Camp, W., van Montagu, M., Sybesma, C., and Inze, D. (1995). Factors affecting the enhancement of oxidative stress tolerance in transgenic tobacco overexpressing manganese superoxide dismutase in the chloroplasts. *Plant Physiol.* 107, 737–750. doi: 10.1104/pp.107.3.737

Sofi, P. A., Ara, A., Gull, M., and Rehman, K. (2019). "Canopy temperature depression as an effective physiological trait for drought screening," in *Drought-Detection and Solutions*, (London: IntechOpen). doi: 10.5772/intechopen.85966

Song, Y., Miao, Y., and Song, C. P. (2014). Behind the scenes: the roles of reactive oxygen species in guard cells. *New Phytol.* 201, 1121–1140. doi: 10.1111/nph.12565

Srivastava, A. K., and Suprassana, P. (2015). "Redox-regulated mechanisms: implications for enhancing plant stress tolerance and crop yield," in *Elucidation of Abiotic Stress Signaling in Plants*, Vol. 1, eds K. Girdhar and Pandey (Functional Genomics Perspectives).

Stewart, B. A., Koohafkan, P., and Ramamoorthy, K. (2006). *Dryland Agriculture*, 2nd Edn. Madison: American Society of Agronomy.

Strock, C. F., Burridge, J. D., Niemiec, M. D., Brown, K. M., and Lynch, J. P. (2021). Root metaxylem and architecture phenotypes integrate to regulate water use under drought stress. *Plant Cell Environ.* 44, 49–67. doi: 10.1111/pce.13875

Tamary, E., Nevo, R., Naveh, L., Levin-Zaidman, S., Kiss, V., Savidor, A., et al. (2019). Chlorophyll catabolism precedes changes in chloroplast structure and proteome during leaf senescence. *Plant Direct.* 3, 1–18. doi: 10.1002/pld3.127

Temam, D., Uddameri, V., Mohammadi, G., Hernandez, E. A., and Ekwaro-Osire, S. (2019). Long-term drought trends in ethiopia with implications for dryland agriculture. *Water* 11:2571. doi: 10.3390/w11122571

Teran, J. C. B. M., Konzen, E. R., Medina, V., Palkovic, A., Tsai, S. M., Gilbert, M. E., et al. (2019). Root and shoot variation in relation to potential intermittent drought adaptation of Mesoamerican wild common bean (*Phaseolus vulgaris* L.). *Ann. Bot.* 124, 917–932. doi: 10.1093/aob/mcy221

Tiwari, M., Pandey, V., Singh, B., and Bhatia, S. (2021a). Dynamics of miRNA mediated regulation of legume symbiosis. *Plant Cell Environ.* 44, 1279–1291. doi: 10.1111/pce.13983

Tiwari, M., Singh, B., Yadav, M., Pandey, V., and Bhatia, S. (2021b). High throughput identification of miRNAs reveal novel interacting targets regulating chickpea-rhizobia symbiosis. *Environ. Exp. Bot.* 186:104469.

Tiwari, M., Yadav, M., Singh, B., Pandey, V., Nawaz, K., and Bhatia, S. (2021c). Evolutionary and functional analysis of Two-Component System in chickpea reveals CaRR13, a TypeB RR, as positive regulator of symbiosis. *Plant Biotechnol. J.* 19, 2415–2427. doi: 10.1111/pbi.13649

Tripathi, P., Rabara, R. C., Reese, R. N., Miller, M. A., Rohila, J. S., Subramanian, S., et al. (2016). A toolbox of genes, proteins, metabolites and promoters for improving drought tolerance in soybean includes the metabolite coumestrol and stomatal development genes. *BMC Genomics* 17:102. doi: 10.1186/s12864-016-2420-0

Ullah, A., Sun, H., Yang, X., and Zhang, X. (2017). Drought coping strategies in cotton: increased crop per drop. *Plant Biotechnol. J.* 15, 271–284. doi: 10.1111/pbi.12688

Verma, G., Srivastava, D., Tiwari, P., and Chakrabarty, D. (2019). "ROS modulation in crop plants under drought stress," in *Reactive Oxygen, Nitrogen and Sulfur Species in Plants: Production, Metabolism, Signaling and Defense Mechanisms*, 1st Edn, Vol. 1, eds M. Hasanuzzaman, V. Fotopoulos, K. Nahar, and M. Fujita (Hoboken, NJ: John Wiley & Sons Ltd).

Viola, I. L., Camoirano, A., and Gonzalez, D. H. (2016). Redox-dependent modulation of anthocyanin biosynthesis by the TCP transcription factor TCP15 during exposure to high light intensity conditions in Arabidopsis. *Plant Physiol.* 170, 74–85. doi: 10.1104/pp.15.01016

Wallace, J. G., Zhang, X. C., Beyene, Y., Semagn, K., Olsen, M., Prasanna, B. M., et al. (2016). Genome-wide association for plant height and flowering time across 15 tropical maize populations under managed drought stress and well-watered conditions in Sub-Saharan Africa. *Crop. Sci.* 56, 2365–2378. doi: 10.2135/cropsci2015.10.0632

Wang, F., Chen, H. W., Li, Q. T., Wei, W., Li, W., Zhang, W. K., et al. (2015). GmWRKY27 interacts with GmMYB174 to reduce expression of GmNAC29 for stress tolerance in soybean plants. *Plant J.* 83, 224–236. doi: 10.1111/tpj.12879

Wang, H., Liang, W., and Huang, J. (2013). Putrescine mediates aluminum tolerance in red kidney bean by modulating aluminum-induced oxidative stress. *Crop Sci.* 53, 2120–2128. doi: 10.2135/cropsci2013.04.0215

Wang, Y., Huang, Y., Fu, W., Guo, W., Ren, N., Zhao, Y., et al. (2020). Efficient physiological and nutrient use efficiency responses of maize leaves to drought stress under different field nitrogen conditions. *Agronomy* 10:523.

Waszczak, C., Carmody, M., and Kangasjärvi, J. (2018). Reactive oxygen species in plant signaling. *Annu. Rev. Plant Biol.* 69, 209–236. doi: 10.1146/annurev-arplant-042817-040322

Weng, X., Wang, L., Wang, J., Hu, Y., Du, H., Xu, C., et al. (2014). Grain number, plant height, and heading date is a central regulator of growth, development, and stress response. *Plant Physiol.* 164, 735–747.

Weraduwage, S. M., Kim, S. J., Renna, L. C., Anozie, F. D., Sharkey, T., and Brandizzi, F. (2016). Pectin methylesterification impacts the relationship between photosynthesis and plant growth. *Plant Physiol.* 171, 833–848. doi: 10.1104/pp.16.00173

Williams, A. P., Cook, E. R., Smerdon, J. E., Cook, B. I., John, T., Abatzoglou, J. T., et al. (2020). Large contribution from anthropogenic warming to an emerging North American megadrought. *Science* 368, 314–318. doi: 10.1126/science.aaz9600

Wituszynska, W., Ślesak, I., Vanderauwera, S., Szechyńska-Hebda, M., Kornaś, A., Van Der Kelen, K., et al. (2013). LESION SIMULATING DISEASE1, ENHANCED DISEASE SUSCEPTIBILITY1, and PHYTOALEXIN DEFICIENT4 conditionally regulate cellular signaling homeostasis, photosynthesis, water use efficiency, and seed yield in Arabidopsis. *Plant Physiol.* 161, 1795–1805. doi: 10.1104/pp.112.208116

Xie, Y., Mao, Y., Duan, X., Zhou, H., Lai, D., Zhang, Y., et al. (2015). Arabidopsis HY1-modulated stomatal movement: an integrative hub for its functionally associated with ABI4 in the dehydration-induced ABA responsiveness. *Plant Physiol.* 170, 1699–1713. doi: 10.1104/pp.15.01550

Xu, Y., Xu, Q., and Huang, B. (2015). Ascorbic acid mitigation of water stress-inhibition of root growth in association with oxidative defense in tall fescue (Festuca arundinaceaSchreb.). *Front. Plant Sci.* 6:807. doi: 10.3389/fpls.2015.00807

Yan, J., Wang, J., Tissue, D., Holaday, S., Allen, R., and Zhang, H. (2003). Photosynthesis and seed production under water-deficit conditions in transgenic tobacco plants that overexpress an ascorbate peroxidase gene. *Crop Sci.* 43, 1477–1483.

Ye, Q., and Steudle, E. (2006). Oxidative gating of water channels (aquaporins) in corn roots. *Plant Cell Environ.* 29, 459–470. doi: 10.1111/j.1365-3040.2005.01423.x

Ye, W., Hossain, M. A., Munemasa, S., Nakamura, Y., Mori, I. C., and Murata, Y. (2013). Endogenous abscisic acid is involved in methyl jasmonate-induced reactive oxygen species and nitric oxide production but not in cytosolic alkalization in Arabidopsis guard cells. *Plant Physiol.* 170, 1212–1215. doi: 10.1016/j.jplph.2013.03.011

You, J., and Chan, Z. (2015). ROS Regulation during abiotic stress responses in crop plants. *Front. Plant Sci.* 6:1092. doi: 10.3389/fpls.2015.01092

You, J., Zong, W., Hu, H., Li, X., Xiao, J., and Xiong, L. (2014). A STRESS-RESPONSIVE NAC1-regulated protein phosphatase gene rice protein Phosphatase18 modulates drought and oxidative stress tolerance through abscisic acid-independent reactive oxygen species scavenging in rice. *Plant Physiol.* 166, 2100–2114. doi: 10.1104/pp.114.251116

Yu, Y., Zhou, W., Liang, X., Zhou, K., and Lin, X. (2019). Increased bound putrescine accumulation contributes to the maintenance of antioxidant enzymes and higher aluminum tolerance in wheat. *Environ. Pollut.* 252, 941–949. doi: 10.1016/j.envpol.2019.06.045

Zandalinas, S. I., Fichman, Y., Devireddy, A. R., Sengupta, S., Azad, R. K., and Mittler, R. (2020). Systemic signaling during abiotic stress combination in plants. *Proc. Natl. Acad. Sci. U.S.A.* 117, 13810–13820. doi: 10.1073/pnas.2005077117

Zhang, H., Liu, Y., Wen, F., Yao, D., Wang, L., Guo, J., et al. (2014). A novel rice C2H2-type zinc finger protein, ZFP36, is a key player involved in abscisic acid-induced antioxidant defence and oxidative stress tolerance in rice. *J. Exp. Bot.* 65, 5795–5809. doi: 10.1093/jxb/eru313

Zhang, J., Jiang, H., Jin, J., and Zhang, X. (2018). The responses of plant leaf CO2/H2O exchange and water use efficiency to drought: a meta-analysis. *Sustainability.* 10:551.

Zhang, X., Liu, X., Zhang, D., Tang, H., Sun, B., Li, C., et al. (2017). Genome-wide identification of gene expression in contrasting maize inbred lines under field drought conditions reveals the significance of transcription factors in drought tolerance. *PLoS One* 12:e0179477. doi: 10.1371/journal.pone.0179477

Zhang, Y., Tan, J., Guo, Z., Lu, S., He, S., Shu, W., et al. (2009). Increased abscisic acid levels in transgenic tobacco over-expressing 9cis-epoxycarotenoid dioxygenase influence H2O2 and NO production and antioxidant defenses. *Plant Cell Environ.* 32, 509–519. doi: 10.1111/j.1365-3040.2009.01945.x

Zhang, Z., Cao, B., Gao, S., and Xu, K. (2019). Grafting improves tomato drought tolerance through enhancing photosynthetic capacity and reducing ROS accumulation. *Protoplasma* 256, 1013–1024. doi: 10.1007/s00709-019-01357-3

Zhang, Z., Zhang, Q., Wu, J., Zheng, X., Zheng, S., Sun, X., et al. (2013). Gene knockout study reveals that cytosolic ascorbate Peroxidase 2(OsAPX2) plays a critical role in growth and reproduction in rice under drought, salt and cold stresses. *PLoS One* 8:e57472. doi: 10.1371/journal.pone.0057472

Zheng, Y., Zhan, Q., Shi, T., Liu, J., Zhao, K., and Gao, Y. (2020). The nuclear transporter SAD2 plays a role in calcium- and H2O2-mediated cell death in Arabidopsis. *Plant J.* 101, 324–333. doi: 10.1111/tpj.14544

Zhou, H., Chen, Y., Zhai, F., Zhang, J., Zhang, F., Yuan, X., et al. (2020). Hydrogen sulfide promotes rice drought tolerance via reestablishing redox homeostasis and activation of ABA biosynthesis and signaling. *Plant Physiol. Biochem.* 155, 213–220. doi: 10.1016/j.plaphy.2020.07.038

Zhou, T., Yang, X., Wang, L., Xu, J., and Zhang, X. (2014). GhTZF1 regulates drought stress responses and delays leaf senescence by inhibiting reactive oxygen species accumulation in transgenic Arabidopsis. *Plant Mol. Biol.* 85, 163–177. doi: 10.1007/s11103-014-0175-z

Zhou, W., Zheng, W., Lv, H., Wang, Q., Liang, B., and Li, J. (2022). Foliar application of pig blood-derived protein hydrolysates improves antioxidant activities in lettuce by regulating phenolic biosynthesis without compromising yield production. *Sci. Hortic.* 291:110602. doi: 10.1016/j.scienta.2021.110602

Zhu, M., Zhu, N., Song, W., Harmon, A. C., Assmann, S. M., and Chen, S. (2014). Thiol-based redox proteins in abscisic acid and methyl jasmonate signaling in *Brassica napus* guard cells. *Plant J.* 78, 491–515. doi: 10.1111/tpj.12490

Zhu, T., Deng, X., Zhou, X., Zhu, L., Zou, L., Li, P., et al. (2016). Ethylene and hydrogen peroxide are involved in brassinosteroid-induced salt tolerance in tomato. *Sci. Rep.* 6:35392. doi: 10.1038/srep35392

Zuniga, F., Jaime, M., and Salazar, C. (2021). Crop farming adaptation to droughts in small-scale dryland agriculture in Chile. *Water Resour. Econ.* 34:100176. doi: 10.1016/j.wre.2021.100176

Conflict of Interest: The authors declare that the research was conducted in the absence of any commercial or financial relationships that could be construed as a potential conflict of interest.

Publisher's Note: All claims expressed in this article are solely those of the authors and do not necessarily represent those of their affiliated organizations, or those of the publisher, the editors and the reviewers. Any product that may be evaluated in this article, or claim that may be made by its manufacturer, is not guaranteed or endorsed by the publisher.

frontiers in Plant Science

ORIGINAL RESEARCH
published: 31 January 2022
doi: 10.3389/fpls.2021.814658

Differences in Water Consumption of Wheat Varieties Are Affected by Root Morphology Characteristics and Post-anthesis Root Senescence

Xuejiao Zheng, Zhenwen Yu, Yu Shi and Peng Liang*

National Key Laboratory of Crop Biology, Agronomy College, Shandong Agricultural University, Tai'an, China

Selecting high-yielding wheat varieties for cultivation can effectively increase water use efficiency (WUE) in the Huang–Huai–Hai Plain, where is threatened by increasing water shortages. To further identify the difference in water use and its relationship with root morphology and senescence characteristics, wheat varieties with different yield potentials—Yannong 1212 (YN), Jimai 22 (JM), and Liangxing 99 (LX)—were studied in a high-yielding wheat field. The water consumption percentage (CP) in YN decreased from planting to anthesis; however, crop evapotranspiration and CP increased from anthesis to maturity compared with JM and LX. In YN, a higher soil water consumption from anthesis to maturity in the 0–100 cm soil layer was partly attributed to the greater root weight density in the 20–60 cm soil layer. In topsoil (0–40 cm), root length density, root surface area density, and root diameter at 20 days after anthesis, root superoxide dismutase activity, and root triphenyl tetrazolium chloride reduction activity during mid grain filling stage were higher in YN than in JM and LX. YN had the highest grain yields of 9,840 and 11,462 kg ha^{-1} and increased grain yield and WUE by 12.0 and 8.4%, respectively, as compared with JM, and by 30.3 and 21.3%, respectively, as compared with LX. Ensuring more soil water extraction post-anthesis by increasing roots in the 20–60 cm soil profile, improving root morphology traits, and alleviating root senescence in the topsoil during mid-grain filling stage will assist in selecting wheat varieties with high yield and WUE.

Keywords: winter wheat, yield potential, water use, root morphology, root senescence

OPEN ACCESS

Edited by:
Thorsten M. Knipfer, University of British Columbia, Canada

Reviewed by:
Quan Xie, Nanjing Agricultural University, China
Min Zhu, Yangzhou University, China

****Correspondence:***
Yu Shi
shiyu@sdau.edu.cn

Specialty section:
This article was submitted to Crop and Product Physiology, a section of the journal Frontiers in Plant Science

Received: *14 November 2021*
Accepted: *06 December 2021*
Published: *31 January 2022*

Citation:
Zheng X, Yu Z, Shi Y and Liang P (2022) Differences in Water Consumption of Wheat Varieties Are Affected by Root Morphology Characteristics and Post-anthesis Root Senescence. Front. Plant Sci. 12:814658. doi: 10.3389/fpls.2021.814658

INTRODUCTION

The Huang–Huai–Hai Plain (3HP), as the main wheat production region in China, owns only 40% of the agricultural land in the country; however, it accounts for about 61% of the total wheat production of the country (Sun et al., 2011; Xu et al., 2018). In this area, the precipitation received during the full wheat growth season ranges from 100 mm to 180 mm, which can only meet 25–40% of the total water requirement of wheat (Iqbal et al., 2014). Groundwater is used on 64% of the irrigated area, and excessive extraction has led to a rapid decline in groundwater table (Zhang et al., 2010). Improving water use efficiency (WUE) is a crucial approach for food security in regions such as the 3HP, where water shortage is a major challenge for agriculture

(Brauman et al., 2013; Rashid et al., 2019). Therefore, reasonable irrigation strategies have been proposed (i.e., regulating irrigation frequency and timing, applying deficit irrigation, and supplemental irrigation) for increasing WUE and maintaining high wheat production (Wang, 2017; Meena et al., 2019a; Zhao et al., 2020). However, studies have shown that renewing varieties is an effective way to increase yield and WUE (Faralli et al., 2019; Meena et al., 2019b), and it is necessary to study the physiological characteristics of wheat varieties with high yield and high WUE.

The variation of wheat varieties in yield and WUE has been reported in some studies (Zeleke and Nendel, 2016; Ma'arup et al., 2020). When wheat yield ranging from 6,475 to 7,275 kg ha^{-1} under the irrigation of 190 and 230 mm in two wheat varieties, using a greater yield and WUE wheat variety Shijiazhuang 8 could increase the WUE up to 17.8 kg ha^{-1} mm^{-1} by reducing the irrigation amount without decreasing the yield (Liu et al., 2016). Zhang et al. (2010) reported that the WUE of wheat is estimated to increase from 10.0 to 12.0 kg ha^{-1} mm^{-1} for the early 1970s varieties to 14.0–15.0 kg ha^{-1} mm^{-1} for the 2000s varieties in the 3HP, and the positive relationship between grain yield and WUE for all the varieties indicated that using a higher-yielding variety has the potential to improve WUE, thereby saving water. However, limited information is available on the variation of WUE in water consumption characteristics between varieties with different yield levels during the entire growing season. There is a need to develop high-yielding wheat varieties because achieving greater yield from the same water resources contributes to higher WUE (Zhang et al., 2017).

Increased grain yield could be achieved by breeding deeper-rooted wheat varieties in specific farming systems as root distribution in the soil is directly associated with soil water uptake (Wasson et al., 2012; Severini et al., 2020). In rice, increased root length density is required for achieving high crop yield and WUE (Yang et al., 2012), and inadequate root length could accelerate the senescence of above-ground plants during the grain filling stage (Liu et al., 2018). However, Fang et al. (2021) reported that in the semi-arid region on the Loess Plateau, modern wheat varieties with yields between 5,814 and 6,115 kg ha^{-1} had less root biomass and root length density in the 0–40 cm soil layer, which reduced pre-anthesis water uptake but increased soil water extraction after anthesis, contributing to the increases in grain yield and WUE. Regulating root morphology characteristics by irrigation technologies can influence the uptake of soil water during the post-anthesis phase, that have major effects on wheat yield and WUE (Ali et al., 2019). However, the onset of wheat senescence during post-anthesis is inevitable (Nehe et al., 2020). Guaranteeing wheat water uptake during this phase can provide important advantages in yield formation (Li et al., 2019). Much attention has been paid to the effects of root morphology characteristics on crop yield and WUE; however, little information is available about the root senescence traits post-anthesis and its relationship with the soil water uptake and grain yield of wheat varieties with different yield levels.

Wheat varieties have been replaced 8–9 times in the main wheat production regions of China since the 1950s, with great improvement in yield potential (He et al., 2018). The average wheat yield in Shandong, Henan, and Hebei Provinces, as the main wheat production regions in the 3HP, varied from 6,052.5 to 6,484 kg ha^{-1} from 2014 to 2017 (Ministry of agriculture and rural affairs of the People's Republic of China, 2016, 2019). Widely planted winter wheat varieties, Jimai 22 (JM) and Liangxing 99 (LX), in the 3HP are important parental resources for the current wheat variety improvement in China (Yang Z. Z. et al., 2020). The well-adapted wheat variety, Yannong 1212 (YN), has broken the yield record of winter wheat twice in China and showed a high yield of over 12,000 kg ha^{-1} at eight different locations in the 3HP since 2015 (Dazhong Daily, 2020). The recorded grain yield of YN was 11,001 kg ha^{-1}, which was 19.5% and 34.4% higher than the varieties JM and LX in a previous study (Liang et al., 2018). However, few studies have been conducted to investigate the differences in water consumption characteristics, root morphology, and senescence traits, underlying yield superiority of YN to JM and LX. Moreover, clarifying the difference in water use of wheat varieties and its relationships with root morphology and senescence characteristics may also contribute to the improvement of new varieties with high yield and high WUE in future breeding programs. The objectives of this study were to: identify the water consumption characteristics associated with high-yielding and high WUE wheat varieties and clarify the relationships among root morphology and post-anthesis senescence characteristics, water use, and wheat production.

MATERIALS AND METHODS

Experimental Site

Field experiments were carried out from 2017 to 2019 in Shijiawangzi village, Yanzhou (116°41′E, 35°42′N), Shandong Province, China. This region has a typical and representative environment of the 3HP. The average annual groundwater depth is 25 m, and the soil type is Haplic luvisol (FAO classification system). Before sowing, the soil layer (0–20 m) contained 19.2 g kg^{-1} organic matter, 1.2 g kg^{-1} total nitrogen (N), 166.3 mg kg^{-1} hydrolyzable N, 56.2 mg kg^{-1} available phosphorus, and 204.3 mg kg^{-1} available potassium. The soil bulk density and field capacity in the 0–200 cm soil layer before sowing are shown in **Supplementary Table 1**. Precipitation during the wheat-growing seasons in 2017–2018 and 2018–2019 are shown in **Supplementary Figure 1**.

Experimental Design

Seeds of three winter wheat varieties with different yield potentials—YN, JM, and LX—were used in the present study. Among the three wheat varieties, YN was approved by National Crop Variety Approval Committee in 2020 (Ministry of agriculture and rural development of the People's Republic of China, 2020). JM and LX have been sown in a cumulative area of 60 million ha due to the excellent performance in wheat production. JM (since 2015) and LX (from 2010 to 2015) were successively employed as control varieties in the performance test of new cultivars in the 3HP (Yang Z. Z. et al., 2020). A randomized design with three replications was implemented. Each experimental plot was 2 m × 30 m in size with a 2.0 m

buffer zone between plots to minimize the effects of adjacent plots. The straw of the preceding maize crop was crushed and returned into the cropland. A base fertilizer of 105 kg ha^{-1} N, 150 kg ha^{-1} P_2O_5, and 150 kg ha^{-1} K_2O were applied before sowing, and at the jointing stage of wheat production, 165 kg ha^{-1} N was ditched. Wheat seeds were sown on October 23, 2017, and October 10, 2018, with a population of 270 plant m^{-2} and 180 plant m^{-2}, respectively, while wheat plants were harvested on June 7, 2018, and June 11, 2019. Experimental plots were irrigated with 60 mm of water each in the pre-winter, jointing, and anthesis stages, totaling 180 mm of water during the growing season.

Sampling and Measurements

Soil Water Content and Crop Evapotranspiration

In all experimental plots, soil from the surface to 200 cm depth was sampled at 20 cm intervals using a soil corer. Measurements of soil samples were taken at pre-planting, a day before irrigation at both the jointing and anthesis stages, and at maturity from each treatment with three replicates. The soil water content of each 20 cm soil layer was determined by using the oven-drying method described by Gardner (1986).

The crop water consumption or crop evapotranspiration (ET) of winter wheat for the whole growing season or an individual growth period was based on the equation described by Chattaraj et al. (2013):

$$ET = \Delta SW + I + P - D - R$$

Where ET (mm) is the crop evapotranspiration, $_{\Delta}$ SW (mm) is the soil water consumption of 0–200 cm soil profile between two specific growth stages, I (mm) is the irrigation amount, P (mm) is the precipitation amount, D (mm) is downward flux below the crop root zone, and R (mm) is surface runoff. In this experimental site, owing to the presence of a low groundwater table (average annual of 25 m) below the ground surface, capillary rise, drainage, and runoff were not calculated. Drainage and runoff are negligible in the 3HP, including in this experimental site (Lv et al., 2011).

The water consumption percentage (CP) for a given growth period was the ratio of the water consumption amount or ET of that period to the total crop evapotranspiration during the whole growth periods of wheat (ET_C) (Xu et al., 2018).

Root Weight Density

Roots were sampled from each treatment with three replicates at anthesis, using an auger with a 10 cm internal diameter, at 20 cm intervals down to a 100 cm depth. At each plot, two cores were collected within and between the wheat rows. The roots from the core sections, with mixtures of roots and soil in each 20 cm soil layer, were collected following the method described by Jha et al. (2017). Root samples were oven-dried at 80°C until a constant weight was reached. The root weight density (RWD) was calculated according to Feng et al. (2017).

Root Morphology Characteristics and Biochemical Assays

Root samples in the 0–40 cm soil layer were collected at 20 cm intervals from each pot with three replicates at anthesis, 10 and 20 days after anthesis (DAA), using an auger with a 10 cm internal diameter. Each sample included two cores that collected within and between the wheat rows. Root samples were collected and refrigerated at −80°C. Half of the root samples were used to measure root length, root surface area, and root diameter measurements using an Epson V700 scanner (Seiko Epson Corp., Japan) and WinRHIZO 2013 software (Regent Instruments Canada Inc., Canada). Root length density and root surface area density were calculated according to He et al. (2019). The remaining root samples were used for the measurements of root malondialdehyde (MDA) concentration, superoxide dismutase (SOD) activity, and root activity. Root MDA concentration and SOD activity were assayed using the methods described by Guo et al. (2015). Root activity was determined following the method of Man et al. (2016) and represented by the triphenyl tetrazolium chloride (TTC) reduction activity.

Grain Yield

At maturity, grain yield was determined by the plants harvested from a 5 m^2 area in each plot and sun-dried to 12.5% moisture content before being recorded.

Water Use Efficiency

The WUE was calculated as follows (Ma et al., 2019):

$$WUE = Y/ETc$$

Where WUE (kg ha^{-1} mm^{-1}) represents the crop water use efficiency, Y (kg ha^{-1}) is the grain yield, and ET_C (mm) is the total crop evapotranspiration during the whole growing periods of wheat.

Statistical Analysis

Statistical analysis was performed using standard ANOVA in SPSS 22.0 (IBM, New York, NY, United States). The normality of data and the homogeneity of variances were checked by using the Shapiro–Wilk test and Levene's test, respectively. ANOVA was conducted to compare the effects of different treatments on the measured variables. The means were compared using Duncan's test at $\alpha = 0.05$ to identify significant effects.

RESULTS

Crop Evapotranspiration in Different Growth Periods

As shown in **Table 1**, the ET_C of YN was significantly higher than that of JM and LX in both years. There was no significant difference in ET from planting to jointing stages in all wheat varieties in 2017–2018. Compared with JM and LX, the CP from planting to jointing of YN was 4.9 and 7.8% lower in 2017–2018, and 5.6 and 8.1% lower in 2018–2019, respectively. ET from jointing to anthesis did not differ significantly among YN, JM, and LX, despite that YN had the lowest CP from jointing to anthesis. ET and CP from anthesis to maturity, both ranked in the decrease order of YN > JM > LX, in both years.

TABLE 1 | Total crop evapotranspiration during the whole growing periods of wheat (ET_C), crop evapotranspiration, and water consumption percentage in different growth periods in the 2017–2018 and 2018–2019 growing seasons.

Year	Treatments	ET_C	Planting-Jointing		Jointing-Anthesis		Anthesis-Maturity	
		(mm)	ET (mm)	CP (%)	ET (mm)	CP (%)	ET (mm)	CP (%)
2017–2018	YN	546.2a	193.1a	35.35c	140.2a	25.67b	212.9a	38.98a
	JM	522.8b	194.4a	37.18b	142.4a	27.24a	186.0b	35.58b
	LX	499.6c	191.4a	38.32a	139.9a	28.00a	168.3c	33.68c
2018–2019	YN	658.4a	168.6b	25.61b	171.6a	26.07b	318.1a	48.32a
	JM	644.8b	175.0a	27.14a	174.3a	27.04a	295.4b	45.82b
	LX	623.8c	173.8ab	27.87a	172.0a	27.57a	278.0c	44.56c

YN, Yannong 1212; JM, Jimai 22; LX, Liangxing 99; ET, crop evapotranspiration; CP, water consumption percentage. Values followed by a different letter are significantly different (Duncan's test, $p < 0.05$) within the treatments in each year.

Soil Water Consumption in Different Growth Periods

The soil water consumption from planting to jointing of YN was lower than that of JM in 2018–2019 (**Figure 1**). The soil water consumption from jointing to anthesis among the three varieties did not differ significantly in both years. The soil water consumption values from anthesis to maturity in YN were 79.1 mm and 61.6 mm in 2017–2018 and 2018–2019, respectively, which were significantly higher than that of JM and LX in both years.

Soil Water Consumption in the 0–200 cm Soil Layer From Anthesis to Maturity

The highest soil water consumption in the 0–100 cm soil layer from anthesis to maturity was observed in YN, followed by JM, and finally, LX (**Figure 2**). Soil water consumption from the 100 to 120 cm soil layer in JM and LX did not differ with that of YN in 2017–2018 but were both lower than that of YN in 2018–2019. No significant differences were found in the soil water consumption of the 120–200 cm soil layer from anthesis to maturity among YN, JM, and LX in both years.

Root Weight Density in the 0–100 cm Soil Layer

The RWD in the 0–40 cm soil layer accounted for 78.8–83.9% of the total RWD (i.e., in the entire 0–100 cm soil layer) in both years (**Figure 3**). In both years, the RWD of all three wheat varieties significantly decreased with an increase in soil depth at anthesis. The RWD from the 0 to 20 cm soil layer in YN did not differ with that of JM in both years but was higher than that of LX in 2018–2019. Compared to JM and LX, YN had greater RWD in the 20–60 cm soil layer in both years. The RWD in the 60–100 cm soil layer did not differ between YN and JM, which were both higher than that of LX.

Root Morphology Characteristics

In the 0–20 cm soil layer, there were no significant differences in root length density and root diameter at 0 DAA among wheat varieties in both years (**Table 2**). YN and JM had greater root length density, root surface area density, and root diameter at 10 DAA than those of LX. Maximum values for root length density, root surface area density, and root diameter at 20 DAA were observed in YN, followed by JM with the lowest in LX.

In the 20–40 cm soil layer, YN and JM had higher root length density, root surface area density, and root diameter at 0 DAA than LX in both years (**Table 2**). The root surface area density at 10 DAA of YN showed 6.5% and 27.6%, and 8.1% and 34.7% higher than that of JM and LX, in 2017–2018 and 2018–2019, respectively. The root diameter at 10 DAA of YN was 4.2% and 8.3% greater than that of JM, and 13.6% and 18.2% higher than that of LX in 2017–2018 and 2018–2019, respectively. Root length density, root surface area density, and root diameter at 20 DAA were manifested in the following order: YN > JM > LX in both years.

Root Senescence Characteristics

In the 0–20 cm soil layer, there was no significant difference in MDA concentration at 0 DAA among wheat varieties in both years (**Figures 4A,B**); however, compared with LX, YN, and JM had lower MDA concentration of root at 10 DAA. The MDA concentration of root at 20 DAA was manifested in the following order: LX > JM > YN. The MDA concentration trend in the 20–40 cm soil layer was similar to that at 0–20 cm. In the 0–20 cm soil layer, SOD activity at 0 DAA in YN did not differ to that of JM in both years but was higher than that of LX in 2017–2018 (**Figures 4C,D**). The SOD activity at 10 and 20 DAA were ranked in the order: YN > JM > LX. In the 20–40 cm soil layer, the differences of roots among wheat varieties were non-significant for SOD activity at 0 DAA in 2017–2018. The highest SOD activity of root at 10 and 20 DAA was obtained in YN, whereas the lowest was obtained in LX in both years.

Root Triphenyl Tetrazolium Chloride Reduction Activity

In the 0–20 cm soil layer, root triphenyl tetrazolium chloride reduction activity (RTTC) at 0 DAA in YN did not differ with that of JM in both years but was higher than that of LX in 2018–2019 (**Table 3**). Compared with JM and LX, YN showed higher RTTC at 10 and 20 DAA. In the 20–40 cm soil layer, the differences of RTTC at 0 DAA among wheat varieties were non-significant in both years. Compared with JM and LX, YN had higher RTTC at 10 DAA by 14.7% and 34.9% in 2017–2018 and by 12.2%

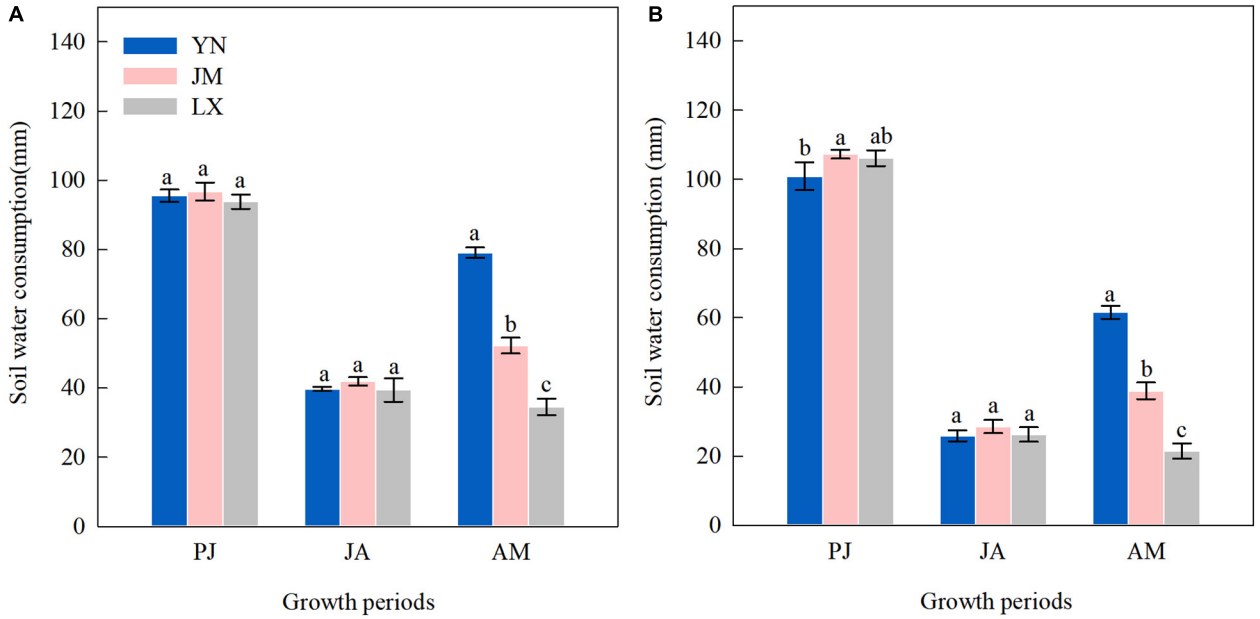

FIGURE 1 | Soil water consumption in different growth periods of wheat varieties in the 2017–2018 **(A)** and 2018–2019 **(B)** growing seasons. YN, Yannong 1212; JM, Jimai 22; LX, Liangxing 99; PJ, planting to jointing; JA, jointing to anthesis; AM, anthesis to maturity. The different letters in the figure indicate significant differences (Duncan's test, $p < 0.05$). Vertical bars represent the standard deviation of the means.

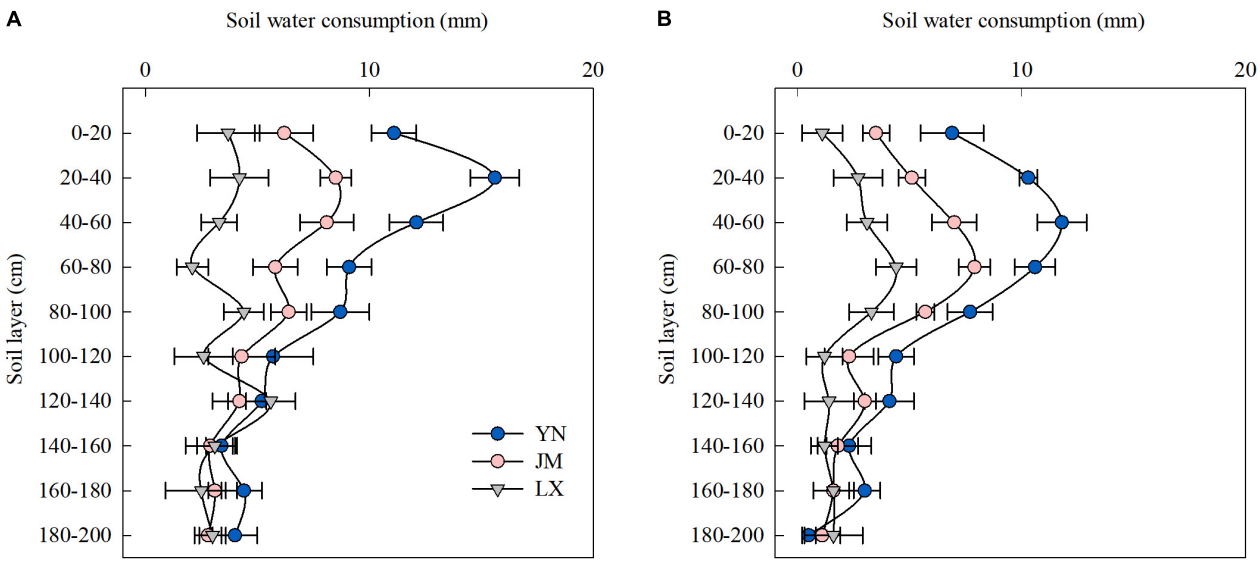

FIGURE 2 | Soil water consumption in the 0–200 cm soil layer from anthesis to maturity of wheat varieties in the 2017–2018 **(A)** and 2018–2019 **(B)** growing seasons. YN, Yannong 1212; JM, Jimai 22; LX, Liangxing 99. Vertical bars represent the SD of the means.

and 27.5% in 2018–2019, respectively. RTTC at 20 DAA was manifested in the following order: YN > JM > LX.

Grain Yield and Water Use Efficiency

Over the 2-year experimental period, the grain yields in YN were 10.8% and 13.1% higher than in JM, respectively, and 28.3% and 32.3% higher than in LX, respectively (**Figure 5**). In both years, the WUE was manifested in the following order: YN > JM > LX.

DISCUSSION

The wheat crop is more sensitive to a water deficit during the reproductive stage than the vegetative growth stage (Ma et al., 2019). Harmsen et al. (2009) indicated that crop evapotranspiration was significantly correlated with crop production. Water consumption in winter wheat reaches peaks during the heading and filling stages to maintain normal growth

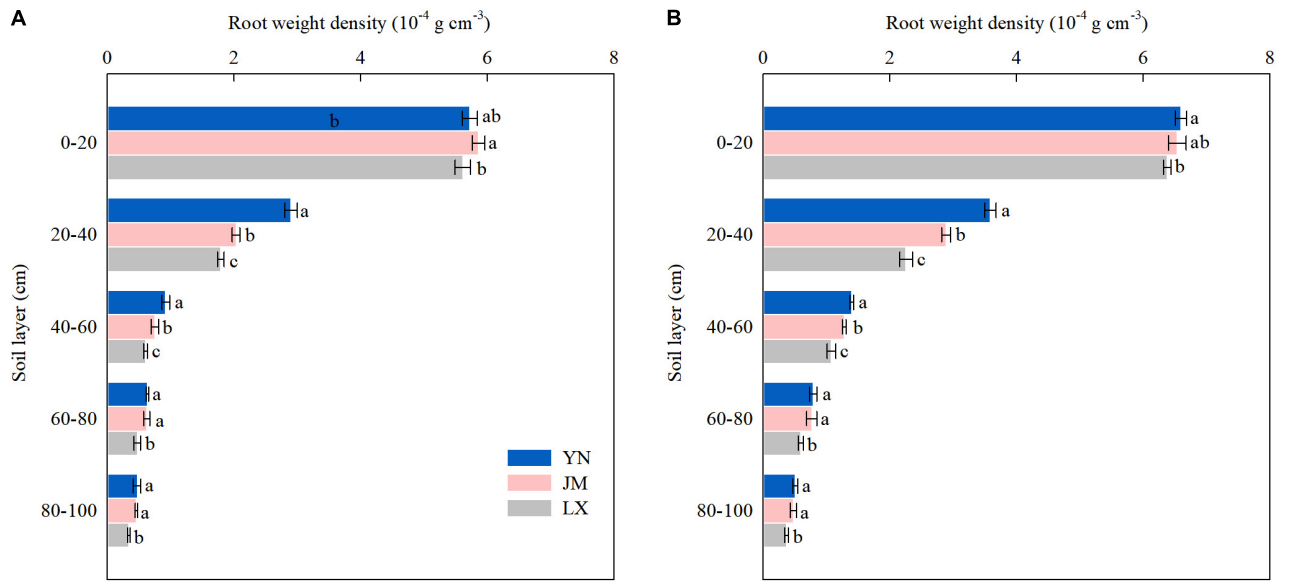

FIGURE 3 | Root weight density in the 0–100 cm soil layer at anthesis of wheat varieties in the 2017–2018 **(A)** and 2018–2019 **(B)** growing seasons. YN, Yannong 1212; JM, Jimai 22; LX, Liangxing 99. The different letters in the figure indicate significant differences (Duncan's test, $p < 0.05$). Vertical bars represent the SD of the means.

TABLE 2 | Root morphology characteristics of winter wheat in the 0–40 cm soil layer after anthesis of wheat varieties in the 2017–2018 and 2018–2019 growing seasons.

Year	Root traits	Treatments	0–20 cm soil layer			20–40 cm soil layer		
			0 DAA	10 DAA	20 DAA	0 DAA	10 DAA	20 DAA
2017–2018	Root length density (cm cm^{-3})	YN	1.39a	1.26a	1.09a	0.79a	0.70a	0.62a
		JM	1.40a	1.26a	1.03b	0.80a	0.68a	0.59b
		LX	1.39a	1.18b	0.88c	0.76b	0.62b	0.53c
	Root surface area density (mm^2 cm^{-3})	YN	12.82ab	10.30a	8.21a	6.43a	5.37a	4.21a
		JM	12.99a	10.19a	7.24b	6.53a	5.04b	3.49b
		LX	12.72b	8.60b	5.52c	5.83b	4.21c	2.81c
	Root diameter (mm)	YN	0.29a	0.26a	0.24a	0.26a	0.25a	0.22a
		JM	0.30a	0.26a	0.22b	0.26a	0.24b	0.19b
		LX	0.29a	0.23b	0.20c	0.24b	0.22c	0.17c
2018–2019	Root length density (cm cm^{-3})	YN	1.47a	1.39a	1.17a	0.89a	0.81a	0.69a
		JM	1.47a	1.39a	1.08b	0.90a	0.79a	0.65b
		LX	1.46a	1.26b	0.94c	0.85b	0.70b	0.57c
	Root surface area density (mm^2 cm^{-3})	YN	14.44a	12.52a	9.74a	7.71a	6.52a	5.13a
		JM	14.39a	12.47a	8.35b	7.81a	6.03b	4.52b
		LX	13.98a	10.33b	6.46c	6.69b	4.84c	3.63c
	Root diameter (mm)	YN	0.31a	0.29a	0.27a	0.28a	0.26a	0.24a
		JM	0.31a	0.29a	0.25b	0.28a	0.24b	0.22b
		LX	0.30a	0.26b	0.22c	0.25b	0.22c	0.20c

YN, Yannong 1212; JM, Jimai 22; LX, Liangxing 99; DAA, days after anthesis. Values followed by a different letter are significantly different (Duncan's test, $p < 0.05$) within the treatments in each year.

and grain production (Jin et al., 2017). In this study, on average, ET accounted for 26.9–37.0%, 26.9–27.0%, and 36.1–46.2% of ET_C from planting to jointing, jointing to anthesis, and anthesis to maturity stages, respectively (**Table 1**). Compared to YN, JM, and LX with lower yields both had higher CP from planting to jointing and from jointing to anthesis but a lower CP from anthesis to maturity stages (**Figure 5** and **Table 1**). The significant increases in CP from anthesis to maturity stages of JM and LX in the following year may be due to the monthly precipitation fluctuations (**Supplementary Figure 1**) because the water requirement of winter wheat can be influenced by interannual precipitation variability (Zhao et al., 2020). A previous study

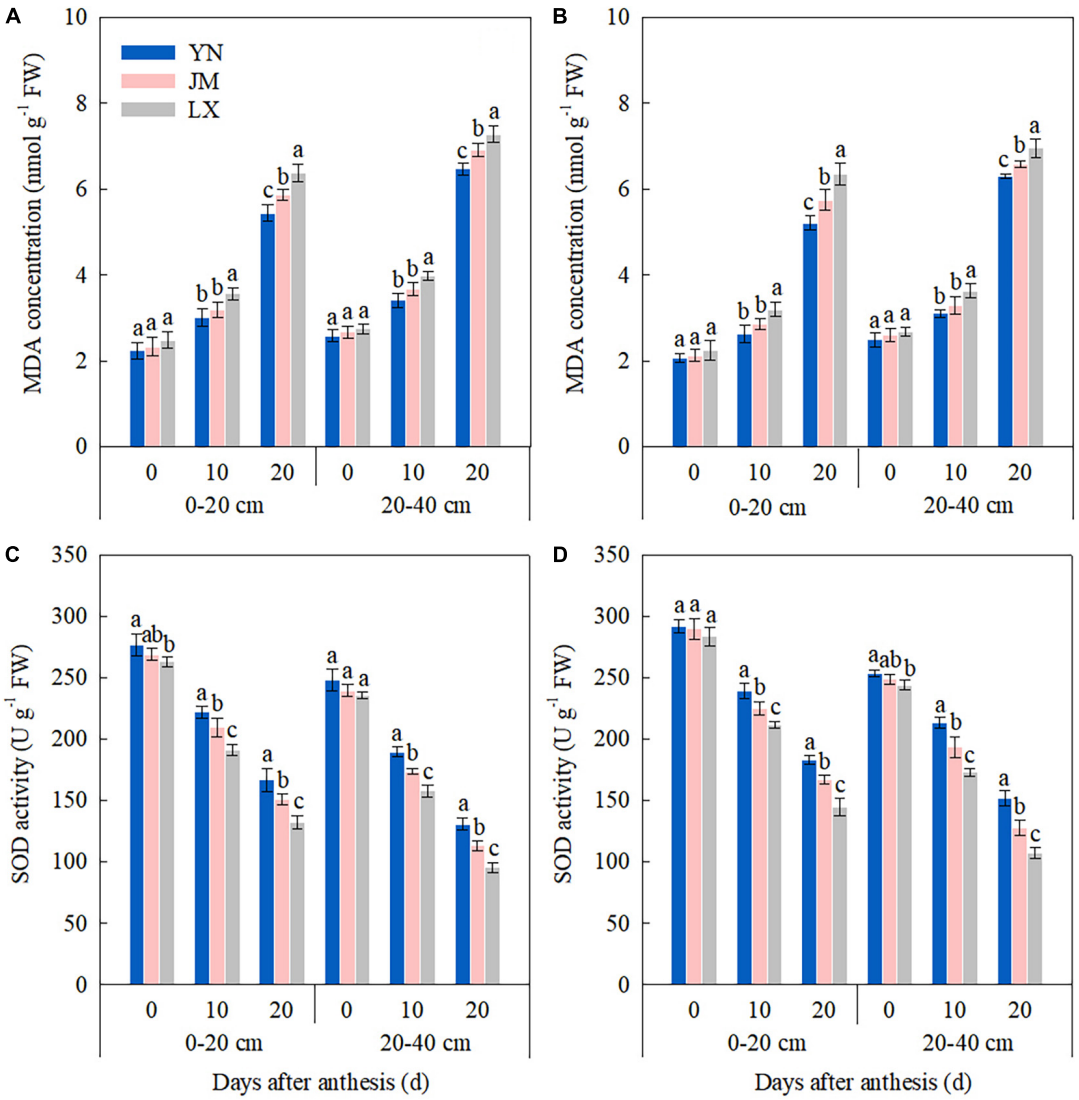

FIGURE 4 | Malondialdehyde (MDA) concentration and superoxide dismutase (SOD) activity of root in 0–20 and 20–40 cm soil layers after anthesis in 2017–2018 **(A,C)** and 2018–2019 **(B,D)** growing seasons. YN, Yannong 1212; JM, Jimai 22; LX, Liangxing 99. The different letters in the figure indicate significant differences (Duncan's test, $p < 0.05$). Vertical bars represent the SD of the means.

showed that wheat yield and WUE in the water shortage area could increase by increasing post-anthesis water use amount and ratio via a reasonable irrigation strategy (Xu et al., 2018). In this study, compared with JM and LX, YN showed lower CP from planting to anthesis but had higher ET and CP from anthesis to maturity under the same irrigation measures (**Table 1**), indicating that the post-anthesis ET and CP should be considered when selecting varieties for cultivation in the 3HP. Further, high-yielding YN can coordinate pre- and post-anthesis water use and improve the water consumption ratio after anthesis, which is beneficial to the formation of grain yield.

As precipitation cannot meet wheat water demand in 3HP, available soil water is required as an additional sources of water supply (Yang M. D. et al., 2020; Shirazi et al., 2022). The differences in the root system of wheat influenced the soil water extraction during the whole growth season of wheat (Středa et al., 2012). Over 85% consumption of the available soil water stored in the 0–50 cm layer at planting occurs due to high root density and evaporation (Shunqing et al., 2003). Wheat varieties with a higher probability of extracting water from deeper soil profiles at the vegetative phase could provide an early indication of plant productivity and lead to higher yield (Corneo et al., 2018). Thapa et al. (2020) showed that under limited irrigation conditions, water used from deeper soil layers significantly contributed to wheat yield compared to water only drawn from the shallower profile, especially in the late growing season. In this study, the differences of soil water extraction from anthesis to maturity among wheat varieties were focused in the upper 100 cm soil profile in both seasons (**Figure 2**). The higher ET and CP during anthesis to maturity shown by YN was attributed to the additional

TABLE 3 | Root triphenyl tetrazolium chloride (TTC) reduction activity of winter wheat in the 0–40 cm soil layer after anthesis of wheat varieties in the 2017–2018 and 2018–2019 growing seasons.

Year	Treatments	Root TTC reduction activity ($\mu g\ g^{-1}\ h^{-1}$)					
		0–20 cm soil layer			20–40 cm soil layer		
		0 DAA	10 DAA	20 DAA	0 DAA	10 DAA	20 DAA
2017–2018	YN	73.7a	60.2a	45.2a	59.3a	52.2a	32.6a
	JM	72.4a	51.7b	37.2b	56.1a	45.5b	25.9b
	LX	70.8a	43.6c	32.0c	55.7a	38.7c	20.7c
2018–2019	YN	80.6a	61.7a	53.7a	61.7a	53.3a	39.1a
	JM	75.8ab	52.5b	48.0b	60.2a	47.5b	35.5b
	LX	71.4b	46.8c	42.2c	58.8a	41.8c	31.8c

YN, Yannong 1212; JM, Jimai 22; LX, Liangxing 99; DAA, days after anthesis. Values followed by a different letter are significantly different (Duncan's test, $p < 0.05$) within the treatments in each year.

soil water consumption in the 0–100 cm soil layer (**Table 1** and **Figure 2**). This could be partly credited to the greater RWD of YN in the 20–60 cm soil layer at anthesis (**Figure 3**), because root distribution can greatly affect water extraction by crops, and root dry weight in deep soil layer had positive relationships with grain yield and WUE (Kang et al., 2014; Fang et al., 2017). In this study the vertical distribution of RWD in YN was not only conducive to the use of water in the 20–60 cm soil layer but was also beneficial to promoting the use of water from the deeper soil layers (60–100 cm), contributing to the improved water use pattern of YN. Measurements for the 0–20 cm soil layer have not been included in this relation in this study, which, due to the extractable water, may include the evaporative loss from the soil surface.

Most of the root distribution was in the top 0–40 cm layer of the soil profile (Fang et al., 2021). Our results supported the result that 78.8–83.9% of the total RWD (i.e., in the entire 0–100 cm soil layer) was distributed in the 0–40 cm soil layer (**Figure 3**). The enhancement of shallow root growth for high-yielding wheat production has been proposed for its role in the absorption of soil nutrients concentrated in the upper layers and the capture of precipitation (Hermanska et al., 2015; Becker et al., 2016). Fang et al. (2021) reported that wheat varieties with large root biomass and root length density in the 0–40 cm soil layer had negative effects on post-anthesis soil water use under rainfed conditions in the semi-arid area on the Loess Plateau. However, Qin et al. (2019) indicated that modern wheat varieties are better adapted on irrigated land than older varieties, due to the increased root biomass at shallow depth assisting water uptake to support greater shoot biomass and grain yield. While root biomass is not directly equivalent to root surface area, it could be assumed that a more extensive root systems could have greater biomass as well as an increased surface area (McGrail and McNear, 2021). In this study compared to JM and LX, high-yielding YN had more water consumption after anthesis and showed better root morphology characteristics in the topsoil (0–40 cm) during mid grain filling stage (root length density, root surface area density, and root diameter at 20 DAA) (**Table 2**), indicating that wheat varieties with better root morphology characteristics during mid grain filling stage could contribute to the increases in soil water absorption and wheat yield. This result is consistent with the findings of Feng et al. (2017), who showed that better root morphology characteristics were beneficial for high yield.

Hu et al. (2018) reported that under water stress conditions, the drought-tolerant wheat genotype, JM-262, showed higher antioxidase activity and a greater root system to uptake more water at the seedling stage. In sunflower (*Helianthus annuus* L.), root senescence during the grain filling stage precedes the canopy senescence that is closely links with yield formation (Lisanti et al., 2013). Our results showed that compared with JM and LX, YN had higher SOD and RTTC at 10 and 20 DAA both in 0–20 and 20–40 cm soil layers (**Figure 4** and **Table 3**), indicating

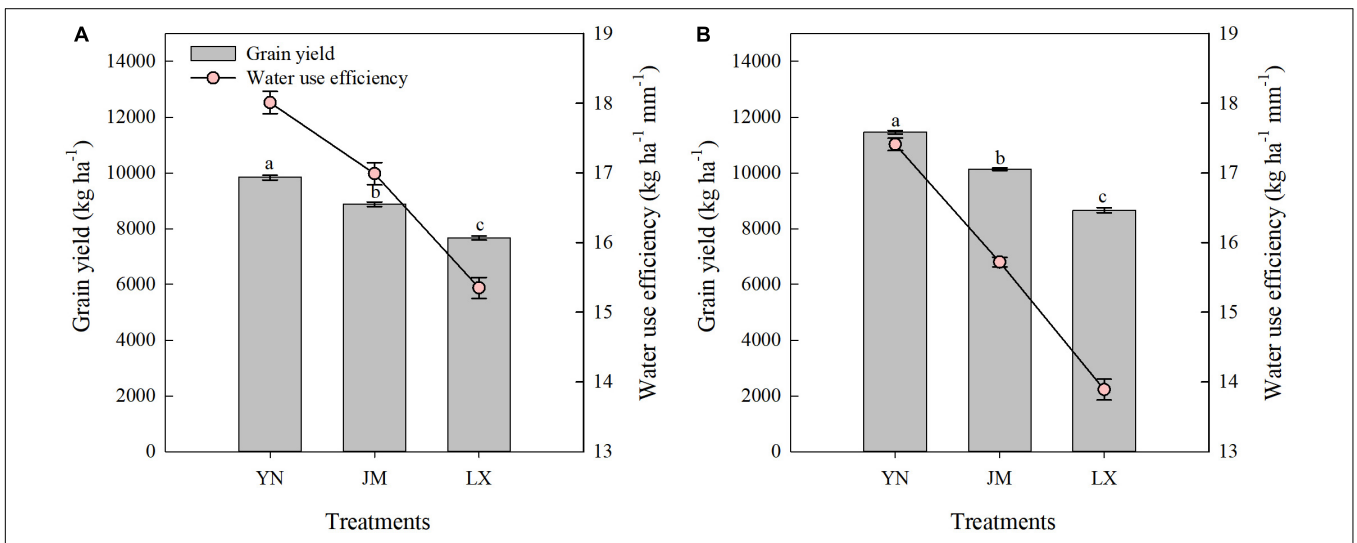

FIGURE 5 | Grain yield and water use efficiency of wheat varieties in the 2017–2018 **(A)** and 2018–2019 **(B)** growing seasons. YN, Yannong 1212; JM, Jimai 22; LX, Liangxing 99. The different letters in the figure indicate significant differences (Duncan's test, $p < 0.05$). Vertical bars represent the SD of the means.

that selecting high-yielding YN with alleviated root senescence in the upper soil layers during mid grain filling period could also contribute to the increases in soil water absorption post-anthesis and wheat yield. Because Man et al. (2016) reported that root TTC reduction activity and root SOD activity post-anthesis were strongly positively correlated with soil water consumption after anthesis, grain yield and WUE. And studies performed in rice (Liu et al., 2021) and maize (Wang et al., 2019) have been clearly demonstrated that delayed root senescence can contribute to the yield enhancement by optimizing resource acquisition from the soil.

Ensuring water use after anthesis largely improved dry matter production, which accelerated grain formation, and hence, grain yield (Xu et al., 2018). Thapa et al. (2020) showed that wheat with a grain yield of 4,807 kg ha^{-1} extracted 165 mm of stored soil water, while only 70 mm of stored soil water was extracted in wheat with a grain yield of 2,933 kg ha^{-1}. Additional consumption of 10.5 mm soil water after anthesis has been shown to increase grain yield by 620 kg ha^{-1} under moderate post-anthesis stress (Kirkegaard et al., 2007). Our study showed that compared to JM and LX, additional consumption of 22.7–44.6 mm soil water after anthesis in YN increased grain yield by 960–2797 kg ha^{-1} (**Figures 1**, **5**). The WUE in YN were 6.0% and 10.8% higher than in JM, respectively, and 17.3% and 25.3% higher than in LX, respectively, in 2017–2018 and 2018–2019. Besides producing the same grain yield from less water resources, an increased WUE in crop production can also be achieved through increased grain yield by cultivar replacement (Zhang et al., 2017; Yan et al., 2021). In this study, the increase in WUE of YN was attributed to the increased grain yield, because YN increased SWC_{AM} and obtained the highest ET_C (**Figure 1** and **Table 1**).

CONCLUSION

The high-yielding wheat variety YN with high WUE showed higher the ET and CP after anthesis and extracted more soil water in the 0–100 cm soil layer post-anthesis. Moreover, compared with JM and LX, YN obtained larger RWD in the 20–60 cm soil layer at anthesis, better root morphology characteristics, greater root antioxidant enzyme activity and higher RTTC in the 0–40 cm soil layer during mid grain filling stage. Thus, improving root development [shown as larger root distribution in 20–60 cm soil profile, improved root morphology traits and alleviated root senescence in the topsoil (0–40 cm) during the mid grain filling phase] helps to increase soil water extraction post-anthesis and should be considered as a critical strategy for breeding wheat varieties with high yield and high WUE.

DATA AVAILABILITY STATEMENT

The raw data supporting the conclusions of this article will be made available by the authors, without undue reservation.

AUTHOR CONTRIBUTIONS

YS and ZY conceived and design the study and revised the manuscript. XZ and PL performed the experiments. XZ analyzed the data and wrote the manuscript. All authors have made good contributions to this work.

FUNDING

This study was supported by the National Natural Science Foundation of China (No. 31771715), China Agriculture Research System of MOF and MARA (No. CARS-03), and Field Station Union Project of Chinese Academy of Sciences (No. KFJ-SW-YW035).

SUPPLEMENTARY MATERIAL

The Supplementary Material for this article can be found online at: https://www.frontiersin.org/articles/10.3389/fpls.2021.814658/full#supplementary-material

REFERENCES

Ali, S., Xu, Y. Y., Ma, X. C., Ahmad, I., Manzoor Jia, Q. M., et al. (2019). Deficit irrigation strategies to improve winter wheat productivity and regulating root growth under different planting patterns. *Agric. Water Manag.* 219, 1–11. doi: 10.1016/j.agwat.2019.03.038

Becker, S. R., Byrne, P. F., Reid, S. D., Bauerle, W. L., McKay, J. K., and Haley, S. D. (2016). Root traits contributing to drought tolerance of synthetic hexaploid wheat in a greenhouse study. *Euphytica* 207, 213–224. doi: 10.1007/s10681-015-1574-1

Brauman, K. A., Siebert, S., and Foley, J. A. (2013). Improvements in crop water productivity increase water sustainability and food security-a global analysis. *Environ. Res. Lett.* 8:024030. doi: 10.1088/1748-9326/8/2/024030

Chattaraj, S., Chakraborty, D., Garg, R. N., Singh, G. P., Gupta, V. K., Singh, S., et al. (2013). Hyperspectral remote sensing for growth-stage-specific water use in wheat. *Field Crops Res.* 144, 179–191. doi: 10.1016/j.fcr.2012.12.009

Corneo, P. E., Kertesz, M. A., Bakhshandeh, S., Tahaei, H., Barbour, M. M., and Dijkstra, F. A. (2018). Studying root water uptake of wheat genotypes in different soils using water $\delta^{18}O$ stable isotopes. *Agric. Ecosyst. Environ.* 264, 119–129. doi: 10.1016/j.agee.2018.05.007

Dazhong Daily (2020). With yields of over 800 kg per mu in successive years, Yannong 1212 has achieved a new breakthrough in high-yield breeding technology. Available online at: https://3g.163.com/dy/article/FGEV87NM0530WJTO.html (accessed December 2, 2021).

Fang, Y., Du, Y., Wang, J., Wu, A., Qiao, S., Xu, B., et al. (2017). Moderate drought stress affected root growth and grain yield in old, modern and newly released cultivars of winter wheat. *Front. Plant Sci.* 8:672. doi: 10.3389/fpls.2017.00672

Fang, Y., Liang, L. Y., Liu, S., Xu, B. C., Siddique, K. H., Palta, J. A., et al. (2021). Wheat cultivars with small root length density in the topsoil increased post-anthesis water use and grain yield in the semi-arid region on the Loess Plateau. *Eur. J. Agron.* 124:126243. doi: 10.1016/j.eja.2021.126243

Faralli, M., Cockram, J., Ober, E., Wall, S., Galle, A., Van Rie, J., et al. (2019). Genotypic, developmental and environmental effects on the rapidity of gs in wheat: impacts on carbon gain and water-use efficiency. *Front. Plant Sci.* 10:492. doi: 10.3389/fpls.2019.00492

Feng, S., Gu, S., Zhang, H., and Wang, D. (2017). Root vertical distribution is important to improve water use efficiency and grain yield of wheat. *Field Crops Res.* 214, 131–141. doi: 10.1016/j.fcr.2017.08.007

Gardner, W. H. (1986). "Water content," in *Methods of Soil Analysis: Part 1-Physical and Mineralogical Methods-Agronomy Monograph No. 9, 2nd edition, Soil Sci. Soc, Amer*, ed. A. Klute (Madison, WI: Wiley), 493–544.

Guo, Z., Shi, Y., Yu, Z., and Zhang, Y. (2015). Supplemental irrigation affected flag leaves senescence post-anthesis and grain yield of winter wheat in the Huang-Huai-Hai Plain of China. *Field Crops Res.* 180, 100–109. doi: 10.1016/j.fcr.2015.05.015

Harmsen, E. W., Miller, N. L., Schlegel, N. J., and Gonzalez, J. E. (2009). Seasonal climate change impacts on evapotranspiration, precipitation deficit and crop yield in Puerto Rico. *Agric. Water Manag.* 96, 1085–1095. doi: 10.1016/j.agwat.2009.02.006

He, J., Shi, Y., Zhao, J., and Yu, Z. (2019). Strip rotary tillage with a two-year subsoiling interval enhances root growth and yield in wheat. *Sci. Rep.* 9:11678. doi: 10.1038/s41598-019-48159-4

He, Z. H., Zhuang, Q. S., Cheng, S. H., Yu, Z. W., Zhao, Z. D., and Liu, X. (2018). Wheat production and technology improvement in China. *J. Agric.* 8, 99–106.

Hermanska, A., Streda, T., and Chloupek, O. (2015). Improved wheat grain yield by a new method of root selection. *Agron. Sustain. Dev.* 35, 195–202. doi: 10.1007/s13593-014-0227-4

Hu, L., Xie, Y., Fan, S., Wang, Z., Wang, F., Zhang, B., et al. (2018). Comparative analysis of root transcriptome profiles between drought-tolerant and susceptible wheat genotypes in response to water stress. *Plant Sci.* 272, 276–293. doi: 10.1016/j.plantsci.2018.03.036

Iqbal, M. A., Shen, Y., Stricevic, R., Pei, H., Sun, H., Amiri, E., et al. (2014). Evaluation of the FAO AquaCrop model for winter wheat on the North China Plain under deficit irrigation from field experiment to regional yield simulation. *Agric. Water Manag.* 135, 61–72. doi: 10.1016/j.agwat.2013.12.012

Jha, S. K., Gao, Y., Liu, H., Huang, Z. D., Wang, G. S., Liang, Y. P., et al. (2017). Root development and water uptake in winter wheat under different irrigation methods and scheduling for North China. *Agric. Water Manag.* 182, 139–150. doi: 10.1016/j.agwat.2016.12.015

Jin, X., Yang, G., Xue, X., Xu, X., Li, Z., and Feng, H. (2017). Validation of two Huanjing-1A/B satellite-based FAO-56 models for estimating winter wheat crop evapotranspiration during mid-season. *Agric. Water Manag.* 189, 27–38. doi: 10.1016/j.agwat.2017.04.017

Kang, L. Y., Yun, S. C., and Li, S. Q. (2014). Effects of phosphorus application in different soil layers on root growth, yield, and water-use efficiency of winter wheat grown under semi-arid conditions. *J. Integr. Agric.* 13, 2028–2039. doi: 10.1016/S2095-3119(14)60751-6

Kirkegaard, J. A., Lilley, J. M., Howe, G. N., and Graham, J. M. (2007). Impact of subsoil water use on wheat yield. *Aust. J. Agric. Res.* 58, 303–315. doi: 10.1071/ar06285

Li, J. P., Zhang, Z., Liu, Y., Yao, C. S., Song, W. Y., Xu, X. X., et al. (2019). Effects of micro-sprinkling with different irrigation amount on grain yield and water use efficiency of winter wheat in the North China Plain. *Agric. Water Manag.* 224:105736. doi: 10.1016/j.agwat.2019.105736

Liang, P., Shi, Y., Zhao, J. Y., Wang, X. Z., and Yu, Z. W. (2018). Differences of canopy light interception characteristics and yield in different yield potential wheat varieties. *J. Triticeae Crops* 38, 1189–1194.

Lisanti, S., Hall, A. J., and Chimenti, C. A. (2013). Influence of water, deficit and canopy senescence pattern on *Helianthus annuus (L.)* root functionality during the grain-filling phase. *Field Crops Res.* 154, 1–11. doi: 10.1016/j.fcr.2013.08.009

Liu, B. T., Li, H. L., Li, H. B., Zhang, A. P., and Rengel, Z. (2021). Long-term biochar application promotes rice productivity by regulating root dynamic development and reducing nitrogen leaching. *GCB Bioenergy* 13, 257–268. doi: 10.1111/gcbb.12766

Liu, E. K., Mei, X. R., Yan, C. R., Gong, D. Z., and Zhang, Y. O. (2016). Effects of water stress on photosynthetic characteristics, dry matter translocation and WUE in two winter wheat genotypes. *Agric. Water Manag.* 167, 75–85. doi: 10.1016/j.agwat.2015.12.026

Liu, H. Y., Wang, W. Q., He, A. B., and Nie, L. X. (2018). Correlation of leaf and root senescence during ripening in dry seeded and transplanted rice. *Rice Sci.* 25, 279–285. doi: 10.1016/j.rsci.2018.04.005

Lv, L., Wang, H., Jia, X., and Wang, Z. (2011). Analysis on water requirement and water-saving amount of wheat and corn in typical regions of the North China Plain. *Front. Agric. China* 5:556–562. doi: 10.1007/s11703-011-1149-4

Ma, S., Zhang, W., Duan, A., and Wang, T. (2019). Effects of controlling soil moisture regime based on root-sourced signal characteristics on yield formation and water use efficiency of winter wheat. *Agric. Water Manag.* 221, 486–492. doi: 10.1016/j.agwat.2019.05.019

Ma'arup, R., Trethowan, R. M., Ahmed, N. U., Bramley, H., and Sharp, P. J. (2020). Emmer wheat (*Triticum dicoccon Schrank*) improves water use efficiency and yield of hexaploid bread wheat. *Plant Sci.* 295:110212. doi: 10.1016/j.plantsci.2019.110212

Man, J., Shi, Y., Yu, Z., and Zhang, Y. (2016). Root growth, soil water variation, and grain yield response of winter wheat to supplemental irrigation. *Plant Prod. Sci.* 19, 193–205. doi: 10.1080/1343943x.2015.1128097

McGrail, R. K., and McNear, Jr. D. H (2021). Two centuries of breeding has altered root system architecture of winter wheat. *Rhizosphere* 19:100411. doi: 10.1016/j.rhisph.2021.100411

Meena, R. P., Karnam, V., Tripathi, S. C., Jha, A., Sharma, R. K., and Singh, G. P. (2019a). Irrigation management strategies in wheat for efficient water use in the regions of depleting water resources. *Agric. Water Manag.* 214, 38–46. doi: 10.1016/j.agwat.2019.01.001

Meena, R. P., Karnam, V., Rinki, R. S., Sharma, R. K., Tripathi, S. C., Singh, G. P., et al. (2019b). Identification of water use efficient wheat genotypes with high yield for regions of depleting water resources in India. *Agric. Water Manag.* 223:105709. doi: 10.1016/j.agwat.2019.105709

Ministry of agriculture and rural affairs of the People's Republic of China (2016). *China Agriculture Statistical Report 2015*. Beijing: China Agriculture Press.

Ministry of agriculture and rural affairs of the People's Republic of China (2019). *China Agriculture Statistical Report 2017*. Beijing: China Agriculture Press.

Ministry of agriculture and rural development of the People's Republic of China (2020). *Announcement No. 295 Of Ministry Of Agriculture And Rural Development Of The People's Republic Of China*. Available online at: http://www.moa.gov.cn/nybgb/2020/202006/202007/t20200706_6347888.htm (accessed December 2, 2021).

Nehe, A. S., Misra, S., Murchie, E. H., Chinnathambi, K., Tyagi, B. S., and Foulkes, M. J. (2020). Nitrogen partitioning and remobilization in relation to leaf senescence, grain yield and protein concentration in Indian wheat cultivars. *Field Crops Res.* 251:107778. doi: 10.1016/j.fcr.2020.107778

Qin, X., Feng, F., Wen, X., Siddique, K. H. M., and Liao, Y. (2019). Historical genetic responses of yield and root traits in winter wheat in the yellow-Huai-Hai River valley region of China due to modern breeding (1948-2012). *Plant Soil.* 439, 7–18. doi: 10.1007/s11104-018-3832-1

Rashid, M. A., Jabloun, M., Andersen, M. N., Zhang, X. Y., and Olesen, J. E. (2019). Climate change is expected to increase yield and water use efficiency of wheat in the North China Plain. *Agric. Water Manag.* 222, 193–203. doi: 10.1016/j.agwat.2019.06.004

Severini, A. D., Wasson, A. P., Evans, J. R., Richards, R. A., and Watt, M. (2020). Root phenotypes at maturity in diverse wheat and triticale genotypes grown in three field experiments: relationships to shoot selection, biomass, grain yield, flowering time, and environment. *Field Crops Res.* 255:107870. doi: 10.1016/j.fcr.2020.107870

Shirazi, S. Z., Mei, X. R., Liu, B. C., and Liu, Y. (2022). Estimating potential yield and change in water budget for wheat and maize across Huang-Huai-Hai Plain in the future. *Agric. Water Manag.* 260:107282. doi: 10.1016/j.agwat.2021.107282

Shunqing, A., Gengshan, L., and Anhong, G. (2003). Consumption of available soil water stored at planting by winter wheat. *Agric. Water Manag.* 63, 99–107. doi: 10.1016/s0378-3774(03)00176-8

Středa, T., Dostál, V., Horáková, V., and Chloupek, O. (2012). Effective use of water by wheat varieties with different root system sizes in rain-fed experiments in Central Europe. *Agric. Water Manag.* 104, 203–209. doi: 10.1016/j.agwat.2011.12.018

Sun, Q., Kröbel, R., Müller, T., Römheld, V., Cui, Z., Zhang, F., et al. (2011). Optimization of yield and water-use of different cropping systems for sustainable groundwater use in North China Plain. *Agric. Water Manag.* 98, 808–814. doi: 10.1016/j.agwat.2010.12.007

Thapa, S., Xue, Q., Jessup, K. E., Rudd, J. C., Liu, S., Devkota, R. N., et al. (2020). Soil water extraction and use by winter wheat cultivars under limited irrigation in

a semi-arid environment. *J. Arid Environ.* 174:104046. doi: 10.1016/j.jaridenv.2019.104046

Wang, D. (2017). Water use efficiency and optimal supplemental irrigation in a high yield wheat field. *Field Crops Res.* 213, 213–220. doi: 10.1016/j.fcr.2017.08.012

Wang, H., Xu, R. R., Li, Y., Yang, L. Y., Shi, W., Liu, Y. J., et al. (2019). Enhance root-bleeding sap flow and root lodging resistance of maize under a combination of nitrogen strategies and farming practices. *Agric. Water Manag.* 224:105742. doi: 10.1016/j.agwat.2019.105742

Wasson, A. P., Richards, R. A., Chatrath, R., Misra, S. C., Prasad, S. V. S., Rebetzke, G. J., et al. (2012). Traits and selection strategies to improve root systems and water uptake in water-limited wheat crops. *J. Exp. Bot.* 63, 3485–3498. doi: 10.1093/jxb/ers111

Xu, X., Zhang, M., Li, J., Liu, Z., Zhao, Z., Zhang, Y., et al. (2018). Improving water use efficiency and grain yield of winter wheat by optimizing irrigations in the North China Plain. *Field Crops Res.* 221, 219–227. doi: 10.1016/j.fcr.2018.02.011

Yan, J. K., Zhang, N. N., Kang, F. R., Wang, J. W., and Wang, X. L. (2021). Cultivar replacement increases water use efficiency in foxtail millet in Shaanxi Province, China. *Plant Physiol. Biochem.* 164, 73–81. doi: 10.1016/j.plaphy.2021.04.036

Yang, J. C., Zhang, H., and Zhang, J. H. (2012). Root morphology and physiology in relation to the yield formation of rice. *J. Integr. Agric.* 11, 920–926. doi: 10.1016/s2095-3119(12)60082-3

Yang, M. D., Leghari, S. J., Guan, X. K., Ma, S. C., Ding, C. M., Mei, F. J., et al. (2020). Deficit subsurface drip irrigation improves water use efficiency and stabilizes yield by enhancing subsoil water extraction in winter wheat. *Front. Plant Sci.* 11:508. doi: 10.3389/fpls.2020.00508

Yang, Z. Z., Wang, Z. H., Hu, Z. L., Xin, M. M., Yao, Y. Y., Peng, H. R., et al. (2020). Comparative analysis of the genomic sequences between commercial wheat varieties Jimai 22 and Liangxing 99. *Acta Agron. Sin.* 46, 1870–1883.

Zeleke, K. T., and Nendel, C. (2016). Analysis of options for increasing wheat (*Triticum aestivum L.*) yield in south-eastern Australia: the role of irrigation, cultivar choice and time of sowing. *Agric. Water Manae.* 166, 139–148. doi: 10.1016/j.agwat.2015.12.016

Zhang, X., Chen, S., Sun, H., Wang, Y., and Shao, L. (2010). Water use efficiency and associated traits in winter wheat cultivars in the North China Plain. *Agric. Water Manag.* 97, 1117–1125. doi: 10.1016/j.agwat.2009.06.003

Zhang, X., Qin, W., Chen, S., Shao, L., and Sun, H. (2017). Responses of yield and WUE of winter wheat to water stress during the past three decades-A case study in the North China Plain. *Agric. Water Manag.* 179, 47–54. doi: 10.1016/j.agwat.2016.05.004

Zhao, J., Han, T., Wang, C., Jia, H., Worqlul, A. W., Norelli, N., et al. (2020). Optimizing irrigation strategies to synchronously improve the yield and water productivity of winter wheat under interannual precipitation variability in the North China Plain. *Agric. Water Manag.* 240:106298. doi: 10.1016/j.agwat.2020.106298

Conflict of Interest: The authors declare that the research was conducted in the absence of any commercial or financial relationships that could be construed as a potential conflict of interest.

Publisher's Note: All claims expressed in this article are solely those of the authors and do not necessarily represent those of their affiliated organizations, or those of the publisher, the editors and the reviewers. Any product that may be evaluated in this article, or claim that may be made by its manufacturer, is not guaranteed or endorsed by the publisher.

frontiers in Plant Science

ORIGINAL RESEARCH
published: 08 February 2022
doi: 10.3389/fpls.2021.788651

Impact of Combining Long-Term Subsoiling and Organic Fertilizer on Soil Microbial Biomass Carbon and Nitrogen, Soil Enzyme Activity, and Water Use of Winter Wheat

Yonghui Yang[1,2,3], Minjie Li[1,2,4], Jicheng Wu[1,2,3,4], Xiaoying Pan[1,2,3], Cuimin Gao[1,2,3] and Darrell W. S. Tang[5]*

[1] Institute of Plant Nutrition and Resource Environment, Henan Academy of Agricultural Sciences, Zhengzhou, China, [2] Yuanyang Experimental Station of Crop Water Use, Ministry of Agriculture, Yuanyang, China, [3] Field Scientific Observation and Research Station of Water Saving Agriculture in the Yellow River Basin of Henan Province, Yuanyang, China, [4] Department of Bioengineering, School of Life Sciences, Zhengzhou University, Zhengzhou, China, [5] Soil Physics and Land Management Group, Wageningen University and Research, Wageningen, Netherlands

Reductions in soil productivity and soil water retention capacity, and water scarcity during crop growth, may occur due to long-term suboptimal tillage and fertilization practices. Therefore, the application of appropriate tillage (subsoiling) and fertilization (organic fertilizer) practices is important for improving soil structure, water conservation and soil productivity. We hypothesize that subsoiling tillage combined with organic fertilizer has a better effect than subsoiling or organic fertilizer alone. A field experiment in Henan, China, has been conducted since 2011 to explore the effects of subsoiling and organic fertilizer, in combination, on winter wheat (*Triticum aestivum* L.) farming. We studied the effects of conventional tillage (CT), subsoiling (S), organic fertilizer (OF), and organic fertilizer combined with subsoiling (S+OF) treatments on dry matter accumulation (DM), water consumption (ET), water use efficiency (WUE) at different growth stages, yield, and water production efficiency (WPE) of winter wheat over 3 years (2016–2017, 2017–2018, 2018–2019). We also analyzed the soil structure, soil organic carbon, soil microbial biomass carbon and nitrogen, and soil enzymes in 2019. The results indicate that compared with CT, the S, OF and S+OF treatments increased the proportion of >0.25 mm aggregates, and S+OF especially led to increased soil organic carbon, soil microbial biomass carbon and nitrogen, soil enzyme activity (sucrase, cellulose, and urease). S+OF treatment was most effective in reducing ET, and increasing DM and WUE during the entire growth period of wheat. S+OF treatment also increased the total dry matter accumulation (Total DM) and total water use efficiency (total WUE) by 18.6–32.0% and 36.6–42.7%, respectively, during these 3 years. Wheat yield and WPE under S+OF treatment increased by 11.6–28.6% and 26.8–43.6%, respectively, in these 3 years. Therefore, S+OF in combination was found to be superior to S or OF alone, which in turn yielded better results than the CT.

Keywords: subsoiling, organic fertilizer, combined amendments, soil microbial biomass carbon and nitrogen, water use, yield

OPEN ACCESS

Edited by:
Italo F. Cuneo, Pontificia Universidad Católica de Valparaíso, Chile

Reviewed by:
Junhng Xie, Gansu Agricultural University, China
Nobuhito Sekiya, Mie University, Japan

****Correspondence:***
Yonghui Yang
yangyongh2020@126.com

Specialty section:
This article was submitted to Crop and Product Physiology, a section of the journal Frontiers in Plant Science

Received: *03 October 2021*
Accepted: *16 December 2021*
Published: *08 February 2022*

Citation:
Yang Y, Li M, Wu J, Pan X, Gao C and Tang DWS (2022) Impact of Combining Long-Term Subsoiling and Organic Fertilizer on Soil Microbial Biomass Carbon and Nitrogen, Soil Enzyme Activity, and Water Use of Winter Wheat. Front. Plant Sci. 12:788651. doi: 10.3389/fpls.2021.788651

INTRODUCTION

Water scarcity and seasonal drought are major constraints on agricultural development globally. Henan province, the main wheat producing region of China, accounts for a quarter of total wheat production in the country (Wu et al., 2003). In addition, due to historical rotary tillage practices, the soil structure has become suboptimal for agriculture: evaporation rates have increased and the soil moisture retention capacity has decreased (Hemmat and Eskandari, 2004; Vita et al., 2007), which further exacerbates the imbalance between water supply and demand. Thus, wheat yields in the area are severely limited by water deficiency. Therefore, improving the utilization efficiency of limited water resources and alleviating the damage caused by drought stress to crops has become an important issue (Li et al., 2015).

Effective tillage and fertilization measures can improve soil properties, increase the water use efficiency of the crop, and increase yields (Sang et al., 2016; Wang et al., 2016; Bottinelli et al., 2017; Zhang et al., 2017). Subsoiling can break the bottom of the plow layer, deepen the soil tillage layer, improve soil pore characteristics, enhance soil infiltration and moisture retention capacity, and increase water use efficiency (Zheng et al., 2011; Sang et al., 2014) and crop yields (Mohanty et al., 2007; Yan et al., 2011; Hu et al., 2013; Yang et al., 2016; Li et al., 2019). Studies have shown that subsoiling can maintain higher physiological activity in flag leaves, increase the accumulation of dry matter in the middle and later stages of wheat growth, and delay the senescence of wheat plants (Zhang et al., 2008; Chu et al., 2012). In addition, Piovanelli et al. (2006) and Kuzyakov and Xu (2013) found that subsoiling can improve crop root growth, which helps maintain optimal plant growth, increases the activity of urease and sucrase in the soil (Sun et al., 2019), while also increasing root stubble and root secretions, which in turn increase the growth and capacity of microorganisms in the soil, thereby activating soil nutrients and promoting nutrient absorption by crops.

The application of organic fertilizers can also improve soil fertility and soil structure, and increase soil water storage and retention capacity, which then improves photosynthetic capacity, water use efficiency and crop yield (Lu et al., 2011; Karami et al., 2012; Liu et al., 2013). Wang et al. (2020) found that organic fertilizers increased grain yield and water use efficiency by an average of 18 and 20% compared to inorganic fertilizer. Studies have also shown that organic fertilizer can improve photosynthetic capacity and delay leaf senescence, which beneficial for increasing the accumulation of dry matter above ground (Dordas, 2009; Bogard et al., 2010). Furthermore, organic fertilizers are a source of carbon, nitrogen, and microorganisms, which provides energy and material for the growth of microorganisms in the soil, and increases the microbial composition of carbon and nitrogen in the soil (Elfstrand et al., 2007). Liang et al. (2010) showed that compared with non-fertilization, the long-term application of organic fertilizer can increase microbial carbon and nitrogen content in the soil by 1.4–2.7 times and 1.9–2.5 times, respectively. However, Zhang et al. (2013) found that single application of organic fertilizer had no significant impact on microbial carbon volume in the soil. Some studies (Bu et al., 2006; Rehana et al., 2008) have shown that long-term application of organic fertilizer can improve the activity of different types of enzymes in the soil, especially urease, sucrase and protease (Pu et al., 2020).

As discussed above, most prior studies have focused on the effects of solely subsoiling or organic fertilizer treatment. Few studies have systematically studied the impact of long-term application of these treatments and the combined application of subsoiling and organic fertilizer, on soil structure, soil microbial biomass carbon and nitrogen, soil enzyme activity, soil water and water use of crops, and any possible correlations between these outcomes. We hypothesize that subsoiling combined with organic fertilizer has a better effect on physical and chemical properties and water use of wheat than subsoiling or organic fertilizer alone, in alleviating or resolving crop damage due to seasonal drought and water scarcity. This study is based on 3 years of results from a long-term experiment, and studies the influence of the individual practices and their combined application on crop water production efficiency (WPE) and yield. We aim to also investigate the mechanisms underlying the effects of these practices, to provide a theoretical basis that would lead to efficient crop water use and yield increases in the region and other geographically similar regions in China and elsewhere. To accomplish this, we analyze the effects of these treatments on soil microbial biomass carbon and nitrogen, soil enzyme activity, dry matter accumulation, and water use efficiency at various growth stages of winter wheat, and perform correlation analyses on these experimental outcomes.

MATERIALS AND METHODS

Experiment Location

The experiments analyzed in this study were conducted at the Tongxu Experimental Station (144°26′58.47″E; 34°25′44. 26″ N, 62 m above sea level) of the Water Saving Agricultural Base in the east of Henan province from 2016 to 2019, as part of a long-term experiment started in October 2011. The annual average temperature is 14.2℃. The mean annual precipitation is 675.9 mm, of which approximately 60% is received from July to September. The region is topographically flat with uniform fertility. According to the international texture classification system, the soil type is mostly sand and loam [59.1% sand (2–0.02 mm), 22.5% silt (0.02–0.002 mm), with 18.4% clay (<0.002 mm)] derived from loess soils. At the start of the present experiment, the organic matter, total nitrogen, nitrate nitrogen, ammonium nitrogen, available phosphorus, available potassium, and bulk density in top layer of soil (0–20 cm) were 11.4 g kg^{-1}, 0.81 g kg^{-1}, 74.31 mg kg^{-1}, 55.89 mg kg^{-1}, 19.8 mg kg^{-1}, 90.3 mg kg^{-1}, and 1.3 g cm^{-1}, respectively. Crop rotation between wheat and maize has been employed in the area for over 50 years. **Figure 1** shows the precipitation and atmospheric temperature during the wheat growing seasons for

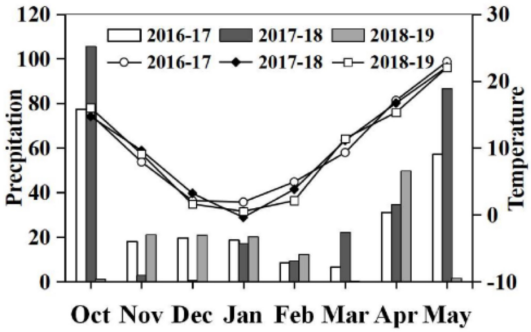

FIGURE 1 | Precipitation and temperature during the growing period of wheat in three seasons (2016–2017, 2017–2018, and 2018–2019).

the years of 2016–2019, and illustrates the rainy growth seasons of 2016–2017 and 2017–2018, and the dry growth season of 2018–2019.

Experimental Design

In the experiment, a randomized split-plot design was adopted, divided into 12 plots with three replicates: CT (conventional tillage, 15 cm deep, plowing with a rotavator), S (subsoiling, 30 cm deep, loosening the plow bottom layer and the core soil layer with a deep loosening machine without turning the soil layer), OF (organic fertilizer, 15 cm deep, plowing with a rotavator), S+OF (organic fertilizer combined with subsoiling, 30 cm deep, loosening the plow bottom layer and the core soil layer with a deep loosening machine without turning the soil layer). The nitrogen, phosphorus and potassium contents of the organic fertilizer were, respectively, 1.5, 1.2, 0.8%. The plot size was 33.6 m^2 (5.6 m × 6 m) with wheat spaced 20 cm apart sown at 195 kg hm^{-2}. Urea (N, 225 kg hm^{-2}), calcium superphosphate (P, 105 kg hm^{-2}) and potassium chloride (K, 75 kg hm^{-2}), and the total amount of N, P, K applied to all treatments were identical. 50% of the nitrogen fertilizer was applied before sowing, and the remaining 30 and 20% were applied at the jointing and booting stage, respectively. Irrigation was carried out at the jointing stage and grouting stage, respectively, with the amount of irrigation being 60 mm. The wheat cultivars were Bainong 207 in 2016–2017, and Zhengmai 369 in 2017–2018 and 2018–2019. Wheat was sown in the middle of October and harvested in early June.

Sampling and Measurements

Measurement of Soil Water Storage

Soil samples in the soil profile (0–100 cm layer) were collected using soil augers at the sowing, booting, anthesis and harvest stages of wheat, while soil water storage was measured with the oven drying method.

Equations (1) and (2) are used to calculate the soil quality water content and soil water storage (Zhang et al., 2019).

$$SWC(\%) = \frac{W1 - W2}{W2} \times 100 \quad (1)$$

$$Soil\ water\ storage(mm) = \Sigma SWC_i \cdot D_i \cdot H_i \ \ i(1, n) \quad (2)$$

where SWC represents the soil water content (%), $W1$(g) represents wet soil weight, $W2$ (g) represents dried soil weight, D_i (g cm^{-3}) is the soil bulk density of layer i, and H_i (mm) represents the soil depth. The water consumption at each growth stage was calculated with Equations (3) and (4) (Guo et al., 2015; Wang et al., 2019).

$$\Delta S = 10\Sigma(SWC_{il} - SWC_{i2}) \cdot D_i \cdot H_i \quad (3)$$

$$ET_{1-2} = 10\sum_{i=1}^{n}(SWC_{il} - SWC_{i2})D_iH_i + I + P \quad i(1,n) \quad (4)$$

where SWC_{il} and SWC_{i2} represent the soil water content at the bottom of layer i, and the soil moisture at the top of layer i, respectively; D_i (g cm^{-3}) is the soil bulk density of layer i, H_i (mm) represents the soil depth; ET_{1-2} (mm) is water consumption amounts during a growth stage (mm), and I and P represent the irrigation (mm) and precipitation during the growth period of wheat, respectively.

Dry Matter Accumulation and Water Use Efficiency

The 1 m double-rows of wheat plant samples were collected at the jointing stage, booting stage, anthesis stage and harvesting stage, then dry matter was measured with the oven drying method at 70℃. After calculating the dry matter accumulation per unit area, the water use efficiency (WUE) was computed as:

$$WUE = DM/ET \quad (5)$$

where WUE and DM are the water use efficiency and dry matter accumulation of wheat.

Grain Yield and Components

At the harvest stage, the number of ears per 0.5 m^2 in each plot was calculated; wheat plants from a randomly chosen 4 m^2 area in each plot were harvested and then threshed, air-dried and weighted to calculate the grain yield, and converted into grain yield per unit area. In addition, 10 wheat plants were randomly selected from each plot, their grain numbers were counted, and the grain numbers per ear were calculated. The yield WPE is:

$$WPE = Y/ET \quad (6)$$

where WPE is yield WPE; Y is the grain yield; ET is the total water consumption during the entire growth period of wheat.

Determination of Soil Microbial Biomass Carbon and Nitrogen, Soil Enzyme Activity, Soil Organic Carbon, and Soil Aggregates

Determination of soil microbial biomass carbon and soil microbial biomass nitrogen was determined with the chloroform fumigation extraction method (Vance et al., 1987; Christianson,

TABLE 1 | Effects of subsoiling, organic fertilizer and subsoiling combined with organic fertilizer on the dry matter accumulation (DM) at different growth stages of winter wheat in the three seasons of 2016–2019.

Year	Treatments	STJ	JTB	BTA	ATH	Total DM
2016–2017	CT	2487.0c	4170.4c	2640.0c	3175.7c	12473.0c
	S	2869.6b	4521.7b	3304.3a	3434.8b	14130.4b
	OF	3163.5a	4652.2ab	2977.4b	3256.5c	14049.7b
	S+OF	3269.6a	4700.0a	3269.6a	3555.7a	14794.8a
2017–2018	CT	2837.0c	4614.8c	2572.2c	3366.5c	13390.4c
	S	3104.3b	5021.7b	3515.2b	4063.0b	15704.3b
	OF	3287.0ab	5259.1a	3427.8b	3991.3b	15965.2b
	S+OF	3334.8a	5438.3a	3642.6a	4412.2a	16827.8a
2018–2019	CT	1944.3c	3888.7d	2580.0c	2654.8c	11067.8c
	S	2347.8b	4343.5c	3208.7ab	3482.6b	13382.6b
	OF	2415.2b	4523.0b	3087.1b	3675.5a	13700.9b
	S+OF	2556.5a	4884.8a	3332.6a	3834.8a	14608.7a

STJ, sowing to jointing; JTB, jointing to booting; BTA, booting to anthesis; ATH, anthesis to harvest; Total DM, the total dry matter accumulation. CT, conventional tillage; S, subsoiling; OF, organic fertilizer; S+OF, organic fertilizer organic fertilizer combined with subsoiling. Different lowercase letters within a column mean significant difference between treatments at three seasons by LSD test ($P < 0.05$).

1988; Moore et al., 2000). 3,5-dinitro salicylic acid was used to determine soil sucrase and cellulase activity (Guan, 1986; Qin et al., 2020), while soil urease activity was determined with the indigo phenol ratio method (Wang et al., 2009; Qin et al., 2020), and protease activity was determined with the ninhydrin contrast color method (Guan, 1986; Qin et al., 2020). The soil total organic carbon content was determined using a heavy cadmium acid potassium outside heating method (Westerman, 1990). The size distribution of water-stable aggregates was determined using the wet sieving method (Elliot, 1986). The aggregated soil was separated into different size fractions by gently shaking the samples into the water through a range of sieves to obtain the aggregate size fractions <0.25, 0.25∼0.5, 0.5∼1.0, 1.0∼2.0, 2.0∼3.0, 3.0∼5.0, and >5 mm.

STATISTICAL ANALYSIS

The experimental data was statistically analyzed using SPSS 19.0. Three replicates were calculated for each treatment, and ANOVA was applied to compare whether different treatments were significantly different at $P < 0.05$ in **Tables 1**, **2** and **Figures 2**–**7**. The relationships between dry matter accumulation, soil water and soil organic carbon, soil microbial biomass carbon and nitrogen, and soil enzyme activity are described with the linear regression functions listed in **Table 3**. The relationships between yield of wheat and soil organic carbon, soil microbial biomass carbon and nitrogen, and soil enzyme activity are described with the linear regression functions listed in **Table 4**. The relationship between yield, WPE and dry matter accumulation, WUE of wheat at different growth stages under different treatments are described with the linear regression functions listed in **Table 5**.

RESULTS

Effects of Combining Subsoiling and Organic Fertilizer on Physical and Chemical Properties of the Soil

Soil Structure

As shown in **Table 6**. Subsoiling (S), organic fertilizer (OF), and organic fertilizer combined with subsoiling (S+OF) increased the proportion of 0.5–1, 1–2, 2–3, 3–5, and >5 mm aggregates significantly. S+OF treatment showed a larger effect on >3 mm aggregates than S and OF treatments. However, the proportion of <0.25 mm aggregates under CT and S treatments was higher than that under OF and S+OF. S+OF resulted in the highest proportion of >0.25 mm aggregate compared to other treatments.

Soil Organic Carbon

Figure 2 shows that across the growth period of wheat, soil organic carbon first decreased (wintering stage), then increased (anthesis stage) and finally decreased again (filling and harvest). S, OF and S+OF treatments increased soil organic carbon compared to CT at the different growth stages of wheat, and there was no difference between the S and OF treatments. The organic carbon content under S+OF treatment was the highest. This indicates that subsoiling coupled with organic fertilizer was more effective at increasing soil organic carbon compared to solely S or OF treatment.

Soil Microbial Biomass Carbon and Nitrogen

Figure 3 shows that across the growth period of wheat, the content of microbial carbon and nitrogen in the soil first decreased, then increased, and finally decreased again. Soil microbial biomass carbon and nitrogen at the jointing stage were lowest, and that at the anthesis stage was highest, compared to other growth stages. Compared to the other treatments, S+OF treatment was more beneficial for soil microbial biomass carbon and nitrogen.

Soil Enzyme Activity

From **Figures 4**, **5**, S+OF treatment improved sucrase activity, cellulase activity and urease activity of wheat compared to the other treatments. However, protease activity of S treatment was the highest compared to other treatments throughout all growth stages of wheat except the anthesis stage.

Effects of Combining Subsoiling and Organic Fertilizer on Soil Water Storage

As shown in **Figure 6**, it was found that in comparison with CT and OF, S and S+OF significantly increased soil water storage during the various growth periods of wheat during two experiment years (2016–2017, 2017–2018). Furthermore, water storage under S and S+OF treatments at the harvest stage increased by 27.2, 28.9, and 35.6%, 33.0% compared with CT in these 2 years, respectively. At the harvest stage, the soil water storage under OF and S+OF treatments increased by 32.1, 5.7, and 46.6%, 17.3% compared to CT and S treatments, respectively.

TABLE 2 | Differences in spike length, number of spikes, number of grains per ear, kilo-grain weightiness, yield and WPE of wheat between subsoiling, organic fertilizer and subsoiling combined with organic fertilizer in three seasons of 2016–2019.

Year	Treatments	Yield components				Yield ($kg.hm^{-2}$)	WPE ($kg.hm^{-2}.mm^{-1}$)
		Spike length (cm)	Number of spikes ($\times 10^4.hm^{-2}$)	Number of grains per ear	1,000-grain weightiness (g)		
2016–2017	CT	7.0c	439.1d	38.0c	43.5b	7025.8d	16.5c
	S	8.0a	608.7b	45.3a	43.2bc	7718.2b	20.0ab
	OF	7.7b	473.9c	42.4b	42.7c	7386.5c	18.7b
	S+OF	7.5b	625.2a	40.6b	44.7a	7841.4a	21.0a
2017–2018	CT	6.3c	520.4c	37.1c	43.1c	7578.3c	17.0c
	S	7.0a	640.9b	43.1a	46.6b	9087.4b	23.1ab
	OF	6.9ab	630.5b	41.3b	45.2b	9018.6b	22.5b
	S+OF	6.7b	700.0a	42.3ab	48.7a	9355.5a	24.1a
2018–2019	CT	6.8c	437.0c	31.5c	42.1c	6591.2c	16.3d
	S	7.3b	513.1b	36.5b	44.3ab	7593.2b	20.1c
	OF	7.4ab	530.4b	37.9ab	44.0b	7625.4b	21.0b
	S+OF	7.6a	600.0a	39.7a	45.9a	8475.8a	23.5a

WPE, yield water production efficiency; CT, conventional tillage; S, subsoiling; OF, organic fertilizer; S+OF, organic fertilizer organic fertilizer combined with subsoiling. Different lowercase letters within a column mean significant difference between treatments at three seasons by LSD test ($P < 0.05$).

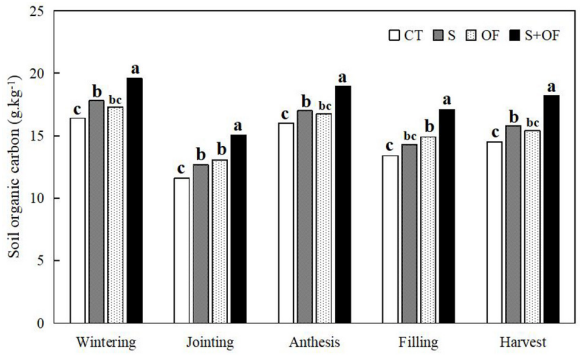

FIGURE 2 | Effects of subsoiling, organic fertilizer and subsoiling combined with organic fertilizer on soil organic carbon at different growth stages of winter wheat in 2019. CT, conventional tillage; S, subsoiling; OF, organic fertilizer; S+OF, organic fertilizer combined with subsoiling. Different lowercase letters in the same growth stage indicate significant differences among treatments by LSD test ($P < 0.05$).

In addition, during the 3-year experiment, S+OF treatment led to the highest soil water storage.

Effects of Combining Subsoiling and Organic Fertilizer on Dry Matter Accumulation

As shown in **Table 1**, during the 3 years of experimentation, OF and S+OF treatment markedly improved the dry matter accumulation (DM) at the STJ (from sowing to jointing) and JTB (from jointing to booting) stages. Compared to CT, the DM in OF and S+OF in the three seasons increased by 15.9–27.2%, 17.5–31.5%, and 11.6–16.3%, 12.7–25.6%, respectively. In addition, DM under S+OF treatment was the largest, followed by S treatment at the BTA (from booting to anthesis) and ATH (from anthesis to harvest) stages in 2016–2018. However, DM under OF and S+OF treatment was significantly higher than that of other treatments at the ATH stage in 2018–2019. The maximum total DM occurred under S+OF treatment in all three seasons. S+OF was more beneficial in increasing DM during the different growth stages, and the total DM of wheat.

Effects of Combining Subsoiling and Organic Fertilizer on Water Consumption and Water Use Efficiency

As shown in **Figures 7A,B**, OF and S+OF treatments significantly reduced water consumption (ET) and increased water use efficiency (WUE) during STB (from sowing to booting). Compared with CT, WUE in OF and S+OF treatments was larger by 11.5–19.0% and 24.0–25.1%, respectively. At the BTA and ATH stages, S+OF treatment has the lowest ET and the highest WUE, followed by S treatment, except for the ATH stage in 2018–2019. However, ET under OF treatment was significantly lower than that under S and CT treatments at the ATH stage in 2018–2019, and WUE under OF treatment increased by 47.6 and 19.6% compared to S and CT, respectively. Moreover, S+OF treatment reduced the total ET[T(a)], while the total WUE [T(b)] under S+OF was significantly higher than other treatments during the whole growth period of wheat. The present study shows that S+OF treatment improves water storage and moisture retention, reduces ET, and increases the WUE of wheat. Therefore, the combination of S+OF led to greatly increased WUE.

Effects of Combining Subsoiling and Organic Fertilizer on Wheat Yield and Yield Water Production Efficiency

Our results (**Table 2**) show that compared to CT, the spike length and the number of grains per ear under S treatment during 2016–2017 and 2017–2018 increased by 14.9, 19.1, and 8.2%, 16.1%,

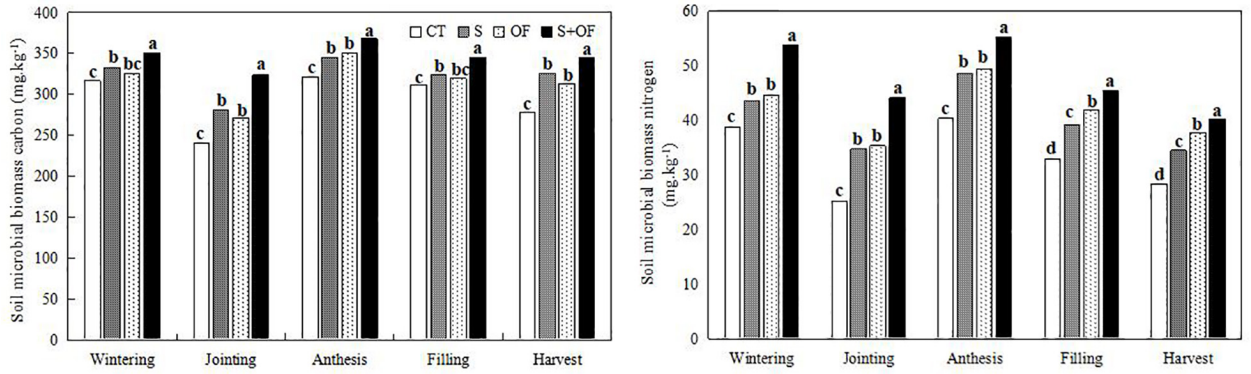

FIGURE 3 | Effects of subsoiling, organic fertilizer and subsoiling combined with organic fertilizer on soil microbial biomass carbon and soil microbial biomass nitrogen at different growth stages of winter wheat in 2019. CT, conventional tillage; S, subsoiling; OF, organic fertilizer; S+OF, organic fertilizer combined with subsoiling. Different lowercase letters in the same growth stage indicate significant differences among treatments by LSD test ($P < 0.05$).

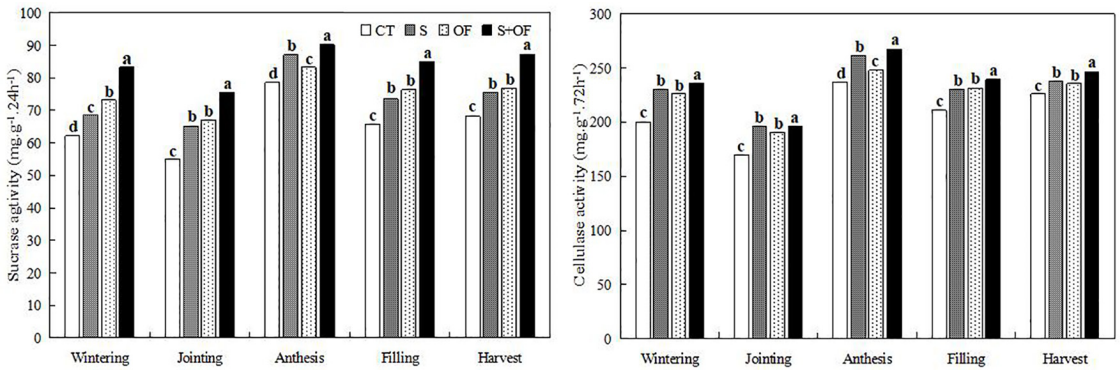

FIGURE 4 | Effects of subsoiling, organic fertilizer and subsoiling combined with organic fertilizer on sucrase activity and cellulase activity of soil at different growth stages of winter wheat in 2019. CT, conventional tillage: S, subsoiling; OF, organic fertilizer; S+OF, organic fertilizer combined with subsoiling. Different lowercase letters in the same growth stage indicate significant differences among treatments by LSD test ($P < 0.05$).

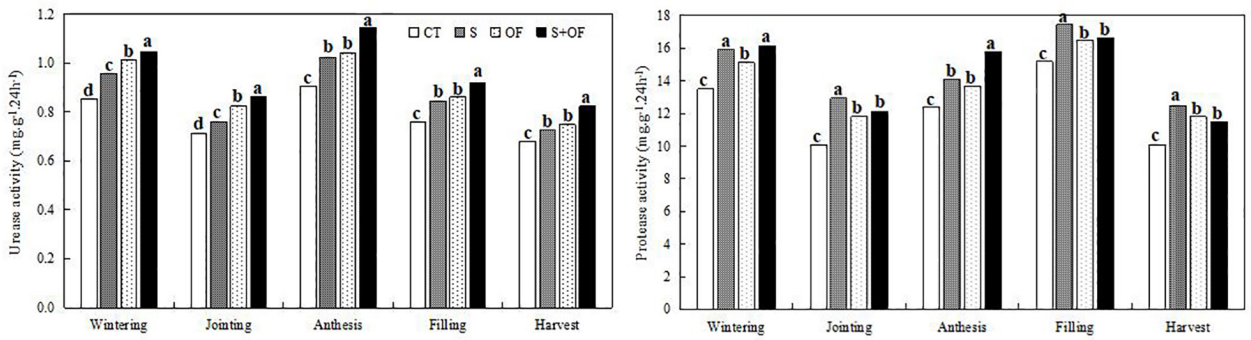

FIGURE 5 | Effects of subsoiling, organic fertilizer and subsoiling combined with organic fertilizer on urease activity and protease activity of soil at different growth stages of winter wheat in 2019. CT, conventional tillage; S, subsoiling; OF, organic fertilizer; S+OF, organic fertilizer combined with subsoiling. Different lowercase letters in the same growth stage indicate significant differences among treatments by LSD test ($P < 0.05$).

respectively, while those under S+OF treatment during 2018–2019 increased by 13.1 and 26.0%, respectively. Additionally, the number of spikes and the 1,000-grain weightiness under S+OF treatment were significantly higher than under other treatments. Compared with CT, the number of spikes and the 1,000-grain weightiness under S+OF treatment in all three seasons larger by 30.7–48.5% and 2.6–13.0%, respectively. The wheat yield and yield WPE of S+OF treatment were the highest in all three

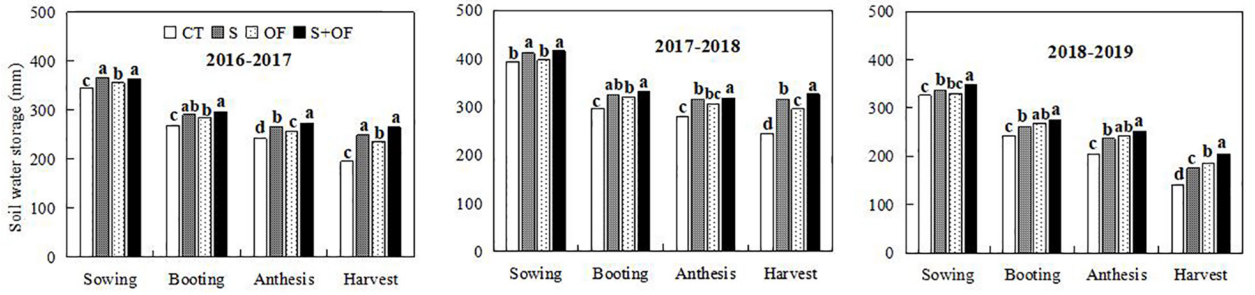

FIGURE 6 | Effects of subsoiling, organic fertilizer and subsoiling combined with organic fertilizer on soil water storage (0–100 cm) at different growth stages of wheat in the three seasons of 2016–2019. CT, conventional tillage; S, subsoiling; OF, organic fertilizer; S+OF, organic fertilizer combined with subsoiling. Different lowercase letters in the same growth stage indicate significant differences among treatments by LSD test ($P < 0.05$).

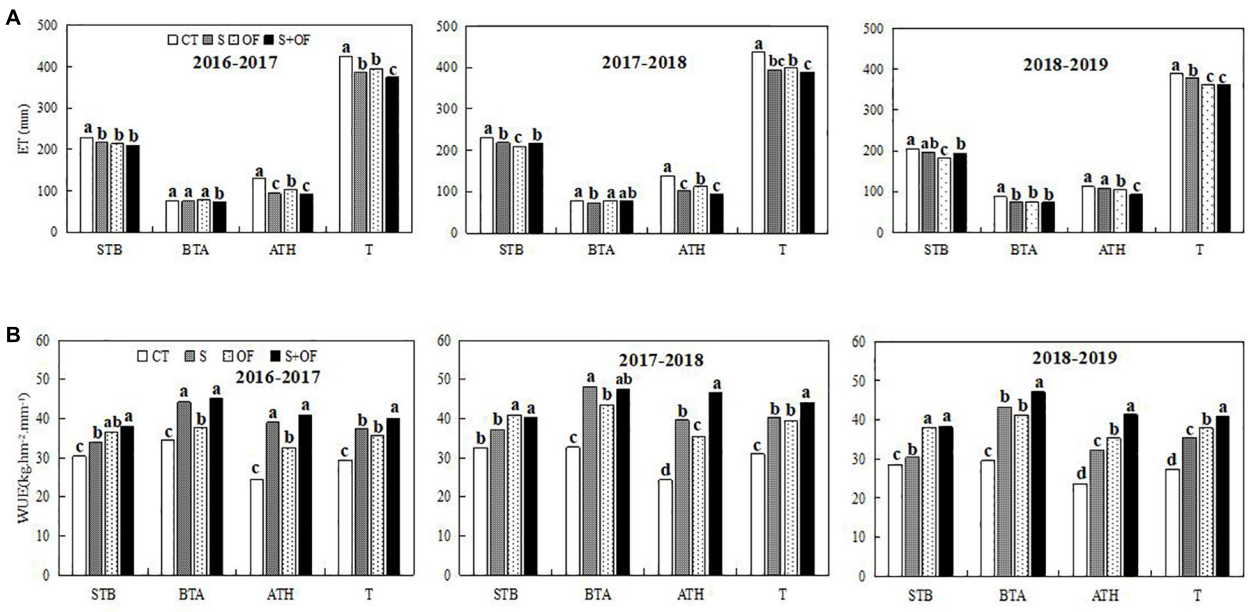

FIGURE 7 | Effects of subsoiling, organic fertilizer and subsoiling combined with organic fertilizer on water consumption (ET) **(A)** and water use efficiency (WUE) **(B)** at different growth stages of winter wheat in the three seasons of 2016–2019. Note: STB, sowing to booting; BTA, booting to anthesis; ATH, anthesis to harvest; T(A), the total ET; T(B), the total WUE. CT, conventional tillage; S, subsoiling; OF, organic fertilizer; S+OF, organic fertilizer combined with subsoiling. Different lowercase letters in the same growth stage indicate significant differences among treatments by LSD test ($P < 0.05$).

seasons, which was 11.6–28.6% and 26.8–43.6% larger compared to CT. In addition, the yield and WPE under S treatment were higher than those under OF and CT treatment in 2016–2018, while the yield and WPE under OF treatment were higher than those under S and CT treatment in 2018–2019.

Correlation Analysis of Dry Matter Accumulation, Soil Water Storage and Soil Organic Carbon, Soil Microbial Biomass Carbon and Nitrogen, and Soil Enzyme Activity

From **Table 3**, dry matter accumulation showed significant ($P < 0.05$) or extremely significant ($P < 0.01$) positive correlations with organic carbon content, soil microbial biomass carbon and nitrogen, sucrase, cellulase, urease and protease activity. Soil water storage showed significant ($P < 0.05$) or extremely significant ($P < 0.01$) positive correlations with soil microbial biomass carbon and nitrogen, urease and protease activity.

Correlation Analysis of Wheat Yield and Soil Organic Carbon, Soil Microbial Biomass Carbon and Nitrogen, and Soil Enzyme Activity

Soil organic carbon, soil microbial biomass carbon and nitrogen, sucrase, cellulase, urease, protease at different growth stages had

TABLE 3 | Relationships among dry matter accumulation, soil water storage and soil organic carbon, soil microbiomass carbon and nitrogen, and soil enzyme activity.

Index	Organic carbon	Soil microbial biomass carbon	Soil microbial biomass nitrogen	Sucrase activity	Cellulase activity	Urease activity	Protease activity
Dry matter accumulation	0.892**	0.858**	0.807**	0.894**	0.928**	0.780**	0.326
Soil water storage	0.384	0.698*	0.828**	0.542	0.475	0.884**	0.713**

**Means significant correlation at 0.05 level, and **means extremely significant correlation at 0.01 level.*

TABLE 4 | Relationships among yield of wheat and soil organic carbon, soil microbiomass carbon and nitrogen, and soil microorganisms enzyme activity.

Index	Wintering	Jointing	Anthesis	Filling
Soil organic carbon	0.969*	0.978*	0.960*	0.959*
Soil microbiomass carbon	0.963*	0.988*	0.987*	0.953*
Soil microbiomass nitrogen	0.977*	0.999**	0.992**	0.968*
Sucrase	0.968*	0.994**	0.948	0.989*
Cellulase	0.920	0.864	0.905	0.958*
Urease	0.943	0.928	0.995**	0.988*
Protease	0.898	0.695	0.988*	0.628

**Means significant correlation at 0.05 level, and **means extremely significant correlation at 0.01 level.*

TABLE 5 | Relationships among yield, WPE, dry matter accumulation, WUE of wheat at different growth stages under different treatments.

Treatments	Parameters	Yield			WPE		
		STB	BTA	ATH	STB	BTA	ATH
CT	DM	0.962**–	0.182	0.934**	0.234	0.275	0.299
	WUE	0.722*	0.516	0.214	0.129	0.280	0.278
S	DM	0.889**	0.916**	0.948**	0.727*	0.715*	0.882**
	WUE	0.868**	0.966**	0.822**	0.718*	0.881**	0.732*
OF	DM	0.745*	0.959**	0.877**	0.288	0.887**	0.943**
	WUE	0.887**	0.823**	0.557	0.810**	0.832**	0.790*
S+OF	DM	0.660	0.907**	0.969**	0.275	0.690*	0.813**
	WUE	0.819**	0.633	0.971**	0.655	0.624	0.842**

*DM, Dry matter accumulation; WUE, water use efficiency; WPE, yield water production efficiency; STJ, sowing to jointing; JTB, jointing to booting; BTA, booting to anthesis; ATH, anthesis to harvest. CT, conventional tillage; S, subsoiling; OF, organic fertilizer; S+OF, organic fertilizer organic fertilizer combined with subsoiling. WPE, water production efficiency. *Means significant correlation at 0.05 level, and **means extremely significant correlation at 0.01 level.*

positive correlations with the yield and WUE of wheat (**Table 4**). From **Table 4**, organic carbon content, soil microbial biomass carbon nitrogen, and sucrase at different stages of wheat showed significant ($P < 0.05$) or extremely significant ($P < 0.01$) positive correlations with yields. Cellulase and urease during the filling and harvest stages showed significant ($P < 0.05$) or extremely significant ($P < 0.01$) positive correlations with yield. Urease and protease at anthesis stage showed significant ($P < 0.05$) or extremely significant ($P < 0.01$) positive correlations with yield.

Correlation Analysis of Dry Matter Accumulation, Water Use Efficiency at Different Growth Stages and Yield, Water Production Efficiency of Wheat at Different Growth Stages

Water use efficiency (WUE) and dry matter accumulation (DM) were correlated with wheat yield and WPE (**Table 5**). At the STB stage, DM and WUE in the all treatments were significantly ($P < 0.05$) or extremely significantly ($P < 0.01$) positively correlated to yields, except between DM and yield under S+OF treatment. DM of S, OF, and S+OF was extremely significantly ($P < 0.01$) positively correlated with the yield, and the WUE of the S and OF treatments were extremely significantly ($P < 0.01$) and positively correlated with the yield at the BTA stage. At the ATH stage, DM in all treatments were extremely significantly ($P < 0.01$) and positively correlated with yield, and the regression coefficient of S+OF treatment was higher ($R^2 = 0.969$). In addition, the correlation between WUE and yield under S and S+OF treatments were also significant ($P < 0.01$) and positive. Moreover, DM and WUE under S treatment were significantly ($P < 0.05$) and positively correlated with WPE at the STB stage. At the BTA stage, DM and WUE under S and OF treatments were significantly ($P < 0.05$) or extremely significantly ($P < 0.01$) and positively correlated with WPE. At the ATH stage, DM and WUE under S, OF and S+OF treatments were significantly ($P < 0.05$) or extremely significantly ($P < 0.01$) and positively correlated with WPE.

TABLE 6 | The proportion of different diameters of aggregates under subsoiling, organic fertilizer and subsoiling combined with organic fertilizer.

Treatments	The proportion of different diameters of aggregates (%)							
	>5 mm	3–5 mm	2–3 mm	1–2 mm	0.5–1 mm	0.25–0.5 mm	<0.25 mm	>0.25 mm
CT	25.0bc	4.7c	3.5b	4.6c	7.5b	9.4c	43.2a	54.8d
S	26.2b	5.7b	4.2a	5.3b	6.7c	10.4b	42.5a	58.4c
OF	24.3c	5.8b	4.3a	7.0a	10.4a	12.9a	35.2b	64.8b
S+OF	34.4a	6.6a	4.4a	5.4b	7.7b	8.5d	33.1b	66.9a

CT, conventional tillage; S, subsoiling; OF, organic fertilizer; S+OF, organic fertilizer organic fertilizer combined with subsoiling. Different lowercase letters within a column mean significant difference between treatments by LSD test ($P < 0.05$).

DISCUSSION

Effects of Combining Subsoiling and Organic Fertilizer on Soil Structure, Microbial Biomass Carbon and Nitrogen and Soil Enzymes

Subsoiling, organic fertilizer, and the combination of these two practices improved soil aggregate structure, microbial biomass carbon and nitrogen and soil enzymes. We found that S, OF and S+OF treatments increased the proportion of >0.5 mm aggregates significantly. Among these, S+OF treatment was most beneficial for increasing the proportion of >0.25 mm aggregates because of the synergistic effects of the combination of S+OF: subsoiling provides loose soil conditions (Yang et al., 2021b) and leads to increased water availability in the root zone, which promotes crop root growth and increases soil organic carbon (Yang et al., 2021b), while organic fertilizers provide nutrients to the crop and soil microorganisms (Spedding et al., 2004; Wang et al., 2015) and thereby promote microbial activity (Piovanelli et al., 2006; Kuzyakov and Xu, 2013) and increase soil organic carbon (Yang et al., 2021a). These factors in turn increased soil structure stability, increased soil water retention, and improved crop growth. The combination of S+OF this results in a positive feedback loop of crop growth and improvements in soil physical properties.

Microbial biomass carbon and nitrogen in the soil can directly or indirectly participate in soil biochemical processes, and plays an extremely important role in the transformation of substances and the energy cycle in the soil (Turner et al., 2001; Nsabimana et al., 2004). In this study, we found that throughout the process of wheat growth, changes in the content of soil microbial biomass carbon and nitrogen had the same trend as soil organic carbon. Soil microbial biomass carbon at the jointing stage and soil microbial nitrogen at the jointing and harvest stages were lowest, and that at the anthesis stage was highest, compared to other growth stages. Previous research has shown that the application of organic fertilizer can effectively increase the carbon content of soil microbes during the crop growth stage, with a 23.0% increase in average annual content (Li et al., 2017). We found that compared to CT, S, and OF treatments, S+OF treatment led to more soil microbial biomass carbon and nitrogen. This indicates that compared to individual application of subsoiling tillage or organic fertilizer, their combination better improves the physical and chemical characteristics of the soil, increases root exudates, promotes nutrient absorption by crop roots, and enhances soil microbial activity and reproduction (Yu, 2015), and microbial biomass quantity (Kuzyakov and Xu, 2013).

Soil enzymes are good catalysts for nutrient metabolism in the soil. Enzyme activity can reflect the extent of decomposition and transformation of substances in the soil, and also reflect changes to soil fertility due to farmland management measures (Zhang et al., 2014). Studies have shown that subsoiling can significantly improve the activity of urease and sucrase in the soil (Huang et al., 2013), while organic fertilizer improves the activity of urease, sucrase, and cellulase in the soil (He et al., 2020). We found that S+OF improved sucrase activity, cellulase activity and urease activity of wheat to a greater extent, compared to sole application of either subsoiling or organic fertilizer. However, protease activity was the highest under S treatment throughout all growth stages of wheat except the anthesis stage. Subsoiling, which creates small disturbances to the soil, increases soil porosity, promotes gas exchange, increases water retention, and facilitates enzyme activity in the soil (Jiang et al., 2012; Nie et al., 2015). Organic fertilizers can increase the carbon content of the soil, and increase root exudates and microbial activity, which increases enzyme activity in the soil (Rehana et al., 2008; Pu et al., 2020). Therefore, the combination of subsoiling combined with organic fertilizer (S+OF) is a good practice to improve the activity of urease, sucrase, and cellulase in the soil and promote crop growth.

Effects of Combining Subsoiling and Organic Fertilizer on Soil Water Storage and Dry Matter Accumulation

Soil water retention is a critical factor and important parameter for evaluating soil productivity, as it has a decisive influence on crop growth conditions and yield (Fu et al., 2005; Yang et al., 2021c). Subsoiling and organic fertilizer can improve soil structure, and promote water storage and infiltration to deeper soil (Hemmat and Eskandari, 2004; Wang et al., 2019; Hu et al., 2013; Liu et al., 2013). In this study, it was found that in comparison with CT and OF, S and S+OF significantly increased soil water storage during the various growth periods of wheat during two experimental years (2016–2017, 2017–2018). This may be due to the better infiltration and soil water retention capacities induced by subsoiling (Hu et al., 2013). Compared to CT and S treatments, OF and S+OF treatments were more effective at increasing soil water storage in 2018–2019, because organic fertilizers improve the soil water retention capacity and moisture content by improving the organic matter content and soil physical properties (Karami et al., 2012). Thus, the application of organic fertilizer leads to higher soil water storage when comparing treatments subject to the same tillage process in the dry growth season. In addition, during the 3-year experiment, S+OF treatment led to the highest soil water storage during the growth stage of wheat, which may be because the synergies between subsoiling and organic fertilizer significantly improved soil and water conservation capacity (Bolan et al., 2003). Therefore, S+OF treatment appears to be most effective at increasing soil water retention capacity.

The accumulation of dry matter during the growth period provides the fundamental materials required for crop formation, which ultimately determines grain yield (Ding et al., 2005; Liu et al., 2009; Hou et al., 2012). Different tillage and cultivation measures can improve the dry matter accumulation ability of wheat by improving soil moisture (Zheng et al., 2013). We found that, during the 3 years of experimentation, OF and S+OF treatment markedly improved dry matter accumulation (DM) at the STJ (from sowing to jointing) and JTB (from jointing to booting) stages. Our results show that the input of organic fertilizer increased DM before the booting stage, which agrees with Yang et al. (2016). This is because organic fertilizer leads

to more balanced crop water demand and soil water supply (Liu et al., 2013), improves the effective water content, promotes the transformation of soil organic nutrients, and improves the absorption and utilization of crop nutrients and water, thus promoting the growth of wheat and increasing DM (Dordas, 2009). In addition, our results also show that the application of organic fertilizer may increase post-anthesis DM during the dry growth season (2018–2019). The reason for this may be that organic fertilizer enhanced deep soil water usage in arid years, which promotes ear development and grain filling (Lu et al., 2011; Ni et al., 2013; Wang et al., 2017), thereby resulting in increased DM. However, among different practices, application of organic fertilizer coupled with subsoiling (S+OF) was more beneficial in increasing DM than sole subsoiling due to double advantage for soil microbes, soil properties and water retention mentioned above.

Effects of Combining Subsoiling and Organic Fertilizer on Water Consumption, Water Use Efficiency, and Water Production Efficiency of Wheat

Miriti et al. (2012) reported that when subject to identical tillage practices, the water use efficiency under organic fertilizer treatment was 26% higher than without organic fertilizer. In this study, OF and S+OF treatments significantly reduced ET and increased WUE during STB (from sowing to booting). These results agree with several previous studies (Lu et al., 2011; Miriti et al., 2012; Zhang et al., 2016; Wang et al., 2017). This may because organic fertilizers help conserve water and soil moisture, reduce inter-plant evaporation and promote the absorption and utilization of water by roots (Lu et al., 2011). In addition, we found that OF treatment led to reduced ET and increased WUE during ATH compared to S treatment during the dry growth season, thus increasing wheat yield. Moreover, S+OF treatment reduced the total ET, while the total WUE under S+OF treatment was significantly higher than other treatments. The present study shows that S+OF treatment improves water storage and moisture retention, reduces ET, and increases the WUE of wheat. This is due to an improvement in infiltration, reduction in surface runoff and soil erosion, and increase in WUE due to subsoiling (Mcconkey et al., 1997; Hu et al., 2013). Furthermore, organic fertilizer could also increase WUE (Miriti et al., 2012; Zhang et al., 2016). Therefore, the combination of S+OF led to greatly increased WUE.

The increased soil water storage, post-anthesis DM and the number of spikes and 1,000-grain weight caused by subsoiling (Huang et al., 2009; Zheng et al., 2011; Yang et al., 2016), and the benefits of organic fertilizer in improving soil physical properties, increasing soil water storage capacity, reducing evaporation, and improving crop yields (Sang et al., 2016) and the absorption and utilization of water (Lu et al., 2011; Miriti et al., 2012; Liu et al., 2013; Wang et al., 2017), suggests that the two individual practices in S+OF provide mutually complementary benefits to wheat growth. Therefore, compared to S and OF treatments, S+OF treatment optimized yield components (number of spikes and 1,000-grain weightiness), which led to a higher number of spikes, 1,000-grain weightiness and total DM and lower ET, and increased WPE and wheat yield.

Correlation analyses indicate that high dry matter accumulation and soil water improved soil microbial biomass carbon and nitrogen and soil enzyme activity, which improves soil organic carbon and soil structure and promotes crop growth. We found that the increment in soil microbial biomass carbon and nitrogen at the different growth stages of winter wheat, and the increment in soil sucrase, cellulase, urease and protease activity after anthesis stage of winter wheat were beneficial to increase yield and WPE of winter wheat based on the correlation analysis. In addition, we also found that dry matter accumulation at the different growth stages of winter wheat had a critical and positive impact on yields and WPE under S, OF and S+OF treatments, especially after the anthesis stage under S+OF treatment (**Table 5**), and that improvements in WUE after the booting stage under S, OF and S+OF treatments, especially after the anthesis stage under S+OF treatment (**Table 5**), led to increased wheat yield and WPE, in agreement with previous studies (Zheng et al., 2008; Yang et al., 2016). Zheng et al. (2008) reported that the dry matter accumulation of winter wheat after anthesis accounted for more than 80% of total grain yield. This is also reflected in our results, which show that S+OF treatment was highly effective at increasing DM and WUE post-anthesis, thereby increasing yield and WPE. Thus, appropriate agricultural practices such as S+OF can effectively improve soil organic carbon, promote soil microbial biomass carbon and nitrogen and soil enzyme activity, thereby increasing wheat production.

CONCLUSION

Subsoiling (S), organic fertilizer (OF) and subsoiling combined with organic fertilizer (S+OF) are treatments that improve soil structure. Among them, S+OF is most beneficial in increasing the proportion of >0.25 mm aggregates, which leads to higher soil structural stability. In addition, S+OF is also the most effective measure in increasing soil organic carbon content, soil microbial biomass carbon, soil microbial biomass nitrogen and sucrase activity, cellulase activity, urease activity and protease activity. Furthermore, S+OF also improved the absorption and utilization of water and DM, wheat yields, and WPE, more significantly compared to other treatments, regardless of rainfall availability. Correlation analyses indicate that long-term continuous amendments are beneficial for improving wheat yield and WPE because they improve soil organic carbon, soil microbial biomass carbon and nitrogen, soil enzyme activity, dry matter accumulation and soil water storage. Therefore, subsoiling combined with organic fertilizer is an effective measure for improving the soil and increasing yield and WPE of winter wheat production under the experimental conditions. Further research is necessary to determine the effects of long-term application of S+OF on the mechanisms of the interactions between microbial variety, and microbial quantity, soil properties, and water availability, so as to build a more informed scientific basis for applying S+OF in farmland.

DATA AVAILABILITY STATEMENT

The raw data supporting the conclusions of this article will be made available by the authors, without undue reservation.

AUTHOR CONTRIBUTIONS

YY wrote the main manuscript. ML wrote the part of the manuscript. JW revised and gave some advice for the manuscript. XP performed most of the experiments. CG prepared the figure and table of the manuscript. DT edited language and modified the main manuscript. All authors reviewed the manuscript.

FUNDING

This work was funded by the National Key R&D Program of China (Grant no. 2017YFD0301102), the National Natural Science Foundation of China (Grant no. U1404404), and Research Project of China Institute of Water Resources and Hydropower Research (Grant no. MK2019J02).

REFERENCES

Bogard, M., Allard, V., Brancourt, H. M., Heumez, E., Machet, J. M., Jeuffroy, M. H., et al. (2010). Deviation from the grain protein concentration-grain yield negative relationship is highly correlated to post-anthesis N uptake in winter wheat. *J. Exp. Bot.* 61, 4303–4312. doi: 10.1093/jxb/erq238

Bolan, N. S., Adriano, D. C., Natesan, R., and Koo, B. J. (2003). Effects of organic amendments on the reduction and phytoavailability of chromate in mineral soil? *J. Environ. Qual.* 32, 120–128. doi: 10.2134/jeq2003.0120

Bottinelli, N., Angers, D. A., Hallaire, V., Michot, D., Guillou, C. L., Heddadj, D., et al. (2017). Tillage and fertilization practices affect soil aggregate stability in a humic cambisol of Northwest France. *Soil Till. Res.* 170, 14–17. doi: 10.1016/j.still.2017.02.008

Bu, Y. S., Miao, G. Y., Zhou, N. J., Shao, H. L., and Wang, J. C. (2006). Analysis and comparison of effects of plastic film mulching and straw mulching on soil fertility. *Sciatic Agric. Sin.* 39, 1069–1075. doi: 10.3321/j.issn:0578-1752.2006.05.031

Christianson, C. B. (1988). Factors affecting N release of urea from reactive layer coated urea. *Fertil. Res.* 16, 273–284. doi: 10.1007/BF01051376

Chu, P. F., Yu, Z. W., Wang, D., Zhang, Y. L., and Wang, Y. (2012). Effect of tillage mode on diurnal variations of water potential and chlorophyll fluorescence characteristics of flag leaf after anthesis and water use efficiency in wheat. *Acta Agron. Sin.* 38, 1051–1061. doi: 10.3724/SP.J.1006.2012.01051

Ding, L., Wang, K. J., Jiang, G. M., Liu, M. Z., Niu, S. L., and Gao, L. M. (2005). Post-anthesis changes in photosynthetic traits of maize hybrids released in different years. *Field Crops Res.* 93, 108–115. doi: 10.1016/j.fcr.2004.09.008

Dordas, C. (2009). Dry matter, nitrogen and phosphorus accumulation, partitioning and remobilization as affected by N and P fertilization and source-sink relations. *Eur. J. Agron.* 30, 129–139. doi: 10.1016/j.agwat.2019.105934

Elliot, E. T. (1986). Aggregate structure and carbon, nitrogen, and phosphorus in native and cultivated soils. *Soil Sci. Soc. Am. J.* 50, 627–633. doi: 10.2136/sssaj1986.03615995005000030017x

Elfstrand, S., Hedlund, K., and Martensson, A. (2007). Soil enzyme activities,microbial community composition and function after 47 years of continuous green manuring. *Applied Soil Ecology*, 35, 610–621. doi: 10.1016/j.apsoil.2006.09.011

Fu, G. Z., Li, C. H., Wang, J. Z., Wang, Z.L., Cao, H. M., Jiao, N. Y., and Wang, X. D. (2005). Effects of stubble mulching and tillage management on leaf senescence metabolism and grain yield in summer maize. *Acta Bot. Boreal.-Occident. Sin.* 1, 155–160. doi: 10.1360/biodiv.050022

Guan, S. Y. (1986). *Soil Enzymes and Research Methods*. Beijing: Agricultural Press.

Guo, Z., Shi, Y., Yu, Z., and Zhang, Y. (2015). Supplemental irrigation affected flag leaves senescence post–anthesis and grain yield of winter wheat in the Huang–Huai–Hai Plain of China. *Field Crop Res.* 180, 100–109. doi: 10.1016/j.fcr.2015.05.015

He, M., Wang, Y. C., Wang, L. G., Cheng, Q., Wang, L. M., Li, Y. H., et al. (2020). Effects of Subsoiling combined with fertilization on the fractions of soil active organic carbon and soil active nitrogen, and enzyme activities in black soil in northeast China. *Acta Pedol. Sin.* 2020, 446–456. doi: 10.11766/trxb201810180282

Hemmat, A., and Eskandari, I. (2004). Conservation tillage practices for winter wheat-fallow farming in the temperate continental climate of northwestern Iran. *Field Crops Res.* 89, 123–133. doi: 10.1016/j.fcr.2004.01.019

Hou, P., Gao, Q., Xie, R. Z., Li, S. K., Meng, Q. F., Kirkby, E. A., et al. (2012). Grain yields in relation to N requirement:optimizing nitrogen management for spring maize grown in China. *Field Crops Res.* 129, 1–6. doi: 10.1016/j.fcr.2012.01.006

Hu, H. Y., Ning, T. Y., Li, Z. J., Han, H. F., Zhang, Z. Z., Qin, S. J., et al. (2013). Coupling effects of urea types and subsoiling on nitrogen-water use and yield of different varieties of maize in northern China. *Field Crops Res.* 142, 85–94. doi: 10.1016/j.fcr.2012.12.001

Huang, H. Q., Wang, J. Y., Ling, D. J., Duan, M. X., and Wang, W. J. (2013). Study on relationship between soil catalase activity and soil chemical properties under different land use patterns-Take leizhou peninsula for example. *Southw. China J. Agric. Sci.* 26, 2412–2416. doi: 10.3969/j.issn.1001-4829.2013.06.045

Huang, M., Wu, J. Z., Li, Y. J., Yao, Y. Q., Zhang, C. J., Cai, D. X., et al. (2009). Effects of tillage pattern on the flag leaf senescence and grain yield of winter wheat under dry farming. *Chin. J. Appl. Ecol.* 20, 1355–1361.

Jiang, X., He, D. X., Ren, H. Z., Liu, Q. R., and Hu, M. (2012). Effects of different patterns of rotational tillage on soil bulk density in wheat field and wheat root development. *J. Triticeae Crops* 32, 711–715.

Karami, A., Homaee, M., Afzalinia, S., Ruhipour, H., and Basirat, S. (2012). Organic resource management: impacts on soil aggregate stability and other soil physico-chemical properties. *Agric. Ecosyst. Environ.* 148, 22–28. doi: 10.1016/j.agee.2011.10.021

Kuzyakov, Y., and Xu, X. (2013). Competition between roots and microorganisms for nitrogen: mechanisms and ecological relevance. *New Phytol.* 198, 656–669. doi: 10.1111/nph.12235

Li, C. B., Wang, H. Y., Zhao, W., Xu, M. M., Yuan, J. H., and Li, X. Q. (2017). Effect of straw returned to the field with microbial fungus agent and organic fertilizer on microbial carbon content of black soil. *Jiangsu Agric. Sci.* 45, 265–268. doi: 10.15889/j.issn.1002-1302.2017.05.069

Li, C. X., Liu, Q., Shao, Y., Ma, S. C., Li, S. S., Li, X. B., et al. (2019). Effects of organic materials returning and nitrogen fertilizer reduction on nitrogen utilization and economic benefits of wheat. *Agric. Res. Arid Areas* 37, 214–220.

Li, M. H., Zhou, Y. X., Zhou, L., Yang, J., and Wang, Y. H. (2015). Comparative advantage changes of regional wheat production in China and analysis of influencing factors. *China J. Agric. Resourc. Regional Plann.* 36, 7–15. doi: 10.7621/cjarrp.1005-9121.20150502

Liang, B., Zhou, J. B., and Yang, X. Y. (2010). Changes of soil microbial biomass carbon and nitrogen,and mineral nitrogen after a long-term different fertilization. *Plant Nutr. Fertil. Sci.* 16, 321–326. doi: 10.11674/zwyf.2010.0209

Liu, C. A., Li, F. M., Zhou, L. M., Zhang, R. H., Lin, S. L., Wang, L. J., et al. (2013). Effect of organic manure and fertilizer on soil water and crop yields in newly-built terraces with loess soils in a semi-arid environment. *Agric. Water Manag.* 117, 123–132. doi: 10.1016/j.agwat.2012.11.002

Liu, W. D., Chen, X. Y., Yin, J., and Du, P. X. (2009). Effect of sowing date and planting density on population trait and grain yield of winter wheat cultivar Yumai 49-198. *J. Triticeae Crops* 29, 464–469. doi: 10.7606/j.issn.1009-1041.2009.03.097

Lu, W. T., Jia, Z. K., Zhang, P., Cai, T. Y., Li, R., Hou, X. Q., et al. (2011). Effects of organic fertilization on winter wheat photosynthetic characteristics and water

use efficiency in semi-arid of southern Ningxia. *Plant Nutr. Fertil. Sci.* 17, 1066–1074. doi: 10.11674/zwyf.2011.0498

Mcconkey, B. G., Ulrich, D. J., and Dyck, F. B. (1997). Slope position and subsoiling effects on soil water and spring wheat yield. *Can. J. Soil Sci.* 77, 83–90. doi: 10.4141/S95-067

Miriti, J. M., Kironchi, G., Esilaba, A. O., Hengd, L. K., Gachened, C. K. K., and Mwangic, D. M. (2012). Yield and water use efficiencies of maize and cowpea as affected by tillage and cropping systems in semiarid Eastern Kenya. *Agric. Water Manag.* 115, 148–155. doi: 10.1016/j.agwat.2012.09.002

Mohanty, M., Bandyopadhyay, K. K., Painuli, D. K., Ghosh, P. K., Misra, A. K., and Hati, K. M. (2007). Water transmission characteristics of a vertisol and water use efficiency of rainfed soybean (Glycine max (L.) Merr.) under subsoiling and manuring. *Soil Till. Res.* 93, 420–428. doi: 10.1016/j.still.2006.06.002

Moore, J. M., Klose, S., and Tabatabai, M. A. (2000). Soil microbial biomass carbon and nitrogen as affected by cropping systems. *Biol. Fertil. Soils* 31, 200–210. doi: 10.1007/s003740050646

Ni, Y. J., Ren, D. C., Ge, J., Huang, J. Y., Zhang, F. J., Huang, S. H., et al. (2013). Effects of straw mulching plus nitrogen fertilizer on grain filling rate and grain yield in wheat 'Zhoumai22'. *Chin. Agric. Sci. Bull.* 29, 105–108. doi: 10.3724/SP.J.1006.2015.00468?

Nie, L. P., Guo, L. W., Niu, H. Y., Wei, J., Li, Z. J., and Ning, T. Y. (2015). Effects of rotational tillage on tilth soil structure and crop yield and quality in maize-wheat cropping system. *Acta Agron. Sin.* 41, 468–478. doi: 10.3724/SP.J.1006.2015.00468

Nsabimana, D., Haynes, R. J., and WAllis, F. M. (2004). Size activity and catabolic diversity of the soil biomass as affected by land use. *Appl. Soil Ecol.* 26, 81–92. doi: 10.1016/j.apsoil.2003.12.005

Piovanelli, C., Gamba, C., Brandi, G., Simoncini, S., and Batistoni, E. (2006). Tillage choices affect biochemical properties in the soil profile. *Soil Till. Res.* 90, 84–92. doi: 10.1016/j.still.2005.08.013

Pu, Q. M., Yang, P., Deng, Y. C., Xiang, C. Y., Lin, B. M., Liu, L. S., et al. (2020). Effects of different fertilization methods on soil enzyme activity, soil nutrients and quality of spring cabbage. *J. Agric. Sci. Technol.* 22, 130–139.

Qin, X., Liu, Y., Huang, Q., Zhao, L., and Xu, Y. (2020). Effects of sepiolite and biochar on enzyme activity of soil contaminated by cd and atrazine. *Bull. Environ. Contam. Toxicol.* 104, 642–648. doi: 10.1007/s00128-020-02833-w

Rehana, R., Kukal, S. S., and Hira, G. S. (2008). Soil organic carbon and physical properties as affected by long-term application of FYM and inorganic fertilizers in maize-wheat system. *Soil Ellage Res.* 101, 31–36. doi: 10.1016/j.still.2008.05.015

Sang, X. G., Wang, D., and Lin, X. (2016). Effects of tillage practices on water consumption characteristics and grain yield of winter wheat under different soil moisture conditions. *Soil Till. Res.* 163, 185–194. doi: 10.1016/j.still.2016.06.003

Sang, X. G., Wang, D., and Yu, Z. W. (2014). Effects of subsoiling and harrowing on water consumption characteristics and grain yield of winter wheat under condition of supplemental irrigation. *J. Triticeae Crops* 34, 1239–1244. doi: 10.7606/j.issn.1009-1041.09.012

Spedding, T. A., Hamel, C., Mehuys, G. R., and Madramootoo, C. A. (2004). Soil microbial dynamics in maize-growing soil under different tillage and residue management systems. *Soil Biol. Biochem.* 36, 499–512. doi: 10.1016/j.soilbio.2003.10.026

Sun, K., Liu, Z., Hu, H. Y., Li, G., Liu, W. T., Yang, L., et al. (2019). Effect of organic fertilizer and rotational tillage practices on soil carbon and nitrogen and maize yield in wheat-maize cropping system. *Acta Agron. Sin.* 45, 401–410. doi: 10.3724/SP.J.1006.2019.83028

Turner, B. L., Bristow, A. W., and Haygarth, P. M. (2001). Rapid estimation of microbial biomass in grassland soil by ultraviolet absorbance. *Soil Biol. Biochem.* 33, 913–919. doi: 10.1016/S0038-0717(00)00238-8

Vance, E. D., Brookes, P. C., and Jenkinson, D. S. (1987). An extraction method for measuring soil microbial biomass C. *Soil Biol. Biochem.* 19, 703–707. doi: 10.1016/0038-0717(87)90052-6

Vita, P. D., Paolo, E. D., Fecondo, G., Fonzo, N. D., and Pisante, M. (2007). No-tillage and conventional tillage effects on durum wheat yield, grain quality and soil moisture content in Southern Italy. *Soil Till. Res.* 92, 69–78. doi: 10.1016/j.still.2006.01.012

Wang, B., Zhang, Y. H., Hao, B. Z., Xu, X. X., Zhao, Z. G., Wang, Z. M., et al. (2016). Grain yield and water use efficiency in efficiency in extremely-late sown winter wheat cultivars under two irrigation regimes in the North China Plain. *PLoS One* 11:e0153695. doi: 10.1371/journal.pone.0153695

Wang, L. L., Li, Q., Coulter, J. A., Xie, J. H., Lou, Z. Z., Zhang, R. Z., et al. (2020). Winter wheat yield and water use efficiency response to organic fertilization in northern China: a meta-analysis. *Agric. Water Manag.* 229:2020. doi: 10.106/j.2019.105934

Wang, L. L., Wang, S. W., Chen, W., Li, H. B., and Deng, X. P. (2017). Physiological mechanisms contributing to increased water-use efficiency in winter wheat under organic fertilization. *PLoS One* 12:e0180205. doi: 10.1371/journal.pone.0180205

Wang, Q. Y., Zhou, D. M., and Long, C. (2009). Microbial and enzyme properties of apple or chard soil as affected by long-term application of copper fungicide. *Soil Biol. Biochem.* 41, 1540–1590. doi: 10.1016/j.soilbio.2009.04.010

Wang, Y. D., Hu, N., Xu, M. G., Li, Z. F., and Lou, Y. L. (2015). 23-year manure and fertilizer application increasessoil organic carbon sequestration of a rice-barley cropping system. *Biol. Fert. Soils* 51, 583–591. doi: 10.1007/s00374-015-1007-2

Wang, Y. H., Liu, H., Huang, Y., Wang, J. F., Wang, Z. Z., Gu, F. X., et al. (2019). Effects of cultivation management on the winter wheat grain yield and water utilization efficiency. *Sci. Rep.* 9:12733. doi: 10.1038/s41598-019-48962-z

Westerman, R. L. (1990). *Soil Testing and Plant Analysis*, 3rd Edn. Madison, WI: Soil Science Society of America. doi: 10.1097/00010694-197506000-00011

Wu, J. C., Zhang, C. M., Wang, Z. Y., Li, T. L., and Xue, Y. F. (2003). Research and application of techniques of highly-effective utilization of precipitation resource in west Henan. *Agric. Res. Arid Areas* 21, 152–155.

Yan, J. T., Kang, Y. L., and Tian, Z. H. (2011). Effects of tillage depth on winter wheat growth and water use in dry land. *J. Henan Agric. Sci.* 40, 81–83. doi: 10.3969/j.issn.1004-3268.2011.10.023

Yang, Y. H., Wu, J. C., Zhang, Y. T., Pan, X. Y., Ding, J. L., Zhang, J. M., et al. (2016). Effects of tillage, moisture conservation on water use and yield in wheat at different growth stages. *Acta Agric. Boreali Sin.* 31, 184–190. doi: 10.7668/hbnxb.2016.03.027

Yang, Y. H., Wu, J. C., Zhao, S. W., Mao, Y. P., Zhang, J. M., Pan, X. Y., et al. (2021b). Impact of long-term sub-soiling tillage on soil porosity and soil physical properties in the soil profile. *Land Degrad. Dev.* 32, 2892–2905. doi: 10.1002/ldr.3874

Yang, Y. H., Wu, J. C., Zhao, S. W., Gao, C. M., Pan, X. Y., Tang, D. W. S., et al. (2021a). Effects of long-term super absorbent polymer and organic manure on soil structure and organic carbon distribution in different soil layers. *Soil Till. Res.* 206:104781. doi: 10.1016/j.still.2020.104781

Yang, Y. H, Wu, J. C., Du, Y-L., Gao, C. M., Pan, X. Y., Tang, D. W. S., and Van der Ploeg, M. (2021c). Short- and long-term straw mulching and subsoiling affect soil water, photosynthesis, and water use of wheat and maize. *Front. Agron.* 3:708075. doi: 10.3389/fagro.2021.708075

Yu, H. (2015). *Study on the Regulation Effect of Straw Returning on Soil Microorganisms and Maize*. Jilin: Jilin Agricultural University.

Zhang, H. Q., Yu, X. Y., Zhai, B. N., Jin, Z. Y., and Wang, Z. H. (2016). Effect of manure under different nitrogen application rates on winter wheat production and soil fertility in dryland. *IOP Conf. Ser. Earth Environ. Sci.* 39:012048. doi: 10.1088/1755-1315/39/1/012048

Zhang, J., Yao, Y. Q., Lu, J. J., Jin, K., Wang, Y. H., Wang, Y. H., et al. (2008). Soil carbon change and yield increase mechanism of conservation tillage on sloping drylands in semi-humid arid area. *Chin. J. Eco Agric.* 16, 297–301. doi: 10.3724/SP.J.1011.2008.00297

Zhang, L., Li, Y. J., Fu, Z. G., Jiao, N. Y., and Zhang, Y. Y. (2014). Effects of rotational tillage on spatial and temporal variation of soil enzyme activities in winter wheat field. *J. Triticeae Crops* 34, 1104–1110. doi: 10.7606/j.issn.1009-1041.2014.08.013

Zhang, R., Zhang, G. L., Ji, Y. Y., Li, G., Chang, H., and Yang, D. L. (2013). Effects of different fertilizer application on soil active organic carbon. *Environ. Sci.* 34, 277–282.

Zhang, Y. J., Wang, R., Wang, H., Wang, S. L., Wang, X. L., and Li, J. (2019). Soil water use and crop yield increase under different long-term fertilization practices incorporated with two-year tillage rotations. *Agriculture Water Management* 221, 362–370. doi: 10.1016/j.agwat.2019.04.018

Zhang, Y. Q., Wang, J. D., Gong, S. H., Xu, D., and Sui, J. (2017). Nitrogen fertigation effect on photosynthesis, grain yield and water use efficiency of winter wheat. *Agric. Water Manag.* 179, 277–287. doi: 10.1016/j.agwat.2016.08.007

Zheng, C. Y., Cui, S. M., Wang, D., Yu, Z. W., Zhang, Y. L., and Shi, Y. (2011). Effects of soil tillage practice on dry matter production and water use efficiency in wheat. *Acta Agron. Sin.* 37, 1432–1440. doi: 10.1016/S1875-2780(11)60039-4

Zheng, C. Y., Yu, Z. W., Ma, X. H., Wang, X. Z., and Bai, H. L. (2008). Water consumption characteristics and dry matter accumulation and distribution in high-yielding wheat. *Acta Agron. Sin.* 34, 1450–1458. doi: 10.3724/SP.J.1006.2008.01450

Zheng, C. Y., Yu, Z. W., Zhang, Y. L., Wang, D., Shi, Y., and Xu, Z. Z. (2013). Effects of subsoiling and supplemental irrigation on dry matter production and water use efficiency in wheat. *Acta Ecol. Sin.* 33, 2260–2271. doi: 10.5846/stxb201112211941

Conflict of Interest: The authors declare that the research was conducted in the absence of any commercial or financial relationships that could be construed as a potential conflict of interest.

Publisher's Note: All claims expressed in this article are solely those of the authors and do not necessarily represent those of their affiliated organizations, or those of the publisher, the editors and the reviewers. Any product that may be evaluated in this article, or claim that may be made by its manufacturer, is not guaranteed or endorsed by the publisher.

frontiers in Plant Science

ORIGINAL RESEARCH
published: 14 February 2022
doi: 10.3389/fpls.2022.834520

Integrated Analysis of Osmotic Stress and Infrared Thermal Imaging for the Selection of Resilient Rice Under Water Scarcity

Naima Mahreen[1], Sumera Yasmin[1], M. Asif[2], Sumaira Yousaf[3], Mahreen Yahya[1], Khansa Ejaz[1], Hafiz Shahid Hussain[1], Zahid Iqbal Sajjid[1] and Muhammad Arif[2]*

[1] Soil and Environmental Biotechnology Division, National Institute for Biotechnology and Genetic Engineering College, Pakistan Institute of Engineering and Applied Sciences (NIBGE-C, PIEAS), Faisalabad, Pakistan, [2] Agricultural Biotechnology Division, National Institute for Biotechnology and Genetic Engineering College, Pakistan Institute of Engineering and Applied Sciences (NIBGE-C, PIEAS), Faisalabad, Pakistan, [3] Nuclear Institute for Agriculture and Biology College, Pakistan Institute of Engineering and Applied Sciences (NIAB-C, PIEAS), Faisalabad, Pakistan

The climate change scenario has increased the severity and frequency of drought stress, which limits the growth and yield of rice worldwide. There is a dire need to select drought-tolerant rice varieties to sustain crop production under water scarcity. Therefore, the present study effectively combined morpho-physiological and biochemical approaches with the technology of infrared thermal imaging (IRTI) for a reliable selection of drought-tolerant genotypes. Initially, we studied 28 rice genotypes including 26 advance lines and three varieties for water stress tolerance under net house conditions. Three genotypes NIBGE-DT-02, KSK-133, and NIBGE-DT-11 were selected based on the Standard Evaluation System (SES) scoring for drought tolerance. NIBGE-DT-02 showed tolerance to polyethylene glycol (20%) induced osmotic stress indicated by a minimum reduction in seedling length, biomass, chlorophyll content, and increased leaf proline content as compared to susceptible varieties under a hydroponic system. NIBGE-DT-02 was further evaluated for water withholding at varying growth stages, i.e., 30 and 60 days after transplantation (DAT) in pots under net house conditions. NIBGE-DT-02 showed a significantly lower reduction (35.9%) in yield as compared to a susceptible variety (78.06%) under water stress at 60 DAT with concomitant induction of antioxidant enzymes such as peroxidase, catalase, and polyphenol oxidase. A significant increase (45.9%) in proline content, a low increase (7.5%) in plant temperature, along with a low reduction in relative water content (RWC) (5.5%), and membrane stability index (MSI) (9%) were observed under water stress at 60 DAT as compared to the well-watered control. Pearson correlation analysis showed the strong correlation of shoot length with MSI and root length with RWC in rice genotypes at the later growth stage. Furthermore, Regression analysis indicated a negative correlation between plant temperature of NIBGE-DT-02 and proline, RWC, MSI, and peroxidase enzyme under variable water stress conditions. All these responses collectively validated the adaptive response of selected genotypes under water stress during different growth stages. Tolerant genotypes can be used in breeding programs aimed at improving

OPEN ACCESS

Edited by:
Italo F. Cuneo, Pontificia Universidad Católica de Valparaíso, Chile

Reviewed by:
Parviz Ehsanzadeh, Isfahan University of Technology, Iran
Mona F. A. Dawood, Assiut University, Egypt

***Correspondence:**
Sumera Yasmin
sumeraimran2012@gmail.com

Specialty section:
This article was submitted to Plant Abiotic Stress, a section of the journal Frontiers in Plant Science

Received: *13 December 2021*
Accepted: *17 January 2022*
Published: *14 February 2022*

Citation:
Mahreen N, Yasmin S, Asif M, Yousaf S, Yahya M, Ejaz K, Shahid Hussain H, Sajjid ZI and Arif M (2022) Integrated Analysis of Osmotic Stress and Infrared Thermal Imaging for the Selection of Resilient Rice Under Water Scarcity. Front. Plant Sci. 13:834520. doi: 10.3389/fpls.2022.834520

drought tolerance and can expand rice cultivation. Furthermore, this study provides a foundation for future research directed to utilize IRTI as a fast and non-destructive approach for the selection of potent rice genotypes better adapted to water scarcity from wide germplasm collection.

Keywords: osmotic stress tolerance, plant temperature, water deficit, infrared thermal imaging, proline

INTRODUCTION

Rice (*Oryza sativa* L.) is an important staple food consumed by more than half of the global human population. It plays a predominant role by providing 50–80% of the daily calories (Fukagawa and Ziska, 2019). It is estimated that annually, 520 million metric tons of rice grains (milled) are produced worldwide (FAOSTAT, 2021) while its grain yield is ≈ 2,562 Kg/ha in Pakistan (Suleri and Iqbal, 2019). In the recent era, climate change is a global problem because many countries around the world are becoming more vulnerable to natural disasters (Tan et al., 2021). As agriculture depends on climate cycles and weather patterns, climate change has caused negative effects on crop productivity and economic returns from the agricultural land (Kavadia et al., 2020).

Rice production has significantly been exposed to a number of abiotic stresses like drought, flood, high temperature, salinity, and heavy metals due to global climate change (Yadav et al., 2020). Among different abiotic stresses, drought is the most challenging as it reduces up to 70% of the rice production globally (Lum et al., 2014). Water scarcity affected one-third of the world's total rice cultivated area (Kumbhar et al., 2015). The severity of drought is very complex and depends on various causes such as the frequency of rainfall, evaporation, and soil moisture (Oladosu et al., 2019).

Many studies have been reported water stress causing changes in plants' physiological and biochemical responses, i.e., effects on mineral nutrition, transpiration rate, plant water relations, enzymatic activities, rate of photosynthesis, pigment degradation, stomatal conductance, and process of grain filling (Anjum et al., 2017). In water stress conditions, induction of reactive oxygen species (ROS) stimulates in plants causing DNA mutation, cellular oxidative damages, peroxidation of lipids, and protein denaturation (Sgherri et al., 1996; Hasanuzzaman et al., 2020). Water scarcity is linked with oxidative damage and mechanical interruption during the penetration of plant roots in drought-stressed hard soils. Collectively, these factors affect morpho-physiological and biochemical attributes of plants that ultimately result in reduced crop yield (Wilkinson and Davies, 2010).

Responses of rice genotypes to water stress are complex and widely varied with stress duration, growth stage, and type of genotype. It has been documented that flowering is delayed if water stress occurred between panicle initiation and pollen meiosis due to the delay in the development of flowers and other parts (Ji et al., 2012). Many studies have been reported that water scarcity in rice is more sensitive for seedling and booting/flowering stages (Sridevi and Chellamuthu, 2015). Less reduction in the yield of rice is observed if water stress occurs at a vegetative stage but the same stress can cause a severe yield decrease if it occurs at the time of fertilization (Raza et al., 2019). The water stress tolerance of plants at the initial stages of development is of prime importance, because good seed germination and better growth of seedlings under water deficit conditions may show potential tolerance at later growth stages to attain higher yields (Sun et al., 2020).

Rice is a water-demanding crop during the irrigated ecosystem. It needs about three to five thousand liters of water for irrigation to harvest 1 kg paddy rice in Pakistan (Sabar and Arif, 2014). To overcome the adverse effects of climate change on water availability, there is a prime need for the development or identification of suitable rice genotypes tolerant to water scarcity that can give sustainable yield under water-stressed conditions (Fahad et al., 2017). In most of the studies for screening tolerance to drought, water deficit condition is usually induced either by (1) withholding irrigation to grown plants in fields or soil pots in greenhouse experiments covered with shelter or (2) elevated the osmotic potential for grown plants in hydroponics with variable osmoticums, e.g., polyethylene glycol (PEG) (Cai et al., 2020).

A better understanding of rice morphological, biochemical, and molecular mechanisms involved in tolerance to water scarcity is extremely important to improve the rice genotypes (Panda et al., 2021). The standard evaluation scoring system (SES) was used as a primary criterion to screen rice genotypes for water stress tolerance or susceptibility (International Rice Research Institute [IRRI], 2014). Several morpho-physiological parameters, for example, root and shoot lengths, fresh and dry weights, relative water content, membrane stability index (MSI), chlorophyll, and proline content are being used for screening the genotypes for water stress tolerance (Lekshmy et al., 2021). A complex antioxidant system including both enzymatic and non-enzymatic antioxidants is a protection mechanism adopted by plants to avoid the damaging effects of ROS (Hasanuzzaman et al., 2020).

Plant physiological and biochemical attributes for screening drought tolerance and susceptibility are complex, labor-demanding, and time-consuming. Infrared thermal imaging (IRTI) emerged as a promising, user-friendly, and non-destructive technique to measure crop physiological status related to water availability (Wedeking et al., 2016). Imaging-guided expert systems have been recently used in agriculture to analyze the response of different crops (soybean, maize, lentil, and rice) to biotic and abiotic stresses (Pineda et al., 2021). Infrared thermography is a high throughput facility that may contribute to the precise selection of next-generation rice crops to combat adverse climate conditions (Kim et al., 2020).

Keeping in view the importance of reliable *in situ* method for the selection of drought-tolerant superior rice genotypes from a wide collection, the present research was conducted to

screen rice genotypes for water stress tolerance ability under PEG-induced osmotic stress at the seedling level in hydroponic nutrient solution and to study the yield components of the selected genotype by imposing water stress (water withholding for 15 days) at early and later growth stages, respectively, in pot experiments. Therefore, the preliminary objective of the present study was to integrate morphological, physiological, and biochemical screening approaches with improved *in situ* methods, i.e., infrared thermal imaging for precise selection of drought-tolerant rice genotypes. Secondly, the objective was to evaluate the selected genotypes under water deficit conditions at different growth stages to ensure their tolerance throughout the whole crop season. The results obtained will be employed for the improvement of the rice crop in future breeding programs to address the food security issues in this alarming situation of climate change.

MATERIALS AND METHODS

Collection of Plant Material Used

A total of twenty-eight rice genotypes including one tolerant (IR-55419-04), one susceptible (Super Basmati) check variety, and 26 advance lines were used for screening their drought tolerance (**Supplementary Table 1**). Among these, NIBGE-DT-02 and NIBGE-DT-11 were the offspring of Super Basmati as drought-susceptible and IR-55419-04 as drought-tolerant parents (Mumtaz et al., 2019; Sabar et al., 2019). The NIBGE-DB lines were the offspring of NIBGE-BR18 as the drought-susceptible and NIBGE-DT-02 as the drought-tolerant parent. Healthy seeds of 28 genotypes were obtained from Agricultural Biotechnology Division (ABD), National Institute for Biotechnology and Genetic Engineering (NIBGE) Faisalabad.

Initial Screening of Rice Genotypes in a Pot Experiment Under Rainout Zone

The experiment was conducted under natural net house conditions at NIBGE (11° 26′ N 73°16′ E) during the rice-growing season (July-October, 2019). The nurseries of 28 genotypes were sown. For the healthy seedlings, recommended management practices were done (Zahid et al., 2020). Earthen pots (12-inch diameter, 14-inch heigh) were filled with homogenized 12 kg soil (textured loamy, non-sterilized, EC 3.1 mS cm^{-1}, and pH 6.45). The pots were water-saturated for a few days to settle down the soil before transplanting the rice seedlings. The level of the soil 5 cm below the edge of pots was set aside. The experiment with three replicates was laid out in randomized completely block design (RCBD). The experimental pots were then divided into two groups, i.e., well-irrigated (control) and 15 days water-stressed. Seedlings of thirty-five days were transplanted in pots. The recommended dose of nitrogen (N) half and phosphorous (P) full in the form of urea and diammonium phosphate (DAP) were applied at a rate of 50 and 150 mg/kg of the soil, respectively, before transplantation. The remaining N dose was applied after 15 days of transplantation. The pots of control treatments were normally irrigated for the whole duration of the experiment while pots of stress treatment were watered for the first 30 days after transplantation (DAT) and then subjected to water stress (pots without watering) for the next 15 days. Water stress-treated pots were protected from rain during the stress period, i.e., 15 days, and re-irrigated after stress imposition.

After 15 days of water stress, a modified standard evaluation system (SES) scoring of rice genotypes at the seedling stage (**Supplementary Table 2**) was used to evaluate stress symptoms on leaves. This scoring differentiates the tolerant, moderately tolerant, and susceptible genotypes according to their ability to tolerate water scarcity (International Rice Research Institute [IRRI], 2014).

Screening of Osmotic Stress Tolerance at Seedling Stage Under Hydroponic Conditions

Three genotypes on the basis of their phenotypic response were selected and a drought tolerance score was observed in their initial screening in pots under net house conditions. These genotypes (NIBGE-DT-02, NIBGE-DT-11, and KSK-133) were further screened under control and polyethylene glycol (PEG) induced osmotic stress hydroponic conditions (**Supplementary Table 3**). The experiment was carried out in a growth room maintained with 16 h day length, 28°C day, and 23°C night with 460 μ mol/m2/s light intensity. The seeds were surface sterilized with 2% NaOHCl for 5 min, washed thrice with sterilized distilled water then soaked for 3 h in sterilized distilled water to get proper germination. Seeds were placed at an equal distance from each other on filter paper already moistened with sterilized distilled water in Petri plates for germination. The Petri plates were kept in a growth room for 4 days.

Uniform seedlings with good germination were transferred into 96-hole containing seedling boxes filled with sterilized distilled water of the same volume. Twenty-four germinated seedlings of each genotype were placed in 12 holes (two seeds in each hole) in three boxes, separately. All the boxes were labeled and placed on racks supplemented with sterilized water in a growth room for 4 days. Rice seedlings were then shifted to one-fourth of Hoagland solution (Gómez-Luciano et al., 2012) for the next 4 days. In each box, the same level of the nutrient solution was maintained by adding the solution. To decipher the variation in genotypes for drought tolerance, 8 days post-transplantation (DPT) rice seedlings were then subjected to drought stress. Drought stress was imposed by elevating the osmotic potential (PEG-simulated drought) in boxes by adding 5% PEG-8,000 in one-fourth Hoagland solution. The plants grown only in Hoagland solution of one-fourth concentration were considered as a control. Then osmotic potential elevated to 10, 15, and 20%, respectively. The duration for each stress level was 4 days. The experiment was conducted in a complete randomized design (CRD) with three replicates. Afterward, the twenty-eight-day-old plants along with the roots were taken from the boxes to study different morphological traits, i.e., root/shoot lengths, fresh and dry weights. The plants were frozen for further analysis, i.e., different physio-biochemical parameters.

Morphological Parameters

The morphological parameters of rice seedlings were studied at the end of the 20% PEG (−0.5 MPa)-simulated osmotic stress. Three plants from each replicate of the control and stressed were collected randomly and studied root/shoot lengths and fresh weights. After recording the fresh weights, the roots and shoots were kept in the oven at 70°C for 48 h to measure their respective dry weights (at 14% water content) (Wimberly, 1983).

Physiological Parameters

After the morphological analysis, physiological responses in plant leaves were analyzed. Ten leaves per replicate of the control and stressed plants were collected and chopped to make a composite sample (Motaleb et al., 2018).

Leaf Chlorophyll Content

The amount of chlorophyll a, b, and t (total chlorophyll) was calculated in the leaves of the control and stressed plants using the methods described by Arnon (1949) and Davies (1976). Leaf sample (0.1 g) was ground in 80% chilled acetone and incubated at 10°C for 24 h. After 24 h, the sample was centrifuged at 14,000 × *g* for 5 min. The absorbance of the supernatant was measured at 470,645, and 663 nm.

Leaf Proline Content

Proline content ($\mu molg^{-1}$ fresh weight) was measured with the method described by Bates et al. (1973). A leaf sample (0.5 g) from a homogenized sample of each replicate was ground in 3% 5-Sulfosalicylic acid, followed by centrifugation at 13,000 rpm for 10 min. The supernatant (2 mL) was added to a test tube with 2 mL of acid ninhydrin, 2 mL of glacial acetic acid, and 2 mL of 6 M phosphoric acid then incubated in a water bath at 100°C for 1 h. After 1 h, the reaction mixture was then cooled in an ice bath for 10 min. Toluene (4 mL) was added to the reaction mixture and mixed vigorously with a test tube stirrer for 20–30 s. The organic toluene phase (upper layer) containing the chromophore was collected and the absorbance of pink to red color developed was estimated at 520 nm using a spectrophotometer (Carry60 UV-Vis, Agilent Technologies, United States). Proline concentration was determined using a standard curve developed with different concentrations of L-proline (Bates et al., 1973).

Validation of Tolerant Rice Genotype for Drought Tolerance in a Pot Experiment Under Rainout Zone

Based on the findings from both the initial screening in a pot experiment followed by hydroponically PEG-simulated screening for drought tolerance, the rice genotype (NIBGE-DT-02) was selected for further validation in a pot experiment not only for their tolerance to water scarcity but also for physio-biochemical and yield parameters. The experiment was conducted under natural net house conditions at NIBGE (11° 26′ N 73°16′ E) during the rice-growing season (July-October, 2020). The growth and experimental conditions were the same as described above in see section "Initial Screening of Rice Genotypes in a Pot Experiment Under Rainout Zone." The pots were divided into two sets for two-stage water stress imposition, i.e., (1) well-watered-control and water-stressed for 15 days after 30 DAT (2) well-watered-control and water-stressed for 15 days after 60 DAT. Water stress treatment pots were protected from rain during stress periods. The plants' physiological and morphological responses were measured and also preserved for biochemical analysis at the end of each stress period. At the stage of harvesting, rice yield and yield attributes were calculated from both sets of control and water-stressed plants.

Application of Infrared Thermal Imaging for Measuring Plant Temperature

Infrared (IR) thermal images were taken with a FLIR E6 camera (FLIR Systems Inc., North Billerica, MA, United States). Plants were studied for thermal imaging before and after stress imposition, i.e., 5, 10, and 15 days after stress (DAT) at both early and later growth stages. The FLIR E6 camera was with IR emissivity ranging from0.1 to 0.95, the temperature ranged from −20 to 250°C, spectral ranged 7.5–13 μm, resolution 19,200 pixels (160 × 120), auto hot/cold detection modes, and < 0.06°C thermal sensitivity. The images were taken from a distance of 1.5 m from the plants and simultaneously, visual color images were also saved automatically. A styrofoam sheet was used to minimize the plant background temperature. IR thermal images were analyzed using IR 4.1 FLIR research and development software (FLIR Systems Inc.). The images were taken at 11:00 am, which is the period of high photosynthesis efficiency at Faisalabad (11° 26′ N 73°16′ E). Three-four thermal images from the plant were taken from each of the genotypes per replicate and temperature was averaged.

Plant Morphological Responses to Water Deficit Treatments

After the onset of water-stress for 15 days during the early and later growth stages, the plants were sampled for morphological analysis. In this experiment, the root-shoot lengths and the plant fresh and dry weights were measured as described above in see section "Morphological Parameters."

Plant Physio-Biochemical Responses to Water Stress

Different physiological traits of stressed and non-stressed plants were measured after both stages of water deficit treatment from homogenized leaf samples as described in see section "Physiological Parameters." Chlorophyll content and proline content analysis were carried out as described above in see sections "Leaf Chlorophyll Content" and "Leaf Proline Content," respectively.

Leaf Relative Water Content Analysis

Leaf relative water content (RWC) was estimated according to Barrs and Weatherley (1962). For this parameter, the youngest fully expanded leaves were removed and weighed immediately for measurement of the fresh weight (FW). Then, the leaf segments were soaked 4–6 h in distilled water to measure the turgid weight (TW), and the dry weight (DW) leaf segments were oven-dried for 24 h at 70°C. Three leaves were included from each replication.

The RWC% was calculated by this formula: RWC = (FW–DW/TW–DW) × 100.

Leaf Chlorophyll Content Using Soil and Plant Analyzer Development (SPAD) Meter

Chlorophyll content was measured by using a chlorophyll meter (Model: SPAD 502 plus, Japan). SPAD meter was used to measure the chlorophyll contents in the leaves before and after 5, 10, and 15 days during both stages of water stress. The chlorophyll SPAD meter readings were taken from three random positions of one leaf and three different leaves per plant and three plants were selected per replication (Cai et al., 2020).

Membrane Stability Index (MSI)

Membrane stability was determined according to the method proposed by Sairam et al. (1997). The leaf discs (1 g) of0.5 cm size were cut from the fully expanded upper leaf washed with distilled water and placed in a test tube containing 15 mL distilled water and incubated at 24°C for 12 h. The electrolytic conductivity (EC) of the solution was measured (C1). The samples were autoclaved

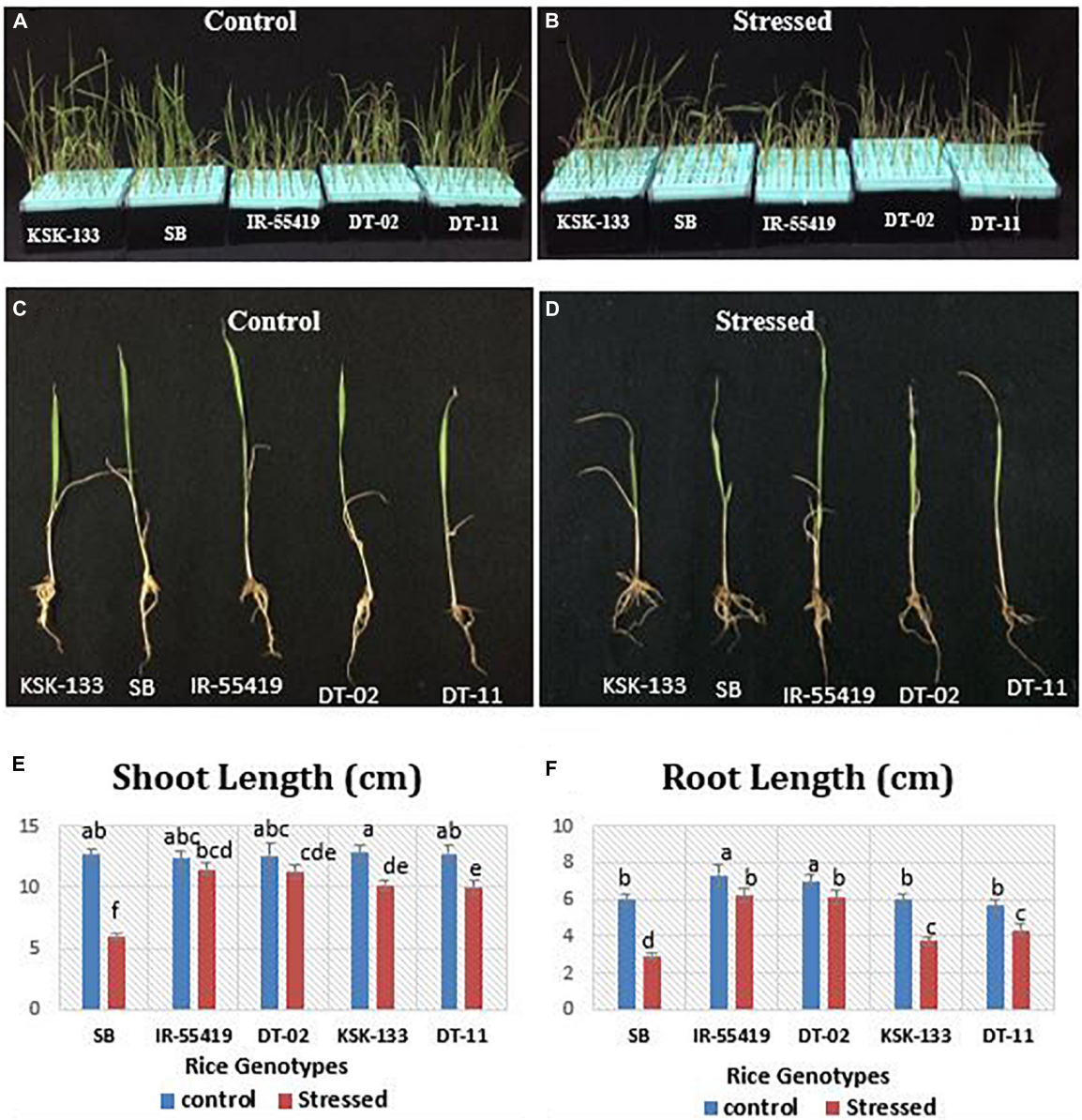

FIGURE 1 | Effect of osmotic stress on rice growth parameters under hydroponic conditions. Rice genotypes: Super Basmati (SB), IR-55419-04, NIBGE-DT-02, KSK-133, and DT-11. **(A)** Control-all tested rice genotypes without osmotic stress. **(B)** Stressed-osmotic stressed [20% Polyethylene Glycol (PEG)] rice seedlings in the hydroponic culture conditions. Morphological response of panel **(C)**. Plants of all tested genotypes under control- (without stress) and panel **(D)**. Plants of all tested genotypes under PEG mediated stressed. Graphical representation of panel **(E)** shoot lengths. **(F)** Root lengths under control-(without stress) and stressed-(20% PEG mediated osmotic stress).

at 120°C for 20 min and the EC of the solution was measured after cooling (C2).

MSI (%) was calculated with the following formula: MSI = [1–(C1/C2)] × 100.

Analysis of Enzymatic Antioxidants

After the morphological and physio-biochemical analysis, the leaves of rice genotypes were comparatively studied for the activities of different antioxidant enzymes.

Catalase (CAT) Activity

Catalase (CAT) activity was determined according to the method described by Zhang et al. (2007). Leaf tissues (0.1 g) from the homogenized sample were ground with 2 ml (0.1 M) sodium phosphate buffer of pH 6.0. Then the homogenate was centrifuged at 13,000 × *g* for 10 min. The supernatant was collected and stored at −18°C until further use. The supernatant (100 μl) was treated with the reaction mixture containing 200 mL of H_2O_2 and 30 mL (0.1 M sodium phosphate buffer) having pH 6.0 at room temperature. Distilled water (1.9 ml) with 100 μl sample and 1 ml substrate were added in a cuvette to determine its absorbance at 240 nm using a spectrophotometer (M350, UV visible double beam, CamSpec, United Kingdom). Enzyme activity was expressed on a fresh weight basis, i.e., units/g f. wt.

Peroxidase (POD) Activity

For POD estimation, the suspension was prepared by weighing 0.1 g leaves from the homogenized leaf sample, grinding them with a pestle and mortar with 2 ml (0.1 M) sodium phosphate buffer having pH 6.0. Then centrifuged at 13,000 × *g* for 10 min. The supernatant was collected for further analysis and stored at −18°C. The activity of POD was estimated according to the method described by Chance and Maehly (1955). Sodium phosphate buffer (2.8 ml of 50 mM), 800 μl (40 mM) H_2O_2, 200 μl guaiacol (substrate), and 60 ml of distilled water were added to prepare the substrate buffer. Substrate buffer (3 ml) and 100 μl supernatant were placed in a cuvette and absorbance at 470 nm were measured. One unit of POD activity was described by a variation of 0.01-unit min^{-1}.

Phenylalanine Ammonia-Lyase (PAL) Activity

Phenylalanine ammonia-lyase (PAL) enzyme activity was estimated by the method described by Zucker (1965). Leaf tissues (0.1 g) from the homogenized leaf sample were ground with 1 ml (0.1 M) sodium borate buffer of pH 8.8. The homogenate was centrifuged at 13,000 × *g* for 10 min. The supernatant was collected and stored at −18°C for further analysis. The enzyme extract (62.5 μl) and sodium borate buffer (800 μl) were added to the test tube, along with 700 μl (12 mM) phenylalanine. The test tubes were incubated in a water bath at 40°C for 1 h. A 5N HCL (200 μl) was added to stop the reaction. Then, (0.5 ml) of 1 M *Trans*-cinnamic acid (TCA) was added and light absorbance was estimated at 290 nm.

Polyphenol Oxidase (PPO) Activity

For the estimation of PPO, 0.1 g leaves from the homogenized sample were ground in pestle and mortar with (2 ml) 0.1 M sodium phosphate buffer of pH 6.0 and centrifuged at 13,000 × *g*

TABLE 1 | Effect of PEG mediated osmotic stress on growth parameters of different rice genotypes under hydroponics.

	Control					Stressed				
Rice genotypes	**Super Basmati**	**IR-55419-04**	**NIBGE-DT-02**	**KSK-133**	**NIBGE-DT-11**	**Super Basmati**	**IR-55419-04**	**NIBGE-DT-02**	**KSK-133**	**NIBGE-DT-11**
Parameters										
Shoot length	12.70 ± 0.36^{ab}	12.33 ± 0.5^{abc}	12.63 ± 0.93^{abc}	12.83 ± 0.67^{a}	12.77 ± 0.65^{ab}	6.00 ± 0.50^{f}	11.47 ± 0.64^{bcd}	11.30 ± 0.80^{cde}	10.17 ± 0.38^{de}	10.00 ± 0.56^{e}
Root length	6.00 ± 0.30^{b}	7.33 ± 0.58^{a}	7.03 ± 0.35^{a}	6.00 ± 0.30^{b}	5.67 ± 0.29^{b}	2.79 ± 0.15^{d}	6.23 ± 0.40^{b}	6.10 ± 0.36^{b}	3.77 ± 0.21^{c}	4.37 ± 0.32^{c}
Shoot fresh weight	0.027 ± 0.003^{bcd}	0.031 ± 0.005^{ab}	0.032 ± 0.003^{a}	0.023 ± 0.003^{de}	0.020 ± 0.002^{ef}	0.019 ± 0.002^{ef}	0.028 ± 0.004^{abc}	0.027 ± 0.004^{cd}	0.018 ± 0.003^{f}	0.016 ± 0.004^{f}
Shoot dry weight	0.015 ± 0.002^{bcd}	0.019 ± 0.002^{ab}	0.020 ± 0.002^{a}	0.013 ± 0.001^{cde}	0.010 ± 0.002^{ef}	0.009 ± 0.001^{def}	0.016 ± 0.002^{bc}	0.016 ± 0.001^{cde}	0.010 ± 0.002^{cde}	0.008 ± 0.001^{f}
Root fresh weight	0.032 ± 0.003^{bc}	0.042 ± 0.004^{a}	0.036 ± 0.004^{abc}	0.042 ± 0.004^{a}	0.033 ± 0.003^{bc}	0.023 ± 0.002^{de}	0.039 ± 0.003^{ab}	0.032 ± 0.003^{c}	0.029 ± 0.003^{cd}	0.020 ± 0.004^{e}
Root dry weight	0.018 ± 0.002^{c}	0.031 ± 0.003^{a}	0.030 ± 0.002^{a}	0.030 ± 0.002^{a}	0.019 ± 0.002^{c}	0.012 ± 0.001^{de}	0.030 ± 0.002^{a}	0.024 ± 0.003^{b}	0.015 ± 0.002^{cd}	0.009 ± 0.001^{e}

Evaluation of osmotic stress on growth parameters: SL-Shoot Length (cm), RL-Root Length (cm), SFW-Shoot Fresh Weight (g), SDW-Shoot Dry Weight (g), RFW-Root Fresh Weight (g), RDW-Root Dry Weight (g), of different rice genotypes: SB (Super Basmati), IR-55419-04, NIBGE-DT-02, KSK-133 and NIBGE-DT-11 under hydroponic conditions. Control- plants grown under sterilized water for 4 days followed by 1/4th Hoagland solution for whole experiment, Stressed-plants grown under sterilized water for 4 days followed by 1/4th Hoagland solution with 5, 10, 15, and 20% PEG mediated osmotic stress, respectively, and duration for each stress level was 4 days. A 28 days old seedlings were removed to measure growth parameters. Data represented as means and means are an average of three biological replicates and there were ten plants per replicate. Means with same letter differ non-significantly at p = 0.01 while different letters show statistical significance according to LSD.

for 10 min. The supernatant was taken and stored at −18°C for further analysis. PPO activity was estimated by the method described by Mayer et al. (1965). In the reaction cuvette (1.0 ml), 0.1 M sodium phosphate buffer and (1.0 ml) 0.01 M L-tyrosine (substrate) in HCl were added with (0.9 mL) distilled water. The sample (100 μl) was used to measure the absorbance at 280 nm using a spectrophotometer. The change in absorbance was measured after every 30 s for 2 min and PPO enzyme activity was expressed in $min^{-1}g^{-1}$ of fresh weight.

Effect of Water Stress on Yield Attributes

Plants of each genotype from both stress treatments and controls were manually harvested at maturity. The harvested plants were measured for different growth and yield parameters, i.e., plant height, number of tillers per plant, paddy weight per plant, and paddy yield per pot.

Statistical Analysis

Data from pot experiments and hydroponic experiments were statistically analyzed by ANOVA and differences between osmotic stressed and controls were compared by the least significant difference (LSD) at 5% (for pot experiment) and 1% confidence level (for the hydroponic experiment) using the software STATISTIX 10.0 (Tallahassee, FL, United States). Pearson correlation coefficient was used for the assessment of associations between different studied plant traits. For interactive studies, the regression analysis of IR temperature with proline content, SPAD, MSI, and RWC were studied using SPSS software (SPSS Inc., NY, United States).

RESULTS

Initial Screening of Rice Genotypes Under Net House Conditions

Depending on the visual symptoms of the leaves after 15 days period of water stress imposition, SES scoring was done for all the tested genotypes, i.e., highly tolerant (HT), tolerant (T), moderately tolerant (MT), moderately susceptible (MS), susceptible (S), and highly susceptible (HS). For the evaluation of water-stressed rice leaves, IR-55419-04 and Super Basmati were used as tolerant and susceptible check varieties, respectively. Highly tolerant genotypes were scored as 0, tolerant genotypes as 1, moderately tolerant genotypes as 3, moderately susceptible as 5, susceptible as 7, and highly susceptible as 9 (**Supplementary Table 1**). After water stress of 15 days, susceptible rice genotypes showed leaf drying followed by chlorosis to dead seedlings (**Supplementary Figures 1A–F**). Among 26 genotypes 3 were identified as tolerant, 9 moderately tolerant, 5 moderately susceptible, 6 susceptible, and 3 as highly susceptible (**Supplementary Table 1**).

Screening of Osmotic Stress Tolerance Under Hydroponic Conditions

Three genotypes were selected on the basis of their phenotypic response and drought tolerance score observed in their initial screening in pots under net house conditions. These genotypes (NIBGE-DT-02, NIBGE-DT-11, and KSK-133) were further screened under control and PEG-simulated osmotic stress hydroponic conditions (**Supplementary Table 3**).

Morphological Responses of Rice Genotypes to Osmotic Stress

The rice genotypes growing in nutrient solution along with 20% PEG-8000 were studied for shoot and root length (**Figures 1A,B**). A significant reduction in shoot and root lengths of susceptible genotypes [Super Basmati (SB), NIBGE-DT-11 followed by KSK-133] was observed as compared to tolerant control (IR-55419-04) (**Figures 1C,D**). The mean values of root length (RL) and shoot length (SL) under osmotic stress showed significant differences among all the tested genotypes (**Figures 1E,F**). Percent reduction in RL was maximum in SB, i.e., 53.5% followed by KSK-133 (37.2%) and NIBGE-DT-11 (22.9%). At 20%-PEG mediated osmotic stress, the RL ranged from 6.23 to 6.10 cm for IR-55419-04 and NIBGE-DT-02, respectively (**Table 1**).

Osmotic stress treatment significantly reduced shoot fresh weight (SFW) and root fresh weight (RFW) in all the tested

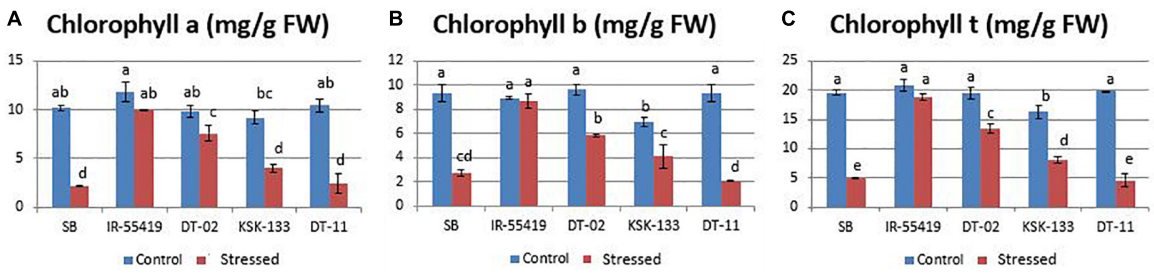

FIGURE 2 | Effect of PEG-induced osmotic stress under hydroponics on chlorophyll a, b, and t of rice genotypes. Genotypes: SB, IR-55419, DT-02, DT-11, and KSK-133. **(A)** Chlorophyll-a content of control-(non-stressed) and stressed-20% PEG induced osmotically stressed plants. **(B)** Chlorophyll-b content of control-(non-stressed) and stressed-20% (PEG) induced osmotically stressed plants. **(C)** Chlorophyll-t (total chlorophyll) of control-(non-stressed) and stressed-20% Polyethylene glycol (PEG) induced osmotic stressed plants in mg/g FW (fresh weight). Ten leaves per plant were homogenized to make a composite sample and three plants per replicate were used. Data represented as mean and means are an average of three biological replicates. According to the least significant difference, means followed by the same letter differ non-significantly at $p = 0.01$ while different letters show statistical significance of genotypes under control and stressed conditions.

genotypes except NIBGE-DT-02 as compared to the tolerant control. SFW at the maximum level of stress ranged from 0.016 to 0.019 g for SB and NIBGE-DT-11, respectively (**Table 1**). IR-55419-04 showed a minimum percent reduction in the RFW (7.1%) as compared to NIBGE-DT-11 (39.4%). The least reduction in shoot dry weight (SDW) was observed in IR-55419-04 (15.8%) and NIBGE-DT-02 (20%) while KSK-133 and SB showed higher reduction, i.e., 40 and 23.1%, respectively. A similar pattern was observed for root dry weight (RDW) (**Table 1**).

Physiological Responses of Rice Genotypes to Osmotic Stress

Chlorophyll a, b, and total chlorophyll contents were reduced variably in all genotypes under stress conditions as compared to their respective well-watered controls (**Figures 2A–C**). Higher chlorophyll content with less percent reduction was observed in tolerant check variety (IR-55419-04) followed by NIBGE-DT-02 under osmotic stress. A significant percent decrease in chlorophyll was observed in SB (78.7%) followed by NIBE-DT-11 (76.9%) (**Table 2**).

An increase in proline content (11.11–22.7%) under osmotic stress showed significant genotypic variability. A significant increase in proline concentration was observed in NIBGE-DT-02 (20 $\mu molg^{-1}$ fresh weight). While least percent increase in proline accumulation was observed in NIBGE-DT-11 (11.8%) as compared to the tolerant control (**Table 2**).

Validation of Rice Genotypes in Pots Under Rain Out Zone

Thermal Imaging of Rice Genotypes Response to Water Stress

Results of infrared thermal imaging detected small differences in whole plant temperature of rice genotypes under water stress conditions (**Figures 4A–F**). During the early and later stages, the plant temperature was almost similar for all the genotypes at 0 days after stress (DAS). At 0DAS, the average temperature during early-stage stress was about 31.9 ± 0.73°C and the later stage was 30.9 ± 0.66°C, respectively. From 0DAS to 15DAS, in response to water stress, the plant temperature changed gradually in all genotypes during both stages of water withholding. The effect of water stress at 15DAS was significant in SB with higher values of IR temperature (14.7%) during the later growth stage (**Table 3**).

Morphological Responses of Rice Genotypes to Water Stress

The relative reduction was observed in the growth parameters of rice genotypes under water-stressed conditions, i.e., for 15 days at 30 DAT (**Figures 3A,B**) and second at 60 DAT (**Figures 3C,D**) as compared to non-stressed plants. The least and maximum relative reduction was observed in the shoot and root lengths of positive control IR-55419-04 and SB, respectively, under water scarcity. Plant FW was drastically reduced in SB at 15DAS during both stages of water stress. The least reduction in fresh and dry weights under water

TABLE 2 | Influence of PEG mediated osmotic stress on chlorophyll and proline contents of different rice genotypes under hydroponic conditions.

	Control				Stressed						
Rice genotypes	**CHL a***	**CHL b***	**CHL t***	**Proline****	**CHL a***	**CHL b***	**CHL t***	**Proline****	**% decrease in CHL a**	**% decrease in CHL b**	**% decrease in CHL t**	**% increase in Proline**
SB	10.15 ± 0.24^{ab}	9.29 ± 0.69^{a}	19.56 ± 0.45^{a}	16 ± 0.50^{c}	2.16 ± 0.08^{d}	2.72 ± 0.23^{cd}	4.91 ± 0.15^{e}	18 ± 1.07^{b}	78.70%	70.70%	74.90%	11.11%
IR-55419	11.78 ± 1.01^{a}	8.90 ± 0.11^{a}	20.83 ± 0.92^{a}	17 ± 1.48^{b}	10.00 ± 0.05^{ab}	8.69 ± 0.60^{a}	18.82 ± 0.65^{a}	22 ± 2.56^{a}	15.10%	2.30%	9.60%	22.70%
DT-02	9.78 ± 0.61^{ab}	9.61 ± 0.43^{a}	19.50 ± 1.04^{a}	16 ± 0.68^{b}	7.59 ± 0.83^{c}	5.82 ± 0.08^{b}	13.51 ± 0.77^{c}	20 ± 1.05^{a}	22.40%	39.40%	30.70%	20%
KSK-133	9.20 ± 0.73^{bc}	6.95 ± 0.35^{b}	16.26 ± 1.09^{b}	14 ± 0.88^{c}	4.02 ± 0.38^{d}	4.08 ± 0.98^{c}	8.15 ± 0.59^{d}	16 ± 1.74^{b}	56.30%	41.30%	49.90%	12.50%
DT-11	10.46 ± 0.68^{ab}	9.29 ± 0.69^{a}	19.88 ± 0.01^{a}	15 ± 0.77^{c}	2.42 ± 0.99^{d}	2.13 ± 0.04^{d}	4.58 ± 1.04^{e}	17 ± 2.20^{b}	76.90%	77.10%	76.90%	11.80%

*Effect of osmotic stress on physiological parameters: CHL a-Chlorophyll a, CHL b- Chlorophyll b, CHL t-Chlorophyll t, *- mg/g FW, **- µM/g. f. wt., of different rice genotypes: SB (Super Basmati), IR-55419, DT-02, KSK-133, and DT-11 under hydroponic conditions. Control- plants grown under sterilized water for 4 days followed by 1/4th Hoagland solution for the whole experiment, Stressed-plants grown under sterilized water for 4 days followed by 1/4th Hoagland solution with 5, 10, 15, and 20% PEG mediated osmotic stress, respectively, and duration for each stress level was 4 days. A 28 days old seedlings were removed to measure chlorophyll and proline contents. Data represented as means and means are an average of three biological replicates and there were ten plants per replicate. Means with the same letter differ non-significantly at p = 0.01 while different letters show statistical significance according to LSD.*

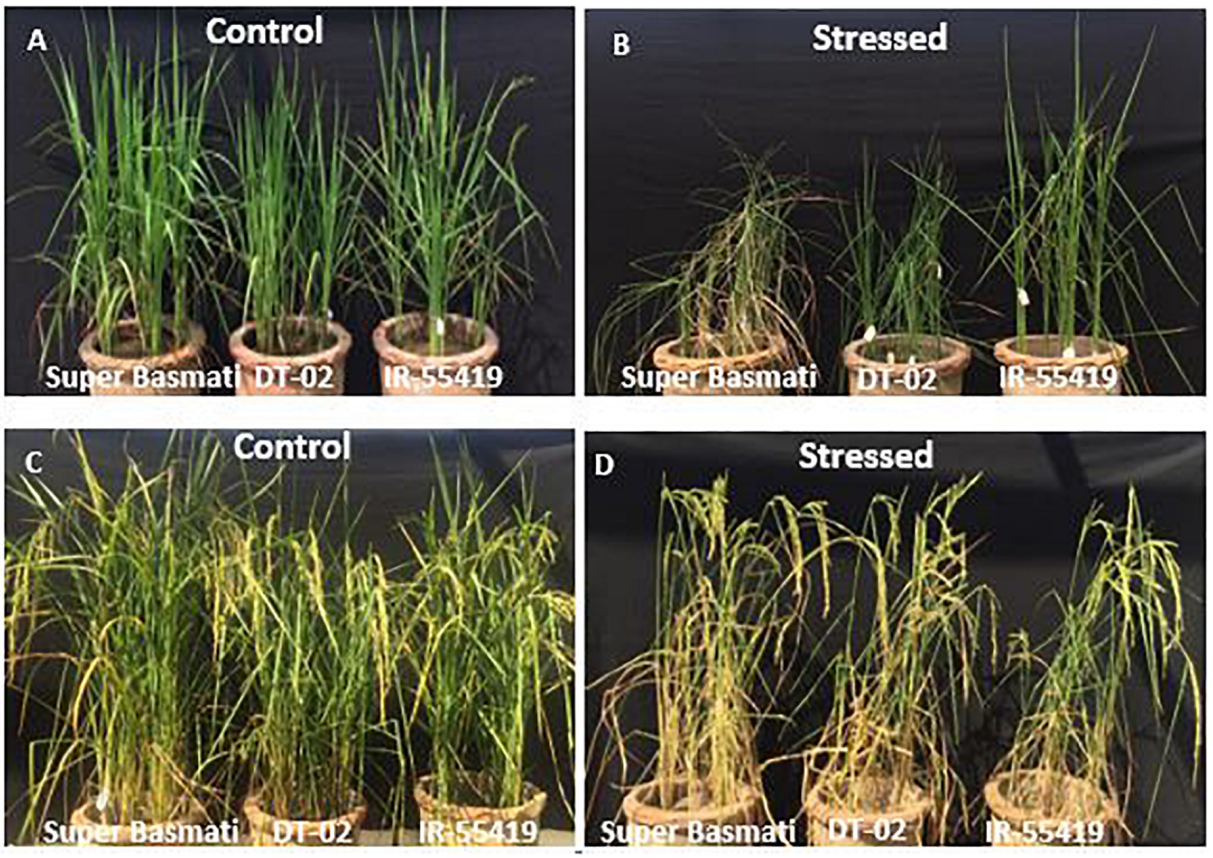

FIGURE 3 | Pictorial view of water stress treatments to rice genotypes during early and later growth stages under net house conditions. Genotypes: SB, IR-55419, and DT-02. **(A)** Control-well irrigated rice plants till 30 days after transplantation (DAS). **(B)** Stressed-water stress rice plants (water withholding for 15 days after 30 DAS) under net house culture conditions. **(C)** Control-well irrigated rice plants till 60 days after transplantation (DAS). **(D)** Stressed-water stress rice plants (water withholding for 15 days after 60 DAS) under net house conditions.

scarcity was observed in IR-55419-04 and NIBGE-DT-02 (**Figures 5A–F**).

Physio-Biochemical Responses of Rice Genotypes to Water Stress

Relative Water Content and Membrane Stability Index (MSI)

The percent RWC of the leaves was measured in the control and stressed plants to understand the effect of water stress on experimental rice genotypes. RWC% was found to be decreased dramatically under drought stress (**Table 4A**). In the control plants, RWC% was found almost in a similar pattern in all genotypes while water stress resulted in a progressive decline in RWC% values. Under the stress conditions, the highest RWC% during both stages of water scarcity were observed in the genotype IR-55419, followed by DT-02. A maximum percent decrease (45.5 and 43.7%) in RWC was found in genotype SB during water stress at 30 DAT and 60 DAT, respectively (**Table 4A**).

Increased electrolyte leakage (EL) under water scarcity points toward the increase in the plant cell membrane injury. Water stress caused a decrease in MSI during the period of stress and the magnitude of the decline in MSI for susceptible rice genotype (SB-70.20%, 42.90%) was greater than that of the tolerant genotype NIBGE-DT-02 (35.90%, 9%) during water stress at 30 DAT and 60 DAT, respectively (**Table 4A**).

Proline and Chlorophyll Content

Under water stress proline concentrations (μ molg^{-1} FW) of rice, genotypes were increased to a variable extent as compared to their respective controls during both stages of stress treatments. The water stress-tolerant genotype NIBGE-DT-02 accumulated the highest concentration (46.72, 56.25 μ molg^{-1} FW) of proline at 15DAS during water stress at 30 DAT and 60 DAT, respectively. SB showed the least percent increase (19.87, 35.02%) in proline content in both stages of water stress (**Table 4A**).

Rice genotypes for chlorophyll a, b, and total chlorophyll differed variably under water scarcity. Higher values of chlorophyll contents after positive control were observed in NIBGE-DT-02 during the early and later stages of water stress. SB showed the highest percent reduction in total chlorophyll content (39.14, 34.50%) in water stress at 30 DAT and 60 DAT, respectively (**Table 4B**).

The SPAD values from the leaves of rice genotypes showed a similar pattern with the chlorophyll contents of respective

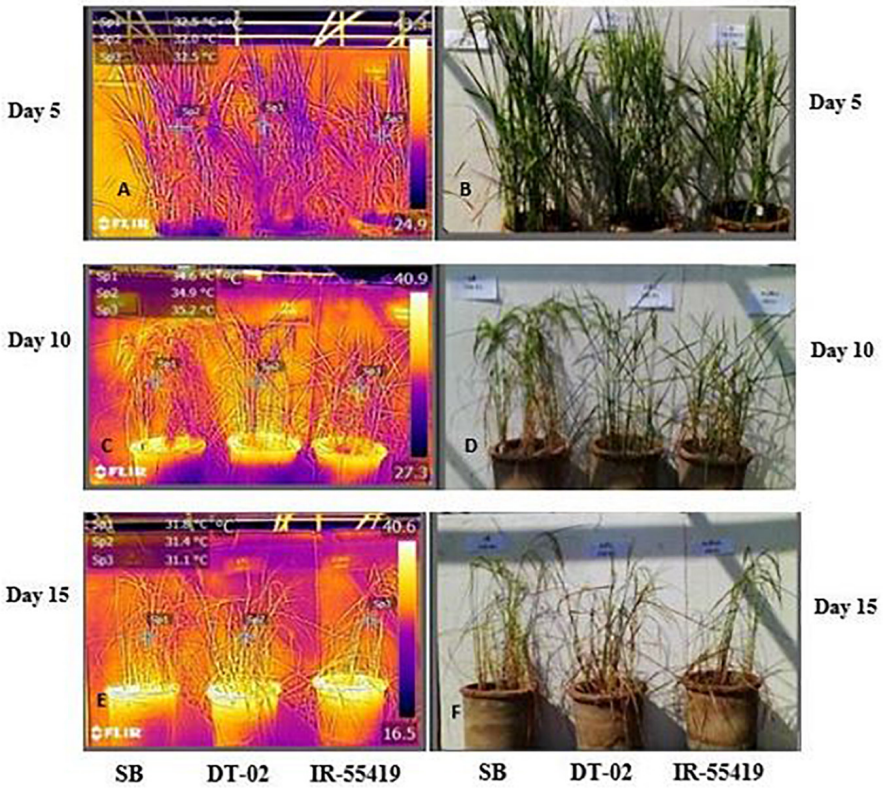

FIGURE 4 | Visual and infrared thermal images of rice genotypes taken by a FLIR T-E6 camera in a net house pot experiment. Genotypes: SB, NIBGE-DT-02, IR-55419-04. **(B,D,F)** Visual images of plants taken at day 5, 10, and 15 after water stress. **(A,C,E)** Thermal images of plants taken at day 5, 10, and 15 after water stress. IR-thermal images were analyzed using IR 4.1 FLIR research and development software (FLIR Systems Inc.).

TABLE 3 | Infrared thermal imaging to study the effect of water stress on plant temperature during early and later growth stages under net house conditions.

	IR temperature before stress (°c)	IR temperature 5DAS (°c)	% increase in IR-temperature at 5 DAS	IR temperature 10DAS (°c)	% increase in IR-temperature at 10 DAS	IR temperature 15DAS (°c)	% increase in IR-temperature at 15 DAS
Water stress at 30 DAT							
Super Basmati	31.8 ± 0.87^{a}	34.0 ± 0.94^{a}	6.50%	35.7 ± 0.52^{a}	10.90%	37.3 ± 0.47^{a}	14.70%
DT-02	31.9 ± 0.73^{a}	33.0 ± 0.85^{b}	3.30%	33.9 ± 0.35^{b}	5.90%	34.7 ± 0.61^{b}	8.10%
IR-55419	31.6 ± 0.57^{a}	32.9 ± 0.40^{b}	3.90%	32.9 ± 0.71^{b}	3.90%	34.2 ± 0.82^{b}	7.60%
Water stress at 60 DAT							
Super Basmati	30.4 ± 0.42^{a}	32.9 ± 0.73^{a}	7.60%	34.1 ± 0.94^{a}	10.60%	35.0 ± 0.64^{a}	13.10%
DT-02	30.8 ± 0.54^{a}	31.9 ± 0.47^{b}	3.40%	32.4 ± 0.78^{b}	4.90%	33.3 ± 0.59^{b}	7.50%
IR-55419	30.9 ± 0.66^{a}	31.1 ± 0.54^{c}	0.64%	32.0 ± 0.61^{b}	3.40%	33.0 ± 0.47^{b}	6.40%

Effect of water withholding for 15 days at 30 days after transplantation (DAT) and 60 DAT on IR (Infrared temperature) of rice plants of different genotypes. Before stress-no stress imposed, 5DAS-(5 days after stress), 10DAS-(10 days after stress), and 15DAS-(15 days after stress). Data represented as means and means are an average of three biological replicates and there were four images per replicate. Means with the same letter differ non-significantly at p = 0.01 while different letters show statistical significance according to LSD.

genotypes. The least percent reduction in SPAD values was observed for NIBGE-DT-02 (5%) later stage (60 DAT) water stress (**Table 4B**).

Enzymatic Antioxidants

The results showed that the concentration of antioxidant enzyme was found maximum in the tolerant and minimum in susceptible rice genotypes under water scarcity. However, the accumulation of enzymes varied between all the tested genotypes. Under water stress, the highest accumulation of antioxidants (CAT:0.36, POD:276.03, PAL:0.21, and PPO: 19.57 units g^{-1} f. wt.) during water stress at 30 DAT (**Figures 6A–D**) and (CAT:0.47, POD:280, PAL:0.73, and PPO:18.86 units g^{-1} f. wt.) at 60 DAT water stress (**Figures 7A–D**) were recorded in NIBGE-DT-02 followed by the positive control (IR-55419-04). The susceptible genotype (SB) under stress showed less

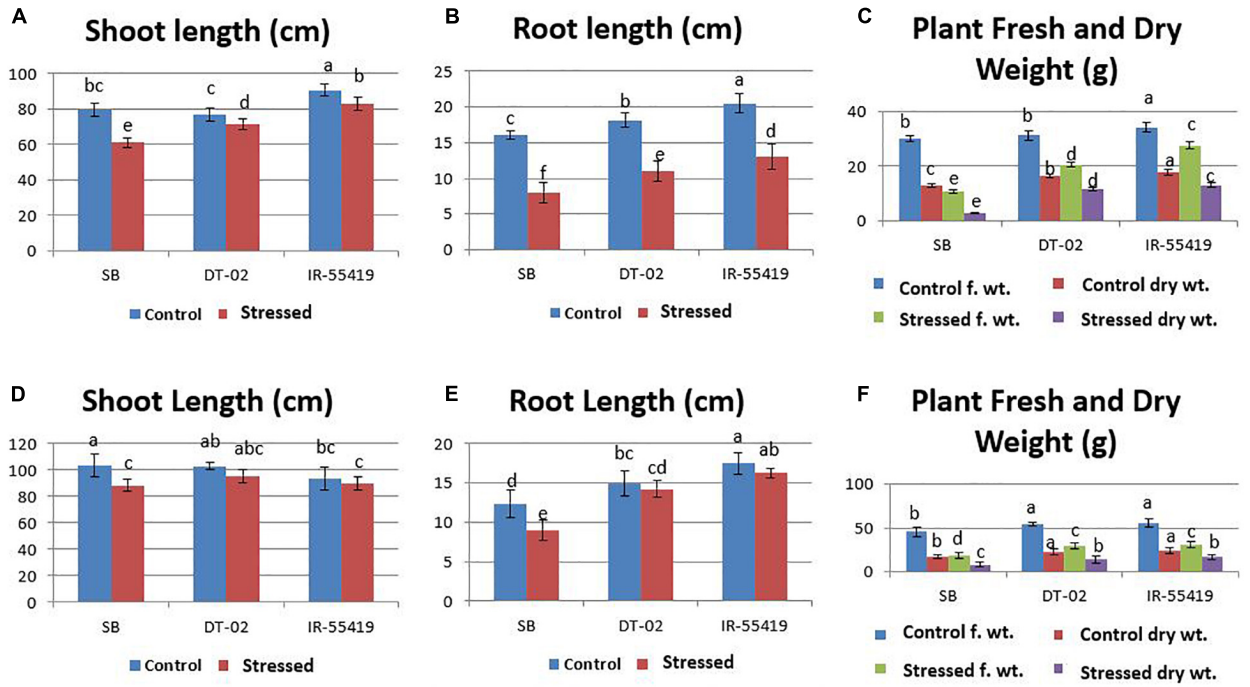

FIGURE 5 | Effect of water stress on rice growth parameters under net house conditions. **(A)** Shoot length (cm). **(B)** Root length (cm). **(C)** Plant fresh and dry weight under control-fully irrigated and stressed-water with holding for 15 days at 30 days after transplantation (DAT). **(D)** Shoot length (cm). **(E)** Root length (cm). **(F)** Plant fresh and dry weight under control-fully irrigated and stressed-water with holding for 15 days at 60 DAT. Rice genotypes: SB, IR-55419, and DT-02. Bars indicate the SD of three biological replicates and each replicate has three plants. Data represented as means and means followed by the same letter differ non-significantly and with different letters show statistical significance at $p = 0.05$ according to LSD.

TABLE 4A | Effect of water stress on relative water content (RWC), membrane stability index (MSI) and proline content of rice genotypes during early and later growth stages under net house conditions.

	Control			Stressed			% decrease in MSI	% decrease in RWC	% increase in Proline
	MSI	RWC	Proline*	MSI	RWC	Proline*			
Water stress at 30 DAT									
Super Basmati	38.65 ± 3.76^{a}	68.08 ± 1.22^{b}	23.62 ± 0.98^{d}	11.50 ± 3.57^{d}	37.09 ± 2.56^{c}	29.48 ± 1.07^{c}	70.20%	45.50%	19.87%
DT-0-2	22.72 ± 3.42^{b}	52.30 ± 5.07^{ab}	29.52 ± 1.20^{c}	14.67 ± 1.54^{cd}	45.07 ± 4.54^{b}	46.72 ± 2.3^{a}	35.40%	13.80%	36.80%
IR-55419	17.61 ± 1.51^{a}	60.40 ± 5.49^{a}	27.00 ± 1.01^{d}	16.83 ± 1.19^{a}	55.79 ± 1.04^{a}	40.09 ± 1.59^{b}	21.50%	7.60%	32.65%
Water stress at 60 DAT									
Super Basmati	15.27 ± 1.49^{a}	55.73 ± 3.68^{a}	29.89 ± 1.51^{c}	8.71 ± 0.34^{c}	31.39 ± 3.99^{c}	46.00 ± 1.39^{b}	42.90%	43.70%	35.02%
DT-02	12.29 ± 0.95^{b}	78.32 ± 0.76^{a}	30.43 ± 1.06^{c}	11.18 ± 0.53^{bc}	73.99 ± 1.43^{ab}	56.25 ± 1.40^{a}	9%	5.50%	45.90%
IR-55419	19.09 ± 2.16^{bc}	73.29 ± 1.51^{ab}	17.52 ± 0.49^{e}	16.40 ± 0.47^{bcd}	70.84 ± 4.98^{b}	30.07 ± 1.41^{c}	14.10%	3.30%	41.70%

*Evaluation of water stress on MSI-Membrane stability index, RWC-Relative Water Content, and proline *- μM/g. f. wt., of different rice genotypes: Super Basmati, IR-55419, and DT-02 under net house conditions. Control- well-irrigated plants, Stressed-water stress for 15 days at 30 DAT, and water stress for 15 days at 60 DAT. After each water stress plants were removed to measure MSI, RWC, and proline content. Data represented as means and means are an average of three biological replicates and each replicate has three plants (ten leaves per plant). Data represented as means and means with the same letter differ non-significantly and with different letters differ significantly at p = 0.05 according to LSD.*

accumulation of defense-related enzymes as compared to non-stressed conditions.

Effect of Water Stress on Rice Yield

Irrespective of rice genotype, water stress reduced the plant height. A high reduction in plant height was recorded in SB while less reduction was observed in IR-55419 followed by DT-02 under water stress conditions as compared to their respective controls in both stages of stress. Drought stress reduced the number of tillers per plant in all tested rice genotypes. Maximum reduction in tiller number was recorded in drought susceptible genotype SB. Drought stress significantly reduced the grain yield in SB (82.30%) during water stress at 30 DAT while the least reduction in NIBGE-DT-02 (35.90%) during water stress at 60 DAT (**Table 5**). Percent decrease in plant height in all genotypes was more during early-stage water

TABLE 4B | Effect of water stress on chlorophyll content and SPAD values in different rice genotypes during early and later growth stages in a pot experiment under net house conditions.

	Control				Stressed					
	CHL a*	CHL b*	CHL t*	SPAD values	CHL a*	CHL b*	CHL t*	SPAD values	% decrease in CHL a	% decrease in CHL b	% decrease in CHL t	% decrease in SPAD values
Water stress at 30 DAT												
Super Basmati	26.06 ± 0.55^{a}	15.13 ± 0.73^{a}	41.52 ± 1.28^{a}	81.97 ± 0.55^{a}	15.02 ± 0.72^{e}	10.07 ± 0.21^{d}	25.27 ± 0.52^{d}	71.17 ± 0.86^{c}	42.40%	33.40%	39.14%	13.80%
DT-02	23.20 ± 0.83^{b}	13.75 ± 0.42^{bc}	37.25 ± 1.26^{b}	81.82 ± 0.74^{a}	18.76 ± 0.90^{d}	12.58 ± 0.31^{c}	31.57 ± 1.22^{c}	77.60 ± 0.52^{b}	19.13%	8.50%	15.20%	5.20%
IR-55419	23.36 ± 0.69^{b}	13.97 ± 0.30^{ab}	37.63 ± 0.60^{b}	82.02 ± 0.94^{a}	20.80 ± 0.69^{c}	12.92 ± 0.63^{bc}	33.99 ± 1.63^{c}	79.10 ± 0.58^{a}	10.90%	7.50%	9.70%	3.60%
Water stress at 60 DAT												
Super Basmati	32.79 ± 0.56^{ab}	23.22 ± 0.14^{c}	56.42 ± 0.71^{c}	81.79 ± 0.41^{a}	21.04 ± 0.38^{e}	15.67 ± 0.45^{e}	36.97 ± 0.83^{f}	74.15 ± 0.48^{c}	35.80%	32.50%	34.50%	9.30%
DT-02	31.37 ± 0.85^{c}	18.53 ± 0.11^{d}	50.30 ± 0.97^{d}	81.83 ± 0.14^{a}	28.12 ± 0.38^{d}	17.68 ± 0.48^{d}	46.15 ± 0.86^{e}	77.73 ± 0.35^{b}	10.40%	3.90%	8.30%	5%
IR-55419	33.39 ± 0.22^{a}	29.33 ± 0.54^{a}	63.11 ± 0.76^{a}	81.79 ± 0.24^{a}	31.89 ± 0.50^{bc}	27.36 ± 0.65^{b}	59.63 ± 0.14^{b}	79.89 ± 0.47^{a}	4.50%	6.70%	5.50%	2.30%

*Evaluation of water stress on CHL a-Chlorophyll a, CHL b- Chlorophyll b, CHL t-Chlorophyll t, *-mg/g FW, SPAD- Soil and Plant Analyzer Development, of different rice genotypes: Super Basmati, IR-55419, and DT-02 under net house conditions. Control- well-irrigated plants, Stressed-water stress for 15 days at 30 DAT, and water stress for 15 days at 60 DAT. After each water stress plants were removed to measure MSI, RWC, and proline content. Data represented as means and means are an average of three biological replicates and each replicate has three plants (ten leaves per plant). Data represented as means and means with the same letter differ non-significantly and with different letters differ significantly at p = 0.05 according to LSD.*

stress as compared to a later stage, while percent reduction in plant fresh weight was more during early-stage water scarcity because of low tillering so in correspondence to this percent decrease in grain yield was more during water stress at 30 DAT (**Table 5**).

Correlation Analysis Among Morpho-Physiological and Biochemical Traits

Pearson's correlation analysis was performed on different morphological and physio-biochemical traits of water-stressed plants (studied during early and later growth stage water stress). The results indicated that (at $p < 0.05$) positive correlation among all the tested genotypes with different traits was expressed in bold form while the negative correlation with a negative sign. So, on this basis, a significant correlation with multiple traits related to stress tolerance was easily identified during both stage stress conditions (**Tables 6A,B**). A negative correlation was observed between infrared (IR) temperature with (proline content, SPAD values, MSI and POD) during early-stage and with (RWC, proline content, MSI and PAL) during later-stage water stress (**Figures 8**, **9A–D**).

DISCUSSION

In the scenario of climatic shift, water scarcity is one of the most common abiotic stresses that hinders rice growth through alteration in many morphological, physiological, and biochemical responses (Chaudhry and Sidhu, 2021). Usually, rice genotypes are being selected on the basis of their tolerance to water scarcity using different drought-related morpho-physiological and biochemical approaches (Panda et al., 2021). The present study effectively combined these approaches with the useful tool of SPAD meter with further validation of drought tolerance in rice genotypes using the technology of infrared thermal imaging. Furthermore, the selected genotype was subjected to water scarcity at early (vegetative) as well as later (reproductive) growth stages to ensure its tolerance throughout the whole crop season.

In our experiment, initially, 28 rice genotypes including one tolerant (IR-55419-04) and one susceptible check (Super Basmati) variety with 26 advance lines were screened for water stress tolerance in pots under net house conditions. Among the tested genotypes, 3 were identified as tolerant, 9 moderately tolerant, 5 moderately susceptible, 6 susceptible, and 3 as highly susceptible to water deficit conditions (**Supplementary Table 1**). Three promising genotypes (NIBGE-DT-02, NIBGE-DT-11, and KSK-133) were selected based on the standard evaluation system (SES) scoring for drought tolerance (**Supplementary Table 3**). SES scoring for rice genotypes is a reliable measure of drought tolerance and reflects dehydration in plant tissues (Swapna and Shylaraj, 2017). The results of the present study in pots under net house conditions showed that water withholding for 15 days at 30 days after transplantation significantly affected the plants' phenotypic response as indicated by leaf drying to dead seedlings (**Supplementary Table 2**).

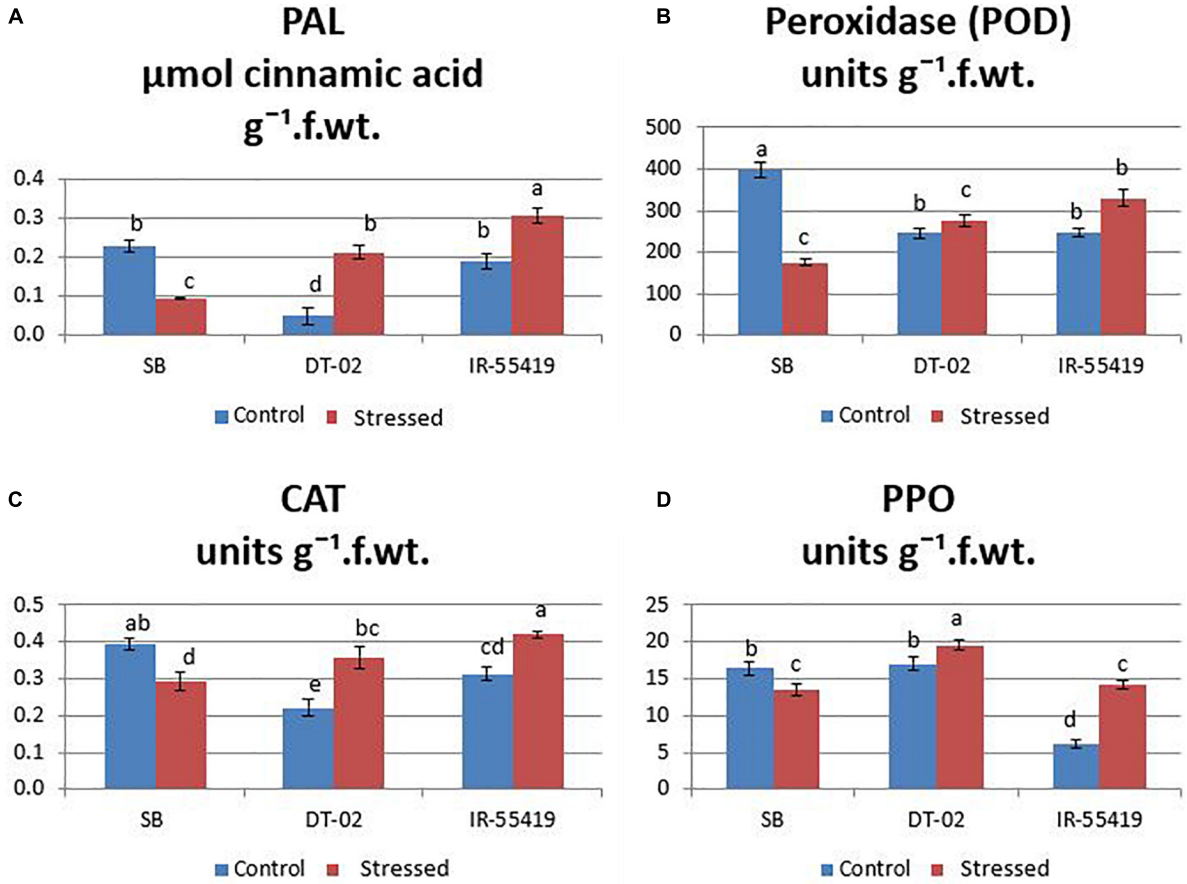

FIGURE 6 | Induction of defense-related enzymes. **(A)** Phenylalanine ammonia lyase (PAL). **(B)** Peroxidase (POD). **(C)** Catalase (CAT). **(D)** Polyphenol oxidase (PPO) in rice plants of genotypes SB, IR-55419 and DT-02 under control-fully irrigated and stressed-water with holding for 15 days at 30 days after transplantation (DAT). Bars indicate the SD of three biological replicates and each replicate has three plants (ten leaves per plant). Data represented as means and means with the same letter differ non-significantly at $p = 0.05$ according to LSD.

Three selected genotypes (NIBGE-DT-02, NIBGE-DT-11, and KSK-133) were subjected to Polyethylene glycol (PEG-20%) mediated osmotic stress under a hydroponic system in a growth room experiment. PEG-induced osmotic stress reduced all the growth parameters of rice genotypes to a variable extent (Nahar et al., 2018). In the present study, a higher level of PEG (20%) stress reduced the growth attributes of all the tested rice genotypes, the maximum reduction in the shoot length (21.7%) of NIBGE-DT-11 and in the root length (37.2%) of KSK-133 was observed (**Table 1**). Shirazi et al. (2019) reported that the reduction in growth parameters was also reflected in the physiological responses of susceptible rice genotypes, i.e., IR-8 and B-60-B. Genotype NIBGE-DT-02 achieved better growth in hydroponics osmotic stress as well as under variable water withholding stages in pots under net house conditions. NIBGE-DT-02 showed a minimum reduction in the shoot (10.5%) and root (13.2%) lengths under hydroponics (**Table 1**). Franco et al. (2011) ratified the better root growth of plants under stress conditions as an important index for the selection of drought-tolerant cultivars. In the present study, NIBGE-DT-02 revealed a minimum reduction in root growth concomitant with the least reduction in plant fresh and dry weights under 15-days water withholding at 30 and 60 DAT (**Figures 5A–F**).

Chlorophyll is an important plant photosynthetic pigment, determining plant growth and development. Under osmotic stress, a significant decrease in chlorophyll a (76.9%) and b (77.1%) were observed in the genotype NIBGE-DT-11. Genotypes NIBGE-DT-02 showed the least reduction in chlorophyll a (22.4%) and chlorophyll t (30.7%) under osmotic stress as compared to the susceptible check variety (**Table 2**). Nahar et al. (2018) reported that rice variety (SN09) showed significantly minimum chlorophyll a and b content as compared to the tolerant variety (SN03) under PEG (20%) induced stress. Moreover, NIBGE-DT-02 showed a minimum reduction in chlorophyll a (10.4%), b (3.9%), and t (8.30%), while a similar pattern of NIBGE-DT-02 was observed with a minimum (5%) reduction in SPAD values under 15-days water withholding at 60 days after transplantation (**Table 4B**). According to Nahakpam (2017), the reduction in chlorophyll content might be due to the formation of active oxygen species (AOS) that affects the stability of the chloroplast membrane and causes the chlorophyll degradation under water stress conditions.

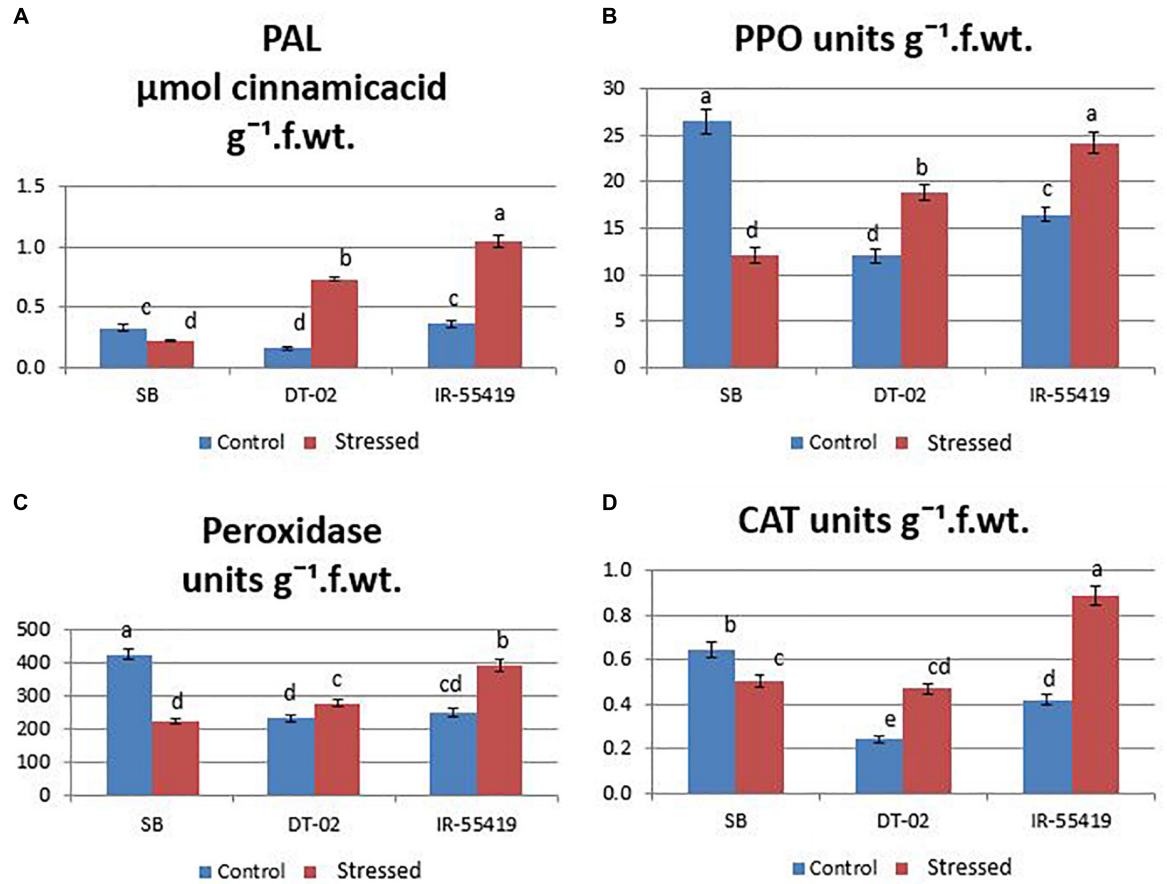

FIGURE 7 | Induction of defense-related enzymes. **(A)** Phenylalanine ammonia-lyase (PAL). **(B)** Polyphenol oxidase (PPO). **(C)** Peroxidase (POD). **(D)** Catalase (CAT) in rice plants of genotypes SB, IR-55419, and DT-02 under control-fully irrigated and stressed-water withholding for 15 days at 60 days after transplantation (DAT). Bars indicate the SD of three biological replicates and each replicate has three plants (ten leaves per plant). Data represented as means and means with the same letter differ non-significantly at $p = 0.05$ according to LSD.

Plants produced proline as an important osmolyte to maintain protein conformation and stabilize the membranes at a low level of leaf water potential. Likewise, an increased accumulation of proline was observed in genotype NIBGE-DT-02 (20%) followed by the tolerant check variety (22.7%) as compared to the susceptible check variety (**Table 2**). In plants, the relative increase of proline content under drought stress has been proposed as a potential indicator for the selection of drought-tolerant varieties (Dien et al., 2019). Abdula et al. (2016) reported that the increased biosynthesis of proline enhanced abiotic stress tolerance in rice genotypes. In this study maximum increase in proline content was observed in genotype NIBGE-DT-02 during early (32.65%) and later (41.7%) growth-stage water stress followed by tolerant check variety (**Table 4**). As reported by Saha et al. (2019), proline is a key factor involved in the mechanism of tolerance against 10 days of water stress as BRRI-dhan-56 showed 3.7 folds increase in proline accumulation under water withholding at 21 days after sowing.

Relative water content (RWC) is considered as an effective physiological parameter to measure the water content of plants under control and water deficit conditions (Gupta et al., 2020; Zhu et al., 2020). According to Puangbut et al. (2018) the drought-tolerant variety maintained higher RWC as indicated by low reduction (21.6%) in comparison with the susceptible variety (35%). In our present study, tolerant genotype NIBGE-DT-02 exhibited less reduction in RWC (5.5%) with the maximum accumulation of proline osmolyte (45.9%) under water deficit conditions at 60 DAT (**Table 4A**). Swapna and Shylaraj (2017) stated that the ability to retain water content (74.37%) in rice variety (Neeraja) under drought stress may be due to osmolyte accumulation in cells or due to rigidness of cell wall.

The increase in EL values points toward the increase in the cell membrane injury induced by the water stress (Al-Ashkar et al., 2016). In the present study highest electrolyte leakage (EL) was observed in Super Basmati as indicated by maximum reduction (70.2%) in membrane stability index (MSI) under water stress at 30 days after transplantation. NIBGE-DT-02 (35.4%) followed by tolerant check variety IR-55419-04 (21.5%) exhibited the least reduction in MSI under 15 days water stress at 30 DAT (**Table 4A**).

TABLE 5 | Effect of water stress on yield attributes of rice genotypes during early and later growth stages in a pot experiment under net house conditions.

	Control				Stressed				% decrease in plant height	% decrease in plant weight	% decrease in grain weight
	Plant Height*	No. of tillers per plant	Plant weight**	Grain weight***	Plant Height*	No. of tillers per plant	Plant weight**	Grain weight***			
Water stress at 30 DAT											
Super Basmati	111.50 ± 3.70^{a}	9.8 ± 2.5^{ab}	70.10 ± 2.46^{a}	27.95 ± 2.1^{a}	81.50 ± 1.29^{e}	3.8 ± 0.5^{c}	18.85 ± 0.91^{f}	4.95 ± 3.0^{e}	26.90%	73.11%	82.30%
DT-02	91.75 ± 1.71^{c}	9.8 ± 1.5^{ab}	42.90 ± 2.03^{b}	34.05 ± 1.34^{a}	73.75 ± 3.30^{f}	5.8 ± 2.8^{c}	20.00 ± 1.19^{ef}	11.85 ± 0.92^{cd}	19.60%	53.40%	65.20%
IR-55419	87.25 ± 2.99^{d}	10.5 ± 2.4^{a}	43.68 ± 2.10^{b}	31.25 ± 3.46^{a}	72.50 ± 2.08^{f}	5.3 ± 1.3^{c}	25.68 ± 1.33^{c}	16.6 ± 1.13^{bc}	16.90%	41.20%	46.88%
Water stress at 60 DAT											
Super Basmati	100.50 ± 4.80^{a}	12 ± 1.83^{a}	58.58 ± 2.77^{a}	29.85 ± 4.6^{a}	87.75 ± 1.71^{b}	6 ± 0.82^{b}	29.50 ± 1.29^{e}	6.55 ± 0.92^{e}	12.60%	49.60%	78.06%
DT-02	97.50 ± 4.20^{a}	11.8 ± 2.06^{a}	61.13 ± 2.60^{a}	16.95 ± 1.1^{bc}	88.00 ± 2.16^{b}	6.5 ± 0.58^{b}	35.23 ± 1.50^{cd}	10.85 ± 0.5^{d}	9.70%	42.40%	35.90%
IR-55419	79.25 ± 1.71^{c}	10.5 ± 1.91^{a}	58.65 ± 3.00^{a}	20.2 ± 1.8^{b}	75.00 ± 1.83^{d}	7.3 ± 0.50^{b}	37.88 ± 1.62^{bc}	15.1 ± 1.3^{cd}	5.40%	35.40%	25.20%

*Evaluation of water stress on yield attributes: *plant height (cm), no. of tillers, **plant weight (g) and ***grain weight (g), of rice genotypes: Super Basmati, IR-55419, and DT-02 under net house conditions. Control-well-irrigated plants, Stressed-water stress for 15 days at 30 DAT, and water stress for 15 days at 60 DAT. After each water stress plants were removed to measure MSI, RWC, and proline content. Data represented as means and means are an average of three biological replicates and each replicate has three plants. Data represented as means and means with the same letter differ non-significantly and with different letters differ significantly at p = 0.05 according to LSD.*

In this study, the plants were also studied for the induction of stress-related antioxidant enzymes. The plants of NIBGE-DT-02 showed a significant increase in PAL enzyme activity (0.73 μmol cinnamic acid/g F. wt.) with a concomitant increase in POD, CAT, and PPO (units/g. F. wt.) under 15 days water stress at 60 DAT as compared to its well-watered control (**Figure 7**). Sahebi et al. (2018) reported that in rice, water scarcity leads to the formation of ROS in various cellular compartments (mitochondria, chloroplast, and peroxisomes). The enhanced activities of ROS scavengers might be one strategy of this genotype for reducing oxidative damage and improving the drought resistance in rice plants (Sachdev et al., 2021).

Sabar and Arif (2014) reported significant variation in rice genotypes for yield-related attributes. Severe water scarcity at vegetative (early) and reproductive (later) growth stages is needed to screen segregating germplasm because stress imposition of different types exposed the genetic variation of genotypes due to the underlying different mechanisms of drought tolerance (Mumtaz et al., 2019). In our experiment, water stress imposed during the early growth stage coincides more or less with the onset of vegetative (before flowering) and later growth stage stress with the reproductive stage. Wang et al. (2017) reported that biomass production is largely affected under vegetative growth stage water scarcity. In the present study, the percent decrease in plant height in all genotypes was more during the early-stage water stress as compared to the later stage, while percent reduction in plant fresh weight was more during early-stage water scarcity because of low tillering so in correspondence to this percent decrease in grain yield was more during water stress at 30 days after transplantation (**Table 5**).

Correlation analysis between morphological, physiological, and biochemical traits of stressed rice plants indicated that root length was strongly correlated with PAL, relative water content, (chl b), catalase, and plant dry weight while relative water and proline contents strongly correlated with catalase, PAL, and membrane stability index. These results depicted that an increase in root growth had significant effects on plant physiological and biochemical responses to early-stage water stress (**Table 6A**). Proline and relative water contents have been proposed as key factors involved in the mechanism of tolerance to water stress (Saha et al., 2019). The strong correlation between RWC and RL under water stress during both growth stages (**Tables 6A,B**) showed that RL played a significant role in plant survival under low water potential and these traits (RWC and proline) could be used as a good marker to determine drought tolerance in rice plants. Furthermore, in the present study regression analysis showed a negative correlation between plant temperature (IRTI) and proline content (r^2 = 0.97) under 15-days water stress condition at 30 days after transplantation while plant temperature under water stress at 60 DAT also had a strong correlation with RWC (r^2 = 0.99). Previously, Carroll et al. (2017) argued that plant temperature increases with decreased plant available water. Though it is normal for plant temperature to rise during the day and reduce throughout the night in relative to well-watered control, the

TABLE 6A | Correlation matrix for morphological and physio-biochemical traits during early-stage water stress in a pot experiment under net house conditions.

Traits	PPO	SL	RWC	PAL	CAT	PDW	CHL b	POD	CHL a	MSI	RL	PFW	CHL t	Proline
PPO	1													
SL	0.08	1												
RWC	0.02	1	1											
PAL	0.15	1	**0.99**	1										
CAT	0.15	1	**0.99**	1	1									
PDW	0.47	**0.92**	**0.89**	**0.94**	**0.94**	1								
CHL b	0.49	**0.91**	**0.88**	**0.94**	**0.93**	1	1							
POD	0.27	**0.98**	**0.97**	**0.99**	**0.99**	**0.98**	**0.97**	1						
CHL a	0.27	**0.98**	**0.97**	**0.99**	**0.99**	**0.98**	**0.97**	1	1					
MSI	0.21	**0.99**	**0.98**	1	1	**0.96**	**0.95**	1	1	1				
RL	0.21	**0.99**	**0.98**	1	1	**0.96**	**0.96**	1	1	1	1			
PFW	0.19	**0.99**	**0.98**	1	1	**0.96**	**0.95**	1	1	1	1	1		
CHL t	0.35	**0.96**	**0.94**	**0.98**	**0.98**	**0.99**	**0.99**	1	1	**0.99**	**0.99**	**0.99**	1	
Proline	0.31	**0.97**	**0.96**	**0.99**	**0.99**	**0.98**	**0.98**	1	1	**0.99**	1	**0.99**	1	1

Relationship of water-stressed- 15 days of water stress at 30 DAT, morphological and physio-biochemical traits: SL-Shoot length, RL-Root length, RWC-Relative water content, PFW-plant fresh weight, PDW-plant dry weight, CAT-catalase, POD-peroxidase, PPO- Polyphenol oxidase, PAL-Phenylalanine ammonia-lyase, CHL a-chlorophyll a, CHL b-chlorophyll b, CHL t-total chlorophyll and MSI-membrane stability index. Values in bold differ from 0 with level of significance p = 0.05.

TABLE 6B | Correlation matrix for morphological and physio-biochemical traits during later-stage water stress in a pot experiment under net house conditions.

Traits	Proline	PAL	CAT	POD	PPO	SL	MSI	CHL b	CHL t	PFW	PDW	CHL a	RL	RWC
Proline	1													
PAL	**0.99**	1												
CAT	0.69	**0.75**	1											
POD	0.53	0.51	**0.78**	1										
PPO	0.61	0.59	**0.77**	**0.97**	1									
SL	−0.29	−0.43	−0.43	0.22	0.17	1								
MSI	−0.03	−0.19	−0.53	0	−0.01	**0.86**	1							
CHL b	0.37	0.38	0.43	0.45	0.52	−0.09	−0.2	1						
CHL t	0.36	0.32	0.3	0.5	0.55	0.21	0.12	**0.95**	1					
PFW	−0.27	−0.37	−0.44	0	0.01	0.67	0.58	0.49	0.68	1				
PDW	−0.04	−0.13	−0.33	−0.01	0.03	0.48	0.5	0.63	0.79	**0.95**	1			
CHL a	0.3	0.21	0.1	0.49	0.52	0.53	0.48	0.76	**0.93**	**0.81**	**0.86**	1		
RL	0.48	0.41	0.01	0.13	0.22	0.14	0.34	0.74	**0.83**	0.65	**0.84**	**0.83**	1	
RWC	0.5	0.41	−0.07	0.12	0.21	0.26	0.51	0.59	**0.74**	0.64	**0.81**	**0.82**	**0.97**	1

Relationship of water-stressed- 15 days of water stress at 60 DAT, morphological and physio-biochemical traits: SL-Shoot length, RL-Root length, RWC-Relative water content, PFW-plant fresh weight, PDW-plant dry weight, CAT-catalase, POD-peroxidase, PPO- Polyphenol oxidase, PAL-Phenylalanine ammonia-lyase, CHL a-chlorophyll a, CHL b-chlorophyll b, CHL t-total chlorophyll and MSI-membrane stability index. Values in bold differ from 0 with level of significance p = 0.05.

water-stressed plants have less evaporation cooling with lower rates of transpiration and hence have a higher temperature at daytime. Thus, the measurement of plant temperature quantifies the degree of plant water stress if compared to the well-watered control plants. In this study, all the rice genotypes showed a variable decline in RWC (**Table 3**) and an increase in plant temperature (**Table 4A**) of water-stressed plants as compared to the non-stressed plants. The rice genotype NIBGE-DT-02 showed less percent decrease (5.5%) in RWC and less percent increase (7.5%) in IR temperature as compared to the susceptible variety under water stress at 60 DAT (**Tables 3**, **4A**). Saleem et al. (2020) reported that the ability of a plant to keep leaf temperature cooler was associated with drought stress tolerance.

The correlation between marker traits (proline and RWC) and plant temperature highlighted the significance of infrared thermal imaging as an effective tool for the indication of drought tolerance in plants. These findings provide a foundation for future research directed to utilize the IRTI approach for the selection of potent rice genotypes better adapted to water scarcity from a wide germplasm collection. Additionally, drought stress affects more or less at every growth stage causing a reduction in yield attributes. The selected genotype NIBGE-DT-02 (drought-tolerant introgression) of the recipient variety Super Basmati (aromatic, long-grain, and sensitive to water stress) was improved significantly and comparatively more tolerant to water stress irrespective of the growth stage as this genotype gave significantly higher yield than the susceptible

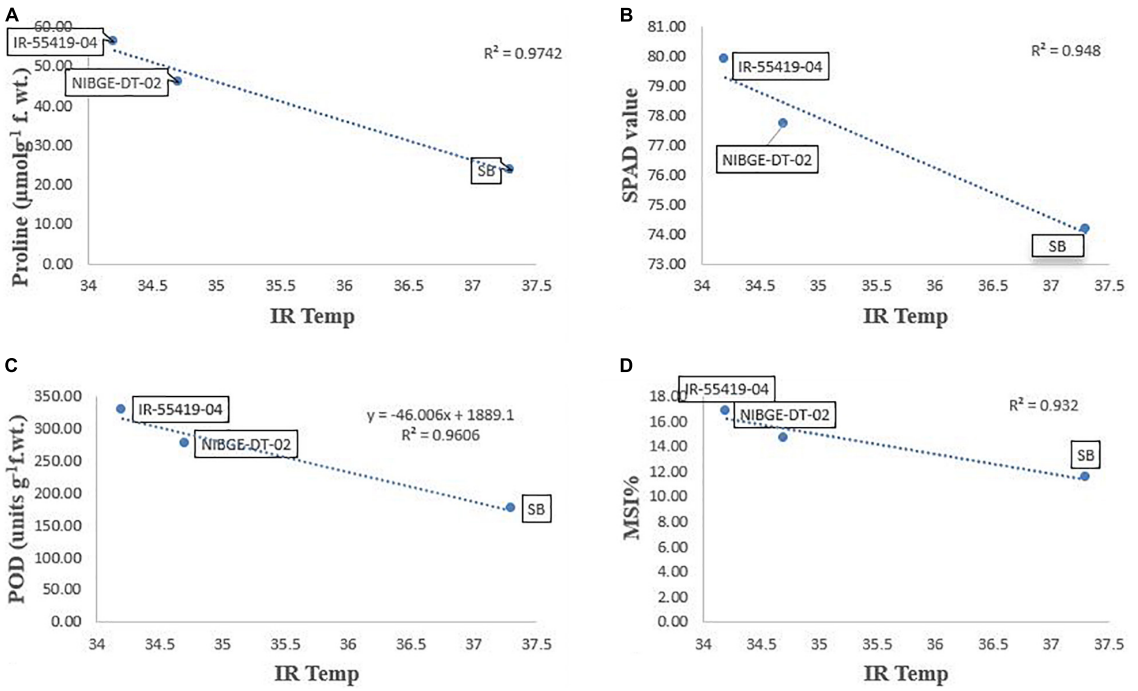

FIGURE 8 | Correlation analysis of Infrared (IR) temperature with different traits for three tested genotypes under early-stage stress conditions. **(A)** Relationship between IR-temperature and proline content. **(B)** Relationship between IR-temperature and SPAD values. **(C)** Relationship between IR-temperature and POD enzyme. **(D)** Relationship between IR-temperature and MSI%. Relationships were studied by correlation analysis using SPSS software. Means are an average of four biological replicates at $p = 0.05$ according to the LSD.

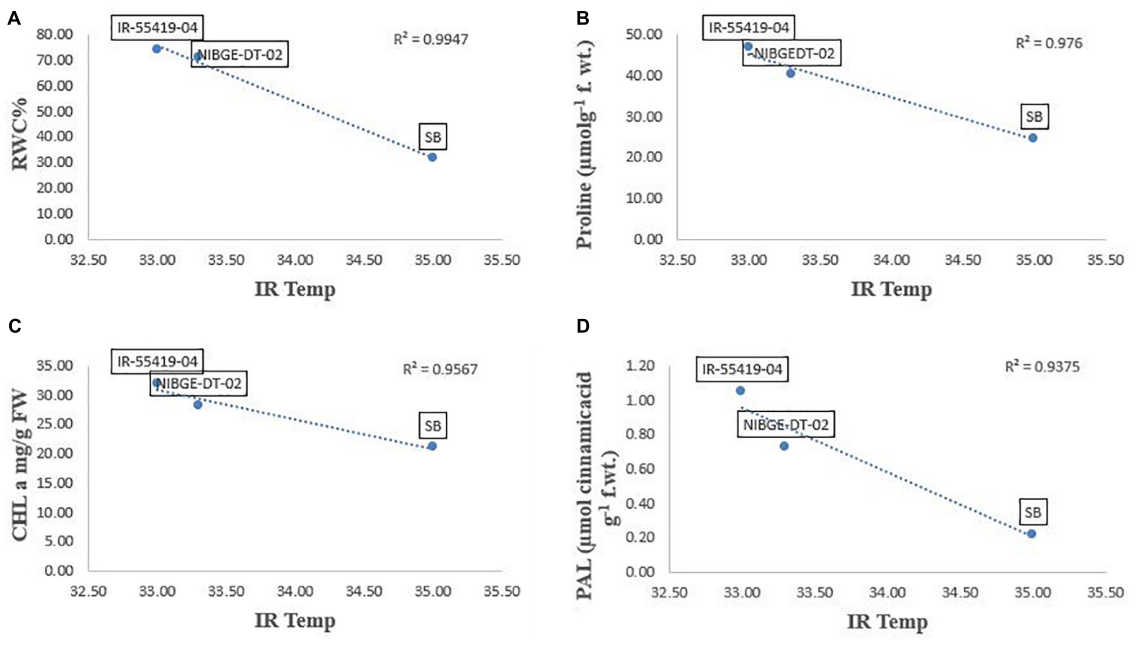

FIGURE 9 | Correlation analysis of Infrared (IR) temperature with different traits for three tested genotypes under later-stage stress conditions. **(A)** Relationship between IR-temperature and RWC%. **(B)** Relationship between IR-temperature and proline content. **(C)** Relationship between IR-temperature and chlorophyll a (CHL a). **(D)** Relationship between IR-temperature and PAL enzymes. Relationships were studied by correlation analysis using SPSS software. Means are an average of four biological replicates at $p = 0.05$ according to the LSD.

genotype. Consequently, sustainable rice production under this climatic shift will bring more opportunities for food security and prosperity of the country.

CONCLUSION

Drought stress has been increased drastically due to climate change, which limits the growth and yield of rice worldwide. Therefore, the present study aimed for the reliable selection of drought-tolerant genotypes by integrating morpho-physiological and biochemical approaches with *in situ* technology of infrared thermal imaging (IRTI) to sustain crop production under water scarcity. The selected rice genotype NIBGE-DT-02 has significant production of osmoregulator (proline), antioxidants, relative water content, better yield, and tolerance to water stress irrespective of the growth stage. Our study suggests that the correlation between infrared thermal imaging and different physio-biochemical responses provides a foundation for future research directed to utilize the IRTI approach for the selection of potent rice genotypes better adapted to water scarcity from wide germplasm collection. These findings can further be utilized for breeding programs to address the food security issues in this alarming situation of climate change.

DATA AVAILABILITY STATEMENT

The original contributions presented in the study are included in the article/**Supplementary Material**, further inquiries can be directed to the corresponding author.

AUTHOR CONTRIBUTIONS

NM did the overall execution of the experiment, analytical work, collection of infrared thermal images and software analysis, collection of data after morpho-physiological and biochemical analysis of leaves, organization of resulting data, and writing up and revision of manuscript. SYa and MAr contributed to the planning, designing and finalization of basic idea of experiments and overall supervision during analytical work, revised, and finalized the manuscript. MAs did the arrangement and provision of rice seeds, contributed in study basic idea and planning of net house experiment, and help in data collection. MY and KE performed data analysis and reviewed the manuscript. SYo helped in plant biochemical analysis and data execution. ZS and HS helped in the analysis of plant stress physiological responses. All authors contributed to the article and approved the submitted version.

ACKNOWLEDGMENTS

We are highly grateful to Mohy ud din (Technical assistant, NIAB) for his help in plant biochemical analysis. Thanks are due to Qaiser Zaman and M. Sarwar (Technical assistant, NIBGE) for their help in the lab and net house experiments.

SUPPLEMENTARY MATERIAL

The Supplementary Material for this article can be found online at: https://www.frontiersin.org/articles/10.3389/fpls.2022.834520/full#supplementary-material

Supplementary Figure 1 | Initial screening of rice genotypes under net house conditions. **(A)** Control-well irrigated rice plants till 30 days after transplantation (DAT). **(B)** Stressed-water stress rice plants (water withholding for 15 days after 30 DAT) under net house conditions. **(C)** Control-well irrigated five rice genotypes viz, IR-55419-04, NIBGE-DT-02, SB, NIBGE-DT-11, and KSK-133 selected from initial screening. **(D)** Stressed-water stress five rice genotypes viz, IR-55419-04, NIBGE-DT-02, SB, NIBGE-DT-11, and KSK-133. **(E)** Control-leaves of plants of genotypes IR-55419-04, NIBGE-DT-02, SB, NIBGE-DT-11, and KSK-133, respectively, under well water conditions. **(F)** Stressed- leaves of plants of genotypes IR-55419-04, NIBGE-DT-02, SB, NIBGE-DT-11 and KSK-133, respectively, under water deficit conditions.

REFERENCES

Abdula, S. E., Lee, H. J., Ryu, H., Kang, K. K., Nou, I., Sorrells, M. E., et al. (2016). Overexpression of BrCIPK1 gene enhances abiotic stress tolerance by increasing proline biosynthesis in rice. *Plant Mol. Biol. Rep.* 34, 501–511. doi: 10.1007/s11105-015-0939-x

Al-Ashkar, I. M., Zaazaa, E. I, El Sabagh, A., and Barutçular, C. (2016). Physio-biochemical and molecular characterization for drought tolerance in rice genotypes at early seedling stage. *J. Exp. Biol. Agric. Sci.* 4, 675–687. doi: 10.18006/2016.4.675.687

Anjum, S. A., Ashraf, U., Tanveer, M., Khan, I., Hussain, S., Shahzad, B., et al. (2017). Drought induced changes in growth, osmolyte accumulation and antioxidant metabolism of three maize hybrids. *Front. Plant Sci.* 8:69. doi: 10.3389/fpls.2017.00069

Arnon, D. I. (1949). Copper enzymes in isolated chloroplasts. Polyphenoloxidase in *Beta vulgaris*. *Plant Physiol.* 24:1.

Barrs, H. D., and Weatherley, P. E. (1962). A re-examination of the relative turgidity technique for estimating water deficits in leaves. *Aust. J. Biol. Sci.* 15, 413–428. doi: 10.1071/BI9620413

Bates, L. S., Waldren, R. P., and Teare, I. D. (1973). Rapid determination of free proline for water-stress studies. *Plant Soil* 39, 205–207. doi: 10.1007/BF00018060

Cai, K., Chen, X., Han, Z., Wu, X., Zhang, S., Li, Q., et al. (2020). Screening of worldwide barley collection for drought tolerance: the assessment of various physiological measures as the selection criteria. *Front. Plant Sci.* 11:1159. doi: 10.3389/fpls.2020.01159

Carroll, D. A., Hansen, N. C., Hopkins, B. G., and Dejonge, K. C. (2017). Leaf temperature of maize and Crop Water Stress Index with variable irrigation and nitrogen supply. *Irrig. Sci.* 35, 549–560. doi: 10.1007/s00271-017-0558-4

Chance, B., and Maehly, A. C. (1955). Assay of catalase and peroxidase. *Methods Enzymol.* 2, 764–775. doi: 10.1016/S0076-6879(55)02300-8

Chaudhry, S., and Sidhu, G. P. S. (2021). Climate change regulated abiotic stress mechanisms in plants: a comprehensive review. *Plant Cell Rep.* 1–31. doi: 10.1007/s00299-021-02759-5

Davies, B. H. (1976). *Chemistry and Biochemistry of Plant Pigments*, Vol. II, ed. T. W. Goodwin, New York, NY: Academic Press, 28.

Dien, D. C., Mochizuki, T., and Yamakawa, T. (2019). Effect of various drought stresses and subsequent recovery on proline, total soluble sugar and starch metabolisms in Rice (*Oryza sativa* L.) varieties. *Plant Prod. Sci.* 22, 530–545. doi: 10.1080/1343943X.2019.1647787

Fahad, S., Bajwa, A. A., Nazir, U., Anjum, S. A., Farooq, A., Zohaib, A., et al. (2017). Crop production under drought and heat stress: plant responses and management options. *Front. Plant Sci.* 8:1147. doi: 10.3389/fpls.2017.01147

FAOSTAT (2021). *Food and Agriculture Data FAOSTAT Provides Free Access to Food and Agriculture Data for Over 245 Countries and Territories and Covers all FAO Regional Groupings from 1961 to the Most Recent Year Available*. Available online at: http://faostat.fao.org (accessed December, 2021).

Franco, J. A., Banon, S., Vicente, M. J., Miralles, J., and Martinez-Sanchez, J. J. (2011). Root development in horticultural plants grown under abiotic stress conditions: a review. *J. Hortic. Sci. Biotechnol.* 86, 543–556. doi: 10.1080/14620316.2011.11512802

Fukagawa, N. K., and Ziska, L. H. (2019). Rice: importance for global nutrition. *J. Nutr. Sci. Vitaminol.* 65, S2–S3. doi: 10.3177/jnsv.65.s2

Gómez-Luciano, L. B., Su, S., Wu, C., and Hsieh, C. H. (2012). Establishment of a rapid screening method for drought tolerance of rice genotypes at seedling stage. *J. Int. Coop.* 7, 107–122.

Gupta, A., Rico-Medina, A., and Cano-Delgado, A. I. (2020). The physiology of plant responses to drought. *Science* 368, 266–269.

Hasanuzzaman, M., Bhuyan, M. H. M., Zulfiqar, F., Raza, A., Mohsin, S. M., Mahmud, J. A., et al. (2020). Reactive oxygen species and antioxidant defense in plants under abiotic stress: revisiting the crucial role of a universal defense regulator. *Antioxidants* 9:681. doi: 10.3390/antiox9080681

International Rice Research Institute [IRRI] (2014). *Standard Evaluation System for Rice*, 5th Edn. Los Banos: International Rice Research Institute.

Ji, K., Wang, Y., Sun, W., Lou, Q., Mei, H., Shen, S., et al. (2012). Drought-responsive mechanisms in rice genotypes with contrasting drought tolerance during reproductive stage. *J. Plant Physiol.* 169, 336–344. doi: 10.1016/j.jplph.2011.10.010

Kavadia, A., Omirou, M., Fasoula, D., Trajanoski, S., Andreou, E., and Ioannides, I. M. (2020). Genotype and soil water availability shape the composition of AMF communities at chickpea early growth stages. *Appl. Soil Ecol.* 150:103443. doi: 10.1016/j.apsoil.2019.103443

Kim, S. L., Kim, N., Lee, H., Lee, E., Cheon, K. S., Kim, M., et al. (2020). High-throughput phenotyping platform for analyzing drought tolerance in rice. *Planta* 252, 1–18. doi: 10.1007/s00425-020-03436-9

Kumbhar, S. D., Kulwal, P. L., Patil, J. V., Sarawate, C. D., Gaikwad, A. P., and Jadhav, A. S. (2015). Genetic diversity and population structure in landraces and improved rice varieties from India. *Rice Sci.* 22, 99–107. doi: 10.1016/j.rsci.2015.05.013

Lekshmy, V. S., Vijayaraghavareddy, P., Nagashree, A. N., Ramu, V. S., Ramegowda, V., Makarla, U., et al. (2021). Induction of acquired tolerance through gradual progression of drought is the key for maintenance of spikelet fertility and yield in rice under semi-irrigated aerobic conditions. *Front. Plant Sci.* 11:632919. doi: 10.3389/fpls.2020.632919

Lum, M. S., Hanafi, M. M., Rafii, Y. M., and Akmar, A. S. N. (2014). Effect of drought stress on growth, proline and antioxidant enzyme activities of upland rice. *J. Anim. Plant Sci.* 24, 1487–1493.

Mayer, A. M., Harel, E., and Shaul, R. B. (1965). Assay of catechol oxidase, a critical comparison of methods. *Phytochemistry* 5, 783–789. doi: 10.1016/S0031-9422(00)83660-2

Motaleb, K. Z. M., Shariful Islam, M., and Hoque, M. B. (2018). Improvement of physicomechanical properties of pineapple leaf fiber reinforced composite. *Int. J. Biomater.* 2018:7384360. doi: 10.1155/2018/7384360

Mumtaz, M. Z., Saqib, M., Abbas, G., Akhtar, J., and Ul-Qamar, Z. (2019). Drought stress impairs grain yield and quality of rice genotypes by impaired photosynthetic attributes and K nutrition. *Rice Sci.* 27, 5–9.

Nahakpam, S. (2017). Chlorophyll stability: a better trait for grain yield in rice under drought. *Indian J. Ecol.* 44:77.

Nahar, S., Sahoo, L., and Tanti, B. (2018). Screening of drought tolerant rice through morpho-physiological and biochemical approaches. *Biocatal. Agric. Biotechnol.* 15, 150–159. doi: 10.1016/j.bcab.2018.06.002

Oladosu, Y., Rafii, M. Y., Samuel, C., Fatai, A., Magaji, U., Kareem, I., et al. (2019). Drought resistance in rice from conventional to molecular breeding: a review. *Int. J. Mol. Sci.* 20:3519. doi: 10.3390/ijms20143519

Panda, D., Mishra, S. S., and Behera, P. K. (2021). Drought tolerance in rice: focus on recent mechanisms and approaches. *Rice Sci.* 28, 119–132. doi: 10.1016/j.rsci.2021.01.002

Pineda, M., Barón, M., and Perez-Bueno, M. L. (2021). Thermal imaging for plant stress detection and phenotyping. *Remote Sens.* 13:68. doi: 10.3390/rs13010068

Puangbut, D., Jogloy, S., Vorasoot, N., and Craig, K. (2018). Root distribution pattern and their contribution in photosynthesis and biomass in Jerusalem artichoke under drought conditions. *Pak. J. Bot.* 50, 879–886.

Raza, A., Razzaq, A., Mehmood, S. S., Zou, X., Zhang, X., Lv, Y., et al. (2019). Impact of climate change on crops adaptation and strategies to tackle its outcome: a review. *Plants* 8:34. doi: 10.3390/plants8020034

Sabar, M., and Arif, M. (2014). Phenotypic response of rice (*Oryza sativa*) genotypes to variable moisture stress regimes. *Int. J. Agric. Biol.* 16, 32–40.

Sabar, M., Shabir, G., Shah, S. M., Aslam, K., Naveed, S. A., and Arif, M. (2019). Identification and mapping of QTLs associated with drought tolerance traits in rice by a cross between Super Basmati and IR55419-04. *Breed. Sci.* 69, 169–178. doi: 10.1270/jsbbs.18068

Sachdev, S., Ansari, S. A., Ansari, M. I., Fujita, M., and Hasanuzzaman, M. (2021). Abiotic stress and reactive oxygen species: generation, signaling, and defense mechanisms. *Antioxidants* 10:277. doi: 10.3390/antiox10020277

Saha, S., Begum, H. H., and Nasrin, S. (2019). Effects of drought stress on growth and accumulation of proline in five rice varieties (*Oryza sativa* L.). *J. Asiat. Soc. Bangladesh Sci.* 45, 241–247. doi: 10.3329/jasbs.v45i2.46597

Sahebi, M., Hanafi, M. M., Rafii, M. Y., Mahmud, T. M. M., Azizi, P., Osman, M., et al. (2018). Improvement of drought tolerance in rice (*Oryza sativa* L.): genetics, genomic tools, and the WRKY gene family. *Biomed Res. Int.* 2018:3158474. doi: 10.1155/2018/3158474

Sairam, R. K., Deshmukh, P. S., and Shukla, D. S. (1997). Tolerance of drought and temperature stress in relation to increased antioxidant enzyme activity in wheat. *J. Agron. Crop Sci.* 178, 171–178. doi: 10.1111/j.1439-037X.1997.tb00486.x

Saleem, M. A., Qayyum, A., Malik, W., and Amjid, M. W. (2020). "Molecular breeding of Cotton for Drought Stress Tolerance," in *Cotton Production and Uses*, eds S. Ahmad and M. Hasanuzzaman (Singapore: Springer), 495–508. doi: 10.1007/978-981-15-1472-2

Sgherri, C. L., Pinzino, C., and Navari-Izzo, F. (1996). Sunflower seedlings subjected to increasing stress by water deficit: changes in O2•– production related to the composition of thylakoid membranes. *Physiol. Plant.* 96, 446–452.

Shirazi, M., Khan, M., and Arif, M. (2019). Effects of peg induced water stress on growth and physiological responses of rice genotypes at seedling stage. *Pak. J. Bot.* 51, 2013–2021. doi: 10.30848/PJB2019

Sridevi, V., and Chellamuthu, V. (2015). Growth analysis and yield of rice as affected by different System of Rice Intensification (SRI) practices. *Int. J. Res. Appl. Nat. Soc. Sci.* 3, 29–36.

Suleri, A. Q., and Iqbal, M. (2019). "National food security challenges and strategies in Pakistan: cooperation for technology and trade," in *Regional Cooperation for Sustainable Food Security in South Asia*, eds N. Kumar and J. George (London: Routledge), 211–226.

Sun, Y., Wang, C., Chen, H. Y., and Ruan, H. (2020). Response of plants to water stress: a meta-analysis. *Front. Plant Sci.* 11:978. doi: 10.3389/fpls.2020.00978

Swapna, S., and Shylaraj, K. S. (2017). Screening for osmotic stress responses in rice varieties under drought condition. *Rice Sci.* 24, 253–263. doi: 10.1016/j.rsci.2017.04.004

Tan, B. T., Fam, P. S., Firdaus, R. B., Tan, M. L., and Gunaratne, M. S. (2021). Impact of climate change on rice yield in Malaysia: a panel data analysis. *Agriculture* 11:569. doi: 10.3390/agriculture11060569

Wang, S., Callaway, R. M., Zhou, D. W., and Weiner, J. (2017). Experience of inundation or drought alters the responses of plants to subsequent water conditions. *J. Ecol.* 105, 176–187. doi: 10.1111/1365-2745.12649

Wedeking, R., Mahlein, A. K., Steiner, U., Oerke, E. C., Goldbach, H. E., and Wimmer, M. A. (2016). Osmotic adjustment of young sugar beets (*Beta vulgaris*) under progressive drought stress and subsequent rewatering assessed by metabolite analysis and infrared thermography. *Funct. Plant Biol.* 44, 119–133. doi: 10.1071/FP16112

Wilkinson, S., and Davies, W. J. (2010). Drought, ozone, ABA and ethylene: new insights from cell to plant to community. *Plant Cell Environ.* 33, 510–525.

Wimberly, J. E. (1983). *Technical Handbook for the Paddy Rice Postharvest Industry in Developing Countries*. Los Banos: International Rice Research Institute.

Yadav, S., Modi, P., Dave, A., Vijapura, A., Patel, D., and Patel, M. (2020). "Effect of abiotic stress on crops," in *Sustainable Crop Production*, eds M. Hasanuzzaman, M. Fujita, M. C. M. Teixeira Filho, T. A. R. Nogueira, and F. S. Galindo (London: IntechOpen). doi: 10.5772/intechopen.88434

Zahid, A., Ali, S., Ahmed, M., and Iqbal, N. (2020). Improvement of soil health through residue management and conservation tillage in rice-wheat cropping system of Punjab, Pakistan. *Agronomy* 10:1844. doi: 10.3390/agronomy10121844

Zhang, F. Q., Wang, Y. S., Lou, Z. P., and Dong, J. D. (2007). Effect of heavy metal stress on antioxidative enzymes and lipid peroxidation in leaves and roots of two mangrove plant seedlings (*Kandelia candel* and *Bruguiera gymnorrhiza*). *Chemosphere* 67, 44–50. doi: 10.1016/j.chemosphere.2006.10.007

Zhu, R., Wu, F., Zhou, S., Hu, T., Huang, J., and Gao, Y. (2020). Cumulative effects of drought–flood abrupt alternation on the photosynthetic characteristics of rice. *Environ. Exp. Bot.* 169:103901. doi: 10.1016/j.envexpbot.2019.103901

Zucker, M. (1965). Induction of phenylalanine deaminase by light and its relation to chlorogenic acid synthesis in potato tuber tissue. *Plant Physiol.* 40:779.

Conflict of Interest: The authors declare that the research was conducted in the absence of any commercial or financial relationships that could be construed as a potential conflict of interest.

frontiers in Plant Science

ORIGINAL RESEARCH
published: 24 February 2022
doi: 10.3389/fpls.2022.818769

Applying Plant Hydraulic Physiology Methods to Investigate Desiccation During Prolonged Cold Storage of Horticultural Trees

Rebecca A. Sheridan[1] and Lloyd L. Nackley[2,3]**

[1]Weyerhaeuser, Federal Way, WA, United States, [2]North Willamette Research and Extension Center, Oregon State University, Corvallis, OR, United States, [3]Department of Horticulture, Oregon State University, Corvallis, OR, United States

Plant nursery production systems are a multi-billion-dollar, international, and horticultural industry that depends on storing and shipping live plants. The storage environment represents potentially desiccating and even fatal conditions for dormant, bareroot, and deciduous horticulture crops, like orchard trees, forestry trees, ornamental trees, and grapevines. When tree mortality is considered within a plant hydraulic framework, plants experiencing water stress are thought to ultimately die from hydraulic failure or carbon starvation. We hypothesized that the hydraulic framework can be applied to stored crops to determine if hydraulic failure or carbon starvation could be attributed to mortality. We used deciduous trees as model species because they are important horticultural crops and provide a diversity of hydraulic strategies. We selected cultivars from six genera: *Acer*, *Amelanchier*, *Gleditsia*, *Gymnocladus*, *Malus*, and *Quercus*. For each cultivar, we measured stem hydraulic conductance and vulnerability to embolism. On a weekly basis for 14 weeks (March–June), we removed trees of each cultivar from cold storage (1–2°C). Each week and for each cultivar, we measured stem water potential and water content ($n = 7$) and planted trees to track survival and growth ($n = 10$). At three times during this period, we also measured non-structural carbohydrates. Our results showed that for four cultivars (*Acer*, *Amelanchier*, *Malus, and Quercus*), the stem water potentials measured in trees removed from storage did not exceed stem P_{50}, the water potential at which 50% of stem hydraulic conductivity is lost. This suggests that the water transport system remains intact during storage. For two cultivars (*Gleditsia* and *Gymnocladus*), the water potential measured on trees out of storage exceeded stem P_{50}, yet planted trees from all weeks survived and grew. In the 14 weeks, there were no significant changes or directional trends in stem water potential, water content, or NSC for most cultivars, with a few exceptions. Overall, the results show that the trees did not experience detrimental water relations or carbon starvation thresholds. Our results suggest that many young deciduous trees are resilient to conditions caused by prolonged dormancy and validate the current storage methods. This experiment provides an example of how a mechanistically based understanding of physiological responses can inform cold storage regimes in nursery tree production.

Keywords: arboriculture, chilling hours, water relations, non-structural carbohydrates, nursery management, urban forestry, vulnerability curves

OPEN ACCESS

Edited by:
Thorsten M. Knipfer, University of British Columbia, Canada

Reviewed by:
Tom De Swaef, Institute for Agricultural, Fisheries and Food Research (ILVO), Belgium
Claudia Cocozza, University of Florence, Italy

****Correspondence:***
Rebecca A. Sheridan
Rebecca.Sheridan@Weyerhaeuser.com
Lloyd L. Nackley
Lloyd.Nackley@OregonState.edu

Specialty section:
This article was submitted to Plant Abiotic Stress, a section of the journal Frontiers in Plant Science

Received: *19 November 2021*
Accepted: *01 February 2022*
Published: *24 February 2022*

Citation:
Sheridan RA and Nackley LL (2022) Applying Plant Hydraulic Physiology Methods to Investigate Desiccation During Prolonged Cold Storage of Horticultural Trees. Front. Plant Sci. 13:818769. doi: 10.3389/fpls.2022.818769

INTRODUCTION

The plant nursery industry produces billions of plants and trees, which are then shipped to global destinations (Haase et al., 2020). Making them unique among crops, plants grown in nursery production systems are often moved great distances in the middle of their lifecycle, which generates novel physiological stress to these otherwise stationary lifeforms. For this to be feasible, nursery professionals take advantage of natural phenophases, for example, harvesting and transferring dormant deciduous species. Many plant nurseries (hereafter referred to as nurseries) are located where favorable conditions and consistent seasonal cues induce winter dormancy. A wide variety of orchard species, forestry species, and ornamental species are produced in a nursery production system known as "bareroot" in which trees are excavated (aka "lifted") in late fall and winter, stored at or just below freezing temperatures during winter, and shipped in the spring. Plants grown and sold in nursery systems must be able to withstand prolonged storage conditions without significant detrimental effects on growth and survival after planting (Maclennan and Fennessy, 2006; Dumroese et al., 2016). Decades of commercial trial and error have created rough guidelines for safe storage practices for bareroot plants. However, there is a need for relevant, mechanistic information about how long trees can tolerate cold storage without damage or death. We believe that investigating the impacts of desiccation and carbon depletion in cold storage through a plant hydraulic framework will help provide meaningful guidelines to this multi-billion-dollar annual industry (United State Department of Agriculture, 2020).

How long seedlings can be kept in cold storage is one of the key physiological questions for optimizing nursery production (Grossnickle et al., 2020). For example, more time in storage allows for the accumulation of chilling hours, which can lead to faster bud break and increased root growth after planting (Harris et al., 1993; Nanninga et al., 2017). The two key risks of storage are desiccation and carbon starvation due to respiration, in the absence of external causes of mortality, such as pests and pathogens (Mckay, 1997). Winter desiccation can impact performance in the growing season if the hydraulic function cannot be restored (Niu et al., 2017). Dormant trees rely on carbohydrate reserves for respiration and tissue development (Tixier et al., 2019). The physiological effects of cold storage have been well studied for conifer seedlings but are not understood as well for deciduous trees (Ritchie, 1982; Cannell et al., 1990; McKay, 1994). Developing parameters such as the length of time deciduous trees will tolerate cold storage conditions without a loss of plant vigor requires careful evaluation of multiple physiological traits (Jacobs et al., 2008). Even then, recommendations may vary by species and by variety or ecotype within species (Overton et al., 2013). Decisions about planting windows to avoid frost damage and ensure access to the planting site are made all the more difficult due to the unpredictable impacts of climate change (Chmura et al., 2011; Fargione et al., 2021). Nursery professionals may need to keep trees in cold storage for longer than is the current practice to respond dynamically to a changing climate.

A framework of tree mortality that considers the trade-offs between hydraulic failure and carbon starvation has been considered extensively (Sevanto et al., 2014; Adams et al., 2017). This "hydraulic framework" has been applied to explain tree mortality as a result of drought (Choat et al., 2018). Plant water relations and xylem function are typically studied in actively growing (i.e., non-dormant) seedlings and trees (Landsberg and Waring, 2017). However, the same physiological processes are important for the survival of dormant deciduous trees: the combined effects of water stress and low carbohydrate reserves can compromise winter cold tolerance, leading to a greater likelihood of mortality (Galvez et al., 2011). Water relations and carbon balance and the interactions of these fluxes coming out of the winter are also important to ensure function in the next growing season (Améglio et al., 2004; Tomasella et al., 2017).

Nursery production systems that use cold storage provide a unique opportunity to study the confounding physiological challenges that trees face through winter. Given the prevalence of cold storage in nursery production, it is important to understand the plant responses to develop research-based management practices that maintain plant health. Therefore, our objectives were to examine the patterns of plant water relations and NSC dynamics during storage for cultivated varieties (cultivars) of six genera of deciduous trees, *Acer, Gleditsia, Gymnocladus, Malus,* and *Quercus*. We selected these six genera as model species because they are high value and widely sold horticultural crops and provide a diversity of hydraulic strategies. We wanted to identify if these trees reach physiological thresholds that correlate with mortality during extended cold storage. If so, would the impacts from cold storage be evident in post-planting performance?

We had the following expectations for the plant physiological metrics that we measured in this experiment: stem water potential and stem water content would decline over an extended time in cold storage due to desiccation. Total stem NSC would also decline over time in cold storage, due to respiration. As a result of the compound impacts of desiccation and carbon depletion due to extended time in cold storage, height growth after outplanting would be diminished for trees that were in storage longer. In trees where the stem water potential dropped low enough to cause significant hydraulic failure in the xylem, we expected growth and survival after planting would be negatively affected.

MATERIALS AND METHODS

Starting March 19, 2020, we obtained trees from the cold storage facility at a commercial shade tree nursery in Canby, Oregon (45.21, −122.73). Retrieving trees from the storage facility continued every week until June 18, 2020, for a total of 14 weeks. The stored trees had been harvested in fall 2019 and washed of all soil in a process called bare-rooting. While in cold storage, the trees were stored at 1-2° C. The coolers were turned off the week of June 8, 2020. Each week, we transported the trees to Oregon State University's North

Willamette Research and Extension Center (NWREC) in Aurora, Oregon (45.28, −122.75) for sampling and planting. Upon arrival at NWREC, we randomly sorted the trees into planting and destructive sampling cohorts. Ten trees were planted each week. For each of the seven trees selected for destructive sampling, we measured stem water potential, water content for the terminal stem segment, and non-structural carbohydrates in the terminal stem segment.

We evaluated six cultivars: Red Sunset® maple (*Acer rubrum* "Franksred"); Prairie fire crabapple (*Malus* "Prairifire"); red oak (*Quercus rubra*); Skyline® honeylocust (*Gleditsia triacanthos* "Skycole"); Autumn Brilliance® serviceberry (*Amelanchier x grandiflora*); and Kentucky coffeetree (*Gymnocladus dioicus*). Due to logistical challenges, not all cultivars were planted at all weeks; additional details and planting and sampling timing can be found in **Table 1**.

Planting and Field Measurements

Each week, we planted 10 trees in a field at NWREC. The field has loam soil (47% sand; 32% silt; and 21% clay). Depending on the exact size of the weekly shipment, three to seven of the trees planted had the terminal shoot removed for other measurements described below; the remaining trees were planted without any pruning. We measured height at planting, and again on November 30, 2020, and calculated the incremental growth. Additionally, we monitored mortality and phenological development after planting.

Environmental Conditions

Temperature and precipitation were tracked by an U.S. Bureau of Reclamation AgriMet weather station that is located adjacent to the field and displayed in **Figure 1** (AgriMet, 2016). Drip irrigation was installed within several weeks of each planting to mitigate any impacts of drought. By June 30, 2020, all trees were on drip irrigation.

Physiological Measurements

Physiological measurements were made on seven individuals of each cultivar at each transplanting date.

Stem Water Potential

We measured midday stem water potential on the terminal shoot using a pressure chamber (Model 1505D-EXP, PMS Instruments, Albany, OR). Stem water potential can be reliably measured on dormant deciduous trees and used to track winter water stress (Milliron et al., 2018).

Water Content

We calculated the water content of the plant tissue using the following equation:

$$WC\left(\frac{g}{g}\right) = \frac{Fresh\ Weight - Dry\ Weight}{Dry\ Weight}$$

For stem water content, we weighed the same terminal stem segment used in the water potential measurements. Immediately after the stem water potential measurement, we put the stem segment into a plastic bag until measuring the fresh weight. We then dried the plant tissues in a drying oven at 75°C for 7 days, then weighed the samples.

Non-structural Carbohydrates:

Samples of the same stem segments used for water relations measurements were also used to analyze non-structural carbohydrates (NSC) by a lab at Oregon State University that specializes in this type of analysis. To extract the NSC, the samples were ground to a fine powder in a Wiley mill. The soluble carbohydrates were extracted in deionized water; starch was extracted with ethanol and an A-AMG (amyloglucosidase) enzyme solution. NSC content of the samples was quantified by measuring absorbance at 630 nm using a microplate multiscan reader (Leyva et al., 2008).

Stem Hydraulic Conductance and Vulnerability Curves

We measured stem hydraulic conductance and vulnerability to embolism on three samples for each of the species, except *Quercus*. We cut a stem segment of approximately 20 cm, less

TABLE 1 | Cultivated species (cultivars) represented within this experiment and the corresponding dates for planting and NSC sampling.

Species	Cultivar name	Stock type	First planting date	Mid-season NSC sample date	Last planting date	Xylem anatomy
Acer rubrum 'Franksred'	Red Sunset® maple	4-foot whips; 4- and 5-foot branched saplings	March 19, 2020	April 30, 2020	June 18, 2020	Diffuse porous
Amelanchier x. grandiflora	Autumn Brilliance® serviceberry	3- and 4-foot whips	April 2, 2020	April 30, 2020	May 21, 2020	Diffuse porous
Gleditsia triacanthos 'Skycole'	Skyline® honeylocust	3- and 4-foot whips	March 19, 2020	April 30, 2020	May 21, 2020	Ring porous
Gymnocladus dioicus	Kentucky coffeetree	4-foot whips	April 2, 2020	April 30, 2020	May 28, 2020	Ring porous
Malus 'Prairifire'	Prairie fire crabapple	5-foot whips on hardy rootstock	March 19, 2020	April 30, 2020	May 21, 2020	Diffuse porous
Quercus rubra	Red oak	4-foot whips	March 19, 2020	April 30, 2020	June 18, 2020	Ring porous

Planting dates vary due to logistical issues that differed by cultivar. Xylem anatomy is also listed (InsideWood, 2004; Wheeler, 2011).

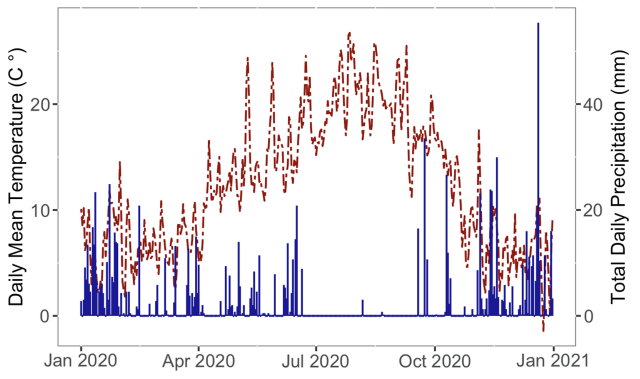

FIGURE 1 | Daily mean temperature (left axis, red dashed line) and total daily precipitation (right axis, blue solid line) at the planting location over the first growing season after planting.

TABLE 2 | Vulnerability curve parameters for five cultivars. Stem P_{12}, P_{50}, and P_{88} are modeled from the vulnerability curves shown in **Figure 2**.

	Stem P_x	Estimate	95% Confidence Interval	
Acer	P_{12}	−1.37	−1.12	−1.61
	P_{50}	−2.52	−2.34	−2.69
	P_{88}	−3.77	−3.42	−4.24
Amelanchier	P_{12}	−1.70	−1.21	−2.21
	P_{50}	−4.53	−4.16	−4.97
	P_{88}	−8.66	−7.24	−11.38
Gleditsia	P_{12}			
	P_{50}	−0.33	−0.26	−0.40
	P_{88}	−0.70	−0.57	−0.88
Gymnocladus	P_{12}			
	P_{50}	−0.60	NA	NA
	P_{88}	−0.75	NA	NA
Malus	P_{12}	−1.67	−1.40	−1.95
	P_{50}	−3.56	−3.36	−3.76
	P_{88}	−5.85	−5.35	−6.51

N = 3 for each cultivar. For Gleditsia and Gymnocladus, the stem P_{50} was higher than −1 MPa and P_{12} was not estimated from the collected data.

than 15 mm in diameter (small enough to fit the cavitation chamber), and without side branches from the middle of the tree. The initial cuts were made underwater because the unplanted trees could be laid within a basin of water. We immediately brought the stem segments into the lab, removed the bark, and recut the ends underwater. We then vacuum infiltrated stems overnight in 0.2 µm filtered deionized water to remove initial emboli.

Stem-Specific Conductivity

We measured stem conductance using the gravity-feed method with 0.2 µm filtered deionized water. We measured flow through the stem using an electronic balance (Explorer Ex224, Ohaus Corp., Parsippany, NJ) connected to a computer running the R-based program conductR (Smith, 2018). When the flow rate stabilized, we recorded flow as the average of the last four readings. To calculate hydraulic conductivity, we used the slope of the volume flow rate ($kg\,s^{-1}$) vs. the pressure gradient ($MPa\,m^{-1}$); then, to standardize to stem-specific conductivity, the hydraulic conductivity was divided by stem cross-sectional area (k_s, $kg\ m^{-1}\ s^{-1}\ MPa^{-1}$).

Vulnerability to Embolism

We used the air-injection method to measure stem vulnerability to embolism (Sperry and Saliendra, 1994). After the maximum stem conductivity was measured as described above, we inserted the stem segment into the cavitation chamber accessory for the PMS pressure chamber and pressurized for 10 min. After there were no longer bubbles exiting the stem due to pressurization, flow through the stem was measured again. The pressure was increased by 0.25 MPa intervals for *Gleditsia* and *Gymnocladus* and 0.5 MPa intervals for the other four cultivars. In between each pressure interval, stem-specific conductivity was again measured. Using conductR, the percent loss of stem-specific conductivity relative to maximum was plotted against the pressure applied by the pressure chamber to create vulnerability. We increased pressures in the cavitation chamber until 90% of stem-specific conductivity was lost, so the maximum pressurization varied for each cultivar. Vulnerability curves and water potential thresholds at which 12, 50, and 88% of stem-specific conductivity were lost (P_{12}, P_{50}, P_{88}) were modeled using the R package fitPLC (Duursma and Choat, 2017).

Statistical Analysis

Each cultivar was analyzed separately for several reasons: the trees came from different nursery sources, the range of planting dates varied by species, and in a few cases, the sample size varied by species at planting. To test if there was a linear relationship between the week of planting and the plant physiological metrics, we used linear regression. The four physiological metrics, which were tested individually, were as: stem water potential, stem water content, total stem NSC, and height growth after planting. We used the software R version (4.0.2) for all statistical analyses.

RESULTS

The year 2020 started with warmer than average temperatures (**Figure 1**). By March 19th, when planting began, temperature closely followed the 30 year average [U.S.A. National Phenology Network (NPN), 2020]. In this region, most rainfall occurs from October through June, with a dry period from July to September. The region in which this project is located experienced moderate to severe drought conditions during the experiment (U.S. Drought Monitor, 2021). The trees were irrigated through the summer dry period.

Stem P_{12}, P_{50}, and P_{88}, as estimated from the vulnerability curves are reported in **Table 2**. Stem vulnerability curves showed two types of responses (**Figure 2**). *Gleditsia* and *Gymnocladus* demonstrated vulnerability to embolism at relatively mild water potentials (>−2.0 MPa). *Acer*, *Amelanchier*, and *Malus* were not as susceptible to embolism until more extreme water potentials (<−2.0 MPa). We did not build hydraulic vulnerability curves for the *Quercus* cultivar in this experiment due to the

methodological challenges associated with hydraulic conductivity measurements with *Quercus* stems (Cavender-Bares and Holbrook, 2001). For this analysis, we use previously reported stem P_{50} values for *Q. rubra* ($P_{50} = -2.5$ MPa; Cochard and Tyree, 1990).

For one cultivar., *Amelanchier*, there was evidence of a significant negative effect of planting week on stem water potential ($\beta = -0.22$, $F_{1,51} = 35.84$, $p < 0.01$; **Figure 3**). *Amelanchier* was the cultivar we had the most logistical issues with procuring, so the effect is evaluated over only 8 weeks. *Amelanchier* also had the most negative stem P_{50}, so despite a decline in stem water potential over time in cold storage, measured stem water potentials did not come close to exceeding stem P_{50} in the time frame we tested. For all other cultivars, there was no evidence of a significant effect of planting week on stem water potential (**Table 3**). Two cultivars—*Gleditsia* and *Gymnocladus*—had stem water potentials that exceeded stem P_{50} from the very first week of the experiment. For *Acer*, *Amelanchier*, *Malus*, and *Quercus*, median stem water potential did not exceed stem P_{50}.

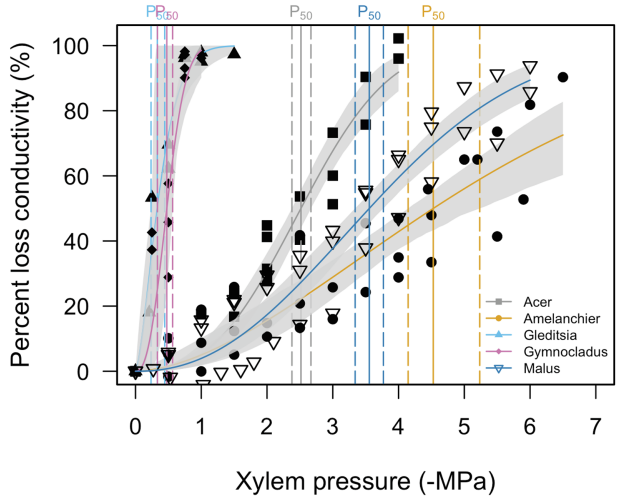

FIGURE 2 | Stem vulnerability curves for five cultivars. Gray shading around each curve shows the 95% confidence interval of the curve ($n = 3$). Stem P_{50} for each species is indicated by a solid vertical line and 95% confidence intervals are indicated by a dashed vertical line. *Quercus* is not included (see text for details).

For all six cultivars, there was no evidence of a significant effect of the planting dates in the stem water content (**Figure 4**). The parameters of the linear regression model are given in **Table 3**. Stem water content is expressed in grams of water in fresh tissue to grams of dry plant tissue; with most stem water content values falling around or above 1 g/g, this indicates that the fresh tissue is over 50% water content, by weight.

Based on the expectation that total NSC would diminish over time in storage due to respiration, we evaluated the effect of the week of removal from cold storage and planting on total NSC concentration (mg/g DW). There was evidence of a significant positive effect of planting week on total NSC for *Amelanchier* ($\beta = 8.21$, $F_{1,16} = 9.43$, $p < 0.01$). In contrast, for *Gymnocladus*, there was evidence of a significant negative effect of planting week on total NSC ($\beta = -16.68$, $F_{1,19} = 5.40$, $p < 0.05$). There was no evidence of a significant effect of planting week on total NSC for the other cultivars (**Table 3**). Among the cultivars, there was no clear pattern of a shift

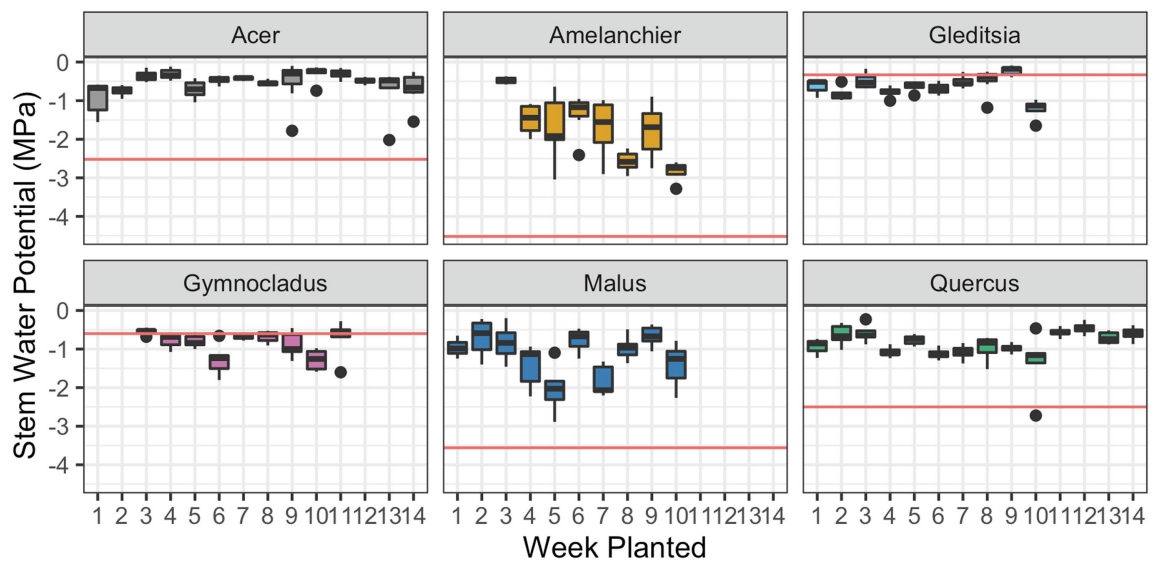

FIGURE 3 | Stem water potential at the time of removal from cold storage and subsequent planting. Box plots show median, interquartile range, and minimum and maximum range for each week of planting. Solid red lines indicate stem P_{50} for each species, estimated by the stem vulnerability curves. There was evidence of a significant negative effect of planting date on stem water potential for *Amelanchier* ($p < 0.01$; details in text and **Table 3**). For all other cultivars, there was no evidence of a significant effect of planting date on stem water potential.

TABLE 3 | Linear regression results for stem water potential, water content, total NSC, and incremental field growth for each cultivar.

	Stem ψ (MPa)				Stem WC (g/g)				Total NSC (mg/g DW)				Field Growth (cm)			
	β	R^2	$F_{df1, df2}$	p	β	R^2	$F_{df1, df2}$	p	β	R^2	$F_{df1, df2}$	p	β	R^2	$F_{df1, df2}$	p
Acer	0.01	0.01	$1.14_{1,96}$	0.29	0.00	0.02	$1.58_{1,96}$	0.21	7.73	0.17	$3.96_{1,19}$	0.06	0.06	0.00	$0.05_{1,138}$	0.82
Amelanchier	−0.22	0.41	$35.85_{1,51}$	**<0.01**	0.00	0.00	$0.20_{1,51}$	0.66	8.21	0.37	$9.43_{1,16}$	**<0.01**	0.74	0.01	$0.59_{1,72}$	0.44
Gleditsia	0.01	0.11	$0.71_{1,64}$	0.40	0.01	0.03	$1.91_{1,65}$	0.17	−13.25	0.05	$0.83_{1,16}$	0.38	−0.36	0.00	$0.25_{1,93}$	0.62
Gymnocladus	−0.03	0.04	$2.21_{1,57}$	0.14	0.00	0.00	$0.08_{1,60}$	0.77	−16.67	0.22	$5.40_{1,19}$	**<0.05**	−0.06	0.00	$0.08_{1,88}$	0.77
Malus	−0.03	0.02	$1.05_{1,68}$	0.31	0.01	0.04	$2.78_{1,68}$	0.10	6.31	0.04	$0.75_{1,19}$	0.40	−1.67	0.10	$10.91_{1,98}$	**<0.01**
Quercus	0.01	0.02	$2.33_{1,96}$	0.13	0.00	0.01	$0.81_{1,96}$	0.32	5.053	0.05	$0.92_{1,19}$	0.35	−2.03	0.12	$18.53_{1,138}$	**<0.01**

N varies by cultivar and metric, so degrees of freedom are given with the F-statistics. Results where $p < 0.05$ are highlighted in bold.

between starch concentration and soluble sugars concentration (**Figure 5**).

In the case of four out of six of the cultivars, there was no significant effect of the planting date on the height growth in the season that followed planting (**Figure 6**; **Table 3**). There was evidence of a significant negative effect of planting date on height growth for *Malus* ($\beta = -1.67$, $F_{1,98} = 10.91$, $p < 0.01$) and *Quercus* ($\beta = -2.03$, $F_{1,138} = 18.53$, $p < 0.01$). The significant effect of planting date on height in these cultivars is driven by the absence of height growth in the latest-planted trees. Additionally, we observed frequent terminal stem die-back in planted *Malus*. However, there was not a higher incidence of mortality at the later planting dates. We observed that bud flush followed the timing of planting. None of the cultivars had broken bud in cold storage, but the *Acer* trees had bloomed in storage before the first planting date. At the end of the growing season, we observed that leaf senescence occurred across a gradient, beginning several days earlier in the early-planted trees than the late-planted trees.

DISCUSSION

Contrary to previous work, we did not observe the effects of extended cold storage on growth after planting for most of the cultivars we tracked in this experiment. For two cultivars, *Malus* and *Quercus*, there was a negative relationship between the timing of planting and incremental height growth, but this could not be tied to a change in water relations or carbon depletion. For all cultivars, survival was high when the trees were planted into an irrigated, weeded environment. The managed planting site probably helped tree performance: stressful environmental conditions at the planting site are more likely to expose detrimental impacts from the nursery production process (Grossnickle et al., 2020). However, the consistent height growth in the field helps to rule out other detrimental effects of extended storage on physiological traits that we did not measure within the experiment. The range of planting dates tested in this experiment extended from the operational standard, in early to mid-spring, to beyond what commercial growers would consider feasible, at the beginning of summer. In other research, extended time in cold storage and desiccation during storage have been tied to poor outplanting performance and changes in physiology for nursery-grown plants (Tung et al., 1986; Deans et al., 1990; Mena-Petite et al., 2001; Overton et al., 2013).

We expected that trees with a stem water potential that exceeded P_{50} or more in storage would have detrimental effects on growth and survival after planting. Hydraulic failure occurs when there is extensive xylem embolism, which reduces a stem's capacity to conduct water. For angiosperm species, lethal water potentials correlated with 80–100% loss of xylem hydraulic conductance (PLC; Choat et al., 2018). Short of catastrophic hydraulic failure, chronically high PLC (e.g., P_{60}) may also precede mortality (Sperry and Love, 2015). Therefore, P_{50} is a conservative threshold for stem water potentials beyond which we might expect to see detrimental effects to plant growth

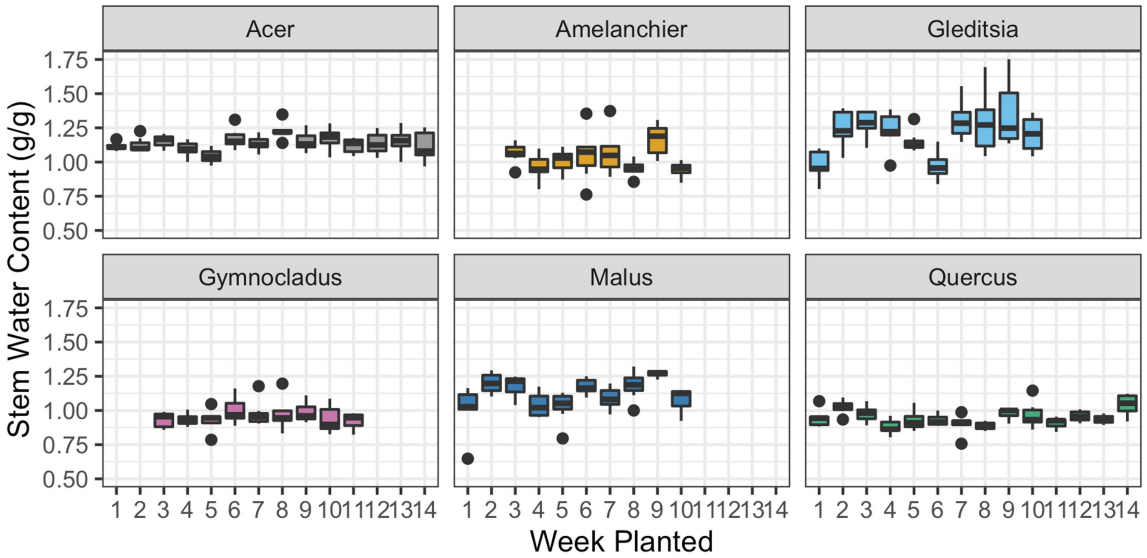

FIGURE 4 | Stem water content at the time of removal from cold storage and subsequent planting. Box plots show median, interquartile range, and minimum and maximum range for each week of planting. One outlier for *Gleditsia* has been removed in this figure, but not the statistical analysis. There was no evidence of a significant effect of planting date on stem water content for any cultivar.

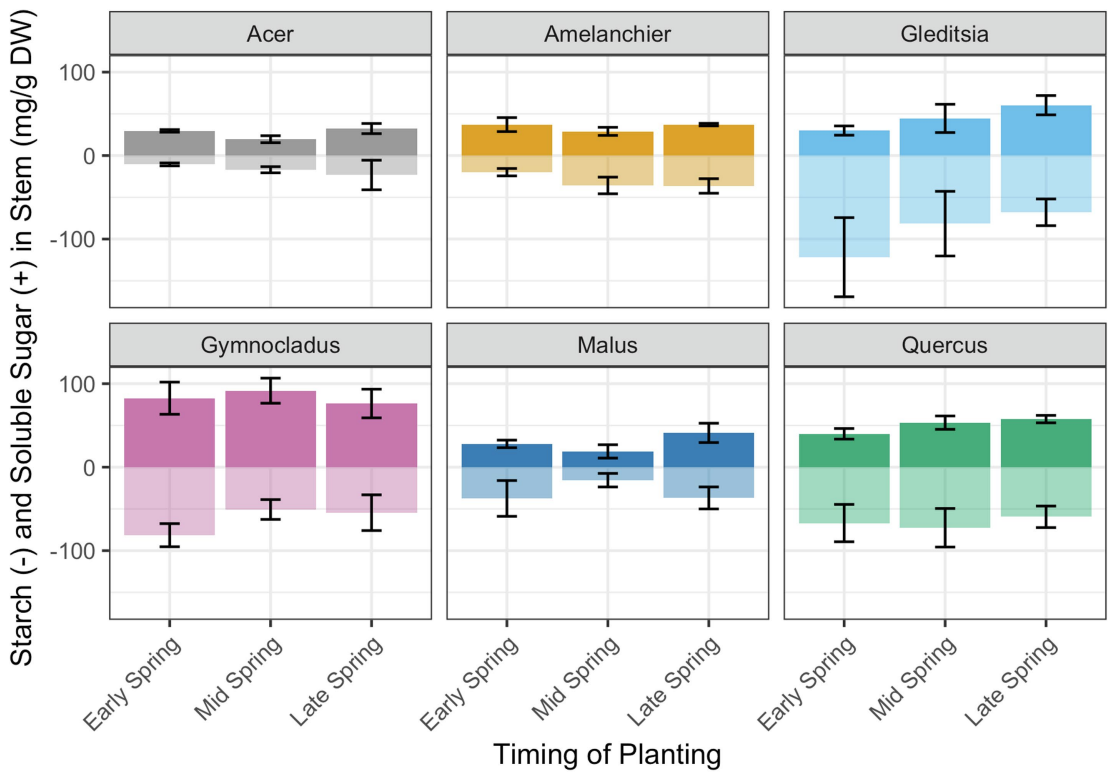

FIGURE 5 | Total non-structural carbohydrate concentration and relative proportion of starch (transparent bars, below midline) and soluble sugars (solid bars, above midline). The specific dates for the timing of planting categories are in **Table 1**. There was evidence of a significant positive relationship of planting week on total NSC concentration for *Amelanchier* ($p < 0.01$; details in text and **Table 1**) and evidence of a significant negative relationship for *Gymnocladus* ($p < 0.05$; details in text and **Table 1**). Error bars indicate standard deviation for soluble sugar and starch concentration separately. Soluble sugars and starch concentrations were not tested separately in linear regression models.

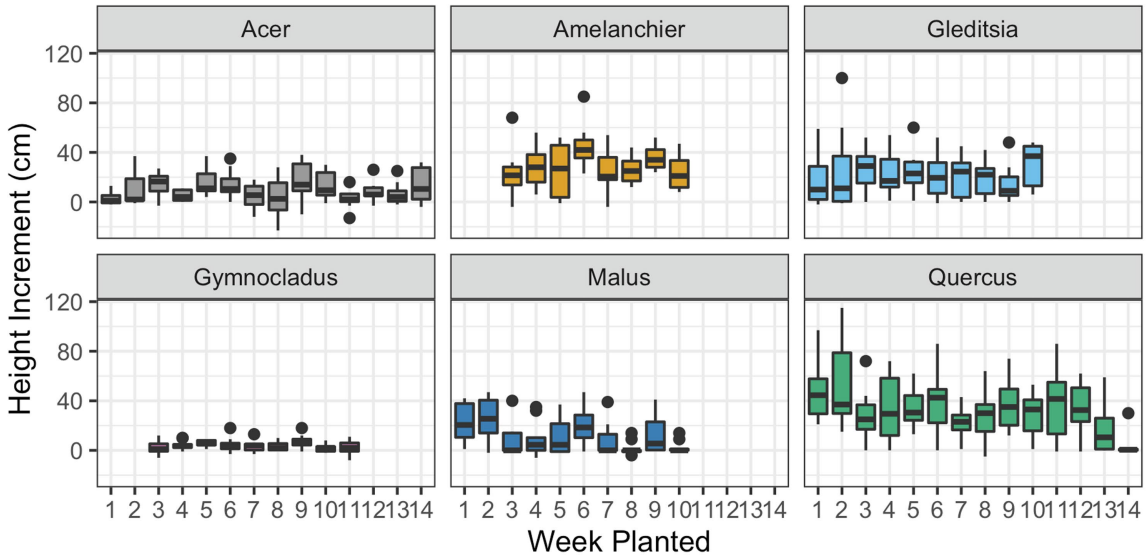

FIGURE 6 | Incremental height growth by the time of plantings. Height was measured for each tree at planting and in late fall 2020 and the difference is given here. Box plots show median, interquartile range, and minimum and maximum range for each week of planting. Negative height increments suggest die-back of the terminal stem. There was evidence of a significant effect of planting date on height growth for *Malus* and *Quercus* ($p < 0.01$; details in text and **Table 3**).

and survival. From the first measurements in mid-March, the stem water potential measurements in *Gleditsia* and *Gymnocladus* were below stem P_{50}, as determined by the hydraulic vulnerability curves. However, these trees grew without issue after outplanting. The stem water potential measurements for the remaining four cultivars did not exceed stem P_{50} values. Though there was a negative relationship between *Amelanchier* and planting date, there were not detrimental effects observed in the growth of this cultivar.

For this experiment, the recovery of the hydraulic system in conjunction with spring growth is particularly important. The loss of stem hydraulic conductance during winter may not impact growth in all species, particularly ring-porous species. Spring recovery of hydraulic function can occur with growth of new xylem vessels and possibly by refilling of embolized conduits (Christensen-Dalsgaard and Tyree, 2014). Some trees can experience over 90% PLC by early spring, but regain stem conductance following leaf expansion and earlywood growth (Jaquish and Ewers, 2001; Christensen-Dalsgaard and Tyree, 2014). In ring-porous species, including the *Gymnocladus*, *Gleditsia*, and *Quercus* cultivars in this experiment, building a new tree ring in the spring allows for full recovery of hydraulic conductance (Urli et al., 2012). This is likely the reason that *Gymnocladus* and *Gleditsia* grew without issue after planting, despite experiencing stem water potentials in cold storage that exceeded P_{50}.

However, the growth of new xylem is not the only strategy for hydraulic recovery. Diffuse-porous trees, represented by the *Malus*, *Acer*, and *Amelanchier* cultivars in this experiment, are more likely to rely on the development of positive xylem pressure for spring recovery of hydraulic conductivity (Hacke and Sauter, 1996; Niu et al., 2017). Trees held in cold storage maintained at a constant temperature may miss seasonal temperature changes that initiate physical processes that create xylem pressure (Schenk et al., 2021). Additionally, trees kept in storage before planting do not have access to soil water for the creation of positive root pressure, which can contribute to hydraulic recovery (Zhu et al., 2000; Jaquish and Ewers, 2001). Therefore, diffuse-porous trees might be particularly susceptible to damage if physiological thresholds are crossed in cold storage. In orchard settings, *Malus* cultivars at 70% PLC mid-winter had subsequent damage and die-back (Beikircher et al., 2016). High winter PLC in peach (*Prunus persica* Batsch) trees led to low rates of bud break as well as arrested growth of new shoots (Améglio et al., 2002). The *Malus* grown in our experiment experienced frequent terminal stem die-back. However, we did not observe a relationship between tip mortality and planting dates.

There is evidence to suspect that cultivated plants could be more vulnerable to hydraulic failure than wild-type species (Beikircher et al., 2013). Nursery practices, such as fertilization and irrigation, can change the xylem anatomy of plants, which impacts hydraulic function and vulnerability (Beikircher et al., 2019; Sloan et al., 2020). Grafting, rootstock choice, and selection for traits such as rapid growth will affect tree vigor, anatomy, and subsequently, hydraulic physiology and vulnerability to embolism (Beikircher et al., 2013). Plant growth is pushed in nursery production because larger plants are more valuable. Yet rapid growth, especially late-season, is less suberized and more at risk of desiccation than early-season growth and is more vulnerable to hydraulic failure (Beikircher and Mayr, 2013).

As was generally the case with stem water potential, we saw no trend in stem water content over the extended time in storage. Desiccation in cold storage represents a threat to nursery-grown trees, given the importance of stem water

content to tree growth after planting. Through the winter, stem tissues can lose up to half of their water content, impacting the onset of water stress (Charrier et al., 2015). Many storage rooms in nursery production systems are essentially very large refrigerators and do not have humidity controls. A common practice is for growers to occasionally spray the plants with a hose or mulch with wetted shredded paper. Both methods are imprecise and can lead to desiccating conditions. Even though we did not see detrimental effects for the trees in this experiment, we still recommend nursery growers monitor the water content of roots and stems during the time in storage to track tree status. Water is needed in the stem before bud break for starch hydrolysis, cell growth, cell expansion, and the resumption of water flow through the stem if conductance has been lost (Améglio et al., 2002; Copini et al., 2019). Water is also necessary for mobilizing non-structural carbohydrates (NSC) reserves for survival and growth, another crucial component of winter survival (Tomasella et al., 2017). During the growing season, water stored in roots, branches, and leaves can buffer xylem tensions created by water stress and help preserve hydraulic function (Scholz et al., 2011; Cuneo et al., 2016; Knipfer et al., 2019); stored water during the dormant season may play a similar buffering role.

We did not see a consistent trend in total NSC concentrations among the cultivars for the time intervals at which we measured NSC. In the two cultivars where there was evidence of a significant effect of planting date on total NSC, yet the trends were contradictory, with a positive relationship between the metrics for *Amelanchier* and a negative relationship for *Gymnocladus*. While there are known methodological challenges to NSC measurements, the results reported here originate from one lab, allowing us to compare among them (Landhäusser et al., 2018). The expected pattern of NSC reserves through the winter starts with high levels at the end of the growing season, then a slow decline through the dormant season to meet respiratory demands, with a final rapid decline at leaf-out or earlywood formation (Dietze et al., 2014). Predictably, the starting NSC condition for plants in storage is an important factor for the carbon dynamics over time in storage (Christiaens et al., 2015). Extended time in cold storage means additional energy demands for maintenance respiration, which can impair outplanting performance (Cannell et al., 1990; Villar-Salvador et al., 2015). NSC was first measured in early spring, when the first trees were removed from cold storage and planted, so we did not capture the expected peak NSC concentration. Future studies on carbon dynamics in these cultivars would benefit from NSC measurements when trees are first put into storage.

In this experiment, the soluble sugars and starch concentrations were highly variable for all cultivars. The balance of starch and soluble sugars is also expected to shift over the dormant season: starch acts as a reservoir of energy for future use, while soluble sugars are used to perform immediate functions such as osmoregulation (Martínez-Vilalta et al., 2016). While reduced NSC levels may not be the ultimate cause of mortality, they can contribute to weakened trees that succumb to other stresses (Charrier et al., 2015). NSC reserves may have an osmotic role in stem pressure formation that leads to hydraulic recovery (Strati et al., 2003; Améglio et al., 2004; Yin et al., 2018; Zhang et al., 2018). Carbon depletion can also contribute to reduced water stress tolerance and slower resumption of growth (Jiang et al., 1995). Seedlings and saplings start with relatively small NSC reserves going into the dormant season, putting them at higher risk of mortality (Losso et al., 2018). On top of that, nursery trees face unique risks: pruning at the time of nursery lifting removes NSC sinks in the roots and branches (Charrier et al., 2015). If trees survive until planting, concerns about NSC reserves lessen: the leaves of deciduous trees can become autonomous from stored C reserves soon after bud break and do not rely on stored carbohydrates for long (Hoch et al., 2003).

Nursery-grown trees are important not only for the horticultural industry but also, in tree planting projects, one of our best solutions for addressing climate change (Bastin et al., 2019). Maintaining urban forests, wildland restoration, and reforestation are challenged by the environmental conditions associated with climate change, like extreme heatwaves, that make it more difficult for trees to survive after planting. Warm autumn temperatures delay dormancy and planting windows are more unpredictable (Beil et al., 2021; Fargione et al., 2021). Extreme weather puts even more pressure on nursery professionals to understand how plant physiology, including water relations and carbon dynamics, responds to each stage of the nursery production process (Sheridan and Nackley, 2021). An understanding of plant hydraulic physiology will also guide decisions about how to manage tree production and planting under warmer, drier future climate conditions (Losso et al., 2018). While we were not able to identify specific physiological thresholds or trends among the deciduous cultivars we tracked in this experiment, we present the first hydraulic response to cold storage data for these important genera and demonstrate how plant physiology can be integrated into nursery practices to guide plant production.

DATA AVAILABILITY STATEMENT

The raw data supporting the conclusions of this article will be made available by the authors, without undue reservation.

AUTHOR CONTRIBUTIONS

RS and LN: conceptualization, investigation, methodology, writing original draft, and writing-review and editing. RS: formal analysis and data curation. LN: funding acquisition. All authors contributed to the article and approved the submitted version.

FUNDING

Funding for this project was provided in part by the Oregon Association of Nurseries and the Oregon Department of Agriculture nursery research program grant no. K11920.

ACKNOWLEDGMENTS

We thank Brian Hill, Dean and Louis Nackley, Luke and Owen Van Lehman, and Hannah Velazquez for assistance with project installation, field maintenance, and data collection.

Thanks to Hans Nelson & Sons Nursery and Bailey Nurseries for providing plant material. Special thanks to Sam, Rich, and Claudia, and the rest of the team at J. Frank Schmidt and Son Co. for donating plant material and providing cooler space to store trees.

REFERENCES

Adams, H. D., Zeppel, M. J. B., Anderegg, W. R. L., Hartmann, H., Landhäusser, S. M., Tissue, D. T., et al. (2017). A multi-species synthesis of physiological mechanisms in drought-induced tree mortality. *Nat. Ecol. Evol.* 1, 1285–1291. doi: 10.1038/s41559-017-0248-x

AgriMet (2016). Aurora, Oregon AgriMet Weather Station (arao) Available at: https://www.usbr.gov/pn/agrimet/agrimetmap/araoda.html. (Accessed May 31, 2021).

Améglio, T., Bodet, C., Lacointe, A., and Cochard, H. (2002). Winter embolism, mechanisms of xylem hydraulic conductivity recovery and springtime growth patterns in walnut and peach trees. *Tree Physiol.* 22, 1211–1220. doi: 10.1093/treephys/22.17.1211

Améglio, T., Decourteix, M., Alves, G., Valentin, V., Sakr, S., Julien, J. L., et al. (2004). Temperature effects on xylem sap osmolarity in walnut trees: evidence for a vitalistic model of winter embolism repair. *Tree Physiol.* 24, 785–793. doi: 10.1093/treephys/24.7.785

Bastin, J.-F., Finegold, Y., Garcia, C., Mollicone, D., Rezende, M., Routh, D., et al. (2019). The global tree restoration potential. *Science* 365, 76–79. doi: 10.1126/science.aax0848

Beikircher, B., De Cesare, C., and Mayr, S. (2013). Hydraulics of high-yield orchard trees: A case study of three Malus domestica cultivars. *Tree Physiol.* 33, 1296–1307. doi: 10.1093/treephys/tpt096

Beikircher, B., Losso, A., Gemassmer, M., Jansen, S., and Mayr, S. (2019). Does fertilization explain the extraordinary hydraulic behaviour of apple trees? *J. Exp. Bot.* 70, 1915–1925. doi: 10.1093/jxb/erz070

Beikircher, B., and Mayr, S. (2013). Winter peridermal conductance of apple trees: Lammas shoots and spring shoots compared. *Trees Struct. Funct.* 27, 707–715. doi: 10.1007/s00468-012-0826-0

Beikircher, B., Mittmann, C., and Mayr, S. (2016). Prolonged soil frost affects hydraulics and phenology of apple trees. *Front. Plant Sci.* 7:867. doi: 10.3389/fpls.2016.00867

Beil, I., Kreyling, J., Meyer, C., Lemcke, N., and Malyshev, A. V. (2021). Late to bed, late to rise—warmer autumn temperatures delay spring phenology by delaying dormancy. *Glob. Chang. Biol.* 27, 5806–5817. doi: 10.1111/gcb.15858

Cannell, M. G. R., Tabbush, P. M., Deans, J. D., Hollingsworth, M. K., Sheppard, L. J., Philipson, J. J., et al. (1990). Sitka spruce and Douglas fir seedlings in the nursery and in cold storage: root growth potential, carbohydrate content, dormancy, frost hardiness and mitotic index. *Forestry* 63, 9–27. doi: 10.1093/forestry/63.1.9

Cavender-Bares, J., and Holbrook, N. M. (2001). Hydraulic properties and freezing-induced cavitation in sympatric evergreen and deciduous oaks with contrasting habitats. *Plant Cell Environ.* 24, 1243–1256. doi: 10.1046/j.1365-3040.2001.00797.x

Charrier, G., Ngao, J., Saudreau, M., and Améglio, T. (2015). Effects of environmental factors and management practices on microclimate, winter physiology, and frost resistance in trees. *Front. Plant Sci.* 6:259. doi: 10.3389/fpls.2015.00259

Chmura, D. J., Anderson, P. D., Howe, G. T., Harrington, C. A., Halofsky, J. E., Peterson, D. L., et al. (2011). Forest responses to climate change in the northwestern United States: Ecophysiological foundations for adaptive management. *For. Ecol. Manag.* 261, 1121–1142. doi: 10.1016/j.foreco.2010.12.040

Choat, B., Brodribb, T. J., Brodersen, C. R., Duursma, R. A., López, R., and Medlyn, B. E. (2018). Triggers of tree mortality under drought. *Nature* 558, 531–539. doi: 10.1038/s41586-018-0240-x

Christensen-Dalsgaard, K. K., and Tyree, M. T. (2014). Frost fatigue and spring recovery of xylem vessels in three diffuse-porous trees in situ. *Plant Cell Environ.* 37, 1074–1085. doi: 10.1111/pce.12216

Christiaens, A., De Keyser, E., Lootens, P., Pauwels, E., Roldán-Ruiz, I., De Riek, J., et al. (2015). Cold storage to overcome dormancy affects the carbohydrate status and photosynthetic capacity of Rhododendron simsii. *Plant Biol.* 17, 97–105. doi: 10.1111/plb.12195

Cochard, H., and Tyree, M. T. (1990). Xylem dysfunction in *Quercus*: vessel sizes, tyloses, cavitation and seasonal changes in embolism. *Tree Physiol.* 6, 393–407. doi: 10.1093/treephys/6.4.393

Copini, P., Vergeldt, F. J., Fonti, P., Sass-Klaassen, U., Den Ouden, J., Sterck, F., et al. (2019). Magnetic resonance imaging suggests functional role of previous year vessels and fibres in ring-porous sap flow resumption. *Tree Physiol.* 39, 1009–1018. doi: 10.1093/treephys/tpz019

Cuneo, I. F., Knipfer, T., Brodersen, C. R., and McElrone, A. J. (2016). Mechanical failure of fine root cortical cells initiates plant hydraulic decline during Drought. *Plant Physiol.* 172, 1669–1678. doi: 10.1104/pp.16.00923

Deans, J. D., Lundberg, C., Tabbush, P. M., Cannell, M. G. R., Sheppard, L. J., and Murray, M. B. (1990). The influence of desiccation, rough handling and cold storage on the quality and establishment of Sitka spruce planting stock. *Forestry* 63, 129–141. doi: 10.1093/forestry/63.2.129

Dietze, M. C., Sala, A., Carbone, M. S., Czimczik, C. I., Mantooth, J. A., Richardson, A. D., et al. (2014). Nonstructural carbon in Woody plants. *Annu. Rev. Plant Biol.* 65, 667–687. doi: 10.1146/annurev-arplant-050213-040054

Dumroese, R. K., Landis, T. D., Pinto, J. R., Haase, L., Wilkinson, K. W., and Davis, A. S. (2016). Meeting forest restoration challenges: using the target plant concept. *Reforesta* 1, 37–52. doi: 10.21750/REFOR.1.03.3

Duursma, R., and Choat, B. (2017). Fitplc - an R package to fit hydraulic vulnerability curves. *J. Plant Hydraul.* 4:e002. doi: 10.20870/jph.2017.e002

Fargione, J., Haase, D. L., Burney, O. T., Kildisheva, O. A., Edge, G., Cook-Patton, S. C., et al. (2021). Challenges to the reforestation pipeline in the United States. *Front. For. Glob. Chang.* 4:629198. doi: 10.3389/ffgc.2021.629198

Galvez, D. A., Landhäusser, S. M., and Tyree, M. T. (2011). Root carbon reserve dynamics in aspen seedlings: does simulated drought induce reserve limitation? *Tree Physiol.* 31, 250–257. doi: 10.1093/treephys/tpr012

Grossnickle, S. C., Kiiskila, S. B., and Haase, D. L. (2020). Seedling ecophysiology: five questions to explore in the nursery for optimizing subsequent field success. *Tree Plant. Notes* 63, 112–127.

Haase, D. L., Pike, C., and Enebak, S. (2020). Forest nursery seedling production in the United States — fiscal year 2019. *Tree Plant. Notes* 63, 26–31.

Hacke, U., and Sauter, J. J. (1996). Xylem dysfunction during winter and recovery of hydraulic conductivity in diffuse-porous and ring-porous trees. *Oecologia* 105, 435–439. doi: 10.1007/BF00330005

Harris, J. R., Bassuk, N. L., and Whitlow, T. H. (1993). Effect of cold storage on bud break, root regeneration and shoot extension of Douglas fir, paper birch and green ash. *J. Environ. Hortic.* 11, 119–123. doi: 10.24266/0738-2898-11.3.119

Hoch, G., Richter, A., and Körner, C. (2003). Non-structural carbon compounds in temperate forest trees. *Plant Cell Environ.* 26, 1067–1081. doi: 10.1046/j.0016-8025.2003.01032.x

InsideWood (2004). InsideWood. Available at: http://insidewood.lib.ncsu.edu/search. (Accessed June 27, 2021).

Jacobs, D. F., Wilson, B. C., Ross-Davis, A. L., and Davis, A. S. (2008). Cold hardiness and transplant response of *Juglans nigra* seedlings subjected to alternative storage regimes. *Ann. For. Sci.* 65, 606–606. doi: 10.1051/forest:2008036

Jaquish, L. L., and Ewers, F. W. (2001). Seasonal conductivity and embolism in the roots and stems of two clonal ring-porous trees, *Sassafras albidum* (Lauraceae) and *Rhus typhina* (Anacardiaceae). *Am. J. Bot.* 88, 206–212. doi: 10.2307/2657011

Jiang, Y., MacDonald, S. E., and Zwiazek, J. J. (1995). Effects of cold storage and water stress on water relations and gas exchange of white spruce (*Picea glauca*) seedlings. *Tree Physiol.* 15, 267–273. doi: 10.1093/treephys/15.4.267

Knipfer, T., Reyes, C., Earles, J. M., Berry, Z. C., Johnson, D. M., Brodersen, C. R., et al. (2019). Spatiotemporal coupling of vessel cavitation and discharge of stored xylem water in a tree sapling. *Plant Physiol.* 179, 1658–1668. doi: 10.1104/pp.18.01303

Landhäusser, S. M., Chow, P. S., Turin Dickman, L., Furze, M. E., Kuhlman, I., Schmid, S., et al. (2018). Standardized protocols and procedures can precisely and accurately quantify non-structural carbohydrates. *Tree Physiol.* 38, 1764–1778. doi: 10.1093/treephys/tpy118

Landsberg, J. J., and Waring, R. H. (2017). Water relations in tree physiology: where to from here? *Tree Physiol.* 37, 18–32. doi: 10.1093/treephys/tpw102

Leyva, A., Quintana, A., Sánchez, M., Rodríguez, E. N., Cremata, J., and Sánchez, J. C. (2008). Rapid and sensitive anthrone-sulfuric acid assay in microplate format to quantify carbohydrate in biopharmaceutical products: method development and validation. *Biologicals* 36, 134–141. doi: 10.1016/j.biologicals.2007.09.001

Losso, A., Bär, A., Dämon, B., Dullin, C., Ganthaler, A., Petruzzellis, F., et al. (2018). Insights from *in vivo* micro-CT analysis: testing the hydraulic vulnerability segmentation in *Acer pseudoplatanus* and *Fagus sylvatica* seedlings. *New Phytol.* 221, 1831–1842. doi: 10.1111/nph.15549

Maclennan, L., and Fennessy, J. (2006). Plant Quality A Key to Success in Forest Establishment. *Proceedings of the COFORD Conference*, 20-21 September 2005, Mount Wolseley Hotel, Tullow, Co Carlow.

Martínez-Vilalta, J., Sala, A., Asensio, D., Galiano, L., Hoch, G., Palacio, S., et al. (2016). Dynamics of non-structural carbohydrates in terrestrial plants: A global synthesis. *Ecol. Monogr.* 86, 495–516. doi: 10.1002/ecm.1231

McKay, H. M. (1994). Frost hardiness and cold-storage tolerance of the root system of *Picea sitchensis*, *Pseudotsuga menziesii*, *Larix kaempferi* and *Pinus sylvestris* bare-root seedlings. *Scand. J. For. Res.* 9, 203–213. doi: 10.1080/02827589409382832

Mckay, H. M. (1997). A review of the effect of stresses between lifting and planting on nursery stock quality and performance. *New For.* 13, 363–393. doi: 10.1023/A:1006563130976

Mena-Petite, A., Ortega-Lasuen, U., González-Moro, M., Lacuesta, M., and Muñoz-Rueda, A. (2001). Storage duration and temperature effect on the functional integrity of container and bare-root *Pinus radiata* D. *Don stock-types. Trees-Struct. Funct.* 15, 289–296. doi: 10.1007/s004680100104

Milliron, L., Olivos, A., Saa, S., Sanden, B. L., and Shackel, K. A. (2018). Dormant stem water potential responds to laboratory manipulation of hydration as well as contrasting rainfall field conditions in deciduous tree crops. *Biosyst. Eng.* 165, 2–9. doi: 10.1016/j.biosystemseng.2017.09.001

Nanninga, C., Buyarski, C. R., Pretorius, A. M., and Montgomery, R. A. (2017). Increased exposure to chilling advances the time to budburst in north American tree species. *Tree Physiol.* 37, 1727–1738. doi: 10.1093/treephys/tpx136

Niu, C. Y., Meinzer, F. C., and Hao, G. Y. (2017). Divergence in strategies for coping with winter embolism among co-occurring temperate tree species: the role of positive xylem pressure, wood type and tree stature. *Funct. Ecol.* 31, 1550–1560. doi: 10.1111/1365-2435.12868

Overton, E. C., Davis, A. S., and Pinto, J. R. (2013). Insights into big sagebrush seedling storage practices. *Nativ. Plants J.* 14, 225–230. doi: 10.3368/npj.14.3.225

Ritchie, G. A. (1982). Carbohydrate reserves and root growth potential in Douglas-fir seedlings before and after cold storage. *Can. J. For. Res.* 12, 905–912. doi: 10.1017/CBO9781107415324.004

Schenk, H. J., Jansen, S., and Hölttä, T. (2021). Positive pressure in xylem and its role in hydraulic function. *New Phytol.* 230, 27–45. doi: 10.1111/nph.17085

Scholz, F. G., Phillips, N., Bucci, S. J., Meinzer, F. C., and Goldstein, G. (2011). "Hydraulic Capacitance: Biophysics and Functional Significance of Internal Water Sources in Relation to Tree Size," in *Size- and Age-Related Changes in Tree Structure and Function*. eds. F. C. Meinzer, B. Lachenbruch and T. E. Dawson (New York: Springer), 341–384.

Sevanto, S., McDowell, N. G., Dickman, L. T., Pangle, R., and Pockman, W. T. (2014). How do trees die? A test of the hydraulic failure and carbon starvation hypotheses. *Plant Cell Environ.* 37, 153–161. doi: 10.1111/pce.12141

Sheridan, R. A., and Nackley, L. L. (2021). A primer on plant hydraulic physiology for nursery professionals. *Tree Plant. Notes* 64, 70–79.

Sloan, J. L., Burney, O. T., and Pinto, J. R. (2020). Drought-conditioning of quaking Aspen (*Populus tremuloides* Michx.) seedlings During nursery production modifies seedling anatomy and physiology. *Front. Plant Sci.* 11:557894. doi: 10.3389/fpls.2020.557894

Smith, D. D. (2018). Conduct R. Available at: https://uwmadison.app.box.com/v/conductR. (Accessed March 1, 2020).

Sperry, J. S., and Love, D. M. (2015). What plant hydraulics can tell us about responses to climate-change droughts. *New Phytol.* 207, 14–27. doi: 10.1111/nph.13354

Sperry, J. S., and Saliendra, N. (1994). Intra-and inter-plant variation in xylem cavitation in *Betula occidentalis*. *Plant Cell Environ.* 17, 1233–1241. doi: 10.1111/j.1365-3040.1994.tb02021.x

Strati, S., Patiño, S., Slidders, C., Cundall, E. P., and Mencuccini, M. (2003). Development and recovery from winter embolism in silver birch: seasonal patterns and relationships with the phenological cycle in oceanic Scotland. *Tree Physiol.* 23, 663–673. doi: 10.1093/treephys/23.10.663

Tixier, A., Gambetta, G. A., Godfrey, J., Orozco, J., and Zwieniecki, M. A. (2019). Non-structural carbohydrates in dormant Woody perennials; The tale of winter survival and spring arrival. *Front. For. Glob. Chang.* 2:18. doi: 10.3389/ffgc.2019.00018

Tomasella, M., Häberle, K. H., Nardini, A., Hesse, B., Machlet, A., and Matyssek, R. (2017). Post-drought hydraulic recovery is accompanied by non-structural carbohydrate depletion in the stem wood of Norway spruce saplings. *Sci. Rep.* 7, 14308–14313. doi: 10.1038/s41598-017-14645-w

Tung, C.-H., Wisniewski, L., and DeYoe, D. (1986). Effects of prolonged cold storage on phenology and performance of Douglas-fir and noble fir 2 + 0 seedlings from high-elevation sources. *Can. J. For. Res.* 16, 471–475. doi: 10.1139/x86-084

U.S. Drought Monitor (2021). Available at: https://droughtmonitor.unl.edu/. (Accessed May 31, 2021).

U.S.A. National Phenology Network (NPN). (2020). Phenology Visualization Tool. Available at: https://www.usanpn.org/data/visualizations. (Accessed May 31, 2021).

United State Department of Agriculture (USDA) (2020). 2019 Census of Horticultural Specialties. Available at: https://www.nass.usda.gov/Publications/AgCensus/2017/Online_Resources/Census_of_Hortculture_Specialties/HORTIC.pdf. (Accessed October 31, 2021).

Urli, M., Porté, A. J., Cochard, H., Guengant, Y., Burlett, R., and Delzon, S. (2012). Xylem embolism threshold for catastrophic hydraulic failure in angiosperm trees. *Tree Physiol.* 33, 672–683. doi: 10.1093/treephys/tpt030

Villar-Salvador, P., Uscola, M., and Jacobs, D. F. (2015). The role of stored carbohydrates and nitrogen in the growth and stress tolerance of planted forest trees. *New For.* 46, 813–839. doi: 10.1007/s11056-015-9499-z

Wheeler, E. A. (2011). InsideWood - a web resource for hardwood anatomy. *IAWA J.* 32, 199–211. doi: 10.1163/22941932-90000051

Yin, X. H., Sterck, F., and Hao, G. Y. (2018). Divergent hydraulic strategies to cope with freezing in co-occurring temperate tree species with special reference to root and stem pressure generation. *New Phytol.* 219, 530–541. doi: 10.1111/nph.15170

Zhang, W., Feng, F., and Tyree, M. T. (2018). Seasonality of cavitation and frost fatigue in *Acer mono* maxim. *Plant Cell Environ.* 41, 1278–1286. doi: 10.1111/pce.13117

Zhu, X. B., Cox, R. M., and Arp, P. A. (2000). Effects of xylem cavitation and freezing injury on dieback of yellow birch (*Betula alleghaniensis*) in relation to a simulated winter thaw. *Tree Physiol.* 20, 541–547. doi: 10.1093/treephys/20.8.541

Conflict of Interest: The authors declare that the research was conducted in the absence of any commercial or financial relationships that could be construed as a potential conflict of interest.

Publisher's Note: All claims expressed in this article are solely those of the authors and do not necessarily represent those of their affiliated organizations, or those of the publisher, the editors and the reviewers. Any product that may be evaluated in this article, or claim that may be made by its manufacturer, is not guaranteed or endorsed by the publisher.

frontiers | Frontiers in Plant Science

ORIGINAL RESEARCH
published: 18 April 2022
doi: 10.3389/fpls.2022.833041

Stable Soil Moisture Improves the Water Use Efficiency of Maize by Alleviating Short-Term Soil Water Stress

Li Niu[1†], Zhuan Wang[1†], Guolong Zhu[1,2], Kefan Yu[1], Ge Li[1] and Huaiyu Long[1]*

[1] Institute of Agricultural Resources and Regional Planning, Chinese Academy of Agricultural Sciences, Beijing, China,
[2] Beijing Liangxiang Lanxin Hydraulic Engineering & Design Co., Ltd, Beijing, China

Weaker temporal variation of soil moisture can improve crop water use efficiency (WUE), but its physiological mechanism was still unclear. To explore the mechanism, an organized experiment was conducted in Beijing from June to September. From the jointing stage to maturity stage of maize, stable soil moisture (SSM) and fluctuating soil moisture (FSM) were established with Pressure Potential Difference-Crop Initiate Drawing Water (PCI) and manual irrigation (MI), respectively, to explore the physiological mechanism of SSM to improve maize WUE. Among them, PCI treatments were set with 3 pressure differences of -5, -10, and -15 kPa, and MI treatment was watering every 3 days with the irrigation amount of 9.3 mm. The results showed that (1) after water treatment, the average soil water content of PCI-5 kPa, PCI-10 kPa, PCI-15 kPa, and MI treatments were 53% field capacity (FC), 47, 38, and 78% FC, respectively. It was SSM with weak temporal variation under PCI treatments, and FSM with medium temporal variation under MI treatment. (2) PCI treatments reduced the content of proline, malondialdehyde, and abscisic acid in each organ of maize. (3) Compared with FSM 78% FC, the maize root activity at the filling stage of 53% FC SSM and 47% FC SSM increased significantly by 57.1 and 28.6%, respectively, and the carbon isotope discrimination value ($\Delta^{13}C$) in bracts of the two treatments increased by 18.3 and 10.4%, respectively. (4) There was a very significant positive correlation between WUE based on biomass (WUE_b) and $\Delta^{13}C$ in bracts. In conclusion, a large temporal variation of soil moisture was an important factor that caused water stress in maize. Under SSM treatments, the accumulation of abscisic acid, proline, and malondialdehyde was synergistically reduced. SSM improved the WUE of maize by alleviating short-term soil water stress caused by the fluctuation of soil moisture.

Keywords: temporal variation of soil moisture, negative pressure irrigation, crop initiate drawing water, maize, physiological response

OPEN ACCESS

Edited by:
Thorsten M. Knipfer, The University of British Columbia, Canada

Reviewed by:
Hadi Pirasteh-Anosheh, National Salinity Research Center, Agricultural Research, Education and Extension Organization, Iran
Mohammad Nauman Khan, Huazhong Agricultural University, China

***Correspondence:**
Huaiyu Long
longhuaiyu@caas.cn

[†]These authors have contributed equally to this work

Specialty section:
This article was submitted to Crop and Product Physiology, a section of the journal Frontiers in Plant Science

Received: *10 December 2021*
Accepted: *02 February 2022*
Published: *18 April 2022*

Citation:
Niu L, Wang Z, Zhu G, Yu K, Li G and Long H (2022) Stable Soil Moisture Improves the Water Use Efficiency of Maize by Alleviating Short-Term Soil Water Stress. Front. Plant Sci. 13:833041. doi: 10.3389/fpls.2022.833041

INTRODUCTION

Maize is not only the most productive food crop but also an important source of feed in China, which plays an important role in meeting human dietary needs (Klopfenstein et al., 2013; Hou et al., 2021). The water consumption of maize during the whole growth period was relatively large. Xiao's study suggested that summer maize with a yield of 10,500–12,000 kg/hm^2 had a water requirement

of 3500–4000 m^3 (Xiao et al., 2008). At present, water shortage is a worldwide problem (Zhang Y. et al., 2019). Therefore, it is of great significance for water conservation to study the water-saving irrigation technology of maize and its water-saving mechanism.

Previous studies on the relationship between soil moisture and crops generally believed that crops have compensation effect of water deficit (Shan and Xu, 1991) and root–shoot communication mechanisms (Kang et al., 2007). Based on the two mechanisms, crops will undergo a series of physiological and biochemical reactions to avoid the harm of soil water stress, thereby improving crop yields and water use efficiency (WUE). The field trials results revealed that compared with full irrigation, maize had the highest WUE when 20–30% water deficit was applied (Liu et al., 2017). Plants respond to water deficits by regulating endogenous hormones, osmotic regulating substances, and membrane lipid peroxidation products, thereby improving WUE. Proline functions as an osmotic regulating substance, the hydrophilic protective substance of enzymes and cell structure, and free radical scavenger to protect cells under stress conditions (Naeem et al., 2018). In the case of water deficit, proline gets accumulated in plants to reduce water potential and avoid the harmful effects of water stress (Maggio et al., 2002). In response to water stress, excessive accumulation of reactive oxygen species will oxidize polyunsaturated fatty acids in membrane lipids and produce malondialdehyde (MDA) in plants. The chain polymerization of MDA with membrane proteins leads to the increase of membrane permeability and the destruction of the membrane system (Tayyab et al., 2020), which leads to the damage of ion channels, membrane proteins, and related enzymes. Therefore, MDA content can be used to evaluate the degree of lipid damage (Ma et al., 2015). The content of MDA increases with the decrease of soil water content (100, 60, and 30% FC) (Khazaei et al., 2020). Abscisic acid (ABA) is produced by the root and transported to shoot underwater stress, which regulates the stomatal aperture of leaves (Buckley, 2019), and is regarded as an important signal substance of plants in response to soil water stress. Furthermore, the accumulation of ABA in plants can inhibit the transpiration rate, root growth rate, and grain fertility (Pilet and Saugy, 1987; Wang H. et al., 2020), thus affecting the WUE (Liao et al., 2018). In addition, salicylic acid (SA) also played an important role in responding to water deficits. Previous research revealed that SA improved the tolerance of plants to drought stress by enhancing the antioxidant protection system and increasing the content of osmotic regulators (Saheri et al., 2020; Sedaghat et al., 2020). SA levels were significantly elevated in maize seedlings with water withholding for 7 days (Guo et al., 2021) and spraying 1 mM SA in the early stage of drought can alleviate the effects of drought stress and ensure the growth of maize seedlings (Bijanzadeh et al., 2019).

Root activity not only affected the growth and development of plants, but also reflected the stress resistance of plants, and the root activity first increased and then decreased with the decrease of soil water content (Wu et al., 2017). Carbon isotope discrimination value ($\Delta^{13}C$) was used to reflect the water status of crops and soil and characterize the physiological state of crops, which have a certain relationship with plant osmotic regulation and WUE (Yang and Li, 2018). It was expected to become a simple and fast method to characterize crop WUE. The relationship between WUE and $\Delta^{13}C$ had been extensively studied. In a previous study of wheat, the $\Delta^{13}C$ in grains was negatively correlated with leaf instantaneous WUE, total biomass WUE, and yield WUE (Wang et al., 2013). The research of maize indicated that the $\Delta^{13}C$ of leaves and grains at the filling stage was negatively correlated with the WUE based on grain yield (Yang and Li, 2018). While the research on maize genome seemed to give the reason: the carbon isotope composition, WUE, and drought sensitivity of maize are controlled by a common genome segment (Avramova et al., 2019).

In summary, the relationship between maize physiological response, WUE, and $\Delta^{13}C$ based on the theory of water deficit compensation effect was mostly studied under traditional irrigation technology. The soil water content was constantly undergoing the process of gradually changing from "high" to "low" and suddenly from low to high. The time variation of soil moisture was very large, and it was difficult to accurately describe the relationship between soil moisture and crops. Batista et al. (2013) had proposed a device to stabilize soil moisture using electricity. Recently, the negative pressure irrigation technology had been identified as Pressure Potential Difference-Crop Initiate Drawing Water (PCI) technology (Long et al., 2020), which can accurately, continuously, and stably control soil water content without any energy consumption. Previous studies had indicated that PCI can effectively improve crop yield and WUE compared with traditional irrigation (Bian et al., 2018; Zhao et al., 2019; Wang Z. et al., 2020; Yang et al., 2020; Zhu et al., 2020). However, the soil moisture under PCI is in a relatively stable state, and the effect of water deficit compensation does not exist in theory. The mechanism of crops' efficient use of water under the condition of stable soil moisture (SSM) was not clear. Physiological and gene expression responses of plants under different SSMs were compared in *Petunia* (Kim et al., 2012), while the differences in the effects of stable and fluctuating soil moisture (FSM) on plants were not compared.

In this experiment, PCI technology and manual irrigation were used to form SSM and FSM, respectively. By observing malondialdehyde, proline, plant hormone, root activity, $\Delta^{13}C$, and WUE under different treatments, the physiological response of maize to temporal variations of soil moisture was explored. It is expected to lay the foundation for revealing the physiological mechanism of SSM to improve crop WUE.

MATERIALS AND METHODS

Study Site

The maize pot experiment was conducted from June to September, 2018, in the rain shelter house in the Chinese Academy of Agricultural Sciences (39.9°N, 116.3°E) in Beijing, China. The annual average temperature and precipitation of this site were 10–12°C and 565 mm, respectively, and it has a warm and semi-humid continental monsoon climate.

Pressure Potential Difference-Crop Initiate Drawing Water System

The PCI system (Patents, China ZL201610329413.3) is composed of four parts: a negative pressure generator, a water tank, a water delivery pipe, and a water seepage device (**Figure 1**). The heavy liquid-type negative pressure valve was used as a negative pressure generator to control the water supply pressure. The water tank was a sealed cylindrical PVC bucket (inner diameter 19 cm, height 50 cm) with a tube installed on it to observe the water level. The water delivery pipe is a transparent silicone hose connecting the water tank and the water seepage device. The water seepage device is a porous clay pipe (with an inner diameter of 1 cm, an outer diameter of 1.8 cm, and a length of 23 cm) that is water permeable and airtight. The water seepage device was buried in the middle of the potting bucket, 10 cm deep from the soil surface, and slightly inclined downward until the tail was about 1 cm lower than the head, which is conducive to the air discharge from the clay pipe. With the growth of crops and the absorption of soil moisture, the soil matrix potential decreases. The PCI system will start to irrigate when the soil matrix potential is lower than the negative pressure in the clay pipe because water will always move from the high potential region (PCI system) to the low potential region (soil). Here, the water level of the tank drops, and the air volume above the tank increases, thereby reducing the pressure in the tank and allowing the outside air to enter the tank through the silicone tube. Through this process, the dynamic balance of soil matrix potential and irrigation pressure is realized by the PCI system, thereby maintaining the soil moisture stability (**Figure 1**).

Pots and Soil

Considering the specifications of the clay pipe and the uniformity of soil moisture distribution throughout the pot, pots with length, width, and height of 42, 26, and 25 cm were used for the experiment. The clay pipe was inserted into the middle of the soil through a hole (10 cm from the soil surface) punched in the middle of one side of the pot at an angle of 5–10° to the horizontal. Each pot was filled with 25 kg of soil and the texture of which was loamy clay. The basic physical and chemical properties of the soil are shown in **Table 1**.

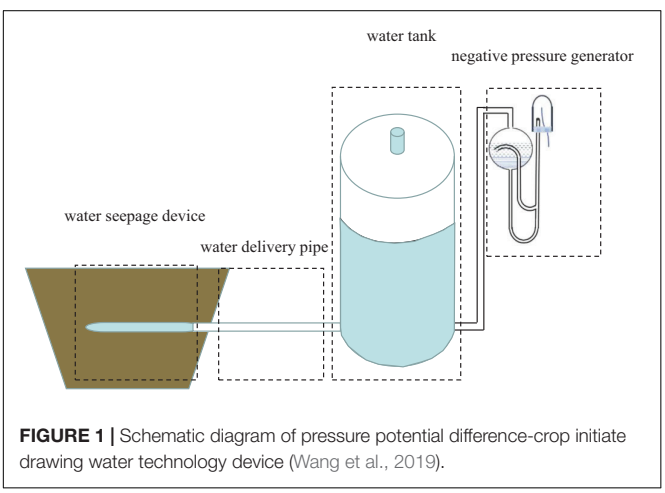

FIGURE 1 | Schematic diagram of pressure potential difference-crop initiate drawing water technology device (Wang et al., 2019).

Experimental Design

Four treatments were established in this experiment, which was PCI-5 kPa, PCI-10 kPa, and PCI-15 kPa treatment and manual irrigation treatment (MI), with four replicates per treatment. The maize cultivar "Zheng dan 958" was sown on June 25, 2018. Before sowing, each pot was applied with 2.3 g of urea, 8.5 g of superphosphate, 2.8 g of potassium sulfate, and 3 L of water. Six seeds were sown in each pot, and the seedlings were thinned at the third leaf stage, leaving one seedling per pot. The top application was applied with 4.7 g of urea per pot at the twelfth leaf stage. The water consumption of summer maize in the local field was 5.0–7.0 mm/day (Xiao et al., 2008). Considering that there was no water leakage in potting soil, an irrigation amount of 1 L was given to each pot every 2 days, equivalent to 3.1 mm/day, before the jointing stage. The PCI system was activated at the jointing stage until maturity. Then the PCI treatments were irrigated through the PCI system, and the MI treatment was surface irrigated manually every 3 days with the irrigation amount of 9.3 mm.

Sampling and Measurements

Soil Moisture

The soil moisture was measured every 4 days at the period of 17:00 to 18:00 from silking stage (2 weeks after the PCI system was initiated) to maturity. Three points were evenly taken around each maize plant using a soil moisture rapid measuring instrument (SU-LB, Beijing Meng Chuang Wei Ye Technology Co., Ltd., Beijing, China) with a measuring depth of 0–6 cm.

Soil Moisture Stability

The temporal variation coefficient (CV) is calculated as follows:

$$CV = \sigma/m \quad (1)$$

Where σ is the SD of soil moisture observed at different times, and μ is the average value of soil moisture observed at different times. If $CV \leq 0.1$, the soil moisture belongs to weak variations if $0.1 < CV < 1$, it belongs to medium variation, and if $CV \geq 1$, it belongs to strong variation (Zhu et al., 2020).

The fluctuation coefficient (δ) of soil moisture was calculated as follows:

$$\delta = \Sigma[|\theta_i - \theta_{i-1}|/((\theta_i + \theta_{i-1})/2)]/(n-1) \quad (2)$$

Where θ_i is the observed value of soil water content (%) at i moment, θ_{i-1} is the observed value of soil water content (%) at the last moment before i, and n is the observation times of soil water content. The fluctuation coefficient reflects the stability of soil moisture, and the smaller the value is, the more stable the soil moisture is (Zhu et al., 2020).

Physiological Characteristics

Plant Water Content and Stomatal Conductance

At the grain filling stage, the root, stem, leaf, bract, and cob were sampled and weighed immediately to obtain fresh weight.

TABLE 1 | Soil basic physical and chemical properties.

Soil texture			Field capacity (V/V)	Soil bulk density	Alkaline hydrolysis nitrogen	Available phosphorus	Available potassium	OM	EC	pH
Sand	Silt	Clay								
%	%	%	(%)	(g cm^{-3})	(mg kg^{-1})	(mg kg^{-1})	(mg kg^{-1})	(g kg^{-1})	(μs cm^{-1})	(%)
52.9	22.5	24.5	22.36	1.1	93.53	34.26	194.02	16.04	129.2	6.66

Then, the samples were heated at 105°C for 30 min and dried to constant weight at 70°C. The samples were weighed to obtain the dry weight.

$$\text{Plant water content} = (\text{fresh weight} - \text{dry weight}) \times 100\% / \text{fresh weight}$$

The stomatal conductance was measured using a Li-6400 portable photosynthesis instrument (LI-COR, Lincoln, NE, United States) with an LED light source between 9:00 and 11:00 AM on a sunny day (Niu et al., 2020).

Malondialdehyde and Proline

Sampling was performed from 9:00 to 11:00 AM at the grain filling stage. The ear leaves of maize were sampled and immersed in liquid nitrogen immediately and then transferred to a –80°C freezer for later use. For the quantification of MDA, ear leaf (0.5 g) was determined by thiobarbituric acid method with the absorbance recorded at 450, 532, and 600 nm using a UV–vis spectrophotometer (Saheri et al., 2020). For the quantification of proline, ear leaf (0.5 g) was extracted with 5 ml of 3% sulfo SA solution, and the homogenate was heated in a boiling water bath for 10 min and then cooled. The cooled homogenate was centrifuged at 3,000 *g* for 10 min. Next, 2 ml of the supernatant was added with 2 ml of distilled water, 2 ml of glacial acetic acid, and 4 ml of 2.5% ninhydrin solution, and the mixture was put into a boiling water bath for 60 min and then cooled. The cooled mixture was added with 4 ml of toluene to extract the red substance. After standing the mixture, the toluene phase was used to measure the absorbance at a wavelength of 520 nm, and the proline content was calculated according to a standard curve (Saheri et al., 2020).

Abscisic Acid and Salicylic Acid

For the detection of ABA and SA, the ear leaf (50 mg) was ground with liquid nitrogen and added with 0.5 ml methanol/water/formic acid (15:4:1, V/V/V) at 4°C. The extract was vortexed for 10 min and centrifuged at 14,000 rpm for 5 min at 4°C. The supernatant was collected, and the extraction process was repeated. The combined extracts were dried with a stream of nitrogen and redissolved with 80% (v/v) methanol. The extract was ultraphoniced for 1 min and filtrated (PTFE, 0.22 μm; Anpel). The ABA and SA content were detected by an LC–ESI–MS/MS system (HPLC, Shim-pack UFLC SHIMADZUCBM30A system[1]; MS, AppliedBiosystems 6500 Triple Quadrupole[2]) (Guo et al., 2021).

[1]www.shimadzu.com.cn/

[2]www.appliedbiosystems.com.cn/

Root Activity and $\Delta^{13}C$

The roots were taken out from the soil and washed with 0.01 mol/L phosphate-buffered saline. After washing, the roots were wiped dry and stored at 4°C for later use. The root activity of maize was measured with the triphenyl tetrazolium chloride method using 0.5 g fresh root as soon as possible (Khan et al., 2014). For the quantification of $\Delta^{13}C$, the ear leaf was dried at 80°C to constant weight, then the dried leaf was ground to a fine powder and passed through a 0.15-mm sieve. A 1 mg of the sample was determined by the combination of element analyzer (Flash 2000 HT, Thermo Fisher Scientific, Waltham, United States) and isotope mass spectrometer (Delta V advantage, Thermo Fisher Scientific, United States) (Gao et al., 2018). Four biological replicates were performed for the physiological indicators.

Water Consumption of Plant

The water consumption of the plant was calculated according to the theory of water balance:

$$ET_k = M_k - \Delta W = M_k - (\theta m_k - \theta m_{k-1}) \times m_s/\rho_w \quad (3)$$

In the formula, ET_k is the water consumption (L) of maize in the kth period, M_k is the irrigation amount (L) in the kth period, ΔW is the change of soil water storage (L), θm_k is the mass water content of soil (%) at the kth moment, θm_{k-1} is the mass water content of soil (%) at the last moment before k, m_s is the mass of the soil in the pot (kg), and ρ_w is the density of water (1 g.cm^{-3}) (Li et al., 2017).

Water Use Efficiency

At the maturity stage, the shoot and root of maize were put into an oven at 105°C for 30 min and then dried to constant weight at 75°C. The biomass and grain yield were measured, respectively. WUE was calculated as follows:

$$\text{Biomass water use efficiency } (WUE_B) = \text{biomass / total water consumption.}$$

$$\text{Yield water use efficiency } (WUE_Y) = \text{grain yield / total water consumption.}$$

Statistical Analysis

ANOVA and correlation were performed with SPSS 12.5 (SPSS, Chicago, IL, United States), and the least significant difference (LSD) method was used to compare means at $P < 0.05$.

TABLE 2 | Soil volumetric moisture content and its stability parameters under different treatments.

Treatment	The range of soil moisture content (%)	Mean value of soil moisture content (%)	Temporal variation coefficients of soil moisture	Temporal fluctuation coefficients of soil moisture
MI	13.98 (62.5%FC) ~ 19.96 (89.3%FC)	17.40 (78%FC)	0.113	0.120
–5 kPa	10.55 (47.2%FC) ~ 12.89 (57.6%FC)	11.81 (53%FC)	0.068	0.041
–10 kPa	9.12 (40.8%FC) ~ 12.23 (54.7%FC)	10.55 (47%FC)	0.093	0.074
–15 kPa	6.83 (30.5%FC) ~ 9.88 (44.2%FC)	8.59 (38%FC)	0.121	0.066

RESULTS

Soil Moisture and Its Stability

From the silking stage to the maturity stage, the average soil volume water contents of MI, PCI-5 kPa, -10 kPa, and -15 kPa were 17.40% (78% FC), 11.81% (53% FC), 10.55% (47% FC), and 8.59% (38% FC), respectively, indicating that the greater the PCI pressure was, the higher the soil moisture content became. The temporal variation coefficients of soil moisture in the MI, PCI-5 kPa, PCI-10 kPa, and PCI-15 kPa treatments were 0.113, 0.068, 0.093, and 0.121, respectively, and the fluctuation coefficients were 0.120, 0.041, 0.074, and 0.066, respectively. Considering the variation coefficient and fluctuation coefficient, the PCI treatments were SSM with weak time variation, and the MI treatment was FSM with medium time variation (**Table 2** and **Supplementary Figure S1**).

Physiological Characteristics

Proline

Compared with MI treatment, the proline content of each organ tended to decrease under PCI treatments. The stem proline content of the PCI-5 kPa treatment was significantly lower than that of the MI treatment by 31.4%, and the proline content in the bract and cob of all PCI treatments was also significantly lower than that of the MI treatment (**Figure 2**). The bract leaf proline contents of PCI-5 kPa, PCI-10 kPa, and PCI-15 kPa were significantly lower than MI by 29.9, 25.1, and 18.8%, respectively, and the cob proline contents of PCI-5 kPa, PCI-10 kPa, and PCI-15 kPa were significantly lower than MI by 20.0, 16.6, and 12.2%, respectively. In the range of 38% FC to 53% FC under SSM conditions, the proline content in each organ gradually increased with decreasing soil moisture content. Among them, the stem proline contents of the PCI-5 kPa and -10 kPa treatments were lower than that of the -15 kPa treatment by 30.8 and 19.9%, respectively (**Figure 2**). The proline content varied in different organs in the order of bract > cob > leaf > stem > root. The average proline content of bracts was 23.7, 7.1, 3.2, and 1.0 times higher than that of roots, stems, leaves, and cobs, respectively, and that of cobs was 11.3, 3.0, and 1.1 times higher than that of roots, stems, and leaves, respectively.

Malondialdehyde

The root MDA content of the MI treatment was significantly higher than that of the PCI-5 kPa, PCI-10 kPa, and PCI-15 kPa treatments by 38.3, 25.6, and 20.4%, respectively. Moreover, the cob MDA of MI treatment was significantly higher than PCI-5 kPa, PCI-10 kPa, and PCI-15 kPa by 26.3, 24.1, and 16.0%, respectively. Stem MDA in the MI treatment was significantly higher than that in the PCI-5 kPa and PCI-10 kPa treatments by 29.8 and 18.6%, respectively, and bract MDA in the MI treatment was significantly higher than that in the PCI-5 kPa and PCI-15 kPa treatments by 10.1 and 12.4%, respectively. Within the range of 38% FC to 53% FC under SSM conditions, the MDA content of roots, stems, leaves, and cobs increased with decreasing soil water content. Among them, the MDA content in roots and stems at 38% FC was significantly higher than that at 53% FC, while the MDA content in bracts showed a trend of first increasing and then decreasing with decreasing water supply pressure (**Figure 3**). The MDA content differed in different organs of maize. The average MDA content of all treatments in leaves was 0.1, 1.9, 2.7, and 5.2 times higher than that in bracts, stems, cobs, and roots, and that in bracts was 1.5, 2.2, and 4.4 times higher than that in stems, cobs, and roots (**Figure 3**).

Abscisic Acid

The ABA content in the roots of the MI treatment was significantly higher than that of the PCI-5 kPa treatment by 40.3%. In addition, the ABA content in the leaves of the MI treatment was significantly higher than that of the PCI-5 kPa and PCI-15 kPa treatments by 42.1 and 30.1%, respectively; the

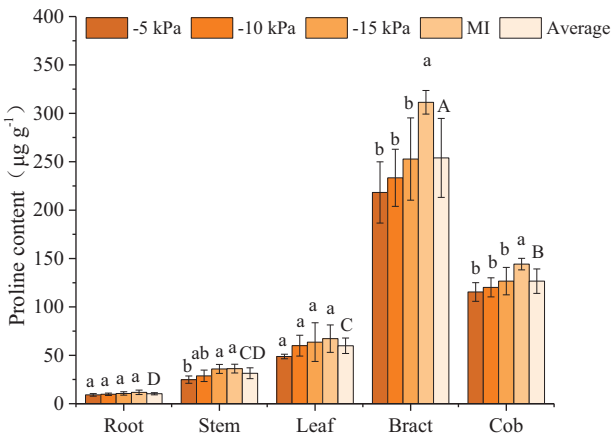

FIGURE 2 | Proline content in different organs of maize under different treatments. Values represent mean ± SD. The least significant difference (LSD) method was used to test differences among treatments or organs at the $P < 0.05$ level. Different lowercase letters indicate significant differences among treatments within the same organ, and different capital letters on the average value of all treatments in each organ indicate significant differences among organs.

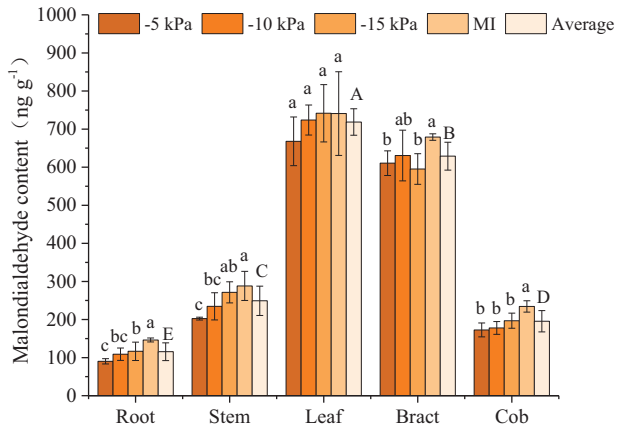

FIGURE 3 | Malondialdehyde content in different organs of maize under different treatments. Values represent mean ± standard deviation. The least significant difference method was used to test differences among treatments or organs at the $P < 0.05$ level. Different lowercase letters indicate significant differences among treatments within the same organ, and different capital letters on the average value of all treatments in each organ indicate significant differences among organs.

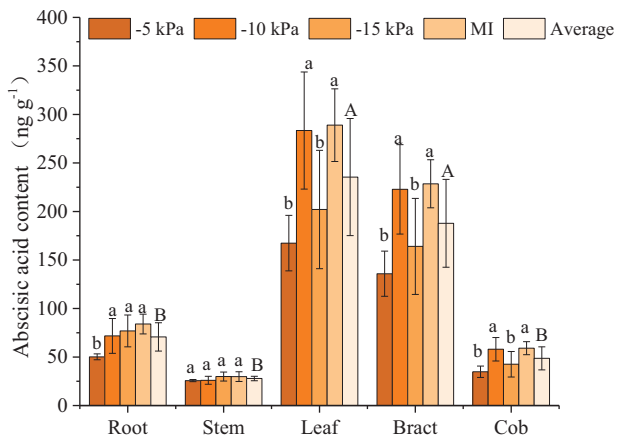

FIGURE 4 | Abscisic acid content in different organs of maize under different treatments. Values represent mean ± SD. The least significant difference method was used to test differences among treatments or organs at the $P < 0.05$ level. Different lowercase letters indicate significant differences among treatments within the same organ, and different capital letters on the average value of all treatments in each organ indicate significant differences among organs.

ABA content in the bract was significantly higher than that by 40.6 and 28.2%; and the ABA content in the cob was significantly higher than that by 41.0 and 28.0%. Under 38% FC to 53% FC of SSM, the ABA content of stems and roots increased with the decrease in soil water content, and the ABA content of the PCI-5 kPa treatment was significantly lower than that of the PCI-10 kPa and PCI-15 kPa treatments. However, the ABA content in maize leaves, bracts, and cobs increased significantly at first and then decreased significantly with decreasing soil water content (**Figure 4**). To compare the ABA content in different organs, the average ABA content of the four treatments in each organ was calculated. The ABA content differed in different organs in the order of leaf > bract > root > cob > stem. The average ABA content in leaves was 7.4, 3.8, 2.3, and 0.3 times higher than that in bracts, roots, cobs, and stems, respectively, and that in bracts was 5.7, 2.9, and 1.7 times higher than that in roots, cobs, and stems, respectively.

Salicylic Acid

In the present study, neither the temporal variation in soil moisture (between SSM and FSM) nor the soil water content variation under SSM had effects on the SA content of maize (**Figure 5**). The content of SA differed among the different organs in the order cob > leaf > bract > root > stem. The average content of SA in the cob was 112.5, 66.0, 22.3, and 9.3% higher than that in the leaf, bract, root, and stem, respectively, while that in the leaf was 94.5, 51.9, and 12.0% higher than that in the bract, root, and stem (**Figure 5**).

Root Activity and Δ ^{13}C

At the grain filling stage, the root activity of maize was significantly affected by soil moisture (**Table 3**). Compared with MI treatment, the root activity under -5 kPa, -10 kPa, and -15 kPa of PCI increased by 57.1, 28.6, and 8.7%, respectively. The root activity of maize increased with the increase in PCI water supply pressure in the range of 38% FC to 53% FC.

As shown in **Table 3**, PCI treatments had significant effects on the $\Delta^{13}C$ of maize bracts but not leaves. Compared with MI treatment, the bract $\Delta^{13}C$ at PCI -5 kPa, -10 kPa, and -15 kPa was significantly increased by 18.3, 10.4, and 9.1%, respectively, indicating that SSM with 53% FC, 47% FC, and 38% FC was more beneficial to the improvement of bracts $\Delta^{13}C$ than FSM with 78% FC. Additionally, in the range of 38% FC to 53% FC under SSM

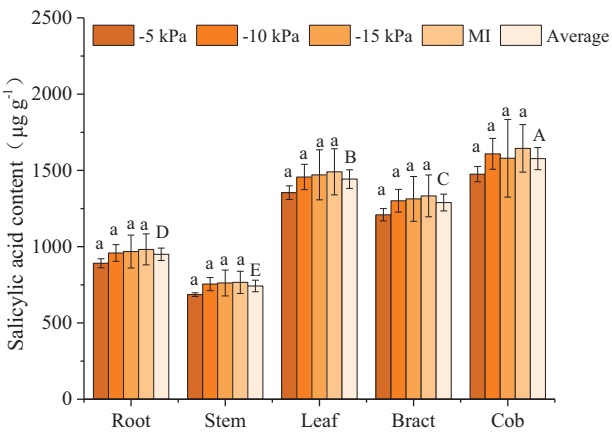

FIGURE 5 | Salicylic acid content in different organs of maize under different treatments. Values represent mean ± SD. The least significant difference method was used to test differences among treatments or organs at the $P < 0.05$ level. Different lowercase letters indicate significant differences among treatments within the same organ, and different capital letters on the average value of all treatments in each organ indicate significant differences among organs.

TABLE 3 | Effects of different treatments on root activity and $\Delta^{13}C$ of maize.

Treatment	Root activity (mg/g/h)	$\Delta^{13}C$ in maize leaf (‰)	$\Delta^{13}C$ in maize bract (‰)
–5 kPa	4.56 ± 0.30^{a}	$5.04 \pm 0.18^{a*}$	4.37 ± 0.07^{a}
–10 kPa	3.73 ± 0.57^{b}	$5.06 \pm 0.18^{a*}$	4.08 ± 0.14^{b}
–15 kPa	3.15 ± 0.58^{bc}	$4.98 \pm 0.15^{a*}$	4.03 ± 0.19^{b}
MI	2.90 ± 0.41^{c}	$4.97 \pm 0.18^{a*}$	3.70 ± 0.09^{c}

Data are the mean ± SD of the observed values, and different lowercase letters within the same column indicate significant differences among the treatments at the $P < 0.05$ level using the least significant difference (LSD) method.
**Indicates a significant difference between $\Delta^{13}C$ in leaves and bracts under the same treatment.*

conditions, bract $\Delta^{13}C$ had an increasing trend with increasing soil water content.

Correlation Analysis

The correlation between $\Delta^{13}C$ and biomass as well as WUE was analyzed. Considering all the treatments, leaf $\Delta^{13}C$ had no significant correlation with biomass, grain yield, or WUE; however, bract $\Delta^{13}C$ showed a significantly positive correlation with biomass and biomass WUE. With MI treatment excluded, the above correlation remains, and the correlation coefficient between biomass and bract $\Delta^{13}C$ is increased (**Table 4**).

The correlations between different physiological indices were further analyzed (**Figure 6**), and the results indicated that root ABA was positively correlated with proline, MDA, ABA, and SA in leaves as well as proline, MDA, and SA in roots and negatively correlated with root activity and bract $\Delta^{13}C$. Moreover, root activity and bract $\Delta^{13}C$ were negatively correlated with proline, MDA, ABA, and SA in leaves, roots, and bracts, and there was no significant correlation between leaf $\Delta^{13}C$ and various physiological indices.

Physiological Response of Maize Under Stable Soil Moisture

The soil moisture fluctuation coefficient was smaller under SSM conditions than under FSM conditions, which reduced the short-term water stress caused by the lower soil moisture, thereby reducing the root ABA content, and improving root activity. On the one hand, due to the lower content of ABA in roots, the amount of ABA transported to the leaves was also lower. As the role of ABA was to promote stomatal closure, less ABA weakened the stomatal limitation of leaves so that the $^{13}CO_2$ absorbed by the leaves was relatively low, and the $\Delta^{13}C$ was relatively increased. The water stress on plants was reduced under SSM conditions, so the accumulation of the osmotic regulating substance (proline) and the membrane lipid peroxidation product (MDA) was lower, which was conducive to the improvement of yield and WUE. On the other hand, higher root activity was favorable for nutrient uptake by roots, thus improving yield and WUE (**Figure 7**).

TABLE 4 | The correlation of $\Delta^{13}C$ with biomass and water use efficiency.

	Dry biomass	Dry grain weight	WUE_B	WUE_Y
L-$\Delta^{13}C$	+0.260 (0.288)	–0.129 (–0.124)	+0.366 (+0.435)	–0.155 (–0.144)
B-$\Delta^{13}C$	+0.625** (+0.733**)	+0.312 (+0.513)	+0.788** (+0.738**)	+0.276 (+0.500)

*L-$\Delta^{13}C$, leaf $\Delta^{13}C$; B-$\Delta^{13}C$, bract $\Delta^{13}C$. Values are Pearson correlation coefficients, + indicates positive correlation, – indicates a negative correlation, ** indicates significant correlation at the $P < 0.01$ level and the values in brackets indicate the correlation coefficient without considering MI treatment.*

DISCUSSION

Physiological Responses of Maize to Temporal Variation in Soil Moisture

Plant roots cannot produce proline, and the proline in roots mainly comes from the transport of leaves (Verslues and Sharp, 1999), so the proline content in roots is the lowest (**Figure 2**). Previous studies suggested that the proline content of maize leaves at the grain filling stage is about 50–60 μg/g under normal water conditions, which increased to 60–100 μg/g under drought treatment (Shemi et al., 2021). The leaf proline content of PCI-5 kPa, -10 kPa, -15 kPa, and MI treatment were 48.8, 59.9, 63.6, and 67.2 μg/g, respectively. Only considering the accumulation of proline, the two treatments PCI-5 kPa and PCI-10 kPa had no water stress, and PCI-15 kPa and MI treatment caused water stress. ABA mainly existed in the leaf at the grain filling stage, and the ABA in the leaf was more sensitive to water treatment than in other organs. Additionally, the ABA was accumulated more in leaf under FSM condition than under SSM condition, which suggested that the maize was subjected to severe water stress under FSM condition than SSM (**Figure 4**). Previous studies under traditional irrigation conditions indicated that proline, MDA, and ABA in maize increased with the decrease of soil water content (Tayyab et al., 2020; Shemi et al., 2021), which was consistent with the changes of proline, MDA, and ABA in most organs of maize under PCI treatment. Interestingly, the average soil water contents and most organ water contents of PCI treatments were lower than that of MI treatment in this experiment (**Table 2** and **Supplementary Table S1**), however, the proline, MDA, and ABA content in most organs of PCI treatments were lower than that of MI treatment at grain filling stage. The main reason was that the soil moistures of PCI treatments were in a stable state, while that of MI treatment was fluctuating. The stability of soil moisture under PCI can compensate for the influence of insufficient soil moisture to a certain extent, and in the case of high content of soil moisture with large temporal variation, maize would also produce adverse physiological reactions (Wang Z. et al., 2020). Previous studies had shown that under mild drought or short-term drought conditions, SA content increased slightly, but the difference was not significant (Guo et al., 2021; Mariotti et al., 2021). With the prolongation of the drought time, the SA content showed a trend of increasing first and then decreasing, and finally slightly higher than the control, but the difference was not significant (Abreu and Munné-Bosch, 2008). In the present study, the SA content

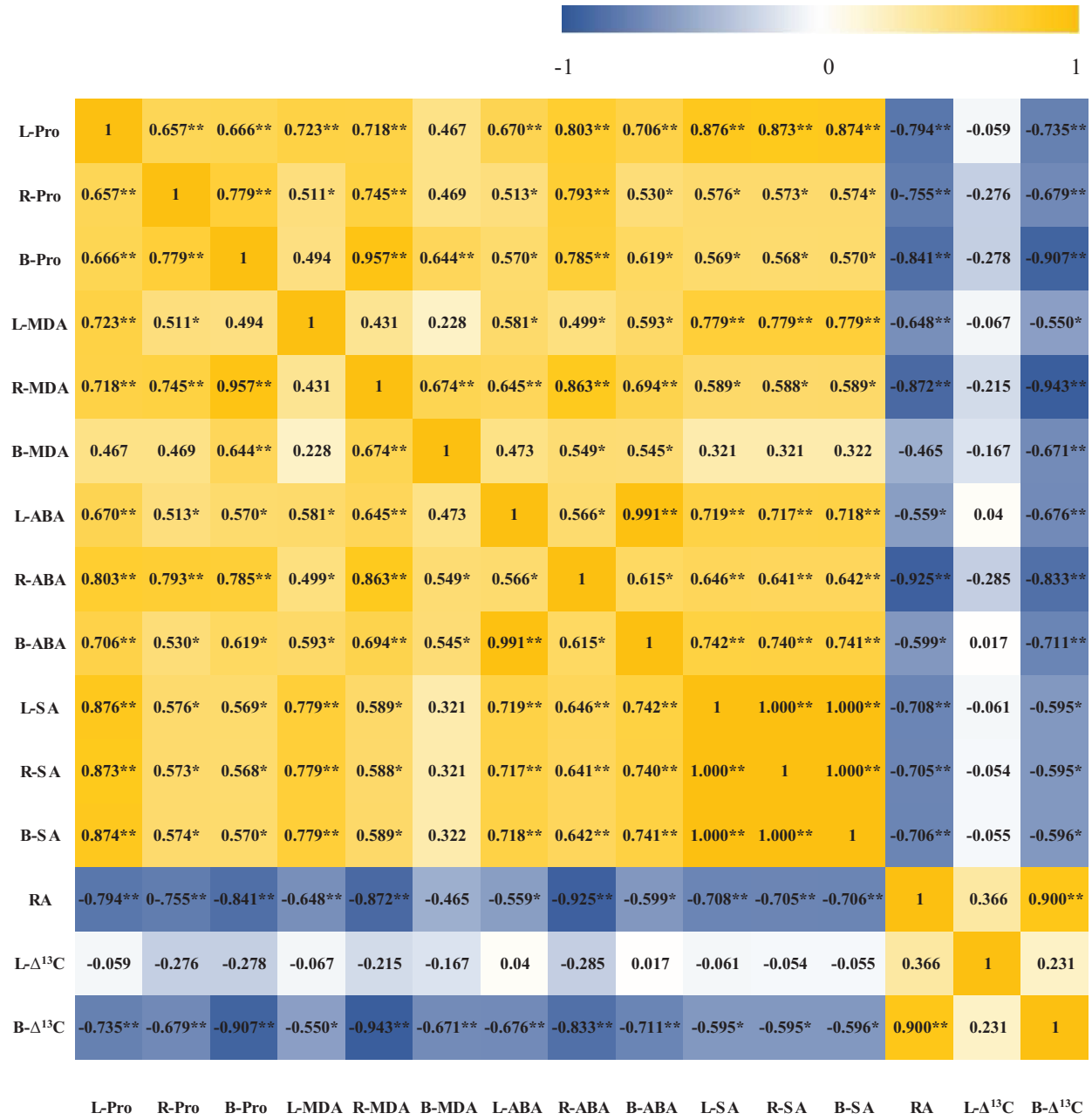

FIGURE 6 | Correlation analysis of various physiological indices. L-Pro, leaf proline; R-Pro, root proline; B-Pro, bract proline; L-MDA, leaf malondialdehyde; R-MDA, root malondialdehyde; B-MDA, bract malondialdehyde; L-ABA, leaf abscisic acid; R-ABA, root abscisic acid; B-ABA, bract abscisic acid; L-SA, leaf salicylic acid; R-SA, root salicylic acid; B-SA, bract salicylic acid; RA, root activity; L-$\Delta^{13}C$, leaf $\Delta^{13}C$; B-$\Delta^{13}C$, bract $\Delta^{13}C$; *represents a significant correlation at the $P < 0.05$ level and **represents a significant correlation at the $P < 0.05$ level.

of −5 kPa, −10 kPa, −15 kPa, and MI treatments also increased gradually, but the difference was not significant, indicating that MI treatment was subjected to mild or short-term drought compared with PCI treatment. The above results indicated that the proline, MDA, and ABA in most organs of maize under PCI treatments increased with the decrease of soil water content, and maize can maintain better physiological characteristics under the condition of SSM with lower water content than that of FSM.

In general, the root activity and $\Delta^{13}C$ increased with the increase of soil water content. A previous study on wheat revealed that the root activity of wheat increased gradually with the soil water content increased from 40% FC to 70% FC (Wu et al., 2017). With the soil moisture measured by tensiometers, it was suggested that the $\Delta^{13}C$ of the top spreading leaf of rice decreased gradually with the soil water potential changed from − 6 to − 8 kPa to − 30 to − 35 kPa (Gao et al., 2018). Only considering

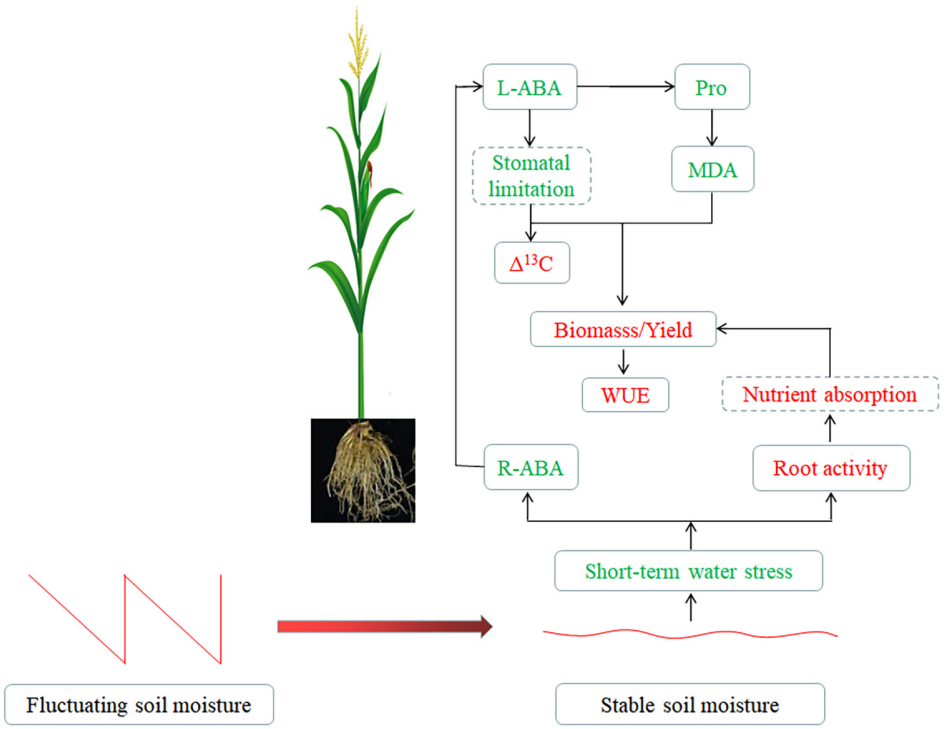

FIGURE 7 | Physiological changes in maize under stable soil moisture. The green font represents the decreased indices or weakened physiological process, and the red font represents the increased index or enhanced physiological process under SSM conditions. The dotted box represents the index or physiological process not measured in this study.

the same temporal variation of soil moisture in SSM, the results in the present study were consistent with the predecessors cited above, that is, in the range of 38% FC to 53% FC under SSM condition, the root activity, and bract $\Delta^{13}C$ at the grain filling stage increased with the increase of soil water content. However, if all the treatments of SSM and FSM were considered, there was a contradiction between the results of the present study and that of the above literature, as bract $\Delta^{13}C$ of SSM with an average moisture content of 53% FC was higher than that of FSM with an average moisture content of 78% FC. The above results indicated that the root activity and bract $\Delta^{13}C$ increased with the increase of water content in the case of similar temporal variation of soil moisture. The SSM can improve the root activity and bract $\Delta^{13}C$ at the grain filling stage with lower water content and make up for the negative effect brought by insufficient water content to a certain extent. The above correlation analysis revealed that ABA, osmotic regulating substances, and MDA decreased synergistically under PCI treatments, indicating that the degree of water stress and membrane lipid peroxidation under PCI treatments was slighter compared with MI treatment.

Correlation Between Water Use Efficiency and $\Delta^{13}C$

Determination of $\Delta^{13}C$ was used as a relatively convenient method to evaluate the WUE of plants under water stress (Gao et al., 2018; Yang and Li, 2018). Carbon isotope discrimination value ($\Delta^{13}C$) reflects the comprehensive information of CO_2 fixation during photosynthesis. Because of the larger molecular weight, the diffusion rate of $^{13}CO_2$ in the air is slower than that of $^{12}CO_2$, and plants preferentially absorb $^{12}CO_2$ when fixing CO_2. As the photosynthesis of maize leaf is stronger than that of bract (Langdale et al., 1988), and $^{12}CO_2$ is preferentially absorbed when photosynthesis is strong, so $^{12}CO_2$ in bract is less than that of leaf, and $\Delta^{13}C$ was smaller than that of the leaf (**Table 3**). Different scholars hold different views on the positive or negative correlation between $\Delta^{13}C$ and biomass as well as WUE (Gao et al., 2018; Yang and Li, 2018), which may be related to the degree or duration of water stress. Underwater stress, CO_2 assimilation is affected by a stomatal limitation or non-stomatal limitation (Sarabi et al., 2019). Under severe or long-term water stress, non-stomatal limitation occurred in leaves (Liang et al., 2019). At this time, photosynthetic activity (ATP content, Rubisco content, and activity) of mesophyll cells decreased (Hou et al., 2015), or the water loss of epidermal cells around stomata was more severe than that of guard cells, which made the stomata passively enlarged and increased intercellular carbon dioxide concentration. With the increase of intercellular carbon dioxide, the utilization ratio of $^{12}CO_2$ increased, and the utilization ratio of $^{13}CO_2$ decreased, resulting in increased $\Delta^{13}C$. In this case, $\Delta^{13}C$ was negatively correlated with biomass and WUE. Under mild or short-term water stress, stomatal limitation occurred in leaves (Zhang Y. J. et al., 2019). In the present study, the stomatal conductivity decreased

in MI treatment (**Supplementary Figure S2**), resulting in decreased intercellular carbon dioxide concentration. With the decreased intercellular carbon dioxide concentration, the utilization ratio of $^{13}CO_2$ increases, and $\Delta^{13}C$ decreases. Lower stomatal conductance may reduce photosynthesis and thus inhibited plant growth and biomass accumulation (**Supplementary Figure S2**). In addition, higher ABA content may promote grain abortion (Wang H. et al., 2020), resulting in lower yield and WUE (**Supplementary Table S2**). Therefore, the bract $\Delta^{13}C$ was positively correlated with biomass and WUE based on biomass (**Table 4**).

Previous studies on wheat had shown that the $\Delta^{13}C$ in leaves, grains, and pedicels were positively correlated with grain yield (Sayre et al., 1995; Merah et al., 1999; Tambussi et al., 2007). The results in the present study revealed that the bract $\Delta^{13}C$ had positive correlations with biomass and grain yield (**Table 4**), which was consistent with previous research results. Studies had shown that in the case of limited water, the correlation between $\Delta^{13}C$ and biomass as well as grain yield was higher than that under adequate water conditions (Gao et al., 2018), and the present study further found that the correlation between bract $\Delta^{13}C$ and biomass of maize was enhanced under SSM. This may be since stomatal characteristics are in different stable states under various SSM, and gas exchange was closely related to biomass accumulation. Bracts play an important role in grain filling and yield formation of maize (Cantrell and Geadelmann, 1981). They have higher carbon assimilation efficiency than leaves to promote the accumulation of photosynthetic products (Fujita et al., 1994). Bracts produce more biomass and grain yield per unit area than leaves (Sawada et al., 1995). This may be the reason why bract $\Delta^{13}C$ had a significant positive correlation with biomass and WUE based on biomass, while the $\Delta^{13}C$ of leaves does not correlate with them. The results of the present study revealed that SSM enhanced the correlation between bract $\Delta^{13}C$ and biomass, and bract$\Delta^{13}C$ was more suitable for evaluating the WUE of maize than leaf $\Delta^{13}C$.

CONCLUSION

In the present study, PCI and manual irrigation were used to form SSM and FSM with different soil moisture content in the pot experiment. The dynamic changes of soil water content from the sixth leaf stage to the maturity stage of maize under different water treatments were observed, and proline, MDA, ABA, SA, root activity, and $\Delta^{13}C$ at the grain filling stage, as well as WUE throughout the growing season, were analyzed. Based on this study, the following conclusions can be drawn:

(1) SSM alleviated short-term or mild soil water stress of maize, thereby synergistically reducing the accumulation of root ABA, shoot ABA, osmotic regulating substances, and membrane lipid peroxidation products.

(2) SSM improved the root activity with even lower soil water content. The root activity of maize under the treatment of 53% FC with weak temporal variation was significantly higher than that of 78% FC with a medium temporal variation.

(3) The WUE of maize under SSM can be evaluated by bract $\Delta^{13}C$. The WUE based on biomass had a significant correlation with bract $\Delta^{13}C$ at grain filling stage rather leaf $\Delta^{13}C$, and SSM enhanced the correlation between $\Delta^{13}C$ and biomass. Therefore, compared with the leaf $\Delta^{13}C$, bract $\Delta^{13}C$ was more suitable for evaluating WUE based on the biomass of maize.

DATA AVAILABILITY STATEMENT

The original contributions presented in the study are included in the article/**Supplementary Material**, further inquiries can be directed to the corresponding author/s.

AUTHOR CONTRIBUTIONS

LN performed the manuscript writing. LN and ZW conducted the data analysis. ZW carried out the experiment. GZ and KY contributed to perform the experiment. GL contributed to the data analysis. HL supervised the study, including design of experiments, data analysis, and manuscript writing. All the authors contributed to the article and approved the submitted version.

FUNDING

This study was supported by the National Key Research and Development Program of China (2018YFE0112300).

SUPPLEMENTARY MATERIAL

The Supplementary Material for this article can be found online at: https://www.frontiersin.org/articles/10.3389/fpls.2022.833041/full#supplementary-material

REFERENCES

Abreu, M. E., and Munné-Bosch, S. (2008). Salicylic acid may be involved in the regulation of drought-induced leaf senescence in perennials: a case study in field-grown Salvia officinalis L. *Plants Environ. Exp. Bot.* 64, 105–112. doi: 10.1016/j.envexpbot.2007.12.016

Avramova, V., Meziane, A., Bauer, E., Blankenagel, S., Grill, E., Eggels, S., et al. (2019). Carbon isotope composition, water use efficiency, and drought sensitivity are controlled by a common genomic segment in maize. *Theor. Appl. Genet.* 132, 53–63. doi: 10.1007/s00122-018-3193-4

Batista, S. C. O., Carvalho, D. F., Rocha, H. S., Santos, H. T., and Medici, L. O. (2013). Production of automatically watered lettuce with a low cost controller. *J. Food Agric. Environ.* 11, 485–489.

Bian, Y., Yang, P. G., Long, H. Y., Ding, Y. H., and Li, D. (2018). Water use efficiency and nutrient absorption of spinach (*Spinacia oleracea* L.) under two material emitters and negative water supply pressures. *J. Plant Nutr. Fertil.* 24, 507–518. doi: 10.11674/zwyf.17171

Bijanzadeh, E., Naderi, R., and Egan, T. P. (2019). Exogenous application of humic acid and salicylic acid to alleviate seedling drought stress in two corn (*Zea mays* L.) hybrids. *J. Plant Nutr.* 42, 1483–1495. doi: 10.1080/01904167.2019.1617312

Buckley, T. N. (2019). How do stomata respond to water status? *New Phytol.* 224, 21–36. doi: 10.1111/nph.15899

Cantrell, R. G., and Geadelmann, J. L. (1981). Contribution of husk leaves to maize grain yield. *Crop Sci.* 21, 544–546. doi: 10.2135/cropsci1981.0011183X002100040017x

Fujita, K., Furuse, F., Sawada, O., and Bandara, D. (1994). Effect of defoliation and ear removal on dry matter production and inorganic element absorption in sweet corn. *Soil Sci. Plant Nutri.* 40, 581–591. doi: 10.1080/00380768.1994.10414297

Gao, Q., Sun, J., Tong, H., Wang, W., Zhang, G., Zhang, Y., et al. (2018). Evaluation of rice drought stress response using carbon isotope discrimination. *Plant Physiol. Biochem.* 132, 80–88. doi: 10.1016/j.plaphy.2018.08.030

Guo, Q., Li, X., Niu, L., Jameson, P. E., and Zhou, W. (2021). Transcription-associated metabolomic adjustments in maize occur during combined drought and cold stress. *Plant Physiol.* 186, 677–695. doi: 10.1093/plphys/kiab050

Hou, F. Y., Zhang, L. M., Xie, B. T., Dong, S. X., Li, A., Zhang, H. Y., et al. (2015). Effect of plastic mulching on the photosynthetic capacity, endogenous hormones and root yield of summer-sown sweet potato (*Ipomoea batatas* (L). Lam.) in Northern China. *Acta Physiol. Plant.* 37:164. doi: 10.1007/s11738-015-1912-x

Hou, P., Liu, Y., Liu, W., Yang, H., Zhao, R., Xie, R., et al. (2021). Quantifying maize grain yield losses caused by climate change based on extensive field data across China. *Resour. Conserv. Recycl.* 174:105811. doi: 10.1016/j.resconrec.2021.105811

Kang, S. Z., Du, T. S., Sun, J. S., and Ding, R. S. (2007). Theory and technology of improving irrigation water use efficiency based on crop growing water demand information. *J. Hydraulic Eng.* 38, 661–667. doi: 10.3321/j.issn:0559-9350.2007.06.004

Khan, A. R., Cheng, Z., Ghazanfar, B., Khan, M. A., and Yongxing, Z. (2014). Acetyl salicylic acid and 24-epibrassinolide enhance root activity and improve root morphological features in tomato plants under heat stress. *Acta Agric. Scand. Sec. B Soil Plant Sci.* 64, 304–311. doi: 10.1080/09064710.2014.906645

Khazaei, Z., Esmaielpour, B., and Estaji, A. (2020). Ameliorative effects of ascorbic acid on tolerance to drought stress on pepper (*Capsicum annuum* L) plants. *Physiol. Mol. Biol. Plants* 26, 1649–1662. doi: 10.1007/s12298-020-00846-7

Kim, J., Malladi, A., and van Iersel, M. W. (2012). Physiological and molecular responses to drought in *Petunia*: the importance of stress severity. *J. Exp. Bot.* 63, 6335–6345. doi: 10.1093/jxb/err313

Klopfenstein, T. J., Erickson, G. E., and Berger, L. L. (2013). Maize is a critically important source of food, feed, energy and forage in the USA. *Field Crops Res.* 153, 5–11. doi: 10.1016/j.fcr.2012.11.006

Langdale, J. A., Zelitch, I., Miller, E., and Nelson, T. (1988). Cell position and light influence C4 versus C3 patterns of photosynthetic gene expression in maize. *Embo J.* 7, 3643–3651. doi: 10.1002/j.1460-2075.1988.tb03245.x

Li, S. P., Wu, X. P., Long, H. Y., Zhang, S. X., and Wang, X. L. (2017). Water and nitrogen use efficiencies of cucumber under negatively pressurized fertigation. *J. Plant Nutr. Fertil.* 23, 416–426. doi: 10.11674/zwyf.16196

Liang, G. T., Bu, J. W., Zhang, S. Y., Jing, G., Zhang, G. C., and Liu, X. (2019). Effects of drought stress on the photosynthetic physiological parameters of *Populus×euramericana "Neva"*. *J. Forest. Res.* 30, 409–416. doi: 10.1007/s11676-018-0667-9

Liao, R. K., Zhang, L. L. Z., Yang, P. L., Wu, W. Y., and Zhang, Z. C. (2018). Physiological regulation mechanism of multi-chemicals on water transport and use efficiency in soil-maize system. *J. Clean. Prod.* 172, 1289–1297. doi: 10.1016/j.jclepro.2017.10.239

Liu, H. J., Wang, X. M., Zhang, X., Zhang, L. W., Li, Y., and Huang, G. (2017). Evaluation on the responses of maize (*Zea mays* L.) growth, yield and water use efficiency to drip irrigation water under mulch condition in the Hetao irrigation District of China. *Agric. Water Manag.* 179, 144–157. doi: 10.1016/j.agwat.2016.05.031

Long, H. Y., Wu, X. P., Zhang, S. X., Wang, J. J., Zhang, R., Drohan, P. J., et al. (2020). Connotation and research progress of crop initiate water drawing technology. *Trans. Chin. Soc. Agric. Eng.* 36, 139–152. doi: 10.11975/j.issn.1002-6819.2020.23.017

Ma, J., Du, G. Y., Li, X. H., Zhang, C. Y., and Guo, J. K. (2015). A major locus controlling malondialdehyde content under water stress is associated with *Fusarium* crown rot resistance in wheat. *Mol. Genet. Genom.* 290, 1955–1962. doi: 10.1007/s00438-015-1053-3

Maggio, A., Miyazaki, S., Veronese, P., Fujita, T., Joly, R., Ibeas, J. I., et al. (2002). Does proline accumulation play an active role in stress-induced growth reduction? *Plant J.* 31, 699–712. doi: 10.1046/j.1365-313x.2002.01389.x

Mariotti, L., Scartazza, A., Curadi, M., Picciarelli, P., and Toffanin, A. (2021). Azospirillum baldaniorum sp245 induces physiological responses to alleviate the adverse effects of drought stress in purple basil. *Plants* 10:1141. doi: 10.3390/plants10061141

Merah, O., Deléens, E., and Monneveux, P. (1999). Grain yield, carbon isotope discrimination, mineral and silicon content in durum wheat under different precipitation regimes. *Physiol. Plant.* 107, 387–394. doi: 10.1034/j.1399-3054.1999.100403.x

Naeem, M., Naeem, M. S., Ahmad, R., Ihsan, M. Z., Shah, F., Ashraf, M. Y., et al. (2018). Foliar calcium spray confers drought stress tolerance in maize via modulation of plant growth, water relations, proline content and hydrogen peroxide activity. *Arch. Agron. Soil Sci.* 64, 116–131. doi: 10.1080/03650340.2017.1327713

Niu, L., Yan, Y., Hou, P., Bai, W., Wang, Y., Zhao, R., et al. (2020). Influence of plastic film mulching and planting density on yield, leaf anatomy, and root characteristics of maize on the Loess Plateau. *Crop J.* 8, 548–564. doi: 10.1016/j.cj.2019.12.002

Pilet, P. E., and Saugy, M. (1987). Effect on root growth of endogenous and applied IAA and ABA: a critical reexamination. *Plant Physiol.* 83, 33–38. doi: 10.1104/pp.83.1.33

Saheri, F., Barzin, G., Pishkar, L., Boojar, M. M. A., and Babaeekhou, L. (2020). Foliar spray of salicylic acid induces physiological and biochemical changes in purslane (*Portulaca oleracea* L.) under drought stress. *Biologia* 75, 2189–2200. doi: 10.2478/s11756-020-00571-2

Sarabi, B., Fresneau, C., Ghaderi, N., Bolandnazar, S., Tangama, M., Streb, P., et al. (2019). Stomatal and non-stomatal limitations are responsible in down-regulation of photosynthesis in melon plants grown under the saline condition: application of carbon isotope discrimination as a reliable proxy. *Plant Physiol. Biochem.* 141, 1–19. doi: 10.1016/j.plaphy.2019.05.010

Sawada, O., Ito, J., and Fujita, K. (1995). Characteristics of photosynthesis and translocation of ^{13}C-Labelled photosynthate in husk leaves of sweet corn. *Crop Sci.* 35, 480–485. doi: 10.2135/cropsci1995.0011183X003500020033x

Sayre, K. D., Acevedo, E., and Austin, R. B. (1995). Carbon isotope discrimination and grain yield for three bread wheat germplasm groups grown at different levels of water stress. *Field Crops Res.* 41, 45–54. doi: 10.1016/0378-4290(94)00105-L

Sedaghat, M., Sarvestani, Z. T., Emam, Y., Bidgoli, A. M., and Sorooshzadeh, A. (2020). Foliar-applied GR24 and salicylic acid enhanced wheat drought tolerance. *Russ. J. Plant Physl.* 67, 733–739. doi: 10.1134/S1021443720040159

Shan, L., and Xu, M. (1991). Water-saving agriculture and its physio-ecological bases. *Chin. J. Appl. Ecol.* 2, 70–76. doi: 10.3969/j.issn.1005-3409.1999.01.002

Shemi, R., Wang, R., Gheith, E., Hussain, H. A., Irfan, M., Hussain, S., et al. (2021). Effects of salicylic acid, zinc and glycine betaine on morpho-physiological growth and yield of maize under drought stress. *Sci. Rep.* 11:3195. doi: 10.1038/s41598-021-82264-7

Tambussi, E. A., Bort, J., and Araus, J. L. (2007). Water use efficiency in C3 cereals under Mediterranean conditions: a review of physiological aspects. *Ann. Appl. Biol.* 150, 307–321. doi: 10.1111/j.1744-7348.2007.00143.x

Tayyab, N., Naz, R., Yasmin, H., Nosheen, A., Sajjad, M., Keyani, R., et al. (2020). Combined seed and foliar pre-treatments with exogenous methyl jasmonate and salicylic acid mitigate drought-induced stress in maize. *PLoS One* 15:e232269. doi: 10.1371/journal.pone.0232269

Verslues, P. E., and Sharp, R. E. (1999). Proline accumulation in maize (*Zea mays* L.) primary roots at low water potentials. II. Metabolic source of increased proline deposition in the elongation zone. *Plant Physiol.* 119, 1349–1360. doi: 10.1104/pp.119.4.1349

Wang, H., Liu, P., Zhang, J., Zhao, B., and Ren, B. (2020). Endogenous hormones inhibit differentiation of young ears in maize (*Zea mays* L.) under heat stress. *Front. Plant Sci.* 11:533046. doi: 10.3389/fpls.2020.533046

Wang, J., Long, H., Huang, Y., Wang, X., Cai, B., and Liu, W. (2019). Effects of different irrigation management parameters on cumulative water supply under negative pressure irrigation. *Agric. Water Manag.* 224, 105743. doi: 10.1016/j.agwat.2019.105743

Wang, Y. Z., Zhang, X. Y., Liu, X. W., Zhang, X. Y., Sun, H., Shao, L. W., et al. (2013). The effects of nitrogen supply and water regime on instantaneous WUE,

time-integrated WUE and carbon isotope discrimination in winter wheat. *Field Crops Res.* 144, 236–244. doi: 10.1016/j.fcr.2013.01.021

Wang, Z., Zhu, G. L., Long, H. Y., Zhang, R. L., and Shen, Z. (2020). Effects of temporal variation of soil moisture on the growth and water use efficiency of maize. *J. Agr. Sci. Tech.* 22, 153–164. doi: 10.13304/j.nykjdb.2019.0648

Wu, Y., Wang, H. Z., Yang, X. W., Meng, Z. J., and He, D. X. (2017). Soil water effect on root activity, root weight density, and grain yield in winter wheat. *Crop Sci.* 57, 437–443. doi: 10.2135/cropsci2015.11.0704

Xiao, J. F., Liu, Z. D., and Chen, Y. M. (2008). Study on the water requirement and water requirement regulation of maize in China. *J. Maize Sci.* 16, 21–25.

Yang, P. G., Bian, Y., Long, H. Y., and Drohan, P. J. (2020). Comparison of emitters of ceramic tube and polyvinyl formal under negative pressure irrigation on soil water use efficiency and nutrient uptake of crown daisy. *Agric. Water Manag.* 228:105830. doi: 10.1016/j.agwat.2019.105830

Yang, W., and Li, P. F. (2018). Association of carbon isotope discrimination with leaf gas exchange and water use efficiency in maize following soil amendment with superabsorbent hydrogel. *Plant Soil Environ.* 64, 484–490. doi: 10.17221/463/2018-PSE

Zhang, Y., Tian, Q., Hu, H., and Yu, M. (2019). Water footprint of food consumption by Chinese residents. *Int. J. Environ. Res. Public Health* 16:3979. doi: 10.3390/ijerph16203979

Zhang, Y. J., Gao, H., Li, Y. H., Wang, L., Kong, D. S., Guo, Y. Y., et al. (2019). Effect of water stress on photosynthesis, chlorophyll fluorescence parameters and water use efficiency of common reed in the Hexi Corridor. *Russ. J. Plant Physl.* 66, 556–563. doi: 10.1134/S1021443719040150

Zhao, X. J., Gao, X., Zhang, S. X., and Long, H. (2019). Improving the growth of rapeseed (*Brassica chinensis* L.) and the composition of rhizosphere bacterial communities through negative pressure irrigation. *Water Air Soil Pollut.* 230:9. doi: 10.1007/s11270-018-4061-1

Zhu, G. L., Wang, Z., Long, H. Y., Zhang, R. L., and Yu, K. (2020). Effect of soil moisture on growth and water use efficiency of cherry radish under negative pressure irrigation. *J. Agr. Sci. Tech.* 22, 127–136. doi: 10.13304/j.nykjdb.2019.0953

Conflict of Interest: GZ was employed by Beijing Liangxiang Lanxin Hydraulic Engineering & Design Co., Ltd.

The remaining authors declare that the research was conducted in the absence of any commercial or financial relationships that could be construed as a potential conflict of interest.

Publisher's Note: All claims expressed in this article are solely those of the authors and do not necessarily represent those of their affiliated organizations, or those of the publisher, the editors and the reviewers. Any product that may be evaluated in this article, or claim that may be made by its manufacturer, is not guaranteed or endorsed by the publisher.

frontiers | Frontiers in Plant Science

ORIGINAL RESEARCH
published: 24 May 2022
doi: 10.3389/fpls.2022.870438

Adapting Grapevine Productivity and Fitness to Water Deficit by Means of Naturalized Rootstocks

Emilio Villalobos-Soublett[1], *Nicolás Verdugo-Vásquez*[1], *Irina Díaz*[2] *and Andrés Zurita-Silva*[1]*

[1] Centro de Investigación Intihuasi, Instituto de Investigaciones Agropecuarias INIA, La Serena, Chile, [2] Centro de Investigación Raihuén, Instituto de Investigaciones Agropecuarias INIA, San Javier, Chile

Climate change effects are unbalanced in all regions and cultivars linked to the wine industry. However, the impact of extreme weather events, such as drought and rising global temperatures, highlight the potential vulnerability in plant productivity, phenology, and crop water requirements that affect quality and harvests. Among adaptative measures for grapevine cultivars in existing or new winegrowing areas, the use of tolerant rootstocks to abiotic stress has been regarded as a mid-term strategy to face emerging constrains. The aim of this study was to compare naturalized or autochthonous rootstocks influence over grapevine cultivar performance and to characterize their response to deficit irrigation conditions. Data was collected from Cabernet Sauvignon and Syrah grafted plants for over 3 growing seasons (2018–2021) from a hyper-arid experimental field in Vicuña, Chile. Morpho-physiological parameters were determined throughout seasons and combinations where significant effects from rootstocks, irrigation treatment, and cultivar were observed over A_n and g_s, thus modifying CO_2 assimilation and intrinsic Water Use Efficiency (WUE_i). Primary productivity and yield were also modified by rootstock depending upon cultivar hydric behavior. Interestingly, cluster and berry traits were unaffected despite how water productivity and integral water stress were modulated by rootstock. In both cultivars, it was observed that trait responses varied according to the irrigation conditions, rootstocks, and their respective interactions, thus highlighting a relative influence of the rootstocks in the processes of adaptation to the water deficit. Moreover, harvest date and acidity were modified by deficit irrigation treatment, and rootstocks did not modify phenological stages. Adaptation of grapevines to expected lower water availability might be improved by using suitable tolerant rootstocks, and maturity index can be modified through irrigation management.

Keywords: ***Vitis vinifera***, **naturalized rootstocks,** ***V. berlandieri*** **×** ***V. rupestris***, **hydric behavior, deficit irrigation, gas exchange, water use efficiency**

OPEN ACCESS

Edited by:
Thorsten M. Knipfer, University of British Columbia, Canada

Reviewed by:
Yaosheng Wang, Chinese Academy of Agricultural Sciences (CAAS), China
Renato De Mello Prado, São Paulo State University, Brazil

***Correspondence:**
Andrés Zurita-Silva
andres.zurita@inia.cl

Specialty section:
This article was submitted to Plant Abiotic Stress, a section of the journal Frontiers in Plant Science

Received: *06 February 2022*
Accepted: *06 April 2022*
Published: *24 May 2022*

Citation:
Villalobos-Soublett E, Verdugo-Vásquez N, Díaz I and Zurita-Silva A (2022) Adapting Grapevine Productivity and Fitness to Water Deficit by Means of Naturalized Rootstocks. Front. Plant Sci. 13:870438. doi: 10.3389/fpls.2022.870438

INTRODUCTION

Among environmental constraints, water scarcity is probably the most important threat all over the world (Jury and Vaux, 2005; Kijne, 2006; Berger et al., 2010), compromising agricultural production at several latitudes (FAO, 2018). Rapidly, the possibilities to generate and to manage new water sources for agriculture will be limited, and the instability of water resources will not

only be detrimental to crop productivity, but will also generate substantial socioeconomic impacts (Postel, 2000; Polade et al., 2017). Considering the competition for water use among agriculture, human consumption, and industrial sectors, crop water demands could double by 2050, whereas the availability of freshwater is predicted to drop by 50%, owing to global climate change (CC; Gupta et al., 2020). Viticulture production is not an exception, since future projections of CC-driven changes or "climate crisis" suggest a lack of water to maintain current levels of production in all regions of the world, which will particularly impact Mediterranean ecosystems (Hannah et al., 2013). Furthermore, suitable zones for grapevine production based on temperature may be greatly affected in the Mediterranean regions (Santillán et al., 2019). Viticulture adaptation to CC in these regions (as most crops do) will require integrated strategies and major adaptive levers to cope with water availability and grapevine productivity and an increase in evapotranspiration that encompass different levels of organization: the crop (cultivar and rootstock), the cropping system (management techniques used), and the farming system, including farmers (del Pozo et al., 2019; Naulleau et al., 2021).

A recent systematic study identified current knowledge to evaluate adaptation strategies in the main vineyards worldwide (Naulleau et al., 2021), whose findings were as follows: (1) evaluation of a combination of adaptation strategies provides better solutions for adapting to CC; (2) multi-scale studies allow local constraints and opportunities to be considered; and (3) only a small number of studies have developed multi-scale and multi-lever approaches to quantify feasibility and effectiveness of adaptation (Naulleau et al., 2021). For instance, ecophysiological studies have contributed to maximize the use and productivity of water, i.e., irrigation technification, regulated deficit irrigation (Hsiao et al., 2007), soil mulch, and optimization of the orchard density and architecture (Ripoche et al., 2010). However, in mid-term, it will be necessary to incorporate increasing productivity, fruit quality and disease tolerance, criteria of water productivity [WP; g (MS)/mm (H_2O) transpired], and water stress tolerance in cultivars and rootstock breeding (Warschefsky et al., 2016; Simonneau et al., 2017; Gupta et al., 2020). Thus, a water shortage scenario will demand to assess interaction effects of cultivar x rootstock x environment and their impacts in fruit attributes associated with its quality (Ibacache et al., 2016; Cochetel et al., 2017; van Leeuwen et al., 2019; Villalobos-González et al., 2019).

Under water deficit conditions, perennial plants display a continuum of mechanisms for dealing with low water availability between two edges: 1) drought evasion, which is found in species bearing high stomatal sensitivity (near-isohydric), or 2) drought tolerance, found in species bearing low stomatal sensitivity response to the ambient (near-anisohydric) and functional and morphological traits toward adaptation such as osmo-regulation (Schultz, 2003; Blum, 2011; Gupta et al., 2020). Stomatal closure is linked to systemic signaling from the roots rather than the shoot, as evidence that root physiological status plays a key role in controlling the shoot behavior (Lawlor, 2002). Traditionally, the plant hormone abscisic acid (ABA) plays an essential function as a phytochemical signal involved in the shoot-root communication, because of drop in soil water potential (Zhang et al., 2006). It is also considered the most prominent player in drought stress, directly affecting stomatal conductance (gs) at the guard cell level (Gupta et al., 2020). The physiological and molecular mechanisms driving the ABA effects are yet to be summarized (Gambetta et al., 2020).

In grapevines, the hydraulic and biochemical modes of stomatal regulation are interdependent, making a strict division between them extremely challenging both theoretically and experimentally (Medrano et al., 2003; Ollat et al., 2016; Buckley, 2019; Gambetta et al., 2020). Moreover, the relative contribution of these mechanisms is still unknown and likely dependent on genotype and environment (Lovisolo et al., 2016; Coupel-Ledru et al., 2017; Hochberg et al., 2018; Dayer et al., 2020). It has also been demonstrated that leaf hydraulic conductance (K_{leaf}) was downregulated by exogenous ABA, with strong variations depending on the genotype (Coupel-Ledru et al., 2017). Interestingly, variation between isohydric and anisohydric genotypes correlated with K_{leaf} sensitivity to ABA, with K_{leaf} being unresponsive to exogenous ABA in the most anisohydric genotypes (Coupel-Ledru et al., 2017). Recent work suggests that all genotypes regulate stomatal conductance to protect against more severe damage, such as petiole or leaf cavitation and leaf shedding (Dayer et al., 2020). However, it is not clear to what extent differences in regulation of vine water use between cultivars result from innate genotypic differences or environmental factors (Hochberg et al., 2018). Likewise, grapevines appear to almost always operate within a "safe" margin of water potentials in which stem cavitation is extremely rare (Charrier et al., 2018). Still, the exact vine mortality thresholds are still unknown. Thus, numerous gaps remain in understanding of what really configures a drought-adapted grapevine cultivar, making it difficult to robustly address future climate challenges (Gambetta et al., 2020). Also, unraveling mechanisms to explain how the regulation of aerial (cultivar) drought tolerance could be enhanced by a root-driven feedback regulation, where the role of rootstock might be crucial to determine such responses and sustain productivity, pointing toward an integrative approach that digs into the complexity of cultivar x rootstock x environment interaction (Franck et al., 2020).

Most of the worldwide vineyards are grafted on commercial rootstocks which are hybrids of mostly three species, namely, *Vitis berlandieri*, *V. riparia*, and *V. rupestris,* that were developed before 1930 from American *Vitis* species to control phylloxera damage (Serra et al., 2014; Berdeja et al., 2015). Rootstocks also provide support for cultivation under challenging soil conditions, including the presence of nematodes and insects, high salinity or active lime, and drought (Meggio et al., 2014; Serra et al., 2014; Walker et al., 2014). Limited long-term information on rootstock effects over yield and its components are available. Nevertheless, it is established that the response is primarily associated with the vigor level conferred to the scion by the rootstock (Dry and Loveys, 1998). This influences bud fruitfulness and vine productivity (Satisha et al., 2010; Ibacache et al., 2016). To sustain grapevine productivity and quality in CC warming, an increase for irrigation water will occur, generating big freshwater demands, considering the low adoption of measurements of RDI

or PRD. Therefore, agricultural adaptation efforts that anticipate these multiple possible effects in Mediterranean agroecosystems are needed (Hannah et al., 2013; Wolkovich et al., 2018). By assessing the current effects of CC on *V. vinifera*, it is key to understand the plasticity associated with the ability to uptake water from soil in the continuous root/vine/environment (Santillán et al., 2019; van Leeuwen et al., 2019).

Although scion-rootstock interactions in drought tolerance have been studied (Serra et al., 2014; Tomás et al., 2014; Bianchi et al., 2020), the diversity of rootstocks adapted to dryer conditions is limited. Recent studies in rootstock effects were evaluated, and differences in fruit yield, pruning weight, budburst, fruit set, bunch weight, berry weight, berry diameter, and rachis weight between nine rootstocks in semiarid conditions were determined along with their effects on nutrient uptake (Ibacache et al., 2016, 2020). Therefore, grapevine rootstocks will undoubtedly play a fundamental role in the adaptation to future CC, especially to water shortage (Serra et al., 2014; Ollat et al., 2016; Delrot et al., 2020) and to improve WP, but mechanisms driving these processes are still elusive. In a grapevine meta-analysis contrasting stomatal conductance in response to water availability, rootstock genotype explained the greatest contribution to variability (19.1%) followed by the scion genotype (16.2%) (Lavoie-Lamoureux et al., 2017). Moreover, the effect of soil water-holding properties was analyzed and showed a scion-dependent effect which was dominant over rootstock effect in predicting gs values. Overall results suggest that a continuum exists in the range of stomatal sensitivities to water stress in *V. vinifera*, rather than an isohydric—anisohydric dichotomy, which is further enriched by diversity of scion-rootstock combinations and interactions with soils and intensity of water deficits (Levin et al., 2020).

In Chile, naturalized rootstocks were collected from arid regions of Northern Chile (Milla-Tapia et al., 2013) and studied in response to water deficit. Some selected genotypes induced significantly higher tolerance for morpho-physiological traits irrespective of scion and seasons associated with higher root growth at early stages (Franck et al., 2020). Further transcriptomic analysis was performed, determining that major differences in transcriptional behavior occurred at root level, suggesting scion-driven transcriptional regulation in response to water deficit (Franck et al., 2020). Despite the importance of grapevine phenology, studies on the effect of rootstock on the development of phenological stages are scarce in literature and have been carried out in few varieties and under different edaphoclimatic conditions (Loureiro et al., 2016; van Leeuwen and Destrac-Irvine, 2017; van Leeuwen et al., 2019).

To understand the effects and expected impacts of CC warming due to water deficit on grapevine productivity and fruit maturity, we conducted a multi-rootstock approach using two contrasting cultivars in regard to hydric behavior grafted on selected naturalized rootstocks to assess the array of response as study model for understanding adaptive responses that might confer better drought adaptation to specific clone/rootstock combinations on vegetative and fruit expression in hyper arid environment.

MATERIALS AND METHODS

Plant Material, Drought Stress Conditions, and Physiological Measurements

The field experiment was conducted during three growing seasons (2018/19, 2019/20, and 2020/21) at an experimental vineyard located at the Vicuña Experimental Center belonging to the Instituto de Investigaciones Agropecuarias (INIA) (30°02′S, 70°41′W, 630 m above sea level; Coquimbo Region, Chile). The climate of the area is classified as hyper-arid, with an average daily temperature of 16.1°C and a mean annual rainfall of 100 mm that concentrates in winter (June–September). The vineyard soil is a sandy loam alluvial Entisol and has a flat topography (<1%). The soil holds moderate depth (>50 cm) with no physical restrictions for root growth. A pit was made, determining that the roots were concentrated in the 30 cm depth. From 0 to 30 cm depth, a soil sample was taken, obtaining the following composition: sand (54.1%), slime (28%), clay (17.85), field capacity (11.2% v v^{-1}), permanent wilting point (5.2% v v^{-1}), pH value (7.3, calcareous soil), organic matter (1.5%), and electrical conductivity (2.3 dS m^{-1} in saturated paste). Cultivars Cabernet Sauvignon (CS, near-isohydric) and Syrah (Sy, near-anisohydric) were grafted onto two naturalized genotypes (R32 and R70) selected in northern Chile for their tolerance to water deficit (Bavestrello-Riquelme et al., 2012; Milla-Tapia et al., 2013; Franck et al., 2020), to commercial tolerant rootstock Ruggeri140 (140Ru), and to self-grafted vines (SG). Both varieties grafted onto rootstocks were assigned in a completely randomized design at planting.

The grapevines were planted during spring 2015 with a spacing of 1 × 2.5 m within north-south oriented rows, trained on a vertical shoot positioning (VSP) trellis system, formed in unilateral cordon, and cane pruned to a Guyot system leaving about 6–8 buds per vine. Due to the low rainfall that was characteristic during the seasons (<100 mm), it was necessary to apply water through irrigation. Thus, grapevines were drip irrigated using one irrigation line per row with emitters supplying water at a rate of 4 l h^{-1} spaced at 1 m (1 emitter per plant) located on the surface, 15 cm from the trunk. Weather variables (air temperature, relative humidity, solar radiation, precipitation, wind speed, and wind direction) were measured at 15 min time during the season, using an automatic meteorological station (Adcon Telemetry, A730, Klosterneuburg, Austria) located near the experimental vineyard (30 m). This information was used to calculate the reference evapotranspiration (ET0) using the Penman–Monteith model (Allen et al., 1998). Then, the actual evapotranspiration (ETa) was calculated by adjusting the ET0 by the crop coefficient (Kc) corresponding to each phenological stage, using the value described by Jara-Rojas et al. (2015). The reference evapotranspiration during the three seasons varied between 792.4 and 797.7 mm (September–April).

The experimental design consisted of two water regime treatments per cultivar with three replicates (blocks) of five grapevines each to cope for soil variability along the vineyard: full irrigation (T0) and 50% deficit irrigation (T1) *via* a drip irrigation system in both cultivars that was randomly distributed within rows. The 50% deficit irrigation was considered since the

observed decline of precipitation over central Chile has been greatly accentuated by an uninterrupted sequence of dry years since 2010, with annual rainfall deficits ranging between 25 and 45% (Garreaud et al., 2020). Field trial received a standard agronomic management used in commercial vineyards in terms of irrigation, fertilization, pruning, pest, and disease management in each growing season.

Nutritional content of the soil was described elsewhere (Verdugo-Vásquez et al., 2021a). In brief, nutritional content of the soil at the beginning of the study was 40 mg kg^{-1} of available N, 8 mg kg^{-1} of available P, 105 mg kg^{-1} of available K, 8.2 meq 100 g^{-1} of available Ca, 2.0 meq 100 g^{-1} of available Mg, 22.0 mg kg^{-1} of available Fe, 7.0 mg kg^{-1} of available Mn, 6.3 mg kg^{-1} of available Zn, 11.4 mg kg^{-1} of available Cu, and 1.8 mg kg^{-1} of available B. The fertilization program consisted of applications of N, P_2O_5, and K_2O (90, 50, 70 kg ha^{-1}, respectively) during each growing season, *via* irrigation (fertigation), dividing the mentioned doses in each irrigation (∼3 per week) during spring and early summer. It was only fertilized with N, P, and K because the other nutrients were at adequate levels. The sources of commercial fertilizers used were "Ultrasol Nit One 25," "potassium sulfate," and "Ultrasol Pro P." Through foliar analyses carried out in veraison, it was determined that there were no deficiencies or excess of nutrients during the development of the study. Therefore, fertilization was not a limitation.

Physiological trait measurements included the stem water potential (Ψ_{stem}) taken from fully mature and healthy leaves (two per replicate) located in the center of the west facing vine canopy between 12:00 and 15:00 h (Solar noon; Coordinated Universal Time UTC−3) from November to March using a pressure chamber (PMS Instrument Co., model 600, Corvallis, Oregon, USA). For these measurements, the leaves were covered with completely hermetic aluminum foil bags for at least 1 h before the measurement. Then, leaves were cut and immediately placed in the chamber. Moreover, to describe the accumulated effect of the deficit irrigation treatments between rootstocks, the water stress integral (SIΨ) was calculated as follows (Myers, 1988):

$$SI\Psi = \left| \sum (\Psi_{stem} - c)\, n \right|$$

Where Ψ_{stem} is the average stem water potential for any interval (MPa day), c is the maximum value of Ψ_{stem} during the season, and n is the number of days in each interval (Moriana et al., 2007).

Also, the stomatal conductance (g_s; mol H_2O $m^{-2}s^{-1}$) and net assimilation rate (A_n; μmol CO_2 m^{-2} s^{-1}) were measured on fully sunny, developed, and healthy leaves located in the mid center of the canopy facing west using a portable infrared gas analyzer (LI−6400, LICOR Inc., Lincoln, Nebraska, USA) equipped with a 6 cm^2 transparent leaf chamber. Environmental conditions in the leaf chamber were photosynthetically active radiation ≥ 2,000 μmol photon m^{-2} s^{-1}, a molar air-flow rate setting at 500 μmol s^{-1}, and a concentration of 400 μmol s^{-1} CO_2 that was kept constant by a CO_2 injector system provided by the manufacturer. These measurements were taken on the same days and times when the Ψ_{stem} was measured. Also, the intrinsic water use efficiency was calculated from the ratio between A_n and g_s (A_n/g_s; WUE_i, μmol CO_2 mol H_2O^{-1}).

Grapevine Phenology Determinations

The phenology observations were made using the scale proposed by Coombe (1995) and followed the procedure described by Verdugo-Vásquez et al. (2016). Briefly, 3 main phenological stages were observed (budburst, flowering, and veraison) through observations made every 5–7 days, expressing the dates of occurrence of the phenological stages in day of the year (DOY) for each cultivar and season. Additionally, the duration of the growth cycle from budburst to veraison was determined by calculating the number of days elapsed between both phenological stages (expressed in days).

Berry Maturity Measurements

From post-veraison (4–15 days after veraison) to harvest (defined when the berries reached between 22 and 23°Brix of total soluble solids), berry samplings (4 dates) were carried out following the procedure described by Verdugo-Vásquez et al. (2018). In each of the sampling dates, berry maturity parameters (total soluble solids, total acidity, and pH) were determined according to the Organization of Vine and Wine (OIV) protocol (International Organisation of Vine and Wine (OIV), 2021). With the evolution curves of total soluble solids, the day of the year when the berries reached 22.5°Brix was determined, recording this day as the harvest date.

Productivity Traits Measurements

At harvest, all bunches of the replicates were manually harvested and weighed in a digital weight scale, recording yield by vine (kg $vine^{-1}$) and the number of bunches per vine. The bunch weight (g) was determined by dividing the yield by the number of bunches per plant. A sample of three clusters per replicate was taken to the laboratory where the following variables were determined: N° berries per bunch, berry weight, rachis length, rachis weight, and caliber. Vines of each replicate were manually pruned in winter, and the pruning weight (kg $vine^{-1}$) was determined. Based on yield and pruning weight obtained, the Ravaz index was calculated as the ratio between yield and pruning weight, representing the balance between vine reproductivity and vegetative activity for each season. Scion trunk circumference (cm) was measured at the end of each season (May) at 30 cm above the ground using a metric tine. Water productivity (kg/m^3) was determined by the quotient between the yield and the water applied per season in each treatment.

Statistical Analysis

Preliminarily, a four-way analysis of variance (ANOVA) considering all the factors (cultivar, season, rootstock, and irrigation) and the double interactions that consider the rootstock factor was performed. This analysis allowed to determine that the cultivar and season factors had a significant effect on most of the variables measured in this study (**Supplementary Table 1**). Therefore, each season and cultivar

were considered separately, like the proposed methodology by Buesa et al. (2021). The variables were analyzed considering a completely randomized design with factorial arrangement, with two factors (rootstock and irrigation) and their interaction (RxI). Variables were subjected to an ANOVA, and the significance of the differences was determined by Tukey's test ($p \leq 0.05$). Additionally, the percentage of variance explained by each factor (for a given variable) was calculated using the quotient between the sum of squares of the factor and the total, multiplied by 100. On the other hand, boxplots of the main variables were performed. ANOVAs and boxplots were made using the Xlstat Software version 2020.3.1 (Addinsoft SARL, Paris, France).

Regression analyses were performed to establish the relationships between A_n vs. g_s, intrinsic Water Use Efficiency (WUE_i) vs. g_s under both treatments, namely, two cultivars and four rootstocks. For the case of WUE_i, the data were transformed with the natural logarithm (ln WUE_i) to increase the linearity of the slope in each cultivar-rootstock regression according to Tortosa et al. (2019).

A meta-analysis was applied to physiological trait responses to deficit irrigation in both cultivars and rootstocks based on Yan et al. (2016) and Zhang et al. (2018). This allowed to determine the different response patterns between cultivars and rootstocks under deficit irrigation, integrating magnitudes of the decline, and integrating results between seasons. The effect size for each observation was calculated as the response ratio (InR) to represent the magnitude of the responses of plant water status to deficit irrigation conditions:

$$InRR = In\left(X_{T1}/X_{T0}\right) = In\left(X_{T1}\right) - In\left(X_{T0}\right) \quad (1)$$

where X_{T1} and X_{T0} are the mean response values of each individual observation in the deficit irrigation treatment and control irrigation conditions, respectively.

The variance of the response ratio (LnR) was calculated as follows:

$$vi = \ln\left[(1/n_{T1}) \times (S_{T1}/X_{T1})^2 + (1/n_{T0}) \times (S_{T0}/X_{T0})^2\right] \quad (2)$$

where n_{T1}, n_{T0}, S_{T1}, S_{T0}, X_{T1}, and X_{T0} are the sample sizes, standard deviations, and mean response values in the deficit irrigation and control irrigation conditions, respectively. To improve the accuracy of LnR and reduce its variability, the mean weighted response ratio (LnRR++) was calculated from LnRR:

$$lnRR_{++} = \sum_{i=1}^{m}\sum_{j=1}^{k} W_{ij}\, lnRR_{ij} / \sum_{i=1}^{m}\sum_{j=1}^{k} W_{ij} \quad (3)$$

where m is the number of groups (e.g., rootstock), k is the number of comparisons in the *i*th group (measurement number throughout the three seasons), and W is the reciprocal of the variance that was considered as the weight of each LnR and calculated as follows:

$$W = 1/vi. \quad (4)$$

The meta-analyses were performed using the R software package (version 3.1.1) (R Development Core Team, 2008). The natural logs of the response ratios (RRs) for the individual and combined treatments were determined by specifying the rootstock as a random factor in the model in the "metafor" package. The effects of deficit irrigation on water status and gas exchange were considered significant if the 95% confidence intervals (CIs) of lnRR did not overlap with zero. The bigger the value is, the greater the influence of T1 on the vines. Therefore, to make the $lnRR_{++}$ more visible, it was calculated the percent change (D, %) as follows:

$$D\,(\%) = \left(e^{lnRR_{++}} - 1\right) \times 100\% \quad (5)$$

RESULTS

Hyper Arid Conditions Exhibited Reduced Variability Among Seasons

Main climatic characteristics of the three growing seasons under study are shown in **Table 1**. Vapor pressure deficit (VPD) showed a similar behavior pattern in the three seasons, increasing as the season progresses (from budburst to harvest, mean values). Within the seasons, Season 3 (S3) was the one that presented the lowest VPD value (mean value Bu-Ha, 12% lower) compared to seasons S1 and S2, which were similar (1.0–1.01 kPa). Reference evapotranspiration (ET_0) showed a similar pattern between seasons, where ∼50% of atmospheric demand (ET_0) occurred in the Flowering-Veraison period (Fl-Ve), with similar values between the different seasons. Growing degree days (GDD) showed a behavior pattern like ET_0 during the three growing seasons. S3 was the one that exhibited the lowest accumulation of GDD from Budburst to Harvest (Bu-Ha). Precipitation and maximum and minimum temperatures for the three growing seasons are shown in **Supplementary Figure 1**. The temperature patterns were similar between seasons, with S3 being the one that presented lowest values of minimum and maximum temperatures on average. Rainfall was concentrated during the winter months, with no rain during spring and summer. S2 was a season with lowest rainfall (7.9 mm), while S1 and S3 had more rainfall (36.2 and 52.3 mm, respectively), but far below the historical mean for the study site (96 mm).

Contrasting Physiological Responses of Cultivars Due to Deficit Irrigation

Overall, the evolution of the gas exchange was rather dynamic throughout the three growing seasons. It only showed significant differences at rootstock level during quite limited days of the season, and mainly observed under deficit irrigation conditions. Under T0 conditions, the A_n of CS and Sy on average were 11.1 and 12.3 μmol CO_2 m^{-2} s^{-1}, respectively, and considered all rootstocks (**Supplementary Figures 2**, **3** for CS and Sy, respectively). Regarding g_s, both cultivars showed an average of 0.2 mol H_2O $m^{-2}s^{-1}$ under T0 conditions. Plant water status displayed the same seasonal pattern than gas exchange (**Supplementary Figures 4**, **5** for CS and Sy, respectively). The average Ψ_{stem} during all growing seasons, regardless of the rootstocks, were −0.9 MPa and −1.0 MPa for CS

TABLE 1 | Vapor pressure deficit (VPD), reference evapotranspiration (ET0), and growing degree days (GDD) for the main phenological stages of both cultivars during 2018–2019 (S1), 2019–2020 (S2), and 2020–2021 (S3) seasons.

Season	Variable		Bu-Fl	Fl-Ve	Ve-Ha	Bu-Ha
S1	VPD (kPa)	Min	0.42	0.63	0.65	0.42
		Max	1.65	1.64	1.50	1.65
		Mean	0.96	1.00	1.03	1.00
	ET0 (mm)	Accumulated	186.2	411.8	199.7	797.7
	GDD (°Cd)	Accumulated	308.5	661.4	414.8	1,384.7
S2	VPD (kPa)	Min	0.32	0.55	0.71	0.32
		Max	1.94	1.82	1.52	1.94
		Mean	0.98	1.02	1.03	1.01
	ET0 (mm)	Accumulated	156.8	444.9	190.8	792.4
	GDD (°Cd)	Accumulated	223.8	743.9	387.9	1,355.7
S3	VPD (kPa)	Min	0.39	0.47	0.61	0.39
		Max	1.57	1.27	1.29	1.57
		Mean	0.85	0.87	0.92	0.88
	ET0 (mm)	Accumulated	182.2	405.2	208.2	795.6
	GDD (°Cd)	Accumulated	267.0	636.6	386.1	1,289.7

Bu, Budburst; Fl, Flowering; Ve, Veraison; Ha, Harvest; Min, Minimum; Max, Maximum.

and Sy, respectively (**Supplementary Figures 6**, **7**). In addition, independent of the cultivar and rootstock combination, it was observed that the stress integral (SIΨ) was significantly higher during the last season (−93 MPa), followed by the second (−170 MPa), and finally the first season (−189 MPa). For CS vines, rootstock R70 (−141MPa) reached an SI significantly higher than showed by 140 Ru (−147 MPa) in average, whereas R32 and SG did not differ between both at the end of the study. This SIΨ was similar in Sy vines grafted on the different rootstocks (**Table 2**). The magnitudes of the T1 effect on physiological parameters during all growing seasons were frequently significant and oscillated to a greater or lesser extent according to the cultivar and rootstock as shown (**Figure 1**). In the case of CS, T1 decreased the A_n of R70, SG, and 140 Ru by 11, 13, and 19%, respectively, while the R32 was not affected. Also, the decrease of g_s in the rootstocks R32, 140 Ru, and R70 by T1 were 25, 26, and 30%, respectively, which were lower than the observed in SG that had a decrease of 31%.

Regarding Ψ_{stem}, the effect of T1 was significant in all rootstocks, with a decrease between 15 and 17%. The WUE_i of CS under T1 was significantly increased by 16, 20, and 25% for SG, R32, and R70, respectively, whereas the effect of T1 was not significant for 140 Ru (9%). Regarding the impact of deficit irrigation (T1) on Sy vines, it was observed that the reductions of A_n were significant and that rootstocks 140 Ru (14%), R70 (17%), and R32 (21%) alleviated these reductions. In turn, the reduction of A_n in these rootstocks was less than the reduction observed in g_s. Instead, the reduction of A_n in SG was greater than that of the other rootstocks and greater than the reduction in its g_s. Moreover, the percentage changes in Ψ_{stem} and WUE_i induced by T1 were significant and similar for all rootstocks, with a decrease and increase close to 20%. On the other hand, the responses of A_n were associated with the variations of g_s through a significant non-linear relationship ($\alpha = 0.05$) under optimal and deficit irrigation conditions for both cultivars and each rootstock as shown in **Figure 2**. In this regard, with a g_s between 0.35 and 0.15 mol H_2O mol m^{-2} s^{-1}, it was observed that the A_n of CS and Sy was 12.0 and 13.4 μmol CO_2 m^{-2} s^{-1} on average. Thus, between g_s values of 0.15 and 0.05 mol H_2O mol m^{-2} s^{-1}, these A_n values decreased to 8.3 and 7.9 μmol CO_2 m^{-2} s^{-1} in C S and Sy, respectively. Moreover, in both cultivars, it was observed that the correlation between A_n and g_s increased with rootstocks under a well irrigated condition (T0). Instead, under deficit irrigation conditions (T1) it was observed that the same correlation decreased with rootstocks (**Figure 1**).

The response of WUE_i to the g_s variations showed a significant relationship ($\alpha = 0.05$) under control and deficit irrigation for both cultivars and each rootstock (**Supplementary Figure 8**). Under mild water stress conditions (g_s between 0.15 and 0.35 mol H_2O m^{-2} s^{-1} as proposed by Medrano et al., 2002), SG and 140 Ru efficiency were 70.5 and 73.1, respectively, whereas the WUE_i for R32 and G7 were 67.2 and 64, respectively. Under similar mild water stress conditions, Sy did not shown differences of WUE_i between rootstocks with a mean value of 65.6 μmol CO_2 mol^{-1} H_2O. Under higher water stress (g_s between 0.05 and 0.15 mol H_2O m^{-2} s^{-1}), CS plants increase their WUE_i to 88.7 μmol CO_2 mol^{-1} H_2O without differences between rootstocks. For Sy vines in the same treatment, it was observed that the WUE_i in R70 was 78.5 μmol CO_2 mol^{-1} H_2O, whereas it was 83.3 μmol CO_2 mol^{-1} H_2O in average for the other rootstocks. On the other hand, these WUE_i responses were linearized by means of natural logarithm. In this regard, the correlation (r) under T0 and T1 conditions were higher for self-grafted plants in CS. In turn, Sy vines showed a higher correlation (r) in plants grafted onto rootstock R32 and SG under T0 and T1 conditions, respectively. Furthermore, it was observed that SG and R70 displayed a lower

TABLE 2 | Effect of different rootstocks and irrigation treatments on mean seasonal values of water stress integral (SIΨ).

	Stress integral (MPa)			
	Cabernet Sauvignon		Syrah	
Rootstock (R)				
R32	−144	ab	−154	a
R70	−141	a	−153	a
140Ru	−147	b	−161	a
SG	−144	ab	−159	a
Treatment (T)				
T0	−133	a	−138	a
T1	−154	B	−174	b
Season (S)				
2018–2019	−180	c	−197	c
2019–2020	−160	b	−179	b
2020–2021	−92	a	−94	a
ANOVA				
R	0.0551		0.0395	
T	<0.001		<0.001	
S	<0.001		<0.0001	
R × S	0.1758		0.3885	
R × T	0.7049		0.1896	
S × T	<0.0001		<0.0001	

T0 (control) indicates that vines were irrigated 100% according to actual evapotranspiration. T1 corresponds to a sustained deficit irrigation in which vines were irrigated with the 50% of actual evapotranspiration throughout the experimental period.

slope when they were in T0 and T1 conditions in both cultivars, respectively (**Figure 3**).

Irrigation Impacts in Phenology Are Influenced by Rootstocks

The percentage of variance explained by rootstocks, irrigation, and interaction for the phenological variables according to cultivar and season are shown in **Table 3** (only the significant ones). As mentioned, in a more complete exploratory analysis, the factor that explained the greatest variance for the phenological variables corresponded to the season. This in turn considered the effect of the season, the cultivar, and their interactions (**Supplementary Table 1**). Regarding the rootstock factor, for both cultivars, there were specific effects on the date of occurrence of the main phenological stages during the 2019–2020 season. The irrigation factor affected the harvest date in both cultivars in two of the three seasons under study. For the interaction (RxI), there were specific effects in both cultivars. For the S1 and S3 seasons, the harvest date in both cultivars was earlier (between 8 and 10 days) in the irrigation treatment T1 (**Figures 4A,C,D,F**). For CS, the budburst date (S2) was affected by the different rootstocks, where 140-Ru presented a later budburst date (4 days later) compared to the other rootstocks (**Figure 4B**). For Sy, during the S2 season, the harvest date was affected by the rootstocks, where R70 presented a later harvest date (8 days later) compared to the other rootstocks (**Figure 4E**).

The percentage of variance explained by rootstocks, irrigation, and interaction for the berry maturity evolution, according to cultivar and season (only the significant ones), is shown in **Table 4**. Rootstock factor affected the evolution of berry maturity, particularly for some dates and seasons, in both cultivars without consistency. On the other hand, the irrigation factor affected the three maturity parameters considered in almost all the dates of the 2018–2019 season (S1) for both cultivars, being more consistent for total soluble solids (TSS) and titratable acidity (TA). For the other seasons, the effect of the irrigation factor was not consistent, with specific effects in some maturity parameters and specific dates in both cultivars (**Table 4**). Regarding the interaction (RxI), it only affected some parameters and specific dates. During the 2018–2019 season (S1), treatment T1 (irrigation) presented for all sampling dates higher values of total soluble solids in both cultivars (**Figures 5A,C**) and lower values of titratable acidity (**Figures 5B,D**) with respect to the control (T0). The differences in total soluble solids were ∼2°Brix, independent of the cultivar and sampling date, while for titratable acidity, the differences were higher in the CS cultivar (0.2%) than in Sy (0.13%).

Productivity Traits Are Modified by Treatment and Influenced by Both Cultivars and Rootstocks

Considering the season effect and its impact as a large source of variation captured in the measurements and experimental set-up and expected influence by cultivar scion (**Supplementary Table 1**; **Table 5**), we also measured the percentage variance in traits explained by rootstocks, irrigation, and their interaction (RxI). The highest variance percentage explained among Rootstock by Irrigation interaction was Pruning Weight trait in both cultivars CS and Sy in two out of three seasons. Particularly, in Season 1 where pruning weight trait were 28.6 and 23.5%, and in Season 3 were 34.1 and 18.5%. In season two, the most significant interaction RxI was the Caliber trait for CS (35.8%), followed by Rachis Length (31.8%) and Bunch number per plant (29.7%) in this cv. No significant interactions in RxI were detected in Sy during Season 2. Irrigation treatments also had a significative impact in several traits during the three seasons considered. The highest variance percentage explained during the first season was Pruning Weight (29.7%), followed by Ravaz Index (18.7%) in CS, Meanwhile, in Sy, the traits displayed a different composition, with Water Productivity with the highest variance explained (44.5%), followed by Yield (36.5%). During the second season, Ravaz Index displayed a higher variance (28.8%), followed closely by Water Productivity (27.7%) in CS vines. Again, during in this season, the highest variance percentages in Sy vines were exhibited by Trunk Circumference (31.1%) and Yield (30.5%). Finally, in the third season, Water Productivity (15.8%) and Trunk Circumference (10.6%) displayed the highest variance in CS vines. In Sy vines, Trunk Circumference (43.9%) displayed the highest variance, followed by Ravaz Index (37.2%).

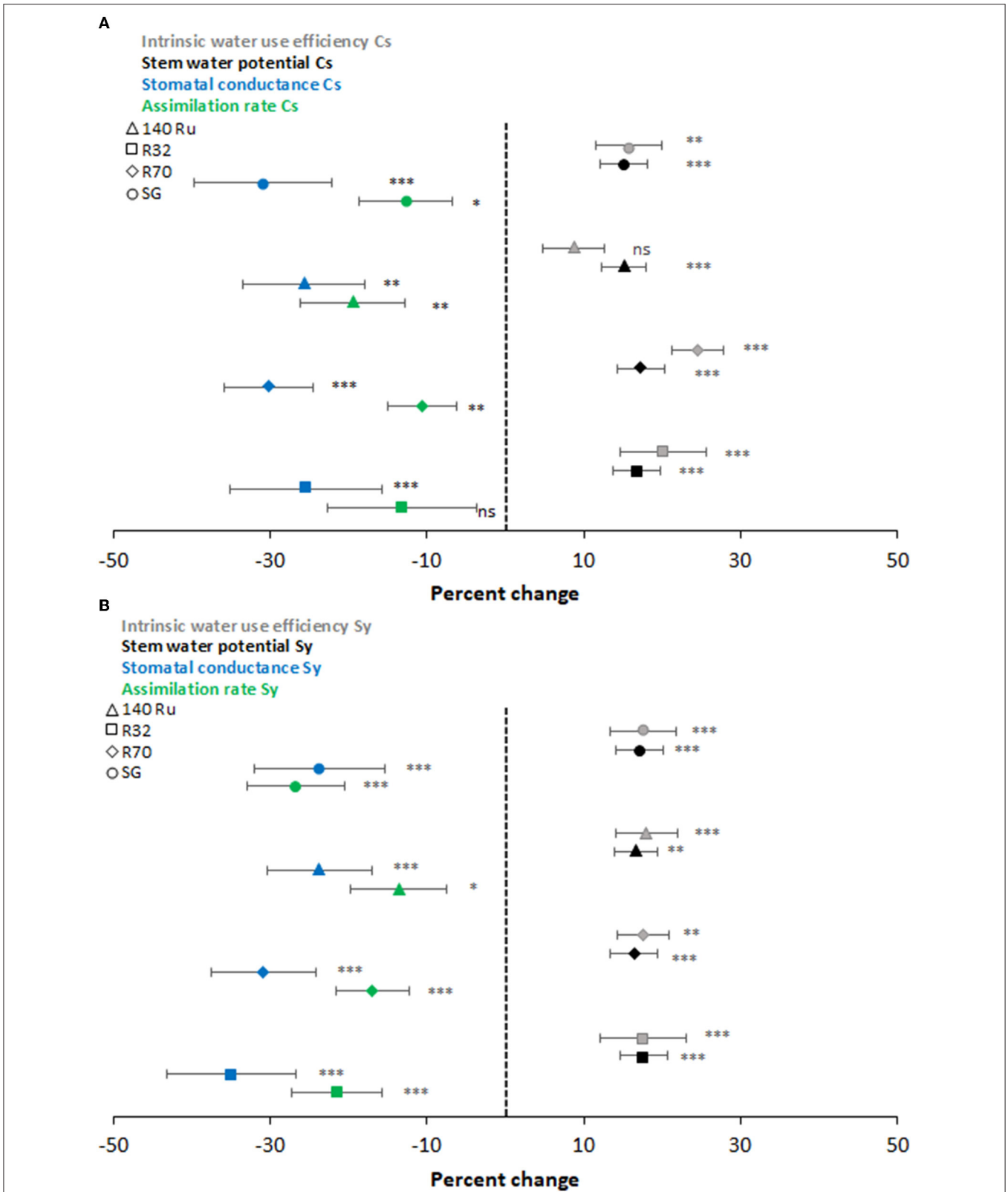

FIGURE 1 | Percent change of intrinsic water-use efficiency (gray), stem water potential (black), stomatal conductance (blue), and assimilation rate (green) under two different moderators: hydric contrasting cultivars (CS—**A**; and Sy—**B**) and rootstocks (140Ru - triangle, R32-square, R70 -diamond, and SG-circle). Asterisks near the symbols specify the significance, and the error bars show the 95% confidence interval (CI).

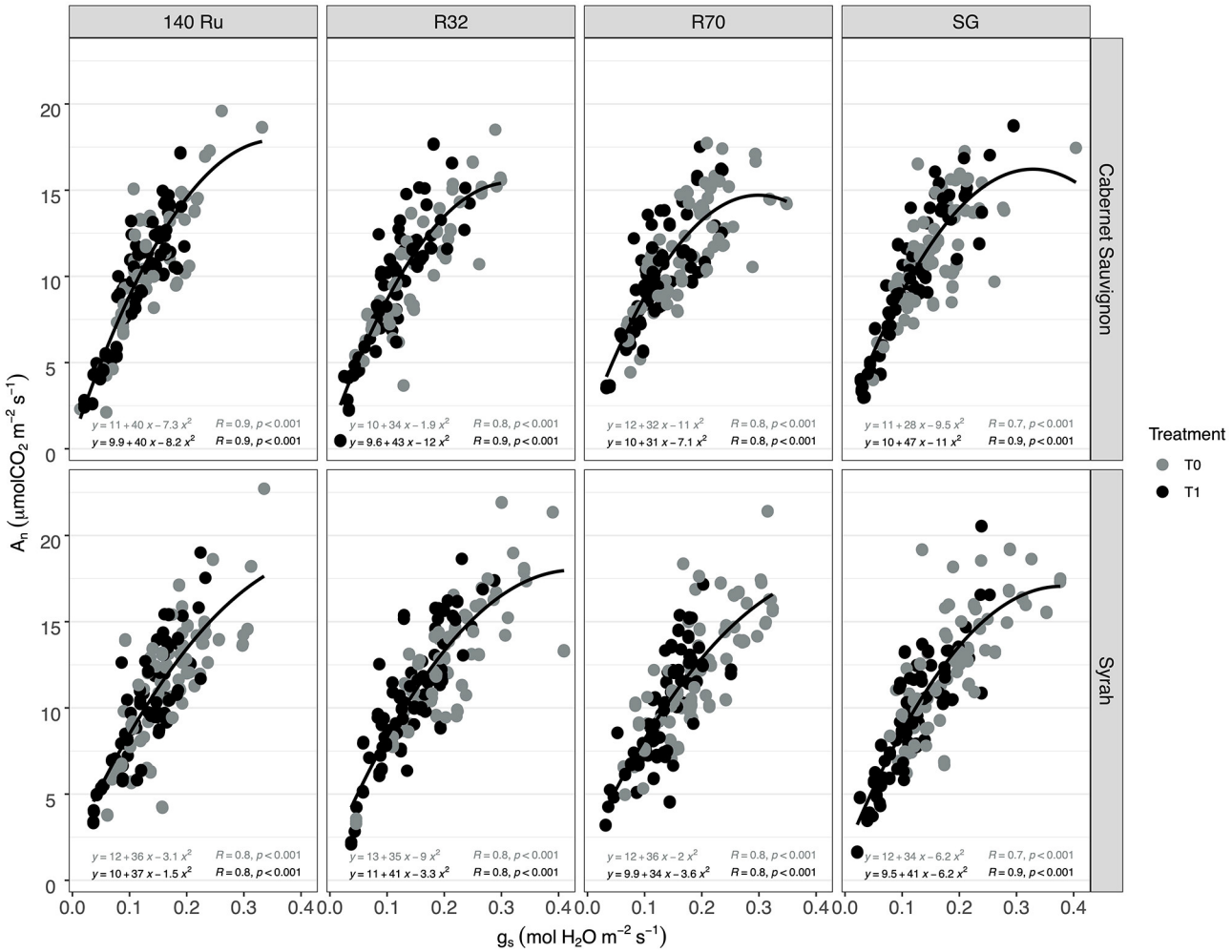

FIGURE 2 | The relationships between photosynthesis (A_n) vs. stomatal conductance (g_s) in two cultivars (Cabernet Sauvignon, CS, and Syrah, Sy) over different rootstocks under two irrigation treatments.

Interestingly, the variance percentages were higher in Sy in response to irrigation treatments.

Rootstock explained a significant amount of variation in most traits measured in CS vines, in contrast to the behavior of Sy that explained most traits in response to Irrigation treatment. As such, the strongest effect for Trunk Circumference (68.7%), Bunch Number per plant (43.8%), Pruning Weight (37.3%), Ravaz Index (35.6%), Yield (35.1%), and Water Productivity (28.8%) were observed in CS vines in Season 1, while only Trunk Circumference (27.8%) and Pruning Weight (21.1%) were significant in Sy vines. During second season, the traits Trunk Circumference (69.2%), Bunch Number per plant (40.3%), Pruning Weight (38.6%), and Water Productivity (31.9%) displayed the strongest effect for CS. No significative effects were determined for Sy during this season. The third season recorded the strongest effect for Trunk Circumference (68.4%), followed by Pruning Weight (56.1%), Yield (50%), and Water Productivity (32.9%) in CS. In turn, Syr effects were significant in Yield (29%), Berry Weight (28.7%), Caliber (25.9%), and Pruning Weight (23.2%) for Season 3.

Rootstock Performance in Deficit Irrigation Is Linked to Cultivar Behavior

Focusing on the traits in which rootstock showed the strongest effect, we plotted the distributions for Water Productivity, Trunk Circumference, Pruning Weight, and Yield among all seasons (**Table 5**) and compared each of the rootstocks using a Tukey test (**Figure 6**). A common trend was observed, which was determined by the interaction with the cultivar scion. Commercial rootstock 140Ru obtained higher results and surpassed R32, R70 and SG (grafted control) in CS vines. Conversely, R32 exceeded the rest of rootstocks considered in the analyses, exhibiting the highest water productivity, trunk

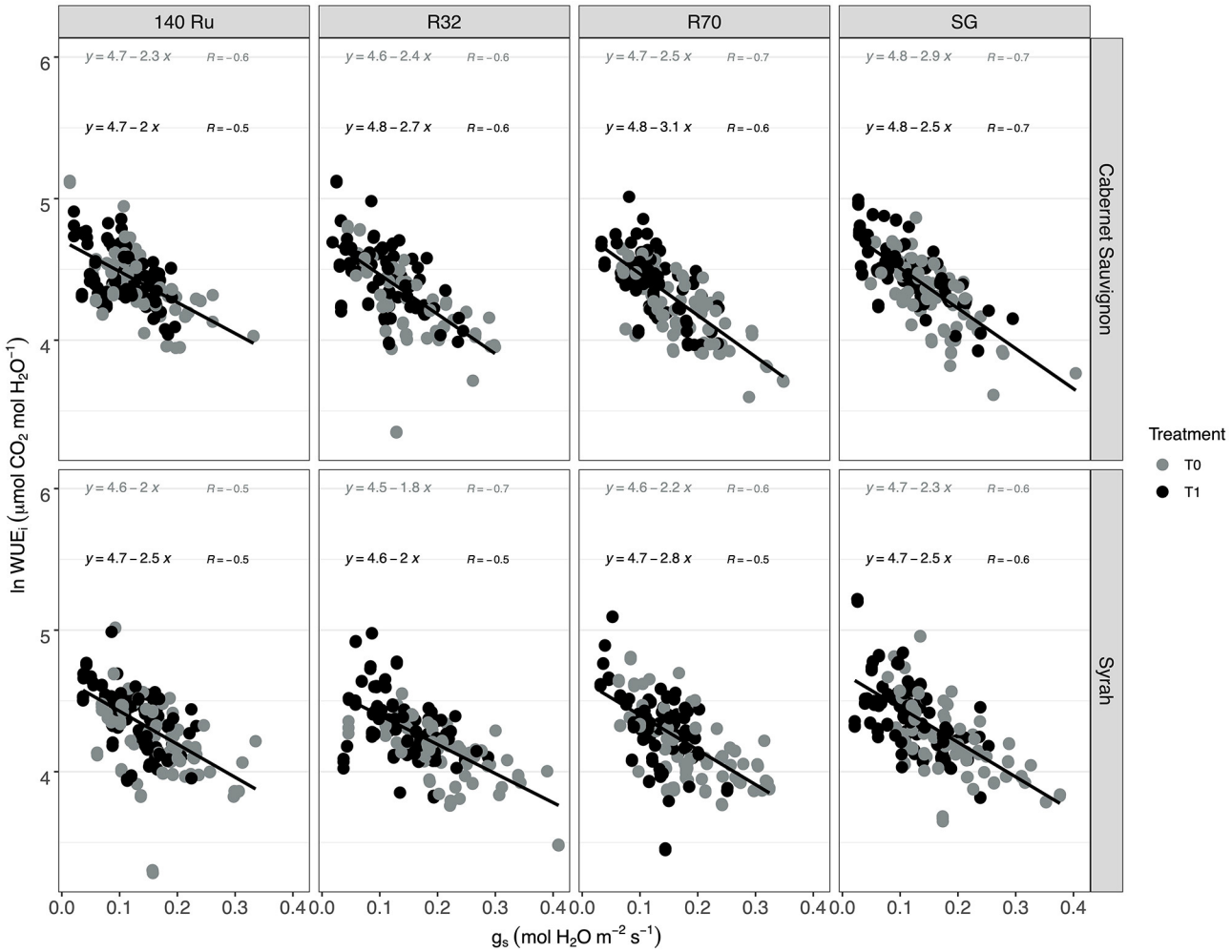

FIGURE 3 | The relationships between linearized intrinsic water use efficiency (ln WUE_i; A_n/g_s) vs. stomatal conductance (g_s) in two cultivars (CS and Sy) over different rootstocks under two irrigation treatments.

circumference, yields and pruning weights in Sy vines, although without significance in WP (but with decreases ranging from 13% to 22%) as shown in **Figure 6**. Trunk circumference in Sy was significantly higher for R32 (12.7 cm average with reductions of 10, 14, and 9% in 140 Ru, R70, and SG, respectively). The average yield for R32 in Sy (4.6 Kg/plant) was significantly higher than the other rootstocks and grafting control evaluated (a comparative decrease of 19, 28, and 22% for 140Ru, R70, and SG, respectively). Another productive trait was pruning weight, where R32 significantly exceeded the other rootstocks tested and controlled by having an average of 1.6 Kg/pl in three seasons compared to other tested rootstocks (0.9, 0.6, and 0.9 Kg/pl in 140 Ru, R70, and SG, respectively) (**Figure 6**). Similar results were observed when considering the behavior of the rootstocks in both cultivars under the T0 treatment (data not shown).

DISCUSSION

This study was designed to determine to what extent the plant water relations are modified by using naturalized rootstocks and whether this fit primary productivity and adaptation to harsh conditions typical of a hyper-arid zone that is expected to occur in Mediterranean regions due to CC (Morales-Castilla et al., 2019; IPCC, 2021). Considering the observed decline of precipitation over central Chile, which has been greatly accentuated by an uninterrupted sequence of dry years from 2010 to the present, with annual rainfall deficits ranging between 25 and 45% (Garreaud et al., 2020), the 50% deficit irrigation was a feasible projected decrease. This ongoing, multiyear dry spell has been referred to as the Central Chile Mega Drought (MD) due to its unprecedented longevity and large spatial extent in the historical record (CR2, 2015). Nevertheless, the phenological, physiological, and productive responses necessarily respond to the climatic conditions that are provisional between the growing seasons. Within the productive variables, grapevine phenology is fundamental for the planning of agricultural practice within the fields. For example, irrigation, fertilization, and the application of phytosanitary and hormonal products are programmed based on the date of occurrence of phenological states such as budburst, flowering, fruit set, and veraison. Indeed, the main factor that

TABLE 3 | Percent of variance explained by each factor (Rootstock and Irrigation) and the interaction (RxI) for the phenological variables in each cultivar and season.

Season	Variable	Cabernet Sauvignon			Syrah		
		R	I	RxI	R	I	RxI
S1	Budburst						
	Flowering						
	Veraison						
	Days Bu-Ve			29.2			
	Harvest (22.5°Brix)		36			27	
S2	Budburst	33.9					30.3
	Flowering						
	Veraison						
	Days Bu-Ve						
	Harvest (22.5°Brix)				37.2		
S3	Budburst						
	Flowering						
	Veraison						
	Days Bu-Ve						
	Harvest (22.5°Brix)		37.1			27	

Only factors which explained a significant portion of the variance ($p < 0.05$) are plotted. The percent variance explained by each factor is indicated using the value (%) and color. Darker colors explain a higher variance in each cultivar and season.
R, Rootstock; I, Irrigation; S1, 2018–2019 season; S2, 2019–2020 season; S3, 2020–2021 season; Days Bu-Ve, Days between budburst and veraison.

affects grapevine phenology is related to temperature (Parker et al., 2011). In this sense, the "season" factor, related to different climatic conditions (**Table 1**), was the most significant for the different phenological stages (**Supplementary Table 1**). The growing degree days accumulation (between budburst and harvest) did not vary between seasons (1,300–1,400 heat units), being like those reported in other wine-growing zones of Chile for the cv CS (Verdugo-Vásquez et al., 2016). Regarding the effect of the use of rootstocks and irrigation on the grapevine phenology, there is little information in literature (Keller et al., 2012; Sabbatini and Howell, 2013). It has been reported that modifications in the date of occurrence due to the use of rootstocks are related to indirect scion response, such as canopy density, as influenced by the rootstock's direct impact on scion vigor (Sabbatini and Howell, 2013). In this study, there were specific effects at the beginning of the season (budburst) for the cv CS (differences <5 days, Season S2), but the differences observed at the beginning of the season were not maintained throughout the season without significant differences for flowering, veraison, and harvest. For cv Sy, the differences due to the use of rootstocks were at the end of the season (harvest), but were also not consistent between seasons. It was observed that there is no consistency in the results between cultivars and seasons, which is why long-term studies are required to determine whether the use of rootstocks allows advancing or delaying phenological stages stably and the mechanisms by which differences are generated. For the "irrigation" factor, there were more consistent results between cultivars and seasons, wherein the decrease in irrigation (T1) advanced harvest date (at the same level of total soluble solids) for both cultivars. This advance was related to the accumulation of sugars, rather than differences in the beginning of the ripening period (veraison) since there were no differences due to the irrigation factor for budburst, flowering and veraison. At the within-field scale, it was determined that soil conditions (slope and total soil water availability) can affect grapevine phenology at the beginning of the season (budburst), and is associated with differences in the initial soil moisture (Li et al., 2016; Verdugo-Vásquez et al., 2021b). However, in this study, despite the differences in the water applied since the beginning of the season and the absence of rain in winter, there were no significant differences due to the irrigation factor for budburst.

Regarding fruit maturity, the "rootstock" factor only modified some specific dates and was not consistent between seasons. Similar results were observed by Keller et al. (2012), as they reported that scion effects and differences due to yearly climate variation far outweighed any differences due to rootstock for fruit maturity. On the other hand, the "irrigation" factor was more consistent in the results, showing that the decrease in irrigation increases the accumulation of sugars in the berries and decreases the titratable acidity, being the earliest harvest, as mentioned above. These results coincide with those reported in literature (Acevedo-Opazo et al., 2010; Cabral et al., 2021; Pérez-Álvarez et al., 2021), according to the time and intensity of water stress (Romero et al., 2022). The differences observed in maturity were more related to the general balance of grapevine (Ravaz index) than to berry weight in this study (**Table 5**).

Previous studies have also experimented with significantly different seasons, which predominate over the physiological parameters, such as Ψ_{stem} and gas exchange, that present dynamic fluctuations itself (Bascuñán-Godoy et al., 2017; Buesa et al., 2017; Romero et al., 2018; Levin et al., 2020). However, there is a high degree of co-regulation in the plant to cope with water deficits through their stomata. Since stomatal closure and regulation of leaf gas exchanges with the atmosphere, it is a key process in response to moderate water deficits both in the soil and in the atmosphere, therefore integrating internal signaling and environmental cues and complex genetic control and thus providing multiple layers of regulation to balance water loss and CO_2 assimilation in dry environments (Chaves et al., 2016; Levin et al., 2020). In a physiological framework, several studies have already reported the different degrees of responses between cultivars, of which CS and Sy display contrast hydric strategy (Hochberg et al., 2012; Franck et al., 2020; Levin et al., 2020). In this fashion, the meta-analysis showed the extent of reductions in physiological parameters measured at T1 in contrast to T0. Thus, when integrating the effect magnitude of water deficit in CS self-grafted plants, it was determined that the decline of g_s was greater than that of the A_n. On the contrary, in Sy self-grafted plants, the decline magnitude was greater in A_n than in g_s (**Figure 1**). On the other hand, the rootstocks alleviated the percentual reductions of A_n caused by T1, which agreed with what was reported by Franck et al. (2020), who observed that the naturalized rootstocks grown in pots and under field conditions displayed a better performance.

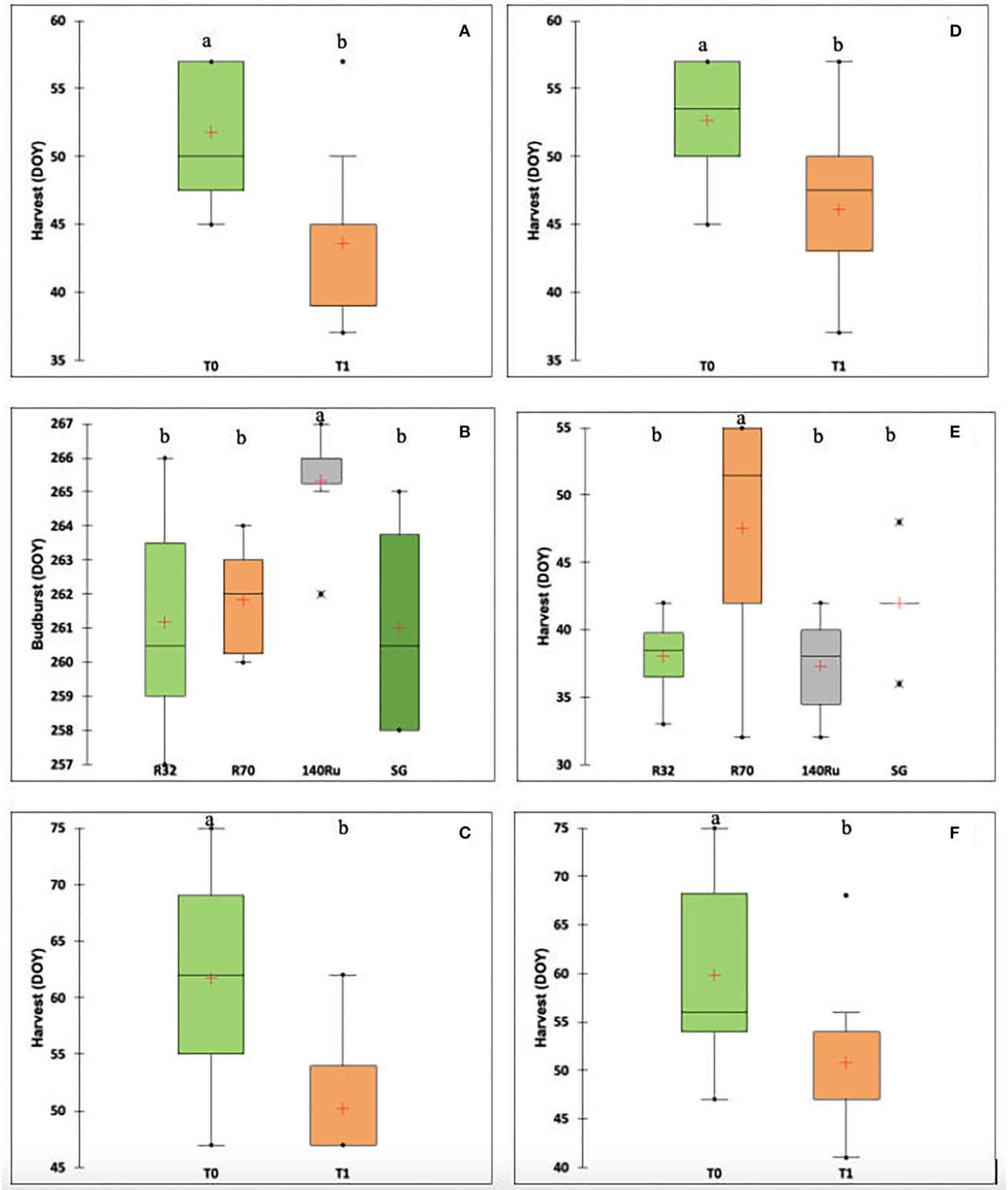

FIGURE 4 | Boxplots showing the distribution of phenological variables by the factor that explained the largest amount of variance for each cultivar and season according to **Table 2**. **(A)** Harvest (Days of the year, DOY) based on to irrigation, cv CS, 2018–2019 season; **(B)** Budburst (DOY) based on to rootstock, cv CS, 2019–2020 season; **(C)** Harvest (DOY) based on to irrigation, cv CS, 2020–2021 season; **(D)** Harvest (DOY) based on to irrigation, cv Sy, 2018–2019 season **(E)** Harvest (DOY) based on to rootstock, cv Sy, 2019–2020 season; and **(F)** Harvest (DOY) based on to irrigation, cv Sy, 2020–2021 season. Within each figure, different lowercase letters present significant differences (p-value < 0.05).

TABLE 4 | Percent of variance explained by each factor (Rootstock and Irrigation) and the interaction (RxI) for the maturity variables in each cultivar and season.

Season	Days post-Veraison	Variable	Cabernet Sauvignon			Syrah		
			R	I	RxI	R	I	RxI
S1	15	TSS	26.9	33.2			30	
		TA	22.9	41.1			47.6	
		pH						
	24	TSS		56			21.4	
		TA		53.4			24.8	
		pH		25.2				
	32	TSS		35.4			34.7	
		TA		74.7			52.4	
		pH		36.1				
	37	TSS		32.1			26.5	
		TA		43.7			45.7	
		pH						
S2	5	TSS					14.6	
		TA						
		pH						47
	12	TSS					16.7	
		TA						
		pH						
	24	TSS				38.3	11.7	
		TA		23.8		44		
		pH		26.7		37.9		
	32	TSS						
		TA	35.5			42.2	13.6	
		pH	41.2					
S3	4	TSS						
		TA						
		pH						
	12	TSS						
		TA					21.6	
		pH						
	22	TSS						
		TA		21.9	35.1		17.8	
		pH						
	30	TSS		21.9			28.9	
		TA		23	35.5		50.3	
		pH						

Only factors which explained a significant portion of the variance ($p < 0.05$) are plotted. The percent variance explained by each factor is indicated using the value (%) and color. Darker colors explain a higher variance in each cultivar and season.
R, Rootstock; I, Irrigation; S1, 2018–2019 season; S2, 2019–2020 season; S3, 2020–2021 season; TSS, Total soluble solids; TA, Titratable Acidity.

During water deficit, photosynthesis is limited by both stomatal closure and impairment of the photosynthetic machinery (i.e., metabolic factors) in order to prevent dehydration, during which root system is the major interface between the plant and water availability of a drying soil (Gambetta et al., 2020). Thus, the rootstocks can contribute to the scion water loss through a combination of hydraulic and hormonal root-to-shoot signaling (Lovisolo et al., 2010). In this sense, the relationship of A_n vs. g_s observed in two contrasting cultivars suggested that different rootstock genotypes (140 Ru, R32, R70) changed the A_n sensitivity to g_s variations given the coefficients r obtained (**Figure 2**). Moreover, in the case of CS, the g_s values (mol H_2O m^2 s^{-1}) in which the A_n reaches the "Plateau" increased with the use of rootstocks (0.17 SG < 0.19 R32 < 0.22 R70 < 0.26 140 Ru). Meanwhile, Sy decreased with R70 (0.23 mol H_2O m^2 s^{-1}), remained with 140 Ru (0.26 mol H_2O m^2 s^{-1}), and increased with R32 (0.29 mol H_2O m^2 s^{-1}), suggesting a modulation effect. Considering A_n and g_s behavior, and from an efficiency perspective (WUE_i), rootstock may also modulate the variability in response to

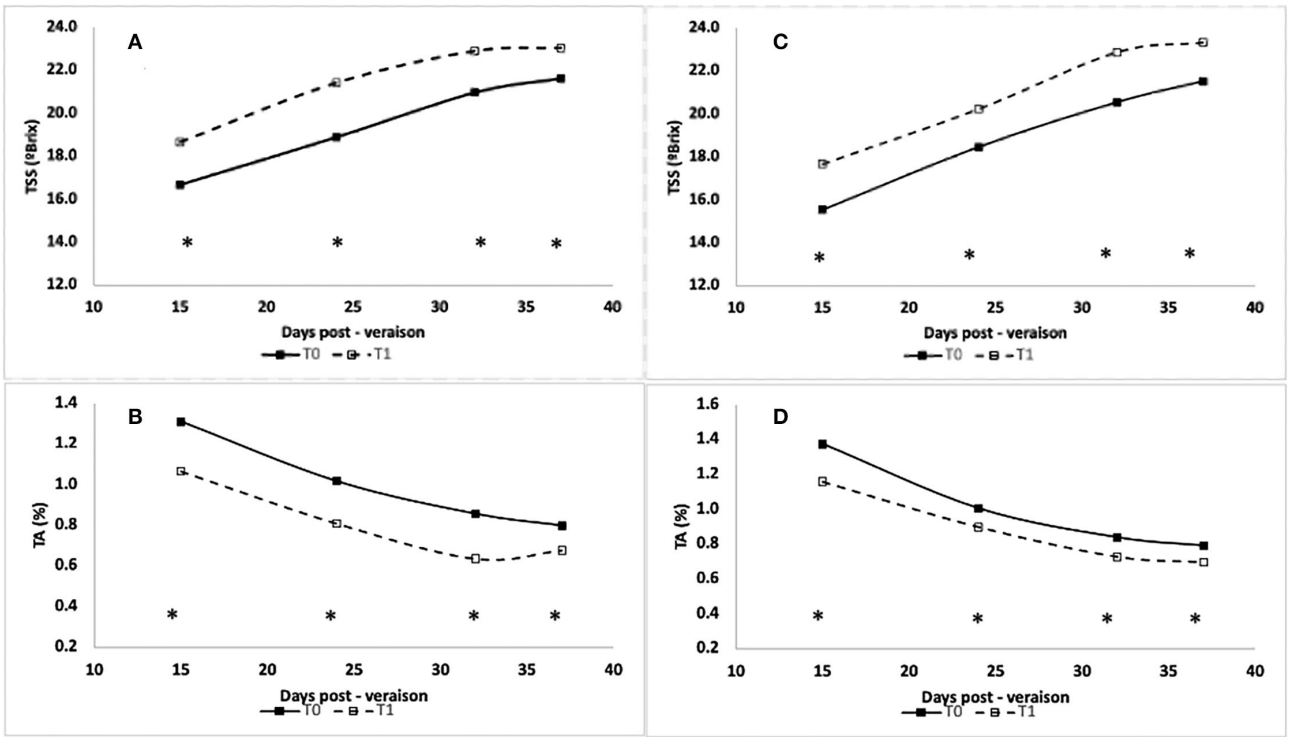

FIGURE 5 | Total soluble solids (TSS, °Brix, **A,C**) and Titratable Acidity (TA, %, **B,D**) measured at different days post—veraison for CS (**A,B**) and Sy (**C,D**) cultivars during the 2018-2019 season (S1). Asterisk (*) represents significant differences (p-value < 0.05).

stomatal closure (correlation r), where calculated slopes demonstrated that 140 Ru and R32 were the most conservative for CS and Sy, respectively, in relation to WUE_i—g_s through regressions lines, enabling to compare the slopes between genotypes to highlight environmental and genetic differences (Tortosa et al., 2019).

It has been described that the regulation of stomatal closure is mediated by hydraulic, chemical, physical, and even electrical signals (Beis and Patakas, 2010). Among these signals, an integrated modeling approach suggested that both hydraulic and chemical signals are likely important for the rootstock-specific stomatal regulation. In addition, the coupled chemical-hydraulic factors most precisely describe the stomatal conductance underlying gas exchange of grafted grapevines, since factors controlling ABA biosynthesis (either in leaves or roots, or root system architecture) caused differences in the hydraulic conductance between the rhizosphere and the soil–root interface (Peccoux et al., 2018). In this sense, this study provides results that reinforces the previous conclusions obtained in which the hydraulic variability between grape cultivars is in turn strongly influenced by the ambient VPD (Villalobos-González et al., 2019; Gambetta et al., 2020). In the face of duration and intensity of water stress given by SIΨ, CS was sensitive to the accumulated effects of deficit irrigation at the end of the growing seasons. A naturalized rootstock R32 showed the least stress, even surpassing 140 Ru, which has been shown to be drought tolerant (Romero et al., 2018). Meanwhile, the SIΨ of Sy was indifferent to deficit irrigation in much of the experimental period. The SIΨ values agrees with what was reported by Zúñiga et al. (2018). However, the stress levels in this study were higher than those previously reported and are explained by the conditions of greater aridity in the experimental site as a natural laboratory for CC adaptation studies.

Nowadays, water use (i.e., the water consumed) and WUE (i.e., the efficiency of this consumed water to assimilate carbon, produce biomass, or fruit yield) are crucial parameters, especially in areas with increasing water scarcity that requires adaptation to CC, such as south Europe, West Asia, Western Australia, Chile, North Africa, and parts of South Africa (FAO, 2018; van Leeuwen et al., 2019; Naulleau et al., 2021). Despite the importance of rootstocks for the total water productivity and WUE of the crop, the variability of WUE in rootstocks has largely been underexplored, in addition to obtaining contradictory results (reviewed by Medrano et al., 2018). Moreover, the main role of rootstocks in plant water economy leads to the consideration of the genetic variability of WUE as a complementary target for current research (Medrano et al., 2018). In this regard, differences based upon the interaction among cultivar scion: commercial rootstock support the necessity of exploring differences both in cultivar hydric behavior and the interaction with the rootstocks, leading to change in crop performances depending on the cultivar (Tortosa et al., 2019; Franck et al., 2020; Romero et al., 2022). Thus, a tolerant rootstock, such as 140 Ru, was superior in the hydric conservative CS vines, whereas R32 overcame

TABLE 5 | Percent of variance explained by each factor (Rootstock and Irrigation) and the interaction (RxI) for the productive variables in each cultivar and season.

Season	Trait	Cabernet Sauvignon			Syrah		
		R	I	RxI	R	I	RxI
S1	Yield	35.1	18.5			36.5	
	N° Bunch per plant	43.8					
	Bunch Weight					33.4	
	N° Berries per bunch	-	-	-	-	-	-
	Berry weight	-	-	-	-	-	-
	Rachis length	-	-	-	-	-	-
	Rachis weight	-	-	-	-	-	-
	Caliber	-	-	-	-	-	-
	Water productivity	28.8	16.2			44.5	
	Pruning weight	37.3	29.7	28.6	21.1	27.2	23.5
	Trunk circumference	68.7		24.4	27.8	21	
	Ravaz index	35.6	18.7				
S2	Yield	57.7		29.9		30.5	
	N° Bunch per plant	40.3	10.6	29.7			
	Bunch weight					28.4	
	N° Berries per bunch						
	Berry weight						
	Rachis length			31.8			
	Rachis weight					22.9	
	Caliber			35.8		14.3	
	Water productivity	31.9	27.7				
	Pruning weight	38.6					
	Trunk Circumference	69.2	6	19.7		31.1	
	Ravaz index		28.8				
S3	Yield	50			29		
	N° Bunch per plant						
	Bunch weight						
	N° Berries per bunch						
	Berry weight				28.7	32.1	
	Rachis length						
	Rachis weight						
	Caliber				25.9	33.6	16.7
	Water productivity	32.9	15.8			20.3	
	Pruning weight	56.1	7.4	34.1	23.2	28.2	18.5
	Trunk circumference	68.4	10.6	17.2		43.9	
	Ravaz index					37.2	

Only factors which explained a significant portion of the variance ($p < 0.05$) are plotted, and percentage of variance explained is indicated using the value (%) and color. Darker colors explain a higher variance in each cultivar and season.
R, Rootstock; I, Irrigation; S1, 2018–2019 season; S2, 2019–2020 season; S3, 2020–2021 season. - data not available.

the 140 Ru performance in Sy vines, which were measured in traits such as water productivity, trunk circumference, and yields and pruning weights (**Figure 6**). Latter results may indicate enhanced abilities for water uptake and assimilation since near-anisohydric cultivars bears a "risky strategy" of water use. Indeed, 140 Ru exhibited better adaptive behavior as CS vines maintained slight unchanged A_n, g_s, and WUE_i levels under both well-watered and persistent water stress conditions. This might be associated to greater root water-uptake capacity and whole-plant hydraulic conductance, translating to high productivity and vigor (Romero and García-García, 2020; Romero et al., 2022). With respect to normal rainfall scenarios which could represent the T0 irrigation treatment (100% ETa applied), it was observed that rootstocks behavior differed in each cultivar under these conditions. For cv CS, 140 Ru was the one that presented the best behavior regarding the productive variables analyzed (N° bunches per plant, pruning weight, trunk circumference, among others), while R32 was the one that presented the best behavior with respect to the productive variables analyzed for cv Sy (yield, trunk circumference, water productivity, among

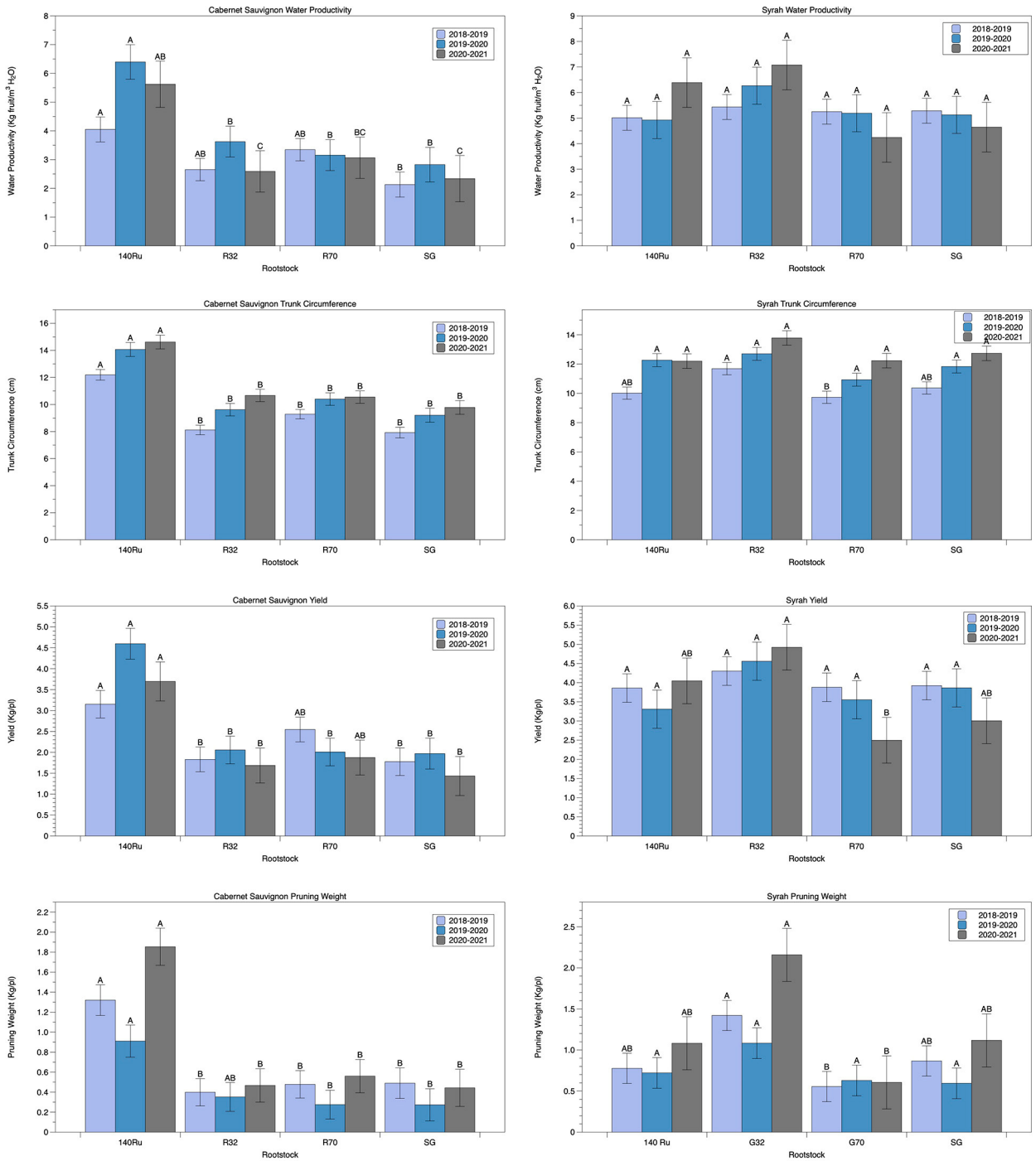

FIGURE 6 | Functional responses of selected rootstocks for productivity attributes, including Water Productivity, Trunk Circumference, Yield, and Pruning Weight among seasons and cultivars. Within each panel, different letters represent significant differences (p-value < 0.05).

others). These results highlight the need to carry out studies that consider different rootstock-scion combinations under different edaphoclimatic conditions.

In concert, CS displayed a conservative behavior in terms of lower g_s and high rates of A_n-enhanced WUE_i (Zamorano et al., 2021). Conversely, cv Sy showed increased WUE_i due to

reduced g_s near-anisohydric behavior. This was characterized by less prone to rapid stomatal closure under water stress maintaining higher stomatal aperture and exhibiting substantial reductions in Ψ_{stem}. Thus, adjusting locally with lower stomata sensitivity to drought-induced ABA and being more dependent on hydraulic signals such as leaf water status (Coupel-Ledru et al., 2017). In this regard, the integral water stress observed in this study highlighted this condition since cv Sy was the one that accumulated more stress. This cultivar is efficient in terms of water use but shows limited heat dissipation due to its reduced g_s, which can favor the occurrence of leaf sunburn under severe heat stress and drought (Costa et al., 2012). Other authors have demonstrated the mechanisms by which rootstocks modify the mentioned productive variables and found that the grafted plant modifies the absorption of light, increasing the assimilation of carbon compounds and therefore increasing the yield (Corso et al., 2016; Bascuñán-Godoy et al., 2017).

Recently, a signaling communication peptide has been identified in response to drought, where CLE25 peptide is produced in the roots and moves systemically through the plant vasculature to leaves to drive ABA production by activating biosynthetic enzyme NCED3 (Takahashi et al., 2018). This burst of ABA synthesis leads to stomatal closure and improved water balance, thereby promoting drought survival. This insight into small-peptide signaling in Arabidopsis may help to unravel conserved mechanisms in crops for root-to-shoot mobilization of stress signals (Gupta et al., 2020). Hence, the interaction with the rootstock and the ability of this to later explore and uptake water is fundamental for efficiently facing water deficit. Many traits and mechanisms are involved in the response of a rootstock by scion combination to water demand/water availability ratio. Hence, determining the optimal combination may enhance this adaptative processes. Rootstocks can differ by their capacity to extract water from the soil, which is primary linked to root biomass and to the hydraulic conductivity of the roots (Gomès et al., 2021). Lately, adaptation of viticulture requires a proper exploration of an optimal interaction of cultivar and rootstock, particularly when exploring new geographical areas, new training systems, new management practices, or new varieties, both for rootstocks and scions (Gomès et al., 2021). There are additional studies of water productivity in vineyards, but knowledge of the effect of irrigation reductions and its combined effect with grafted vines using rootstocks on secondary metabolism is still growing (Cáceres-Mella et al., 2018).

Hence, adaptations to CC require modifications in genotypes and viticulture techniques that can influence both phenology expression and grape ripening since rootstocks are able to trigger transcriptional changes on berry secondary metabolism which is relevant for berry composition and sensory properties (Berdeja et al., 2015). Moreover, studies for rootstocks conferring higher drought tolerance to the scion, driving carbon flux toward both accumulation of phenolic compounds, and alteration of anthocyanin profile, thereby altering grape quality at harvest, might be a target (Zombardo et al., 2020). In this regard, rootstocks that have novel drought tolerance mechanisms (i.e M4 rootstock) have shown greater synthesis of phenolic compounds such as stilbenes and flavonoids with enhanced capacity to scavenge and regulate the reactive oxygen species (ROS) levels that are generated under stress conditions and cause oxidative damage (Corso et al., 2015). In the naturalized R32 rootstock tissues grafted to cv Sy, the upregulation of genes of Phenylpropanoid metabolic process and pigment accumulation was determined in response to water deficit (Franck et al., 2020), enhancing plant survival in the presence of abiotic stress. M-rootstocks have also displayed adaptive traits, such as reducing the stomatal conductance and stem water potential while maintaining high photosynthetic activity with high Water Use Efficiency in water-limiting conditions (Bianchi et al., 2020). The capacity of M4 to satisfy the water demand of the scion under limited water availability has shown a delayed stomatal closure, allowing higher photosynthetic activity, which is also related to a reduced activation of ABA signaling both in the root and the leaf level (Prinsi et al., 2021). Therefore, the use of drought tolerant genotypes (scion, clones, and rootstocks) represents an environmentally friendly and cost-effective tool for adaptation to a changing climate (van Leeuwen et al., 2019).

CONCLUSIONS

Rootstock did not modify the main phenological stages, while irrigation treatment allowed modifying the harvest date. Moreover, harvest date and acidity were modified by deficit irrigation treatment and rootstocks did not modulate phenological stages. Adaptation of grapevines to expected lower water availability might be improved by using suitable tolerant rootstocks. In addition, maturity index can be modified through irrigation management.

The regulation and behavior of several physiological parameters related to the plant water status were contrasting among the cultivars studied. In turn, this behavior varied depending on how stressful the environmental conditions were between growing seasons. Under water deficit conditions, when photosynthesis was mainly limited by stomatal conductance, rootstocks showed the ability to adjust the sensitivity by which photosynthesis was restricted.

The dynamic responses and grapevine adaptation to water deficit were highly dependent on the cultivar hydric strategy (near-isohydric or near-anisohydric) and the interaction with the rootstock. Hence, the vine fitness performance will be determined by new environmental demands that will be imposed by climatic challenges, and such growth and developmental responses to drought, higher temperatures, or combined abiotic stresses will rely on the proper combination of both cultivar and rootstock.

DATA AVAILABILITY STATEMENT

The raw data supporting the conclusions of this article will be made available by the authors, without undue reservation.

AUTHOR CONTRIBUTIONS

AZ-S conceived and designed the experiments. EV-S conduced the physiological analyses and laboratory determinations with the guidance of AZ-S, NV-V, and ID. AZ-S wrote the manuscript with the help of EV-S, NV-V, and ID. EV-S, NV-V, and AZ-S

prepared all the figures. All authors contributed to the discussion of ideas, revised, and approved the final manuscript.

FUNDING

This work was supported by Consejo Nacional de Ciencia y Tecnología CONICYT–Fondecyt Regular (Grant No. 1140039 2014/INIA) to AZ-S, and by Agencia Nacional de Investigación y Desarrollo ANID—Postdoctoral Fondecyt (Grant No. 3180252 2018/INIA) to NV-V.

ACKNOWLEDGMENTS

Authors are grateful to Elizabeth Pastén and Marco Cabrera for their valuable technical support and support of Instituto de Investigaciones Agropecuarias—INIA.

SUPPLEMENTARY MATERIAL

The Supplementary Material for this article can be found online at: https://www.frontiersin.org/articles/10.3389/fpls.2022.870438/full#supplementary-material

REFERENCES

Acevedo-Opazo, C., Ortega-Farias, S., and Fuentes, S. (2010). Effects of grapevine (*Vitis vinifera* L.) water status on water consumption, vegetative growth and grape quality: an irrigation scheduling application to achieve regulated deficit irrigation. *Agr. Water Manage.* 97, 956–964. doi: 10.1016/j.agwat.2010.01.025

Allen, R. G., Pereira, L. S., Raes, D., and Smith, M. (1998). *Guidelines for Computing Crop Water Requirements*. *FAO Irrigation and Drainage Paper No. 56*. Rome: Crop Evapotranspiration.

Bascuñán-Godoy, L., Franck, N., Zamorano, D., Sanhueza, C., Carvajal, D. E., and Ibacache, A. (2017). Rootstock effect on irrigated grapevine yield under arid climate conditions are explained by changes in traits related to light absorption of the scion. *Sci. Hortic.* 218, 284–292. doi: 10.1016/j.scienta.2017.02.034

Bavestrello-Riquelme, C., Cavieres, L., Gallardo, J., Ibacache, A., Franck, N., and Zurita-Silva, A. (2012). Evaluation of drought stress tolerance in four naturalized grapevine genotypes (*Vitis vinifera*) from northern Chile. *Idesia Arica* 30, 83–92. doi: 10.4067/S0718-34292012000300011

Beis, A., and Patakas, A. (2010). Differences in stomatal responses and root to shoot signalling between two grapevine varieties subjected to drought. *Funct. Plant Biol.* 37, 139–146. doi: 10.1071/FP09034

Berdeja, M., Nicolas, P., Kappel, C., Dai, Z. W., Hilbert, G., Peccoux, A., et al. (2015). Water limitation and rootstock genotype interact to alter grape berry metabolism through transcriptome reprogramming. *Hort. Res.* 2, 15012–15013. doi: 10.1038/hortres.2015.12

Berger, B., Parent, B., and Tester, M. (2010). High-throughput shoot imaging to study drought responses. *J. Exp. Bot.* 61, 3519–3528. doi: 10.1093/jxb/erq201

Bianchi, D., Caramanico, L., Grossi, D., Brancadoro, L., and Lorenzis, G. D. (2020). How do novel M-rootstock (*Vitis* Spp.) genotypes cope with drought? *Plants* 9, 1385. doi: 10.3390/plants9101385

Blum, A. (2011). Drought resistance – is it really a complex trait? *Funct. Plant Biol.* 38, 753–757. doi: 10.1071/FP11101

Buckley, T. N. (2019).. How do stomata respond to water status? *New Phytol.* 1, 1285–1216. doi: 10.1111/nph.15899

Buesa, I., Mirás-Avalos, J. M., Paz, J. M. D., Visconti, F., Sanz, F., Yeves, A., et al. (2021). Soil management in semi-arid vineyards: combined effects of organic mulching and no-tillage under different water regimes. *Eur. J. Agron.* 123, 126198. doi: 10.1016/j.eja.2020.126198

Buesa, I., Pérez, D., Castel, J., Intrigliolo, D. S., and Castel, J. R. (2017). Effect of deficit irrigation on vine performance and grape composition of *Vitis vinifera* L. cv. Muscat of Alexandria. *Aust. J. Grape Wine Res.* 23, 251–259. doi: 10.1111/ajgw.12280

Cabral I. L., Carneiro, A., Nogueira, T., and Queiroz, J. (2021). Regulated deficit irrigation and its effects on yield and quality of *Vitis vinifera* L., touriga francesa in a hot climate area (Douro Region, Portugal). *Agriculture* 11, 774. doi: 10.3390/agriculture11080774

Cáceres-Mella, A., Ribalta-Pizarro, C., Villalobos-González, L., Cuneo, I. F., and Pastenes, C. (2018). Controlled water deficit modifies the phenolic composition and sensory properties in Cabernet Sauvignon wines. *Sci. Hortic.* 237, 105–111. doi: 10.1016/j.scienta.2018.04.008

Charrier, G., Delzon, S., Domec, J.-C., Zhang, L., Delmas, C. E. L., Merlin, I., et al. (2018). Drought will not leave your glass empty: Low risk of hydraulic failure revealed by long-term drought observations in world's top wine regions. *Sci. Adv.* 4, eaao6969. doi: 10.1126/sciadv.aao6969

Chaves, M. M., Costa, J. M., Zarrouk, O., Pinheiro, C., Lopes, C. M., and Pereira, J. S. (2016). Controlling stomatal aperture in semi-arid regions – the dilemma of saving water or being cool? *Plant Sci.* 251, 54–64. doi: 10.1016/j.plantsci.2016.06.015

Cochetel, N., Escudié, F., Cookson, S. J., Dai, Z., Vivin, P., Bert, P.-F., et al. (2017). Root transcriptomic responses of grafted grapevines to heterogeneous nitrogen availability depend on rootstock genotype. *J. Exp. Bot.* 68, 4339–4355. doi: 10.1093/jxb/erx224

Coombe, B. G. (1995). Growth Stages of the Grapevine: adoption of a system for identifying grapevine growth stages. *Aust. J. Grape Wine Res.* 1, 104–110. doi: 10.1111/j.1755-0238.1995.tb00086.x

Corso, M., Vannozzi, A., Maza, E., Vitulo, N., Meggio, F., Pitacco, A., et al. (2015). Comprehensive transcript profiling of two grapevine rootstock genotypes contrasting in drought susceptibility links the phenylpropanoid pathway to enhanced tolerance. *J. Exp. Bot.* 66, 5739–5752. doi: 10.1093/jxb/erv274

Corso, M., Vannozzi, A., Ziliotto, F., Zouine, M., Maza, E., Nicolato, T., et al. (2016). Grapevine rootstocks differentially affect the rate of ripening and modulate auxin-related genes in cabernet sauvignon berries. *Front. Plant Sci.* 7, 69. doi: 10.3389/fpls.2016.00069

Costa, J. M., Ortuño, M. F., Lopes, C. M., and Chaves, M. M. (2012). Grapevine varieties exhibiting differences in stomatal response to water deficit. *Funct. Plant Biol.* 39, 179–189. doi: 10.1071/FP11156

Coupel-Ledru, A., Tyerman, S. D., Masclef, D., Lebon, E., Christophe, A., Edwards, E. J., et al. (2017). Abscisic acid down-regulates hydraulic conductance of grapevine leaves in isohydric genotypes only. *Plant Physiol.* 175, 1121–1134. doi: 10.1104/pp.17.00698

CR2 (2015). *Report to the Nation: The Central Chile Mega-Drought. Technical Report from the Center for Climate and Resilience Research*. Santiago-Chile, 30. Available online at: http://www.cr2.cl/megasequia (accessed March 16, 2022).

Dayer, S., Herrera, J. C., Dai, Z., Burlett, R., Lamarque, L. J., Delzon, S., et al. (2020). The sequence and thresholds of leaf hydraulic traits underlying grapevine varietal differences in drought tolerance. *J. Exp. Bot.* 71, 4333–4344. doi: 10.1093/jxb/eraa186

del Pozo, A., Brunel-Saldias, N., Engler, A., Ortega-Farías, S., Acevedo-Opazo, C., Lobos, G. A., et al. (2019). Climate change impacts and adaptation strategies of agriculture in mediterranean-climate regions (MCRs). *Sustain.* 11, 2769–2716. doi: 10.3390/su11102769

Delrot, S., Grimplet, J., Carbonell-Bejerano, P., Schwandner, A., Bert, P.-F., Bavaresco, L., et al. (2020). "Genetic and genomic approaches for adaptation of grapevine to climate change." in *Genomic Designing of Climate-Smart Fruit Crops*, eds C. Kole (Springer, Cham), 1–114.

Dry, P. R., and Loveys, B. R. (1998). Factors influencing grapevine vigour and the potential for control with partial rootzone drying. *Aust. J. Grape Wine Res.* 4, 140–148. doi: 10.1111/j.1755-0238.1998.tb00143.x,

FAO, Food and Agriculture Organization of the United Nations. (2018). *The Impact of Disasters and Crises on Agriculture and Food Security*. Availbale online at: http://www.fao.org/emergencies/resources/documents/resources-detail/en/c/1106859/ (accessed June 23, 2020).

Franck, N., Zamorano, D., Wallberg, B., Hardy, C., Ahumada, M., Rivera, N., et al. (2020). Contrasting grapevines grafted into naturalized rootstock suggest scion-driven transcriptomic changes in response to water deficit. *Sci. Hortic.* 262, 109031. doi: 10.1016/j.scienta.2019.109031

Gambetta, G. A., Herrera, J. C., Dayer, S., Feng, Q., Hochberg, U., and Castellarin, S. D. (2020). The physiology of drought stress in grapevine: towards an integrative definition of drought tolerance. *J. Exp. Bot.* 71, 4658–4676. doi: 10.1093/jxb/eraa245

Garreaud, R. D., Boisier, J. P., Rondanelli, R., Montecinos, A., Sepúlveda, H. H., and Veloso-Aguila, D. (2020). The central chile mega drought (2010–2018): a climate dynamics perspective. *Int. J. Climatol.* 40, 421–439. doi: 10.1002/joc.6219

Gomès, É., Maillot, P., and Duchêne, É. (2021). Molecular tools for adapting viticulture to climate change. *Front. Plant Sci.* 12, 633846. doi: 10.3389/fpls.2021.633846

Gupta, A., Rico-Medina, A., and Caño-Delgado, A. I. (2020). The physiology of plant responses to drought. *Science* 368, 266–269. doi: 10.1126/science.aaz7614

Hannah, L., Roehrdanz, P. R., Ikegami, M., Shepard, A. V., Shaw, M. R., Tabor, G., et al. (2013). Climate change, wine, and conservation. *Proc. Natl. Acad. Sci.* 110, 6907–6912. doi: 10.1073/pnas.1210127110

Hochberg, U., Degu, A., Fait, A., and Rachmilevitch, S. (2012). Near isohydric grapevine cultivar displays higher photosynthetic efficiency and photorespiration rates under drought stress as compared with near anisohydric grapevine cultivar. *Phys. Plant.* 147, 443–452. doi: 10.1111/j.1399-3054.2012.01671.x

Hochberg, U., Rockwell, F. E., Holbrook, N. M., and Cochard, H. (2018). Iso/anisohydry: a plant–environment interaction rather than a simple hydraulic trait. *Trends Pl. Sci.* 23, 112–120. doi: 10.1016/j.tplants.2017.11.002

Hsiao, T. C., Steduto, P., and Fereres, E. (2007). A systematic and quantitative approach to improve water use efficiency in agriculture. *Irrig. Sci.* 25, 209–231. doi: 10.1007/s00271-007-0063-2

Ibacache, A., Albornoz, F., and Zurita-Silva, A. (2016). Yield responses in Flame seedless, Thompson seedless and Red Globe table grape cultivars are differentially modified by rootstocks under semi arid conditions. *Sci. Hortic.* 204, 25–32. doi: 10.1016/j.scienta.2016.03.040

Ibacache, A., Verdugo-Vásquez, N., and Zurita-Silva, A. (2020). "Chapter 21. Rootstock: Scion combinations and nutrient uptake in grapevines," in *Fruit Crops: Diagnosis and Management of Nutrient Constraints,* eds A. K. Srivastava, C. Hu (Cambridge: Elsevier Inc.) 297–316.

International Organisation of Vine and Wine (OIV) (2021). *International Code Of Œnological Practices*. Available online at: https://www.oiv.int/public/medias/7713/en-oiv-code-2021.pdf (accessed January 28, 2022).

IPCC (2021). "Climate change 2021: the physical science basis," in *Contribution of Working Group I to the Sixth Assessment Report of the Intergovernmental Panel on Climate Change*, eds V. Masson-Delmotte, P. Zhai, A. Pirani, S. L. Connors, C. Péan, S. Berger, N. Caud, Y. Chen, L. Goldfarb, M. I. Gomis, M. Huang, K. Leitzell, E. Lonnoy, J. B. R. Matthews, T. K. Maycock, T. Waterfield, O. Yelekçi, R. Yu, and B. Zhou (Cambridge University Press). In Press.

Jara-Rojas, F., Ortega-Farías, S., Valdés-Gómez, H., and Acevedo-Opazo, C. (2015). Gas exchange relations of ungrafted grapevines (cv. Carménère) growing under irrigated field conditions. *South African J Enol. Viticult.* 36, 231–242.

Jury, W. A., and Vaux, H. (2005). The role of science in solving the world's emerging water problems. *Proc. Natl. Acad. Sci*. 102 15715–15720. doi: 10.1073/pnas.0506467102

Keller, M., Mills, L. J., and Harbertson, J. F. (2012). Rootstock effects on deficit-irrigated winegrapes in a dry climate: vigor, yield formation, and fruit ripening. *Am. J. Enol. Viticult.* 63, 29–39. doi: 10.5344/ajev.2011.11078

Kijne, J. W. (2006). Abiotic stress and water scarcity: identifying and resolving conflicts from plant level to global level. *Field Crop Res.* 97, 3–18. doi: 10.1016/j.fcr.2005.08.011

Lavoie-Lamoureux, A., Sacco, D., Risse, P., and Lovisolo, C. (2017). Factors influencing stomatal conductance in response to water availability in grapevine: a meta-analysis. *Physiol. Plant.* 159, 468–482. doi: 10.1111/ppl.12530

Lawlor, D. W. (2002). Limitation to photosynthesis in water stressed leaves: stomata vs. metabolism and the role of ATP. *Ann. Bot.* 89, 871–885. doi: 10.1093/aob/mcf110

Levin, A. D., Williams, L. E., and Matthews, M. A. (2020). A continuum of stomatal responses to water deficits among 17 wine grape cultivars (*Vitis vinifera*). *Funct. Plant Biol.* 47, 11–25. doi: 10.1071/FP19073

Li, T., Hao, X., and Kang, S. (2016). Spatial variability of grapevine bud burst percentage and its association with soil properties at field scale. *PLoS ONE* 11, e0165738. doi: 10.1371/journal.pone.0165738

Loureiro, M. D., Moreno-Sanz, P., García, A., Fernández, O., Fernández, N., and Suárez, B. (2016). Influence of rootstock on the performance of the Albarín Negro minority grapevine cultivar. *Sci. Hortic.* 201, 145–152. doi: 10.1016/j.scienta.2016.01.023

Lovisolo, C., Lavoie-Lamoureux, A., Tramontini, S., and Ferrandino, A. (2016). Grapevine adaptations to water stress: new perspectives about soil/plant interactions. *Theor. Exp. Plant Phys.* 28, 53–66. doi: 10.1007/s40626-016-0057-7

Lovisolo, C., Perrone, I., Carra, A., Ferrandino, A., Flexas, J., Medrano, H., et al. (2010). Drought-induced changes in development and function of grapevine (*Vitis* spp.) organs and in their hydraulic and non-hydraulic interactions at the whole-plant level: a physiological and molecular update. *Funct. Plant Biol.* 37, 98–116. doi: 10.1071/FP09191

Medrano, H., Escalona, J. M., Bota, J., Gulías, J., and Flexas, J. (2002). Regulation of photosynthesis of C3 plants in response to progressive drought: stomatal conductance as a reference parameter. *Ann. Bot.* 89, 895–905. doi: 10.1093/aob/mcf079

Medrano, H., Escalona, J. M., Cifre, J., Bota, J., and Flexas, J. (2003). A ten-year study on the physiology of two Spanish grapevine cultivars under field conditions: effects of water availability from leaf photosynthesis to grape yield and quality. *Funct. Plant Biol.* 30, 607–619. doi: 10.1071/FP02110

Medrano, H., Tortosa, I., Montes, E., Pou, A., Balda, P., Bota, J., et al. (2018). "Genetic improvement of grapevine (*Vitis vinifera* L.) water use efficiency: variability among varieties and clones," in *Water Scarcity and Sustainable Agriculture in Semiarid Environment*, eds I. F. García Tejero, V. H. Durán Zuazo (London: Academic Press), 377–401.

Meggio, F., Prinsi, B., Negri, A. S., Lorenzo, G. S. D., Lucchini, G., Pitacco, A., et al. (2014). Biochemical and physiological responses of two grapevine rootstock genotypes to drought and salt treatments. *Aust. J. Grape Wine Res.* 20, 310–323. doi: 10.1111/ajgw.12071

Milla-Tapia, A., Gómez, S., Moncada, X., León, P., Ibacache, A., Rosas, M., et al. (2013). Naturalised grapevines collected from arid regions in Northern Chile exhibit a high level of genetic diversity. *Aust. J. Grape Wine Res.* 19, 299–310. doi: 10.1111/ajgw.12020

Morales-Castilla, I., Cortazar-Atauri, I. G., de Cook, B. I., Lacombe, T., Parker, A., Leeuwen, C. V., et al. (2019). Diversity buffers winegrowing regions from climate change losses. *Proc. Natl. Acad. Sci.* 117, 2864–2869. doi: 10.1073/pnas.1906731117

Moriana, A., Perez-Lopez, D., Gomez-Rico, A., Salvador Md, L. D., Olmedilla, N., Ribas, F., et al. (2007). Irrigation scheduling for traditional., low-density olive orchards: water relations and influence on oil characteristics. *Agric. Water Manag.* 87, 171–179. doi: 10.1016/j.agwat.2006.06.017

Myers, B. J. (1988). Water stress integral—a link between short-term stress and long-term growth *Tree Physiol.* 4, 315–323. doi: 10.1093/treephys/4.4.315

Naulleau, A., Gary, C., Prévot, L., and Hossard, L. (2021). Evaluating strategies for adaptation to climate change in grapevine production–a systematic review. *Front. Plant Sci.* 11, 607859. doi: 10.3389/fpls.2020.607859

Ollat, N., Peccoux, A., Papura, D., Esmenjaud, D., Marguerit, E., Tandonnet, J.-P., et al. (2016). "Rootstocks as a component of adaptation to environment," in *Grapevine in a Changing Environment*, eds H. Gerós, M. M. Chaves, H. M. Gil, and S. Delrot (Chichester: John Wiley and Sons, Ltd.), 68–108.

Parker, A. K., Cortázar-Atauri, I. G. D., Leeuwen, C. V., and Chuine, I. (2011). General phenological model to characterise the timing of flowering and veraison of *Vitis vinifera* L. *Aust. J. Grape Wine Res.* 17, 206–216. doi: 10.1111/j.1755-0238.2011.00140.x

Peccoux, A., Loveys, B., Zhu, J., Gambetta, G. A., Delrot, S., Vivin, P., et al. (2018). Dissecting the rootstock control of scion transpiration using model-assisted analyses in grapevine. *Tree Physiol.* 38, 1026–1040. doi: 10.1093/treephys/tpx153

Pérez-Álvarez, E. P., Intrigliolo Molina, D. S., Vivaldi, G. A., García-Esparza, M. J., Lizama, V., and Álvarez, I. (2021). Effects of the irrigation regimes on grapevine cv. Bobal in a Mediterranean climate: I. Water relations, vine performance and grape composition, Agr. *Water Manage.* 248, 106772, doi: 10.1016/j.agwat.2021.106772

Polade, S. D., Gershunov, A., Cayan, D. R., Dettinger, M. D., and Pierce, D. W. (2017). Precipitation in a warming world: assessing projected hydro-climate changes in California and other Mediterranean climate regions. *Sci. Rep.* 7, 10783. doi: 10.1038/s41598-017-11285-y

Postel, S. (2000). Entering an era of water scarcity: the challenges ahead. *Ecol. App.* 10, 941–948. doi: 10.1890/1051-0761(2000)0100941:EAEOWS2.0.CO;2

Prinsi, B., Simeoni, F., Galbiati, M., Meggio, F., Tonelli, C., Scienza, A., et al. (2021). Grapevine rootstocks differently affect physiological and molecular responses of the scion under water deficit condition. *Agronomy* 11, 289. doi: 10.3390/agronomy,11020289

R Development Core Team (2008). *R: A Language and Environment for Statistical Computing*. Vienna: R Foundation for Statistical Computing.

Ripoche, A., Celette, F., Cinna, J.-P., and Gary, C. (2010). Design of intercrop management plans to fulfil production and environmental objectives in vineyards. *Eur. J. Agron.* 32, 30–39. doi: 10.1016/j.eja.2009.05.005

Romero, P., Botía, P., and Navarro, J. M. (2018). Selecting rootstocks to improve vine performance and vineyard sustainability in deficit irrigated Monastrell grapevines under semiarid conditions. *Agr. Water Manage.* 209, 73–93. doi: 10.1016/j.agwat.2018.07.012

Romero, P., and García-García, J. (2020). The productive, economic, and social efficiency of vineyards using combined drought-tolerant rootstocks and efficient low water volume deficit irrigation techniques under mediterranean semiarid conditions. *Sustainability* 12, 1930. doi: 10.3390/su12051930

Romero, P., Navarro, J. M., and Ordaz, P. B. (2022). Towards a sustainable viticulture: the combination of deficit irrigation strategies and agroecological practices in Mediterranean vineyards. A review and update. *Agr. Water Manage.* 259, 107216. doi: 10.1016/j.agwat.2021.107216

Sabbatini, P., and Howell, G. S. (2013). Rootstock scion interaction and effects on vine vigor, phenology, and cold hardiness of interspecific hybrid grape cultivars (*Vitis* spp.). *Int. J. Fruit Sci.* 13, 466–477. doi: 10.1080/15538362.2013.789277

Santillán, D., Iglesias, A., Jeunesse, I. L., Garrote, L., and Sotes, V. (2019). Vineyards in transition: a global assessment of the adaptation needs of grape producing regions under climate change. *Sci. Total Environ.* 657, 839–852. doi: 10.1016/j.scitotenv.2018.12.079

Satisha, J., Somkuwar, R. G., and Sharma, J. (2010). Influence of rootstocks on growth yield and fruit composition of Thompson seedless grapes grown in the Pune region of India. *S. Afr. J. Enol. Vitic.* 31, 1–8. doi: 10.21548/31-1-1392

Schultz, H. R. (2003). Differences in hydraulic architecture account for near-isohydric and anisohydric behaviour of two field-grown *Vitis vinifera* L. cultivars during drought. *Pl. Cell Environ.* 26, 1393–1405. doi: 10.1046/j.1365-3040.2003.01064.x

Serra, I., Strever, A., Myburgh, P. A., and Deloire, A. (2014). Review: the interaction between rootstocks and cultivars (*Vitis vinifera* L.) to enhance drought tolerance in grapevine. *Aust. J. Grape Wine R.* 20, 1–14. doi: 10.1111/ajgw.12054

Simonneau, T., Lebon, E., Coupel-Ledru, A., Marguerit, E., Rossdeutsch, L., and Ollat, N. (2017). Adapting plant material to face water stress in vineyards: which physiological targets for an optimal control of plant water status? *OENO One* 51, 167–113. doi: 10.20870/oeno-one.2016.0.0.1870

Takahashi, F., Suzuki, T., Osakabe, Y., Betsuyaku, S., Kondo, Y., Dohmae, N., et al. (2018). A small peptide modulates stomatal control *via* abscisic acid in long-distance signalling. *Nature* 556, 235–238. doi: 10.1038/s41586-018-0009-2

Tomás, M., Medrano, H., Escalona, J. M., Martorell, S., Pou, A., Ribas-Carbó, M., et al. (2014). Variability of water use efficiency in grapevines. *Environ. Exp. Bot.* 103, 148–157. doi: 10.1016/j.envexpbot.2013.09.003

Tortosa, I., Escalona, J. M., Douthe, C., Pou, A., Garcia-Escudero, E., Toro, G., et al. (2019). The intra-cultivar variability on water use efficiency at different water status as a target selection in grapevine: influence of ambient and genotype. *Agr. Water Manage.* 223, 105648. doi: 10.1016/j.agwat.2019.05.032

van Leeuwen, C., and Destrac-Irvine, A. (2017). Modified grape composition under climate change conditions requires adaptations in the vineyard. *OENO One* 51, 147–148. doi: 10.20870/oeno-one.2017.51.2.1647

van Leeuwen, C., Destrac-Irvine, A., Dubernet, M., Duchêne, E., Gowdy, M., Marguerit, E., et al. (2019). An update on the impact of climate change in viticulture and potential adaptations. *Agronomy* 9, 514. doi: 10.3390/agronomy9090514

Verdugo-Vásquez, N., Acevedo-Opazo, C., Valdés-Gómez, H., et al. (2021b). Identification of main factors affecting the within-field spatial variability of grapevine phenology and total soluble solids accumulation: towards the vineyard zoning using auxiliary information. *Precis. Agric.* 23, 253–277. doi: 10.1007/s11119-021-09836-5

Verdugo-Vásquez, N., Acevedo-Opazo, C., Valdés-Gómez, H., Araya-Alman, M., Ingram, B., García de Cortázar-Atauri, I., et al. (2016). Spatial variability of phenology in two irrigated grapevine cultivars growing under semi-arid conditions. *Precis. Agric.* 17, 218–245. doi: 10.1007/s11119-015-9418-5

Verdugo-Vásquez, N., Acevedo-Opazo, C., Valdes-Gomez, H., Ingram, B., García de Cortázar-Atauri, I., and Tisseyre, B. (2018). Temporal stability of within-field variability of total soluble solids of grapevine under semi-arid conditions: a first step towards a spatial model. *OENO One* 52, 15–30. doi: 10.20870/oeno-one.2018.52.1.1782

Verdugo-Vásquez, N., Gutiérrez-Gamboa, G., Villalobos-Soublett, E., and Zurita-Silva, A. (2021a). Effects of rootstocks on blade nutritional content of two minority grapevine varieties cultivated under hyper-arid conditions in northern chile. *Agronomy* 11, 327. doi: 10.3390/agronomy11020327

Villalobos-González, L., Muñoz-Araya, M., Franck, N., and Pastenes, C. (2019). Controversies in midday water potential regulation and stomatal behavior might result from the environment, genotype, and/or rootstock: evidence from Carménère and Syrah grapevine varieties. *Front. Plant Sci.* 10, 1522. doi: 10.3389/fpls.2019.01522

Walker, R. R., Blackmore, D. H., Clingeleffer, P. R., and Emanuelli, D. (2014). Rootstock type determines tolerance of Chardonnay and Shiraz to long-term saline irrigation. *Aust. J. Grape Wine R.* 20, 496–506. doi: 10.1111/ajgw.12094

Warschefsky, E. J., Klein, L. L., Frank, M. H., Chitwood, D. H., Londo, J. P., Wettberg, E. J. B., et al. (2016). Rootstocks: diversity, domestication, and impacts on shoot phenotypes. *Trends Plant Sci.* 21, 418–437. doi: 10.1016/j.tplants.2015.11.008

Wolkovich, E. M., García de Cortázar-Atauri, I., Morales-Castilla, I., et al. (2018). From Pinot to Xinomavro in the world's future wine-growing regions. *Nature Clim. Change* 8, 29–37. doi: 10.1038/s41558-017-0016-6

Yan, W., Zhong, Y., and Shangguan, Z. (2016). A meta-analysis of leaf gas exchange and water status responses to drought. *Sci. Rep.* 6, 917. doi: 10.1038/srep20917

Zamorano, D., Franck, N., Pastenes, C., Wallberg, B., Garrido, M., and Silva, H. (2021). Improved physiological performance in grapevine (*Vitis vinifera* L.) cv. Cabernet Sauvignon facing recurrent drought stress. *Aust. J. Grape Wine R.* 27, 258–268. doi: 10.1111/ajgw.12482

Zhang, J., Jia, W., Yang, J., and Ismail, A. M. (2006). Role of ABA in integrating plant responses to drought and salt stresses. *Field Crops Res.* 97, 111–119. doi: 10.1016/j.fcr.2005.08.018

Zhang, J., Jiang, H., Song, X., Jin, J., and Zhang, X. (2018). The responses of plant leaf CO_2/H_2O exchange and water use efficiency to drought: a meta-analysis. *Sustainability* 10, 551. doi: 10.3390/su10020551

Zombardo, A., Mica, E., Puccioni, S., Perria, R., Valentini, P., Mattii, G. B., et al. (2020). Berry quality of grapevine under water stress as affected by rootstock–scion interactions through gene expression regulation. *Agronomy* 10, 680. doi: 10.3390/agronomy10050680

Zúñiga, M., Ortega-Farías, S., Fuentes, S., Riveros-Burgos, C., and Poblete-Echeverría, C. (2018). Effects of three irrigation strategies on gas exchange relationships, plant water status, yield components and water productivity on grafted Carménère grapevines. *Front. Plant. Sci.* 9, 956–913 doi: 10.3389/fpls.2018.00992

Conflict of Interest: The authors declare that the research was conducted in the absence of any commercial or financial relationships that could be construed as a potential conflict of interest.

Publisher's Note: All claims expressed in this article are solely those of the authors and do not necessarily represent those of their affiliated organizations, or those of the publisher, the editors and the reviewers. Any product that may be evaluated in this article, or claim that may be made by its manufacturer, is not guaranteed or endorsed by the publisher.

Advantages of publishing in Frontiers

OPEN ACCESS
Articles are free to read for greatest visibility and readership

FAST PUBLICATION
Around 90 days from submission to decision

HIGH QUALITY PEER-REVIEW
Rigorous, collaborative, and constructive peer-review

TRANSPARENT PEER-REVIEW
Editors and reviewers acknowledged by name on published articles

Frontiers
Avenue du Tribunal-Fédéral 34
1005 Lausanne | Switzerland

Visit us: www.frontiersin.org
Contact us: frontiersin.org/about/contact

REPRODUCIBILITY OF RESEARCH
Support open data and methods to enhance research reproducibility

DIGITAL PUBLISHING
Articles designed for optimal readership across devices

FOLLOW US
@frontiersin

IMPACT METRICS
Advanced article metrics track visibility across digital media

EXTENSIVE PROMOTION
Marketing and promotion of impactful research

LOOP RESEARCH NETWORK
Our network increases your article's readership